

5. SITE 646¹

Shipboard Scientific Party²

HOLE 646A

Date occupied: 3 October 1985, 1145 UTC

Date departed: 4 October 1985, 1130 UTC

Time on hole: 23 hr, 45 min

Position: 58°12.559'N, 48°22.147'W

Water depth (sea level, corrected m, echo-sounding): 3450.8

Water depth (rig floor, corrected m, echo-sounding): 3461.3

Bottom felt (m, drill pipe): 3461.7

Distance between rig floor and sea level (m): 10.5

Total depth (rig floor; m): 3565.2

Penetration (m): 103.5

Number of cores: 11

Total length of cored section (m): 103.5

Total core recovered (m): 92.4

Core recovery (%): 89

Deepest sedimentary unit cored:

Depth sub-bottom (m): 103.5

Nature: silty clay

Age: Pleistocene

Measured vertical sound velocity (km/s): 1.63 (physical properties)

HOLE 646B

Date occupied: 4 October 1985, 1445 UTC

Date departed: 14 October 1985, 0000 UTC

Time on hole: 9 day, 9 hr, 15 min

Position: 58°12.559'N, 48°22.147'W

Water depth (sea level, corrected m, echo-sounding): 3450.8

Water depth (rig floor, corrected m, echo-sounding): 3461.3

Bottom felt (m, drill pipe): 3458.7

Distance between rig floor and sea level (m): 10.5

Total depth (rig floor; m): 4225.4

Penetration (m): 766.7

Number of cores: 80

Total length of cored section (m): 766.7

Total core recovered (m): 402.86

Core recovery (%): 53

Deepest sedimentary unit cored:

Depth sub-bottom (m): 766.7

Nature: silty clays, clayey silt

Age: late Miocene

Measured vertical sound velocity (km/s): 2.095 (sonic log)

Principal results: Site 646, Holes 646A and 646B, were drilled in a water depth of 3451.2 m, at 58°12.559'N, 48°22.147'W, in the southeastern Labrador Sea. The total depth of penetration was 766.7 mbsf; average recovery was 55.7%. (Hole 646A—APC, 89%; Hole 646B—APC, 74%; XCB, 48%). Two major lithologic units were recovered as follows:

Unit 1 (Cores 105-646A-1H to 105-646A-11H and 105-646B-1H to 105-646B-25X) 0–236.1 mbsf. Age: late Pliocene to Holocene. Description: Unit 1 subdivided into two units as follows:

Subunit 1A (Cores 105-646A-1H to 105-646A-11H and 105-646B-1H to 105-646B-20X) 0–188.2 mbsf. Age: late Pliocene to Holocene. Description: Predominantly greenish gray, dark-gray to light-gray silty clays and clayey silts having as much as 40% carbonate; calcareous nannofossils, foraminifers, and diatoms are common biogenic components. Some thin detrital carbonate to noncarbonate silt and silty clay beds having sharp bases are thinly laminated to cross-laminated. Beds that are relatively rich in detrital carbonate minerals exhibit structures of thin-bedded turbidites. Otherwise, the major lithofacies are homogeneous to bioturbated. Dropstones are common and consist predominantly of mafic volcanics.

Subunit 1B (Cores 105-646B-21X to 105-646B-25X) 188.2–236.1 mbsf. Age: late Pliocene. Description: Predominantly dark-gray to dark greenish gray, poorly sorted, locally granule-bearing muddy sands and silty muds showing vague stratification or size gradation and subtle color banding. Pebbles are common and consist mainly of mafic volcanics but some granitic and gneissic rocks are also present; all are interpreted as being dropstones. The carbonate content aver-

¹ Srivastava, S. P., Arthur, M., Clement, B., et al., *Proc., Init. Repts. (Pt. A), ODP*, 105.

² Ali Aksu, Earth Sciences Department, Memorial University of Newfoundland, St. John's, Newfoundland A1B 3X5, Canada; Michael Arthur (Co-Chief Scientist), Graduate School of Oceanography, University of Rhode Island, Narragansett, RI 02882; Jack Baldauf, Ocean Drilling Program, 1000 Discovery Drive, College Station, TX 77840; Gerhard Bohrmann, Geologisch-Palaeontologisches Institut und Museum der CAU, Olshausenstr. 40, 2300 Kiel, Federal Republic of Germany; William Busch, Department of Geology and Geophysics, University of New Orleans, New Orleans, LA 70148; Tommy Cederberg, University of Copenhagen, Geological Institute, Oester Voldgade 10, DK-1350, Copenhagen, Denmark; Bradford Clement (Co-Chief Scientist), Ocean Drilling Program, 1000 Discovery Drive, College Station, TX 77840; Michel Cremer, Department de Géologie et Océanographie, UA 197, Université de Bordeaux I, Avenue des Facultés, 33405 Talence Cedex, France; Kathleen Dadey, Graduate School of Oceanography, University of Rhode Island, Narragansett, RI 02882; Anne De Vernal, GEOTOP, Sciences de la Terre, Université du Québec à Montréal, L.P. 8888, Succ "A", Montreal, Quebec H3C 3P8, Canada; John Firth, Department of Geology, Florida State University, Tallahassee, FL 32306; Frank Hall, Graduate School of Oceanography, University of Rhode Island, Narragansett, RI 02882-1197; Martin Head, Department of Geology, University of Toronto, Toronto M5A 1A1, Canada; Richard Hiscott, Earth Sciences Department, Memorial University, St. John's, Newfoundland A1B 3X5, Canada; Rich Jarrard, Lamont-Doherty Geological Observatory, Palisades, NY 10964; Michael Kaminski, WHOI/MIT Joint Program in Oceanography, Woods Hole Oceanographic Institution, Clark 1, Woods Hole, MA 02543; David Lazarus, Woods Hole Oceanographic Institution, Department of Geology and Geophysics, Woods Hole, MA 02543; Anne-Lise Monjanel, Université de Bretagne Occidentale, G.I.S. Océanologie et Géodynamique, 6, Av. Victor le Gorgeu, 29283 Brest Cedex, France; Ole Bjorslev Nielsen, Department of Geology, Aarhus University, DK-8000 Aarhus C, Denmark; Surat P. Srivastava (Co-Chief Scientist), Atlantic Geoscience Centre, Geological Survey of Canada, P.O. Box 1006, Dartmouth, Nova Scotia B2Y A42, Canada; Ruediger Stein, Institute of Petroleum and Organic Geochemistry, KFA Julich, P.O. Box 1913, 5170 Julich, Federal Republic of Germany (current address: Institut fuer Geowissenschaften und Lithosphärenforschung, Universitaet Giessen, Senckenbergstr. 3, 6300 Giessen, Federal Republic of Germany); Francois Thiebault, Lab. Dynamique Sédimentaire et Structurale, UA 713 UER, Sciences de la Terre, Université de Lille I, 59655 Villeneuve D'Ascq Cedex, France; James Zachos, Graduate School of Oceanography, University of Rhode Island, Narragansett, RI 02882; Herman Zimmerman, Department of Geology, Union College, Schenectady, NY 12308 (current address: Division of Polar Programs, National Science Foundation, Washington, D.C. 20550).

ages <10%. Detrital carbonate turbidites common to Subunit IA are absent.

Unit II (Cores 105-646B-26X to 105-646B-80X) 236.1–766.7 mbsf. Age: late Miocene to late Pliocene. Description: Mainly consists of dark-gray to greenish-gray silty clay (claystone), clay (claystone), and subordinate clayey silt (siltstone). Some layers contain as much as 50%–60% calcareous nannofossils, but carbonate content commonly varies between 0% and 30%. Strata are moderately to strongly bioturbated (*Zoophycus*, *Planolites*) and have strong mottling in carbonate-rich units. Few laminated silt layers are present.

More than 100 m of double APC cores provides a nearly complete, high-resolution record from 1.2 Ma to present. Fluctuations in carbonate content (0%–40%), vague color variations, magnetic-susceptibility changes, microfossil abundance and diversity, and dropstone abundances record continuous glacial–interglacial cycles. A continuous record through isotope stage 21 is probably contained in APC cores. The onset of major ice rafting at about 2.5 Ma (236 mbsf) coincides with a major change in seismic character. General smoothing and continuous sedimentation of the drift sequence occurred during the late Pliocene to Holocene.

A significant biotic change occurred at the early Pliocene/late Pliocene boundary (3.4 Ma; 314 mbsf). Biosiliceous material is common to abundant above, whereas calcareous nannofossils and planktonic foraminifers are more abundant below. This event probably represents significant cooling of surface water masses over the site accompanied by higher productivity of siliceous plankton. The changes in surface waters also closely correspond to a period of apparent intensification of deep circulation, beginning at about 4.0 Ma, as suggested by erosional modification of the drift sequence and construction of a pronounced ridge observed in the regional seismic lines.

A generally warm early Pliocene is indicated by relatively high and constant carbonate contents and abundant calcareous nannofossils and dinocysts. The Miocene/Pliocene boundary occurs at about 520 mbsf and approximately coincides with a change to highly variable and generally lower carbonate contents below this boundary and coincides with the position of the R2 reflector, which was previously thought to be late early Miocene in age. The R3/R4 seismic reflector, which was originally suggested to be of late Eocene/early Oligocene age, occurs at about 680 mbsf. Although lithology does not change markedly, the depth is closely constrained by velocity information supplied by an excellent sonic log and by physical-properties data. The reflector (actually a pair of reflectors at 680 and 730 mbsf) lies below the level where a significant change in sedimentation rate takes place. Further, it is underlain by an interval of sediment about 50 m thick having a lower density and is characterized by low CaCO₃ contents. The R3/R4 reflector may signify an important change in bottom-water characteristics and intensity of deep circulation during the late Miocene. The possibility of such a change is supported by a significant change in the benthic foraminifer fauna above 680 mbsf.

On the basis of drilling results and interpretation of seismic lines, major drift sedimentation began in this region sometime near the beginning of the late Miocene; earlier abyssal-current erosion and sedimentation in the area are possible but are not constrained by drilling. The advent of major drift sedimentation appears to coincide with increased influx of terrigenous sediments to the region during the latest Miocene, somewhat earlier than the expected flood of terrigenous material seen elsewhere at about 3.4 Ma associated with the transition to a glacial regime. Bottom-current-influenced sediments of the late Miocene–Holocene drift sequence at Site 646 are bioturbated to somewhat homogeneous throughout and possess no persistent features that could be called characteristic or indicative of contourites or current-deposited sediments. The average sedimentation rate is about 9.1 cm/k.y. (91 m/m.y.) in the entire sequence, but bulk accumulation rates decrease in the Pleistocene sequence.

BACKGROUND AND OBJECTIVES

Site 646 is located at proposed site LA-5A (13 km north of site LA-5) on the northwestern flank of Eirik Ridge in the north-eastern Labrador Sea (Fig. 1). The difference between sites LA-5 and LA-5A is the computed depth to the Eocene/Oligocene

boundary (R3/R4), which is about 50 m shallower at site LA-5A. The decision to drill site LA-5A rather than the deeper site LA-5 was an operational decision based on the time available to reach the deep objectives at LA-5, including time required in setting a necessary reentry cone. Because it was not clear that we could accomplish all the objectives at LA-5 in the time that remained, including penetration and recovery of oceanic crust at more than 1500 mbsf, we opted for shallower penetration at LA-5A, followed by drilling of LA-9 (Site 647) where basement of the same age could be cored at shallower depths. Sites 646 and 647 both lie on anomaly 24 crust (Figs. 1 and 4, “Introduction” chapter, this volume), but the depth to basement at Site 647 is only about 800 mbsf. Therefore, Site 646 shares most of the objectives with LA-5, as summarized in following text, except for recovery of the deeper Paleogene sequence and underlying basaltic crust.

Background

Regional Setting

One of the objectives of drilling a set of holes in the Labrador Sea and Baffin Bay during Leg 105, as outlined in the “Introduction” chapter (this volume), is to determine the history of paleocirculation of these basins and thereby establish their effects on the exchange of water between the Arctic and Atlantic oceans before the opening of the Norwegian–Greenland Sea. One site in Baffin Bay and two in the Labrador Sea were chosen for this purpose. Site 646, one of these sites, lies in the south-eastern part of the Labrador Sea, southwest of Greenland. The site was chosen because it lies in a region where maximum influence from the Norwegian Sea Overflow Water (NSOW) is expected and because the top of the older Paleogene section lies at a relatively shallow depth, thereby making it an ideal place for studying the onset of deep, cold bottom-water currents in the North Atlantic.

Despite the uncertainties that may exist about the history of evolution of the Labrador Sea (see “Introduction” chapter, this volume), the region near Site 646 seems to have evolved by seafloor spreading. Such a hypothesis is supported by seismic, gravity, and magnetic observations in this region. Magnetic measurements (Fig. 4, “Introduction” chapter, this volume) show the presence of well-developed magnetic anomalies that closely resemble typical oceanic crustal anomalies 23 to 24. Correlation and identification of the magnetic anomalies in this region (Kristoffersen and Talwani, 1977; Srivastava, 1978) show that they belong to a younger group (anomalies 20 to 24) formed during seafloor spreading between Greenland and North America. The anomalies are symmetrically arranged on either side of the extinct ridge axis, which can be seen in the seismic data as a large V-shaped graben feature. In gravity data (Fig. 2, “Introduction” chapter, this volume), the graben is expressed as a large negative anomaly. Thus, geophysical data near Site 646 show strong evidence that this site lies over early Eocene oceanic crust.

An older group of magnetic anomalies (25 to 33) lies east of Site 646 (Fig. 4, “Introduction” chapter, this volume). These anomalies have a significantly different trend from the younger group of anomalies near the site. Identification and correlation of similar anomalies throughout the Labrador Sea and in the North Atlantic south of the Charlie Gibbs Fracture Zone show that the anomalies on the southwestern margin of Greenland formed during the first stage of opening of the Labrador Sea before the opening of the Norwegian–Greenland Sea, when little or no motion took place between Greenland and Eurasia (Srivastava, 1978). With the opening of the Norwegian–Greenland Sea, the direction of motion between Greenland and North America changed drastically, and this resulted in formation of

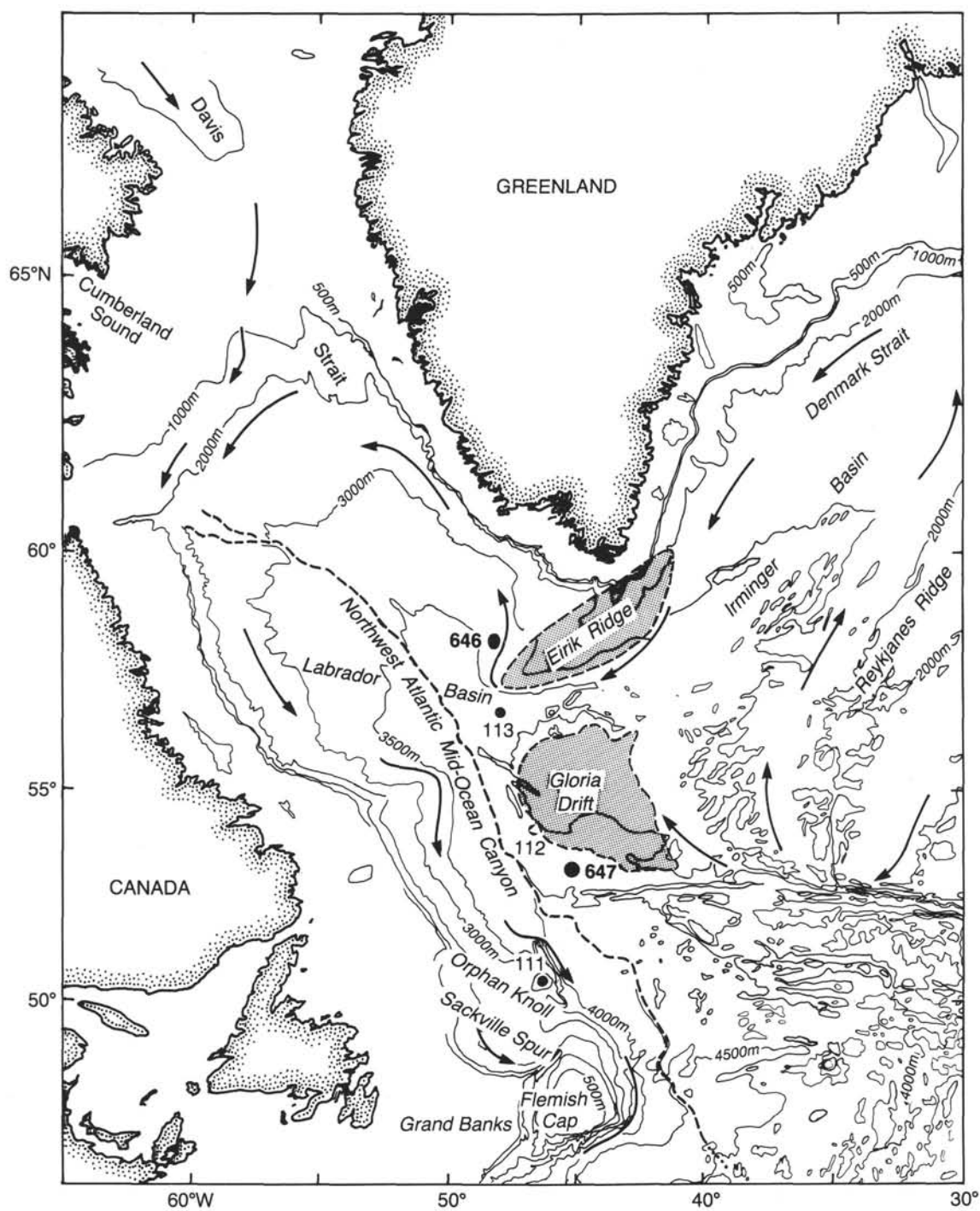


Figure 1. Bathymetric map of the northern North Atlantic, showing the locations of the two major drift deposits (Eirik Ridge and Gloria Drift) and of ODP Sites 646 and 647 and DSDP Sites 111, 112, and 113.

anomalies that exhibit a very different orientation. The change in direction of motion between plates gave rise to excessive volcanism in the Labrador Sea, as evidenced by the presence of large seamounts east of Site 646 (Fig. 2). Not all the anomalies belonging to the older group are observed east of Site 646. Anomaly 31, the first identified anomaly, lies directly adjacent to anomaly 24. This suggests a hiatus of approximately 10 m.y. in this region during the change in direction of motion of Greenland relative to North America.

The region around Site 646 has been extensively surveyed, and gravity, magnetic, and seismic information has been collected along the tracks shown in Figure 3. Some of this data was compiled in the form of contour maps (Figs. 2, 4, and 5). Seismic-reflection data near the site allow definition of several distinct sedimentary units, which are described as follows.

In seismic records (Figs. 6 through 8), the drift sequence near Site 646 is acoustically laminated, whereas acoustic transparency more commonly characterizes many sediment drifts in the

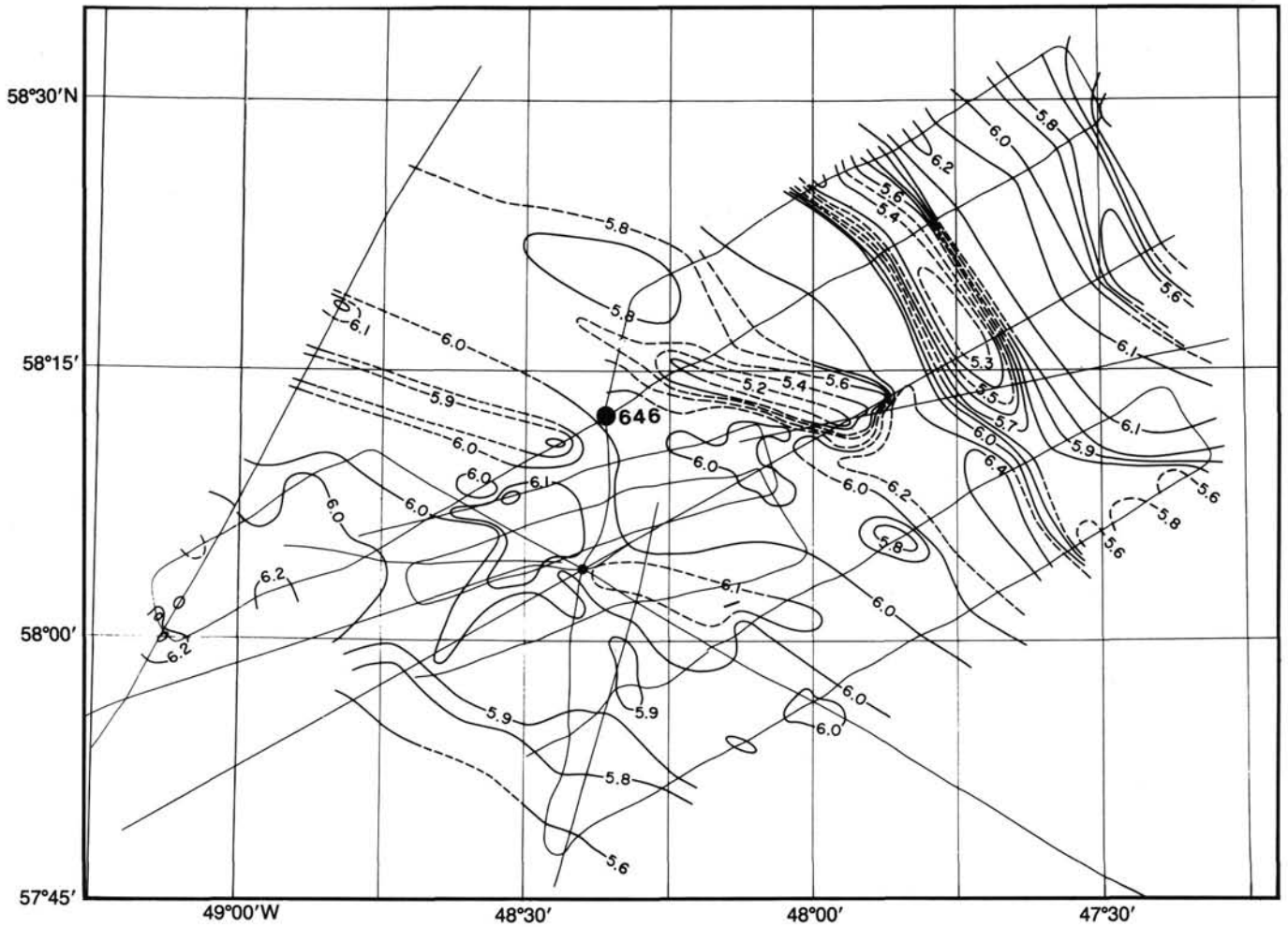


Figure 2. Depth to basement (from the sea surface) near Site 646. Contours in two-way traveltime(s).

North Atlantic. Several informal seismic units can be distinguished (these are shown on multichannel line BGR-2, which crosses single-channel line 14 south of Site 646 but to which we have correlated our reflector units; Fig. 6):

Seismic unit 1. The uppermost interval (unit 1) is about 0.27–0.28 s (250 m) thick at Site 646 and comprises a series of moderate- to high-amplitude reflectors that are parallel to subparallel to the seafloor. The unit varies in thickness over the region from a maximum of about 0.4 s to a minimum of 0.24 s. The thinnest part of the unit occurs at the crest of the subsidiary ridge just south of Site 646; at this point the amplitude of the reflectors also decreases somewhat. The number of internal reflectors increases on the flanks of the ridge.

Seismic unit 2. This unit occurs between 0.27 and 0.45 s bsf (about 250–540 mbsf) at Site 646, but it thickens to the south (Fig. 7), where it reaches a maximum of about 0.47 s thick (about 420 m). Seismic unit 2 has a lenticular shape and comprises a series of slightly northward-dipping (as seen on line 14) subparallel reflectors of very high amplitude. Thicknesses between individual reflectors vary systematically. Reflectors within seismic units 1 and 2 are generally parallel to subparallel to one another except in places where large lenticular wavy features are visible within seismic unit 2. On single-channel profiles, reflectors within seismic unit 2 exhibit stronger amplitudes and are more prominent than those in seismic unit 1 or in units below. On the multichannel lines (BGR2 and 1), seismic unit 2 thins on

the western flank of Eirik Ridge. The thinning is compensated for by thickening of a part of seismic unit 3 that exhibits chaotic internal reflections, perhaps indicating some slumping and/or strong current influence. A feature, probably a partly eroded remnant of an earlier depositional ridge, is the thickest part of seismic unit 2 that underlies the present crest of the subsidiary ridge previously discussed. Although the depth of the uppermost reflector of seismic unit 2 varies, the bottommost reflector lies relatively flat.

Seismic unit 3. The top of this unit and base of seismic unit 2 are marked by a prominent reflector, which is called reflector R2 here, and is of inferred late early Miocene age. A few reflectors, visible within this unit, are parallel to subparallel to the underlying seismic unit 2. Most of seismic unit 3 is acoustically transparent. The base of this unit is marked by a continuous to subcontinuous reflector, identified here as reflector R3 (or R3/R4) of possible Eocene to Oligocene age. The thickness of the unit varies between 0.3 and 0.35 s.

Seismic unit 4. The deepest unit defined in records crossing Site 646 lies below about 0.9 s and extends to the top of the fairly prominent basement reflector that is the top of the oceanic crust at roughly 1.3 s near the site. The top of the unit marked by the R3/R4 reflector is suspected to be equivalent to the R4 reflector of comparable age elsewhere in the northeast Atlantic and at DSDP Site 112 in the southwestern Labrador Sea (where it was assigned an early Oligocene age; see Miller and Tucholke,

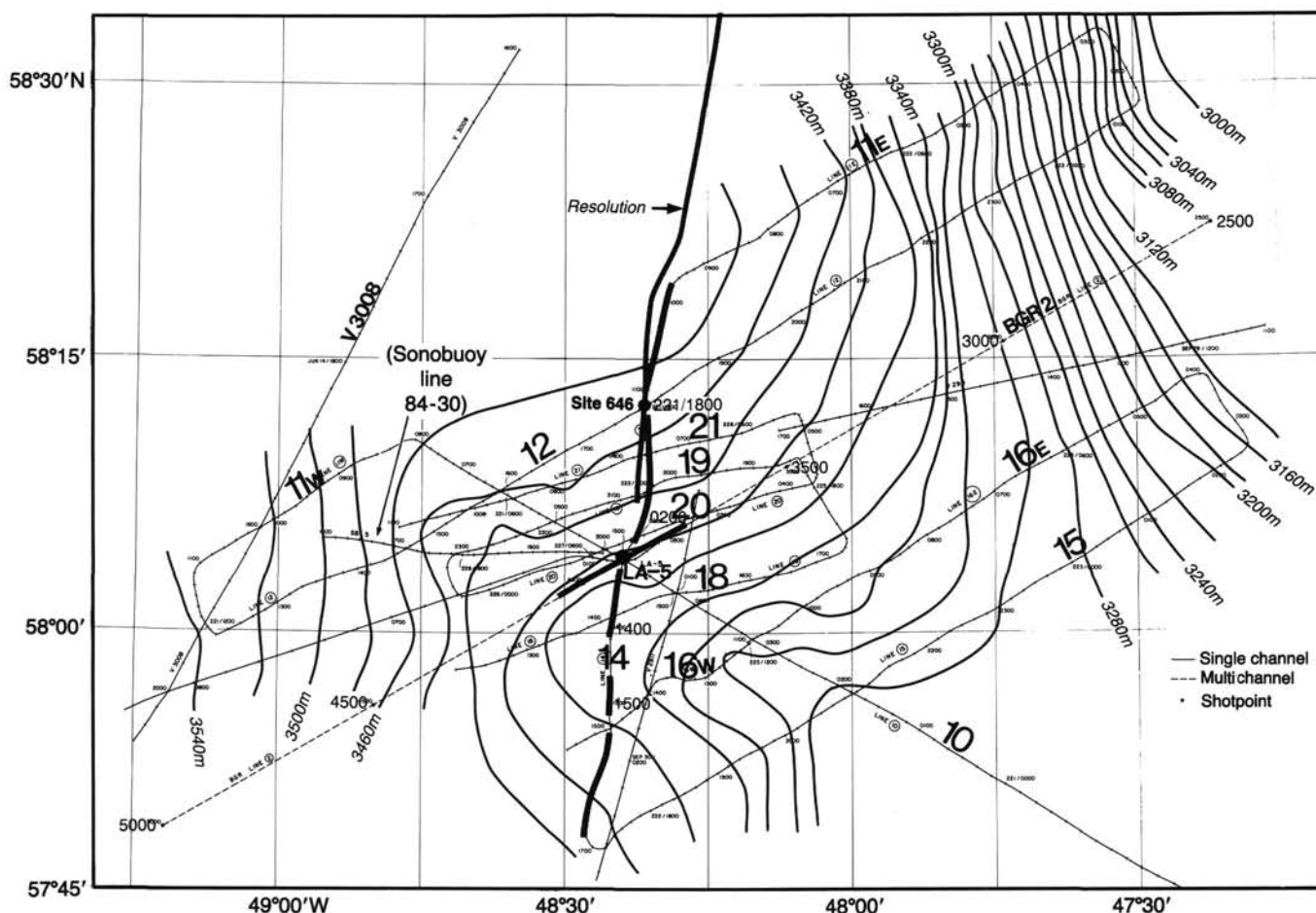


Figure 3. Map showing location of ship track (HD 84-030), along which gravity, magnetic, and bathymetry data were collected during a site survey cruise.

1983). This reflector is assumed to represent the onset of sea-floor erosion in latest Eocene to early Oligocene time, when the Greenland-Scotland Ridge had subsided enough to allow overflow of Arctic waters (NSOW) and the first formation and rapid circulation of bottom water in the North Atlantic (Berggren and Schnitker, 1983; Miller and Tucholke, 1983). The morphology of this reflector surface, as obtained from the compilation of all existing seismic data, is shown in Figure 5. A prominent reflector within the unit has a depth of 1.25 s bsf (Figs. 6 through 8). This deeper reflector terminates against a basement high to the west of early to middle Eocene age, as determined from magnetic-anomaly identification (Fig. 8).

A sedimentary drift deposit, known as Eirik Ridge, lies southeast of the site. The ridge was first delineated from a detailed bathymetric survey by Johnson and Schneider (1969); since then additional seismic and other geophysical data have been collected across the ridge by different agencies. Le Pichon et al. (1971) showed that a basement high, forming part of the Farwell Fracture Zone, underlies this region. From their seismic data, they interpreted that the ridge has developed over a flat-lying unconformity and as such is not controlled by basement-ridge topography. This is contrary to what is observed in some of the multi-channel seismic data from this region (Hinze et al., 1979). A compilation of depths to basement from all available seismic data in this region is shown in Figure 9 together with the main axis of deposition of Eirik Ridge. The magnetic lineations and major fracture zones as obtained from the synthesis of a large amount of magnetic, gravity, and seismic data in this region are also shown

(Kristoffersen and Talwani, 1977; Srivastava, 1978). The axis of deposition of Eirik Ridge lies along the southern flank of the basement high marked by the 5.5-s depth contour. Furthermore, examination of the seismic data in this region suggests the possibility that the major reflector identified as an Oligocene unconformity by Le Pichon et al. (1971) lies at a constant distance above the underlying basement that exhibits substantial relief. Thus we interpret the basement topography as probably having controlled the initial development of Eirik Ridge.

Sedimentary and Paleoclimatic Setting

Eirik Ridge (Johnson and Schneider, 1969) is one of many sediment drifts that occur around the margins of the northern North Atlantic (Fig. 1). Such drifts result from a combination of sediment erosion, redeposition, and smoothing of the sea-floor by strong contour currents (Johnson and Schneider, 1969; Jones et al., 1970). These deep currents originate by cooling and sinking of NSOW (Worthington and Volkmann, 1965; Worthington and Wright, 1970), which spills over the Greenland-Scotland Ridge through major channels at the Denmark Strait (Fig. 1) and the Faeroe-Shetland Trough. The NSOW from the Faeroe-Shetland Trough source follows the base of slope as it flows south around the Reykjanes Ridge and turns north and circulates counterclockwise, influenced by the Coriolis effect, around the Irminger Basin. Along its path, the main body of NSOW is joined by other portions of the overflow that follows the Charlie Gibbs Fracture Zone and pours through the Denmark Straits (Fig. 1). This flow is then diverted around the southern tip of

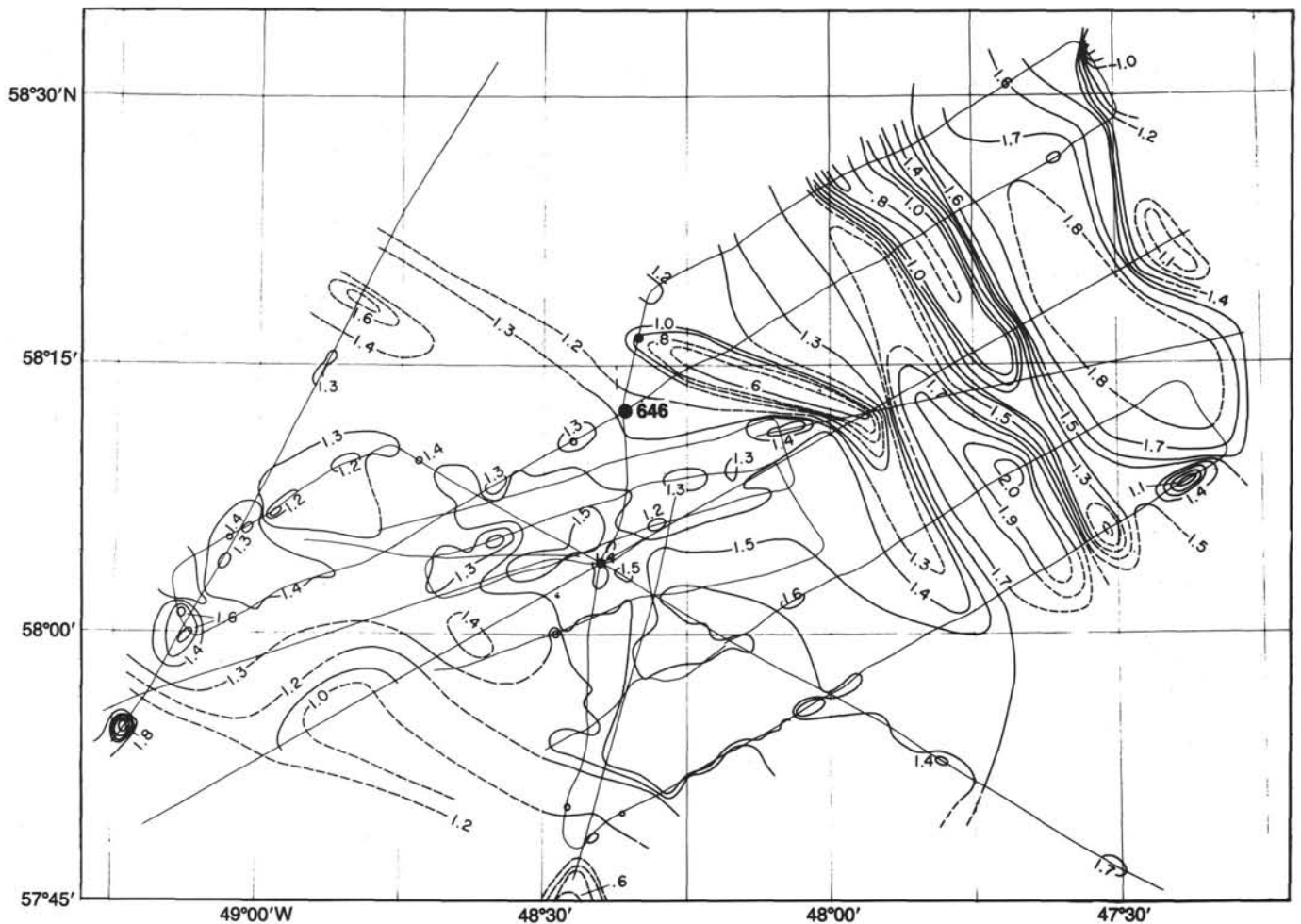


Figure 4. Total thickness of sediment near Site 646. Contours in two-way traveltime(s).

Greenland and turns northwest into the main part of the Labrador Sea. The Eirik Ridge is a depositional feature associated with the flow of NSOW around the southwestern side of Greenland.

Although other workers have suggested that basement structure has not influenced the development of the ridge (Le Pichon et al., 1971; Tucholke and Fry, in press), we observe a close correspondence between the main axis of Eirik Ridge and a fairly prominent basement high, as previously discussed. The basement high may have influenced the initial development of the depositional ridge. Such a hypothesis also explains the contrast between the pronounced bathymetric expression of the Eirik Ridge and the lack of expression in sediment isopachs map of Tucholke and Fry (in press). The total thickness of sediment above basement under Eirik Ridge is about 2 km.

Current velocities of as much as 20 cm/s have been measured in bottom currents in the Labrador Sea (Rabinowitz and Eitrem, 1974). Such currents can transport grain sizes as large as fine sand in traction and can winnow and suspend clay and fine silt. Therefore, the modern sediments of Eirik Ridge are dominantly clayey silts and silty clays (Chough and Hesse, 1985). Bioturbation and mottling account for 90%–95% of the structure of the modern sediments observed in piston cores, although some fine, parallel to wavy or hummocky lamination is present (Chough and Hesse, 1985). The laminated intervals generally lack both grading and systematic upward changes in thickness that are characteristic of fine-grained, laminated turbidites (Stow and Lovell, 1979; Stow, 1982).

We positioned Site 646 off the main axis of Eirik Ridge because we wanted to avoid the thick sedimentary sequence developed there. Site 646 is located on the northern flank of a subsidiary ridge, which, in seismic-reflection lines, exhibits characteristics of a drift sequence. Therefore, although we are unable to observe directly the history of the main depositional ridge in the cores from Site 646, we should be able to carry the ages of the main depositional units into the main drift by using seismic-reflection profiles, mainly the BGR multichannel lines (Fig. 3; see "Seismic Stratigraphy" section, this chapter).

Objectives

In addition to the general paleoclimate- and tectonic-related objectives outlined in the "Introduction" chapter (this volume) our major objectives at Site 646 were as follows:

1. We planned to penetrate the R3/R4 reflector to determine its age and its possible correlation with the R4 reflector identified in the northern North Atlantic by other workers (Roberts, 1975; Roberts et al., 1979; Miller and Tucholke, 1983) as being Eocene/Oligocene in age. The R3/R4 reflector is presumed to result from impedance contrasts across a pronounced hiatus developed by erosion at the onset of generation of strong North Atlantic bottom currents, resulting from overflow and sinking of cool Arctic water masses across the Greenland-Scotland Ridge. The reflector designated as R3/R4 here was identified on the basis of tentative seismic correlations with DSDP Site 112 (Fig. 1). Miller et al. (1982) placed R4 (in the more formal sense),

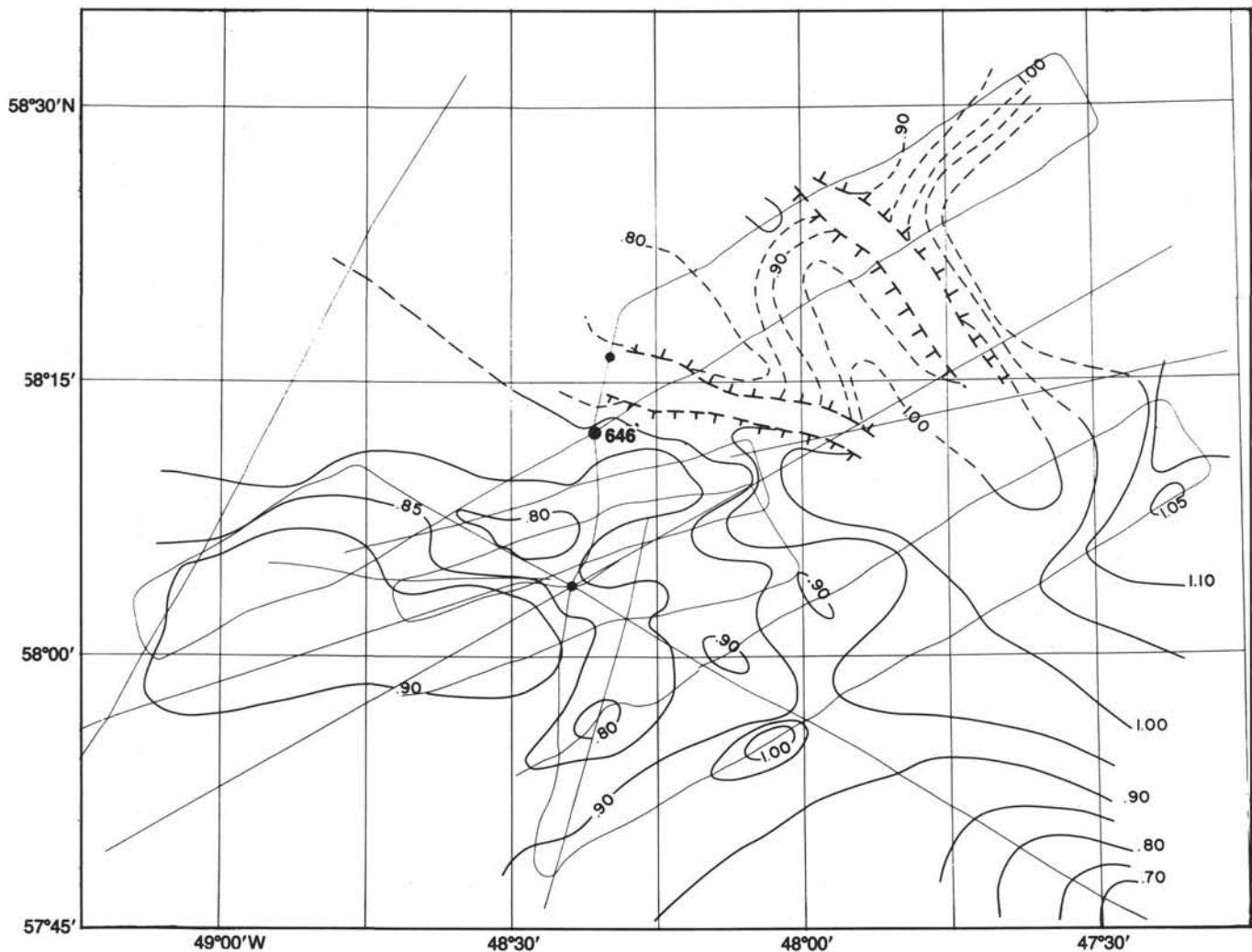


Figure 5. Map of depth to R3 reflector below the seafloor. Contour in two-way traveltime(s).

which occurred at 0.41 s in the seismic lines at Site 112, between 333 and 384 mbsf in the drilled section. The presumed age of the reflector at Site 112 is middle to early Oligocene within a sequence of siliceous silty clays. Miller et al. (1982) suggest that the sequence at Site 112 represents continuous deposition across the Eocene/Oligocene boundary, but they only spot-cored the section. Because so few continuous upper Eocene to middle Oligocene sequences occur in the North Atlantic, or for that matter in any ocean basin, such a sequence should be obtained. The predrilling seismic correlations suggest a substantial thickness of sediment between R3/R4 and reflector R2 (of presumed late early Miocene age) that could contain a continuous Eocene/Oligocene transition. Our goal was to penetrate the R3/R4 reflector and to core some of the interval below it to achieve an understanding of its significance to paleoceanographic changes in the Labrador Sea and the North Atlantic as a whole.

2. Another important objective was to characterize the sediment textures and compositions within a predominantly current-influenced depositional regime. Previous drilling in drift sequences has demonstrated that sedimentation is sufficiently continuous and that good biostratigraphic control is possible (Shackleton et al., 1984; Ruddiman, Kidd, et al., in press). In addition, many continental-margin or open-ocean sediment drifts do not appear to be characterized by a suite of obvious textures and sedimentary structures that might reflect the influence of

strong traction effects of bottom currents. Thus, much debate has arisen on how to recognize contourite deposits in the ancient record where other evidence of strong, deep currents, such as the bathymetric expression of depositional ridges or observations from current meters, is lacking (Stow, 1982, for review; Stow and Holbrook, 1984). We believe that drilling in modern drift deposits is important in documenting the nature of internal stratification and characteristic textures and structures.

In addition, we wanted to examine the history of sedimentation in this drift sequence as a record of the relative importance of current velocity and sediment supply in the buildup and erosion of the drift. Miller and Tucholke (1983) argue that the waning strength of North Atlantic bottom currents resulted in the dominance of drift construction rather than in the formation of hiatuses since the early Oligocene. They state that unconformities are the most convincing evidence of intensified abyssal currents, thereby placing emphasis on the R4 unconformity. However, we believe that sediment supply is also a factor, one that probably has been important since the middle Miocene and particularly since the onset of northern hemisphere glaciation in the middle Pliocene. Drilling at nearby Site 113 illustrates the high Pliocene-Pleistocene sediment supply (Laughton, Berggren, et al., 1972) with more than 200 m of Pleistocene turbidites (about 10 cm/k.y. [100 m/m.y.]) and at least another 650 m of Pliocene turbidites deposited at rates of more than 35 cm/k.y.

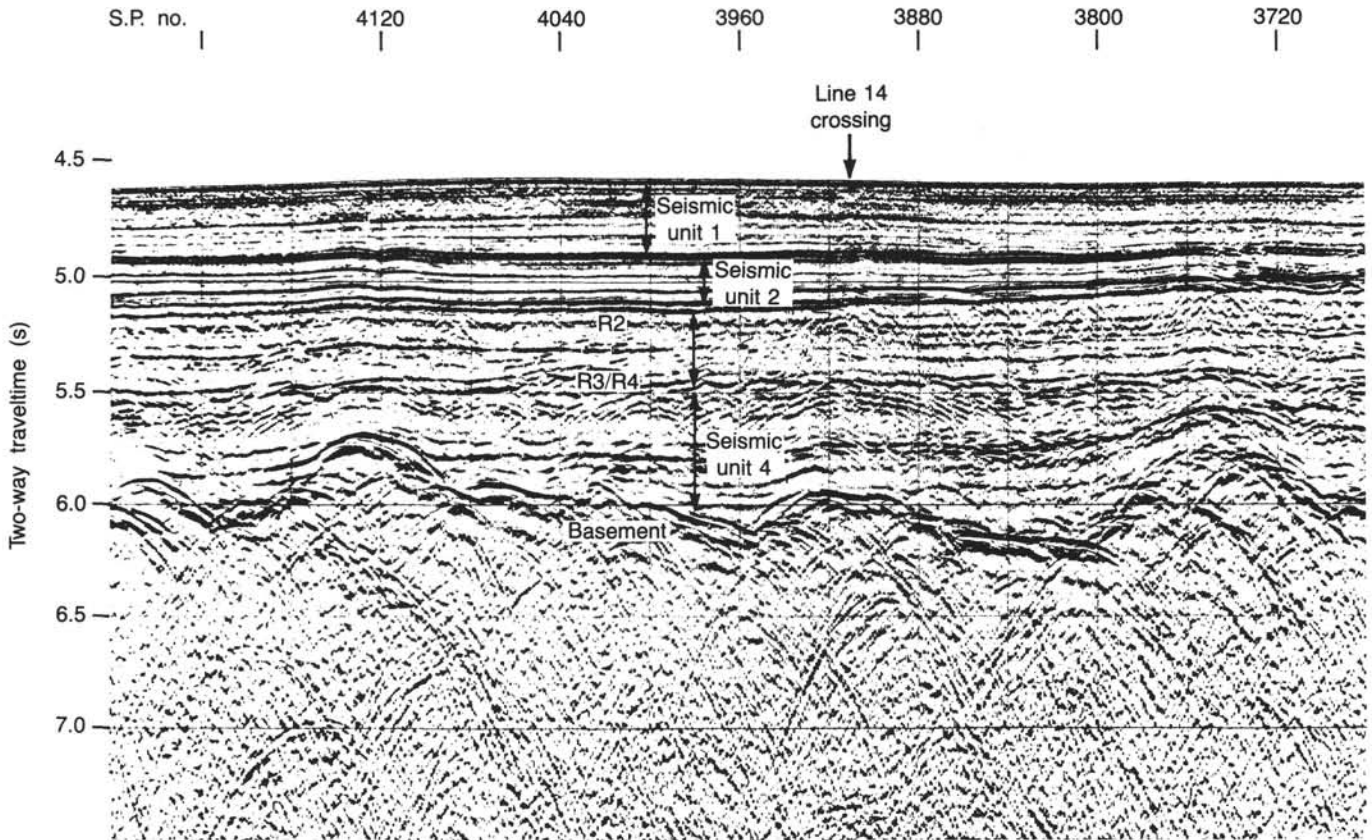


Figure 6. Part of multichannel seismic-reflection profile (BGR-2) near Site 646 showing the division of various sedimentary units. For location see Figure 3.

(350 m/m.y.). The site is located in the Imarssuak Mid-Ocean Canyon (IMOC; Fig. 1).

Other workers offered evidence that the major episode of deep-water formation and a change to the modern pattern of deep circulation in the North Atlantic occurred during the middle Miocene (Shor and Poore, 1979; Schnitker, 1979). Such an explanation, in concert with postulated higher sediment supply, might be advanced to explain the more coherent development of current-controlled sedimentation that occurred above reflector R2 (late early Miocene). Evidence from Site 646 should be useful in testing such models.

3. The timing of the onset of glaciation in the northern hemisphere was also an important objective of the drilling at Site 646. The site lies under the path, at least at present, of icebergs calved from East Greenland ice sheets and therefore should record the development of major continental ice sheets on the western margin of the Norwegian-Greenland Sea. Such information will complement our results of studies in Baffin Bay at Site 645. A timing of 2.5 Ma for the change from predominantly pelagic to terrigenous sediments at DSDP Sites 111 and 112 in the Labrador Sea was given by Backman (1979). A major influx of terrigenous sediment to the IMOC at DSDP Site 113 occurred somewhat earlier during the Pliocene.

4. The apparent high sedimentation rates in the presumed glacial part of the sequence drilled at Site 646 should give us the opportunity for high-resolution studies of glacial-interglacial climatic fluctuations and northward and southward movements of the polar front. A dominant 41-k.y. climatic signal is expected (actually in the transition from 23 to 41 k.y.; Berger, 1978; Rudiman and MacIntyre, 1981a, b). We may also see fluctuations in bottom-current intensity on a glacial-interglacial scale, as indicated by benthic foraminifer faunas and textural changes or

sedimentary structures. Changes in rates of deep-water mass formation resulting from variations in ice cover in the regions of bottom-water sinking have been suggested.

5. A further important result of the drilling at Site 646 will be the assignment of ages to major reflectors and seismic sequences to enable correlations through seismic lines throughout the Labrador Sea region. Such an exercise will provide more constraints on the age of the North Atlantic Mid-Ocean Canyon (NAMOC), as well as data on the basinwide effects of abyssal circulation through time.

OPERATIONS

Approach to Site 646

The transit to Site 646 began at 1845 hr/UTC on 28 September 1985, when *JOIDES Resolution* left Site 645. The original plan called for us to proceed to Site 646 in the Labrador Sea at full speed after completion of work at Site 645 in Baffin Bay. Because of the danger of encountering icebergs and growlers on the way, however, we were asked to follow the ice-surveillance boat *Chester* to Site 646 at its normal cruising speed (9 kt during daylight and 5 kt at night). To derive maximum benefit from this additional transit time, we decided to collect underway geophysical data during the transit. We started our operation about 5 nmi due northwest of Site 645 with the hope of collecting more single-channel digital seismic data directly over the beacon drop area. This, however, was a futile attempt for two reasons: one, we could not definitely locate the beacon when we passed over it because of interference from the ship's noise, the hydrophones that listen to the beacon having been withdrawn into the well, and, two, our 300-psi air gun quit working at about the same time. Instead of making another pass over the site, we de-

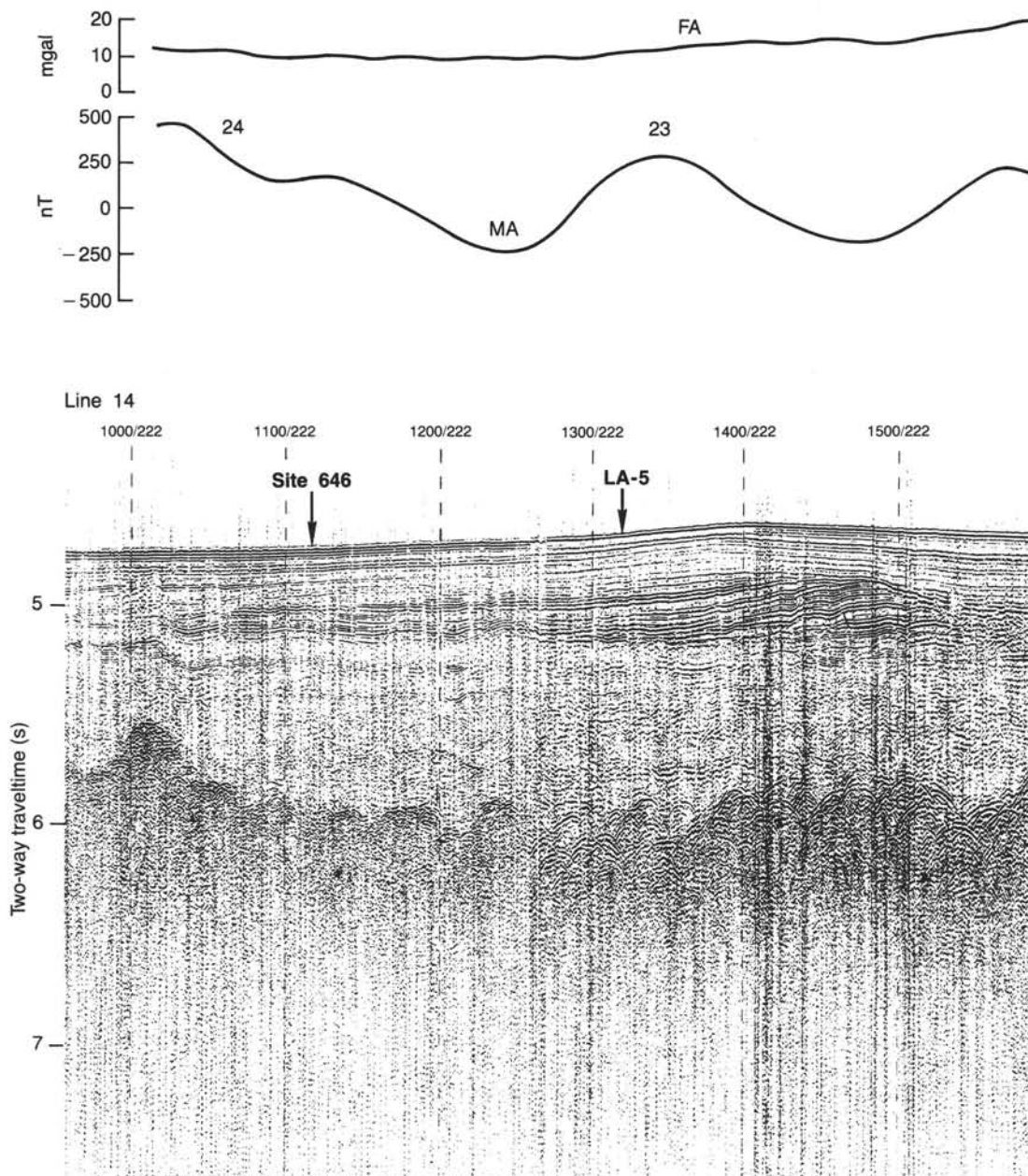


Figure 7. Seismic profile (Hudson line 14) across Site 646 (LA-5A). Shown also are the magnetic and gravity anomalies along this profile. For location see Figure 3.

cided to continue toward the Labrador Sea site while towing seismic gear that was eventually repaired after a few hours. We continuously recorded seismic and magnetic data until noon the next day, when we decided to terminate geophysical-data collection because of the poor quality of the data (lack of deep penetration) and also because we could make better time by increasing our speed during the day.

Several icebergs and growlers were sighted as we moved south. Near Davis Strait, we sighted the last iceberg, breaking up into small pieces and surrounded by a number of growlers that had apparently originated from it.

On 3 October at about 0000 hr UTC, we slowed to 4.5 kt and streamed seismic gear to start recording a single-channel seismic record along a northward continuation of Hudson line 14 (Fig.

3), on which Site 646 had to be located. Despite heavy seas and strong winds (30 kt), we recorded reasonably good-quality data along this track and correlated subsurface features easily between the two sets of data along line 14. After becoming confident that we were proceeding along the right track, we dropped the beacon at the predetermined site location while moving along line 14. The beacon was dropped at 0623 hr UTC, 3 October, and we continued recording seismic data for another hour along line 14 to ensure that no mistake was made in choosing the location where the beacon was dropped. Once we were satisfied with our decision, we pulled in the seismic gear, and the ship returned to the beacon location. The ship was positioned over the beacon at about 1145 hr UTC, 3 October, and we prepared for spudding the first hole at Site 646.

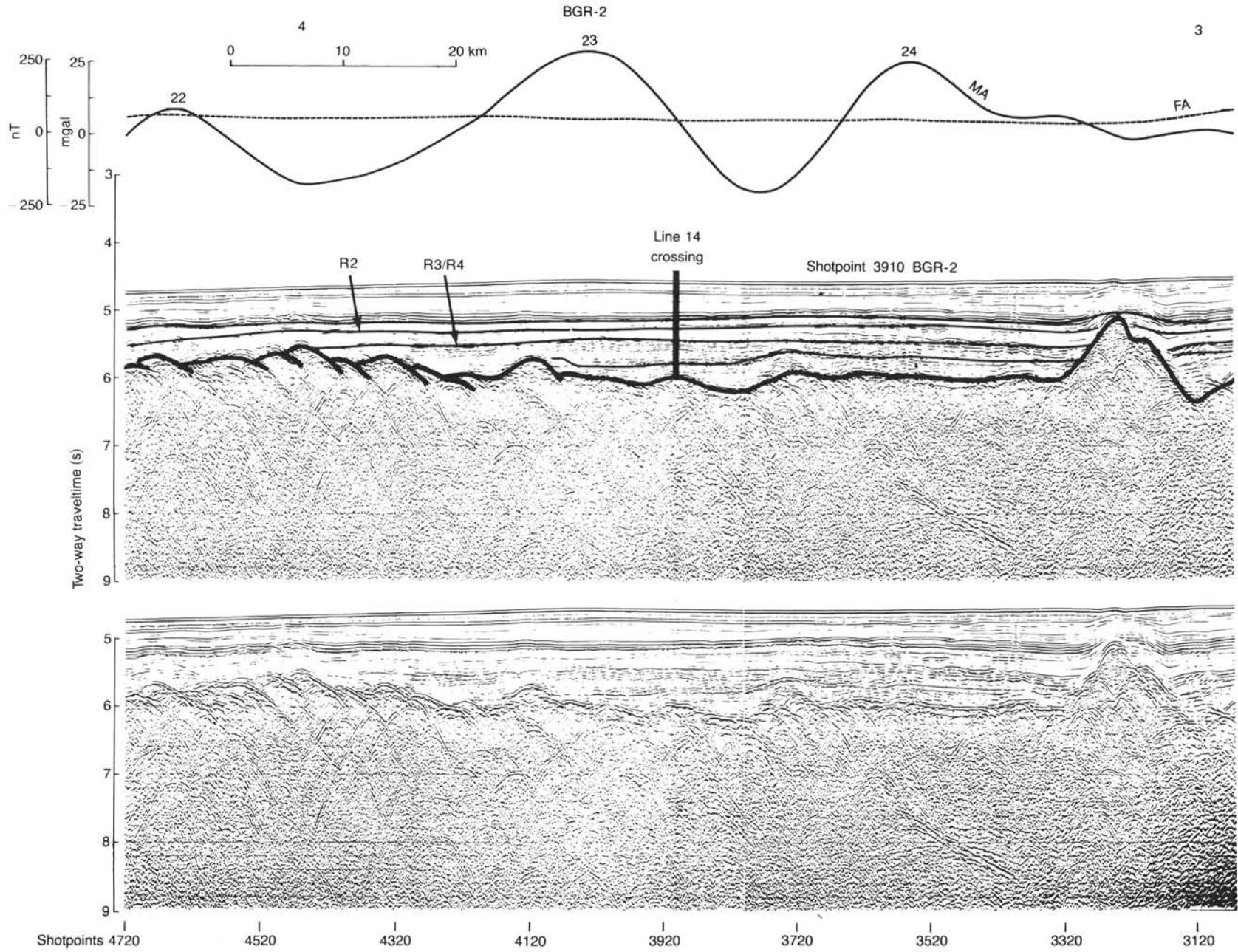


Figure 8. Part of multichannel seismic profile (BGR-2) near Site 646 showing some prominent reflectors. Shown also are the magnetic and gravity anomalies along this profile. For location, see Figure 3.



Figure 9. Map showing the depth to acoustic basement, magnetic lineations, and fracture zones in the southern Labrador Sea near ODP Site 646. Shown also is the axis of deposition of Eirik Ridge. Regions of depth to basement below 5.0 s are darkened. Locations of seismic lines BGR-2, BGR-1, and HD line 14 are also shown. Julian Haab Fracture Zone (J.F.Z.), Farewell Fracture Zone (F.F.Z.), Minna Fracture Zone (M.F.Z.), Leif Fracture Zone (L.F.Z.).

Drilling, Coring, and Logging Operations

Hole 646A

Satellite fixes indicated that we were within a few meters of the designated site. First, we needed to establish the depth of the seafloor below the dual elevator stool (DES), using the read-

ing obtained from the echo-sounder. This was checked and rechecked by several people and was found to be 3461.3 m. The drill string indicated a bottom at 3461 m.

We originally planned to core using the APC followed by XCB coring at this site, but this was initially considered impossible because of the strong winds and high seas (15–20-ft waves)

during the time we were to begin drilling operations. Bumper subs had been used previously for APC drilling in rough weather, and the heave compensator had been used for XCB and rotary drilling. To core using the APC with bumper subs followed by XCB coring using the heave compensator would have involved a round trip because the bumper subs would have had to have been removed before deploying the heave compensator. A decision was made by Lamar Hayes, Operations Superintendent, to try APC drilling using the heave compensator together with the core winch and to keep the sand line taut by adjusting the variac. This was achieved by placing the winch controls in hoist position and by adjusting them to hold in a stalled position. About 95% of the core-line and core-barrel weight was held before the coring-line blowout preventor (BOP) would close. As the heave compensator stroked 6–8 ft to compensate for the ship's vertical heave, the coring winch worked in unison with the heave compensator to maintain constant tension on the coring line above the wireline BOP. The bottom hole assembly (BHA) for APC and XCB was made up with the Monel drill collar for orienting selected APC cores. The first APC core arrived on board at 2100 hr UTC, 3 October. Moderate to heavy seas were encountered throughout drilling of this hole; on the first night, the wind gusted to 50 kt, producing 20-ft swells. Except for a few shattered liners, this new drilling technique, using the combination of the heave compensator with the core winch, worked well.

In-situ heat-flow measurements were made during core runs 4, 7, and 10. The heat-flow-measuring equipment worked well, although we had trouble in playing back the data. Apparently some changes need to be made to the software supplied for playing back the data.

In Hole 646A, 11 cores were collected with a total penetration of 103.5 m, of which 92.4 m of core was recovered, resulting in an 89% recovery. The rate of penetration for Hole 646A is illustrated in Figure 10. Because we wanted to collect double APC cores at this site, we decided to terminate Hole 646A at about 1130 hr UTC, 4 October, and spudded Hole 646B about 100 ft northwest of this site.

Hole 646B

For Hole 646B, the ship was moved 100 ft northwest of Hole 646A, and 14 APC cores were collected at this new site. The first core arrived on board at 1330 hr UTC, 4 October. Cores 105-646B-4H, 105-646B-5H, 105-646B-7H through 105-646B-10H, and 105-646B-12H through 105-646B-14H were collected as oriented cores for paleomagnetic work. Because pulling the core barrel from the bottom was becoming difficult by the fourteenth APC core, we decided to switch to XCB drilling instead (1015 hr UTC, 5 October). A number of problems were encountered as soon as we began XCB coring. Recovery decreased, and many of the cores arrived with shattered liners; some of the liner bottoms were smashed to pieces as if the bottom of the liner had been banged repeatedly against hard rocks. One of the core liners was so badly shattered that it fell apart upon our retrieving the core from the barrel. Many of the cores exhibited drilling biscuits that were presumably caused by some coupling of vertical movement with rotation during drilling. Nearly all cores had slurry and large rocks in their first sections, indicating down-hole sloughing of sediment. Core recovery remained poor for most XCB coring of this hole. Between Cores 105-646B-15X and 105-646B-43X, recovery was 60.8%, and from Cores 105-646B-43X to 105-646B-80X, it was 37.1%; overall recovery was 53%. For the last 20 cores, recovery improved (for details, see Table 1) after the cutting bit on the XCB was replaced by a diamond bit (Acker shoe for Cores 105-646B-66X and following). About 3 hr were lost when the nipple threads were stripped out of the collar between the kelly hose and the top drive on 8 Octo-

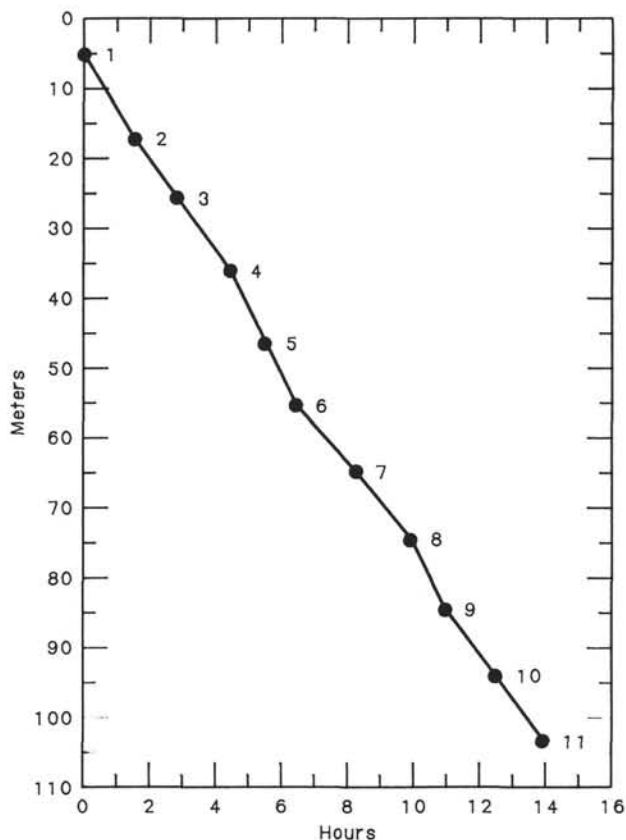


Figure 10. Penetration rate, Hole 646A.

ber. Sediment recovered in the last five cores was highly indurated, and the liner split on the last core upon extraction from the barrel. We were running behind schedule, and it appeared that we would not be able to penetrate below 850 mbsf depth because of drilling difficulties (the bit seemed to be wearing quickly, as evidenced by the dwindling core diameter) without sacrificing objectives at the next hole. We therefore decided to terminate drilling after the eightieth core, having reached beyond the projected depth of the reflector that was our most important deep objective. Drilling was terminated at 1100 hr UTC, 12 October, when the last core was brought on board. The penetration rate at Hole 646B is illustrated in Figure 11.

Preparation for cleaning (wiper trip) and logging the hole got under way. About 7 hr were required to clean the hole, drop the bit, and pull to within 200 m of the mud line before logging could begin. The first logging run consisted of DIL, LSS, GR, and CAL logs and took about 8 hr to complete. The second run, which consisted of NGT, CNTG, and GST logs, took about 10 hr to complete. No bridges were encountered during either of these runs, and we were able to collect some excellent log data. As soon as the logging cables were pulled out of the hole, the entire drill string was retrieved. Tripping out of the hole took longer than usual because the drill pipe had to be sorted and stored in different places for inspection in St. John's. After equipment was secured, the ship departed for Site 647 in the southern Labrador Sea at about 0000 hr UTC, 14 October.

SEDIMENTOLOGY

The strata cored at Site 646 are divided into Unit I (0–236.1 mbsf) and Unit II (236.1–766.7 mbsf) (Fig. 57, "Summary and Conclusions" section, this chapter, and Table 2). Both units are dominantly terrigenous and fine grained; the most common litho-

Table 1. Coring summary, Site 646.

Core no.	Date (Oct. 1985)	Time (local)	Sub-bottom top (m)	Sub-bottom bottom (m)	Length cored (m)	Length recovered (m)	Recovery (%)
Hole 646A							
105-646A-1H	03	1800	0.0	5.0	5.0	5.0	99.8
105-646A-2H	03	1930	5.0	16.5	11.5	9.6	83.0
105-646A-3H	03	2100	16.5	26.2	9.7	7.1	73.5
105-646A-4H	03	2230	26.2	35.8	9.6	9.2	96.1
105-646A-5H	03	2330	35.8	45.5	9.7	9.4	96.7
105-646A-6H	04	0030	45.5	55.1	9.6	9.4	98.0
105-646A-7H	04	0215	55.1	64.8	9.7	8.8	90.8
105-646A-8H	04	0400	64.8	74.4	9.6	8.0	83.0
105-646A-9H	04	0500	74.4	84.1	9.7	7.7	79.6
105-646A-10H	04	0630	84.1	93.8	9.7	9.3	96.3
105-646A-11H	04	0800	93.8	103.5	9.7	8.6	88.7
Hole 646B							
105-646B-1H	04	1215	0.0	9.0	9.0	9.1	100.9
105-646B-2H	04	1330	9.0	14.4	5.4	8.3	153.7
105-646B-3H	04	1445	14.4	24.1	9.7	9.6	98.7
105-646B-4H	04	1600	24.1	33.8	9.7	6.5	66.9
105-646B-5H	04	1715	33.8	43.4	9.6	4.7	48.5
105-646B-6H	04	1830	43.4	53.1	9.7	8.9	91.5
105-646B-7H	04	1945	53.1	62.7	9.6	0.0	0.1
105-646B-8H	04	2100	62.7	72.4	9.7	0.0	0.0
105-646B-9H	04	2315	72.4	82.0	9.6	9.7	100.8
105-646B-10H	05	0015	82.0	91.7	9.7	8.4	86.7
105-646B-11H	05	0145	91.7	101.4	9.7	7.3	74.7
105-646B-12H	05	0245	101.4	111.1	9.7	8.3	85.8
105-646B-13H	05	0400	111.1	120.8	9.7	8.4	87.0
105-646B-14H	05	0515	120.8	130.5	9.7	8.5	87.1
105-646B-15X	05	0745	130.5	140.1	9.6	0.0	0.0
105-646B-16X	05	0945	140.1	149.8	9.7	1.0	9.8
105-646B-17X	05	1130	149.8	159.1	9.3	1.1	12.0
105-646B-18X	05	1330	159.1	168.8	9.7	4.1	42.4
105-646B-19X	05	1500	168.8	178.5	9.7	0.4	4.2
105-646B-20X	05	1645	178.5	188.2	9.7	8.9	92.0
105-646B-21X	05	1830	188.2	197.8	9.6	6.9	72.0
105-646B-22X	05	2000	197.8	207.5	9.7	9.6	99.3
105-646B-23X	05	2145	207.5	217.1	9.6	7.5	77.7
105-646B-24X	05	2315	217.1	226.7	9.6	0.0	0.0
105-646B-25X	06	0100	226.7	236.1	9.4	0.1	1.3
105-646B-26X	06	0300	236.1	246.0	9.9	7.6	77.2
105-646B-27X	06	0445	246.0	255.7	9.7	0.0	0.0
105-646B-28X	06	0645	255.7	265.3	9.6	0.6	6.4
105-646B-29X	06	0845	265.3	275.0	9.7	9.1	93.8
105-646B-30X	06	1045	275.0	284.7	9.7	9.5	97.8
105-646B-31X	06	1230	284.7	294.4	9.7	8.6	88.7
105-646B-32X	06	1445	294.4	304.1	9.7	8.9	91.3
105-646B-33X	06	1645	304.1	313.8	9.7	8.0	82.0
105-646B-34X	06	1845	313.8	323.4	9.6	3.0	31.2
105-646B-35X	06	2100	323.4	333.1	9.7	3.3	33.6
105-646B-36X	06	2300	333.1	342.8	9.7	10.0	103.4
105-646B-37X	07	0100	342.8	352.4	9.6	9.4	98.2
105-646B-38X	07	0300	352.4	362.0	9.6	9.8	102.4
105-646B-39X	07	0500	362.0	371.7	9.7	9.8	100.8
105-646B-40X	07	0745	371.7	381.3	9.6	9.9	103.1
105-646B-41X	07	0945	381.3	391.0	9.7	8.9	91.4
105-646B-42X	07	1145	391.0	400.7	9.7	9.7	100.4
105-646B-43X	07	1400	400.7	410.4	9.7	4.5	46.6
105-646B-44X	07	1645	410.4	420.1	9.7	1.6	16.7
105-646B-45X	07	1915	420.1	429.8	9.7	1.0	10.7
105-646B-46X	07	2200	429.8	439.5	9.7	4.6	47.2
105-646B-47X	08	0445	439.5	449.1	9.6	3.5	36.8
105-646B-48X	08	0745	449.1	458.8	9.7	2.4	25.0
105-646B-49X	08	1045	458.8	468.5	9.7	3.3	33.7
105-646B-50X	08	1400	468.5	478.1	9.6	3.1	32.2
105-646B-51X	08	1615	478.1	487.4	9.3	2.3	24.4
105-646B-52X	08	1930	487.4	497.1	9.7	2.4	24.4
105-646B-53X	08	2215	497.1	506.9	9.8	0.3	2.8
105-646B-54X	09	0045	506.9	516.5	9.6	2.6	26.8
105-646B-55X	09	0330	516.5	526.2	9.7	3.8	38.7
105-646B-56X	09	0630	526.2	535.8	9.1	3.1	33.7
105-646B-57X	09	0930	535.8	545.5	9.7	4.5	46.4
105-646B-58X	09	1300	545.5	555.2	9.7	3.6	36.8
105-646B-59X	09	1600	555.2	564.4	9.2	2.4	26.1
105-646B-60X	09	1845	564.4	574.0	9.6	3.3	33.9
105-646B-61X	09	2145	574.0	583.6	9.6	3.0	30.9
105-646B-62X	10	0100	583.6	593.2	9.6	6.0	62.6
105-646B-63X	10	0400	593.2	602.9	9.7	3.3	33.7
105-646B-64X	10	0645	602.9	612.5	9.6	1.9	20.0
105-646B-65X	10	1015	612.5	622.2	9.7	8.4	86.6
105-646B-66X	10	1400	622.2	631.8	9.6	3.0	31.4
105-646B-67X	10	1745	631.8	641.3	9.5	9.2	96.5
105-646B-68X	10	2045	641.3	650.9	9.6	5.3	55.3
105-646B-69X	10	2315	650.9	660.5	9.6	1.9	20.0
105-646B-70X	11	0145	660.5	670.2	9.7	1.1	11.7
105-646B-71X	11	0430	670.2	679.7	9.5	8.6	90.2
105-646B-72X	11	0745	679.7	689.3	9.6	3.2	33.7
105-646B-73X	11	1115	689.3	699.0	9.7	2.7	27.4
105-646B-74X	11	1415	699.0	708.6	9.6	5.4	56.1
105-646B-75X	11	1700	708.6	718.3	9.7	7.1	72.9
105-646B-76X	11	1945	718.3	727.9	9.6	3.3	33.9
105-646B-77X	11	2245	727.9	737.7	9.8	6.9	70.3
105-646B-78X	12	0145	737.7	747.4	9.7	2.2	22.8
105-646B-79X	12	0430	747.4	757.0	9.6	3.4	35.7
105-646B-80X	12	0800	757.0	766.7	9.7	2.9	29.7

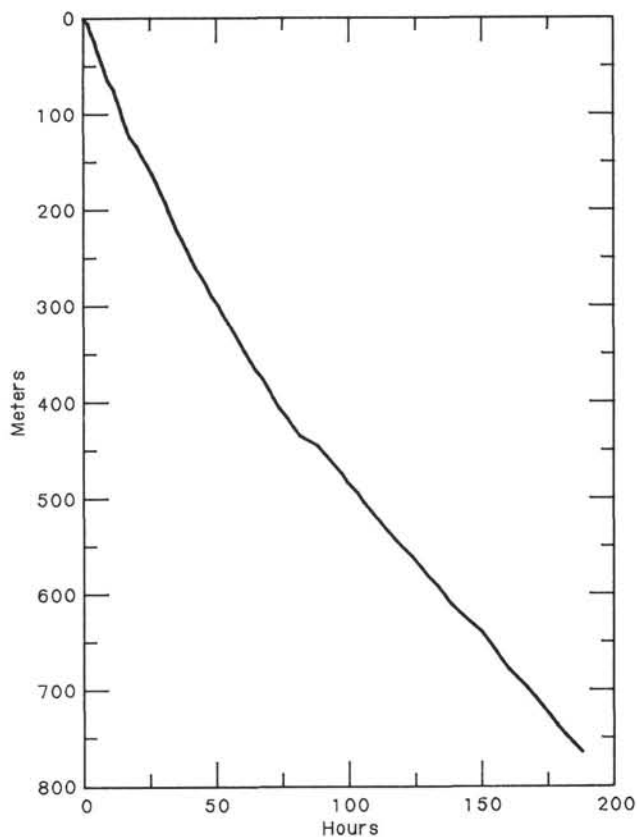


Figure 11. Penetration rate, Hole 646B.

facies (Fig. 12) are silty clay, clayey silt, and clay. Biogenic components include both calcitic and opaline skeletons above 330 mbsf and predominantly calcitic skeletons at greater depths. Nanofossils are volumetrically the greatest biogenic component, locally accounting for as much as half of the sediment volume.

Unit I is characterized by scattered coarse sand, granules, pebbles, and cobbles of inferred ice-rafted origin. Most of the pebbles consist of mafic volcanic rock types. An upper subunit, IA (0–188.2 mbsf), also contains distinctive, thin, laminated and cross-laminated silt and clayey silt beds of two types. The first type consists of <50% detrital carbonate, whereas the second type is predominantly siliciclastic. Otherwise, the sediments of Subunit IA are either homogeneous or bioturbated. There appear, however, to be subtle cyclic variations in grain size and in the content of biogenic carbonate. Subunit IB (188.2–236.4 mbsf) is characterized by poorly sorted, locally granule-bearing muddy sands and silty muds having subtle variations in grain size and a vague color banding.

Unit II is a relatively homogeneous, fine-grained unit, consisting predominantly of silty clays and clays, and locally rich in nanofossils. The sediments only rarely show any primary lamination but rather are moderately to strongly bioturbated throughout.

The base of Unit I is associated with an interval of very poor recovery; hence, the exact nature of the base of the unit is unknown. During continued drilling of Hole 646B, large caved pebbles and cobbles of felsic plutonic rocks (granite, syenite, and so forth) were found at the tops of cores, often in greater abundance and of greater size than caved pebbles of the mafic clast types so common in most of Unit I. This suggests that the interval of poor recovery may contain at least one horizon with abundant, large clasts.

Table 2. Lithologic summary, Site 646.

Unit	Lithology	Sedimentary structures	Interval (mbsf)	Age	Occurrence
IA	Predominantly silty clays and clayey silts with variable amounts of biogenic skeletons to 50%. The most common biogenics are nannofossils, foraminifers, sponge spicules, and diatoms. Thin detriticarbonate and siliciclastic silt and silty clay beds are markers.	The major lithologies are either homogeneous or bioturbated. Dropstones common, predominantly mafic volcanics. Silt and silty clay beds are laminated or cross-laminated; the detrital carbonate beds show structures of thin-bedded turbidites.	0–188.2	late Pliocene–Holocene	105-646A-1H to 105-646A-11H; 105-646B-1H to 105-646B-20X
IB	Poorly sorted, locally granule-bearing muddy sands, and silty muds.	Vague stratification or size gradation, subtle color bands, very poor sorting.	188.2–236.1	late Pliocene	105-646B-21X to 105-646B-25X
II	Predominantly silty clay (claystone), clay (claystone), and clayey silt (siltstone), with layers containing as much as 50%–60% nannofossils — typically much less. Rare glauconite in burrows. Rare micritic limestone beds in lower part.	Slightly to strongly bioturbated, with only rare vague bedding and lamination. Color mottling strongest in carbonate-rich units. <i>Zoophycus</i> , <i>Planolites</i> , <i>Chondrites</i>	236.4–766.7	late Pliocene–late Miocene	105-646B-26X to 105-646B-80X

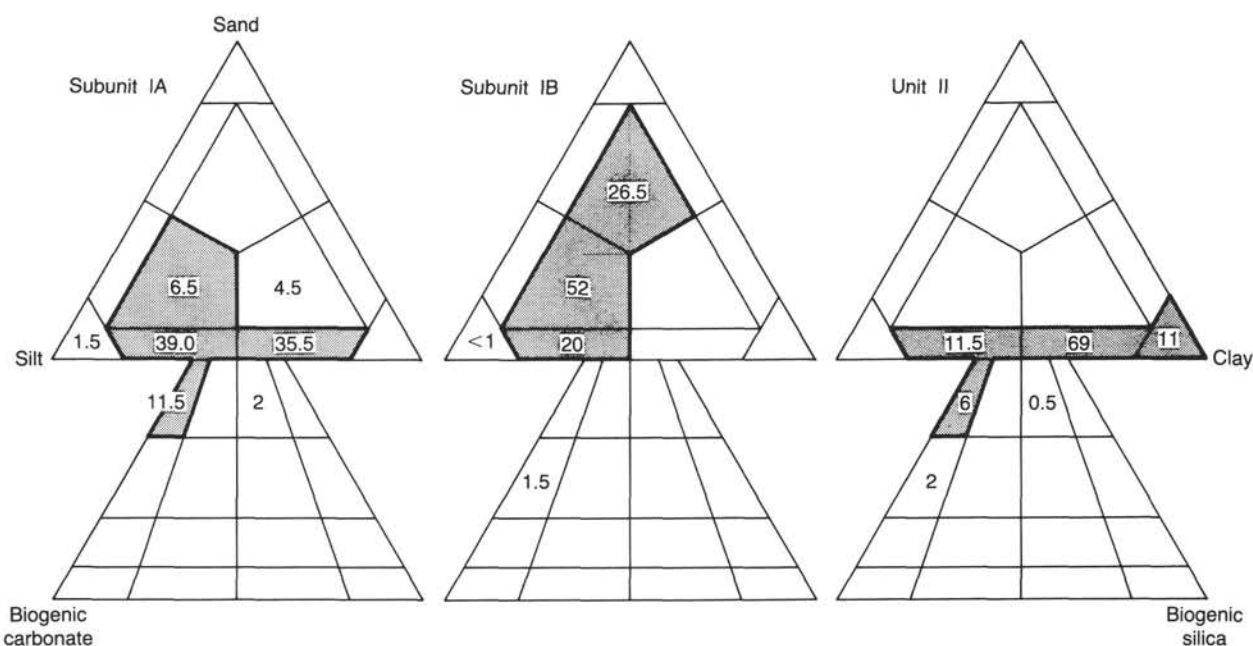


Figure 12. Percentages of recovered sediments assigned to each of the lithologic categories recognized in the classification scheme. The more common lithologies are outlined with a bold line and stippled. Many of the data that are plotted on the “terrigenous” classification diagram have biogenic contents from 10% to 25% and therefore have a name that includes a modifier like “nannofossil-bearing.” Only lithologies with $\geq 25\%$ biogenics are plotted on the lower triangles. For a better appreciation of total biogenic content, see Figure 14.

One of the objectives of drilling this site was to provide samples for high-resolution studies of Pleistocene and Holocene deposition. Such studies require recovery of a complete sediment section. To ensure accurate correlation of sediment horizons in Holes 646A and 646B and to allow exact positioning of cored intervals relative to the seafloor, precise hole-to-hole correlations were attempted. The results are outlined as follows.

Correlation of Holes 646A and 646B

Visual descriptions and examination of color transparencies of whole cores allowed the matching of distinctive thin calcareous silty clay beds and noncalcareous silt beds between Holes 646A and 646B (Table 3). At this site, double coring with the APC corer provided a virtually complete upper Pleistocene–Holocene section.

At the top of both holes, correlation of equivalent beds is possible only if two rather unusual steps are taken:

1. Core 105-646B-2H must be shifted upward to overlap with the base of Core 105-646B-1H. Core 105-646B-2H was taken after washing down below the mud line to the inferred base of Core 105-646B-1H, which may have been incorrectly estimated. Shifting Core 105-646B-2H up to overlap with Core 105-646B-1H is consistent with the fact that the thickness of sediment recovered in Core 105-646B-2H exceeded the amount advanced. An upward shift of Core 105-646B-2H is also necessary for correlation with Core 105-646A-2H (tie points 2 and 3; Table 3).

2. Core 105-646A-1H must be repositioned upward to the top of the 9.5-m stroked interval. This will allow horizons in Core 105-646A-1H to correlate with equivalents in Core 105-646B-1H (tie point 1; Fig. 13). Such a procedure forces the mud line (sampled in Hole 646A but, apparently, not in Hole 646B) above the top of Hole 646B by a small amount, a manipulation that is not unreasonable. Core 105-646A-1H recovered 5.0 m of sediment, which by convention is assumed to have come from

Table 3. Basis for correlation of Holes 646A and 646B.

Basis for depths in Figure 16:

1. Seafloor = 105-646A-1H-1, 46 cm; 105-646B-1H-1, 5 cm.
2. Drilling summary, Hole 646B.

Core	Sub-bottom top
105-646B-3H	1440 cm
105-646B-6H	4340 cm
105-646B-9H	7240 cm

3. Cores 105-646A-3H and 105-646A-7H are unconstrained.
4. Tie-points between Holes 646A and 646B:

	Hole 646A Section	cm	Hole 646B Section	cm
1.	105-646A-1H-2	117	105-646B-1H-2	76
2.	105-646A-2H-1	62	105-646B-2H-5	24
3.	105-646A-2H-2	85	105-646B-2H-6	55
4.	105-646A-2H-4	125	105-646B-3H-1	99
5.	105-646A-2H-6	45	105-646B-3H-3	15
6.	105-646A-4H-2	60	105-646B-4H-4	125
7.	105-646A-4H-6	30	105-646B-5H-2	35
8.	105-646A-4H-6	120	105-646B-5H-2	130
9.	105-646A-5H-5	80	105-646B-6H-2	48
10.	105-646A-5H-6	122	105-646B-6H-3	90
11.	105-646A-6H-2	15	105-646B-6H-6	20
12.	105-646A-6H-2	95	105-646B-6H-6	95
13.	105-646A-8H-4	72	105-646B-9H-2	23
14.	105-646A-9H-1	62	105-646B-9H-5	140
15.	105-646A-10H-2	145	105-646B-10H-6	77
16.	105-646A-10H-5	135	105-646B-11H-2	45
17.	105-646A-11H-6	75	105-646B-12H-2	85

the bottom of the stroked interval; the upper 4.5 m of the stroked interval is inferred to have sampled seawater above the bottom. However, it is conceivable that the drill bit was exactly at the mud line and that the lower 4.5 m of a 9.5-m core washed out of the core liner. Such a scenario is possible because Core 105-646A-1H cored the mud line twice, at 0 cm and at 45 cm; therefore, the bit may have just tapped the seabed before firing. The conclusion that the mud line was cored twice is based on duplication of the upper tens of centimeters in Core 105-646A-1H and on comparison with piston cores taken near the site during the site survey (A. E. Aksu and A. De Vernal, pers. comm., 1985).

Our procedure to improve the hole-to-hole correlation was to determine the position of the mud line in both holes and to assign that position a value of 0 mbsf in the first core of each hole. Hole 646A cored the mud line twice, the lowest mud line being at 46 cm in Section 105-646A-1H-1. Correlation using tie-point 1 suggests that the mud line should be at 5 cm in Section 105-646B-1H-1; the top of this section was disturbed, so it is not surprising that the mud-line lithology was not noted. Figure 13 plots cores from both holes following the criteria of Table 3: (1) The mud lines in both holes are assigned a depth of 0 mbsf. (2) Cores 105-646B-3H and 105-646B-9H, which have full recovery, are positioned at the tops of their cored intervals, while Core 105-646B-6H, having almost full recovery, is positioned 41 cm downward within its cored interval (i.e., from 4340 to 4381 cm; see Table 3). (3) Cores in Hole 646A are plotted to provide the best fit of correlated tie-points. Through this procedure, sub-bottom depths of core tops in Hole 646A provided in the coring summary (Table 1), except Core 105-646-1H, must be repositioned downward by approximately 3.5 m (Table 4). For Hole 646A, Figure 13 violates by small amounts the known advances between successive cores but is the best current estimate of the relative positions of cores in Hole 646A and 646B. Further refinement of the correlation awaits detailed matching of carbonate and stable-isotope curves for the two holes.

Description of Lithologic Units

Lithologic Unit I: Hole 646A (Cores 105-646A-1H to 105-646A-11H), Hole 646B (Cores 105-646B-1H to 105-646B-25X); Holocene-late Pliocene; 0–236.4 mbsf.

The uppermost unit at Site 646 extends from the seafloor to a depth of 236.1 mbsf (Fig. 57, "Summary and Conclusions" section, this chapter). Silty clays, clayey silts, and silty muds, containing variable amounts of scattered gravel-sized rock fragments up to cobble size, characterize this unit. The base of Unit I is defined by the disappearance of this material, as well as most sand-sized detritus. This boundary also corresponds to a change from poorly sorted muddy sediments, characterizing the lower part of Unit I, to the silty clays of Unit II. Recovery, using the APC (Hole 646A and Cores 105-646B-1H to 105-646B-14H) and the XCB corer (Cores 105-646B-15X to 105-646B-25X), averaged 56%; drilling disturbance was moderate to low.

Unit I is divided into two subunits: Subunit IA, Cores 105-646A-1H to 105-646A-11H and 105-646B-1H to 105-646B-20X, 0–188.2 mbsf; and Subunit IB, Cores 105-646B-21X to 105-646B-25X, 188.2–236.4 mbsf. Subunit IA ranges in age from Holocene to late Pliocene, whereas Subunit IB is entirely of late Pliocene age; its base is at about 2.6 ± 0.3 Ma (see "Sediment-Accumulation Rates" section, this chapter).

Subunit IA is characterized by terrigenous silty and clayey sediments with variable amounts of biocarbonate and siliceous skeletal material (Figs. 12 and 14). The major lithologies are gray, and dark-, olive-, and greenish gray clayey silt and biocarbonate-bearing clayey silt (39% of the recovered sediments); dark-gray silty clay and biocarbonate-bearing silty clay (35.5%); and biocarbonate silty clay and clayey silt (11.5%) with a biogenic content to a maximum of 40%–50%. Biogenic carbonate is commonly in the form of nannofossils and foraminifers; biogenic silica consists of sponge spicules and diatom skeletons, usually forming <10% of the sediments. Minor lithologies are (1) silty and clayey muds (11% of recovery), (2) light greenish and pinkish gray layers consisting of about 50% detrital carbonate from 3 to 60 cm thick (3% of recovery), and (3) dark-gray, finely laminated silt and clayey silt layers (1%–2% of recovery). Minor lithologies 2 and 3 are commonly nonbioturbated or only weakly bioturbated and are characterized by lamination and, locally, cross-lamination.

Silty clays of Subunit IA are commonly structureless, except for (1) subtle color mottling, sulfide-rimmed mottles (i.e., halo burrows) and specks caused by bioturbation and (2) local, indistinct color banding. Clayey silts are also relatively homogeneous and moderately bioturbated but show a more pronounced color banding and, in a few places, vague planar laminations. The biogenic component of these sediments consists of nannofossils (as much as 40%), and generally <10% each of foraminifers and siliceous skeletons (sponge spicules, diatoms, and rare radiolarians).

Two types of detriticarbonate layers can be distinguished in Subunit IA; the stratigraphic position of all such beds is plotted in Figure 14 and listed in Table 5. Shore-based XRD analyses indicate that the calcite/dolomite ratio is about 2:1. The first type of layer is characterized by detriticarbonate silty clay or clayey silt (carbonate content as much as 50%) and, in many places, distinct physical sedimentary structures. Each bed grades upward above a sharp base from parallel-laminated (Fig. 15) into a more homogeneous, then mottled, sediment. In several places, the lower part of the mottled layer is greenish with dark greenish gray silt blebs (Fig. 16). A shipboard X-radiograph of a thin slab from a basal-laminated interval reveals several sets of thin to very thin parallel laminae (<1 mm to 5 mm), which appear to be grouped into several normally graded units, each about 0.5–1 cm thick. A thin section from the same slab clearly shows

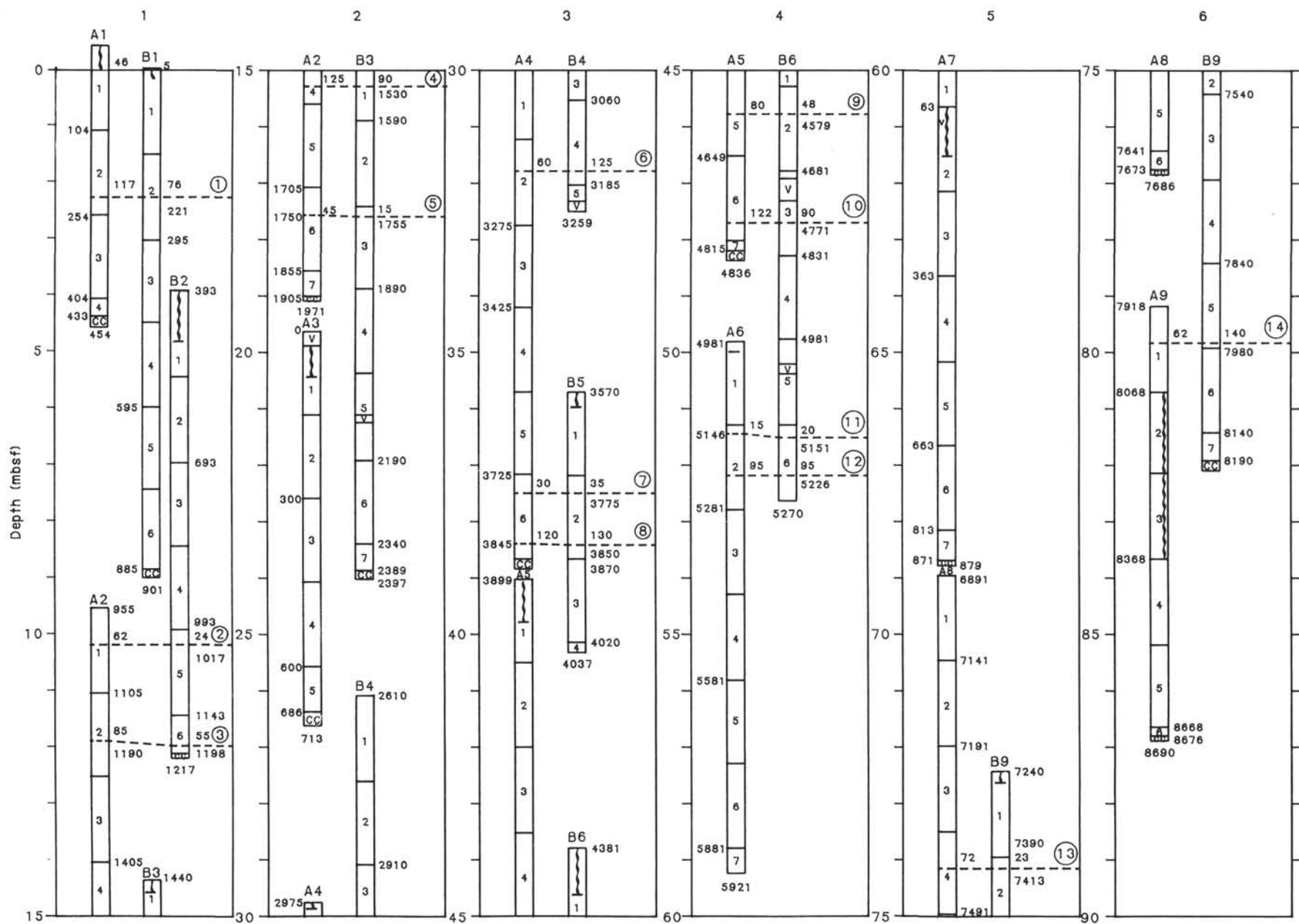


Figure 13. Correlation of the upper parts of Holes 646A and 646B. Sub-bottom depth (mbsf) is indicated to the left of each panel; sub-bottom position is indicated in centimeters for each core top, section break, and core bottom. Tie-points for correlation of cores are circled numbers (see Table 3) and are indicated by sub-bottom position (in centimeters) and by depth in the section (in centimeters) of the marker bed. Cores 105-646A-3H and 105-646A-7H are unconstrained with respect to sub-bottom depth. Centimeter marks for these cores indicate only core length. Core disturbance is indicated by a wavy line or void (v).

Table 4. Estimates of sub-bottom depths of core tops, unless otherwise stated.

Hole 646A		Hole 646B	
Core	Sub-bottom depth (cm)	Core	Sub-bottom depth (cm)
105-646A-1H	Seafloor = 46 cm	105-646B-1H	Seafloor = 5 cm
105-646A-2H	955	105-646B-2H	393
105-646A-3H	1950(?)	105-646B-3H	1440
105-646A-4H	2975	105-646B-4H	2610
105-646A-5H	3899	105-646B-5H	3570
105-646A-6H	4981	105-646B-6H	4381
105-646A-7H	6000(?)	105-646B-7H	—
105-646A-8H	6891	105-646B-8H	—
105-646A-9H	7918	105-646B-9H	7240

these laminae (Fig. 17). These basal laminae consist of well-sorted silt, having a carbonate content as much as 50%. The second type of detrital carbonate layer shows indistinct contacts with no apparent primary physical structures (Fig. 18). Some beds contain scattered granules and sand grains; many others are characterized only by their detrital carbonate content and mottled appearance.

Noncarbonate silt layers (see Table 6 for occurrences) are characterized by both sharp and gradational contacts and are darker than surrounding sediment. They may be thinly parallel-laminated or cross-laminated (Fig. 19). A shipboard X-radiograph of a 20-cm-thick bed (Fig. 20) reveals thinner and more irregular laminations than those found in the detrital carbonate beds. These silts generally contain about 10% heavy minerals and, in some, as much as a few percent of well-preserved sponge spicules and skeletons of foraminifers and diatoms that are of open-ocean, pelagic type. Laminated silt layers are particularly common in Cores 105-646B-13H and 105-646B-14H, and some layers contain thin intervals of very fine sand.

All sedimentary facies in Unit I, except the laminated silt layers, contain variable amounts of coarse sand and gravel-sized material up to cobble size, either dispersed or concentrated in diffuse layers. Soft mud clasts and dark silt and sand pockets were also observed. Most pebbles and cobbles consist of basalt, dolerite, diabase, gabbro, and gneiss clasts and rare felsic plutonic and very rare carbonate clasts.

Subunit IB does not contain the laminated units with detrital carbonate and is characterized by silty muds (52% of recovery), poorly sorted muddy sands (26.5%), and clayey silts (20%) (Fig. 12). The silty muds and clayey silts are locally nannofossil bearing. A 60-cm-thick minor lithology is muddy nannofossil ooze (1.5% of recovery).

The muddy sands of Subunit IB are very poorly sorted, rich in granules, vaguely color banded (Fig. 21), and crudely stratified. A single normally graded interval with a relatively sharp base is the only indication of episodic deposition.

According to examination of approximately 150 smear slides, the sand- and silt-sized fraction of the sediments in Unit I consists primarily of quartz (as much as 70%) and subordinate amounts of relatively fresh feldspar (plagioclase and microcline) and detrital carbonate. Preliminary shore-based XRD analyses of bulk samples, however, indicate that feldspar is roughly twice as abundant as quartz, regardless of mean grain size. Perhaps fresh feldspars were mistaken for quartz in smear slides. Accessory minerals include pyrite, amphibole, epidote, zircon, green and brown biotite, white mica, garnet, and tourmaline. The pronounced greenish color of some layers may result from variations in clay mineralogy; only a few poorly developed glauconitic grains were observed. Available shore-based XRD data, however, indicate little variation in clay mineral composition between cores.

Examination of Figure 14 indicates stratigraphic variation in sediment properties like sand, silt, and clay content, abundance of biogenic constituents, occurrence of detrital carbonate and non-carbonate laminated beds, and abundance of inferred ice-rafted sand and gravel. Total carbonate abundance in the upper six cores of Hole 646A, with gaps filled in from Hole 646B (see "Organic Geochemistry" section, this chapter), also varies cyclically. These variations may be climatically controlled. In an effort to document more precisely the covariance of a few compositional and textural features, we examined smear slides taken at a 40-cm spacing in Core 105-646B-3H (Fig. 22); the lithologic composition in this core is either silty clay or clayey silt, with variable amounts of detrital and biogenic carbonate. Most of the biogenic carbonate is in the form of foraminifers and nannofossils. The detrital carbonate is generally restricted to thin layers (Fig. 22 and Table 5). The resultant curves show fine-scaled cyclicity, particularly in biogenic carbonate content. Figure 23, a photograph of a 24-cm interval from Core 105-646B-3H, illustrates the fine-scaled variations of both grain size and biogenic content that characterize Subunit IA.

Lithologic Unit II: Hole 646B (Cores 105-646B-26X to 105-646B-80X); late Pliocene-late Miocene; 236.1–766.7 mbsf.

Lithologic Unit II begins at the top of Core 105-646B-26X and is dominated by clay-rich sediments (Fig. 12). Recovery averaged 44%, with some long intervals of poor recovery or recovery of only drilling slurry and caved pebbles. Major lithofacies are silty clay (claystone) (69%), clayey silt (siltstone) (11.5%), clay (claystone) (11%), and nannofossil silty clay (claystone) and clayey silt (siltstone) (6%). Minor lithofacies include clayey nannofossil ooze (chalk) (2%) and two thin micritic limestone beds. Nannofossils, the main biogenic component in the unit, have abundances in places reaching about 50%, requiring use of sediment names from our biogenic-classification scheme. In the top 100 m of the unit, siliceous biogenic particles are locally about 10% in smear slides (diatoms, sponge spicules) and disappear below approximately 330 mbsf (see "Biostratigraphy" section, this chapter). In several places, sediment within burrows contains high concentrations of nannofossils.

This unit shows very little variation in either texture or sedimentary structures. From about 310–470 mbsf, the sediments contain a greater proportion of nannofossils (Fig. 14). The main lithofacies in this interval are nannofossil-bearing clay (claystone) and nannofossil-bearing to nannofossil silty clay (claystone); silty clay lithofacies contain more nannofossils than do clay-rich layers. At about 470 mbsf (just above seismic marker R2), quantitative grain-size analyses indicate a slight increase in silt content upward, at the expense of clay content; sand percentage stays more or less constant at < 1%.

Except for a few thin parallel-laminated layers, all sediment is bioturbated, having a wide range of burrow types including *Zoophycos*, *Planolites*, *Chondrites*, and *Cylindrichnus*. The burrows are locally sites for growth of pyrite nodules; some burrows are marked by halos of black iron sulfides.

On the basis of about 150 smear slides, the nonbiogenic silt-sized grains consist of quartz and only minor feldspar above 300 mbsf. Shore-based studies indicate, however, that feldspar content exceeds quartz content, not the reverse. Thin greenish bands and mottles in Cores 105-646B-37X, 105-646B-40X, 105-646B-75X, and 105-646B-77X contain small amounts of glauconitic pellets.

Sediments become increasingly more lithified with depth in Hole 646B, and the arbitrary boundary between soft and hard sediments (e.g., between clays and claystones) is placed at a depth of 450 mbsf. Both above and below this boundary, for

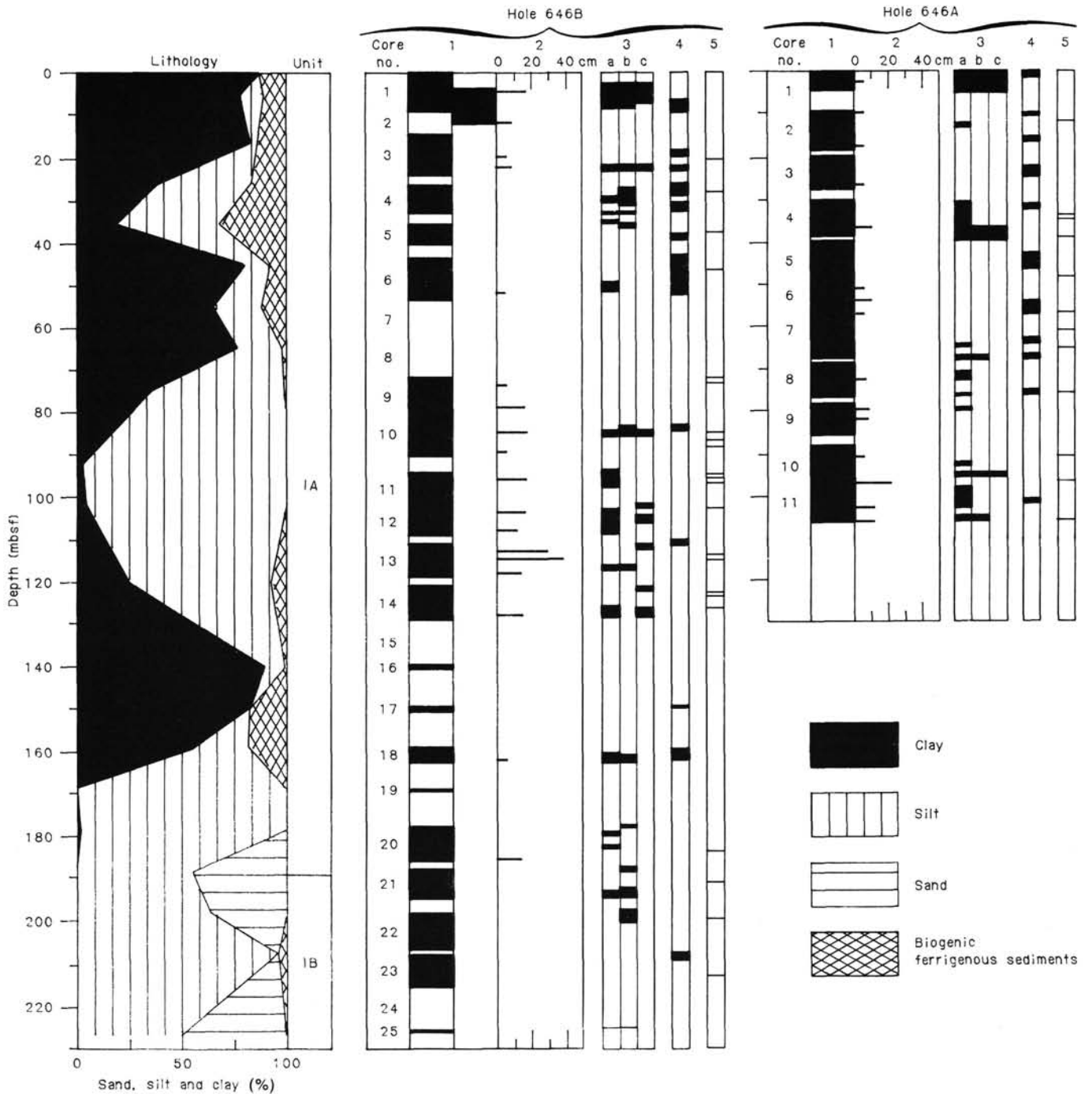


Figure 14. Summary of lithologic variations in Unit I with depth, Holes 646A and 646B. The column on the left shows the percentages in single cores of clay-rich lithologies (clay, silty clay, and clayey mud), silt-rich lithologies (silt, clayey silt, sandy silt, and silty mud), and sand-rich lithologies (sand, silty sand, and muddy sand). For each of Holes 646A and 646B, the numbered columns show the following data: 1, recovery in black; 2, occurrence and thickness of detriticarbonate-rich beds; 3, occurrence of cobbles—a, granules—b, and sand—c; 4, occurrence of biogenic-rich layers ($\geq 10\%$ biogenics); 5, occurrence of dark, noncarbonate, laminated silt layers.

much of Unit II, the sediments are sufficiently brittle to form ubiquitous drilling biscuits.

Interpretation

Sedimentary facies were studied in piston cores from the vicinity of Site 646 by Chough (1978), Chough and Hesse (1976, 1980, 1985, in press, a), and Hesse and Chough (1980). The main depositional processes observed are (1) overspill of turbid currents from the NAMOC, forming finely laminated levee

deposits, (2) slow deposition from thermohaline bottom currents on sediment ridges (e.g., Eirik Ridge; Chough and Hesse, 1985), resulting in thoroughly bioturbated muds, (3) ice rafting, and (4) settling of biogenic carbonate and silica from surface waters.

Lithologic Unit I

Unit I is dominantly terrigenous; some intervals contain significant amounts of biogenic microfossils, mostly nannofossils,

Table 5. Location of detrital carbonate beds.

Hole 646A section	Interval (cm)	Hole 646B section	Interval (cm)
105-646A-1H-2	112-116	105-646B-1H-2	68-78
105-646A-2H-1	53-65	105-646B-1H-3	114-130
105-646A-2H-6	43-47	105-646B-2H-5	15-23
105-646A-3H-2	137-143	105-646B-3H-3	15-19
105-646A-3H-4	5-13	105-646B-3H-6	71-81
105-646A-4H-5	90-100	105-646B-5H-1	57-100
105-646A-4H-5	130-140	105-646B-5H-1	145-150
105-646A-6H-2	5-14	105-646B-5H-2	0-5
105-646A-6H-2	92-95	105-646B-6H-6	10-20
105-646A-6H-4	120-127	105-646B-6H-6	93-95
105-646A-6H-6	100-107	105-646B-9H-2	17-24
105-646A-8H-4	68-72	105-646B-9H-4	55-65
105-646A-9H-1	43-68	105-646B-9H-5	118-140
105-646A-9H-3	80-110	105-646B-10H-3	86-109
105-646A-10H-2	140-146	105-646B-10H-6	71-78
105-646A-10H-5	109-133	105-646B-11H-2	20-40
105-646A-11H-3	85-108	105-646B-12H-2	62-84
105-646A-11H-6	55-77	105-646B-12H-5	53-68
		105-646B-13H-2	6-40
		105-646B-13H-3	103-144
		105-646B-13H-5	23-38
		105-646B-14H-5	54-70
		105-646B-16X-1	44-54
		105-646B-18X-3	64-72
		105-646B-20X-5	75-88

foraminifers, sponge spicules, and diatoms. Variations in the abundance of the biogenic components, which are mainly planktonic, may reflect changes in either surface-water productivity between glacial and interglacial stages (Zimmerman et al., 1984), dissolution, or both. Ice-rafted sand and gravel, as large as cobble size, were dropped from icebergs floating over the site.

Most of the sediments of Subunit IA are fine grained and are either apparently homogeneous or bioturbated. The transport processes that brought the silt and clay fractions to the site are obscured by absence of primary sedimentary structures but probably included ice rafting, bottom currents, low-concentration turbidity currents, and dilute off-shelf lutite flows, forming hemipelagites. Bathymetric maps of the Labrador Sea show a series of slope gulley and small channels northeast of the site on the continental slope of Greenland. These may have funneled low-concentration turbidity currents (lutite flows) to the seafloor (Fig. 24, path 2), and bottom-current transport and bioturbation subsequently destroyed evidence of turbidites. Thin sand-rich layers in the clayey silts and about 5-cm-spaced dark greenish gray bands in much of the sediment suggest a continuous, even deposition rate; no single "event" deposited more than a few centimeters of sediment. Sedimentation rates ("Sediment-Accumulation Rates" section, this chapter) were about 9 cm/k.y. (90 m/m.y.). Complete lack of clear lamination or cross-lamination in the sand-rich layers of Subunit IB is consistent with their emplacement by ice rafting. Chough and Hesse (1985) described sediments from the main part of Eirik Ridge and concluded that bioturbated silts and clays are characteristic of bottom-current-molded sediment drifts. The similarity of large parts of Subunit IA to the descriptions of Chough and Hesse (1985) and the position of Site 646 on the northern flank of Eirik Ridge support an interpretation involving substantial sediment reworking by bottom currents.

Bottom currents are also thought to have promoted deposition of the laminated and cross-laminated noncarbonate silt layers because current-sorted concentrations formed during times of particularly strong bottom-current flow. These units do not show the consistent normal grading characteristic of turbidites and often contain the same open-ocean fauna as the biogenic-bearing finer grained sediments, not the shallow-water, reworked

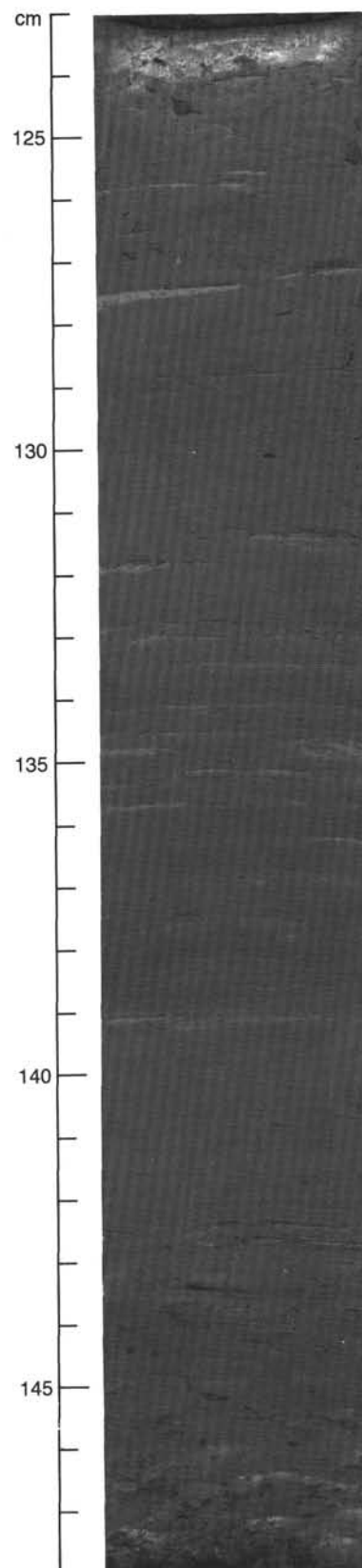


Figure 15. Light greenish gray detritic carbonate clayey silt bed (123-144 cm) with lighter colored laminae of well-sorted carbonate silt. A thin section enlargement of part of this slab is shown in Figure 17. Individual silt-mud couplets are sharp based and graded. Interval shown is Sample 105-646B-13H-3, 123-148 cm.

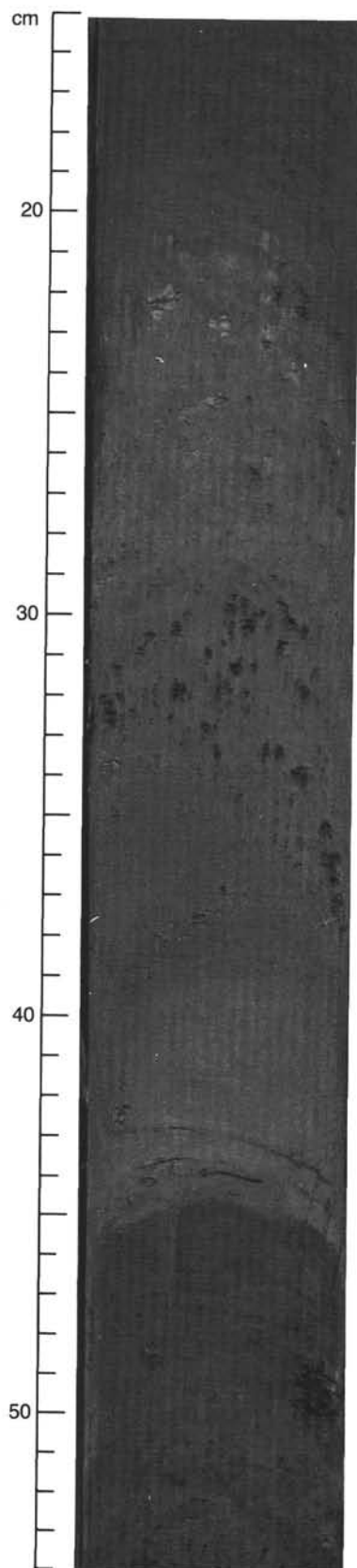


Figure 16. Light-gray detriticarbonate silty clay (35–45 cm), grading upward into a mottled greenish gray detriticarbonate silty clay with dark greenish gray silt pockets (21–45 cm). Interval shown is Sample 105-646B-11H-2, 15–54 cm.



Figure 17. Photographic print, made from a thin section used as a negative, of a sample cut from the slab shown in Figure 15. Note sharp-based silt units, grading upward into silty clay via a laminated division. The lobe on the base of the thickest silt unit is a load cast. A round burrow appearing near the top of the slide contains a large sand grain. Interval shown is Sample 105-646B-13H-3, 137–140 cm. Width of thin section is 2 cm.

fauna expected in turbidites. Our interpretation requires long-term fluctuations in the strength of bottom currents and subtle fluctuations in sedimentation rate to account for the winnowed texture and lack of significant bioturbation in the silt layers. Later, detailed studies may indicate whether changes in bottom-current character are controlled by global climatic or sea-level effects.

Throughout Subunit IA are sharp-based units of clayey silt and silty clay, rich in detritic carbonate, finely laminated, and containing several graded couplets of silt to clay. These units are generally not bioturbated, except at their top. The lack of bioturbation suggests rapid deposition, at least fast enough to exclude burrowers until after deposition of each detriticarbonate unit. We interpret each laminated unit as being a composite bed formed of a succession of thin (<1 cm thick) turbidites. The mineralogy of these inferred turbidites is similar to that of turbidites from DSDP Site 112 (Laughton, Berggren, et al., 1972) and from NAMOC (Chough et al., in press, b), which is located approximately 175 km west of Site 646; the thinly bedded turbidite facies is like that described from piston cores taken on the levees of NAMOC. Local bathymetry is consistent with the origin of the laminated detriticarbonate beds being deposited from turbidity currents that spilled over the levees of NAMOC (Fig. 24, path 1), presumably during times of maximum channel ac-

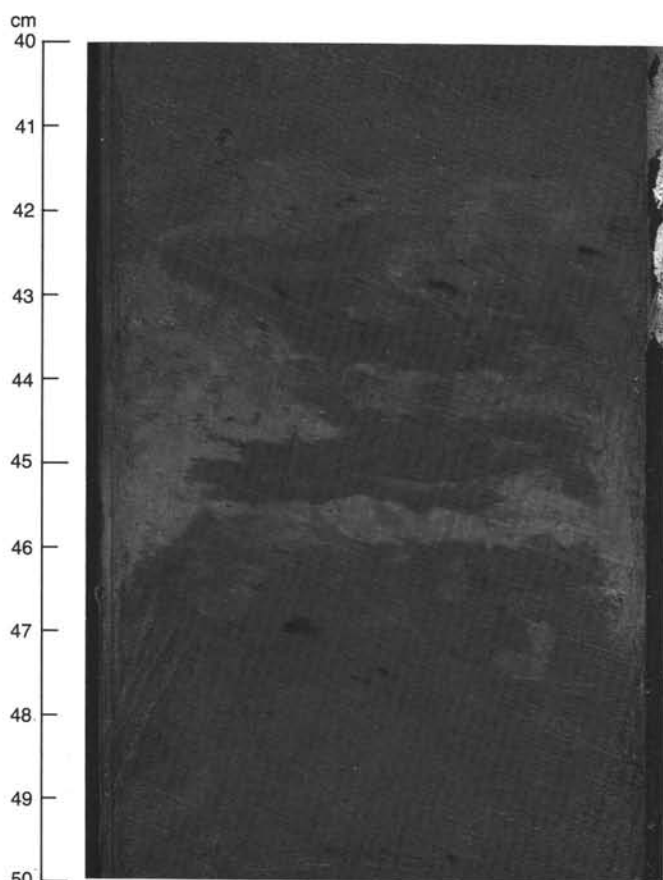


Figure 18. Light-gray detriticarbonate layer (41.5–46.5 cm) without apparent primary physical structures, showing indistinct burrowed contacts with dark-gray, silica-bearing silty clay (40–41.5 cm and 46.5–50 cm). Interval shown is Sample 105-646A-2H-6, 40–50 cm.

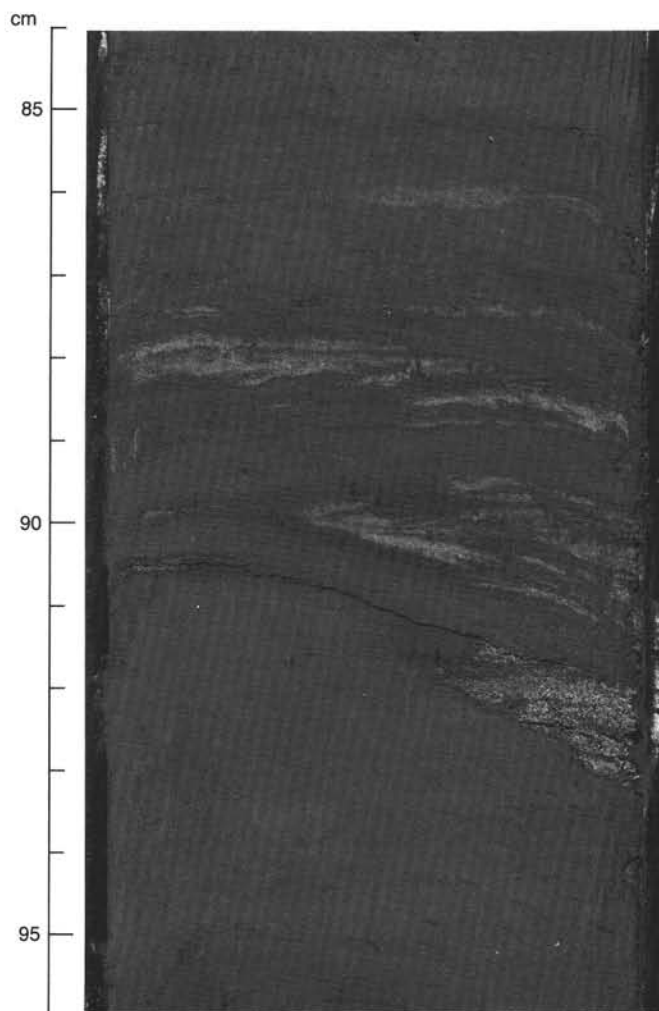


Figure 19. Greenish gray clayey silt with thin layers or lenses of cross-laminated, well-sorted lighter silt to very fine sand (92–93 cm). Interval shown is Sample 105-646B-14H-5, 84–96 cm.

Table 6. Location of laminated, well-sorted silt and fine sand layers.

Hole 646A section	Interval (cm)	Hole 646B section	Interval (cm)
105-646A-2H-2	80–85	105-646B-3H-4	84–90
105-646A-4H-3	113–117	105-646B-4H-2	85–90
105-646A-4H-4	66–76	105-646B-5H-2	37–40
105-646A-4H-4	125–134	105-646B-6H-3	80–88
105-646A-4H-6	30–33	105-646B-9H-1	95–97
105-646A-5H-6	118–123	105-646B-9H-1	127–133
105-646A-6H-5	55–88	105-646B-9H-1	142–144
105-646A-7H-2	90–95	105-646B-10H-1	112–115
105-646A-7H-4	35–40	105-646B-10H-4	72–76
105-646A-8H-4	26–29	105-646B-10H-6	50–54
105-646A-8H-5	58–62	105-646B-11H-2	69–75
105-646A-10H-2	118–135	105-646B-11H-2	105–107
105-646A-10H-6	56–59	105-646B-11H-2	128–132
105-646A-11H-1	104–110	105-646B-12H-2	30–62
105-646A-11H-6	17–46	105-646B-13H-3	29–36
		105-646B-13H-4	68–70
		105-646B-14H-3	15–36
		105-646B-14H-3	50–71
		105-646B-14H-3	84–100
		105-646B-14H-5	79–100
		105-646B-20X-5	138–140
		105-646B-21X-3	123–127
		105-646B-22X-2	54–55
		105-646B-23X-4	55–57
		105-646B-26X-CC	10–15
		105-646B-37X-2	55–70
		105-646B-38X-5	97–105
		105-646B-42X-3	110–123

tivity, interpreted by Chough and Hesse (in press, a) to have been during glacial intervals. The detriticarbonate beds are composite (i.e., formed of many graded couplets), and therefore each corresponds to a pulse of NAMOC activity. The number of these beds is too great for each to reflect a single glacial episode. A more frequent event, flow of meltwater repeatedly during major advances and retreats of continental ice sheets, probably caused these numerous beds. It is noteworthy that cyclicity at Site 645, Baffin Bay, also has a much higher frequency than can be attributed to glacial-interglacial cycles.

Perhaps some of the turbidites did not come from NAMOC but from apparently relict channels that extend into the Davis Strait area, where a source of detrital carbonate may have existed (Fig. 24, path 3). Turbidity currents using this path would be relatively unconstrained below a depth of 3000 m, except by the NAMOC levees on the west and the continental slope of Greenland on the east. If of sufficient thickness, such flows could have reached the site, even though it is at somewhat shallower water depths (about 100 m shallower) than the region just to the west.

A direct correlation exists between the abundance of pebbles and cobbles (dropstones) in Subunit IA and the occurrence of laminated detriticarbonate units. Additionally, the detriticarbonate layers with indistinct contacts and with scattered granules sug-



Figure 20. X-radiograph of a thin slab showing dark-gray laminated silt and clayey silt. Note that the laminations are thicker and more irregular than those found in the calcareous beds. Interval shown is Sample 105-646A-11H-6, 25–45 cm.

gest an association of detrital carbonate supply and ice rafting. These deposits may all be indicators of glacial maxima or early deglaciation because they seem to correlate with relative lows in abundance of biogenic carbonate (Figs. 14 and 22). Laughton, Berggren, et al. (1972) and Latouche and Parra (1979) conclud-

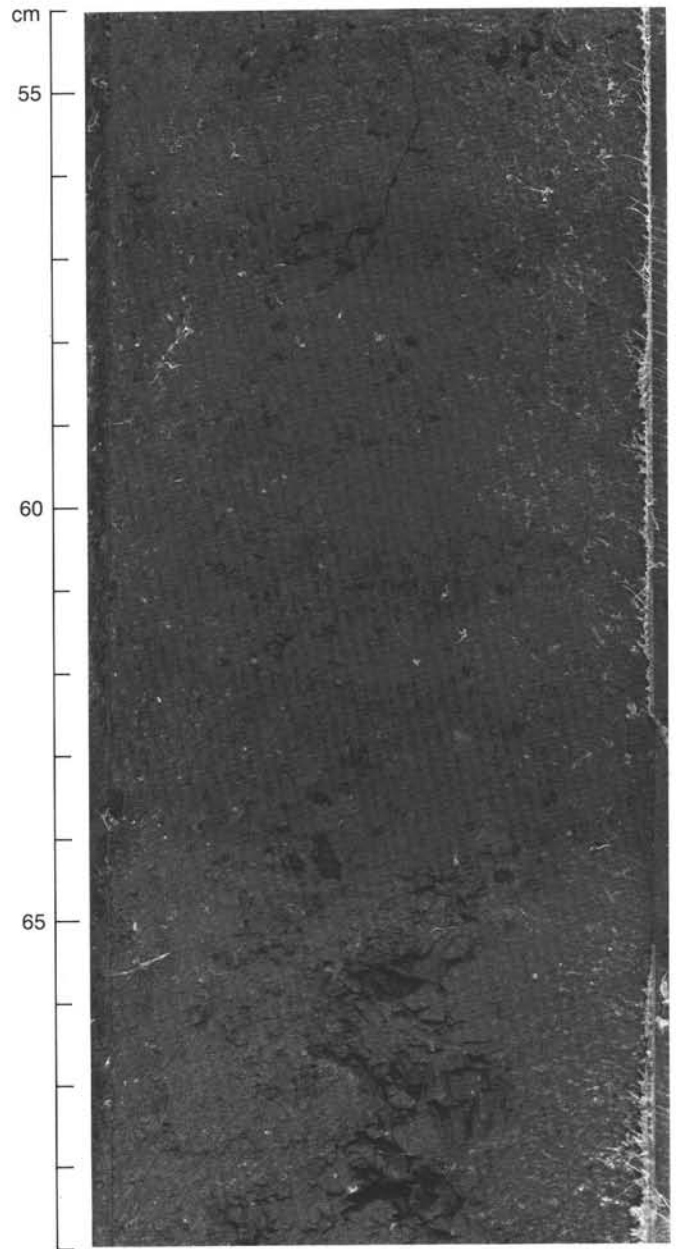


Figure 21. Dark-gray, poorly sorted muddy sand with scattered granules and a few very dark-green bands (56–57 cm, 62–64 cm). Interval shown is Sample 105-646B-21X-4, 54–69 cm.

ed that detrital carbonate turbidites characterize glacial episodes in the Labrador Sea.

The tops of several laminated detrital carbonate units are somewhat greenish, in some places partly the result of inclusion of greenish gray mud clasts. The origin of the greenish minerals, probably either chlorite or poorly crystallized glauconite, is unresolved but may in some way be related to glacial-interglacial cyclicity, perhaps through changes in source area during progressive deglaciation.

Subunit IB is characterized by the presence of very poorly sorted muddy sands, showing little evidence of current activity or of sharp-based events. We interpret these muddy sands as being accumulations of ice-rafted sediments, although we cannot rule out the possibility that some intervals may have been em-

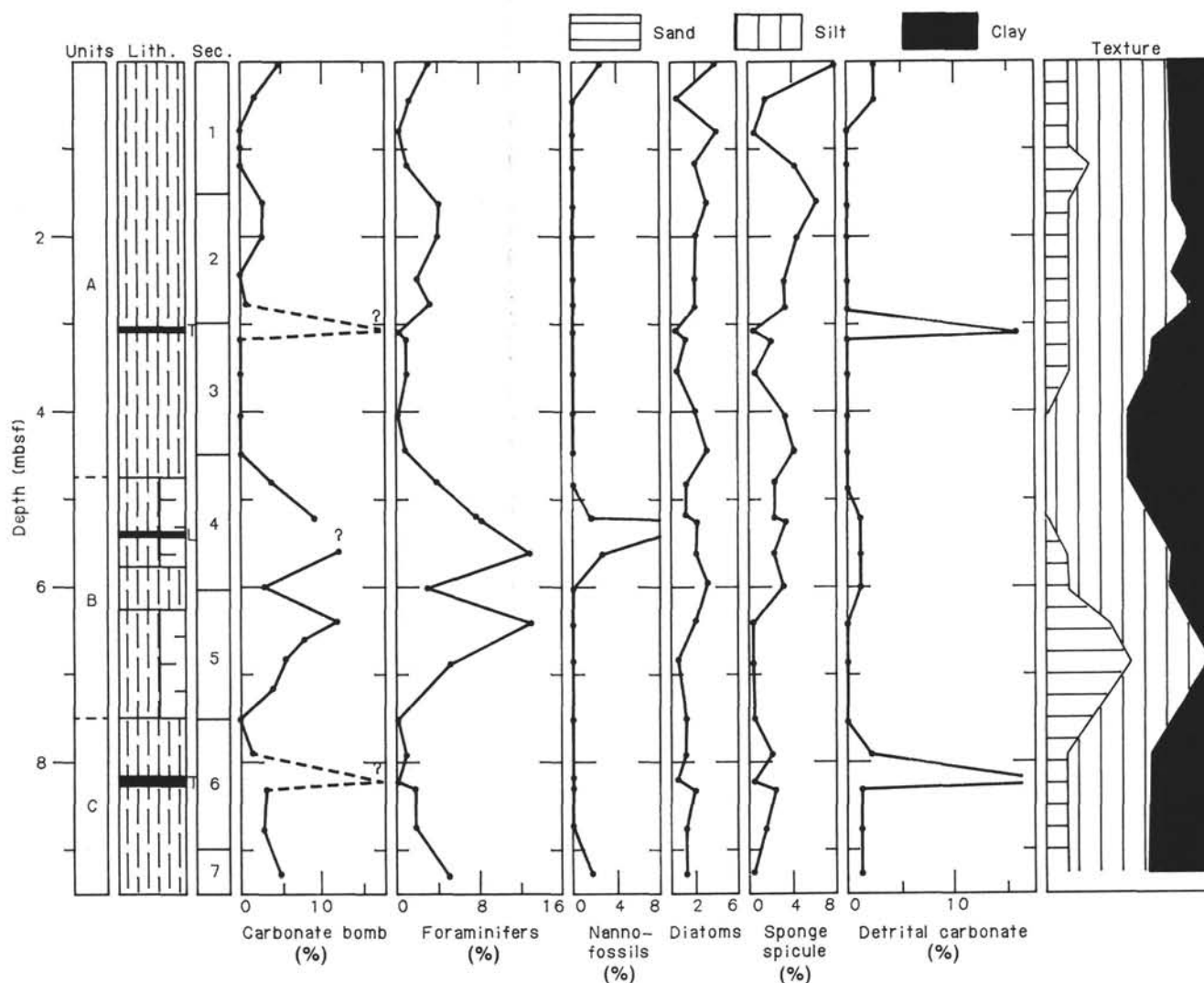


Figure 22. Variation in texture and composition in Core 105-646B-3H, primarily from smear-slide estimates and carbonate-bomb data. In the lithology column (standard core-description form symbols), T = detriticarbonate layers, and L = laminated silt layers. For the carbonate-bomb data, the dashed lines show the effect on the curve of including analyses from the detriticarbonate layers. Intervals A and C are relatively poor in biogenic carbonate, whereas interval B is relatively rich.

placed more quickly by poorly evolved, high-concentration density currents.

Most of the pebbles and cobbles in Unit I are mafic igneous rocks, basalts, dolerites, gabbros, and diabases, probably derived from nearby volcanic rocks on the shelf of southern Greenland (Johnson et al., 1982). Rare carbonate pebbles may have been rafted along the east coast of Greenland by icebergs calved from glaciers on its north coast. Suitable carbonate source rocks are also found around the northern end of Baffin Bay and on the shelves around Baffin Island, but modern surface circulation does not bring icebergs to Site 646 from these Canadian sources. Icebergs in the Labrador Sea drift southward along the western side of the bay. Appearing as cavings in cores through Unit II, large felsic plutonic pebbles that are apparently common in the interval of poor recovery between Units I and II probably came from the Precambrian Shield terranes of eastern Greenland, because currents like those of the present would transport icebergs from western Greenland or Canada away from the site. Note, however, that surface circulation may have been different during the early Pleistocene and late Pliocene, which may have allowed Canadian sources to contribute ice-rafted sediments to the site.

Lithologic Unit II

The uniform fine-grain size of Unit II and the lack of primary physical structures confound any attempt to use facies analysis as a key to understanding the sedimentary environment. Clearly, the depositional rate was slow enough to allow complete or near-complete reworking of the sediment by infauna; the calculated sedimentation rate of Unit II is about 9 cm/k.y. (90 m/m.y.; "Sediment-Accumulation Rates" section, this chapter). These sediments would probably be generally assigned to the category of hemipelagic sediments were it not for seismic evidence ("Seismic Stratigraphy" section, this chapter) that, at least from the top of Unit II to a depth of 490 mbsf (i.e., R2), has the geometric characteristics of a migrating bottom-current drift. From this seismic evidence and the presence of a few laminated silt units above 395 mbsf, we interpret the bulk of Unit II to be contourite or drift deposits. Notice that many sediment drifts, like Unit II, are almost completely bioturbated (Stow and Holbrook, 1984; Chough and Hesse, 1985). The terrigenous detritus may have been carried for some distance along the continental margin of Greenland in a bottom nepheloid layer, and periodic contributions to the nepheloid layer may have been from

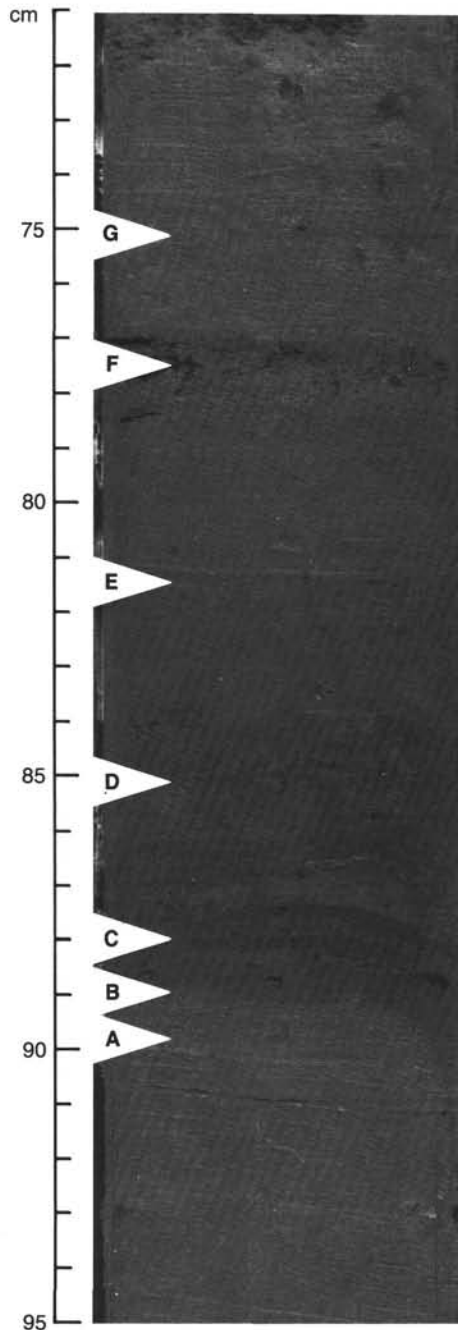


Figure 23. Example of the fine-scale lithologic variations in Core 105-646B-3H that characterize most of Subunit IA. A, nannofossil silty clay, with rare foraminifers and sponge spicules; B, clayey silt, with rare nannofossils, diatoms, and sponge spicules; C, Silt, with rare nannofossils, diatoms, and sponge spicules; D, clayey silt, with common diatoms and sponge spicules; E, nannofossil- and silica-bearing silty clay; F, silty clay, with rare foraminifers, nannofossils, sponge spicules, and pellets; G, nannofossil siliceous silty clay. Interval shown is Sample 105-646B-3H-4, 71–95 cm.

river discharge or from low-concentration turbidity currents or from plumes of turbid water originating on the shelf (storms). Some fine-grained detritus may have been contributed directly from the nearby Greenland margin, perhaps through a series of small slope gulleys.

The minor amount of glauconite found near the base of Unit II is closely associated with burrows. This glauconite may be partly if not entirely authigenic.

History of Glaciation

The first ice-rafted debris occurs at the base of Lithologic Unit I, which has been tentatively assigned an age of 2.6 ± 0.3 Ma ("Sediment-Accumulation Rates" section, this chapter). Within error, this agrees with determinations of the timing of the first introduction of ice-rafted detritus into sediments in the northeastern Atlantic (2.4 Ma; Zimmerman et al., 1984) but could be slightly older. In Unit I at Site 646, most of the *in-situ* pebbles and cobbles appear to have been derived locally from Precambrian or Tertiary volcanic bedrock (basalts, dolerites), inferred by Johnson et al. (1982) to underlie parts of the shelf off the southwest coast of Greenland.

Chough et al. (in press, b) speculate that NAMOC dates from approximately 2.5 Ma (late Pliocene), being initiated and maintained by high sediment yields during glacial events. We find laminated detriticarbonate silty clay and clayey silt turbidites to the base of Subunit IA, tentatively dated at about 2.1 Ma ("Sediment-Accumulation Rates" section, this chapter), agreeing with this suggestion.

Although primarily terrigenous in nature, a cyclical pattern of pelagic/biogenic carbonate characterizes the upper part of the sediment column at this site (Fig. 36, "Organic Geochemistry" section, this chapter; detailed carbonate determinations for the early Pleistocene and Pliocene have not yet been made). Variation of a similar type was described for the North Atlantic by Schott (1935) and, more recently, by Ruddiman and McIntyre (1976) and Roberts, Schnitker, et al. (1984). These cyclical variations in carbonate content have been ascribed to glacial-interglacial control of the depositional regime.

Deposition at Site 646 is influenced by (1) the influx of terrigenous material transported by both ice rafting and bottom currents of various types and (2) the changing pattern of surface productivity and dissolution of microfossils in the water column and on the seafloor. This interplay of sedimentological factors is, in the first instance, controlled by variations in climate and its attendant factors, for example, sea-level rise and fall, ice cover, and the intensity and location of bottom-water production.

As continental areas are approached, the sedimentation rate generally increases, and as high-latitude, glaciated continental areas are approached, deposition rates increase by about an order of magnitude when compared with open-ocean areas (e.g., Holes 646A and 646B; Hole 552A, Roberts, Schnitker, et al., 1984). The high-latitude continentality factor is thought to increase because of ice rafting and glacial-erosional input by down-slope processes on the continental margins, perhaps accentuated in glacial stages by lowered sea level, thus delivering sediment directly to the continental margin. One might expect that this would result in relatively thicker glacial than interglacial intervals in high-latitude areas. Yet, although the study is still preliminary, we see relatively little change in relative rates of sedimentation under the two climatic regimes (Fig. 36). The thickness ratio of glacial to interglacial intervals (perhaps except for inferred isotopic stage 6; the carbonate curve of Figure 36 is used as a proxy for oxygen-isotope variations) appears to be about the same as that for climatic curves generated at more southerly latitudes and under very different sedimentation processes and much lower sedimentation rates. Although a uniform deposition rate is highly unlikely, the climatic imprint on sedimentation rates seems to be overshadowed by the overall high rate of terrigenous influx.

Similarities with Sites 112 and 113

Results from Site 646 can be compared with earlier cores taken at Sites 112 and 113, Leg 12, in the Labrador Sea (Laughton, Berggren, et al., 1972). In Hole 112, two of the recognized lithologic units are of similar age to Lithologic Units I and II of Leg 105. From the top to the base, these Leg 12 units are as follows:

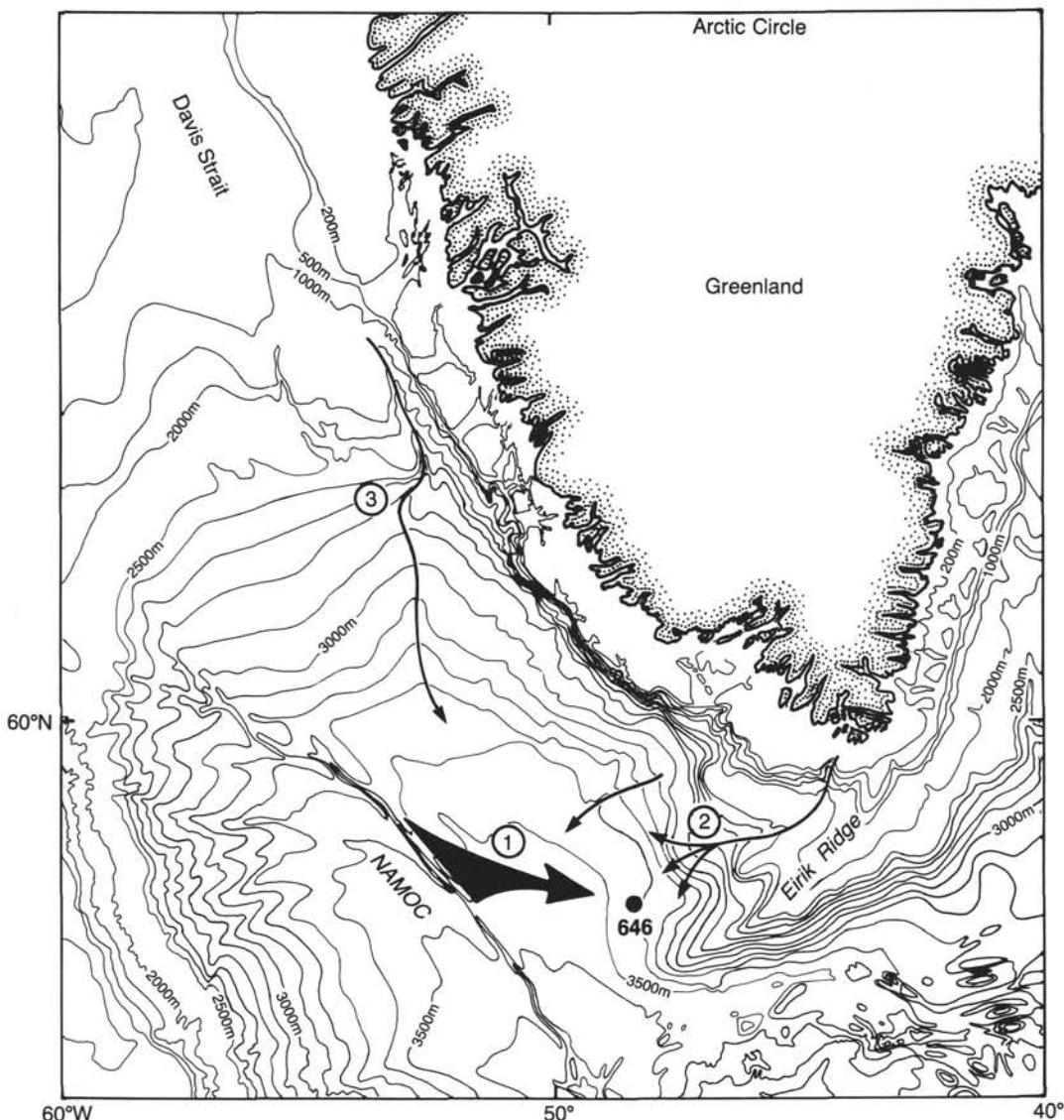


Figure 24. Bathymetric map of the eastern part of the Labrador Sea, in meters (taken from GEBCO Series, International Hydrographic Organization, Chart 504). Site 646 is about 175 km northeast of NAMOC and is nestled against the northwestern flank of Eirik Ridge. Turbidity currents could reach the site (A) by spilling over the eastern levee of NAMOC, either directly west of the site or further north (path 1), (B) directly from slope canyons and gulleys immediately northeast of the site on the Greenland margin (path 2), or (C) from slope channels near the east coast of Greenland just south of Davis Strait, flows being confined between the levees of NAMOC to the west and the continental slope of Greenland to the east (path 3).

Lithologic Unit 5: middle Pliocene to Pleistocene gray terrigenous silty to muddy clay with ice-rafted pebbles, interbedded with hemipelagic silty nannofossil clay and marl (115 cm thick). Sedimentation rate in the Pleistocene strata was about 4.5 cm/k.y. (45 m/m.y.).

Lithologic Unit 4: lower Pliocene gray, pelagic, silty to sandy foraminiferal nannofossil marl and ooze, with an intercalation of terrigenous sandy clay (about 35 m thick).

Site 112 penetrated all but the lower 200 m of a mound-shaped sediment body interpreted by Davies and Laughton (1972) as being a ridge molded by thermohaline bottom currents. Evidence of bottom currents includes broken and hydraulically sorted diatom valves. The sediment-accumulation rate of preglacial

sediments was about 2 cm/k.y. (20 m/m.y.). Inferred turbidite beds at Site 112 are rich in detrital dolomite.

Site 113, lying just southwest of Eirik Ridge in the IMOC, is the closest DSDP site to ODP Site 646. Four recognized units are of similar age to Leg 105 Units I and II. From the top to the base, these are as follows:

Unit 4: upper Pliocene to Pleistocene silty clay and clayey silt and a variable content of microfossils and nannofossils (about 300 m thick).

Unit 3: middle Pliocene, silty, heavy-mineral-rich turbidite sands (about 250 m thick).

Unit 2: middle Pliocene mudflow breccia with reworked Eocene to Pliocene nannofossil clay ooze (thin unit).

Unit 1: upper Miocene to middle Pliocene well-laminated mudstone (about 300 m thick).

Sedimentation rates at Site 113 are about 10 cm/k.y. (100 m/m.y.) in the Pleistocene and about 35 cm/k.y. (350 m/m.y.) in the late Pliocene. The former rate is approximately the same as the rate derived from data at Site 646 ("Sediment-Accumulation Rates" section, this chapter).

In general, the composition and texture of Pleistocene and upper Pliocene sediments at Sites 112 and 113 compare well to those found at Site 646. Facies at Site 113, however, consist of graded beds characteristic of turbidites. Site 112 equivalents are relatively featureless and probably bioturbated like the sediments at Site 646; both sites were drilled into inferred bottom-current drift deposits. Middle Pliocene sediments at Site 113 are turbidites with intercalated debrites (submarine debris-flow deposits) and are therefore not comparable to the uppermost parts of Unit II, which are interpreted as being bottom-current drift deposits. In contrast, upper Miocene to middle Pliocene sediments at Site 113 are finely laminated mudstones, possibly indicating deposition under anaerobic or disaerobic conditions (Laughton, Berggren, et al., 1972) beneath bottom currents in a local depression. At the same time, sediments at Site 646 were being intensively bioturbated under oxygenated bottom waters flowing around the southern tip of Greenland.

BIOSTRATIGRAPHY

Holes 646A and 646B were drilled to a depth of 103.5 and 766.7 mbsf, respectively. Because of time limitations, the core-catcher samples were analyzed mainly for benthic and planktonic foraminifers, calcareous nannofossils, diatoms, radiolarians, dinoflagellates, pollen, and spores. Preliminary examination of core-catcher data indicates that the Pliocene/Pleistocene and Miocene/Pliocene boundaries occur at approximately 131.0 and 520.0 ± 15 mbsf, respectively.

Good lithostratigraphic correlation exists between the upper 11 cores of Hole 646A and the upper 11 cores of Hole 646B (see "Sedimentology" section, this chapter); therefore, in the following summary, the biostratigraphic results of each hole are combined and discussed together (except calcareous nannofossils).

Planktonic Foraminifers

Results

The relative abundance of faunal data from Site 646 is presented in Figure 25. On the basis of planktonic foraminifer stratigraphy, Holes 646A and 646B can be divided into three intervals.

Interval I (0–130.5 mbsf) is a nearly monospecific, high-abundance planktonic foraminifer assemblage, observed down to 64.8 mbsf in Hole 646A (Section 105-646A-7H, CC) and to 62.7 mbsf in Hole 646B (Section 105-646B-7H, CC). The fauna is dominated by sinistral *Neogloboquadrina pachyderma* and minor occurrences of dextral *N. pachyderma*. Sporadic and rare occurrences of *Globigerina bulloides*, *G. quinqueloba*, and *Globigerinita uvula* are also observed in this interval. The quadrate form of *N. pachyderma* (4–4½ chambers in the final whorl) is the dominant morphotype in the samples having smaller proportions of the 5-chamber variety. Very low benthic to planktonic (B/P) ratios (<0.01) and generally <30% test fragmentation observed in the samples suggest a relatively good preservation state of biogenic carbonate on the seafloor. Therefore, it is thought that this assemblage represents the water-mass characteristics during deposition. Between 62.7 mbsf (Section 105-646B-7H, CC) and 130.5 mbsf (Section 105-646B-14H, CC), foraminifers are rare, and except for samples from Sections 105-646B-10H,

CC, and 105-646B-13H, CC, the fauna in samples analyzed consist exclusively of sinistral *N. pachyderma*. Sections 105-646B-10H, CC, and 105-646B-13H, CC, include rare *Globorotalia inflata* and dextral *N. pachyderma*, respectively. All samples examined from this interval exhibit as much as 80% test fragmentation and considerably higher B/P ratios (>5), suggesting higher dissolution of carbonate. This interpretation is supported by pore-water Ca⁺⁺ profiles (see "Inorganic Geochemistry" section, this chapter).

Interval II (130.5–516.5 mbsf), characterized by a higher diversity and abundance assemblage, can be further divided into Subintervals IIa and IIb. Subinterval IIa extends from 130.5 to 304.1 mbsf (Section 105-646B-32X, CC). The fauna is dominated by dextral and sinistral *N. pachyderma* and sinistral *N. atlantica*, *Globigerina bulloides* and *G. quinqueloba* being secondary in abundance. The more reticulate and open *N. pachyderma* appears to be more abundant in the samples, and the dextral form is generally <10% of the fauna. Sporadic and rare occurrences of dextral *N. atlantica*, *N. acostaensis*, *N. humerosa*, *G. umbilicata*, *G. nepenthes*, *Globorotalia inflata*, *G. scitula*, *Globigerinita uvula*, and *Orbulina universa* are also observed in this interval. Subinterval IIb extends from 304.1 to 516.5 mbsf (Section 105-646B-54X, CC). Foraminifer abundances are higher in Subinterval IIb than those in Subinterval IIa. The fauna consists generally of >90% sinistral *N. atlantica* and varying percentages of *N. pachyderma* and *N. humerosa*. Smaller percentages of dextral *N. atlantica* and *Globorotalia bulloides*, *G. nepenthes*, *G. tripartita*, *G. umbilicata*, *Globoquadrina venezuelana*, *Globorotalia margaritae*, *Globorotalia puncticulata*, *G. scitula*, *Globigerinita glutinata*, *Orbulina universa*, and *Pulleniatina primalis* are also found sporadically in the samples as auxiliary species.

Interval III (516.5–766.7 mbsf) is characterized by a lower diversity and abundance assemblage still dominated by *N. atlantica*. Sinistral *N. pachyderma* sl. and *Globigerina bulloides* are secondary in abundance, and *N. continua*, *Globigerina nepenthes*, *Globigerina venezuelana*, *Globorotalia scitula*, *Globorotalia obesa*, and *O. universa* are of lesser quantities. All core-catcher samples analyzed from this interval also contain planktonic foraminifer species that are flattened and partly broken. These species form as much as 30% of the total assemblage and are interpreted as being reworked. A coiling change in *N. atlantica* is observed between Sections 105-646B-77X, CC, and 105-646B-80X, CC. Specimens in Section 105-646B-77X, CC, are predominantly sinistrally coiled, but those in Section 105-646B-80X, CC, are predominantly dextral. The timing of the coiling change is not well constrained chronologically, but occurs within Zone NN11 at Site 407 and near the middle of Zone N16 at Site 116 (Berggren, 1972; Perch-Nielsen, 1972; Martini, 1979; Poore, 1979). This event is probably environmentally controlled and therefore diachronous, so we have accepted an age range of 6.5–9 Ma for this event, on the basis of correlation with the time scale of Berggren et al. (1986).

Chronostratigraphy

The following discussion is based on several assumptions, some or all of which may not be warranted: (1) the sedimentation at the site was continuous, so that the sedimentary record recovered includes the first-appearance datums (FAD) and last-appearance datums (LAD) of the age-diagnostic species involved; (2) the FAD of the species involved show no diachroneity with data from other areas in which the ecological migration occurred at the same time in, for example, the equatorial Atlantic and the Labrador Sea; (3) the late Neogene climatic cooling and the subsequent climatic oscillation had no effect on the synchronicity of the LAD of species; and (4) no re-sedimentation is present, and the faunas observed in the samples are indigenous.

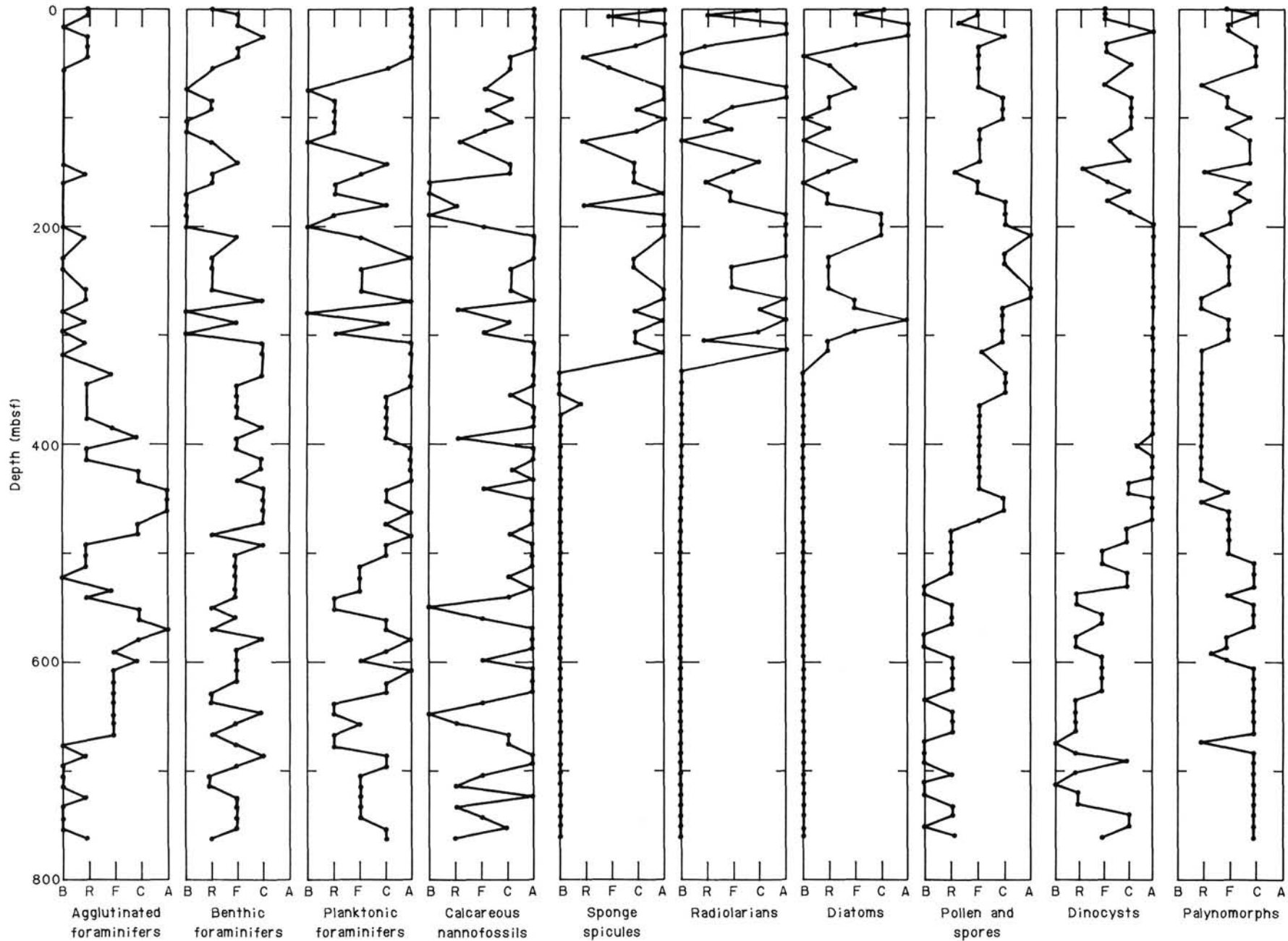


Figure 25. Downhole abundance plots of microfossils. B = barren, R = rare, F = few, C = common, A = abundant.

Although the observed fauna is not diverse, several age-diagnostic species present in the samples allow a tentative framework to be established. On the basis of the last occurrence of *Neogloboquadrina atlantica*, the Pliocene/Pleistocene boundary is tentatively placed at approximately 131 mbsf (between Sections 105-646B-14H, CC, and 105-646B-16X, CC). The presence of *Globorotalia inflata* in Sections 105-646B-16X, CC, and 105-646B-17X, CC, partly supports this boundary placement. However, the first-occurrence depth of this taxon appears to be much higher in the section. Because of the present latitude of Site 646B, the presence of *G. inflata* may be strongly influenced by the paleoclimatic conditions of the northern Labrador Sea. The early/late Pliocene boundary (PL2/PL3) is determined on the basis of the last occurrence of *G. margaritae* and placed at approximately 313.8 m (Section 105-646B-33X, CC). Although slightly lower, the last occurrence of *Globigerina venezuelana* in Section 105-646B-36X, CC, supports this boundary. The PL1/PL2 boundary is placed at the base of Section 105-646B-40X, CC, on the basis of the single occurrence of *Pulleniatiana primalis* and the first occurrence of *G. puncticulata*. The Miocene/Pliocene boundary is tentatively located at approximately 516 mbsf (Section 105-646B-54X, CC), on the basis of the first occurrence of *G. margaritae*.

Paleoenvironment

Data from shorter piston-core tops indicate that the present-day planktonic foraminiferal assemblage in the northeastern Labrador Sea includes as much as 25% subarctic (*G. bulloides*, *G. quinqueloba*, and dextral *N. pachyderma*) and transitional (*Globorotalia inflata*, *Globigerinita uvula*, and *Globigerinita glutinata*) species (Bé and Tolderlund, 1971). This assemblage represents the North Atlantic drift (NAD) fauna, which dominates the Holocene (isotopic stage 1) and the last interglacial (isotopic stage 5) sediments in the Labrador Sea. Glacial stages 2 and 4 are characterized by the dominance of sinistral *N. pachyderma* and the absence of NAD assemblages (Aksu and De Vernal, unpubl. data). The fauna observed in Interval I is dominated by sinistral *N. pachyderma* with <5% subarctic species and can be classified as an arctic planktonic foraminiferal assemblage. No core-catcher samples include "true" interglacial planktonic foraminiferal fauna. Increased dissolution observed between 62.7 and 130.5 mbsf probably altered the fauna; however, the absence of dissolution-resistant temperate-water species such as *Globorotalia inflata* suggests that most sediments recovered in core-catcher samples from Interval I represent glacial and/or interstadial conditions.

In Interval IIa species diversity generally increases, as well as subarctic-water indicator species such as *Globigerina bulloides*, *G. quinqueloba*, and *Globigerinita uvula*. Species diversity is much higher in Interval IIb, and warm subtropical and temperate species such as *Globorotalia margaritae*, *Globorotalia puncticulata*, *Globigerina venezuelana*, and *N. humerosa* are consistently present. The progressive downhole increase of the above-mentioned species suggests warmer oceanic conditions during this interval. The transition from Subinterval IIb to IIa marks the most pronounced decrease of warm-water indicator species and may be interpreted as signifying the onset of northern hemisphere glaciation.

Principally a subarctic fauna, varying in proportions of temperate to warm subtropical species, dominates Interval III.

Benthic Foraminifers

Holes 646A and 646B

Benthic foraminifers were examined from core-catcher samples from Holes 646A and 646B, and abundance data are given in Figure 25. The fauna can be subdivided into two assemblages

on the basis of the occurrence of common or characteristic species. The interval from 0 to about 350 mbsf (Sections 105-646A-1H, CC, to 105-646A-11H, CC, and 105-646B-1H, CC, to 105-646B-34X, CC) contains generally low abundances of benthic taxa compared with Site 645. Eleven core-catcher samples contain no benthic taxa. The assemblage is dominated by *Cibicidoides bradyi*, *Epistominella exigua*, *Fursenkoina fusiformis*, *Melonis barleeanum*, *M. zandaamae*, *Pullenia bulloides*, *P. quinqueloba*, and *Stetsonia horvathi*. Most species in this assemblage possess long or poorly constrained stratigraphic ranges; therefore, they cannot be used for age determinations. *Cassidulina teretis*, the late Pliocene–Holocene species occurring at Site 645, is not found in the samples examined. Sporadic floods of *S. horvathi* are observed in samples from Cores 105-646A-4H to 105-646A-6H, suggesting Arctic affinities. *Elphidium clavatum* is observed in Sections 105-646B-2H, CC, 105-646B-6H, CC, and 105-646B-14H, CC, which suggests redeposition from shallower depths.

This assemblage in the interval from 0 to 350 mbsf shows strongest resemblance to the late Pliocene–Holocene benthic foraminiferal assemblage from the Rockall margins (Murray, 1984), except that typical specimens of *Planulina wuellerstorfi* are very rare in the samples examined. *P. wuellerstorfi* and *C. bradyi* form a series of intergradational forms (D. Schnitker, pers. comm., 1985), but our specimens are closer to the latter species. The fauna can be interpreted as a lower bathyal assemblage, on the basis of the rarity of abyssal species such as *Nuttallides umbonifera* and typical *P. wuellerstorfi*.

A large faunal turnover, marking the second assemblage, occurs in the interval between Sections 105-646B-34X, CC, and 105-646B-40X, CC. Several important species have their local range tops in this interval, and others display changes in their relative abundance. The fauna below is more diverse and is characterized by *Melonis zandaamae*, *M. pompilioides*, *Oridorsalis tener*, *Uvigerina peregrina*, *U. cf. hispida*, *Globocassidulina subglobosa*, *Hoeglundina elegans*, and abundant agglutinated foraminifers. This calcareous fauna more closely resembles a typical North Atlantic deep-water (NADW) assemblage. Murray (1984) reports an increased abundance of *G. subglobosa* and *C. kulenbergi* in the preglacial Pliocene and upper Miocene sediments recovered during Leg 81, which is consistent with the fauna observed at Site 646. Additional samples will further constrain the timing of the faunal change.

The first downcore occurrence of an agglutinated foraminiferal facies begins in Section 105-646B-34X, CC, and becomes abundant in Section 105-646B-45X, CC. The sporadic occurrence of *Eggerella bradyi*, *Siphotextularia* sp., *Karrerella* sp., and *Martinotiella* sp. in the interval above Section 105-646B-34X, CC, is not uncommon, since these are ubiquitous deep-water forms associated with calcareous facies. However, the abundance of morphologically simple, coarsely arenaceous species in the early Pliocene and late Miocene suggests environmental affinity with the Norwegian–Greenland Sea and Baffin Bay. Common agglutinated species include *Hyperammina* spp., *Cyclamina cancellata*, *Cyclamina* sp. cf. *C. arctica*, *Haplophragmoides* spp., *Saccamina sphaerica*, *Recurvoides contortus*, *Cribrostomoides scitulus*, and *Trochamminoides* spp.

The occurrence of agglutinated foraminifers at Site 646 is related to changes in the total organic carbon content of the sediment (see "Organic Geochemistry" section, this chapter), which may suggest higher productivity. Because of the lack of Rock-Eval data, the question of whether the agglutinated facies can be tied to the accumulation rate of marine organic matter, as at Site 645, remains to be resolved. A second faunal break occurs between Section 105-646B-70R, CC, and 105-646B-73R, CC. Agglutinated foraminifers become rare, and the calcareous assemblage is dominated by *Nuttallides umbonifera*. The increased

abundance of this species suggests a possible influx of Antarctic Bottom Water (AABW) at this time.

Calcareous Nannofossils

Calcareous nannofossils are present in most samples examined from Holes 646A and 646B. Many of the species that Martini (1971) used to define her zonal boundaries are present, but some FAD and LAD are difficult to recognize because the zonal species have sporadic occurrences and low abundances. In addition, some zonal species exhibit isolated, rare occurrences above their last common occurrences (LCO). These isolated occurrences may be a result of reworking. In such occurrences, the LCO of the species may better represent the LAD. A few marker species used by Bergen (1982) and Okada and Bukry (1980) were used to augment the zones of Martini (1971), when Martini's primary marker species were not observed (discussion follows).

Hole 646A

Calcareous nannofossil abundance varies dramatically through Hole 646A (Fig. 25). *Gephyrocapsa* spp. and *Coccolithus pelagicus* dominate the assemblages. Present in lesser abundance are *Calcidiscus leptoporus*, *Helicosphaera* spp., and *Umbellosphaera* sp. Zone NN21 of Martini (1971) extends from the top of the hole down to the FAD of *Emiliania huxleyi* in Sample 105-646A-3H-1, 80–82 cm. Zone NN20 occurs between this sample and the LAD of *Pseudoemiliania lacunosa* in Sample 105-646A-4H-6, 96–98 cm. The interval from Sample 105-646A-4H-6, 96–98 cm, to 105-646A-11H, CC, is assigned to Zone NN19.

Hole 646B

Coccolithus pelagicus, small *Gephyrocapsa* spp., and small *Reticulofenestra* spp. dominate the nannofossil assemblages throughout Hole 646B. Above about Section 105-646B-31X, CC, small *Gephyrocapsa* spp. become more common, whereas below this level, small *Reticulofenestra* spp. are more common. These species are not age diagnostic.

Calcareous nannofossil Zone NN21 (Martini, 1971) occurs from the uppermost part of Hole 646B to the FAD of *Emiliania huxleyi* in Section 105-646B-2H, CC. Reworked Cretaceous nannofossils, including *Watzneuria* sp., *Parhabdololithus embergeri*, *P. cretacea*, *Reinhardtites anthophorus*, *Crucellipsis cuvillieri*, and *Eiffelithus turriseiffelli*, occur sporadically down to Section 105-646B-7H, CC. The LAD of *Pseudoemiliania lacunosa* occurs in Sample 105-646B-5H-3, 70–71 cm. The interval from Sample 105-646B-5H-3, 70–71 cm, to 105-646B-18X, CC, is assigned to Zone NN19. Nannofossils are rare to barren in the interval from Section 105-646B-18X, CC, to 105-646B-22X, CC, and the only species present are placoliths such as *C. pelagicus* and *Gephyrocapsa* spp.

The LAD of *Discoaster surculus* occurs in Sample 105-646B-23X-1, 62–64 cm, indicating a zonal assignment of NN16 (upper Pliocene) from this sample down to Sample 105-646B-29X-5, 79–81 cm. The LCO of *Reticulofenestra pseudoumbilica* occurs in Sample 105-646B-29X-5, 79–81 cm. Rare and sporadic occurrences of the species above this sample possibly represent reworking. The LCO of the species is chosen to represent the LAD in Hole 646B. Zones NN14 and NN15 were not separable, because the zonal boundary marker *Amaurolithus tricorniculatus* was not observed.

Discoaster asymmetricus first occurs in Section 105-646B-36X, CC. Martini (1971) used the FAD of this species to distinguish the NN13/NN14 zonal boundary, but Bergen (1982) considered this datum to be unreliable, preferring rather to use the first common occurrence of this species, in accordance with Okada and Bukry (1980), to mark the base of Subzone CN11b (mid-NN15). In this section, *D. pentaradiatus* occurs only sporadically

and in low abundances. Determining whether the first occurrence of *D. pentaradiatus* represents its actual FAD or its first common occurrence is difficult; therefore, Zone NN13 was not distinguished from Zone NN14 in Hole 646B.

Martini (1971) used the FAD of *Ceratolithus rugosus* to mark the NN12/NN13 zonal boundary. Bergen (1982), however, stated that *C. rugosus* is just a *C. cristatus* with calcite overgrowths and that the two forms have the same FAD. Because of the absence of *C. rugosus* and the presence of *C. cristatus* in this section, the FAD of Sample 105-646B-42X-6, 49–51 cm, was used to mark the NN12/NN13 zonal boundary.

A single specimen of *Ceratolithus armatus* and a single broken specimen of *C. acutus* occur in Section 105-646B-49X, CC. Okada and Bukry (1980) used the FAD of *C. acutus*, the oldest ceratolith species, as the base of their Subzone CN10b. This subzone subdivides Martini's Zone NN12 and indicates an age of no older than early Pliocene. *C. acutus* occurs only in Section 105-646B-49X, CC; therefore, this occurrence cannot be reliably used as an FAD. Its presence, however, indicates an age for this sample of no older than early Pliocene. Section 105-646B-49X, CC, is the stratigraphically lowest sample in which an age of no older than Pliocene can be assigned based on nannofossils.

Single specimens of *Discoaster quinqueramus* occur in Sections 105-646B-53X, CC, and 105-646B-54X, CC, and Sample 105-646B-56X-2, 47–49 cm, suggesting a zonal assignment of NN11 (upper Miocene) for these samples. However, the last consistent occurrence of this species is in Section 105-646B-61X, CC, suggesting that the upper three occurrences may be a result of reworking.

Amaurolithus primus has its FAD in Sample 105-646B-62X-1, 76–79 cm. This datum was used by Okada and Bukry (1980) to define their CN9a/CN9b subzonal boundary, which lies within Martini's (1971) Zone NN11. Therefore, the interval from 105-646B-53X, CC, to 105-646B-62X-1, 76–79 cm, can be assigned to Subzone CN9b of Okada and Bukry (1980).

The FAD of *Discoaster quinqueramus*, the zonal boundary marker for the NN10/NN11 zonal boundary, occurs in Sample 105-646B-75X-4, 55–57 cm. The occurrence of *D. berggrenii* down to Sample 105-646B-80X-2, 24 cm, indicates a zonal assignment of CN9a for this interval (Okada and Bukry, 1980) from Sample 105-646B-62X-1, 76–79 cm, to Sample 105-646B-80X-2, 24 cm. Bukry (1978) and Berggren et al. (1986) correlate the base of Subzone CN9a with the base of Zone NN11. Berggren et al. (1986) report a calibrated age of the FAD of *D. quinqueramus*, but no such age for the FAD of *D. berggrenii*. Bergen (1982), however, reports that *D. berggrenii* has an FAD stratigraphically lower than *D. quinqueramus*. The presence of *D. berggrenii* stratigraphically below the lowest occurrence of *D. quinqueramus* in Hole 646B supports the conclusion of Bergen (1982).

Paleoenvironment

The Pleistocene to Holocene interval (including all of Hole 646A and the interval above Section 105-646B-22X, CC, in Hole 646B) is characterized by large fluctuations in nannofossil abundance. The predominance of *Coccolithus pelagicus*, *Gephyrocapsa* spp., and the paucity of warm-water genera such as *Rhabdosphaera* and *Discosphaera* suggest cool-temperate to subarctic conditions in the intervals containing nannofossils.

Discoasters are most abundant in tropical to subtropical regions and rare to absent in arctic regions. In Hole 646B they are present but never abundant in the Pliocene to Miocene interval (below Section 105-646B-22X, CC), suggesting somewhat warmer conditions than in the Pleistocene to Holocene, though not as warm as in tropical or subtropical regions. Because discoasters are more resistant to dissolution than are placoliths, their spo-

radic occurrence in Hole 646B is more likely a result of ecologic exclusion than of dissolution.

Pontosphaera spp., *Scyphosphaera* spp., *Braarudosphaera* spp., and *Discolithina* spp., which are most abundant in near-shore, shelf environments, are rare throughout both Holes 646A and 646B, suggesting that this site has undergone more open-ocean conditions since the Miocene.

Preservation

Preservation of nannofossils is generally good throughout both Holes 646A and 646B (Fig. 26). Changes in preservation appear to be independent of abundance changes, except in intervals of very high abundance (nannofossil oozes), where increased dissolution of placoliths and overgrowths on discoasters and ceratoliths are seen. Intervals barren or nearly barren of all nannofossils occur sporadically throughout the Pliocene and Miocene. Dissolution may have contributed to the poorer preservation of planktonic foraminifers in these same samples.

Diatoms

Biostratigraphy

Holes 646A and 646B

Because of the similarities between the diatom assemblages in Hole 646A and the upper 100 m of Hole 646B, the diatom biostratigraphic results for each hole are combined and discussed together.

Sections 105-646A-1H, CC, 105-646A-2H, CC, and 105-646B-1H, CC through 105-646B-3H, CC, contain common to abundant and moderate to well-preserved diatoms (Figs. 25 and 26). Age-diagnostic species are rare. The occurrence of *Rhizosolenia curvirostris* in samples directly below this interval suggests that Cores 105-646A-1H, 105-646A-2H, and 105-646B-1H through 105-646B-3H are stratigraphically above the last occurrence of *Rhizosolenia curvirostris* (Fig. 27). Therefore, this interval is equivalent to the *Denticulopsis seminae* Zone of Barron (1980);

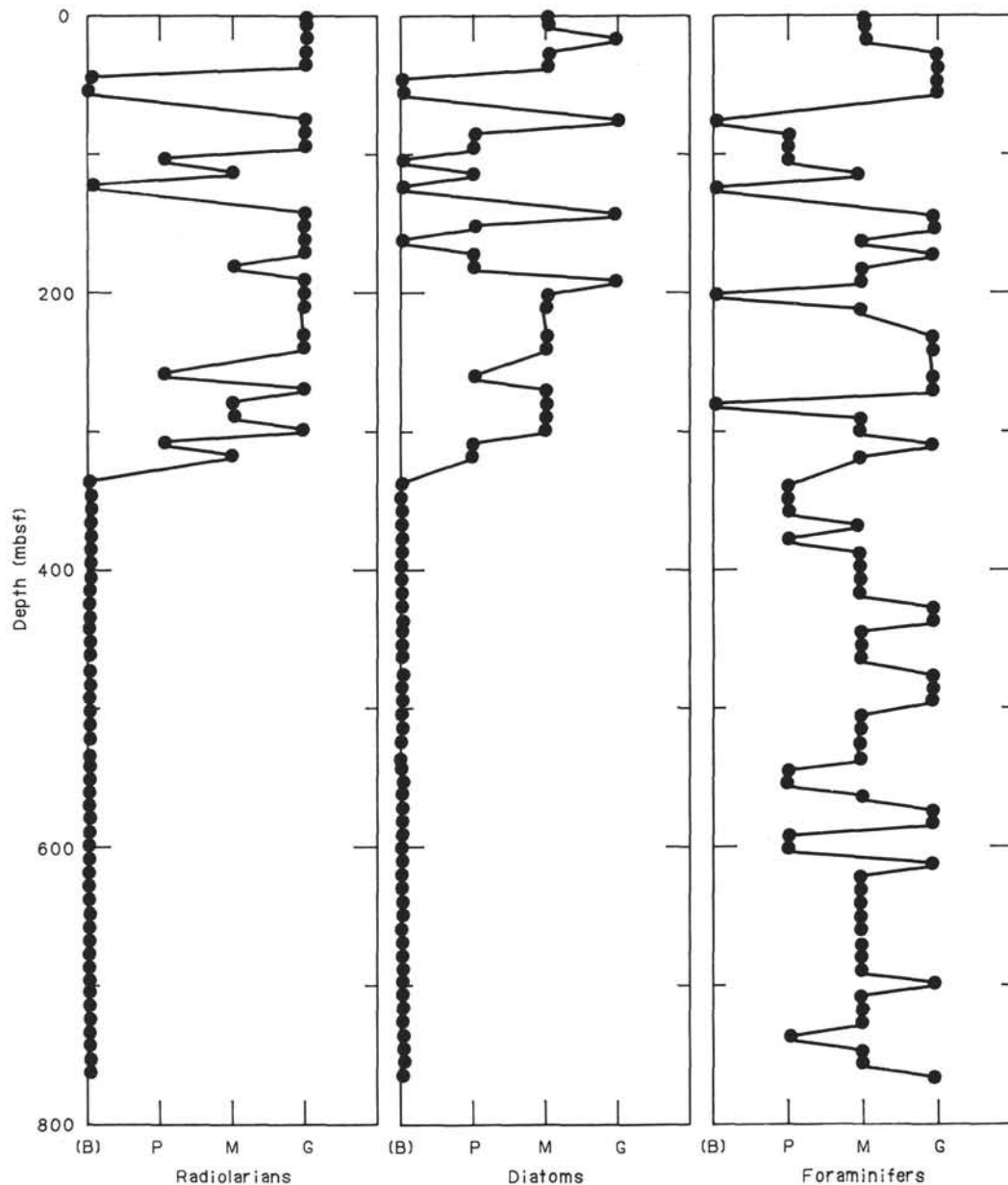


Figure 26. Downhole preservation plots of microfossils. B = barren, P = poor, M = moderate, G = good.

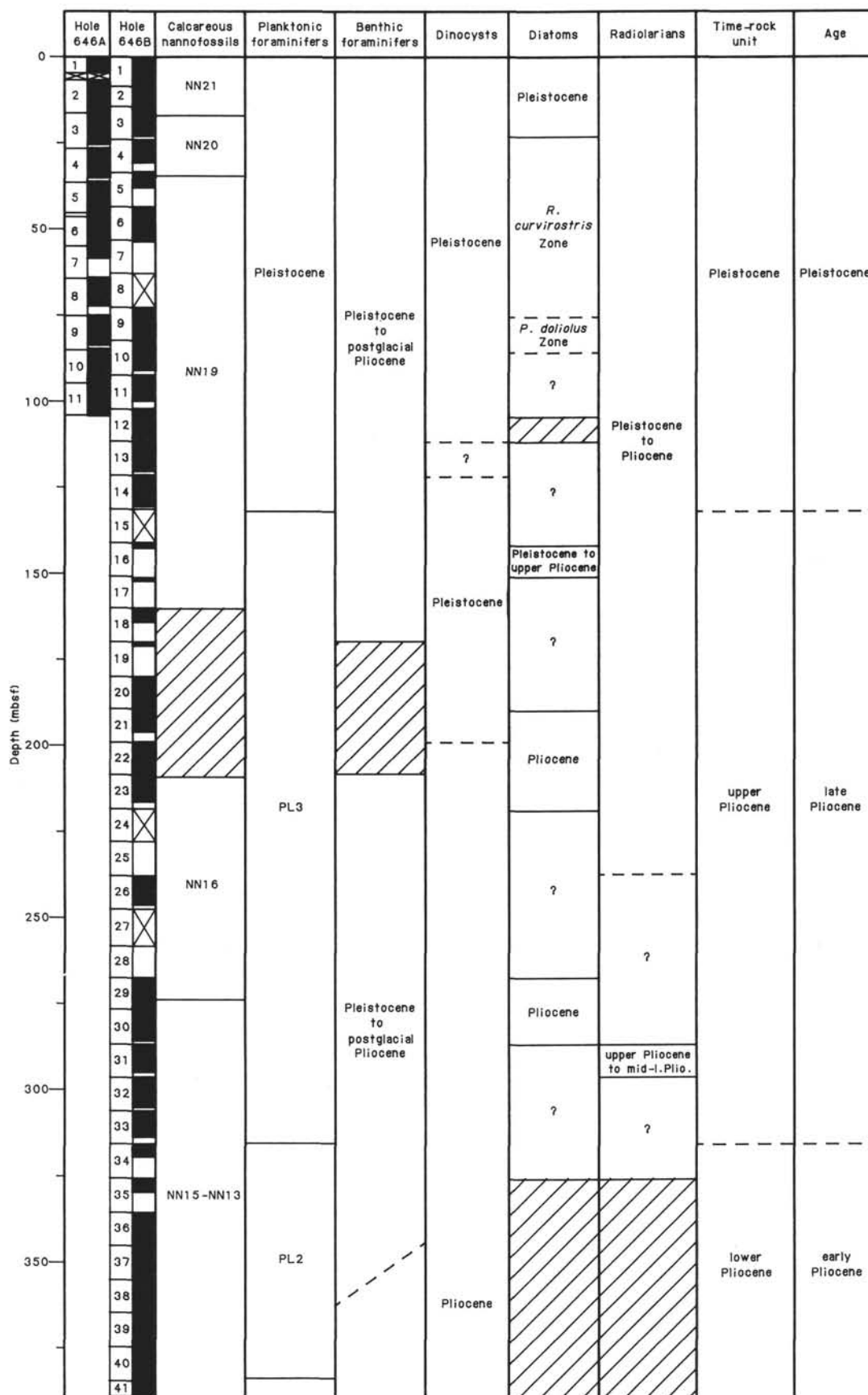


Figure 27. Biostratigraphic summary, Site 646.

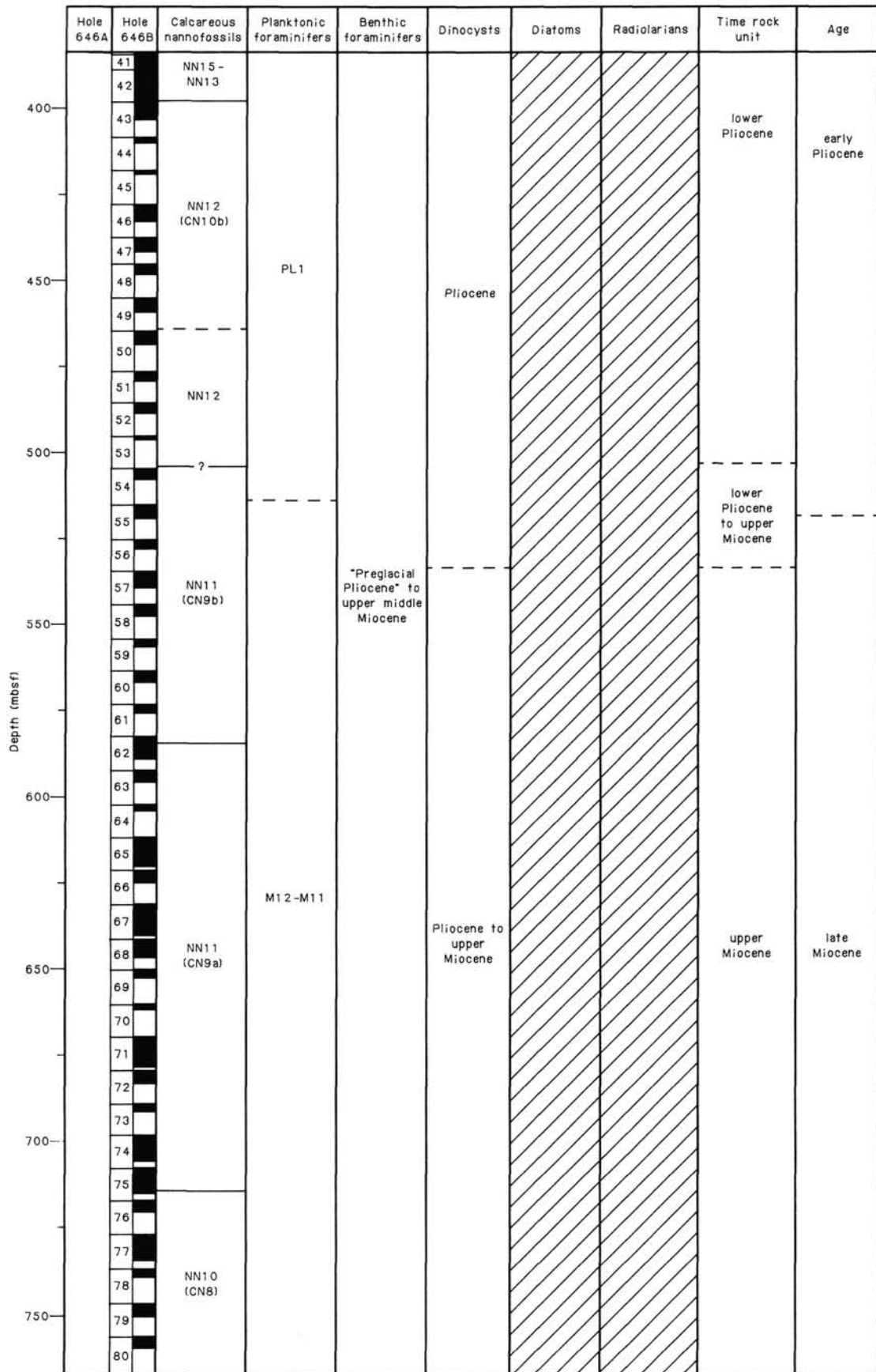


Figure 27 (continued).

however, the zonal species was not observed. This interval can also be assigned to the upper part of the *Nitzschia reinholdii* Zone as used by Baldauf (in press).

The diatom assemblage in this interval is characterized by specimens of *Actinocyclus divisus*, *Nitzschia grunowii*, *Porosira glacialis*, *Rhizosolenia hebetata*, *R. styliformis*, *Thalassiothrix longissima*, *Thalassiosira decipiens*, *T. eccentrica*, *T. gravida*, *T. hyalina*, *T. leptopus*, and *T. trifulta*. In addition, rare specimens of the fresh- to brackish-water species *Melosira islandica* were also observed in Section 105-646A-2H, CC.

Sections 105-646A-3H, CC, through 105-646A-5H, CC, 105-646B-4H, CC, and 105-646B-5H, CC, are assigned to the *Rhizosolenia curvirostris* Zone of Barron (1980), on the basis of the occurrence of *R. curvirostris* throughout this interval. The last occurrence of this species occurs in the North Pacific at about 0.26 Ma (Barron, 1980). The diatom assemblage observed in these samples is similar to that described previously but also includes specimens of *R. barboi* and *Stephanopyxis turris*.

Rare fragments of *Thalassiothrix longissima* are observed in Section 105-646A-6H, CC, and rare fragments of *Actinocyclus divisus*, *Coscinodiscus marginatus*, and *Stephanopyxis turris* occur in Section 105-646B-7H, CC. Sections 105-646A-7H, CC, 105-646A-8H, CC, and 105-646B-6H, CC, are barren of diatoms.

The occurrence of *Pseudoenotia doliolus* and *N. reinholdii* in Section 105-646A-9H, CC, also allows placement of this section into the *Pseudoenotia doliolus* Zone as used by Baldauf (in press). *Nitzschia reinholdii* has a last occurrence in the North Atlantic at about 0.44 Ma, and *P. doliolus* has a first occurrence at about 1.8 Ma (Baldauf, in press).

Rare specimens of *Denticulopsis seminae* are observed in Sections 105-646A-9H, CC, 105-646B-9H, CC, and 105-646B-16X, CC. *D. seminae* is common throughout the Pliocene and Pleistocene of the North Pacific but occurs in the North Atlantic only during about a 400-k.y. interval, which approximates the Jaramillo Subchron (Baldauf, in press). cursory results at Site 646 indicate that this species may have a slightly longer duration at this site than elsewhere in the North Atlantic.

The interval including Sections 105-646A-10H, CC, 105-646A-11H, CC, and 105-646B-10H, CC, through 105-646B-14H, CC, either is barren of diatoms or contains rare fragments of non-age-diagnostic species. Species observed include *Coscinodiscus stellaris*, *Melosira sulcata*, and *Thalassiothrix longissima*.

Section 105-646B-16X, CC, contains few, well-preserved diatoms. The occurrence of *Denticulopsis seminae* suggests a late Pliocene or younger age for this sample. The first occurrence of *D. seminae* in the North Pacific approximates the upper part of the *Denticulopsis seminae* var. *fossilis* Zone of Barron (1980). Additional species observed include *Actinocyclus divisus*, *Coscinodiscus marginatus*, *Melosira sulcata*, *Porosira glacialis*, *Thalassiothrix longissima*, *Thalassiosira eccentrica*, *T. gravida*, and *T. oestrupii*.

Except in Section 105-646B-18X, CC, which is barren of diatoms, only rare, poorly preserved diatoms are observed in Sections 105-646B-17X through 105-646B-20X, CC. Age-diagnostic species were not observed.

Sections 105-646B-21X, CC, through 105-646B-23X, CC, contain few to common diatoms that exhibit moderate to good preservation. The assemblage is dominated by *Stephanopyxis turris*, *Thalassionema nitzschioides*, and *Coscinodiscus marginatus*. The occurrence of *Thalassiosira oestrupii* in these samples suggests that they are Pliocene or younger in age. However, rare specimens of *Thalassiosira antiqua* were observed in Section 105-646B-21X, CC, and together with *T. oestrupii* suggest a Pliocene age for this sample. Other observed species include *Actinocyclus divisus*, *Bacteriastrum hyalinum*, *Coscinodiscus oculus-irridis*, *Melosira sulcata*, *Rhizosolenia styliformis*, *Thalassiosira leptopus*,

T. nordenskioldii, and *T. trifulta*. Sections 105-646B-22X, CC, and 105-646B-23X, CC, contain rare reworked specimens of *Stephanogonia hanzawae* (Miocene).

Rare specimens of *Actinocyclus divisus*, *Rhizosolenia styliformis*, *Stephanopyxis turris*, *Thalassionema nitzschioides*, and *Thalassiosira leptopus* were observed in Section 105-646B-25X, CC. These species have no significant biostratigraphic value.

Sections 105-646B-29X, CC, and 105-646B-30X, CC, contain few, moderately well-preserved diatoms including *Melosira sulcata*, *Rhizosolenia barboi*, *Stephanopyxis turris*, *Thalassionema nitzschioides*, *Thalassiosira leptopus*, *T. oestrupii*, and *Thalassiothrix longissima*. The occurrence of *Thalassiosira oestrupii* in both samples suggests a Pliocene or younger age. Rare specimens of *Actinocyclus ingens* occur in Section 105-646B-29X, CC. Although this species has a sporadic occurrence, ranging stratigraphically into the late Miocene to early Pliocene in the North Pacific, these specimens are most likely reworked. The occurrence of *Stephanogonia hanzawae* also in this sample most likely results from reworking. Rare specimens of the fresh- to brackish-water species *Melosira granulata* occur in Section 105-646B-30X, CC.

The diatom assemblage in both Sections 105-646B-31X, CC, and 105-646B-32X, CC, is similar to that described previously except that *Thalassiosira oestrupii* was not observed. In addition to the previously mentioned species, specimens of *Coscinodiscus marginatus*, *Hemidiscus cuneiformis*, *Melosira clavigeria*, and *Thalassiosira nordenskioldii* were also observed.

Sections 105-646B-32X, CC, through 105-646B-34X, CC, contain rare, poorly preserved (mostly fragmented) diatoms. Fragments of *Actinocyclus divisus*, *Melosira sulcata*, *Stephanopyxis turris*, and *Thalassionema nitzschioides* were observed. Diatoms were not observed in the core-catcher samples examined from Cores 105-646B-36X through 105-646B-80X.

Paleoecology

The diatom assemblage observed in sediments from Site 646 can be divided into three coeval components.

1. Cosmopolitan species such as *Actinocyclus divisus*, *Coscinodiscus marginatus*, *Hemidiscus cuneiformis*, *Melosira sulcata*, *Nitzschia marina*, *N. reinholdii*, *Pseudoenotia doliolus*, *Rhizosolenia hebetata*, *Rhizosolenia styliformis*, *Thalassionema nitzschioides*, *Thalassiosira eccentrica*, *Thalassiosira oestrupii*, and *Thalassiothrix longissima*. These species compose about <90% of the observed assemblage in samples from Site 646.

2. High-latitude species such as *Nitzschia cyclindrus*, *N. grunowii*, *Thalassiosira gravida*, *T. trifulta*, and *T. nordenskioldii*. These species are present in Pliocene through Pleistocene samples from Baffin Bay Site 645 ("Biostratigraphy" section, Site 645 chapter, this volume), the Bering Sea (Baldauf, 1981; Sannetta, 1982), and the North Pacific (Koizumi, 1973). In addition, *T. gravida* and *T. nordenskioldii* also occur in the Norwegian-Greenland Sea (Schrader and Fenner, 1976). These species compose only a minor part (<5%) of the diatom assemblage in samples from Site 646.

3. Middle- to high-latitude species such as *Actinocyclus oculatus*, *Denticulopsis seminae*, *Rhizosolenia barboi*, *R. curvirostris*, *Thalassiosira antiqua*, and *Stephanopyxis horridus*. These species are common in North Pacific sediments; most occur in some sediments from the North Atlantic and Norwegian-Greenland Sea (except *A. oculatus* and *S. horridus*, which have a first-reported occurrence here). These species compose generally <10% of the diatom assemblage at Site 646. *Denticulopsis seminae* is recorded throughout the middle- and high-latitudes of the North Atlantic during the interval approximating the Jaramillo Subchron (Baldauf, in press). The occurrence of this species in the North Atlantic could have resulted either from coevolution

of this species in the Pacific and Atlantic oceans or from open communication and transportation of this species between oceans (see Baldauf, in press, for detailed discussion).

Radiolarians

Strewn slides were prepared from each core catcher and scanned for radiolarians and other biosiliceous components. Radiolarians are commonly abundant and well preserved above about 330 mbsf but absent below this level (Figs. 25 and 26). Within the upper 330 m, radiolarians varied from abundant and well preserved to absent even in samples from adjacent core catchers. Sponge spicules are common in places and in others so abundant as to form the dominant component of the >44- μ m acidified residue. Large centric and pennate diatom frustules are in places common to abundant in the upper 100 m of section but are rare to few below this level.

Biostratigraphy

The Pliocene to Holocene species *Cycladophora davisiana* is abundant in most samples examined above its first occurrence in Section 105-646B-25X, CC (about 235 mbsf). The evolutionary first occurrence of *C. davisiana* is in the early Pliocene of the North Pacific Ocean (Barron et al., 1980; Sakai, 1980) and the Norwegian Sea (Bjørklund, 1976). Other radiolarian stratigraphic indicators are largely absent in Site 646 samples. Age assignments are tentative and are based on rare occurrences (often single specimens) of forms having known stratigraphic utility in other biogeographic provinces. A few specimens of *Sphaeropyle robusta* are seen in Sections 105-646B-22X, CC, and 105-646B-29X, CC. This species ranges from the late Miocene into the latest Pliocene in the North Pacific (Sakai, 1980). A single specimen of *Stylocentron aquilonarium*, which ranges from the early Pliocene to the late Pleistocene in the North Pacific (Sakai, 1980), was seen in Section 105-646B-31X, CC. In the same sample, a single specimen of *Antarctissa whitei* was observed. *A. whitei* is a late Miocene to Pliocene stratigraphic index species in the Norwegian Sea (Bjørklund, 1976). The co-occurrence of these two forms constrains the age of Section 105-646B-31X, CC to middle early Pliocene to latest Pliocene. No other stratigraphic indicators were seen in Site 646 samples.

Paleoenvironment

The composition of the Site 646 radiolarian assemblage is characteristic of high-latitude radiolarian assemblages in other areas of the world oceans, as well as in the North Atlantic. However, certain relatively cosmopolitan forms—such as the Pliocene stratigraphic species *Stichocorys peregrina*—are not seen, suggesting a certain amount of ecological restriction and/or biogeographic distinctiveness.

Cycladophora davisiana

Variations in the abundance of *Cycladophora davisiana* can be used to stratigraphically subdivide the Pleistocene (Morley and Hays, 1979) and can also be used to indicate paleoenvironmental conditions. *C. davisiana* abundances in the modern ocean range from a few percent in most regions to a maximum of 10%–20% in the Bering Sea and Sea of Okhotsk, whereas abundances of *C. davisiana* during the last glacial maximum can be found to reach values of >40%. High abundances of this species thus appear to reflect cold environments and strong seasonal pycnoclines and/or lower-than-average salinities. In core-catcher strewn slide of Sections 105-646B-1H, CC, to 105-646B-4H, CC, the percentage of *C. davisiana* in counts of diagonal tracks varies between 2% (105-646B-4H, CC, N = 202) and 79% (105-646B-3H, CC, N = 290). These values are preliminary and should not be used for stratigraphic or paleoenvironmental interpretation. However, they do suggest that a strati-

graphically and paleoenvironmentally useful "*C. davisiana*" curve from examination of closely spaced samples prepared for quantitative analysis can be obtained by the method of Moore (1973).

Palynology

All core-catcher samples from Holes 646A and 646B were analyzed for their palynomorph content. Pollen, spore, and dinocyst preservation is good in most samples examined. The abundances of dinocysts, pollen, spores, and reworked palynomorphs vary throughout the examined samples.

Dinocysts

A general trend of increasing diversity is observed with depth. Different intervals described as follows are distinguished on the basis of the composition of dinocyst assemblages.

Interval I (0–198 mbsf) has highly variable dinocyst abundances. The assemblages are dominated by *Operculodinium centrocarpum*, *Bitectadodinium tepikiense*, or *Brigantedinium simplex*. *Multispinula minuta*, *Spiniferites* spp. (*S. elongatus*, *S. ramosus*, and *S. mirabilis*), *Nematosphaeropsis labyrinthea*, and *Impagidinium* spp. (*I. aculeatum*, *I. paradoxum*, *I. patulum*, *I. sphaericum*, and *I. pallidum*) have sporadic occurrences throughout this interval.

Interval II (198–540 mbsf) has very abundant dinocysts and relatively high diversity. This interval is characterized by the frequent occurrence of *Filispheera filifera*, *Corrudinium harlandii*, *Nematosphaeropsis oblonga*, cf. *Labyrinthodinium* sp., *Tectadodinium simplex*, *Impagidinium* spp., and *Brigantedinium* spp. *Xandarodinium variabile*, *Operculodinium crassum*, *Operculodinium wallii*, and *Amiculosphaera umbraculata* are present. In addition, some species not described in the literature are common to abundant and are provisionally called *Incertae sedis* sp. I and sp. II, *Dinocyst* sp. I, and *Tectadodinium* sp. I and sp. II.

Interval III (540–738 mbsf) reveals low dinocyst abundance. Cf. *Tectadodinium* spp. are common within this interval. The occurrences of cf. *Labyrinthodinium* sp., *Nematosphaeropsis* spp., and *Impagidinium* spp. are relatively frequent. Specimens of cf. *Eviittosphaerula* sp. are recorded in Sections 105-646B-72X, CC, 105-646B-73X, CC, and 105-646B-76X, CC.

Interval IV (738–767 mbsf) is characterized by the occurrence of *Operculodinium* sp. of Piasecki (1980) and the consistent presence of *Impagidinium maculatum*(?). The species *Tectadodinium* cf. *pellitum* is common.

Biostratigraphy

The dinocyst diversity and concentration are generally high, with few exceptions. Although most of the identified dinocyst species have a long stratigraphic range, a few biostratigraphic interpretations can be made:

1. In the uppermost part of Hole 646B (0–111.1 mbsf), the occurrence of *Multispinula minuta* indicates a Pleistocene age. This arctic species is recorded in the upper Pleistocene sediments of the North Atlantic (Mudie, in press) but occurred also in the lower Pleistocene sediments of the Arctic Ocean (Aksu and Mudie, 1985).
2. *Filispheera filifera* occurs frequently between 120.8 and 620 mbsf, indicating an age of late Miocene to early Pleistocene (Bujak, 1984; Mudie, in press).
3. Below 197.8 mbsf, an important increase in diversity is observed. The occurrence of *Corrudinium harlandii*, *Nematosphaeropsis oblonga*, *Amiculosphaera umbraculata*, and *Tectadodinium simplex* notably indicates a Pliocene or older age (Harland, 1979; Mudie, in press).
4. In the lowest part of Hole 646B (535–766 mbsf), a slight increase of diversity is observed. The assemblage shows similari-

ties with the Miocene assemblages described by Edwards (1985). The presence of common *Brigantedinium* sp. suggests a late Miocene or younger age (Bujak, 1984; Mudie, in press).

Paleoenvironments

High dinoflagellate productivity characterizes the Site 646 area during the Holocene (dinocyst concentrations are about 20,000 cm³ in the surficial sediments from Core HU-75-37; De Vernal, 1986). The mixture of water masses from the NAD and the East Greenland current, in addition to high nutrient input, probably fosters this high phytoplanktonic productivity.

In the upper part of Hole 646B (0–198 mbsf), the dinocyst assemblages show variations in absolute and relative frequencies. Some assemblages are rich and dominated by *Nematosphaeropsis labyrinthea*, *Bitectadodinium tepikiense*, *Operculodinium centrocarpum*, or *Impagidinium* spp.; they suggest the influence of the NAD and the cool-temperate to subarctic conditions. Other assemblages are characterized by the abundance of *Brigantedinium simplex* and reflect low-salinity conditions related to meltwater discharges. Mixed assemblages are also observed, indicating the influence of two components: (1) meltwater and (2) the penetration of the NAD into the Labrador Sea. The variations in dinocyst assemblages suggest changing environmental conditions related to climatic oscillations.

In the 198–540-mbsf interval, very abundant and diverse dinocyst flora is observed, indicating a high primary productivity. The dinocyst assemblages show similarities with the North Atlantic Pliocene assemblages described by Mudie (in press). However, a few species that have yet to be described or reported in the literature are common (dinocyst sp. I, *Incertae sedis* sp. I and II). In this interval (198–540 mbsf), the occurrence of *Operculodinium centrocarpum*, *Filisphaera filifera*, and *Nematosphaeropsis labyrinthea* collectively suggests cool-temperate surficial water masses. In addition, the presence of *Impagidinium aculeatum* and *I. patulum* indicates a slight influence of warm-temperate waters, which is probably related to the penetration of the NAD into the Labrador Sea. In the upper part of the interval (198–246 mbsf), the frequent occurrence of *Brigantedinium simplex* is associated with a low-salinity component and suggests some freshwater input, which could be related to meltwater discharge.

In the 540–680-mbsf interval, the concentrations of dinocysts are relatively low, suggesting a low phytoplanktonic productivity. The occurrences of *Nematosphaeropsis* spp., *Operculodinium* spp., and *Impagidinium* spp. indicate temperate oceanic conditions.

In the lowest part of Hole 646B (680–766 mbsf), an increase in dinocyst concentration and diversity reflects relatively high primary productivity. *Nematosphaeropsis* and *Impagidinium* species indicate temperate oceanic conditions. However, an influence (or input) from neritic low-salinity environments may be seen by the occurrence of *Palaeostomocystis* spp. (Baltes, 1971).

The occurrence of cf. *Evittosphaerula* sp. in Sections 105-646B-72X, CC, to 105-646B-76X, CC, may indicate the influence of Norwegian–Greenland Sea surface waters in the lowest part of Hole 646B. This genus is currently known from only the Beaufort Sea (Bujak and Davies, 1981; Dixon et al., 1984) and the Norwegian–Greenland Sea (Manum, 1976). A similar form was recorded from Spitsbergen (M. Head, pers. comm., 1986).

Pollen and Spores

Pollen and spore abundances vary through Holes 646A and 646B. The more abundant pollen taxa observed are *Pinus* and *Picea*. The high proportions of these bisaccate pollen grains are partly related to a selective effect of long-distance transportation by atmospheric or oceanic circulation. In addition to *Pinus* and *Picea*, *Betula*, *Tsuga*, *Lycopodium*, *Sphagnum*, and *Polypodiaceae* may be relatively well represented.

The vegetation source area is unknown. Nevertheless, detailed studies on piston cores from the Site 646 area (HU-75-37; De Vernal, 1986) have revealed that during late Quaternary, the influx of terrestrial palynomorphs is mainly related to the atmospheric circulation and that the principal source is the southern Labrador coast. However, the atmospheric circulation pattern cannot be assumed to have been uniform during the Neogene. Consequently, the pollen assemblages may be interpreted in terms of paleovegetation as well as in terms of paleoatmospheric circulations. Furthermore, the pollen and spore abundances may be linked, to some extent, to sedimentary processes: the hydrodynamics of palynomorphs seem to be similar to silt-sized detrital particles (Stanley, 1969).

Despite these limitations, a few paleoenvironmental interpretations can be made:

1. In the uppermost 210-m deposits of Site 646, the pollen and spore percentages and concentrations are variable. They suggest the presence of a coniferous boreal forest to open-tundra forest in the source area. The assemblages reflect, therefore, a similar or poorer vegetation than the ones interpreted (coniferous boreal forest) from Holocene sediments (De Vernal, 1986). The variations in pollen assemblages may be related to changes in the density and composition of the vegetation in the same source area or to changes in atmospheric circulation; both possibilities indicate climatic fluctuations.

2. In the approximate 210–410-mbsf interval, the frequent occurrences of *Tsuga* and other thermophilic taxa (*Betula*, *Carpinus/Ostrya*, and *Sciadopitys*) suggest a cool-temperate climate in the source area. The advection of southern air masses in the Labrador Sea may also have occurred.

3. In the lower part of Hole 646B (410–766 mbsf), pollen and spores are rare. The advection of sterile air masses because of long-distance trajectories over areas free of vegetation (the Atlantic Ocean, for example) could have been involved. However, because the silt-size particles are few in this interval (see “Sedimentology” section, this chapter), the low pollen abundance may have been a response to sedimentary processes.

SUMMARY

Biostratigraphy

The biostratigraphic summary chart is presented in Figure 27. The data include a few discrepancies in the placement of the major age boundaries, as discussed in the following text.

The Pliocene/Pleistocene boundary is placed at approximately 131 mbsf by the last occurrence of *Neoglobobulimina atlantica* (planktonic foraminifer), found in Section 105-646B-16X, CC. The Pliocene/Pleistocene boundary is placed at the base of 105-646B-14X, CC, because no core-catcher sample was available from Section 105-646B-15X, CC. Therefore, the boundary suggested by the presence of planktonic foraminifers may actually be in Core 105-646B-15X. Extrapolation using the sedimentation-rate curve (“Sediment-Accumulation Rates” section, this chapter) places the Pliocene/Pleistocene boundary at 128 mbsf.

The early/late Pliocene boundary is placed at about 314 mbsf, on the basis of foraminifer and dinocyst stratigraphies. The last occurrence of *R. pseudoumbilica* (nannofossil) is found in Section 105-646B-26X, CC; however, the base of Zone NN16 is placed about 272.5 mbsf at the top of the consistent occurrence of the taxon (Sample 105-646B-29X-5, 79–81 cm). The last occurrences of the planktonic foraminifer *Globorotalia margaritae* suggests that the early/late Pliocene boundary is at about 313.8 mbsf. Extrapolation using the sedimentation-rate curve places this boundary at 293 mbsf.

The biostratigraphic data cannot precisely identify the Miocene/Pliocene boundary. The nannofossil *Ceratolithus acutus*

occurs only in the Pliocene, marking the base of Zone CN10b. The last occurrence of this taxon is found in Section 105-646B-49X, CC, suggesting that the section above 105-646B-49X, CC, lies in the Pliocene. The last occurrence of *Discoaster quinqueramus* is found in Section 105-646B-53X, CC, indicating an upper Miocene age for the sediments below. The planktonic foraminifer *Neogloboquadrina continuosa* is found only in Sections 105-646B-55X, CC, and 105-646B-56X, CC, suggesting a lower to upper Miocene age for the section. Dinocyst and benthic foraminifer data indicate upper Miocene to lower Pliocene and upper to middle Miocene to "preglacial Pliocene" ages for the interval, respectively. The Miocene/Pliocene boundary is tentatively placed at 520 mbsf, pending further investigation.

Environmental Interpretation

Now that we have dealt with detailed environmental interpretations of individual microfossil groups, we will present general faunal and floral trends. On the basis of downcore microfossil abundances, the sedimentary section cored at Site 646 can be divided into two major intervals (Fig. 25).

Interval A (323.4–766.7 mbsf) is characterized by the absence of all siliceous microfossils (Fig. 25), by the high abundances of nannofossils and planktonic foraminifers, by calcareous and agglutinated benthic foraminifers, and by the variable but generally high abundance of dinoflagellates. The upper boundary of this interval lies approximately 10 m below the tentative Miocene/Pliocene boundary, whereas the base is probably younger than 10 Ma. Except for two short low-abundance intervals, the consistently high abundance of planktonic foraminifers and nannofossils suggests high productivity in the surface waters. This interpretation is supported, at least in the upper part of the interval, by high abundances of dinoflagellates. Both planktonic foraminifers and nannofossils are dominated by cool-temperate to subarctic assemblages, suggesting that surface-water temperatures were comparable to the present-day southern Labrador Sea. Two well-defined intervals containing abundant and diverse agglutinated benthic foraminifers suggest higher productivity.

The first biogenic silica occurs in Section 105-646B-40X, CC, in the form of rare sponge spicules, and becomes increasingly more common and well-preserved (radiolarians and diatoms) in Section 105-646B-39X, CC, and above (Fig. 26). Pore-water silica-concentration data and magnesium/silica ratios (J. Zachos, pers. comm., 1986) suggest that this abrupt increase in the preservation of biogenic silica most likely reflects an increase in surface-water productivity of siliceous microfossils and is not a result of increased dissolution of biogenic silica in the lower part of the hole.

The timing of the increase in the preservation of biogenic silica at Hole 646B approximates 3.5 Ma. Within the Rockall Plateau region, the increase in the preservation of biogenic silica occurs earlier, at about 6.5 Ma (Baldauf, 1984; in press) and suggests that different factors influence silica productivity and preservation between these two regions.

Interval B (0–323.4 mbsf) is characterized by large abundance and diversity fluctuations in all microfossil groups examined. Planktonic foraminifers, nannofossils, dinoflagellates, radiolarians, and diatoms suggest the presence of subarctic water masses during high abundance of microfossils. Rapid changes observed in faunal and floral assemblages suggest that the environment underwent extreme climatic and oceanographic conditions. The temporal resolution obtained by the sampling density is not sufficient to document the nature of these variations.

SEDIMENT-ACCUMULATION RATES

Biostratigraphic and magnetostratigraphic results from Site 646 provide constraints on the rates at which the sediments cored

at this site accumulated. These constraints are plotted in Figure 28, illustrating the age–depth relationships observed at this site.

Biostratigraphic Data

The biostratigraphic information discussed in the "Biostratigraphy" section (this chapter) is summarized in Table 7. Low abundances of biostratigraphically useful species together with, most typically, a relatively coarse sample spacing (only core-catcher samples) cause biostratigraphic datums to have relatively large depth uncertainties, generally ± 10 to several tens of meters. Age uncertainties are also common, particularly for occurrence data based on single samples. The age and depth of all biostratigraphic data are indicated in Table 7 in meters below seafloor (mbsf).

Magnetostratigraphic Data

The magnetostratigraphic results are discussed in the "Paleomagnetism" section (this chapter) and are summarized in Table 7. The polarity reversals observed in the sediments cored at Site 646 are interpreted as being records of geomagnetic-field reversals; therefore the reversal record from this site may be correlated with the geomagnetic-polarity time scale (Berggren et al., 1986). Unfortunately the poor core recovery at this site complicates the correlation of this record with the time scale because large intervals are unsampled. Therefore, correlation of the observed reversal pattern is strongly dependent upon the shipboard biostratigraphic results ("Biostratigraphy" section, this chapter). Within the biostratigraphic framework, however, relatively good agreement is observed between the ages and depths of the reversals that occur in intervals of nearly continuous recovery.

Sediment-Accumulation-Rate Curve

Relatively good agreement exists among the various groups of microfossil biostratigraphic data as well as between the biostratigraphic and magnetostratigraphic data. The sediment-accumulation-rate curve (Fig. 28) is drawn joining the magnetic-reversal boundaries. Three main segments characterize the curve:

1. Between 0 and about 191.5 mbsf, the numerous magnetostratigraphic data allow the calculation of a mean sedimentation rate of 79 m/m.y.
2. Because of uncertainty in the placement of magnetostratigraphic events, two interpretations of the sediment-accumulation rate are given for the interval from 191.5 to 577.0 mbsf. (1) Several small-scale changes in the sediment-accumulation rate are suggested for the interval if only the magnetostratigraphic events are used. This method also suggests that the biostratigraphic events in this interval have a younger age than elsewhere in the Atlantic Ocean. (2) Using the reliable magnetostratigraphic events (M12, M23) that occur above and below this interval for constraints, an average sediment-accumulation rate of 96 m/m.y. is suggested for this interval.
3. In the lower part of Hole 646B (about 577 mbsf), the magnetostratigraphic data allow the calculation of a mean sediment-accumulation rate of about 49 m/m.y. However, these data indicate some short-term fluctuations in the accumulation rates. The mean sedimentation rates of the 640–740-mbsf interval suggest by extrapolation that the lowest sediments (766.7 mbsf) recovered at Site 646 are approximately 10 Ma (or younger).

INORGANIC GEOCHEMISTRY

Interstitial-water samples were collected from 4.4 to 750 mbsf at Site 646. The sampling interval of 10–20 m in the upper 100 m was increased to roughly 30–60-m intervals thereafter. Results of the shipboard chemical analyses of these interstitial-water samples are reported in Table 8 and Figures 29 to 33. Analytical

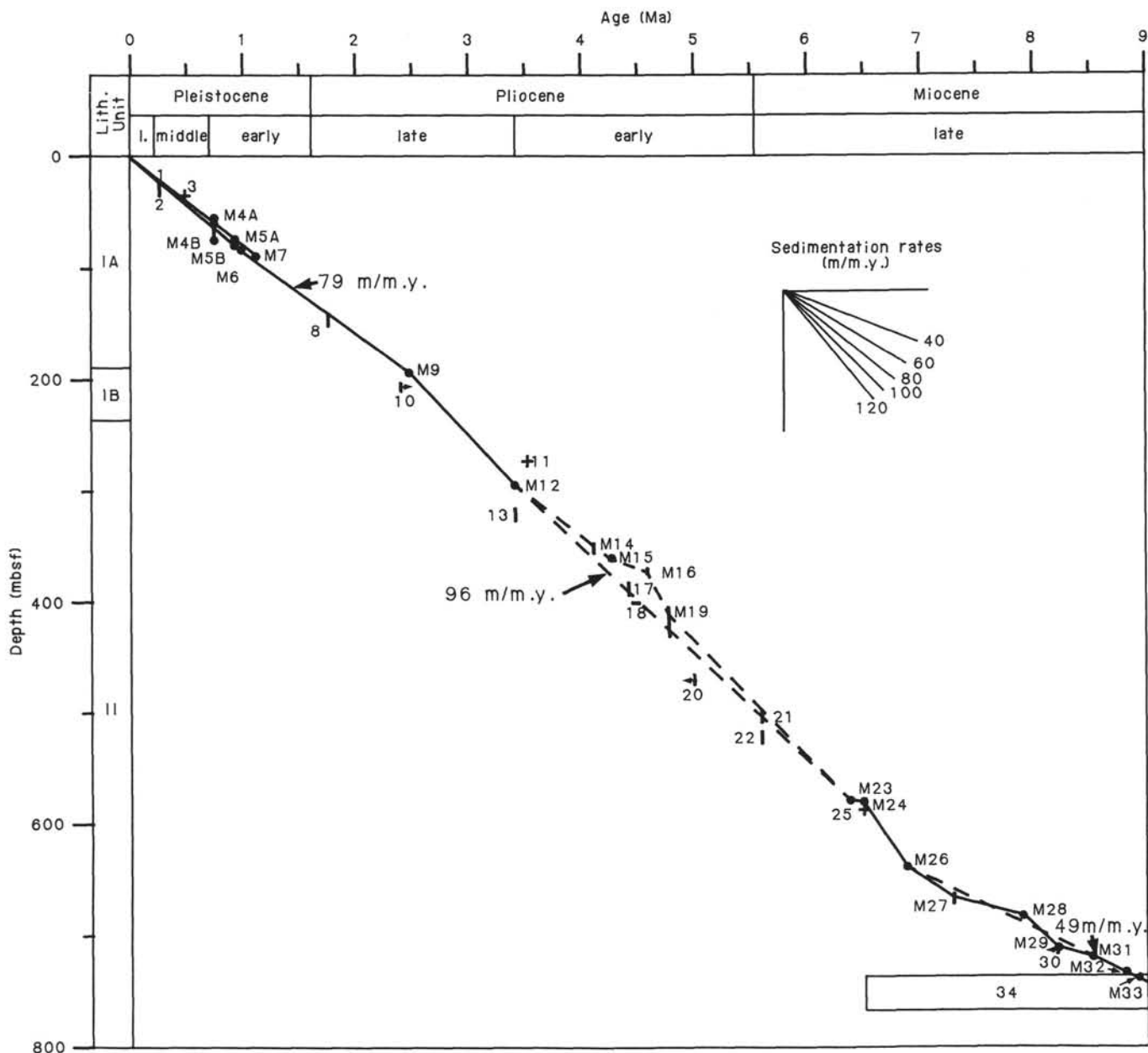


Figure 28. Age versus depth relationships of biostratigraphic and magnetostratigraphic results, Site 646.

methods are summarized in the "Explanatory Notes" chapter (this volume).

Initially, downhole salinity contents at Site 646 become depleted (by 2–3 ‰; Fig. 29) relative to average seawater values (34.9 ‰), and most of the change occurs over the upper 162 m of the sediment column. The most probable origin of this change is the corresponding decrease in sulfate concentrations (Fig. 32). Further downcore salinity values recover slightly, increasing to as much as 34.0 ‰ at 645.7 mbsf. Chlorinity concentrations, which fluctuate by 0.5–1.0 ‰ in upper sections and then show little variation with depth thereafter, display an overall increase of about 0.8 ‰ below 100 mbsf (Fig. 30). These results are similar in trend to those obtained for Site 113 on the mid-Labrador Sea ridge (Manheim et al., 1972), where analyses of limited samples show a decrease in salinity content from 34.7 to 33.9 ‰ and an increase in chlorinity concentrations from 19.1 to 19.6 ‰ from the sediment-water interface to 206 mbsf.

Excluding initial decreases in ion concentration within the upper 30 mbsf, calcium- and magnesium-ion gradients appear to exhibit distinct and inversely correlated downhole trends (Fig. 31). Calcium content increases by 50 mmol from 39.8 to 520 mbsf, whereas magnesium content decreases by 35 mmol over the same interval. Generally, conservative calcium and magnesium concentration depth profiles suggest mass transport of these elements upward through the sediments from layer 2 basalts (Gieskes, 1983). However, the slight nonlinearity of calcium and magnesium gradients at this location indicates that reactions within the sediments have superimposed a secondary chemical signature on the primary chemical profiles. In addition, the change in slope of both calcium- and magnesium-ion gradients coincides with a major change in sediment lithology ("Organic Geochemistry" section, this chapter). Dissolution and recrystallization of carbonate minerals as well as concomitant uptake of magnesium ions into clays may have slightly increased

Table 7. Sub-bottom depths of biostratigraphic and magnetostratigraphic age picks.

No.	Name of datum	Biostratigraphic data	
		Age (Ma)	Depth (mbsf)
1.	FAD <i>Emiliania huxleyi</i>	0.247	17.8–19.3
2.	LAD <i>Rhizosolenia curvirostris</i>	0.26	24.1–33.8
3.	LAD <i>Pseudoemiliania lacunosa</i>	0.475	33.8–37.5
8.	LAD <i>Neogloboquadrina atlantica</i>	1.75	140.1–149.8
10.	LAD <i>Discoaster surculus</i>	>2.4	207.5–208.2
11.	LCO <i>Reticulofenestra pseudoumbilica</i>	3.5	271.0–272.5
13.	LAD <i>Globorotalia margaritae</i>	3.4	313.8–323.4
17.	FAD <i>G. punctulata</i>	4.4	381.3–391.0
18.	FAD <i>Ceratolithus cristatus</i>	<4.5	490.0–401.0
20.	FAD <i>Ceratolithus</i> spp.	<5.0	468.5–478.1
21.	LAD <i>D. quinqueramus</i>	5.6	497.1–506.9
22.	FAD <i>G. margaritae</i>	5.6	516.5–526.2
25.	FAD <i>Amaurolithus primus</i>	6.5	584.2–585.7
30.	FAD <i>Discoaster quinqueramus</i>	<8.2	714.0–715.5
34.	Coiling change <i>N. atlantica</i> (D to S)	6.5–9.0	737.7–766.7
M4A	Brunhes/Matuyama (646A)	0.73	58.70–59.04
M5A	Jaramillo (646A)		
	Top	0.91	72.14–72.34
M7	Cobb Mountain		
	Top	1.12	86.25–86.67
	Bottom		88.85–89.10
M4B	Brunhes/Matuyama (646B)	0.73	52.10–73.86
	Jaramillo		
M5B	Top (646B)	0.91	76.5–78.10
M6	Bottom (646B)	0.98	81.10–83.80
M9	Matuyama/Gauss	2.47	190.40–192.60
M12	Gauss/Gilbert	3.4	292.85–292.95
	Nunivak		
M14	Top	4.10	347.05–352.85
M15	Bottom	4.24	359.45–359.55
	C1		
M16	Top	4.57	367.84–382.85
M19	Bottom	4.77	404.45–429.85
	Chron C6		
M23	Top N1	6.37	577.35–577.44
M24	Bottom N1	6.50	578.44–578.55
	Chron C7		
M26	Top N1	6.85	637.61–637.63
M27	Bottom N3	7.28	661.98–670.25
	Chron C9		
M28	Top N1	7.90	680.14–680.24
M29	Bottom N1	8.21	710.51–710.53
M31	Top N2	8.41	718.53–718.56
	Chron C10		
M32	Bottom N1	8.80	733.06–733.08
	Chron C11		
M33	Top N1	8.92	733.88–740.337

interstitial-water calcium/magnesium ratios. Both processes are plausible because of the highly terrigenous nature of the sequence. Glauconite was noted in some intervals as possible authigenic phases associated with burrows (“Sedimentology” section, this chapter). Eventually, data from oxygen-isotope analyses should provide the necessary information for deciphering the relative influences of pore-water migration from layer 2 basalts and subsequent alteration during sediment diagenesis upon the present interstitial-water chemistry (the oxygen-isotopic composition of pore waters is generally depleted as they migrate through and react with oceanic basalts [Lawrence et al., 1975]).

Variations in sulfate content downhole (Fig. 32) appear to be controlled by bacterial sulfate-reduction processes. Sulfate values decrease from 23 mmol near the sediment-water interface to 1.75 mmol at 162 mbsf. Below this depth, SO_4 concentrations vary slightly and generally remain below 3.0 mmol. Another indicator of sulfate reduction, pyrite, is common at various intervals throughout the hole (“Sedimentology” section, this chapter). Alkalinity values show little correlation with sulfate gradient, suggesting that other processes may be dominating bicarbonate concentration. The downhole decrease in alkalinity values (Fig. 33) suggests uptake of excess bicarbonate along with calcium

and magnesium into authigenic calcite. The relative decrease in alkalinity is small so that the depletion in calcium ion brought about by this process would be negligible relative to the overall magnitude of the aforementioned calcium concentration changes.

During drilling, the presence of drilling slurry between biscuits generated some concern about the possible contamination of interstitial waters by drilling fluids. However, close examination and comparison of the various chemical gradients revealed no evidence of such contamination (i.e., trends toward surface seawaterlike values). In addition, the amount of interstitial water recovered by squeezing declined steadily with depth. If contamination did occur, the effects on interstitial-water chemistry must have been minimal.

ORGANIC GEOCHEMISTRY

Three organic geochemistry sampling and measurement procedures were followed at Site 646: (1) 28 vacutainer samples were analyzed for hydrocarbon gases, (2) 65 sediment samples were used to determine organic and inorganic carbon content (1 sample per core, except in intervals of no recovery, 2 samples per core next to the missing part), and (3) 323 carbonate-bomb measurements were carried out to obtain a high-resolution carbonate record for the late Pleistocene time interval.

Hydrocarbon Gases

We observed neither gas pockets nor evidence of expansion of the sediment within the core liners caused by pressure release. Therefore, gas for vacutainer samples was collected either through the end cap, after allowing several minutes for equilibrium time, or in areas where the core was broken up.

The individual samples and the results are listed in Table 9, and a plot of methane concentration versus depth is shown in Figure 34. Methane was not detected above 180 mbsf. Below 180 mbsf, methane was detected in very scattered occurrences, but a maximum seems to occur between 300 and 400 mbsf. The absolute concentrations are low, <4%, and are probably related to dilution by air because of the aforementioned sampling technique, which can also explain the observed fluctuation in values. Low methane concentration is also expected because of a general low organic carbon content, which averages 0.35%, suggesting little biogenic activity.

Ethane was detected in only two samples (at 82 and 201 mbsf) in very small amounts (23 and 15 ppm); however, this level is near the detection limit.

The first occurrence of methane fits well with the bottom of the sulfate-reducing zone indicated by a decrease in dissolved sulfate in pore water from 0 to 160–180 mbsf (see “Inorganic Geochemistry” section, this chapter). In the sulfate-reducing zone, no bacterial methane production occurs; bacterial production starts in the carbonate-reducing zone below this interval (Claypool and Kaplan, 1974).

Although the minor gas show at this site is purely biogenic in origin and no sign of migrated thermogenic gas has been detected, Section 105-646B-79X, CC, had a strong petroliferous odor. Only a localized patch of drilling slurry exhibited minor fluorescence, suggesting contamination from drilling-related materials.

Organic and Inorganic Carbon

The total organic carbon (TOC) and inorganic carbon (calculated as CaCO_3) were measured by combustion of dried sediment samples by the Perkin Elmer 240C elemental analyzer. Weight percentages of TOC and CaCO_3 were calculated by the difference between the weight percentage of carbon in the whole sample and an acidified fraction of the same sample (see “Explanatory Notes” chapter, this volume).

Organic matter content averages 0.35%, and only minor changes occur downhole (Fig. 35 and Table 10). This result agrees

Table 8. Summary of shipboard interstitial-water chemistry, Site 646. Analyses include pH, alkalinity, salinity, chlorinity, calcium, magnesium, and sulfate-ion concentrations.

Sample interval (cm)	Depth (mbsf)	pH	Alkalinity (meq/dm ³)	Salinity (‰)	Chlorinity (‰)	Ca ⁺⁺ (mmol)	Mg ⁺⁺ (mmol)	Sulfate ⁼ (mmol)
105-646A-1H-3, 140-150	4.40	8.01	5.842	34.8	20.06	9.79	49.78	22.49
105-646A-4H-5, 140-150	33.60	8.38	5.584	33.9	19.76	9.19	44.17	15.79
105-646A-7H-4, 140-150	61.00	7.80	3.820	32.7	19.52	9.49	38.82	10.06
105-646A-10H-4, 140-150	90.00	8.23	5.064	32.7	19.38	11.17	35.59	6.37
105-646B-2H-4, 140-150	9.8	7.99	5.718	34.4	19.70	9.81	49.37	20.70
105-646B-5H-2, 140-150	39.80	8.17	5.228	33.9	19.77	8.88	44.71	14.04
105-646B-9H-5, 140-150	79.80	8.14	4.888	33.5	20.32	10.46	38.32	7.76
105-646B-12H-4, 140-150	107.30	8.27	4.824	32.5	19.56	11.47	34.74	5.50
105-646B-18X-2, 140-150	162.00	7.98	3.889	32.0	20.14	12.32	31.87	1.75
105-646B-21X-4, 140-150	194.10	7.78	4.312	32.0	20.03	15.11	30.63	2.46
105-646B-26X-4, 140-150	242.00	7.60	2.974	32.5	20.27	20.66	27.81	0.98
105-646B-30X-4, 140-150	280.90	7.32	2.855	32.2	20.11	28.43	22.20	1.17
105-646B-33X-4, 140-150	310.0	7.73	1.517	32.3	20.18	34.51	17.99	0.49
105-646B-37X-5, 140-150	350.2	7.94	0.806	32.5	20.18	46.29	11.03	1.80
105-646B-40X-5, 140-150	379.10	7.98	0.689	33.0	20.11	49.60	10.21	1.69
105-646B-43X-2, 140-150	403.60	7.95	0.756	33.0	19.94	54.46	9.85	2.01
105-646B-50X-1, 140-150	469.9	7.84	0.477	33.7	19.44	57.88	10.62	6.95
105-646B-55X-1, 140-150	517.9	7.41	0.439	33.7	20.09	60.45	9.53	2.53
105-646B-58X-2, 140-150	548.4	7.85	1.100	34.1	19.88	55.77	13.59	7.12
105-646B-61X-1, 140-150	575.4	8.08	1.147	33.0	19.74	56.60	13.54	7.82
105-646B-65X-3, 140-150	616.9	7.97	1.175	33.5	19.81	61.88	6.08	3.41
105-646B-68X-3, 140-150	645.7	7.84	0.920	34.0	20.27	59.53	9.98	4.81
105-646B-72X-2, 140-150	682.7	7.83	0.513	32.8	19.80	58.24	7.78	—
105-646B-75X-4, 140-150	714.5	8.23	0.965	32.3	19.58	58.72	7.06	—
105-646B-79X-1, 140-150	748.8	8.11	0.787	32.5	19.59	59.70	7.56	—

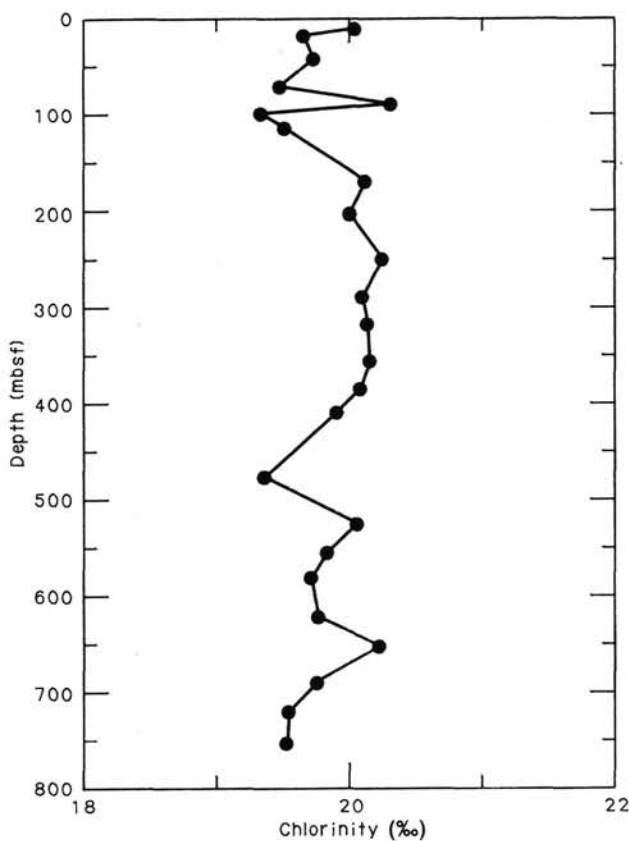
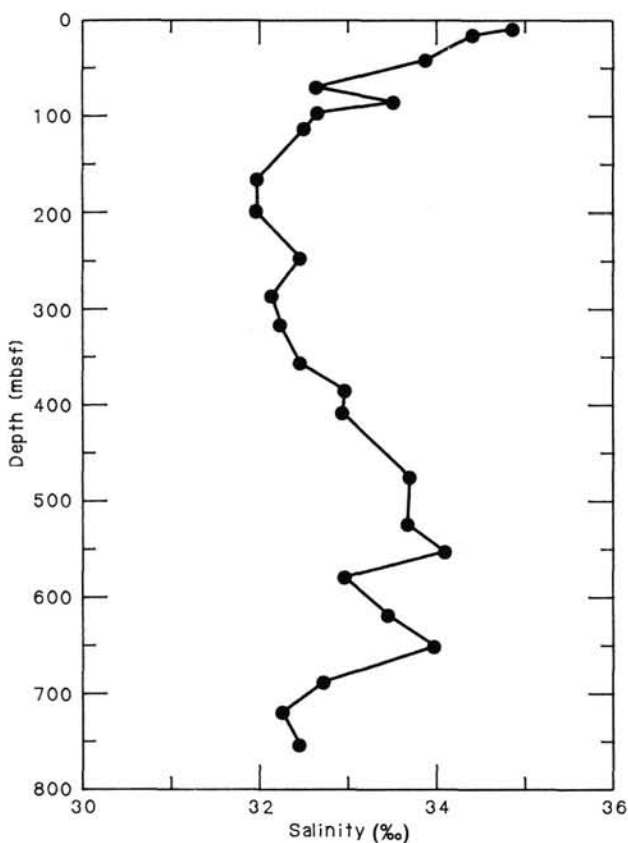


Figure 29. Salinity depth profile, Site 646.

Figure 30. Chlorinity depth profile, Site 646.

with the organic carbon record from Site 113 (Laughton et al., 1972).

Lithologic Unit I is characterized by rapid fluctuations between 0.16% and 0.54% TOC. Unit II has a fairly steady TOC content and an average value of 0.36% (0.18% as a minimum

and 0.53% as a maximum). An inverse relationship exists between organic carbon and carbonate content. Small increases in carbon percentage correlate with decreases in carbonate percentage. This relationship is most pronounced at 300, 480, and 550 mbsf. Rock-Eval data show hydrogen index values < 60 mg HC/g

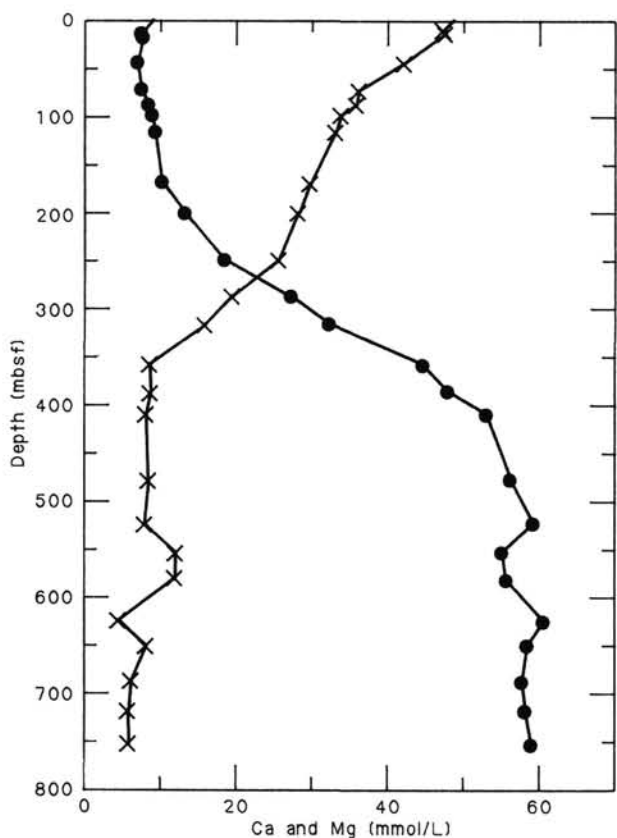


Figure 31. Calcium- and magnesium-ion depth profiles, Site 646. O = calcium, X = magnesium.

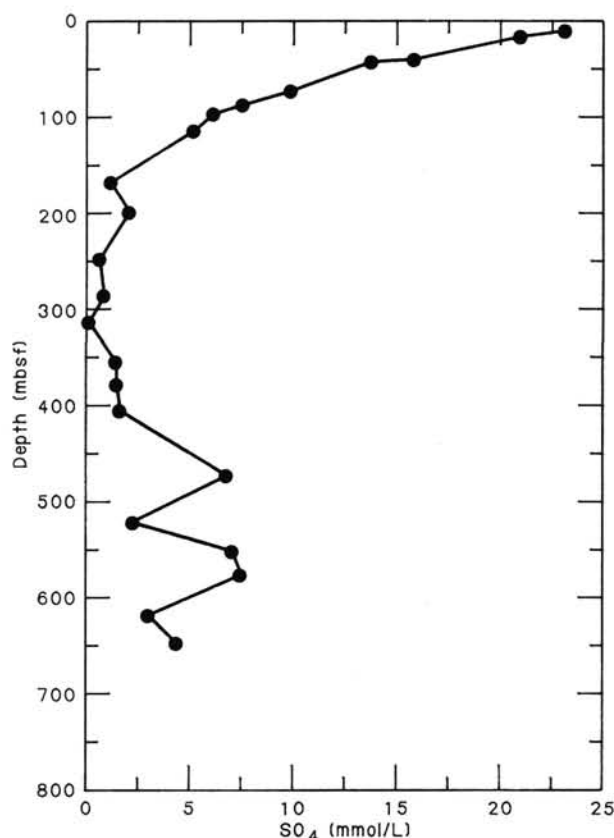


Figure 32. Sulfate depth profile, Site 646.

C_{org} and oxygen index values $>100 \text{ mg CO}_2/\text{g } C_{org}$ (mostly >200), indicating oxidized organic matter (T. Cederberg, pers. comm., 1985).

High-Resolution Late Pleistocene Carbonate Record at Site 646

To obtain a high-resolution record of carbonate fluctuations during late Pleistocene times, inorganic carbon was measured at least every 40 cm in the upper 53 m of Hole 646B. Because of the coring gaps in Cores 105-646B-4H and 105-646B-5H and the lack of recovery in Cores 105-646B-7H and 105-646B-8H of Hole 646B, Cores 105-646A-3H through 105-646A-5H and 105-646A-7H of Hole 646A were densely sampled and measured for carbonate (Fig. 36 and Table 11). The correlation between Hole 646A and Hole 646B (Fig. 36) is based on the occurrences of distinct light detrital-carbonate layers (see "Sedimentology" section, this chapter), the LAD of *Pseudoemiliana lacunosa* (see "Biostratigraphy" section, this chapter), and paleomagnetic reversals (i.e., the Brunhes/Matuyama boundary and the top of the Jaramillo Subchronozone; see "Paleomagnetism" section, this chapter).

The high-resolution carbonate record of the upper 70 m of Site 646 is characterized by cyclic fluctuations between 0% and 40% CaCO_3 (Fig. 36). According to smear slide analyses (see "Sedimentology" section), the carbonate is mainly biogenic. Some layers with high detrital carbonate content occur (black symbols in Fig. 37). These layers are concentrated in intervals of low biogenic carbonate content (see detailed description of Core 105-646B-3H, "Sedimentology" section, this chapter). This type of biogenic carbonate cycle is similar to that observed in other carbonate records from the Atlantic Ocean (Kellogg, 1976; Rudiman and McIntyre, 1981a; Mueller et al., 1983) and to stable

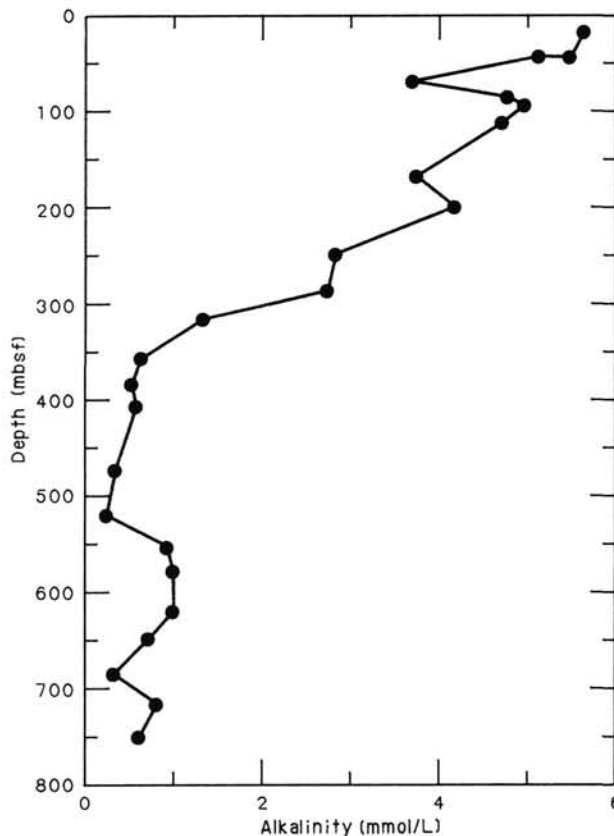
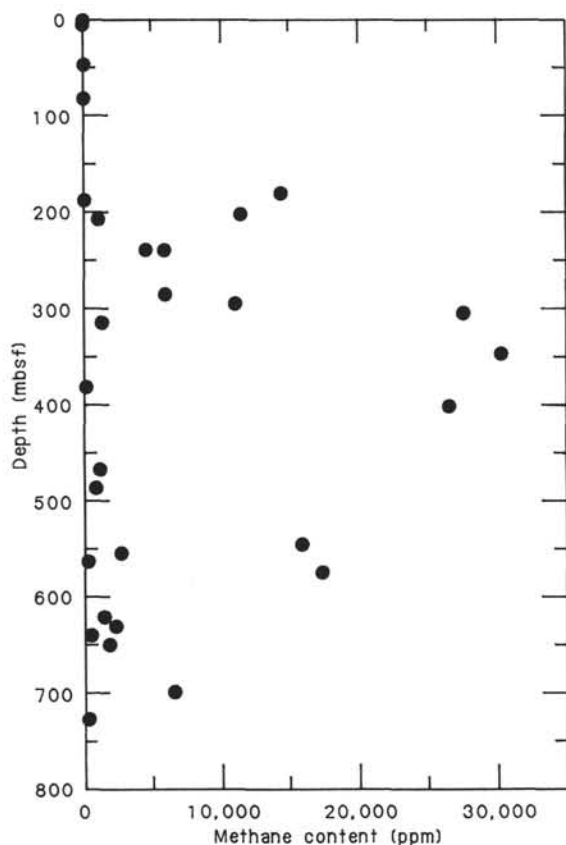


Figure 33. Alkalinity depth profile, Site 646.

Table 9. Methane and ethane content and methane/ethane ratio of gas collected in vacutainers, Site 646.

Sample	Depth (mbsf)	C ₁ (ppm)	C ₂ (ppm)	C ₁ /C ₂
105-646A-1H-1, 142	1.4	23	—	—
105-646A-2H-1, 47	5.5	—	—	—
105-646B-6H-3, 24	46.6	—	—	—
105-646B-10H-1, 0	82.0	—	23	—
105-646B-20X-1, 145	180.0	14348	—	—
105-646B-21X-1, 16	188.0	90	—	—
105-646B-22X-3, 50	201.3	11494	15	766
105-646B-23X-1, 3	207.5	1091	—	—
105-646B-26X-2, 111	238.7	5846	—	—
105-646B-31X-1, 24	284.9	5958	—	—
105-646B-32X-1, 50	294.9	11046	—	—
105-646B-33X-1, 88	305.0	27622	—	—
105-646B-34X-1, 35	314.2	1346	—	—
105-646B-37X-4, 4	347.3	30310	—	—
105-646B-41X-1, 54	381.8	171	—	—
105-646B-43X-1, 85	401.6	26515	—	—
105-646B-50X-1, 31	468.8	1181	—	—
105-646B-52X-1, 17	487.6	882	—	—
105-646B-58X-1, 67	546.2	15843	—	—
105-646B-59X-1, 42	555.6	2698	—	—
105-646B-60X-1, 28	564.7	294	—	—
105-646B-61X-1, 75	574.8	17301	—	—
105-646B-66X-1, 17	622.4	1504	—	—
105-646B-67X-1, 10	631.9	2294	—	—
105-646B-68X-1, 23	641.5	524	—	—
105-646B-69X-1, 28	651.2	1810	—	—
105-646B-74X-1, 35	699.4	6506	—	—
105-646B-77X-1, 24	728.2	300	—	—

**Figure 34. Methane content (ppm) versus depth of gas collected in vacutainers, Site 646.**

oxygen-isotope records (Shackleton and Opdyke, 1976). In the latter, high carbonate values coincide with light $\delta^{18}\text{O}$ values (i.e., interglacial times), and low carbonate values coincide with heavy $\delta^{18}\text{O}$ values (i.e., glacial times). This means that the cyclic changes of biogenic carbonate recorded at Site 646 are probably related to climatic changes. The carbonate maxima C-1, C-3, C-5, C-7, C-11, C-13, C-15, C-17, and C-19 possibly correspond to the stable-isotope (interglacial) stages 1, 3, 5, 7, 11, 13, 15, 17, and 19. The carbonate minima C-2, C-4, C-6, C-8, C-10, C-12, C-14, C-16, C-18, and C-20 possibly correspond to the stable-isotope glacial stages 2, 4, 6, 8, 10, 12, 14, 16, 18, and 20 (Figs. 36 and 37). Assuming linear sedimentation rates of 8.4 cm/k.y. for the uppermost 40 m (Holocene to 0.475 Ma, LAD *P. lacunosa*) and 8.8 cm/k.y. for the interval between 40 and 62 mbsf (0.475–0.73 Ma, Brunhes/Matuyama boundary), the estimated ages of the carbonate maxima and minima intervals are similar to the stable oxygen-isotope stages (Fig. 37; Shackleton and Opdyke, 1976; Savin and Yeh, 1981). A preliminary record of stable oxygen isotopes measured on planktonic foraminifers from Site 646 sediments (A. Aksu, pers. comm., 1985) confirms this interpretation.

PALEOMAGNETICS

Late Miocene to Holocene sediments were cored at Site 646 using both the advanced-piston-corer (APC) and the extended-core-barrel (XCB) techniques. Paleomagnetic studies of these sediments consisted of both remanence and rock-magnetic measurements. The upper sections of both Holes 646A and 646B were cored using the APC and provided relatively undisturbed sediments that were well suited for magnetostratigraphic studies. We oriented several cores from Hole 646B (Cores 105-646B-4H, 105-646B-5H, 105-646B-7H through 105-646B-10H, 105-646B-13H, and 105-646B-14H) using the Eastman-Whipstock multi-shot tool in an effort to provide a true geographic reference for the interval recording the Brunhes and Matuyama and the upper and lower Jaramillo polarity transitions. Unfortunately this attempt failed because the interval containing the Brunhes/Matuyama reversal was lost as a result of poor core recovery. In general, problems with split core liners reduced the usefulness of the other oriented cores.

Magnetostratigraphy

The material recovered at this site proved to be highly magnetic; magnetizations ranged up to $4 \times 10^{-1} \text{ Am}^{-1}$. Because of this, even the split half cores were too strongly magnetized to be measured using the pass-through cryogenic magnetometer without causing the sensors to fluxjump (go off scale). The intensities remained high throughout the section although a slight decreasing trend with depth was observed. Successful pass-through measurements of cores from the lower interval provide constraints on the discrete-sample record.

Progressive alternating-field (AF) demagnetization of pilot samples revealed very simple magnetizations in the upper intervals, as indicated by univectorial magnetizations. Further down-core, however, a strong, downwardly directed overprint was observed. Treatment at a 10–20 millitesla (mT) peak field successfully removed this steep component, isolating a magnetization that decays linearly to the origin with treatment at higher fields. The remaining samples from this site were treated at 10 mT, and the polarities were interpreted on the basis of the inclination record.

The reversals observed in sediments at Site 646 and the bounding samples, sub-bottom depths, and ages are listed in Table 12. The correlation between Holes 646A and 646B is complicated by intervals of poor recovery in both holes, which coincided with the predicted depths of reversal boundaries, and by the possibility that material was double cored in Core 105-646B-2H.

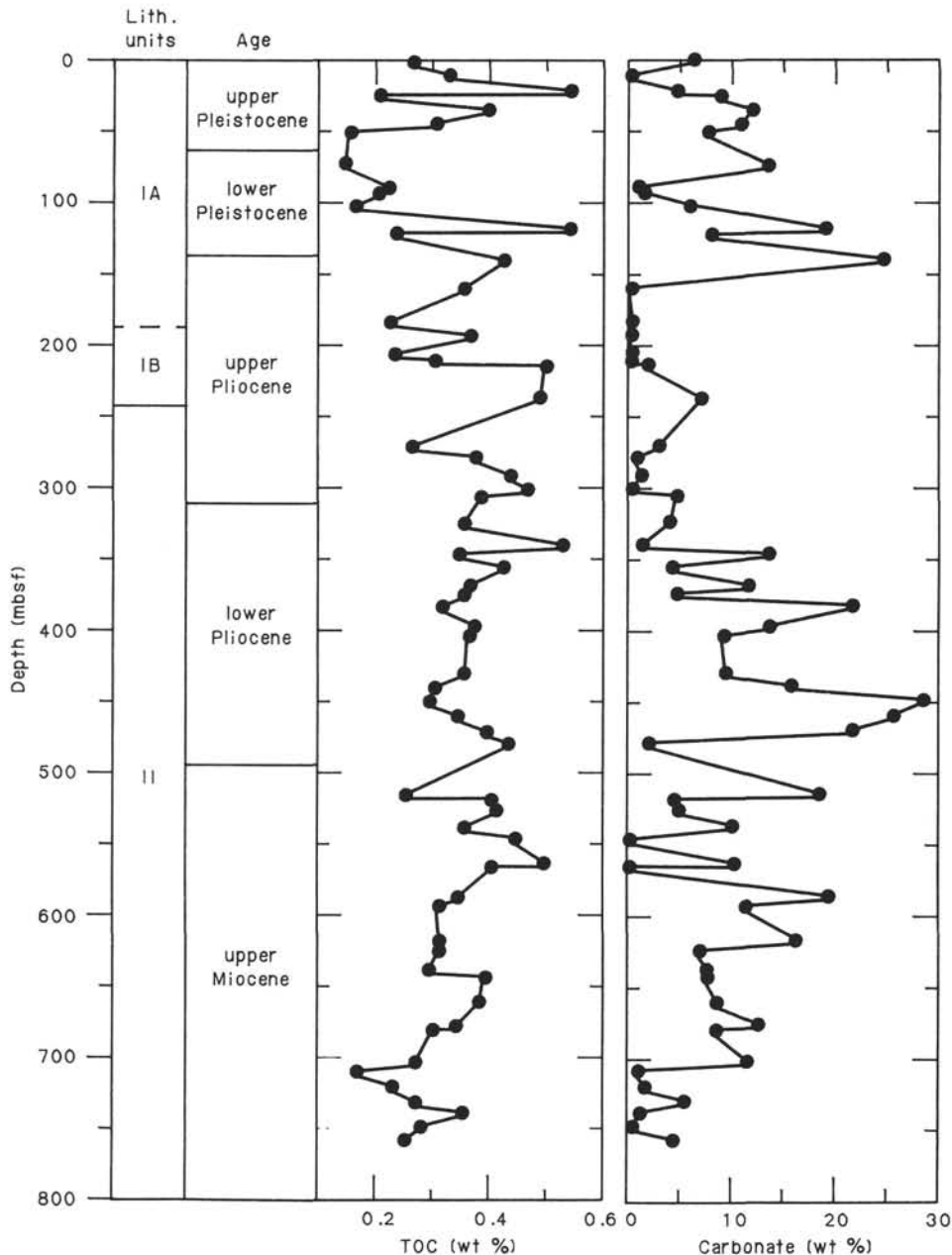


Figure 35. Total organic carbon (TOC) and carbonate content (wt%) versus depth of sediment samples, Hole 646B. Data are identified in Table 10. Roman numerals indicate lithologic units.

As can be seen from Table 12, the depth of the upper Jaramillo reversal in Hole 646B is approximately 5 m deeper than the reversal in Hole 646A. This agrees well with the offset indicated by lithologic correlations between the two holes.

The interval of Hole 646B cored using the XCB proved to be less well suited for magnetostratigraphic studies because of poorer recovery and greater drilling disturbance than observed in the upper, APC interval. Many cores contained drilling biscuits that had apparently rotated within the core barrel. Careful sampling of these sediments, however, provides a coarse polarity record.

The preferred correlation of the polarity reversals observed in the XCB interval of Hole 646B with the geomagnetic time scale (Berggren et al., 1986) is given in Table 12. Because of the large gaps in recovery and between sections of mechanically un-

disturbed sediment, the correlation depends upon the assumption of constant sedimentation rates between biostratigraphic tie-points.

Rock Magnetism

Magnetic-susceptibility analyses were performed on discrete and pass-through samples from Site 646. The susceptibility of 237 discrete samples taken from Holes 646A and 646B was measured. As mentioned in the "Explanatory Notes" chapter (this volume), these samples have not been corrected for mass or volume and will be discussed further by Hall and King (in Part B of this volume). Whole-core measurements were made at 5-cm intervals using the archive half sections of APC Cores 105-646A-1H to 105-646A-8H, 105-646B-4H, and 105-646B-5H.

Table 10. Total organic carbon (TOC) and CaCO₃, both in weight percentage, Core 646B. The samples were measured by combustion of whole sediment sample and acidified sample. Asterisk (*) marks organic carbon sample, all others are physical-properties samples.

Sample	Depth (mbsf)	TOC (wt %)	Carbonate (wt %)
105-646B-1H-1, 88	0.9	0.27	5.6
105-646B-2H-1, 114	10.1	0.33	0.0
*105-646B-3H-5, 119-120	21.6	0.54	3.9
105-646B-4H-1, 50	24.6	0.21	8.3
105-646B-5H-1, 75	34.6	0.40	11.0
105-646B-6H-1, 100	44.4	0.31	10.0
105-646B-6H-5, 75	50.2	0.16	6.9
105-646B-9H-1, 85	73.3	0.15	13.0
*105-646B-10H-5, 119-120	89.2	0.23	0.6
105-646B-11H-1, 105	92.8	0.21	1.1
105-646B-12H-1, 72	102.1	0.17	5.2
*105-646B-13H-5, 119-120	118.3	0.54	18.0
105-646B-14H-5, 75	121.6	0.24	7.3
105-646B-16X-1, 51	140.6	0.43	24.0
105-646B-18X-1, 130	160.4	0.36	0.0
*105-646B-20X-4, 119-120	184.2	0.23	0.0
105-646B-21X-4, 70	193.4	0.37	0.0
*105-646B-22X-6, 119-120	206.5	0.24	0.0
105-646B-23X-3, 75	211.3	0.31	0.0
105-646B-23X-5, 75	214.3	0.50	1.3
105-646B-26X-1, 85	237.0	0.49	6.4
*105-646B-29X-4, 119-120	271.3	0.27	2.3
105-646B-30X-3, 78	278.8	0.38	0.3
105-646B-31X-5, 57	291.3	0.44	0.8
*105-646B-32X-5, 119-120	301.6	0.47	0.0
105-646B-33X-2, 97	306.6	0.39	4.1
105-646B-35X-2, 75	325.7	0.36	3.4
*105-646B-36X-5, 119-120	340.3	0.53	0.8
105-646B-37X-3, 85	346.7	0.35	13.0
105-646B-38X-3, 69	356.1	0.43	3.6
*105-646B-39X-5, 119-120	369.2	0.37	11.0
105-646B-40X-3, 85	375.6	0.36	4.0
105-646B-41X-2, 79	383.6	0.32	21.0
*105-646B-42X-5, 119-120	398.2	0.38	13.0
105-646B-43X-3, 37	404.1	0.37	8.6
105-646B-46X-1, 69	430.5	0.36	8.8
105-646B-47X-1, 65	440.2	0.31	15.0
105-646B-48X-1, 100	450.1	0.30	28.0
105-646B-49X-2, 50	460.8	0.35	25.0
105-646B-50X-3, 43	471.9	0.40	21.0
105-646B-51X-1, 126	479.4	0.44	1.7
105-646B-54X, CC, 25	516.4	0.26	18.0
105-646B-55X-2, 100	519.0	0.41	4.0
105-646B-56X-1, 0-1	526.7	0.42	4.7
*105-646B-57X-2, 119-120	538.5	0.36	9.7
105-646B-58X-1, 147	547.0	0.45	0.0
105-646B-59X, CC, 9	564.1	0.50	10.0
105-646B-60X-2, 26	566.2	0.41	0.0
105-646B-61X-1, 126	575.3	0.45	0.0
*105-646B-62X-3, 119-120	587.8	0.35	19.0
105-646B-63X-1, 110	594.3	0.32	11.0
105-646B-65X-4, 143	618.4	0.32	16.0
105-646B-66X-3, 30	625.5	0.32	6.5
*105-646B-67X-5, 119-120	639.0	0.30	7.1
105-646B-68X-2, 108	643.9	0.40	4.6
105-646B-70X-1, 72	661.2	0.39	8.1
*105-646B-71X-5, 119-120	677.4	0.35	12.0
105-646B-72X-2, 70	680.4	0.31	7.9
*105-646B-74X-3, 119-120	703.2	0.28	11.0
105-646B-75X-2, 50	710.6	0.18	0.5
105-646B-76X-2, 94	720.7	0.24	1.1
*105-646B-77X-3, 119-120	732.1	0.28	5.0
105-646B-78X-2, 1	739.2	0.36	0.6
105-646B-79X-1, 129	748.7	0.29	0.0
105-646B-80X-1, 125	758.3	0.26	3.8

The data presented in the figures are uncorrected for machine drift, which is commonly negligible during the time required to measure a 150-cm section of core.

Laminated silt horizons found in Cores 105-646B-4H, 105-646B-5H, 105-646B-9H, and 105-646B-10H of Hole 646B were sampled for paleocurrent analyses using the anisotropy of the magnetic-susceptibility technique of King and Rees (1962).

These measurements will be performed at the University of Rhode Island.

Results

The results of the magnetic-susceptibility measurements are in $10^{-5} (\times 4\pi\text{SI})$, unless specified in the figure.

Figure 38 shows the susceptibility record of the discrete down-site sample. The record suggests a trend toward increasing susceptibility with depth. This probably results from compaction of the sediments. Given that all other factors remain constant, the susceptibility of a sediment is proportional to the sample permeability (Collinson, 1983). As compaction proceeds and water is expelled, magnetic minerals are brought closer together, increasing their concentrations in each sample.

Figures 39 to 41 give the whole-core susceptibility measurements at Site 646. Because of the density of measurements (every 5 cm), the depths are given in centimeters for easier reading.

Figure 39 shows the results at Hole 646A, measured to a depth of 7050 cm. Because the base of the Brunhes Chronozone is at 5900 cm, our measurements extend into sediment that should be correlative with glacial stage 19.

Spikes in susceptibility intensity seen downcore (e.g., at 3000 cm) are characteristic of low-carbonate silt layers, commonly 5 cm thick. Of the 10 spikes seen in the top 7000 cm of sediment, 7 can be directly correlated to the laminated, well-sorted silt and fine sand layers given in Table 6 ("Sedimentology" section, this chapter). The region of high intensity (values as high as $600 \times 10^{-5} [\times 4\pi\text{SI}]$) at 5200 cm results from a thick-bedded silt unit in Core 105-646A-6H.

Detrital carbonate beds (Table 5, "Sedimentology" section, this chapter) commonly give low susceptibility values ($57\text{--}124 \times 10^{-5} [\times 4\pi\text{SI}]$), except two units. One of these exceptions lies just below the thick silt bed of Core 105-646A-6H and may be influenced by this deposit. The second, in Core 105-646A-3H, is not associated with a silt bed.

These two types of current-deposited units, high and low carbonate, may indicate two different current directions. To test this hypothesis, samples of silt beds from oriented cores taken at Hole 646B will be analyzed for paleocurrent directions by measuring the anisotropy of magnetic susceptibility, using the technique of King and Rees (1962).

Downcore susceptibility measurements were performed on Cores 105-646B-4H and 105-646B-5H, which were oriented with respect to magnetic north. Figure 40 shows the comparison between holes. The correlation lines are based on the tie-points (Fig. 13, "Sedimentology" section, this chapter). The pattern of Core 105-646B-4H appears to correlate with Hole 646A: a peak decreasing to a low with a minor peak at the base, increasing to a high that gradually decreases to the bottom. The susceptibility signal of Core 105-646B-5H is not as easily compared as that of Core 105-646B-4H. The tie-point suggests a correlation with the high at approximately 3500 cm of Hole 646A. The central peaks of each curve relate to silt layers given in Table 6 for each hole and may have been deposited by the same event.

An attempt was made to correlate the variations in susceptibility to downcore lithologic variations in Hole 646A, as determined from core descriptions. There seems to be no apparent correlation between lithology and susceptibility. Carbonate-rich units show as much variability as noncarbonate units.

Figure 41 is a plot of percentage of carbonate versus susceptibility ($\times 10^{-5} (\times 4\pi\text{SI})$). Carbonate analyses performed on cores from Holes 646A and 646B are compared with whole-core susceptibility values from the same depth. The susceptibility values do not vary with carbonate down to approximately 20% carbonate. After this, the susceptibility decreases with carbonate from $15 \times 10^{-5} (\times 4\pi\text{SI})$ to $10 \times 10^{-5} (\times 4\pi\text{SI})$ from 20%

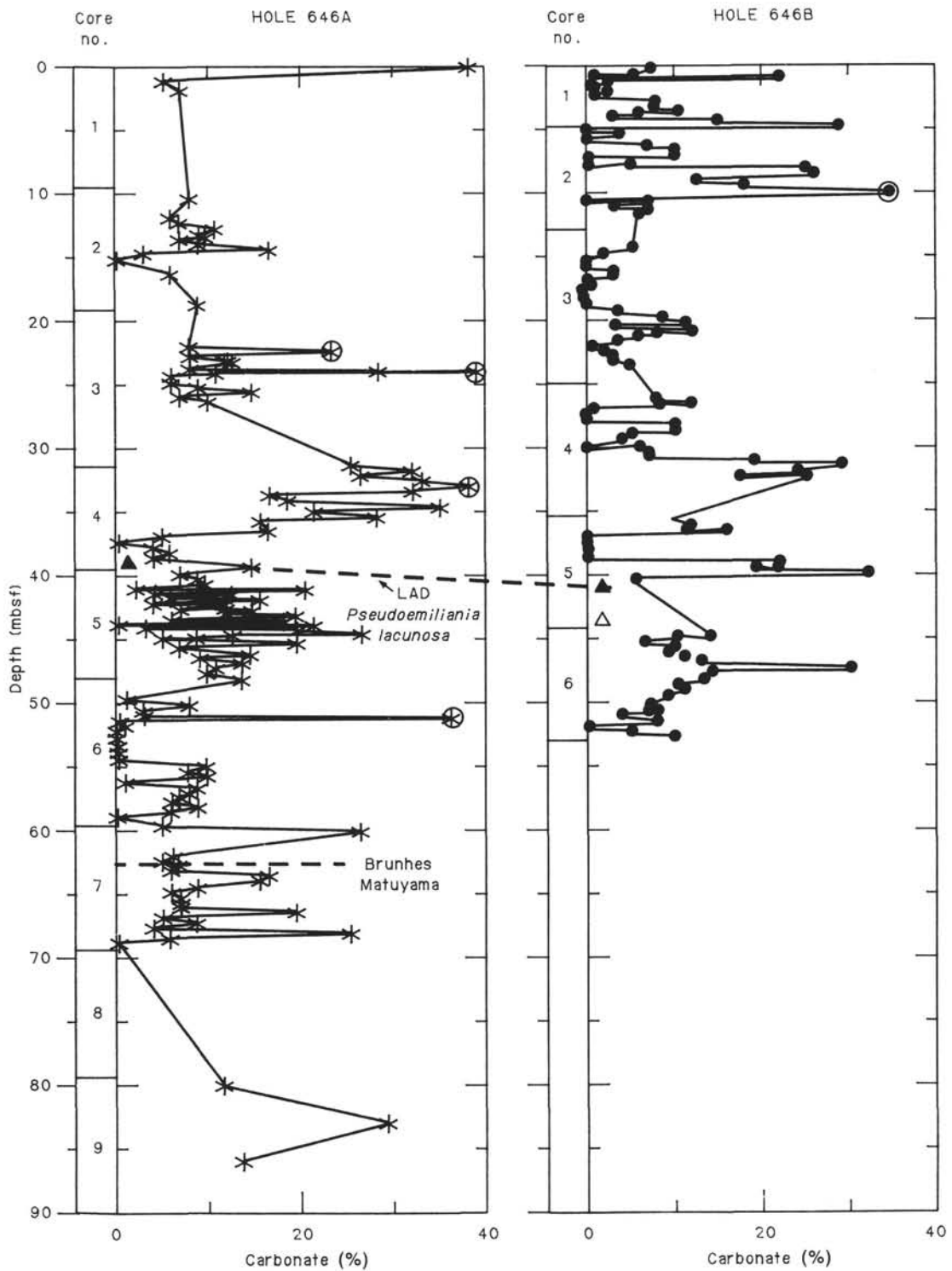


Figure 36. High-resolution carbonate record (wt%) versus depth, upper 70 m of Hole 646A and upper 53 m of Hole 646B. Data are identified in Table 11.

carbonate to 35% carbonate. These data suggest that carbonate dilution is not controlling susceptibility values.

The processes controlling susceptibility downcore are currently unknown. These values may be fluctuating in response to glacial-interglacial variations. Robinson (1986) found a direct correlation between oxygen-isotope stages and rock-magnetic parameters, including susceptibility, in piston cores from the North Atlantic. Closely spaced discrete samples from the upper part

of Site 646 are being studied for rock-magnetic parameters to be compared with other indicators of climatic changes.

PHYSICAL PROPERTIES

Methods

Physical-properties measurements were made on sediments from Holes 646A and 646B at Site 646, following the proce-

Table 11. Carbonate content measured by carbonate-bomb technique and calculated as CaCO₃ (weight percentage). Sediment samples from Holes 646A and 646B.

Sample	Depth (mbsf)	Carbonate (%)
Hole 646A		
105-646A-1H-1, 45	0.00	39.0
105-646A-1H-2, 12	1.17	5.0
105-646A-1H-2, 75	1.80	7.0
105-646A-2H-1, 75	10.30	8.0
105-646A-2H-2, 85	11.90	6.0
105-646A-2H-2, 122	12.27	7.0
105-646A-2H-3, 20	12.75	11.0
105-646A-2H-3, 59	13.14	9.0
105-646A-2H-3, 75	13.30	10.0
105-646A-2H-3, 101	13.56	7.0
105-646A-2H-3, 140	13.95	9.0
105-646A-2H-4, 30	14.35	17.0
105-646A-2H-4, 69	14.74	3.0
105-646A-2H-4, 110	15.15	0.0
105-646A-2H-5, 75	16.30	6.0
105-646A-2H-7, 25	18.80	9.0
105-646A-3H-2, 100	22.00	8.0
105-646A-3H-2, 136	22.36	24.0
105-646A-3H-3, 30	22.80	8.0
105-646A-3H-3, 70	23.20	12.0
105-646A-3H-3, 75	23.25	13.0
105-646A-3H-3, 110	23.60	8.0
105-646A-3H-3, 149	23.99	29.0
105-646A-3H-4, 3	24.03	40.0
105-646A-3H-4, 18	24.18	11.0
105-646A-3H-4, 36	24.36	6.0
105-646A-3H-4, 82	24.82	6.0
105-646A-3H-4, 116	25.16	9.0
105-646A-3H-5, 6	25.56	15.0
105-646A-3H-5, 46	25.96	7.0
105-646A-3H-5, 83	26.33	10.0
105-646A-4H-2, 6	31.31	26.0
105-646A-4H-2, 46	31.71	33.0
105-646A-4H-2, 85	32.10	27.0
105-646A-4H-2, 122	32.47	34.0
105-646A-4H-3, 15	32.90	39.0
105-646A-4H-3, 55	33.30	33.0
105-646A-4H-3, 94	33.69	17.0
105-646A-4H-3, 135	34.10	19.0
105-646A-4H-4, 25	34.50	36.0
105-646A-4H-4, 65	34.90	22.0
105-646A-4H-4, 105	35.30	29.0
105-646A-4H-4, 146	35.71	16.0
105-646A-4H-5, 74	36.49	17.0
105-646A-4H-5, 116	36.91	5.0
105-646A-4H-6, 5	37.30	0.0
105-646A-4H-6, 46	37.71	4.0
105-646A-4H-6, 87	38.12	6.0
105-646A-4H-6, 125	38.50	4.0
105-646A-4H-7, 46	39.21	15.0
105-646A-5H-1, 88	39.87	7.0
105-646A-5H-1, 125	40.24	9.0
105-646A-5H-2, 1	40.50	8.0
105-646A-5H-2, 17	40.66	10.0
105-646A-5H-2, 44	40.93	2.0
105-646A-5H-2, 55	41.04	21.0
105-646A-5H-2, 82	41.31	4.0
105-646A-5H-2, 94	41.43	13.0
105-646A-5H-2, 120	41.69	6.0
105-646A-5H-2, 136	41.85	16.0
105-646A-5H-3, 8	42.07	4.0
105-646A-5H-3, 25	42.24	12.0
105-646A-5H-3, 50	42.49	7.0
105-646A-5H-3, 66	42.65	15.0
105-646A-5H-3, 91	42.90	12.0
105-646A-5H-3, 106	43.05	20.0
105-646A-5H-3, 131	43.30	6.0
105-646A-5H-3, 143	43.42	19.0
105-646A-5H-4, 17	43.66	0.0
105-646A-5H-4, 36	43.85	22.0
105-646A-5H-4, 60	44.09	3.0
105-646A-5H-4, 75	44.24	20.0
105-646A-5H-4, 99	44.48	27.0
105-646A-5H-4, 114	44.63	13.0
105-646A-5H-4, 139	44.88	9.0
105-646A-5H-4, 149	44.98	5.0
105-646A-5H-5, 28	45.27	20.0
105-646A-5H-5, 69	45.68	7.0
105-646A-5H-5, 108	46.07	15.0

Table 11 (continued).

Sample	Depth (mbsf)	Carbonate (%)
Hole 646A (cont.)		
105-646A-5H-5, 149	46.48	9.0
105-646A-5H-6, 35	46.84	14.0
105-646A-5H-6, 79	47.28	11.0
105-646A-5H-6, 119	47.68	10.0
105-646A-5H-7, 9	48.08	14.0
105-646A-6H-1, 20	49.71	1.0
105-646A-6H-1, 60	50.11	8.0
105-646A-6H-1, 100	50.51	3.0
105-646A-6H-1, 140	50.91	3.0
105-646A-6H-2, 10	51.11	37.0
105-646A-6H-2, 30	51.31	0.0
105-646A-6H-2, 72	51.73	1.0
105-646A-6H-2, 109	52.10	0.0
105-646A-6H-2, 149	52.50	0.0
105-646A-6H-3, 43	52.94	0.0
105-646A-6H-3, 120	53.71	0.0
105-646A-6H-4, 10	54.11	0.0
105-646A-6H-4, 50	54.51	0.0
105-646A-6H-4, 91	54.92	10.0
105-646A-6H-4, 131	55.32	8.0
105-646A-6H-5, 20	55.71	10.0
105-646A-6H-5, 63	56.14	1.0
105-646A-6H-5, 101	56.52	9.0
105-646A-6H-5, 141	56.92	8.0
105-646A-6H-6, 31	57.32	7.0
105-646A-6H-6, 70	57.71	6.0
105-646A-6H-6, 113	58.14	9.0
105-646A-6H-6, 149	58.50	6.0
105-646A-6H-7, 35	58.86	0.0
105-646A-7H-1, 5	59.55	5.0
105-646A-7H-1, 45	59.95	27.0
105-646A-7H-2, 95	61.95	6.0
105-646A-7H-2, 135	62.35	5.0
105-646A-7H-3, 13	62.63	7.0
105-646A-7H-3, 54	63.04	6.0
105-646A-7H-3, 94	63.44	17.0
105-646A-7H-3, 138	63.88	16.0
105-646A-7H-4, 36	64.36	9.0
105-646A-7H-4, 75	64.75	6.0
105-646A-7H-4, 115	65.15	7.0
105-646A-7H-5, 4	65.54	7.0
105-646A-7H-5, 47	65.97	7.0
105-646A-7H-5, 84	66.34	20.0
Hole 646B		
105-646B-1H-1, 101	0.96	23.0
105-646B-1H-3, 70	3.65	6.0
105-646B-1H-5, 75	6.70	6.0
105-646B-2H-3, 85	7.78	5.0
105-646B-2H-5, 68	10.61	7.0
105-646B-3H-1, 94	15.34	0.0
105-646B-3H-5, 59	20.99	8.0
105-646B-4H-3, 75	27.85	0.0
105-646B-4H-5, 15	30.25	25.0
105-646B-5H-3, 75	37.55	22.0
105-646B-6H-3, 75	47.15	14.0
105-646B-9H-3, 70	76.07	0.0
105-646B-9H-5, 75	79.10	0.0
105-646B-10H-1, 95	82.95	11.0
105-646B-10H-1, 133	83.33	0.0
105-646B-10H-3, 75	85.75	17.0
105-646B-10H-5, 75	88.75	6.0
105-646B-11H-3, 75	95.45	0.0
105-646B-11H-5, 70	98.40	0.0
105-646B-12H-3, 62	105.02	5.0
105-646B-12H-5, 87	108.27	10.0
105-646B-13H-1, 75	111.85	16.0
105-646B-13H-3, 75	114.85	6.0
105-646B-13H-5, 75	117.85	15.0
105-646B-14H-1, 75	121.55	10.0
105-646B-14H-3, 72	124.52	0.0
105-646B-18X-3, 75	162.85	0.0
105-646B-20X-1, 75	179.25	10.0
105-646B-20X-3, 75	182.25	5.0
105-646B-20X-5, 70	185.20	21.0
105-646B-21X-3, 60	191.80	0.0
105-646B-21X-7, 98	198.18	0.0
105-646B-22X-1, 90	198.70	0.0
105-646B-22X-6, 75	206.05	0.0
105-646B-23X-1, 75	208.25	0.0
105-646B-23X-2, 69	209.69	9.0

Table 11 (continued).

Sample	Depth (mbsf)	Carbonate (%)
Hole 646B (cont.)		
105-646B-26X-3, 85	239.95	8.0
105-646B-26X-5, 75	242.85	0.0
105-646B-29X-1, 72	266.02	0.0
105-646B-29X-5, 77	272.07	9.0
105-646B-30X-1, 73	275.73	12.0
105-646B-30X-5, 82	281.82	0.0
105-646B-31X-1, 76	285.46	7.0
105-646B-31X-3, 79	288.49	9.0
105-646B-32X-1, 75	295.15	0.0
105-646B-32X-3, 16	297.56	0.0
105-646B-32X-5, 72	301.12	0.0
105-646B-33X-4, 105	309.65	0.0
105-646B-36X-1, 112	334.18	12.0
105-646B-36X-3, 90	336.87	5.0
105-646B-36X-5, 78	339.66	0.0
105-646B-37X-1, 69	343.49	3.0
105-646B-37X-5, 72	349.52	3.0
105-646B-38X-1, 30	352.69	8.0
105-646B-38X-5, 84	359.08	12.0
105-646B-39X-1, 70	362.69	18.0
105-646B-39X-3, 70	365.67	3.0
105-646B-39X-5, 71	368.66	6.0
105-646B-40X-6, 102	379.96	12.0
105-646B-40X-7, 75	381.16	7.0
105-646B-41X-4, 74	386.54	9.0
105-646B-42X-2, 95	393.44	3.0
105-646B-42X-5, 99	397.96	15.0
105-646B-48X-1, 0	449.10	3.0
105-646B-49X-2, 50	460.80	27.0
105-646B-56X-1, 40	527.10	6.0
105-646B-57X-3, 76	539.56	7.0
105-646B-62X-1, 53	584.13	7.0
105-646B-62X-4, 53	588.63	22.0
105-646B-65X-1, 141	613.91	13.0
105-646B-67X-2, 39	633.69	0.0
105-646B-69X-1, 140	652.30	22.0
105-646B-71X-1, 78	670.98	4.0
105-646B-71X-5, 95	677.15	4.0
105-646B-73X-1, 95	690.25	19.0
105-646B-73X-2, 66	691.46	33.0
105-646B-74X-1, 93	699.93	13.0
105-646B-74X-3, 60	702.60	4.0
105-646B-75X-4, 97	714.07	0.0
105-646B-77X-4, 133	733.73	4.0
105-646B-78X-2, 1	739.21	1.0
105-646B-79X-1, 129	748.69	1.0
105-646B-80X-1, 125	758.25	5.0
105-646B-1H-1, 39	0.34	8.0
105-646B-1H-1, 88	0.83	5.6
105-646B-1H-1, 80	0.75	1.0
105-646B-1H-1, 101	0.96	23.0
105-646B-1H-1, 120	1.15	3.0
105-646B-1H-2, 8	1.53	0.0
105-646B-1H-2, 50	1.95	3.0
105-646B-1H-2, 90	2.35	1.0
105-646B-1H-2, 130	2.75	8.0
105-646B-1H-3, 20	3.15	8.0
105-646B-1H-3, 60	3.55	11.0
105-646B-1H-3, 70	3.65	6.0
105-646B-1H-3, 100	3.95	3.0
105-646B-1H-3, 140	4.35	15.0
105-646B-1H-4, 30	4.75	29.0
105-646B-2H-1, 100	4.93	0.0
105-646B-2H-1, 114	5.07	0.0
105-646B-2H-1, 140	5.33	4.0
105-646B-2H-2, 30	5.73	0.0
105-646B-2H-2, 70	6.13	7.0
105-646B-2H-2, 110	6.53	10.0
105-646B-2H-3, 0	6.93	10.0
105-646B-2H-3, 39	7.32	0.0
105-646B-2H-3, 79	7.72	0.0
105-646B-2H-3, 85	7.78	5.0
105-646B-2H-3, 121	8.14	25.0
105-646B-2H-4, 9	8.52	26.0
105-646B-2H-4, 50	8.93	12.0
105-646B-2H-4, 90	9.33	18.0
105-646B-2H-5, 20	10.13	35.0
105-646B-2H-5, 60	10.53	0.0
105-646B-2H-5, 68	10.61	7.0
105-646B-2H-5, 100	10.93	3.0
105-646B-2H-5, 140	11.33	7.0
105-646B-2H-6, 30	11.73	6.0

Table 11 (continued).

Sample	Depth (mbsf)	Carbonate (%)
Hole 646B (cont.)		
105-646B-3H-1, 2	14.42	5.0
105-646B-3H-1, 42	14.82	2.0
105-646B-3H-1, 82	15.22	0.0
105-646B-3H-1, 94	15.34	0.0
105-646B-3H-1, 122	15.62	0.0
105-646B-3H-2, 12	16.02	3.0
105-646B-3H-2, 52	16.42	3.0
105-646B-3H-2, 92	16.82	0.0
105-646B-3H-2, 132	17.22	1.0
105-646B-3H-3, 22	17.62	0.0
105-646B-3H-3, 62	18.02	0.0
105-646B-3H-3, 75	18.15	0.0
105-646B-3H-3, 102	18.42	0.0
105-646B-3H-3, 142	18.82	0.0
105-646B-3H-4, 32	19.22	4.0
105-646B-3H-4, 72	19.62	9.0
105-646B-3H-4, 112	20.02	12.0
105-646B-3H-5, 2	20.42	3.0
105-646B-3H-5, 42	20.82	12.0
105-646B-3H-5, 59	20.99	8.0
105-646B-3H-5, 87	21.27	6.0
105-646B-3H-5, 120	21.60	3.9
105-646B-3H-6, 7	21.97	0.0
105-646B-3H-6, 47	22.37	2.0
105-646B-3H-6, 87	22.77	3.0
105-646B-3H-6, 127	23.17	3.0
105-646B-3H-7, 17	23.57	5.0
105-646B-4H-1, 2	26.12	8.0
105-646B-4H-1, 40	26.50	12.0
105-646B-4H-1, 50	26.60	8.3
105-646B-4H-1, 80	26.90	1.0
105-646B-4H-1, 120	27.30	0.0
105-646B-4H-1, 120	27.30	0.0
105-646B-4H-2, 9	27.69	0.0
105-646B-4H-2, 50	28.10	10.0
105-646B-4H-2, 91	28.51	10.0
105-646B-4H-2, 130	28.90	5.0
105-646B-4H-3, 29	29.39	4.0
105-646B-4H-3, 75	29.85	0.0
105-646B-4H-3, 70	29.80	6.0
105-646B-4H-3, 109	30.19	7.0
105-646B-4H-4, 1	30.61	7.0
105-646B-4H-4, 40	31.00	19.0
105-646B-4H-4, 80	31.40	29.0
105-646B-4H-4, 120	31.80	24.0
105-646B-4H-5, 10	32.20	17.0
105-646B-4H-5, 15	32.25	25.0
105-646B-5H-1, 0	35.70	9.0
105-646B-5H-1, 40	36.10	12.0
105-646B-5H-1, 75	36.45	11.3
105-646B-5H-1, 80	36.50	16.0
105-646B-5H-1, 120	36.90	0.0
105-646B-5H-2, 10	37.30	0.0
105-646B-5H-2, 51	37.71	0.0
105-646B-5H-2, 91	38.11	0.0
105-646B-5H-2, 131	38.51	0.0
105-646B-5H-3, 29	38.99	22.0
105-646B-5H-3, 75	39.45	22.0
105-646B-5H-3, 70	39.40	19.0
105-646B-5H-3, 110	39.80	32.0
105-646B-5H-3, 149	40.19	5.0
105-646B-6H-1, 95	44.76	14.0
105-646B-6H-1, 100	44.81	10.2
105-646B-6H-1, 145	45.26	6.0
105-646B-6H-2, 30	45.61	10.0
105-646B-6H-2, 71	46.02	9.0
105-646B-6H-2, 110	46.41	11.0
105-646B-6H-3, 1	46.82	13.0
105-646B-6H-3, 53	47.34	30.0
105-646B-6H-3, 75	47.56	14.0
105-646B-6H-3, 91	47.72	14.0
105-646B-6H-3, 130	48.11	13.0
105-646B-6H-4, 19	48.50	10.0
105-646B-6H-4, 58	48.89	11.0
105-646B-6H-4, 100	49.31	9.0
105-646B-6H-5, 29	50.10	7.0
105-646B-6H-5, 75	50.56	6.9
105-646B-6H-5, 70	50.51	8.0
105-646B-6H-5, 110	50.91	4.0
105-646B-6H-5, 149	51.30	8.0
105-646B-6H-6, 40	51.71	0.0
105-646B-6H-6, 80	52.11	5.0
105-646B-6H-6, 120	52.51	10.0

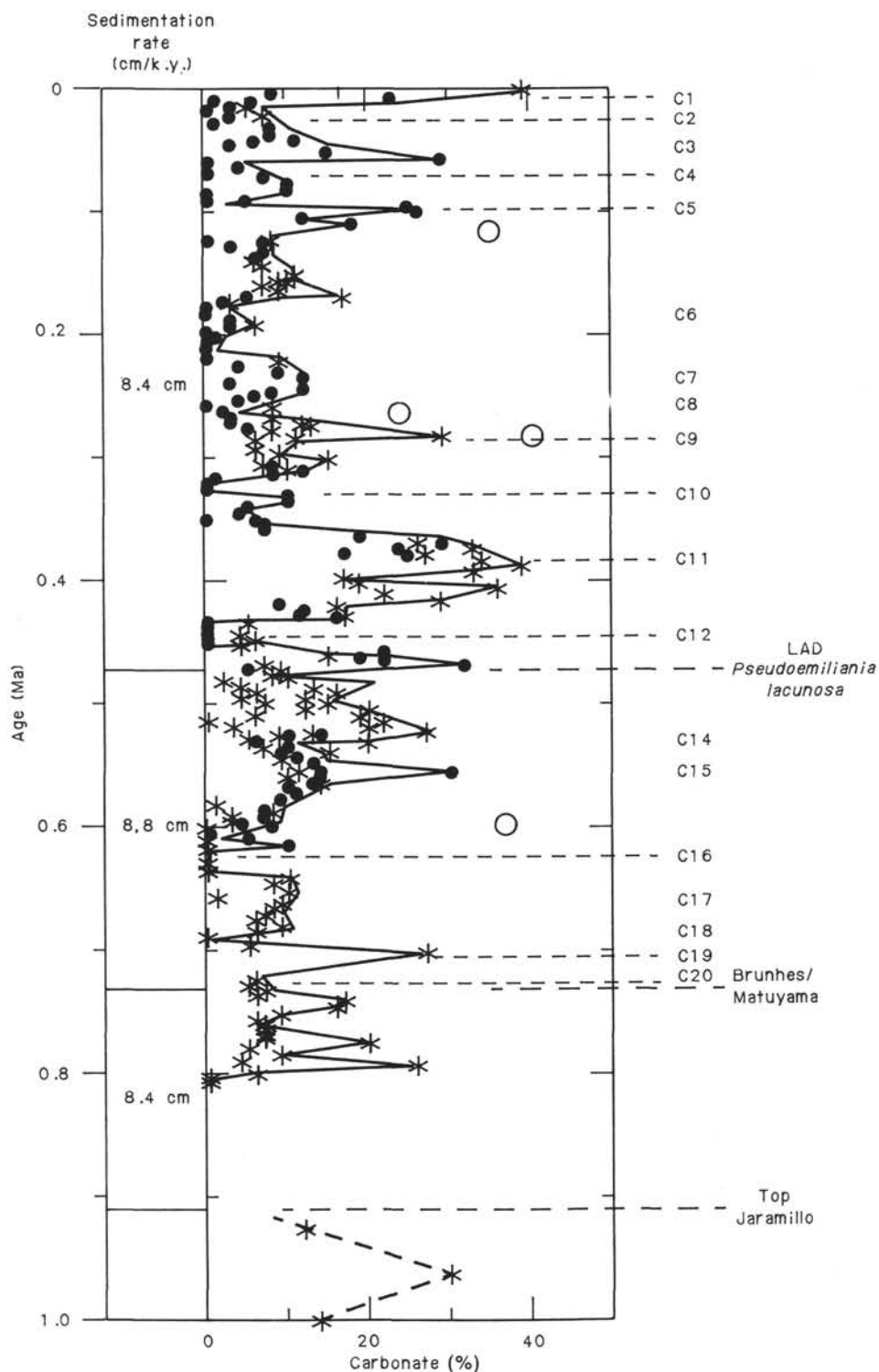


Figure 37. High-resolution carbonate record (wt%) versus age. Asterisks mark data from Hole 646A, closed circles from Hole 646B. Dashed lines mark stratigraphic datum levels. C-1, C-2, and so forth, indicate carbonate stages. Carbonate values from detrital-carbonate-rich layers are marked by large open circles.

dures outlined in the "Explanatory Notes" chapter (this volume). Because of poor core recovery and extensive sediment disturbance below 400 mbsf, the sampling frequency for index properties and compressional-wave velocity decreased. Samples used for the measurements in this interval were selected from well-preserved drilling biscuits that were cleaned of surrounding slurred sediment.

GRAPE Wet-Bulk Density

The GRAPE bulk-density profiles (plots preceding core-description forms, this volume) show a relatively uniform increase in density with depth at Site 646. In profiles from Hole 646A and from depths < 200 mbsf in Hole 646B, individual sediment units that vary in thickness from several centimeters to tens of

Table 12. Paleomagnetic-reversal boundaries, Site 646.

Reversal	Age	Bounding samples	Depth (mbsf)
Hole 646A			
Brunhes/Matuyama	0.73	105-646A-7H-3, 60/105-646A-7H-3, 94	58.70/59.04
Jaramillo	0.91	105-646A-8H-5, 134/105-646A-8H-6, 4	72.14/72.34
Cobb Mountain	1.12	105-646A-10H-2, 65/105-646A-10H-3, 80	86.25/86.67
Top			88.85/89.10
Bottom			
Hole 646B			
Brunhes/Matuyama	0.73	105-646B-6H-6, 120/105-646B-8H-6, 78	52.10/73.86
Jaramillo	0.91	105-646B-9H-3, 106/105-646B-9H-4, 115	76.5/78.10
Top	0.98	105-646B-9H-6, 106/105-646B-10H-2, 30	81.10/83.80
Bottom	2.47	105-646B-21X-2, 69/105-646B-21X-3, 141	190.40/192.60
Matuyama/Gauss	3.4	105-646B-31X-6, 65/105-646B-31X-6, 75	292.85/292.95
Gauss/Gilbert	4.10	105-646B-37X-3, 125/105-646B-38X-1, 35	347.05/352.85
Nunivak	4.24	105-646B-38X-5, 104/105-646B-38X-5, 115	359.45/359.55
Top	4.57	105-646B-39X-4, 134/105-646B-41X-2, 5	367.84/382.85
Bottom	4.77	105-646B-43X-3, 75/105-646B-46X-1, 5	404.45/429.85
Chron C1	6.37	105-646B-61X-3, 35/105-646B-61X-3, 45	577.35/577.44
Top N1	6.50	105-646B-61X-3, 145/105-646B-61X-4, 5	578.44/578.55
Bottom N1	6.85	105-646B-67X-4, 131/105-646B-67X-4, 133	637.61/637.63
Chron C6	7.28	105-646B-70X-1, 148/105-646B-71X-1, 5	661.98/670.25
Top	7.90	105-646B-72X-1, 45/105-646B-72X-1, 55	680.14/680.24
Bottom N1	8.21	105-646B-75X-2, 41/105-646B-75X-2, 43	710.51/710.53
Top N2	8.41	105-646B-76X-1, 23/105-646B-76X-1, 26	718.53/718.56
Chron C7	8.80	105-646B-77X-4, 66/105-646B-77X-4, 68	733.06/733.08
Top N1	8.92	105-646B-77X-4, 148/105-646B-78X-2, 113	733.88/740.33

centimeters can be distinguished. Distinctive silt and carbonate layers used for the visual correlation of Holes 646A and 646B can be identified clearly in the GRAPE records by their higher density. Below 200 mbsf in Hole 646B, the amount of drilling slurry in the cores increased and the quality of the density profiles decreased. Agreement between the GRAPE-estimated bulk density and gravimetrically determined bulk density was good for cores having little disturbance. Cores with small-diameter drilling biscuits and extensive slurried sediment displayed slightly lower GRAPE densities.

Index Properties

Results of index-property measurements in Holes 646A and 646B are shown in Figure 42 and listed in Table 13. The combined results from the two holes show a relatively uniform increase in bulk density and decrease in water content and porosity with depth. Bulk density varies from 1.30 g/cm³ in the upper 10 m of Hole 646A to 2.10–2.20 g/cm³ at the base of Hole 646B, near 750 mbsf. Over this interval, water content decreases from 140% to 25% and dry weight and porosity decrease from 80% to 41%. At Site 646, grain density is more variable than at Site 645; consequently bulk density shows more small-scale fluctuation than does water content. Grain density is higher at Site 646; most values range from 2.70 to 2.85 g/cm³. Carbonate and clay minerals are a larger fraction of the sediment at Site 646, and these constituents generally contribute to increasing the overall grain density (Hamilton, 1974).

The vertical profiles of Hole 646B (Fig. 42) can be divided into three depth ranges that display different density, water-content, and porosity gradients. In terms of bulk density, these ranges are (1) 0–140 mbsf, density increases from 1.40 to 1.95 g/cm³; (2) 140–340 mbsf, density is a nearly constant 1.75 g/cm³; and (3) 340–758 mbsf, density increases from 1.95 to 2.15 g/cm³. Water content and porosity display patterns that are the inverse of the bulk-density variation. Both of these properties are characterized by smoothly decreasing profiles below 340 mbsf, al-

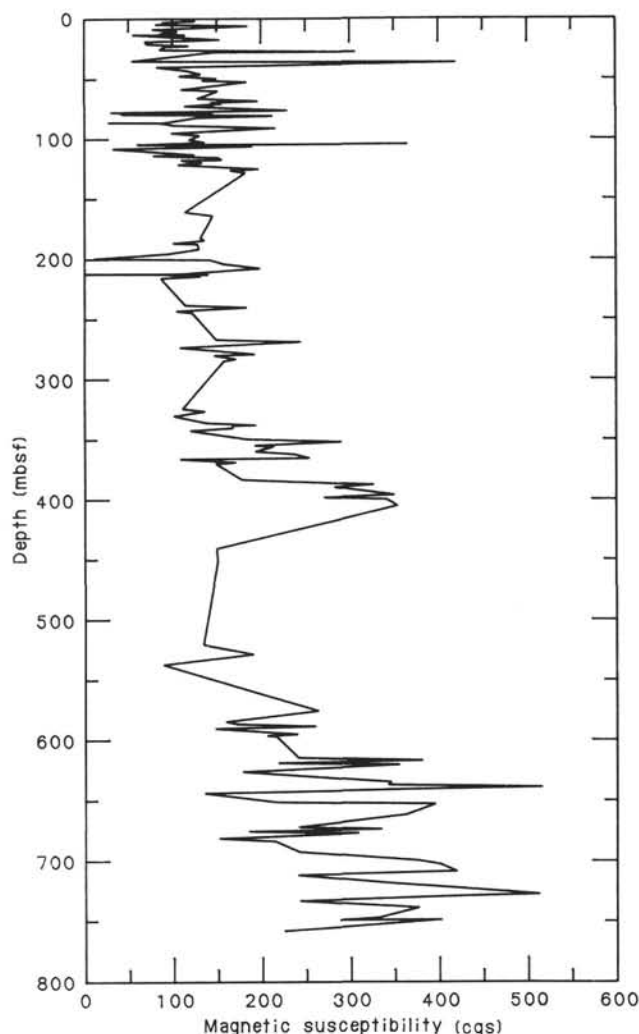


Figure 38. Discrete-sample magnetic susceptibility, Site 646. Measurements of discrete-sample magnetic susceptibility suggest a general down-site increase. This probably results from compaction of the sediment, increasing the amount of magnetic minerals present in a given sample.

though some small but significant reversals are observed near the bottom of the hole.

Changes in the profiles correspond well to sediment texture (see Fig. 57, “Summary and Conclusions” section, this chapter). The upper interval in the vertical profiles (0–140 mbsf) has a nearly equal abundance of silt and clay. Silt and sand are predominant in the middle interval (140–340 mbsf), and from 340 mbsf to the base of Hole 646B, the sediment is predominantly clay.

A good correspondence also exists between the index properties and boundaries between seismic units and prominent reflectors within the units (Fig. 57, “Summary and Conclusions” section, this chapter). The seismic reflectors are located at pronounced density maxima or at intervals of rapidly increasing density below density minima.

Vane Shear Strength

Vane shear strengths increase fairly regularly in both Holes 646A and 646B to a depth of approximately 70–75 mbsf. Below this depth, more scatter is observed (Fig. 42), although low values between 75 and 80 mbsf in Hole 646A (Table 13) are attributed to flow-in disturbance in Core 105-646A-9H. A consistent

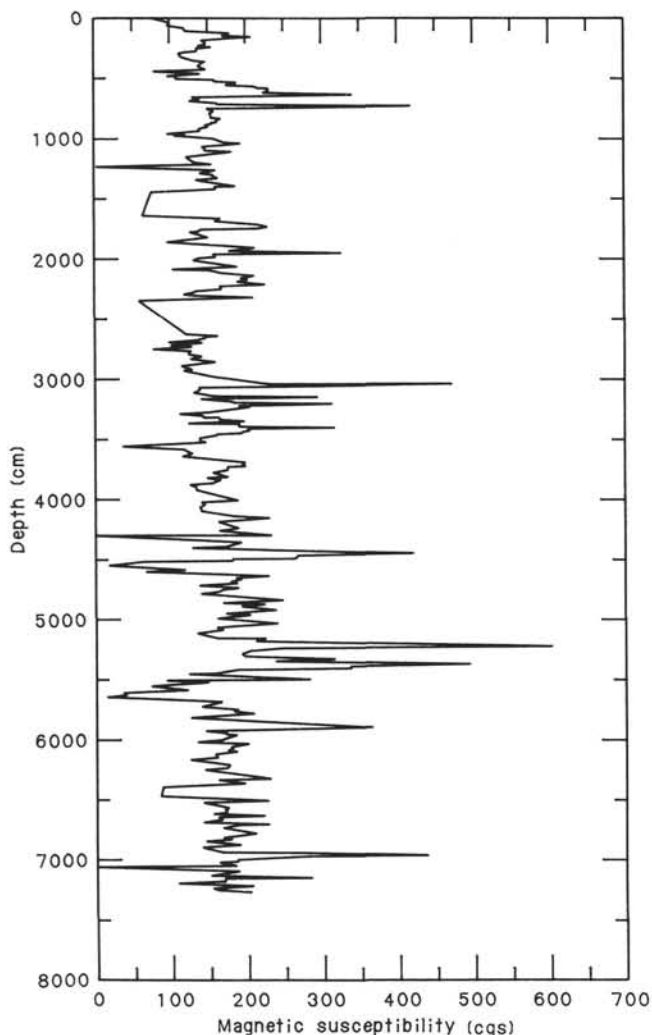


Figure 39. Pass-through (archive half) magnetic-susceptibility measurements, Hole 646A, Cores 105-646A-1H to 105-646A-8H. Magnetic-susceptibility measurements were performed at 5-cm intervals downcore. The scattered large spikes correspond to low-carbonate silt layers found throughout the hole.

inverse relationship between shear strength and water content in Hole 646A exists, but the same correlation is not readily apparent in Hole 646B. The reason for this discrepancy is probably related to the large sampling interval and to normal experimental error.

Despite a rise in scatter below 80 mbsf, shear-strength values in Hole 646B display an increasing trend with depth to about 130 mbsf (Fig. 42). Below this depth, the range of values is even wider, but the base line is low, < 50 kPa, and tends to remain relatively constant with depth. This change coincides with the Pliocene/Pleistocene boundary, a decrease in calcium carbonate content, and a prominent seismic reflector. A concurrent change in index properties below 140 mbsf is observed, and the decrease in shear strength may have a textural or lithologic origin. On the other hand, XCB coring, which was initiated at 130 mbsf, tends to produce a greater degree of disturbance than does the APC coring. This disturbance may be reflected in lower shear strengths.

Thermal Conductivity and Heat Flow

In general, thermal-conductivity values at Site 646 are lower than those measured at Site 645 and range from approximately 2.0 to $3.5 \times 10^{-3} \times \text{cal} \times \text{°C}^{-1} \times \text{cm}^{-1} \times \text{s}^{-1}$. Except two

anomalous values at 3.75 and 52.25 mbsf, conductivity tends to increase steadily with depth in Hole 646A. In addition, excellent agreement in the trends of bulk density and conductivity is observed (Table 13).

Below 100 mbsf, trends in conductivity closely resemble those in bulk density (see Fig. 42), and three broad ranges can be identified. Conductivity values increase with depth to the seismic reflector at approximately 140 mbsf. Below this horizon, measurements display greater scatter but appear to decrease with depth to about 230 mbsf. This range corresponds to a relatively constant or decreasing gradient in bulk density, possibly related to high sedimentation rates and a lower degree of consolidation. Values of both properties again increase steadily with depth to 390 mbsf, where thermal-conductivity measurements were suspended.

Because of changes in temperature and pressure, laboratory-measured thermal conductivities differ from *in-situ* values. Hyndman et al. (1974) suggest an empirical equation employing density, depth, geothermal gradient, and temperature differences to correct for pressure and temperature effects. We used this equation to convert the laboratory measurements to *in-situ* conductivities. The results, displayed in Table 14, are consistent with those reported for shallow depths by Hyndman et al. (1974); all *in-situ* values are lower than laboratory measurements.

Three sub-bottom temperature measurements were conducted during core runs 105-646A-4H, 105-646A-7H, and 105-646A-10H. Plots of temperature versus time, significant events being indicated, appear in Figure 43. The resulting data and measurement depths are displayed in Table 15.

Problems were encountered during the last run of Core 105-646A-10H. Although the probe was held at the bottom of the hole for the same period (10 min) as for the previous two trials, the temperature never stabilized but continued to fall until the time to pullout. As a result, the true temperature is uncertain, and three values have been used. The high temperature value was calculated from an average of all data at 93.8 mbsf. The low value was estimated by fitting a linear-regression line ($r = 0.99$) to this data and extending the time period an additional 5 min. The intermediate temperature represents the final measurement before the probe was withdrawn. Associated geothermal gradients calculated from these data are also reported in Table 15.

A preliminary heat-flow value was computed using the convective-flow equation of Williams et al. (1979):

$$q = -K \, dT/dz,$$

where q = heat flow
 K = thermal conductivity and
 dT/dz = geothermal gradient.

An average *in-situ* thermal conductivity of $2.30 \times 10^{-3} \times \text{cal} \times \text{°C}^{-1} \times \text{cm}^{-1} \times \text{s}^{-1}$ from Hole 646A was employed with the geothermal gradient of 0.074 °C/m . A heat flow of 71.2 mW/m^2 , or 1.68 heat flow units (HFU), was obtained. Error bars were calculated based on variations in geothermal gradient resulting from uncertainties in the temperature measurement in Core 105-646A-10H (Table 15 and Fig. 44).

All three computed heat-flow values are slightly higher than those reported by Hyndman (1973) and Pye and Hyndman (1972) but within the range of variability of their measurements. When plotted on the theoretical curve of Slater and Francheteau (1970), 1.68 HFU corresponds to an age of approximately 45 m.y. The age of Site 646 was estimated at 55–60 m.y. by dating magnetic anomaly 24 (Srivastava et al., 1981).

Compressional-Wave Velocity

Compressional-wave velocities in the upper 100 m of each hole are low and fairly constant (Table 13 and Fig. 42). They av-

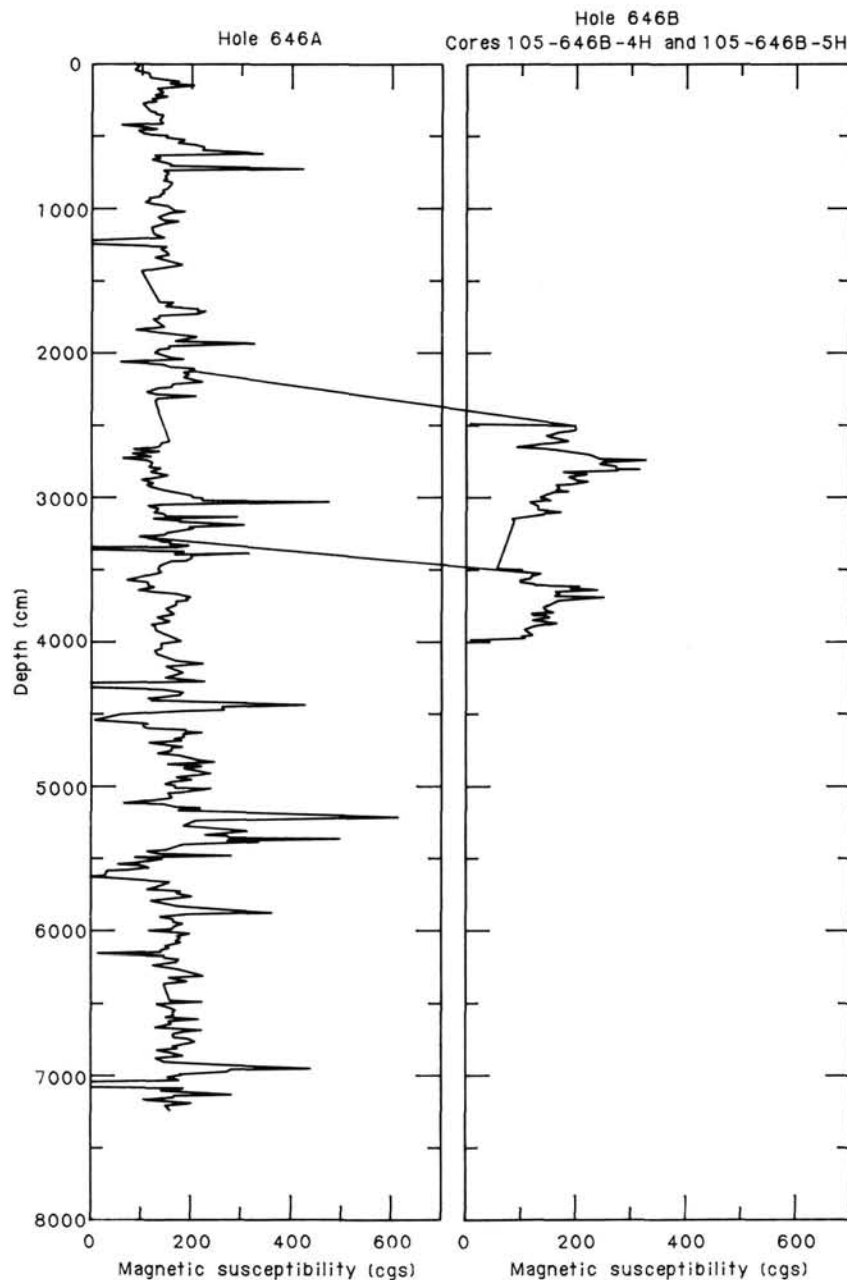


Figure 40. Correlation between Hole 646A and Cores 105-646B-4H and 105-646B-5H. Magnetic-susceptibility analysis was performed on Cores 105-646B-4H and 105-646B-5H. These data are compared with that of Hole 646A. The lines connecting the two graphs represent tie-points from Figure 13. The pattern of change for Core 105-646B-4H appears similar to the pattern for the similar lithology in Hole 646A. The pattern for Core 105-646B-5H is somewhat different from the similar lithology in Hole 646A, but the central spike in both holes represents a silt layer, perhaps deposited from the same event.

erage 1540 m/s, slightly higher than the velocity of sound in water. This is consistent with the high water contents and porosities in the upper section. Below 100 mbsf in Hole 646B, scatter in the measurements becomes more pronounced, but base-line values remain steady to approximately 300 mbsf. Velocity then begins a relatively regular increase with depth to values approaching 2100 m/s near the bottom of the hole. A slight decrease in gradient is indicated at about 475 mbsf.

Although no correlations exist between small-scale variations in velocity and index properties, a general relationship is observed. The gradual increase in velocity with depth clearly is re-

lated to the decline in water content and porosity and the corresponding increasing density of the sediment (Figs. 42 and 45).

Laboratory-measured velocity values tend to exhibit a greater degree of scatter than do those estimated from downhole seismic logs. Gradients with increasing depth and bulk density are similar in both data sets, although laboratory values are generally somewhat lower for equivalent depths and densities (see Fig. 45). A fairly obvious change in slope is evident in the plot of velocity versus density (Fig. 45) at approximately 1.9 g/cm^3 . This density corresponds to about 350 mbsf, where relatively large increases in velocity are observed, particularly in the sonic

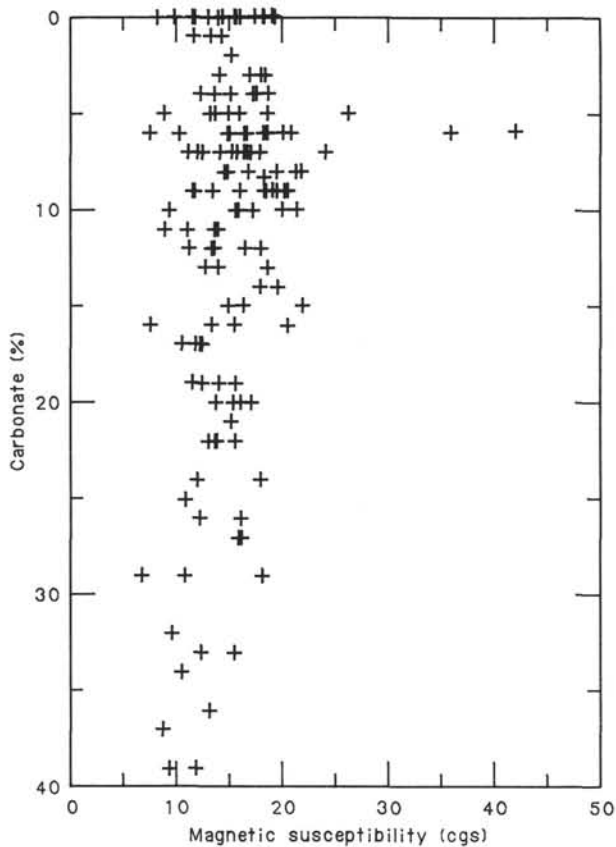


Figure 41. Magnetic susceptibility versus carbonate percentage. Magnetic-susceptibility measurements from the same location as samples used for carbonate analyses are plotted against carbonate percentage. This figure shows no apparent correlation between magnetic susceptibility and carbonate concentration, except perhaps at the high-carbonate range (>20%) where the susceptibility values appear to decrease. Therefore, variations in magnetic susceptibility cannot be the result of only a carbonate dilution effect.

log. This horizon also falls near the early/late Pliocene boundary and is probably a consequence of a similar increase in density resulting from a decrease in biogenic silica and an increase in calcium carbonate below 330 mbsf. Correlations between velocity and seismic reflectors are less prominent and are restricted primarily to gradual velocity increases over depth intervals above certain reflectors (e.g., see reflector R2 in Fig. 57).

Summary

The sediments at Site 646 are characterized by physical properties that are consistent with those determined for other terrigenous sediment sequences. Index properties indicate a relatively uniform dewatering of a sediment column and minimal lithologic variation. An interval of slightly coarser sediment between 140 and 340 mbsf displays somewhat anomalously low bulk density and density gradient. Hydraulic piston coring in Holes 646A and 646B recovered sediments having minimal disturbance. In these sediments, correlation of GRAPE density profiles between holes is possible, and shear-strength values appear accurate.

An increase in shear strength with decreasing water content is observed to depths of 130 mbsf. Below this level, shear strengths decrease possibly as a result of increased sediment disturbance from coring with the XCB system. Thermal-conductivity measurements were conducted regularly and used with sub-bottom temperature measurements in Hole 646A to estimate heat flow. The value determined, 1.68 HFU, is slightly higher

than reported values. Compressional-wave velocity measurements were generally successful and display a fairly steady increase with depth and increasing bulk density. Laboratory measurements tend to be somewhat less than those estimated from down-hole sonic logs, but trends are similar.

DOWNHOLE LOGGING

Downhole logging at Site 646 had two primary purposes: (1) to tie core depths to seismic reflectors through acquisition of reliable sonic velocities and calculation of a synthetic seismogram, and (2) to provide continuous records of lithologic and mineralogic variations. The tie between the cores and the seismic records was particularly important at this site, yet velocity measurements from sources other than logs are contradictory (see "Seismic Stratigraphy" section, this chapter). Poor core recovery and relatively uniform gross lithology hampered sedimentological determination of lithologic variations; downhole logging could detect subtler changes or cycles.

Two logging runs were planned: (1) LSS-DIL-GR-MCD, and (2) GST-CNTG-NGT. The capabilities and limitations of these logging tools are discussed in the "Explanatory Notes" chapter (this volume). The focus of the first run was on velocity (LSS), approximate clay percentage (GR), porosity (DIL), and hole conditions (MCD and LSS). The focus of the second run was on detailed mineralogy (GST and NGT) and porosity (CNTG). Eighteen hours were allotted for logging this site.

Operations

Logging-related operations at Site 646 began at 0800 local time on 12 October 1985. Thorough hole conditioning between 0800 and 1700 included pulling pipe to 100 mbsf and returning to hole bottom, four passes through a bridge 30 m above bottom, circulating, dropping the bit, and pulling pipe to 205 mbsf. This hole conditioning, in conjunction with the use of seawater instead of mud and the apparent lack of expanding clays, resulted in very good hole conditions. Better hole conditions than at Site 645 were anticipated on the basis of (1) more common occurrence at Site 645 of layers that are nearly 100% clay, (2) evidence of core expansion during sampling at Site 645 but not at Site 646, (3) use of mud and polymer at Site 645 but not at Site 646, (4) more thorough hole conditioning at Site 646, and (5) use of the large-diameter XCB bit at Site 646 but smaller-diameter rotary core bit at Site 645. A potential problem was the caving of dropstones from the upper 236 mbsf. These dropstones severely degraded core recovery and increased the amount of core disturbance. Further, they greatly increased the probability that the drill pipe would become stuck if left in one place without rotating or circulating. Thus we abandoned a tentative plan to log first with the GST combination through pipe.

The first tool run was the LSS combination. Logging down at 200 m/hr, all logs except waveforms were recorded from the open-hole interval of 205–742 mbsf. The wireline heave compensator (WHC) was then turned on, parameters were set up for the upward run, and the tool was lowered to set down at about 755 mbsf. The difference between this set-down depth and the deepest drill penetration of 766.7 mbsf implies the presence of about 12 m of cavings in the hole bottom. Recording of upgoing logs began at 751.8 mbsf at only 65 m/hr to test minimum winch speed, then continued at about 500 m/hr until pipe was reached. Only one small bridge was noted. Occurring near the hole bottom, this bridge registered a small increase in wireline tension on the upgoing log. We anticipated this bridge on the basis of hole-conditioning experience. Its only significant effect on operations was a slight decrease in data acquisition near the bottom of the hole on both logging runs, because of the danger that the tools would be trapped by cavings while in the short interval between the bridge and bottom.

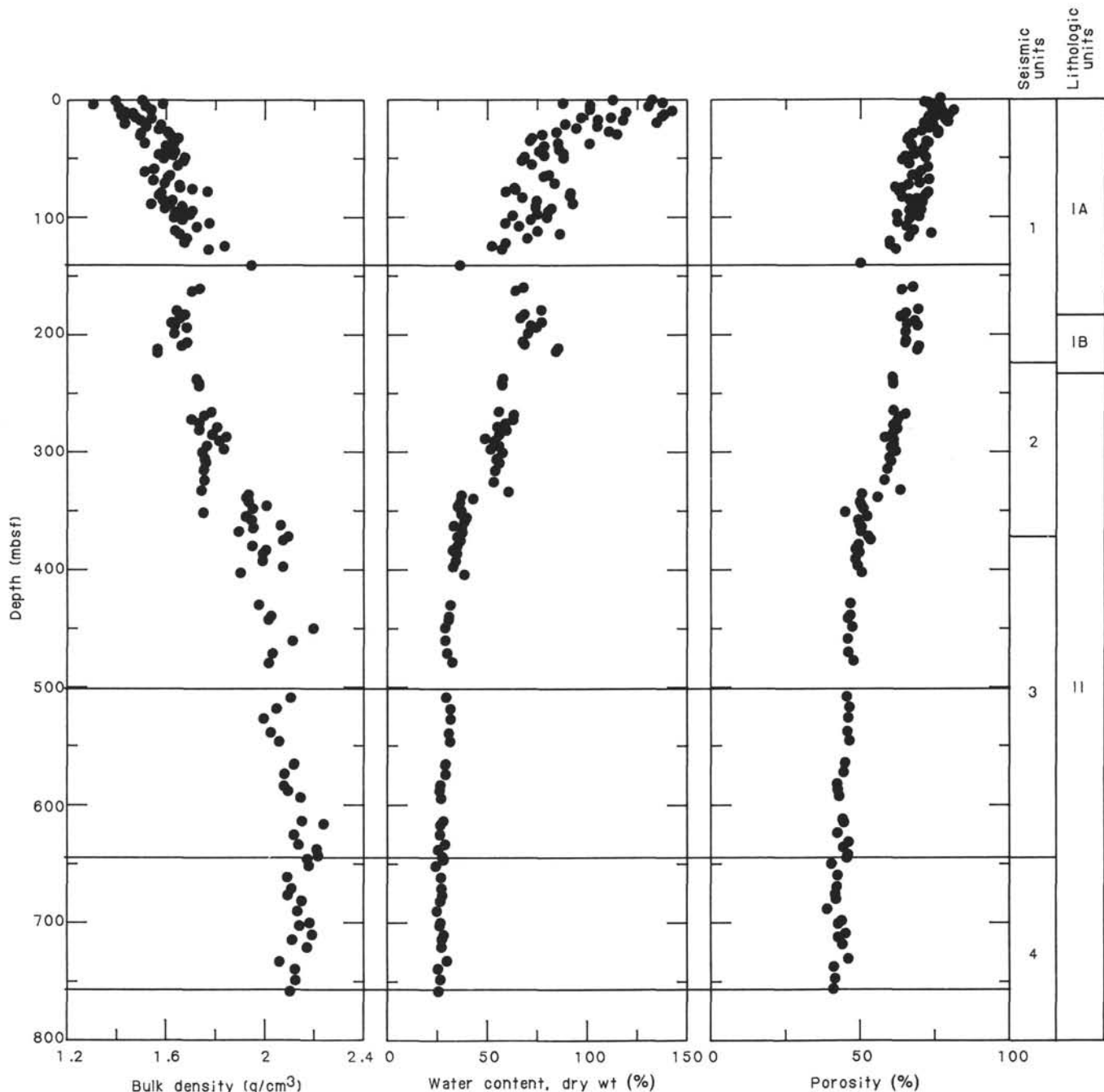


Figure 42. Vertical profiles of the variation of physical properties.

The second logging run, with the GST combination, was delayed by 1.5 hr because a kink was discovered in the wireline on deck. About 30 m of cable was cut off and the pigtail was rebuilt before the second run proceeded. To prevent unnecessary pipe irradiation, the GST was not turned on until 100 m into open hole. Calibrations were attempted first when the tool moved slowly upward and then when the tool stopped. All internal checks on GST calibration quality indicated only marginal reliability; attempts to improve quality failed. Therefore the decision was made to lower the tool rapidly to 362 mbsf and run two passes across an anticipated major lithologic and porosity change at about 340 mbsf. The two passes showed at least fair replication, so logging proceeded with continuation of the second pass

up into the pipe. Partway through this pass, the WHC developed a leak and was turned off. This second pass was terminated at 14 m above seafloor to provide porosity calibration points for the GST and CNTG; potassium, thorium, and uranium zero points for the NGT; and silicon, calcium, and salinity calibration points for the GST. The tool was then lowered at 1200 m/hr to bottom with the GST turned off. After lowering to 756 mbsf, the GST was turned on and recalibrated. Internal consistency tests now showed good quality, and logging up at 170 m/hr began from 743 mbsf. During this upward logging, repair to the WHC was completed and it was turned on. Data acquisition concluded at 234 mbsf. The interval within the pipe was not relogged because of insufficient radioactive cooling time

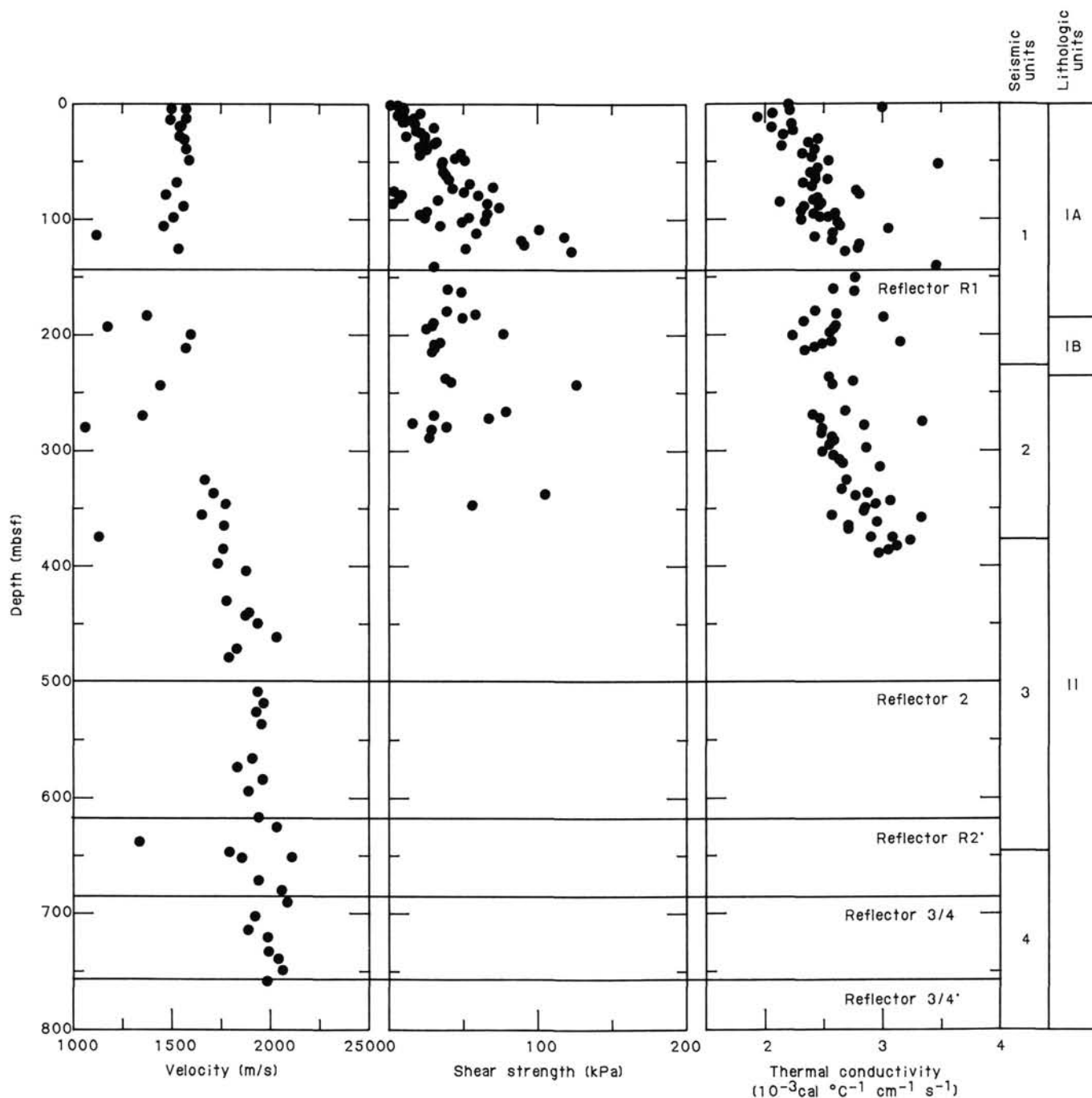


Figure 42 (continued).

(< 8 hr) before the pipe would arrive on deck. Final rig-down concluded at 1300 hr local time on 13 October 1985, 20 hr after initiation of logging rig-up.

Data Processing

Most logs require some processing or editing before they can be used reliably for interpretation of borehole properties. The most common form of editing is removal of inaccuracies caused by enlarged borehole diameter (washouts). At Site 646, excellent hole conditions resulted in little problem with washouts. Data processing at Site 646 included depth shifting, reprocessing of the sonic and GST logs, removal of GST effects on the spectral gamma-ray log, merging of different logging runs, and examination of pipe effects on logs.

Depth Shifting

Log depths are based on length of cable downhole. However, cable stretch or cable slip through the depth meter during lowering and raising of the logging tool can cause small and systematic depth errors. Both logging runs at Site 646 included a gamma-ray log, and comparison of these two logs permits depth justification between runs. Depths of lithologic horizons on the sonic combination run (Run 1) were systematically shallower than corresponding horizon depths on the GST combination run (Run 2). This discrepancy ranged from 2.75 m above 318 mbsf to 3.65 m below 500 mbsf. Consequently, all logs from the sonic run were depth shifted to remove this discrepancy. After depth shifting, relative depth accuracy between runs is about

Table 13. Physical-properties summary, Holes 646A and 646B.

Section	Depth (m)	Bulk density (g/cm ³)	Grain density (g/cm ³)	Water content dry wt. (%)	Porosity (%)	Shear strength (kPa)	Thermal conductivity (× 10 ⁻³ cal × cm ⁻¹ × s ⁻¹)	Velocity (m/s)
105-646A-1H-1	0.90						2.20	
105-646A-1H-1	1.01	1.39	2.74	134	78.5	2.18		
105-646A-1H-3	3.75	1.30	2.73	139	73.9	9.36	2.98	
105-646A-1H-3	4.32							1510
105-646A-2H-1	5.75	1.52	2.81	102	75.0	11.44	2.20	
105-646A-2H-3	8.75	1.54	2.77	102	75.9	22.06	2.06	
105-646A-2H-5	11.75	1.47	2.78	121	78.7	17.99	1.93	
105-646A-2H-5	12.17							1578
105-646A-2H-7	14.75	1.43	2.58	139	81.0			
105-646A-3H-1	17.40						2.22	
105-646A-3H-1	17.60	1.50	2.68	106	75.3	17.99		
105-646A-3H-3	19.52							1549
105-646A-3H-3	20.25	1.43	2.69	136	80.7	30.91	2.05	
105-646A-3H-5	23.00	1.52	2.82	106	76.0	19.61	2.23	
105-646A-4H-1	26.95						2.15	
105-646A-4H-1	27.60	1.61	2.92	85	72.2	12.92		
105-646A-4H-3	29.95	1.62	2.79	78	69.0	25.14	2.44	
105-646A-4H-3	30.67							1574
105-646A-4H-5	32.95	1.65	2.75	73	67.9	33.22	2.36	
105-646A-5H-1	36.47						2.14	
105-646A-5H-1	36.80	1.63	2.90	86	73.6	21.22		
105-646A-5H-3	38.81							1584
105-646A-5H-3	39.55						2.41	
105-646A-5H-3	39.60	1.60	2.73	79	68.9	26.30		
105-646A-5H-5	42.55	1.60	2.78	87	72.6	48.90	2.31	
105-646A-6H-1	46.25						2.38	
105-646A-6H-1	46.30	1.57	2.75	89	72.1	48.90		
105-646A-6H-1	48.51							1596
105-646A-6H-3	49.25	1.68	2.83	69	66.9	51.67	2.53	
105-646A-6H-5	52.25						3.46	
105-646A-6H-5	52.40	1.67	2.79	68	65.9	36.45		
105-646A-7H-1	55.60	1.65	2.80	73	68.2		2.45	
105-646A-7H-3	58.85	1.55	2.73	98	74.6	37.70	2.38	
105-646A-7H-5	61.85	1.51	2.55	95	71.8	39.20	2.42	
105-646A-7H-7	64.25	1.62	2.76	82	71.2		2.42	
105-646A-8H-1	65.55	1.61	2.74	79	69.1	41.06	2.52	
105-646A-8H-3	67.81							1537
105-646A-8H-3	68.55	1.55	2.74	98	75.0	55.62	2.32	
105-646A-8H-5	71.55	1.60	2.82	85	84.7	70.92	2.39	
105-646A-9H-1	75.15	1.66	2.77	64	63.0	5.97	2.76	
105-646A-9H-3	78.15	1.77	2.80	60	64.5	9.69	2.79	
105-646A-9H	78.87							1480
105-646A-9H-5	81.15	1.57	2.71	93	73.6	8.07	2.44	
105-646A-10H-1	84.85						2.13	
105-646A-10H-1	85.43	1.59	2.76	84	71.1	4.89		
105-646A-10H-3	87.85	1.62	2.76	83	71.7	45.21	2.45	
105-646A-10H-3	88.57							1570
105-646A-10H-5	90.85	1.67	2.78	75	69.8	35.84		
105-646A-11H-1	94.55	1.71	2.90	70	68.5	67.19	2.58	
105-646A-11H-3	97.55	1.68	2.90	76	70.5	54.50	2.53	
105-646A-11H-3	98.27							1520
105-646A-11H-5	100.55	1.64	2.51	81	71.5	64.95	2.30	
105-646B-1H-1	0.88	1.50	2.76	114	77.7	6.24		
105-646B-1H-3	3.70	1.58	2.75	89	72.9	11.03		
105-646B-1H-3	4.47							1580
105-646B-1H-5	6.75	1.41	2.74	132	78.2	8.43		
105-646B-2H-1	10.14	1.43	2.95	144	82.6	6.76		
105-646B-2H-3	12.85	1.42	2.69	140	80.8	10.82		
105-646B-2H-3	13.47							1500
105-646B-2H-5	15.68	1.54	2.71	98	74.4	10.19		
105-646B-3H-1	15.34	1.48	2.70	113	76.7	11.65		
105-646B-3H-3	18.15	1.50	2.75	119	79.7	18.10		
105-646B-3H-3	18.87							1556
105-646B-3H-5	20.99	1.58	2.72	90	73.0			
105-646B-4H-1	24.60	1.57	2.77	95	74.5	21.22		
105-646B-4H-3	27.85	1.50	2.97	112	77.7	24.68		
105-646B-4H-3	28.57							1548
105-646B-4H-5	30.25	1.49	2.53	116	78.0	24.91		
105-646B-5H-1	34.55	1.63	2.81	72	67.2	31.83		
105-646B-5H-3	37.55	1.51	2.40	102	74.6	25.84		
105-646B-6H-1	44.40	1.64	2.88	77	69.7	21.91		
105-646B-6H-3	47.15	1.63	2.75	79	70.1	44.98		
105-646B-6H-5	50.15	1.59	2.73	89	73.2	36.45		
105-646B-9H-1	73.25	1.66	2.71	72	67.7	43.83		
105-646B-9H-3	76.10	1.71	2.78	65	65.5	51.67		
105-646B-9H-5	79.15	1.58	2.95	93	74.8	60.90		
105-646B-10H-1	82.75						2.41	
105-646B-10H-1	82.95	1.67	2.76	68	65.8	33.97		
105-646B-10H-3	85.75	1.63	2.68	76	68.5	67.19	2.47	
105-646B-10H-5	88.75	1.54	2.69	94	73.1	75.40	2.33	
105-646B-11H-1	92.55						2.30	
105-646B-11H-1	92.75	1.60	2.66	84	71.2	26.50		
105-646B-11H-3	95.45	1.64	2.54	82	72.3	22.40	2.41	

Table 13 (continued).

Section	Depth (m)	Bulk density (g/cm ³)	Grain density (g/cm ³)	Water content dry wt. (%)	Porosity (%)	Shear strength (kPa)	Thermal conductivity ($\times 10^{-3}$ cal \times °C ⁻¹ \times cm ⁻¹ \times s ⁻¹)	Velocity (m/s)
105-646B-11H-5	98.40	1.70	2.77	63	64.2	25.38		
105-646B-11H-5	98.45						2.47	
105-646B-12H-1	102.12	1.67	2.72	73	68.4	50.02		
105-646B-12H-1	102.15						2.61	
105-646B-12H-3	105.02	1.78	2.85	60	64.8	35.83		
105-646B-12H-3	105.15						2.63	
105-646B-12H-3	105.87							1470
105-646B-12H-5	108.03						3.04	
105-646B-12H-5	108.27	1.73	2.79	67	67.5	102.28		
105-646B-13H-1	111.85	1.64	2.76	77	70.0	59.47	2.57	
105-646B-13H-3	114.12							1130
105-646B-13H-3	114.85	1.66	2.85	88	75.5	120.11	2.42	
105-646B-13H-5	117.85	1.69	2.70	71	68.4	90.96	2.56	
105-646B-14H-1	121.55	1.68	2.49	60	61.5	93.29	2.79	
105-646B-14H-3	124.52	1.84	2.84	53	62.2	52.48		
105-646B-14H-3	124.65						2.78	
105-646B-14H-3	125.27							1550
105-646B-14H-5	127.55	1.78	2.85	58	63.8	124.78	2.68	
105-646B-16X-1	140.61	1.95	2.75	37	51.8	31.48	3.45	
105-646B-17X-1	150.45						2.76	
105-646B-18X-1	160.40	1.74	2.90	69	69.5	41.52	2.58	
105-646B-18X-3	162.85	1.71	2.77	66	66.2	50.02	2.76	
105-646B-20X-1	179.25	1.65	2.75	79	71.2	40.31	2.43	
105-646B-20X-3	182.25	1.68	2.80	70	67.2	59.72	2.61	
105-646B-20X-3	182.97							1390
105-646B-20X-5	185.20	1.66	2.59	68	65.6	50.77		
105-646B-20X-5	185.25						3.00	
105-646B-21X-1	188.95						2.33	
105-646B-21X-1	189.18	1.63	2.80	79	70.2	31.36		
105-646B-21X-3	191.80	1.64	2.65	73	67.5	31.36		
105-646B-21X-3	191.95						2.60	
105-646B-21X-3	192.67							1190
105-646B-21X-4	193.40	1.69	2.74	76	71.2	26.88		
105-646B-21X-5	194.90						2.58	
105-646B-22X-1	198.55						2.55	
105-646B-22X-1	198.70	1.64	2.64	72	67.0	78.39		
105-646B-22X-1	199.27							1615
105-646B-22X-3	201.50						2.23	
105-646B-22X-6	206.05	1.69	2.84	69	67.2	35.84	2.56	
105-646B-22X-7	207.10						3.15	
105-646B-23X-1	208.25	1.67	2.77	70	67.1	32.10	2.49	
105-646B-23X-3	211.20							1590
105-646B-23X-3	211.25	1.57	2.69	87	71.6	32.48	2.42	
105-646B-23X-5	214.25	1.57	2.62	86	71.0	30.61	2.34	
105-646B-26X-1	237.25	1.73	2.71	59	62.7	39.57	2.55	
105-646B-26X-3	240.25	1.74	2.77	58	62.8	43.30	2.75	
105-646B-26X-5	243.15	1.74	2.71	59	62.9	129.16		
105-646B-26X-5	243.25						2.58	1460
105-646B-29X-1	266.02	1.79	2.84	57	63.2	80.46		
105-646B-29X-1	266.05						2.68	
105-646B-29X-3	268.90	1.76	2.89	65	67.4	31.49		
105-646B-29X-3	269.05						2.42	
105-646B-29X-3	269.71							1370
105-646B-29X-5	272.75						2.47	
105-646B-29X-5	272.07	1.71	2.67	64	65.1	68.80		
105-646B-30X-1	275.73	1.74	2.88	60	64.0	17.49		
105-646B-30X-1	275.75						3.33	
105-646B-30X-3	278.75						2.84	
105-646B-30X-3	278.78	1.81	2.58	56	63.0	40.31		
105-646B-30X-3	279.48							1080
105-646B-30X-5	281.75						2.49	
105-646B-30X-5	281.82	1.74	2.87	61	64.5	30.61		
105-646B-31X-1	285.45	1.79	2.90	57	63.2		2.48	
105-646B-31X-3	288.45						2.57	
105-646B-31X-3	288.49	1.85	2.91	50	60.1	28.37		
105-646B-31X-5	291.27	1.82	3.10	55	63.2			
105-646B-31X-5	291.45						2.59	
105-646B-32X-1	295.15	1.77	2.70	57	62.9		2.55	
105-646B-32X-3	298.01	1.84	2.80	53	62.1			
105-646B-32X-3	298.13						2.86	
105-646B-32X-5	301.12	1.75	2.82	59	63.6			
105-646B-32X-5	301.15						2.49	
105-646B-33X-1	304.80						2.58	
105-646B-33X-2	306.57	1.76	2.70	56	61.5			
105-646B-33X-3	307.85						2.63	
105-646B-33X-4	309.65	1.77	2.80	57	62.4			
105-646B-33X-5	310.85						2.66	
105-646B-34X-1	314.55						2.98	
105-646B-34X-2	316.48	1.76	1.56	55	60.9			
105-646B-35X-2	325.50						2.69	
105-646B-35X-2	325.65	1.76	2.78	54	59.9			
105-646B-35X-2	325.98							1683
105-646B-36X-1	333.85						2.65	

Table 13 (continued).

Section	Depth (m)	Bulk density (g/cm ³)	Grain density (g/cm ³)	Water content dry wt. (%)	Porosity (%)	Shear strength (kPa)	Thermal conductivity ($\times 10^{-3} \text{ cal} \times \text{cm}^{-1} \times \text{s}^{-1}$)	Velocity (m/s)
105-646B-36X-1	334.22	1.75	2.59	62	65.6			
105-646B-36X-3	337.00	1.94	2.73	38	52.1	107.28	2.87	
105-646B-36X-3	337.10							1732
105-646B-36X-5	339.85						2.77	
105-646B-36X-5	339.88	1.93	2.91	44	57.5			
105-646B-37X-1	343.49	1.94	2.79	37	51.5			
105-646B-37X-1	343.55						3.07	
105-646B-37X-3	346.55						2.94	
105-646B-37X-3	346.60							1792
105-646B-37X-3	346.65	2.01	2.70	36	52.0	58.31		
105-646B-37X-5	349.52	1.96	2.91	38	52.9		2.85	
105-646B-38X-1	352.70	1.76	2.70	38	46.8			
105-646B-38X-1	353.10						2.84	
105-646B-38X-3	356.09	1.93	2.79	41	54.1			
105-646B-38X-3	356.17						2.57	
105-646B-38X-3	356.20							1671
105-646B-38X-5	359.15						3.33	
105-646B-38X-5	359.24	1.95	2.77	40	51.0			
105-646B-39X-1	362.70	2.07	2.70	34	51.3		2.96	
105-646B-39X-3	365.67						2.71	
105-646B-39X-3	365.70	1.96	2.82	38	52.3			1783
105-646B-39X-5	368.71	1.90	2.77	39	52.1			
105-646B-39X-5	368.73						2.71	
105-646B-40X-1	372.45	2.10	2.96	36	54.6			
105-646B-40X-3	375.40						3.09	
105-646B-40X-3	375.55	2.08	2.92	38	55.5		2.90	
105-646B-40X-3	376.18							1150
105-646B-40X-5	378.45						3.24	
105-646B-40X-6	380.22	1.96	2.73	36	50.7			
105-646B-41X-2	383.59	2.01	2.78	34	50.0		3.13	
105-646B-41X-3	385.78							1780
105-646B-41X-4	386.54	2.00	2.74	36	51.5		3.05	
105-646B-41X-6	389.55						2.97	
105-646B-42X-2	392.45	2.00	2.84	35	50.2			
105-646B-42X-5	397.99	2.08	2.76	34	51.1			1750
105-646B-43X-3	404.07	1.91	2.77	40	52.8			1900
105-646B-46X-1	430.45							1799
105-646B-46X-1	430.49	1.98	2.73	33	48.5			
105-646B-47X-1	440.15	2.03	2.76	32	48.4			1914
105-646B-47X-C	442.94	2.02	2.76	32	47.5			1899
105-646B-48X-1	450.10	2.20	2.88	30	49.3			1959
105-646B-49X-2	460.80	2.12	2.79	30	47.7			
105-646B-49X-2	461.70							2053
105-646B-50X-3	471.93	2.04	2.79	31	47.7			1850
105-646B-51X-1	479.36	2.02	2.79	34	49.6			1810
105-646B-54X-C	509.40	2.11	2.82	30	46.9			1959
105-646B-55X-2	519.00	2.05	2.75	32	48.2			
105-646B-55X-2	519.15							1988
105-646B-56X-1	526.82							1948
105-646B-56X-1	527.60	2.00	2.66	32	47.6			
105-646B-57X-1	526.82							1979
105-646B-57X-3	539.56	2.03	2.77	31	47.4			
105-646B-58X-1	546.97	2.06	2.80	31	47.7			
105-646B-60X-2	566.16	2.12	2.85	29	46.2			1930
105-646B-61X-1	574.00	2.08	2.83	29	45.8			1849
105-646B-62X-1	584.13	2.08	2.73	27	43.8			1980
105-646B-62X-4	588.63	2.10	2.72	27	44.0			
105-646B-63X-1	594.30	2.15	2.72	27	44.5			1912
105-646B-65X-1	613.91	2.15	2.85	28	45.8			
105-646B-65X-4	616.93	2.24	2.92	27	46.2			1960
105-646B-66X-3	625.50	2.12	2.75	26	43.4			2050
105-646B-67X-2	633.69	2.14	2.99	29	47.3			
105-646B-67X-5	638.13	2.21	2.86	26	45.5			1351
105-646B-68X-2	643.88	2.22	2.95	28	47.2			
105-646B-68X-4	646.24	2.17	2.76	28	46.6			
105-646B-68X-4	646.35							1810
105-646B-69X-1	651.94	2.18	2.78	24	41.4			1875
105-646B-70X-1	651.18							2127
105-646B-70X-1	661.22	2.09	2.77	27	43.4			
105-646B-71X-1	671.38	2.11	2.69	27	43.1			1957
105-646B-71X-5	677.15	2.09	2.76	27	42.8			
105-646B-72X-2	680.05							2072
105-646B-72X-2	681.90	2.15	2.70	26	42.9			
105-646B-73X-1	690.25	2.13	2.77	24	40.0			2097
105-646B-74X-1	699.93	2.18	2.88	27	44.9			
105-646B-74X-3	702.60	2.14	2.71	26	43.6			1940
105-646B-75X-2	710.60	2.19	2.88	28	46.2			
105-646B-75X-4	714.07	2.11	2.72	27	43.6			1900
105-646B-76X-2	720.74	2.17	2.76	27	45.1			2000
105-646B-77X-4	732.73	2.06	2.76	30	46.9			2003
105-646B-78X-2	739.20	2.12	2.83	25	41.9			2054
105-646B-79X-1	748.69	2.12	2.80	26	42.3			2075
105-646B-80X-1	758.25	2.10	2.74	25	41.3			1992

Table 14. Laboratory-measured thermal conductivities (K_{lab}) and corresponding computed *in-situ* values ($K_{in situ}$), based on the equation of Williams et al. (1979), Hole 646A.

Depth	K_{lab}	$K_{in situ}$
0.9	2.19	2.13
3.8	2.98	2.90
5.8	2.20	2.13
8.8	2.06	2.00
11.8	1.93	1.87
17.4	2.22	2.16
20.3	2.05	1.99
23.0	2.23	2.17
27.0	2.15	2.09
30.0	2.44	2.38
33.0	2.36	2.30
36.5	2.14	2.09
39.5	2.41	2.35
42.5	2.31	2.25
46.3	2.38	2.32
49.3	2.53	2.47
52.3	3.46	3.38
55.6	2.45	2.40
58.8	2.38	2.33
61.8	2.42	2.37
64.3	2.42	2.37
65.6	2.52	2.47
68.6	2.32	2.27
71.6	2.39	2.34
75.2	2.76	2.71
78.2	2.79	2.74
81.2	2.43	2.39
84.8	2.13	2.10
87.8	2.45	2.41
94.6	2.58	2.54
97.6	2.53	2.49

0.2 m. Absolute depth accuracy is considered to be about 1 m, according to (1) log responses at the 205-mbsf base of pipe and (2) correspondence between the major porosity change at 335-mbsf logging depth and the physical-properties measurements of a similar change between 334.2 and 337.0 mbsf.

Sonic Reprocessing

We obtained excellent-quality raw sonic logs from Site 646. The almost identical values for short and long spacings of travel paths indicate both an absence of problems associated with cycle skipping and a lack of drilling-induced alteration of the borehole wall. The sonic log was reprocessed, using the procedure described in the Site 645 chapter (this volume). For nearly all the log, this reprocessing accomplished little more than an averaging of the short-spaced (DT) and long-spaced (DTL) sonic logs. Reprocessing did correct unreliable data in the topmost 2 m and bottommost 2 m of the logged interval.

GST Reprocessing

The initial GST log was fair to poor quality throughout because the recorded energy spectra were not a constant width throughout the logged interval. Local stretch and compression of the spectra caused the shipboard inversion software to yield an incorrect partitioning of the energy spectra among the six analyzed elements. Post-cruise reprocessing of this GST by R. Dove of Schlumberger included a detailed effort to remove the variability in spectrum width. This reprocessing resulted in a significant improvement in GST log quality, as evidenced by decreased data dispersion within each log and increased consistency with

core data. For example, the lithology-indicator ratio in Figure 46 is based on shipboard determination of the ratio of silicon counts to the sum of silicon and calcium counts. Comparison of this curve to the reprocessed silicon-indicator ratio (silicon counts divided by the sum of silicon, calcium, iron, and sulfur counts) of the log (preceding core-description forms, this chapter) indicates higher dispersion and sudden base-line shifts in the lithology-indicator ratio. Another example is the porosity-indicator-ratio plot of Figure 47, based on the shipboard analysis of the ratio of hydrogen counts to chlorine counts. Comparison of this curve to the neutron curve (Fig. 47) shows both character matches and mismatches. In contrast, correlation of reprocessed hydrogen counts with the neutron log (preceding core-description forms, this chapter) shows significantly closer correspondence.

The reprocessed GST still exhibits several warning signs of less than optimum reliability. The correlation between hydrogen counts and neutron log indicates that hydrogen count is a good porosity indicator, but chlorine count does not correlate with either hydrogen or neutron logs. Chlorinity of interstitial waters is approximately constant throughout Hole 646B (see "Inorganic Geochemistry" section, this chapter); therefore, porosity variations are expected to cause a high correlation between chlorine and hydrogen variations. The lack of an observed correlation between chlorine and hydrogen, coupled with an observed strong inverse correlation of chlorine with both calcium and iron, indicates that the chlorine log is unreliable. Possibly the "chlorine count" is actually a composite of several additional elements, beyond the other five elements solved by the algorithm.

A more significant problem with the GST is the apparent incorrect partitioning between calcium and iron. Trace amounts of pyrite throughout the cored interval suggest that iron should be low throughout the open-hole interval. Iron counts should be much higher in the pipe than in the open hole. Reprocessed iron counts do show a sudden drop at the 205-mbsf base of the pipe, but they also gradually increase beneath this depth to an approximately constant value below 440 mbsf, which is substantially higher than in pipe. Such an increase in iron counts with depth is inconsistent with pyrite variations indicated by both smear slides and GST sulfur counts. This pattern is similar to the observed increase in calcium carbonate from about 260 to 440 mbsf (see "Organic Geochemistry" section, this chapter), yet calcium counts exhibit only a subtle increase over this depth interval. Further, calcium counts exhibit consistently higher values in pipe than in open hole, as well as a positive correlation with pipe thickness, the opposite of the pattern expected for a reliable calcium log. Over short depth intervals, the correlation between calcium and iron is consistently high.

All these observations suggest that the inversion for elemental yields is partitioning incorrectly between iron and calcium. Consequently, iron and calcium counts were summed, then normalized by dividing by the sum of iron, calcium, silicon, sulfur, and background counts. This indicator ratio of iron plus calcium was converted to an approximate calcium-indicator ratio by removing base-line shifts associated with the high iron of the drill pipe and even higher iron of the bottom-hole assembly. Because core data indicate that calcium is much more common than iron, this final curve is considered to be primarily a calcium-indicator ratio (log preceding core-description forms, this chapter). The curve may be a better indicator of calcium variations over short distances than over long distances, but this entire log should be treated with caution.

Editing of NGT Logs

Most of the spectral gamma-ray (NGT) log appears to be reliably indicating variations in potassium, thorium, and uranium concentrations. However, two intervals exhibit artifacts associated with the logging procedure. First, through-pipe logs (<205

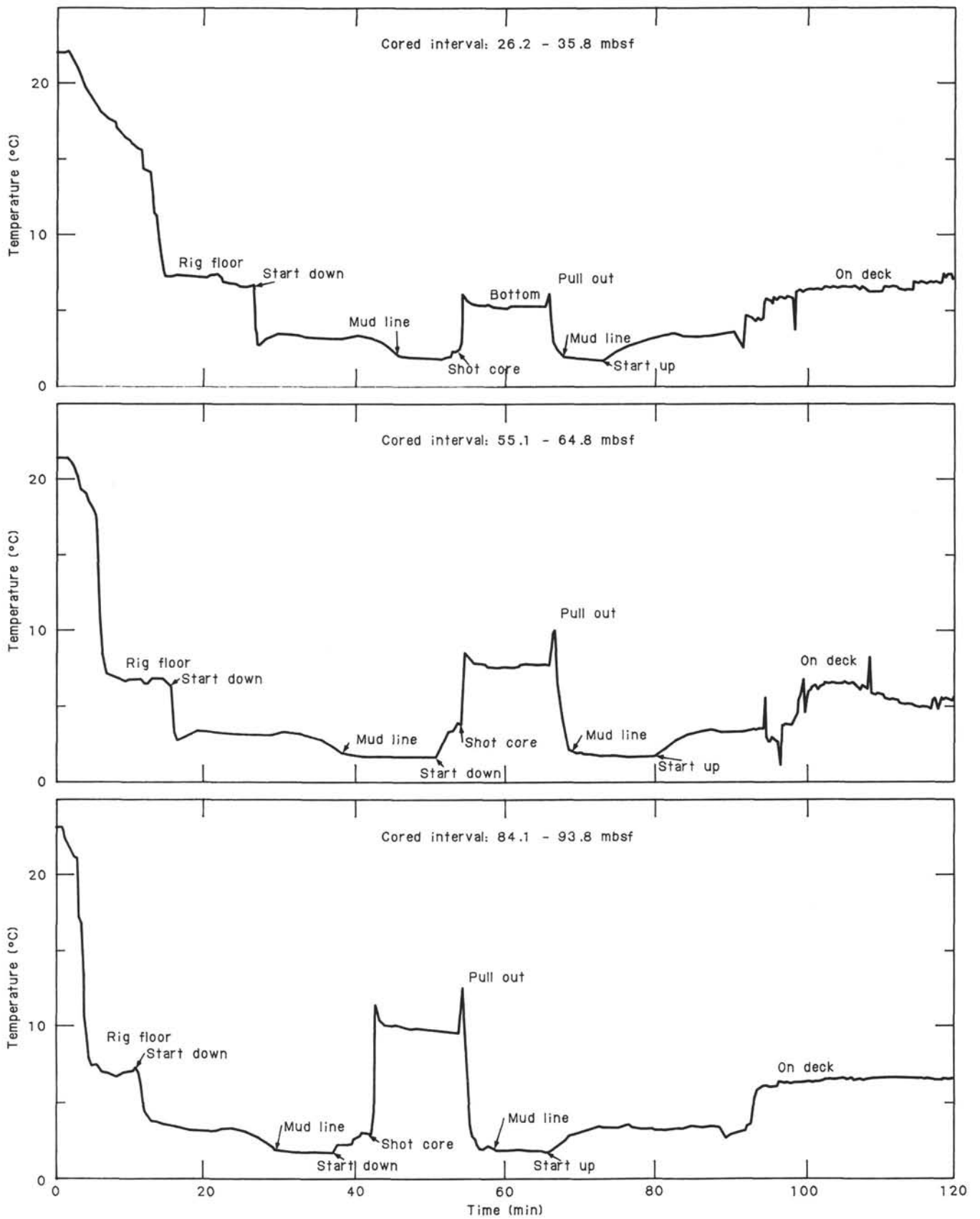


Figure 43. Downhole temperature measurements versus time, Cores 105-646A-4H, 105-646A-7H, and 105-646A-10H.

Table 15. Downhole temperature measurements, associated calculated geothermal gradients, and heat flow, Cores 105-646A-4H, 105-646A-7H, and 105-646A-10H.

Core	Measurement depth (m)	Temp. (°C)	dT/dz (°C/m)	Heat flow (mW/m ²)
105-646A-4H	35.8	5.334		
105-646A-7H	64.8	7.746		
105-646A-10H	93.8	9.742	0.076	73
		9.634	0.074	71.2
		9.60	0.070	67.5

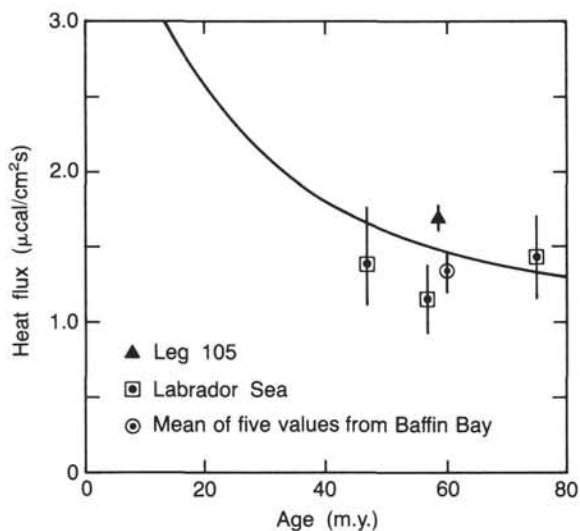


Figure 44. Heat flow versus age of crust. The line is a theoretical curve suggested by Sclater and Francheteau (1970); circled data points were reported by Pye and Hyndman (1972).

mbsf) are attenuated, as described in the next section. Second, the interval 290.2–357.6 mbsf was logged twice with the GST; the second and longer pass is shown in Figures 48 and 49 and the log (preceding core-description forms, this chapter). This interval exhibits a base-line upward shift of potassium, thorium, combined potassium and thorium (CGR), and probably of the thorium/potassium ratio, as well as a downward shift of uranium. These base-line shifts result from a memory effect in the formation of the previous activation of neutrons associated with the first GST pass. At depths of 292 and 298 mbsf, the GST tool was stopped for calibration tests during the first GST pass. These pauses cause large spikes in all NGT logs from the second pass; the spikes in the thorium/potassium ratio and potassium are shown in Figure 46. All edited NGT logs (preceding core-description forms, this chapter) have the spikes removed. However, only the CGR log has had the base-line shift removed, though a base-line shift of the thorium/potassium ratio, potassium, thorium, and uranium curves is appropriate before interpreting differences between the 290.2–357.6-m interval and the adjacent intervals.

Pipe Effects

The second Schlumberger logging run (GST/CNTG/NGT) collects useful data through the drill pipe (0–104 mbsf) and bottom-hole assembly (104–205 mbsf). All curves, however, are somewhat affected by the pipe. The neutron (CNTG) and spectral gamma-ray (NGT) logs are attenuated by passage of neutrons through steel, as are the hydrogen and chlorine counts of the GST. Greater steel thickness increases the GST count rates for

calcium, sulfur, silicon, and of course, iron. In addition to the base-line shifts of these logs at the junctions of pipe and bottom-hole assembly and of bottom-hole assembly and open-hole, narrow spikes occur at 10-m intervals throughout the upper 100 m, corresponding to pipe collars. These spikes are most evident on the hydrogen and neutron logs.

Approximate corrections for pipe were applied to the hydrogen- and calcium-indicator logs (preceding core-description forms, this chapter) by application of base-line shifts for the intervals of 0–104 and 104–205 mbsf. A similar adjustment is appropriate but not applied in CGR, uranium, thorium, potassium, and neutron logs (preceding core-description forms, this chapter). Adjustment of the silica-indicator and sulfur-indicator logs was not applied and is probably not necessary because steel thickness affects the numerator and denominator of each of these ratios by similar percentages. No attempt was made to correct any log for pipe collars because the amplitudes of these spikes show no obvious coherent pattern.

Lithologic Horizons

The sedimentary sequence at Site 646 is marked by several horizons determined on the basis of paleontology (“Biostratigraphy” section, this chapter), lithology (“Sedimentology” section, this chapter), physical properties (“Physical Properties” section, this chapter), or seismic reflectors (“Seismic Stratigraphy” section, this chapter). Changes in a variety of log responses can be used to characterize more fully the nature of these horizons, as well as possibly identify additional significant horizons or lithologic changes. This section examines such changes downhole, beginning at the seafloor. It should be noted that description of a log change as decreasing refers to only the downhole change; this corresponds to an increase with time.

A change from Lithologic Subunit IB to Unit II was placed at about 235–240 mbsf (“Sedimentology” section, this chapter), associated with the base of sediments having numerous dropstones. This boundary may also be the top of seismic unit 2 (“Seismic Stratigraphy” section, this chapter).

A thin unit rich in sand-sized grains forms the lowest part of Subunit IB. The log interval from 227 to 236 mbsf may represent this sandier unit, which on the GST log (preceding core-description forms, this chapter) exhibits lower sulfur and silicon and higher raw iron counts than surrounding intervals. The lower half of this 9-m interval is lower in clay mineral concentration and higher in porosity (from resistivity logs) than bracketing intervals.

The largest change in log responses observable at Site 646 occurs at 335.8 mbsf, corresponding to a change from biogenic silica (diatoms) to biogenic calcite. Several logs show significant base-line shifts at this horizon. A 7% porosity drop here is visible in physical-properties measurements (Fig. 47), associated with a density increase from 1.75 to 1.95 g/cm³ (“Physical Properties” section, this chapter). This porosity increase is even larger in a porosity log created from resistivity, though in other parts of the hole the resistivity porosities agree generally with physical properties (Fig. 47). In contrast, the porosity decrease is small in the GST porosity-indicator ratio and is absent from both neutron porosities and GST hydrogen counts (Figs. 47 and log preceding core-description forms, this chapter). All three of the later porosity indicators detect hydrogen rather than directly detect pore water; thus they cannot distinguish between bound water in clays and free water in pores. These varied porosity responses suggest that total water does not change at the boundary but that the proportion of bound water does increase below the boundary.

The possible increase in bound water could reflect either an increase in clay mineral percentages or a change in type of clay minerals. An increase in total amount of clay minerals is sug-

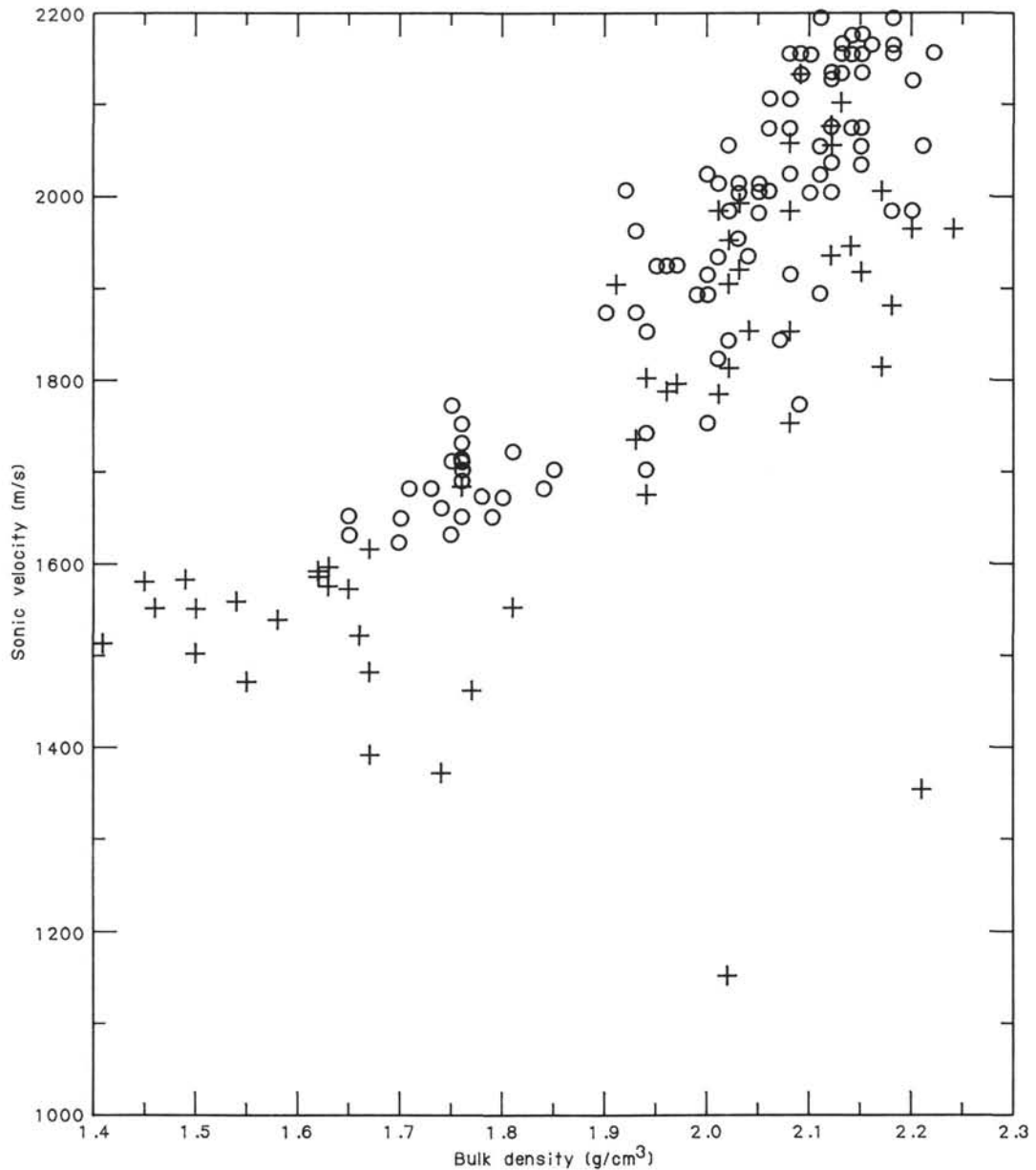


Figure 45. Compressional wave velocity versus bulk density. Plus symbol represents laboratory measurement; Circle corresponds to velocity estimated from sonic log. All bulk-density values are gravimetrically determined.

gested by a base-line shift in the gamma-ray log at this depth (Figs. 46 and 49). However, a change in relative proportions among the different types of clay minerals could also cause this base-line shift. More detailed clay typing through log analysis constrained by X-ray diffraction is required to quantitatively characterize the changes.

Two other significant log changes occur at the 335.8-m boundary: the GST lithology indicator decreases (Fig. 46) and sonic velocities increase (Fig. 48). The GST lithology indicator, which is an uncalibrated measure of the amount of silicon relative to calcium plus silicon, is probably responding to the increase in biogenic calcium carbonate. The drop in diatom concentration has little effect on this lithology indicator because most of the total silicon is present in quartz and clays.

The increase in sonic velocities is accompanied by a major change in the cyclicity of porosity and velocity variations and increases in both frequency and amplitude of variations (Fig.

48). An interval of rapidly fluctuating velocities from 335.8 to 385 mbsf is marked by a wavelength of about 3–6 m in sonic, porosity, and gamma-ray responses (Fig. 49). Cyclical variations in clay mineral percentage are probably causing the porosity variations, whereas both the porosity and mineralogy variations directly affect sonic velocities. The highest velocities and lowest porosities are associated with the clay-rich layers in this interval. This pattern does not hold for the entire hole; for example, in the interval from 280 to 335.8 mbsf, the clay-rich layers have lower velocities and higher porosities than surrounding sediments.

A thin clay-rich bed occurs at 544–549 mbsf. High gamma-ray response, low velocity, high-resistivity porosity, high neutron porosity, high Th/K, and low potassium suggest that this bed may be uncommonly rich in chlorite or montmorillonite.

The rapidly fluctuating velocities and clay percentages noted for the interval from 335.8 to 385 mbsf continue with much smaller amplitude variations but similar frequency down to a

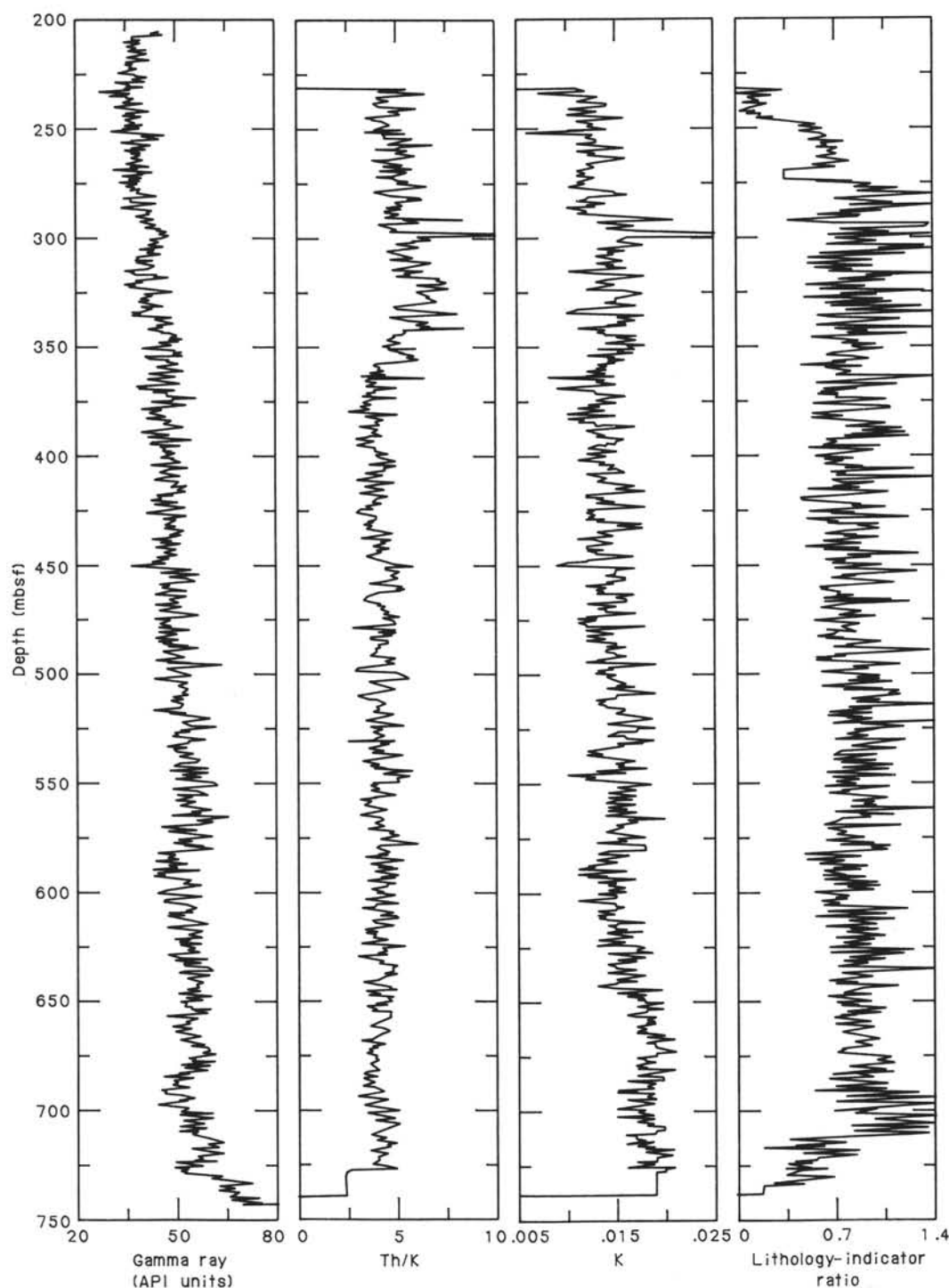


Figure 46. Gamma-ray (GR, API units), thorium/potassium ratio (Th/K, $\times 10^{-4}$), potassium (%K), and lithology-indicator-ratio (silicon counts/silicon plus calcium counts) logs for the open-hole interval, Site 646.

depth of 681 mbsf. Below this depth, a further decrease in amplitude variations occurs. The association between high velocities and low-porosity clay-rich intervals is much poorer than farther uphole, probably because clay mineral composition is fluctuating.

From 712 to 730 mbsf, a silty unit was identified in the cores. This unit is marked on the logs by low velocities, higher resistivity porosities, higher silicon-indicator ratio, and lower calcium-indicator ratio. No consistent change in clay mineralogy is indicated by the thorium/potassium ratio or by potassium content.

A higher uranium content gives the illusion of higher clay content to the gamma-ray response.

The deepest log-response change at Site 646 occurs at 730 mbsf, where a major apparent increase in clay content is visible on the gamma-ray log, accompanied by a modest velocity increase. Unfortunately, the GST combination logging run did not extend sufficiently far below this boundary to confirm the nature of the lithologic change. Uncommonly high clay mineral content is indirectly indicated by the hole-conditioning operations, which encountered the only bridge at Site 646 in this in-

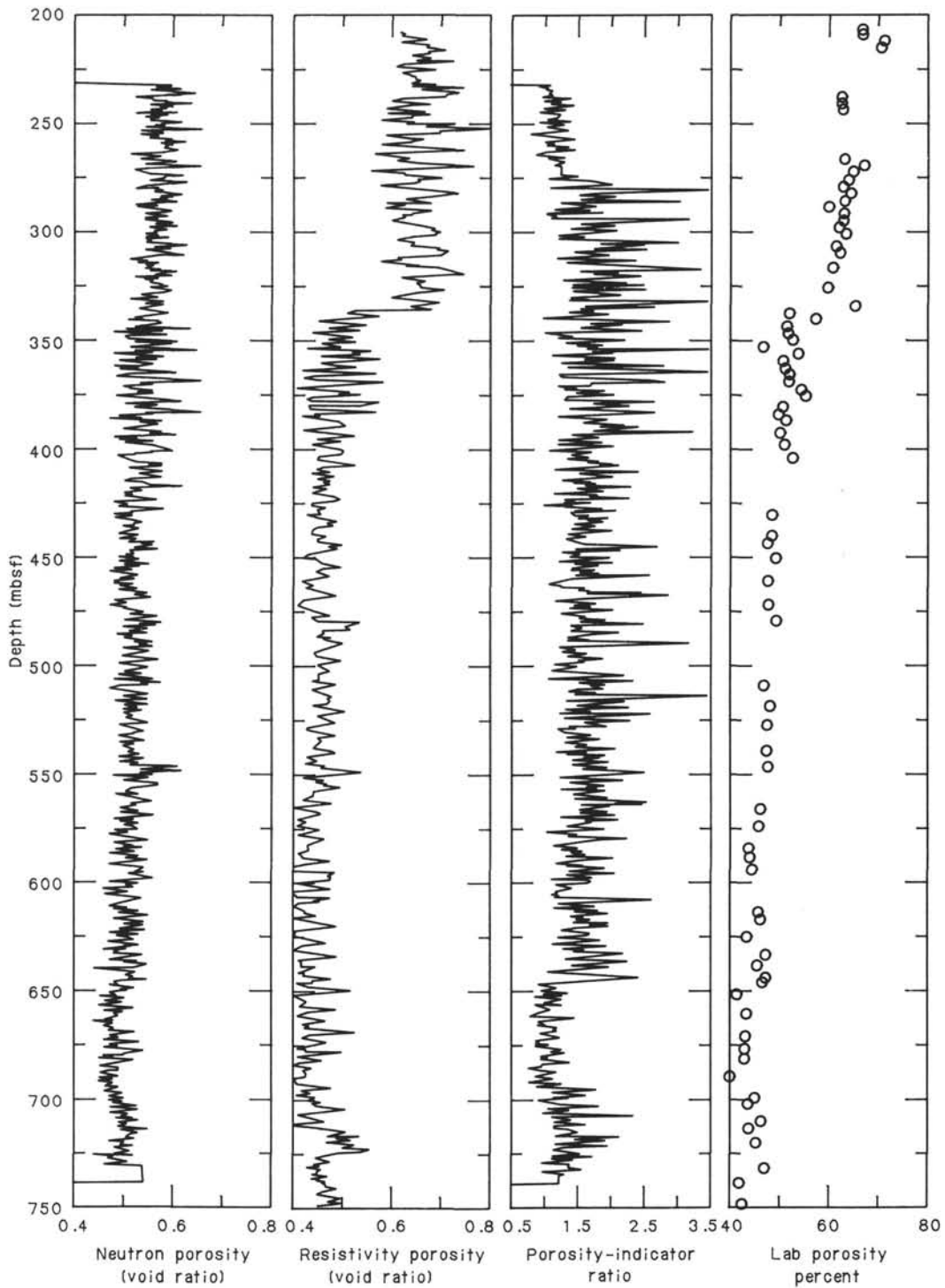


Figure 47. Comparison of four porosity logs: neutron porosity, estimated porosity from resistivity, porosity-indicator ratio (hydrogen counts/silicon plus calcium counts), and laboratory porosities of discrete core samples (from "Physical Properties" section, this chapter). Note that all logs except porosity-indicator ratio are scaled identically. Note also the general similarity of different logs, except near 340 mbsf.

terval. The presence of a unit rich in expanding clays is the most straightforward explanation for the reappearance of this bridge during logging, several hours after it was removed by the drill pipe.

Sediment Velocities

The long-spaced sonic tool provided excellent velocities for the entire interval between 205 and 739.8 mbsf (Fig. 48). The 8-

10 ft and 10-12 ft logs agree almost exactly for nearly the entire interval, indicating an absence of cycle skipping, borehole alteration, and noise tripping except in the short intervals of 205-207.9 and 732.1-738.5 mbsf. The sonic analysis program described in the Site 645 report (this volume) was used on the entire log, but only these two intervals showed substantial change.

As previously discussed, the effect of lithology on velocity at Site 646 is complex and varies with depth. Porosity changes are

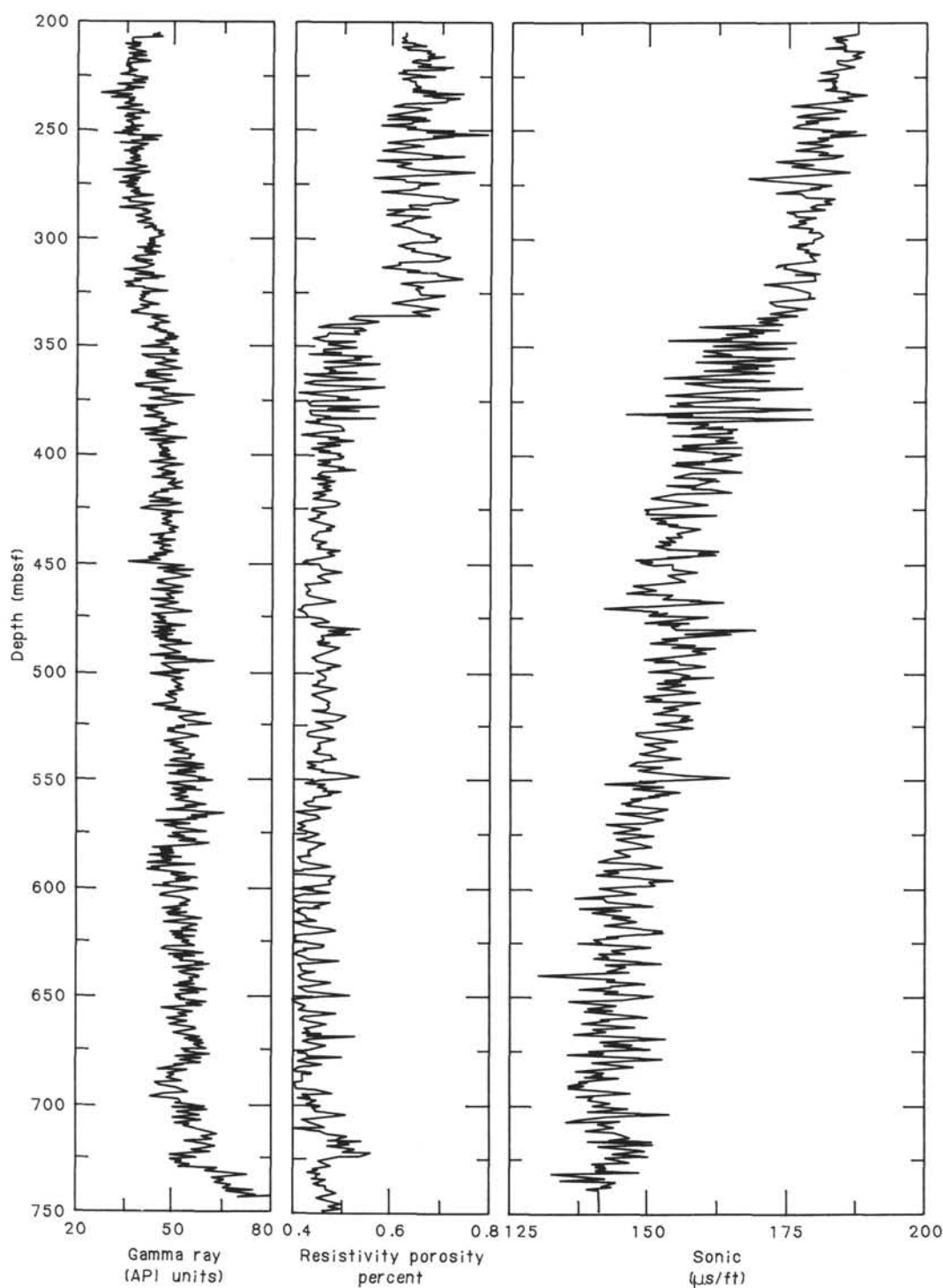


Figure 48. Sonic slowness ($\mu\text{s}/\text{ft}$) and two major factors that may control or influence velocity: porosity (shown calculated from resistivity logs) and clay content (as indicated by gamma-ray log).

a more direct cause of velocity variations. This relationship is well illustrated by the correlation between porosity (from resistivity logs) and velocity (Fig. 49). Figure 50 shows that a different relation appears to exist for the slow, high-porosity sediments above 336 mbsf than for the sediments below that horizon. To examine other factors influencing sediment velocities, the simple dominating porosity effect first must be removed.

Sonic velocities throughout the logged interval are much less than predicted by the equation of Wyllie et al. (1956) for a con-

solidated sediment in which the primary mineralogy is quartz plus calcite (Fig. 50). Raymer et al. (1980) empirically revised the Wyllie equation to predict velocities for porosities $>25\%$ more accurately. As shown by Fig. 50, Site 646 porosities and slowness are more consistent with this relation than with that of Wyllie. Departures from the empirical curve of Raymer et al. (1980) are probably attributable to two factors. First, the Raymer curve is largely an interpolation based on very few data for the porosity range of Figure 49. Second, the Raymer curve is

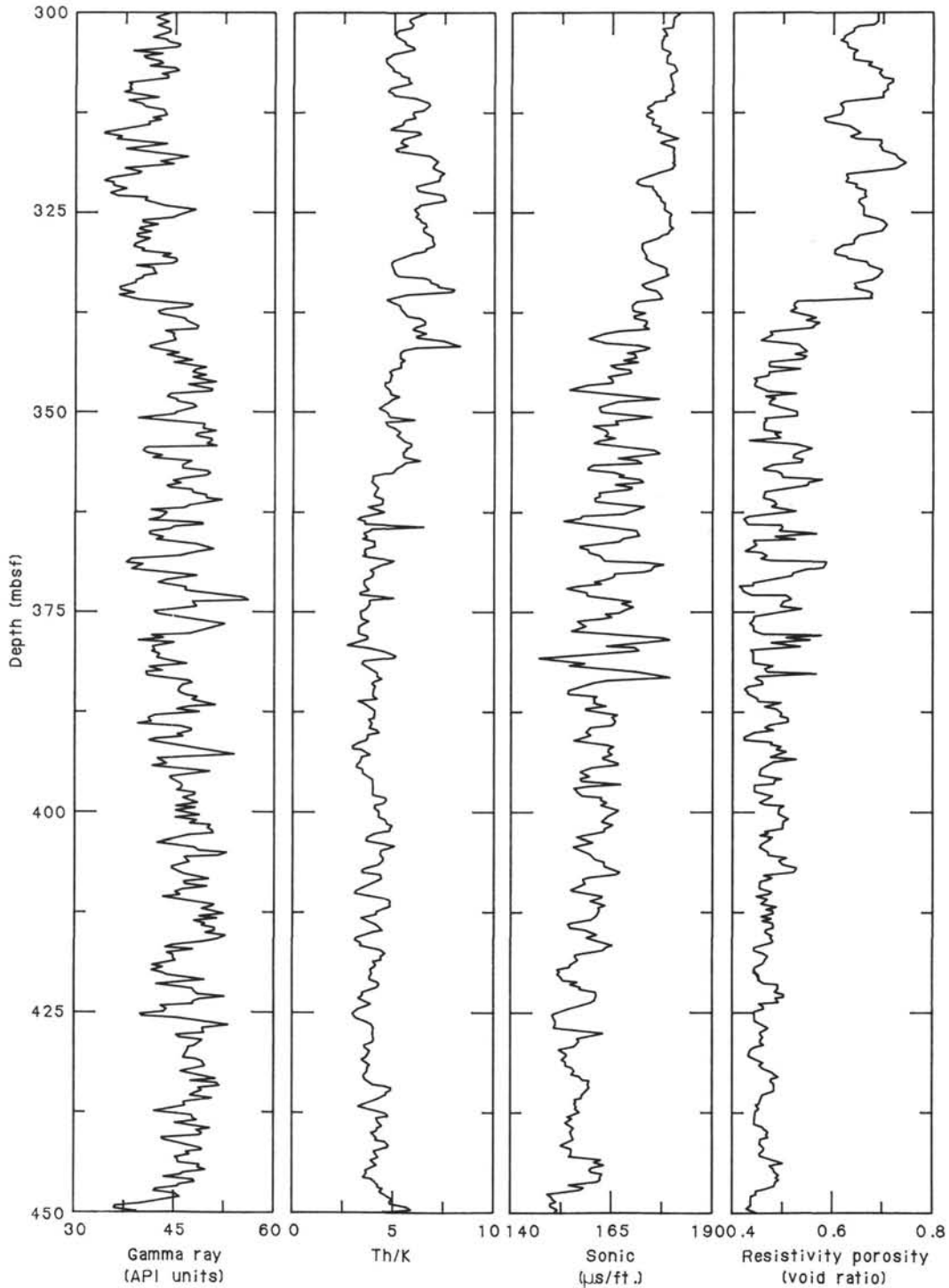


Figure 49. Expanded composite of an interval of Figures 46 and 48, showing the correlation among log responses near the 336-mbsf discontinuity.

made on the basis of quartz sands, yet the mineralogy at Site 646 is considerably more complex.

Synthetic Seismogram

The edited sonic log for 205–739.8 mbsf was used to calculate a synthetic seismogram for Site 646 (Fig. 51). No density logging was attempted at this site, but physical-properties measurements of density are highly correlated ($R = 0.91$) with log values of slowness (“Physical Properties” section, this chapter).

Thus, a constant-density synthetic seismogram can be calculated, with confidence that the sonic log has captured all important impedance variations.

The calculated synthetic seismogram is a one-dimensional convolution, including internal multiples. Attenuation and spherical divergence were not included; thus the synthetic seismogram is most appropriately compared to seismic data that have a low noise and automatic gain control. The starting time of the synthetic seismogram is arbitrary; however, traveltimes from the start to deeper reflectors should be accurate.

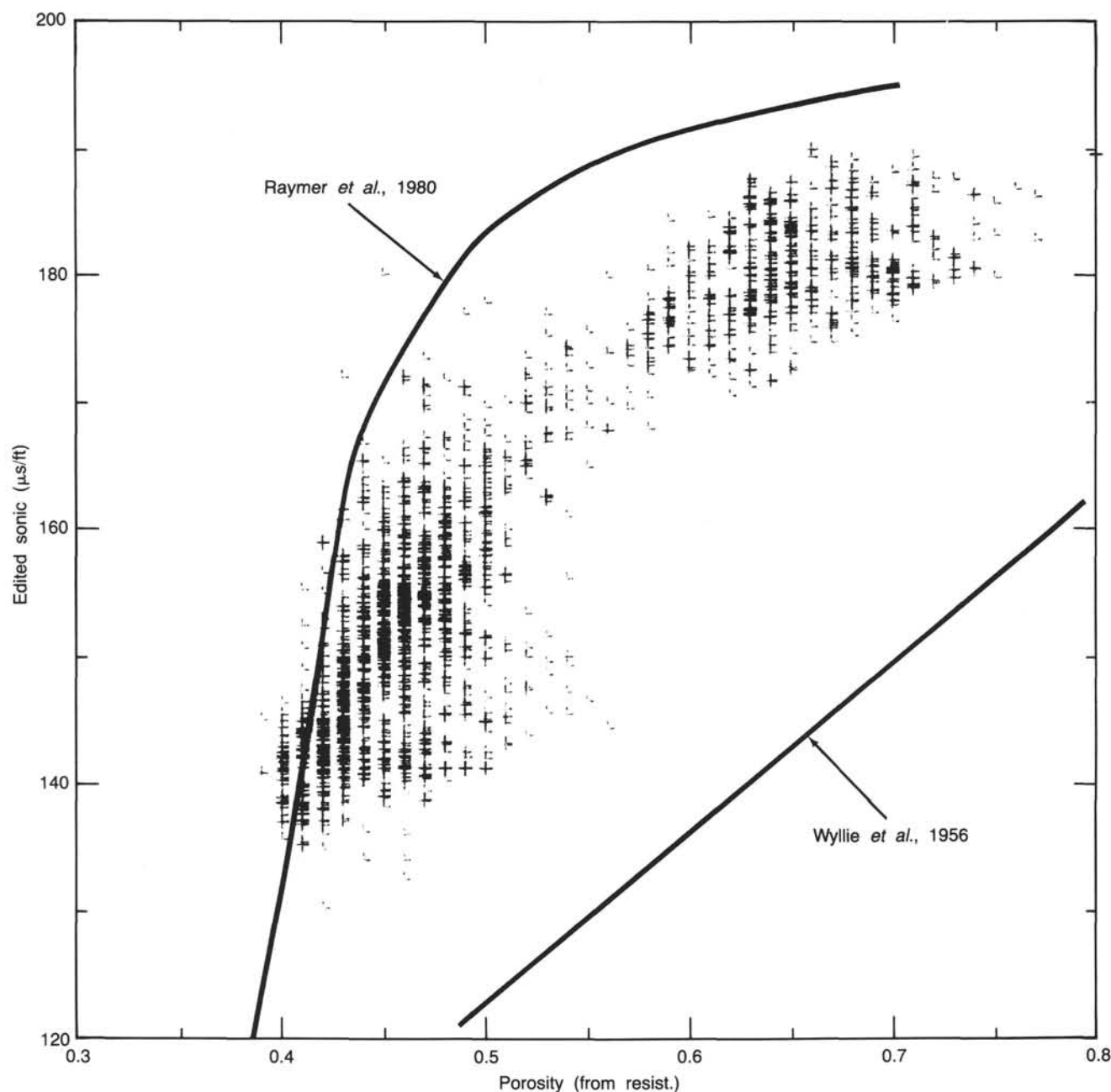


Figure 50. Crossplot of porosity (calculated from resistivity) versus sonic slowness. Note the strong overall correlation, indicating porosity control of velocity variations at this site. Note also the bimodal distribution, resulting from the significant increase in porosity at 336 mbsf. These data are clearly more consistent with the empirical relation of Raymer et al. (1980) than with that of Wyllie et al. (1956).

A 25-Hz zero-phase Ricker wavelet was used in the convolution. This wavelet is probably approximately correct for comparison to a nearby multichannel line. However, the single-channel line that crosses the site undoubtedly has a somewhat more complex wavelet. Therefore, comparison of small reflectors on the seismic line to the synthetic seismogram should be treated with caution.

The short wavelength nature of most velocity variations at the site causes almost all peaks and troughs on the synthetic seismogram to be thin-bed interference patterns. A notable exception is the peak at 336 mbsf, which is caused by a sudden base-line shift downhole toward faster velocities. This shift is

even more apparent in physical-properties measurements of bulk density ("Physical Properties" section, this chapter); thus the peak may be larger than shown. The lowest peak and associated trough on the synthetic seismogram are primarily caused by a 10-m-thick unit described as a silt in the core-description form. This high-porosity unit may be low in clay minerals, as shown in the core descriptions; the high gamma-ray response is caused by uranium rather than by clay minerals. Just above this peak-trough pair, the even larger peak at 690 mbsf apparently results primarily from the gradual velocity increase caused by porosity decrease and clay increase beneath a pair of thin silty(?) beds at 670 and 679 mbsf.

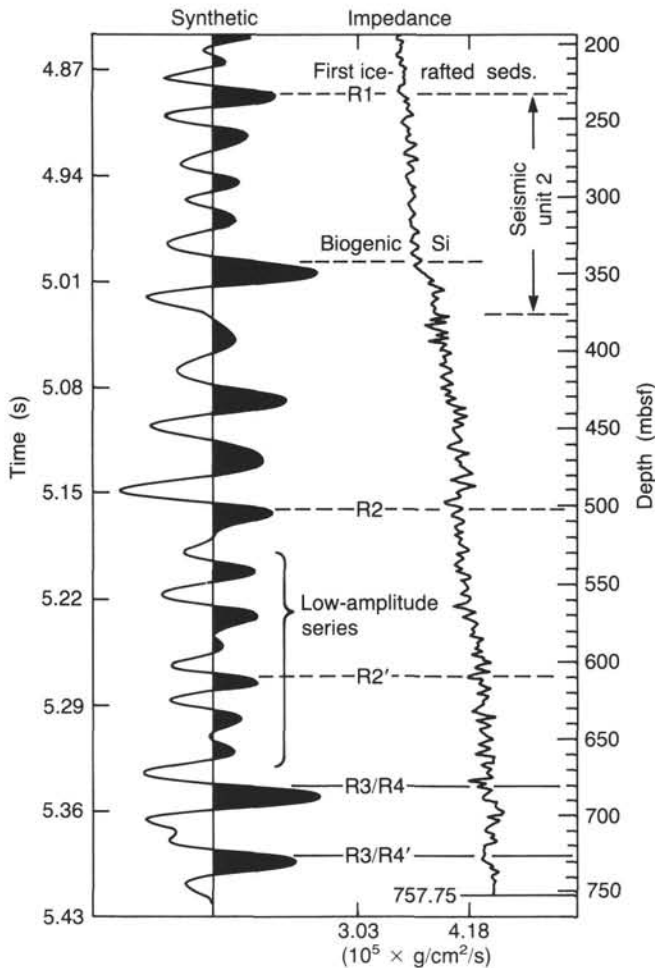


Figure 51. Synthetic seismogram from sonic-log data, Site 646 (see "Downhole Measurements" section, this chapter). Note impedance contrasts and variable amplitudes of reflectors. The synthetic seismogram was constructed assuming constant density across intervals of changing velocity, an assumption that is valid for most intervals, according to inspection of geophysical data.

A comparison of the synthetic seismogram with seismic data near Site 646 is included in the "Seismic Stratigraphy" section (this chapter).

SEISMIC STRATIGRAPHY

Site 646 is located on *Hudson* 84-30 line 14 at 1110 hr, day 222 (Fig. 3, "Background and Objectives" section, this chapter). Examination of this and numerous other lines shot in this region (Figs. 3, 52, and 53) shows the presence of many prominent reflectors. We divided the reflector sequence into four main units according to their uniformity, continuity, and seismic characteristics, as described briefly in "Background and Objectives" (this chapter). Here we discuss the correlation among the drilling results, major reflectors, and seismic units near the site and for the southeastern Labrador Sea as a whole. The implications of this correlation are illustrated for the Eirik Ridge. Because of the previous lack of stratigraphic control, the evolution of Eirik Ridge could not be deciphered.

In addition to the four major seismic units, we identified several reflectors within each unit. We tentatively correlated them with physical-properties measurements made on the cores recovered at this site. For calculations of the depth to each reflector, we used the sonic velocities as obtained from the sonic log (Ta-

ble 16A). Comparison of the velocities obtained from the sonobuoy measurements in this region with those obtained from the log shows good agreement between the two (Table 16A). Seismic records show the presence of high-amplitude reflectors (inferred high-impedance contrasts) at the site (Figs. 52 and 53). Cores from Site 646 neither exhibit drastic lithologic differences across various seismic boundaries as defined here nor do the sonic logs exhibit major steps in velocity. Hence, some of the differences in the acoustic impedance must arise from density and porosity variations. However, a synthetic seismogram (Fig. 51), generated using the sonic log (LLS package) and a "constant density" assumption (see "Downhole Logging" section, this chapter), exhibits impedance contrasts and reflectors of varying amplitudes that fairly closely match the pulse character observed in the multichannel seismic record (Fig. 53). The correlation of the reflector depths with changes in lithology, physical properties, and biostratigraphy (Fig. 54) is surprisingly good. These correlations are discussed as follows for each seismic unit.

Seismic Unit 1

Seismic unit 1 is the uppermost interval of the seismic units and varies in thickness from 0.20 to 0.40 s in the region adjacent to Site 646. At the site, it is about 0.28 s (250 m) thick and comprises moderate- to high-amplitude reflectors that are parallel to subparallel to the seafloor. The thinnest part of the unit occurs at the subsidiary ridge just south of Site 646; at this point, the amplitude of the reflectors also decreases somewhat. The base of the unit lies at a depth of 222 mbsf, marked by a very high amplitude reflector, R1, forming the top of seismic unit 2. R1 correlates well with the bottom of Lithologic Subunit IB (depth 235 mbsf), marking the bottommost occurrence of dropstones. The unit consists predominantly of silty clays and clayey silts and significant amounts of biogenic components. Some sandy layers occur in the lower part. The prominent reflectors as seen throughout this unit probably arise from local variations in the relative proportions of carbonate and clay. Variations in density and porosity profiles resulting from measurements on discrete sediment samples correlate well with the calculated depths to individual reflectors. For example, note the change in density and porosity at the Pleistocene/Pliocene boundary, which gives rise to a moderate-amplitude reflector. Similarly, a marked change in the rate of decrease of water content and porosity and increase in density with depth at 75 mbsf depth correlates well with the occurrence of a pronounced reflector at this depth. Reflectors generally are much more prominent in the upper part of seismic unit 1. These reflectors are late Pleistocene in age (Fig. 53), and may indicate the degree of glacial material present, similar to that observed at Site 645 in Baffin Bay.

The bottom of seismic unit 1 is conformable with the top of seismic unit 2 at the drill site (Fig. 52); however south and east of the site, the two units are separated by an unconformity where the basal reflectors onlap the top of seismic unit 2. The southern end of line 14 in Figure 52 clearly shows a prominent unconformity marked by a prominent reflector, R1, between the two units at the base of an erosional depression. No sonic log data are available from the upper 200 m of the hole for detailed comparison, and the synthetic seismogram cannot accurately depict reflector strength without such data.

Seismic Unit 2

Seismic unit 2 consists of many very high amplitude, parallel to subparallel reflectors that resemble the style expected from a sequence of turbidites. The unit occurs between 0.27 and 0.45 s bsf (about 222–377 mbsf) at Site 646 and thickens to the south, where it reaches a maximum thickness of 0.27 s (about 250 m). Seismic unit 2 has a lenticular shape and comprises a series of slightly northward-dipping subparallel reflectors near the site on

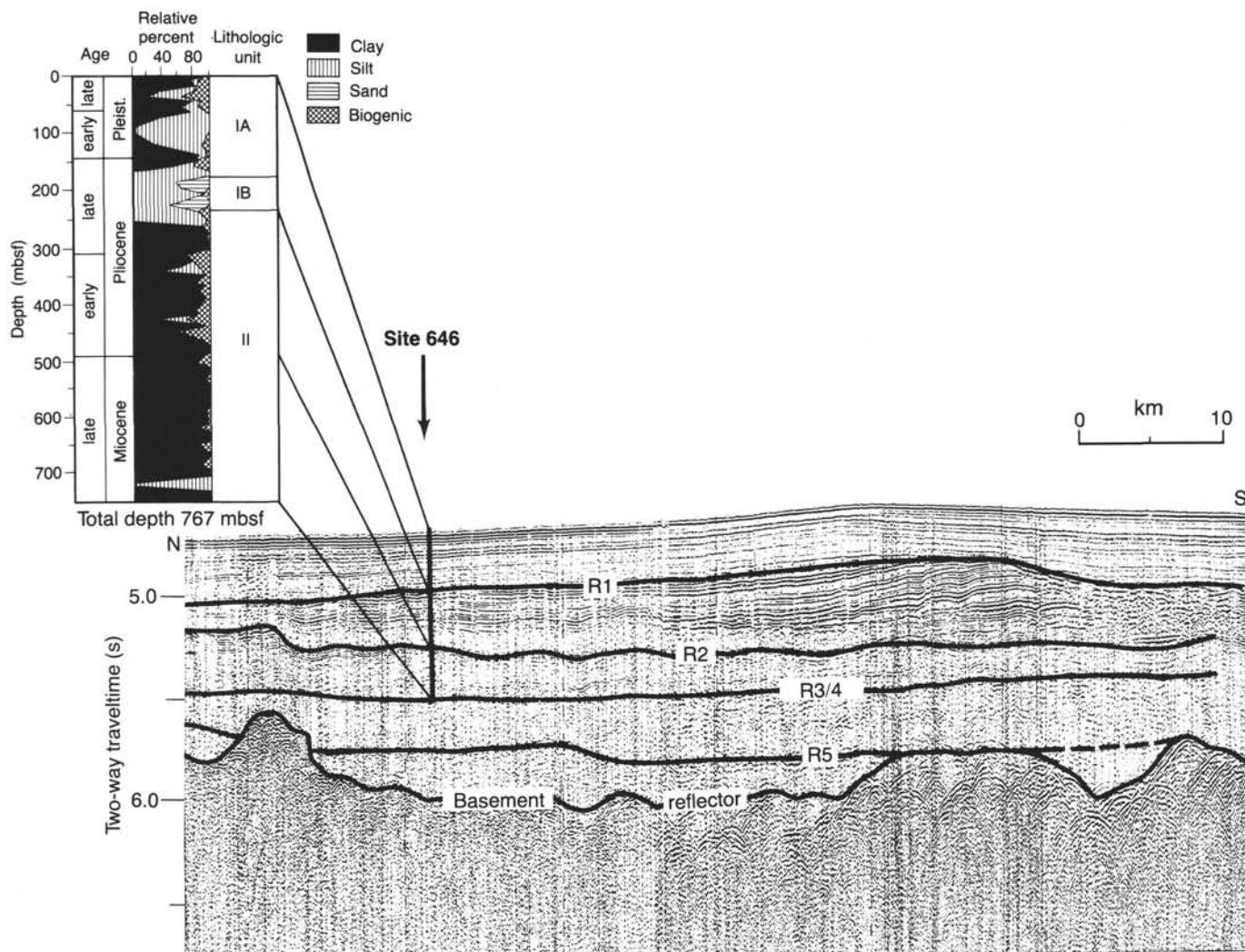


Figure 52. Part of seismic line (HD 84-30, line 14) that crosses Site 646. For location of the site, see Figure 1 ("Background and Objectives" section, this chapter). Shown also here are the major lithological and age units and suggested correlations to the seismic line, at ODP Site 646.

line 14 (Fig. 52). Thicknesses between individual reflectors vary systematically. At many places, migrating sediment waves are visible, indicating a strong influence of bottom currents on the deposition of sediments. Seismic unit 2 seems to have been deposited during a massive influx of sediments, possibly as the result of the same depositional regime that produced the pronounced depositional ridge seen in line 14 (Fig. 52). Seismic unit 2 comprises predominantly silty clays and clayey silts with subordinate, relatively nannofossil-rich beds of the upper part of Lithologic Unit II. The bottom of seismic unit 2 lies conformably on top of seismic unit 3 near Site 646, but, in general, seismic unit 2 is separated from the underlying seismic unit 3 by an erosional unconformity. The seismic expression of the seismic unit 2/3 contact suggests an irregular thickness of the upper part of seismic unit 3 above reflector R2 and therefore indicates possible erosion at the seismic unit 2/3 contact. However, no evidence of a hiatus exists in the stratigraphy across this interval at Site 646.

Density and porosity measurements made on discrete samples from the part of Lithologic Unit II equivalent to seismic unit 2 show variations that may be correlated with depth to various reflectors (Fig. 54). The unit comprises sediments of late to early Pliocene age. Sonic logs exhibit only small changes in velocity in this interval (Table 16B), but substantial reflectors were

generated in a synthetic seismogram (Fig. 51); the most significant occurred at about 340 mbsf. This reflector at 340 mbsf probably represents a pronounced change in physical properties of the sediment, which results from an increase in the proportion of frustules and skeletons of diatoms and radiolarians above this depth and an increase in carbonate content below.

Seismic Unit 3

Seismic unit 3 consists of continuous to discontinuous reflectors. The single-channel profiles exhibit low-amplitude reflectors compared with those in seismic unit 2. However, multichannel data indicate reflectors of moderate amplitude (Fig. 53). Seismic unit 3 lies conformably to unconformably over seismic unit 4, as seen in the multichannel data (Fig. 53). Such character is difficult to see in the single-channel data because of the lack of resolution through this interval. The calculated depth to an important regional reflector, R2, which lies at a depth of 0.05 s (about 502 mbsf) from the top of seismic unit 3, correlates well with the depth of the Miocene/Pliocene boundary (520 mbsf) at Site 646 (Fig. 51). Density and porosity measurements show only small variations and can be related to the changes in the amplitude of the resulting reflectors (e.g., at 0.72 s depth in Fig. 54; see also Fig. 51). The base of this unit is marked by the pres-

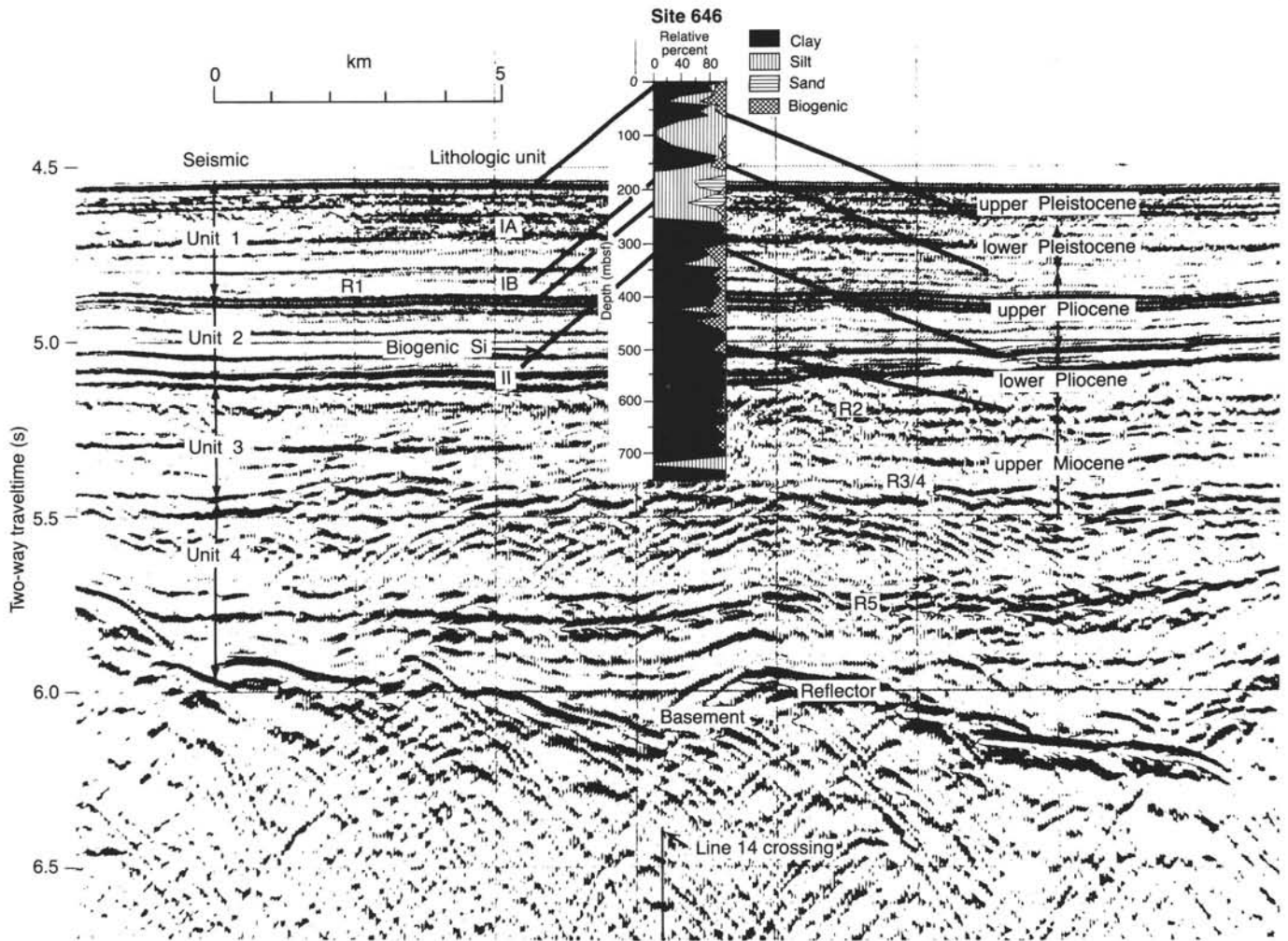


Figure 53. Part of the multichannel line (BGR-2) (Fig. 56) that crosses line 14 (Fig. 52) just south of ODP Site 646. Shown here are the correlations to lithologic units, the seismic units, and the biostratigraphic units as obtained from the drilling results at Site 646.

ence of a high-amplitude reflector doublet that is underlain by many diffractions and is interpreted here as being the R3/R4 reflector.

Seismic Unit 4

Seismic unit 4, the bottommost unit, the top of which lies at a depth of 0.82 s at Site 646, extends downward to the top of the fairly prominent basement reflector that is the top of the oceanic crust at roughly 1.3 s near Site 646. The top of seismic unit 4 is marked by the R3/R4 reflector, which is actually two strong reflectors separated by about 0.05 s and is presumed to be equivalent in age or just younger than the R4 reflector in the northeast Atlantic (Roberts et al., 1979; Miller and Tucholke, 1983). This reflector is assumed to represent the onset of seafloor erosion during the latest Eocene and early Oligocene, which occurred when the Greenland-Scotland Ridge subsided enough to allow overflow of Arctic waters, initiating the formation and rapid circulation of bottom water in the North Atlantic (Berggren and Schnitker, 1983; Miller and Tucholke, 1983). We believe that we recovered only the top 80–90 m of seismic unit 4 below the first reflector of the R3/R4 doublet at Site 646. No marked lithologic change occurs in the 680–730-mbsf interval although sharp changes occur in carbonate content below 680 mbsf and carbonate content decreases sharply to <5% below 695 mbsf.

No velocity measurements are available from laboratory physical-properties studies for the critical 680–730-mbsf interval. Core recovery was generally poor. Fortunately, borehole sonic, resistivity, and gamma-ray logs were run to within 15 m of the bottom of the hole and demonstrated some recognizable but not major changes in rock properties from 680 mbsf to 750 mbsf.

The velocity data from the sonic log were used to generate a synthetic seismogram (Fig. 51), which exhibits two high-amplitude reflectors that occur somewhat shallower (680 and 730 mbsf) than the depth we calculated for R3/R4 (755 mbsf). However, the character of the generated pulse is similar to that of the top of R3/R4 reflector and to a companion reflector (R3/R4') that consistently occurs in the seismic lines at about 0.05 s deeper than the main R3/R4 reflector. The actual seismic pulse is a sharp but moderate positive pulse followed by a broad strong negative pulse and a second strong positive pulse. The synthetic pulse character is similar but suggests that the top reflector is a stronger positive event. The difference in character may simply be the result of the frequencies used in generating the synthetic signal as well as the result of the assumption of constant density across the interval. In fact, the physical-properties data (Fig. 54; "Physical Properties" section, this chapter) show a corresponding small but significant increase in porosity and water content and a decrease in density from about 680 to 730 mbsf. We think

Table 16. Interval velocities and depths to major reflectors.**A. Velocities from sonic logs compared to sonobuoy measurements.**

Reflector depth (two-way travelt ime)	Sonic velocity		Sonobuoy velocity	
		Average velocity (km/s)	Reflector depth (two-way travelt ime)	Average velocity
0		1.47	0	1.47
0.09		1.58	0.54	1.77
0.185	Unit I	1.62		
0.275		1.63	0.86	2.05
0.31		1.68		
0.40	Unit II	1.78	1.20	2.35
0.45		1.83		
0.58		1.93	>1.4	2.40
0.72	Unit III	2.05		
0.82		2.15		

B. Calculated depths, probable depths, and nature of major reflectors cored at Site 646.

Reflector depth (two-way travelt ime)	Average velocity (km/s)	Calculated ^a depth (mbsf)	Probable ^b depth (mbsf)	Comments
0	0(1.49)	—	0	Seafloor
0.09	1.58	71	80	Change in CaCO ₃ content
0.185	1.62	148	144	Plio/Pleistocene boundary
R1	0.275	222	236	Top Lith. Unit II
	0.31	251	252	?
	0.40	331	335	Biogenic Si out/CaCO ₃ in
	0.45	377	377	Bottom seismic unit 2
R2	0.58	502	520	Mio/Pliocene boundary
	0.72	646	615	?
R3/4	0.82	754	680/730	Bottom "drift sequence" (reflector doublet)

^a Calculated depth to reflectors using velocity profile as shown, based on integration of sonic log velocities at Site 646.

^b Probable depth based on inferences from lithologic changes and physical-properties data from Site 646 and results of a synthetic seismogram that utilized data from geophysical logs.

that these data strongly support the contention that we drilled through and dated the R3/R4 reflector at Site 646. Additional information from micropaleontologic studies ("Biostratigraphy" section, this chapter) indicate important changes in the benthic fauna and in preservation and abundance of calcareous planktonic microfossils at 680 mbsf. The implications of this are discussed in the following text and in the "Summary and Conclusions" section (this chapter).

A large hiatus probably exists in the sequence beneath the base of Hole 646B. From the age of the crust that underlies this region (time of magnetic anomaly 24, 55–56 m.y.) and the constraint on the youngest age imposed by our drilling results, seismic unit 4 should contain sediments from late Miocene to early Eocene in age. These constraints indicate, however, that the sedimentation rates must be much lower than that indicated in the lower part of seismic unit 3 (49 m/yr, Fig. 28) or that a significant hiatus must exist in seismic unit 4. A prominent reflector, R5, lies at a depth of 1.25 s bsf within this unit (Fig. 53) and terminates to the west against a basement high of early middle Eocene age, as obtained from magnetic-anomaly identification. The drilling results clearly show that the R3/R4 reflector previously identified by Miller (1982) is not older than early late Miocene and is not equivalent to the R4 reflector of the northeast Atlantic. Furthermore, the R2 reflector occurs near the late Miocene/early Pliocene boundary and signifies the onset of strong bottom-water circulation in the southeastern Labrador Sea.

Discussion

The seismic stratigraphy outlined in previous text provides a means by which we can further interpret the depositional his-

tory in the region. The history of bottom-water circulation and the development of the Eirik Ridge is of primary interest in the southeastern Labrador Sea. We are able to carry our seismic-well ties to the Eirik Ridge through correlations between Hudson line 14, which crosses Site 646 and intersects the multichannel line BGR-2 roughly 16 km south (Fig. 9), through BGR-2 and to a second multichannel line, BGR-1, that runs northwest-southeast, perpendicular to the axis of Eirik Ridge. Two segments of line BGR-1 (Figs. 55 and 56) illustrate the correlations and the continuity of reflection characteristics and major seismic units of Site 646 across Eirik Ridge and to the south in the IMOC region of relatively flat seafloor topography.

The seismic line (Fig. 55) and the basement contour map (Fig. 9) demonstrate that Eirik Ridge is a constructional sedimentary feature, located where it was influenced by the interaction of roughly southwestward-flowing contour currents and having a topography inherited from the basement. A fairly steep southeast-facing slope exists between the younger crust of the extinct spreading center east of the Leif fracture zone, which is now deeply subsided, and the older, more elevated crust on the southwest Greenland margin, which is probably transitional between oceanic and continental crust and/or is partly a constructional volcanic edifice.

A relatively constant thickness of sedimentary strata (about 2 s thick) drapes this basement topography, but most of the existing seafloor relief results from the buildup of the depositional ridge that occurs above the R2 reflector. Because the R2 reflector was dated at Site 646 as being the top of the Miocene and we have no reason to expect that it is of different age here, we think that the major drift-building episode occurred during the early Pliocene to Holocene. No evidence of significant thickness variations exists in underlying units, except where they have been truncated in thickness by erosion, or, as at the lower part of seismic unit 4 (probable Eocene age), where strata have progressively overlapped basement during subsidence.

We have no definitive way to identify a reflector equivalent to R4 elsewhere in the eastern North Atlantic (Roberts, Schnitker, et al., 1984; Miller and Tucholke, 1983) that might represent a period of intensified erosion of the seafloor during the late Eocene and early Oligocene. Reflector R3/R4 in the Eirik Ridge region is of late Miocene age and corresponds to a brief hiatus overlain by sediment of 7.4 Ma age at Site 646. Strata below R3/R4 cored in Site 646 are also of late Miocene age, and therefore much of the upper part of seismic unit 4 below the R3/R4 reflector may also be Miocene in age. No evidence of differential erosion exists beneath any of the reflectors within seismic unit 4, but this does not preclude a substantial hiatus. Undoubtedly, however, the rates of sedimentation below the upper part of seismic unit 4 must be slower than those in the upper Miocene to Holocene interval above (49 m/m.y.).

We can construct the following tentative depositional history of Eirik Ridge and environs on the basis of our seismic interpretations:

1. Deposition of seismic unit 4 filled troughs in the region and progressively overlapped and draped the basement. The top of seismic unit 4 is late Miocene in age, so that this depositional interval probably encompasses the middle Eocene to late Miocene. The seismic records show no major variations in thickness between any two reflectors in the sequence. Therefore, we have no evidence of either major erosional episodes or episodes of construction of current-influenced sedimentary bodies during seismic unit 4 deposition.

2. Deposition of seismic unit 3 occurred during the upper part of the late Miocene and earliest Pliocene. The base of seismic unit 3 is conformable to disconformable with underlying seismic unit 4. A significant change in the rate of sedimenta-

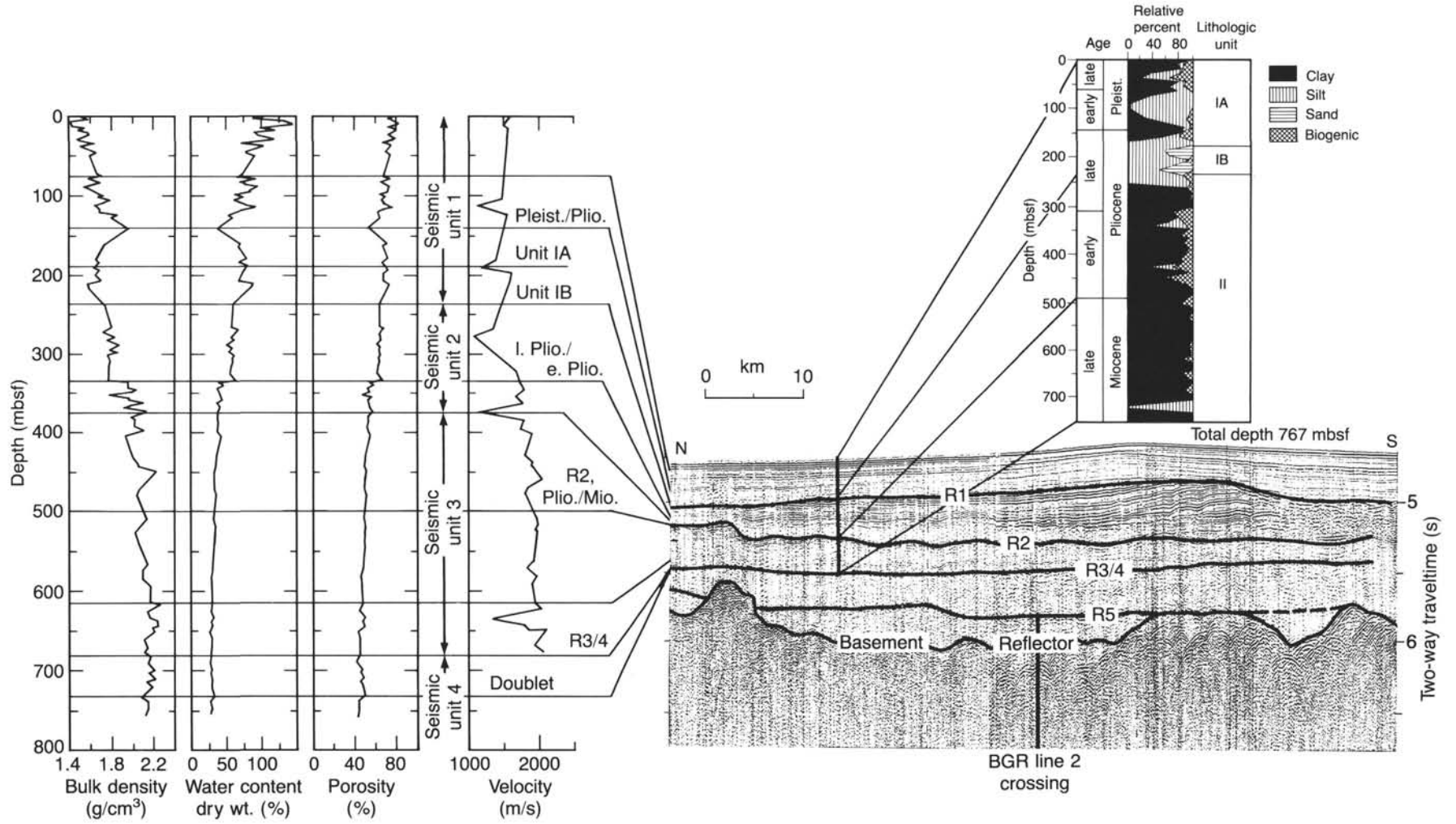


Figure 54. Correlation between physical-properties measurements (density, water content, porosity, velocity), major reflectors, and seismic units. Shown also is the lithology at Site 646.

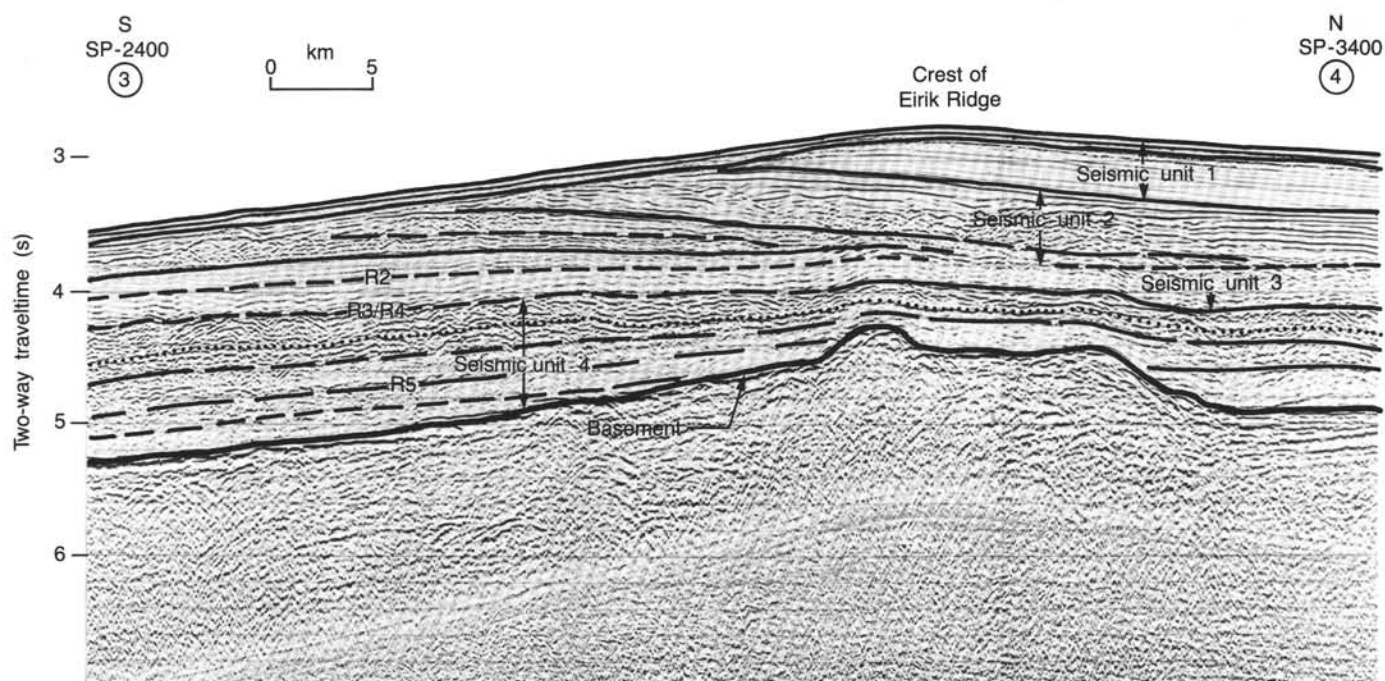


Figure 55. Interpretation of part of multichannel seismic line BGR-1 that crosses the crest of Eirik Ridge between shotpoints 2400 (south) and 3400 (north). Seismic units and reflectors are based on correlations from Site 646 through BGR multichannel line.

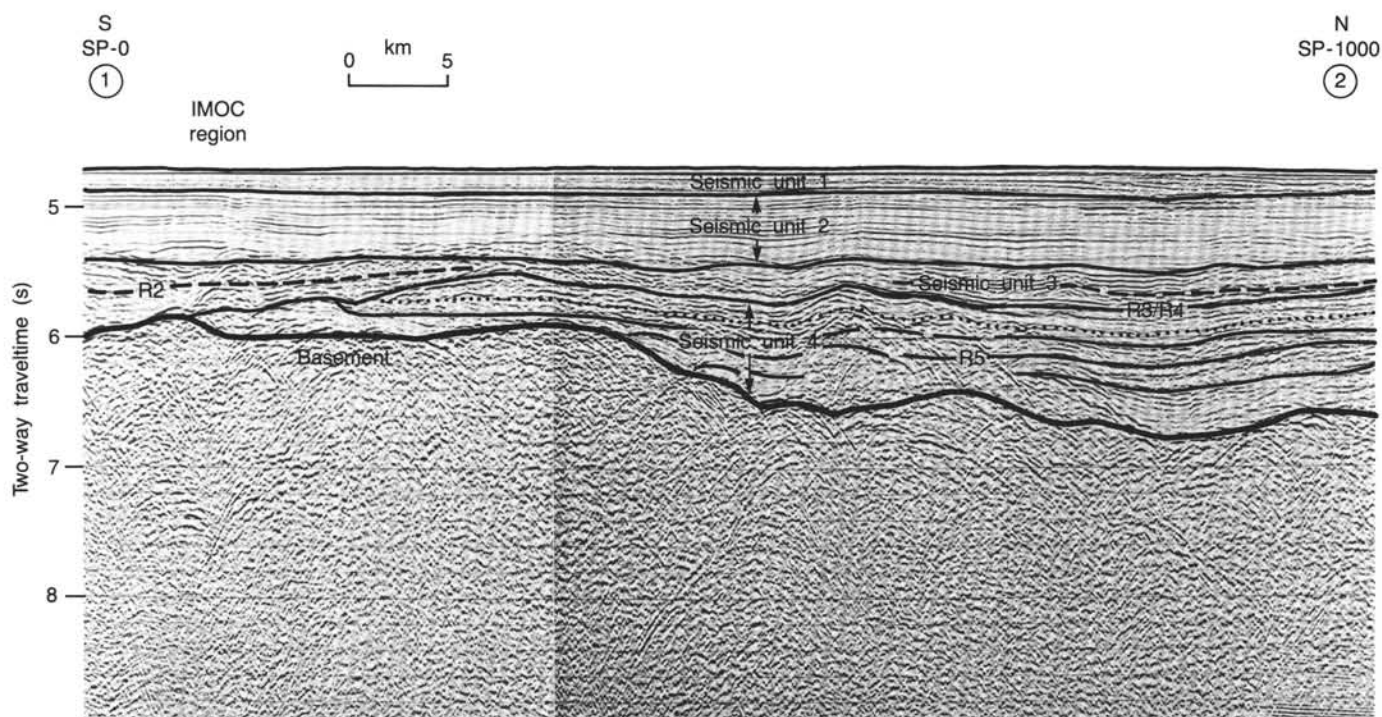


Figure 56. Interpretation of part of multichannel seismic line BGR-1 (south of that shown in Fig. 55) that crosses the IMOC region south of Eirik Ridge (shotpoints 0–1000). Seismic units and reflectors are based on correlation from Site 646 through multichannel line BGR-2.

tion, however, takes place at about 640–650 mbsf (Fig. 28) near the base of seismic unit 3. This suggests a hiatus of variable duration at the R3/R4 reflector over the region. The hiatus could have been caused by erosive currents. The thickness of seismic unit 3 is relatively constant over the region, except where erosion of the upper part has taken place. The R2 reflector occurs within the upper part of seismic unit 3 and lies near the Miocene/Pliocene boundary.

The reflector probably represents a subtle lithologic change at the boundary, mainly an increase in carbonate content above in the early Pliocene section. No evidence of an erosional hiatus at R2 exists either at Site 646 or in the seismic lines. Deposition at apparently high sedimentation rates continued into the early Pliocene, but again no evidence of formation of a depositional ridge or even direct evidence of any current-

controlled deposition occurs until the base of seismic unit 2. However, the high sediment-accumulation rates and the lithologic and textural similarity of strata from seismic unit 3 with those of seismic unit 2 suggest that deposition was controlled by bottom currents but that they were not particularly strong.

3. Deposition of seismic unit 2 in the early Pliocene marked a distinct change in sedimentation in the region. The base of seismic unit 2 lies unconformably above seismic unit 3 over much of the area, except in the lee of the depositional ridges, such as at Site 646 where sedimentation was apparently continuous across the contact between the two units. Buildup of pronounced depositional ridges occurred mainly during the early to early late Pliocene. The seismic line across the Eirik Ridge (Fig. 55) shows the unconformity between seismic units 2 and 3. Strata of seismic unit 2 apparently climbed the slope at the top of seismic unit 3 and progressively built a large dune that began to prograde northward across the present position of Eirik Ridge. A segment of the BGR-1 line to the south (Fig. 56) shows that much of seismic unit 3 was eroded before or during deposition of seismic unit 2. A major flood of sediment, probably from the source region of the IMOC, also occurred during seismic unit 2 time. The increased sediment supply was also observed at DSDP Site 113 just west in the form of Pliocene turbidites, equivalent in age to our seismic unit 2, deposited at rates of 35 cm/k.y. The high sediment supply coupled with apparently increased current velocities caused the episode of drift building. Erosional modification of the Pliocene drift sequence apparently occurred during the late Pliocene, as can be observed in line 14 near Site 646 and in the BGR-1 line (Fig. 55). Several seismic lines show that large sediment waves formed at the top of the drift sequence concomitant with the erosional episode (Fig. 55). The erosion and formation of sediment waves could be the result of a decrease in sediment supply and/or an increase in current velocities.

4. Deposition of seismic unit 1 primarily represents deposition and smoothing of the seafloor under probably less vigorous deep circulation during latest Pliocene and Pleistocene time. Sediments of seismic unit 1 cover the entire region but vary in thickness; they are thickest on the lee side of the depositional ridges.

SUMMARY AND CONCLUSIONS

Background

Drilling in the southeast Labrador Sea, off the southwest coast of Greenland, provides an opportunity to examine the interaction of high-latitude climate and surface and deep circulation of the Paleogene through the Quaternary. The Labrador Sea, along with Baffin Bay, forms an important connection for water-mass exchange between the Arctic and the North Atlantic, perhaps since the Late Cretaceous. During the glacial episode, the southern Labrador Sea probably had repeated major environmental changes as arctic and subarctic surface-water masses competed as the result of glacial-interglacial climatic cycles. In addition, changes in abyssal circulation through time left a record, in the form of drift sequences and unconformities, that can provide important clues to the linkage between tectonic events, climate, and deep-water circulation. Although some drilling was originally done in the Labrador Sea during Leg 12 of the Deep Sea Drilling Project (DSDP), the incomplete recovery of the sedimentary section, as well as the lack of drilling constraints on basement age, did not provide answers to some critical tectonic and paleoceanographic problems. Our first Labrador Sea objective was to drill Site 646 (Holes 646A and 646B), in a water depth of 3451.2 m, at 58°12.559'N, 48°22.147'W, on the northern flank of Eirik Ridge. The total depth of penetration is

766.7 mbsf, and average recovery is 55.7% (Hole 646A—APC, 89%; Hole 646B—APC, 74%; and XCB, 48%).

The major objectives at Site 646 were as follows:

1. To recover a continuous Quaternary sequence to examine the pattern and frequency of variations in surface-water-mass properties tied to cyclic climatic changes. To resolve the changes in sedimentation accompanying these climatic variations, including the relative fluxes resulting from ice rafting, bottom-current winnowing, and resedimentation, and to study the interplay of biogenic silica and carbonate sources.

2. To obtain a complete Neogene sequence recording the inception of ice rafting, which marks the probable time that the major continental ice sheets were built up in the surrounding region, for comparison with the record at Site 645 in Baffin Bay and at other sites in the North Atlantic. We also intended to examine evidence of possible steplike changes in climate and circulation during the late Neogene cooling trend and the changes in surface-water productivity that accompanied them.

3. To penetrate and date two reflectors of regional, and possibly oceanwide, importance: the R2 reflector, which was presumed to be of lower to middle Miocene age and to represent a hiatus caused by intensification of deep circulation at that time, and the R3/R4 reflector, which was hypothesized to be of Eocene to Oligocene or possibly early Oligocene age and was tentatively correlated with the R4 reflector observed and dated elsewhere in the eastern North Atlantic and at Site 112 in the Labrador Sea (Miller and Tucholke, 1983). The R3/R4 reflector was thought to represent a significant erosional unconformity or possibly a lithologic change related to the onset of vigorous deep circulation during latest Eocene to early Oligocene time. Therefore, we also wanted to recover strata above and below the unconformity because we hoped to find a continuous Oligocene section. On a worldwide basis, the details of Oligocene stratigraphy and paleoceanography remain elusive because of the paucity of continuous pelagic sequences.

4. To examine the history of deep circulation and the nature of current-influenced sedimentation through time in a major drift sequence. Of interest are the characteristic textures and sedimentary structures of bottom-current-deposited sediments, the detailed stratigraphy of such units (i.e., is continuous stratigraphic control possible?), and the age of inception of such depositional ridges and their relation to sediment supply and inferred current strength.

General Features and Lithostratigraphic Framework

Two major lithologic units were recovered at Site 646 as follows:

Unit I (Cores 105-646A-1H to 105-646A-11H; 105-646B-1H to 105-646B-25X) 0–236.1 mbsf. Age: late Pliocene to Holocene. Description: Unit I subdivided into two subunits as follows:

Subunit 1A (Cores 105-646A-1H to 105-646A-11H; 105-646B-1H to 105-646B-20X) 0–188.2 mbsf. Age: late Pliocene to Holocene. Description: Predominantly greenish gray, dark-gray to light-gray silty clays and clayey silts having as much as 40% carbonate; calcareous nannofossils, foraminifers, and diatoms are common biogenic components. Some thin detrital carbonate to non-carbonate silt and silty clay beds with sharp bases are thinly laminated to cross-laminated; those beds that are relatively rich in detrital carbonate minerals exhibit structures of thin-bedded turbidites. Otherwise, the major lithofacies are homogeneous to bioturbated. Dropstones are common and consist predominantly of mafic volcanics and hypabyssal intrusives.

Subunit IB (Cores 105-646B-21X to 105-646B-25X) 188.2–236.4 mbsf. Age: late Pliocene. Description: Predominantly dark-gray to dark greenish gray, poorly sorted, locally granule-bearing muddy sands and silty muds showing vague stratification or size gradation and subtle color banding. Pebbles are common, and consist mainly of mafic volcanics, although some granitic and gneissic rocks are also present; all are interpreted as being dropstones. The carbonate content averages <10%. Detrital carbonate turbidites common to Subunit IA are absent.

Unit II: (Cores 105-646B-26X to 105-646B-80X) 236.1–766.7 mbsf. Age: late Miocene to late Pliocene. Description: Mainly consists of dark-gray to greenish-gray silty clay (claystone), clay (claystone), and subordinate clayey silt (siltstone). Some layers contain as much as 50%–60% calcareous nannofossils, but carbonate content typically varies between 0% and 30%. Strata are moderately to strongly bioturbated (*Zoophycos*, *Planolites*), and carbonate-rich units show strong mottling. Few laminated silt layers are present.

Although much of the sedimentary sequence is thought to have been deposited or at least partly transported and reworked by deep currents, little direct evidence appears in the cores of the effects of suspected moderate to strong currents, except for the rare, isolated silt laminae and uncommon laminated silt intervals as thick as 15 cm. Most recovered sediment is moderately to highly bioturbated or homogeneous. The winnowed silt layers typically contain open-ocean biogenic particles; some are rich in heavy minerals. Evenly spaced, diffuse greenish bands (about every 5 cm) are the only other characteristic structure, but their origin is not now understood except that they may have resulted from slight changes in current strength. Silt- and sand-sized terrigenous grains are found mostly in the upper 440 m of the sequence and particularly above 236 mbsf, where ice-rafted pebbles and cobbles also occur. The sequence below this has a generally uniform fine-grained size. Quartz predominates among silt- and sand-sized particles, and feldspar and detrital carbonate grains occur in subordinate amounts. These detrital carbonate grains occur mostly above 236 m as disseminated material but also occur, in Subunit IA only, as an important component of light-green, sharp-based, slightly graded to laminated beds, interpreted as being fine-grained turbidites. Such beds are similar in composition to those recovered at DSDP Site 112 and in the modern NAMOC levee deposits (Chough and Hesse, 1985) and are inferred to have traveled to the vicinity of Site 646 through overflow from NAMOC to the northeast during the latest Pliocene through Pleistocene only (see "Sedimentology" section, this chapter). No other evidence of turbidite sedimentation was observed at Site 646.

The biogenic component of the sediments is relatively minor and is predominantly composed of calcareous nannofossils and lesser amounts of planktonic foraminifers and, above about 330 mbsf, diatoms and radiolarians. Only in the interval between 310 and 470 mbsf (lower Pliocene) do lithologies occur that could be given biogenic modifiers (nannofossil-bearing claystone, silty clay, and a few thin beds of nannofossil ooze). Total carbonate contents range from 0% to 40% over the entire section (Fig. 57) and are highly variable. Lithologic Subunit IA (Pleistocene to Holocene) is characterized by rapidly fluctuating carbonate contents between 0% and 40%, whereas Subunit IB and the top of Unit II (upper Pliocene) have uniformly low carbonate values. Higher values occur between 340 and 480 mbsf in Unit II (lower Pliocene), decreasing to lower values in the upper Miocene to very low values below 695 mbsf. Organic carbon contents are also uniformly low, with values from 0.1% to 0.55% over the entire sequence. The average organic carbon content is about 0.3%.

Stratigraphy and Sedimentation Rates

Zonal markers and first and last occurrences of common planktonic species are relatively abundant throughout the sequence at Site 646 ("Biostratigraphy" section, this chapter). Therefore, the biostratigraphic zonation was much less difficult to accomplish than that at Site 645. Age assignments for the different microfossil groups generally agreed in most of the sequence, except between paleomagnetism and biostratigraphy between 300 and 377.0 mbsf. The exact placement of the Miocene/Pliocene boundary is still in doubt. Siliceous microfossils are common to abundant above about 310 mbsf and absent below 336 mbsf; calcareous nannofossils and planktonic foraminifers are present throughout almost the entire sequence and are common to abundant and generally well preserved. Dinocysts and pollen are also observed in most samples, but their abundance varies considerably, with rare occurrences below about 540 mbsf. All microfossil groups have large abundance variations in the upper 200 m of the sequence.

Paleomagnetic studies are also helpful in constructing a stratigraphy. However, intensities of magnetization in the upper 100 m were too high, even on half cores, to run through the cryogenic magnetometer as configured; below that, the recovery was not good and the cores too disturbed to justify continuous measurement with the cryogenic unit. Even measurement of discrete samples was difficult in some intervals because of rotation of "biscuits" in the cores. Nonetheless, the magnetic-polarity pattern provided significant age constraints ("Paleomagnetism" section, this chapter).

The depths and age of important boundaries are as follows:

1. 59 mbsf—lower Pleistocene/upper Pleistocene (top of Matuyama Chronozone at 0.73 Ma),
2. 131 mbsf—Pliocene/Pleistocene boundary (1.6 Ma),
3. 314 mbsf—lower Pliocene/upper Pliocene boundary (3.4 Ma),
4. 520 mbsf—Miocene/Pliocene boundary (5.3 Ma),
5. 767 mbsf—bottom of hole <10.4 Ma, probably about 8.5 Ma.

The biostratigraphic and magnetostratigraphic data are used to construct a sedimentation-rate curve (Fig. 28, see "Sediment Accumulation Rates" section, this chapter) for the sequence. The simplest interpretation of the data is a series of straight lines fit to the stratigraphic picks that gives average rates of 79 m/m.y. for the late Pliocene and Pleistocene, 96 m/m.y. for the latest Miocene through much of the late Pliocene, and 49 m/m.y. for the rest of the late Miocene. The other noteworthy feature is the drastic change in the sedimentation rates at 640 mbsf in the lower part of Lithologic Unit III.

These sedimentation rates, together with bulk-density data from physical-properties measurements and carbonate and organic carbon data, were used to calculate accumulation rates of various sedimentary components using the method outlined in the "Explanatory Notes" section, this volume) (Figs. 57 and 58). The accumulation rates are plotted g/cm²/k.y. versus time. The most obvious feature is that accumulation rates of all components are steady from the base of the sequence to about the 6.8-Ma level, at which point they abruptly increase and then gradually decrease upsection. There is a significant step-like decrease in accumulation rates in the upper part of the lower Pliocene (3.8 Ma) that continues the decreasing trend to the top of the hole. More detailed data from the Quaternary section illustrate the nature of glacial-interglacial antithetic variations in carbonate and noncarbonate accumulation rates (Fig. 37). Overall, the sedimentation was surprisingly continuous and rapid, and,

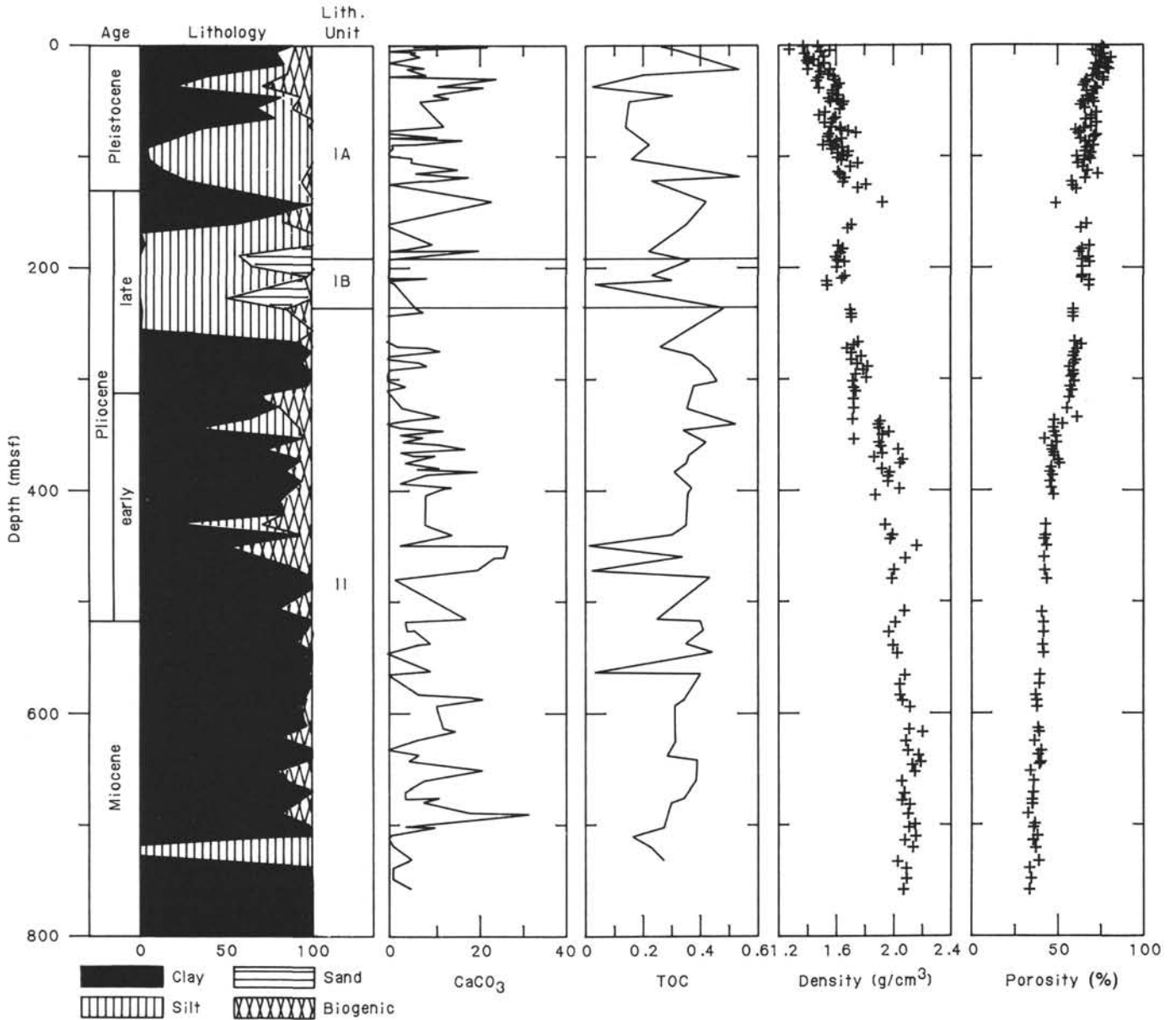


Figure 57. Lithologic columns, age, organic carbon, carbonate contents, density, and porosity, Site 646. No high-resolution carbonate curve is available for the upper 100 m.

although some reworking of microfossils is observed, no evidence of significant stratigraphic mixing occurs that would make zonation of the sequence difficult.

Paleoenvironmental Evolution

Glacial Climate and Sedimentation

More than 100 m of double APC cores provide a nearly complete, high-resolution record from 1.2 Ma to present. Fluctuations in carbonate content (0%–40%), and vague color variations, magnetic-susceptibility changes, microfossil abundance and diversity, and dropstone abundances record continuous glacial-interglacial cycles. Preliminary correlations of carbonate stratigraphy (samples analyzed every 40 cm in the top 70 m) with the oxygen-isotope stages were made assuming that the intervals of higher carbonate content represent interglacial episodes (Rudiman and MacIntyre, 1976; Zimmerman et al., 1984). The APC

cores from Holes 646A and 646B probably contain a continuous record through isotope stage 21. The stage numbers (centers of peaks), shown in Figure 37, were assigned independently using linear interpolation of the sedimentation rates between stratigraphic markers.

These tentative correlations show that a fairly strong glacial-interglacial contrast in surface-water properties and sedimentation existed in this region during the Quaternary but that sedimentation was generally dominated by influx of terrigenous material, either ice rafted or transported by deep currents. The data (Fig. 59) demonstrate that noncarbonate material accumulated three to four times faster than carbonate material (primarily biogenic) during interglacial periods and that the carbonate flux decreased (primarily detrital carbonate during glacial periods) and was even more diluted by increased noncarbonate input during glacial periods. A significant decrease in bulk accumulation rate took place at about 0.4 Ma, which coincides with changes

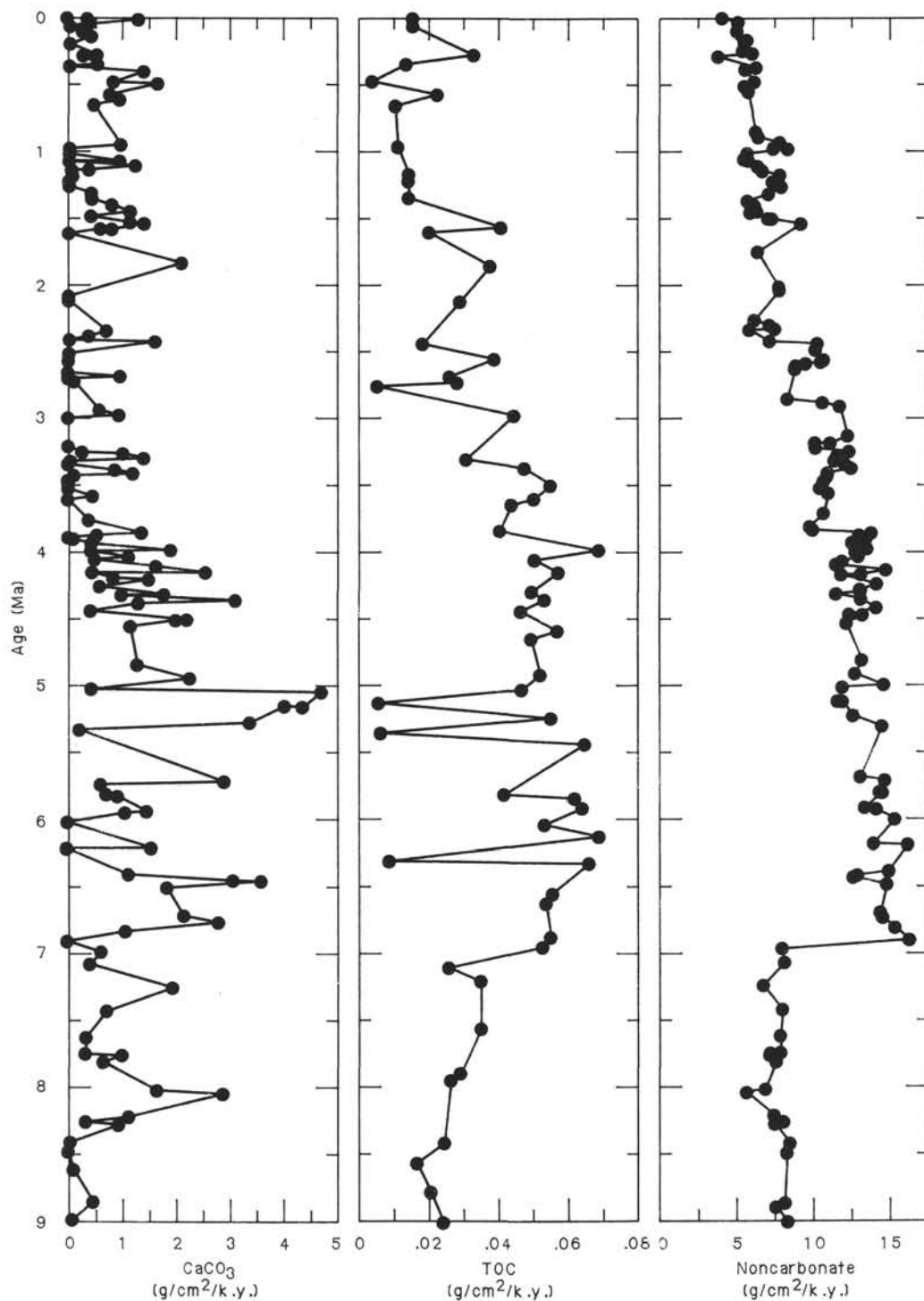


Figure 58. Accumulation rates downhole in $\text{g}/\text{cm}^2/\text{k.y.}$ of bulk sediment, carbonate and noncarbonate fractions, and organic carbon. Accumulation rates were calculated using available carbonate and TOC data (Fig. 57), bulk density from physical-properties measurements, and sedimentation rates shown in Figure 28.

in the abundance and preservation of surface-dwelling biota. The total sediment flux also seems to have been lower during interglacial periods, but such conclusions require confirmation from a study of detailed oxygen-isotope stratigraphy at this sequence. We can now only speculate about the dominant periodicity of the environmental and sedimentary fluctuations. No obvious indication of periodicities shorter than 40–100 k.y. appear in available carbonate data (sampled at about 5-k.y. intervals).

Surface waters over Site 646 during the Quaternary appear to have been generally cold and, at least periodically, of low salinity. The presence of nearly monospecific planktonic foraminiferal fauna indicates arctic-water-mass conditions. Furthermore, a low-abundance dinocyst flora is cyclically dominated by a form that indicates low salinity, as might be expected from influxes of meltwater, and alternates with a subarctic (North Atlantic) assemblage. A rigorous, low-productivity environment is indicated overall. Diatom assemblages primarily consist of cos-

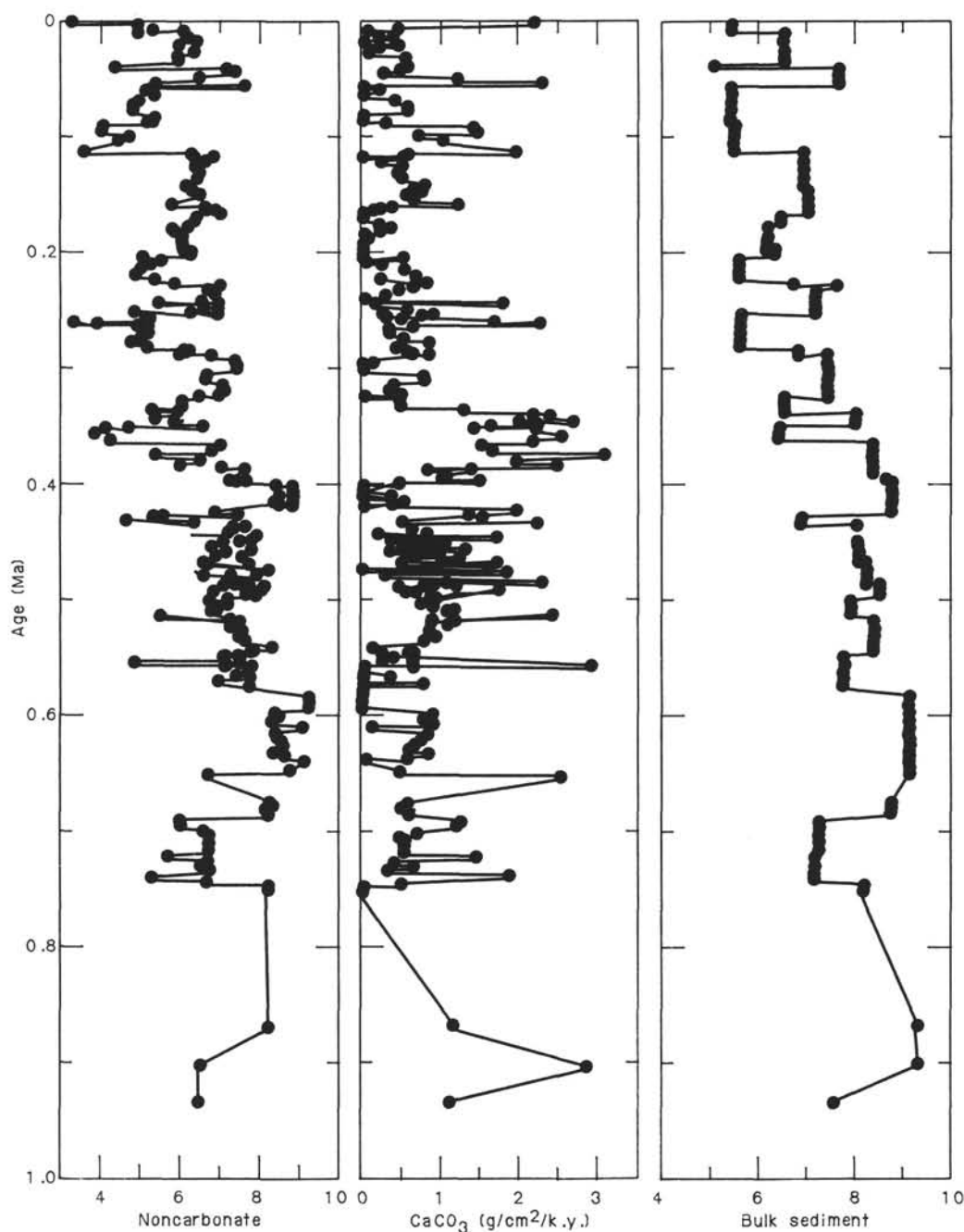


Figure 59. Accumulation rates for the upper 100 m of Site 646, in $\text{g}/\text{cm}^2/\text{k.y.}$ of carbonate, noncarbonate, and bulk sediment. The data and interval sedimentation rates shown in Figure 57 were used along with bulk-density measurements to calculate the accumulation rates.

mopolitan forms having subordinate amounts of arctic and subarctic species. The abundance of the radiolarian *Cycladophora davisiana* over the last 400 k.y. of the sequence may also indicate a strong seasonal pycnocline and cold surface waters of lower-than-normal salinity. Further detailed studies will undoubtedly provide important information about the glacial environment in this part of the Labrador Sea.

Onset of Glaciation and Late Neogene Climate Deterioration

The onset of major ice rafting, in the form of recognizable pebbles, cobbles, and granules interpreted as being dropstones, occurs at about 2.5 Ma (236 mbsf) in Site 646 and coincides with a major change in seismic character. General smoothing

and continuous sedimentation of the drift sequence occurred during the late Pliocene through the Pleistocene but with differential sedimentation on the lee sides of the ridges. No distinct break in sedimentation occurs either in the cores from Site 646 or in the seismic lines associated with the Pliocene/Pleistocene boundary. The age of the first recognizable ice rafting agrees with that established for the northeastern Atlantic (Shackleton et al., 1984) and for the major ice rafting in the Norwegian Sea (Eldholm, Theide, Taylor, et al., in press) but may be somewhat younger than that found at Site 645 in Baffin Bay.

However, the significant biotic change at Site 646 occurred not at the initiation of ice rafting but at the early Pliocene/late Pliocene boundary (3.4 Ma; 314 mbsf). Biosiliceous material is

common to abundant above the boundary, whereas calcareous nannofossils and planktonic foraminifers are more abundant below. This event probably represents significant cooling of surface water masses over the site, accompanied by higher productivity of siliceous plankton. The changes in surface waters also closely correspond to a period of apparent intensification of deep circulation, beginning at about 3.8–4.0 Ma, as suggested by erosional modification of the drift sequence and construction of a pronounced ridge observed in the regional seismic lines. The advent of organized drift sedimentation appears to coincide with increased influx of terrigenous sediments to the region during the latest Miocene (6.8 Ma), earlier than the expected flood of terrigenous material seen elsewhere in the North Atlantic at about 3.4 Ma, associated with the transition to a glacial regime (see following discussion).

A generally warm early Pliocene is indicated by relatively high and constant carbonate contents and abundant calcareous nannofossils and dinocysts. The Miocene/Pliocene boundary occurs at about 520 mbsf and approximately coincides with a change to highly variable and generally lower carbonate contents above this boundary and with the R2 reflector, which was originally assumed to be late early Miocene in age. An interesting feature of the Pliocene sequence is the markedly cyclic variations in carbonate contents, which were inferred from a periodic signal of varying amplitude in an array of geophysical logs (Figs. 46 and 47). These cycles may represent the expression of Milankovitch cycles of about the 100-k.y. period.

The R3/R4 Reflector

The top of seismic unit 4 (Fig. 53) is marked by a reflector, which is actually two strong reflectors separated by about 0.05 s and which was initially presumed to be equivalent in age or just younger than the R4 reflector, in the northeast Atlantic (Roberts et al., 1979; Miller and Tucholke, 1983). Miller (1982) identified this reflector as either the R3 or R4 reflector in this region. It was interpreted to represent the onset of seafloor erosion in latest Eocene–early Oligocene times. This erosion was interpreted to have begun when the Greenland–Scotland Ridge subsided enough to allow overflow of arctic waters, thereby initiating the first formation and rapid circulation of bottom water in the North Atlantic (Berggren and Schnitker, 1983; Miller and Tucholke, 1983). We believe that we recovered only the top 80–90 m of seismic unit 4, including the R3/R4 doublet at Site 646 (“Seismic Stratigraphy” section, this chapter). No single marked lithologic change in the interval cored (680–776 mbsf) appears to correspond to a single R3/R4 reflector. However, carbonate content changes sharply below 680 mbsf and greatly decreases to <5% below 695 mbsf; silt content increases at about 730 mbsf.

Borehole sonic, resistivity, and gamma-ray logs, run to within 15 m of the bottom of the hole, demonstrated recognizable changes in rock properties from 680 to 750 mbsf. A synthetic seismogram generated using the sonic logs exhibits two high-amplitude reflectors that occur somewhat shallower, at 680 and 730 mbsf, than the 754-mbsf depth we originally calculated for R3/R4 (Table 16). The character of the generated pulse is similar to that of the top R3/R4 reflector and the companion reflector (R3/R4') below it. The physical-properties data (“Physical Properties” section, this chapter) show a corresponding small but significant increase in porosity and water content and a decrease in density from about 680 to 730 mbsf. We believe that these data strongly support the contention that we drilled through and dated the R3/R4 reflector at Site 646. However, the late Miocene (about 8.2 Ma) age of that reflector is much younger than expected. Biostratigraphic data indicate important changes in the benthic fauna and preservation and abundance of calcareous planktonic microfossils at 680 mbsf.

The expected Eocene/Oligocene hiatus may be present in the sequence beneath the bottom of the hole at Site 646 (i.e., beneath 766.7 mbsf). From the age of the crust that underlies this region (magnetic anomaly 24, 55–56 m.y.) and from the constraint on bottom-hole age imposed by our drilling results, seismic unit 4, at an inferred depth of 680 mbsf and deeper, should contain sediments from late Miocene to early Eocene age. These constraints indicate, however, that the sedimentation rates must be much lower (about 15 m/m.y.) than those encountered in the upper sequence (49 m/m.y.) or that a significant hiatus must be within seismic unit 4.

The drilling results clearly show that the R3/R4 reflector, as identified from earlier studies in the region of Site 646, is not older than early late Miocene and is not equivalent to the R4 reflector of the northeast Atlantic, as defined by Miller and Tucholke (1983).

History of Deep-Water Circulation

The history of bottom-water circulation and its effect on the development of drift deposits like the Eirik Ridge is of primary interest in the study of the southeastern Labrador Sea. To relate the findings from Site 646 to the history of deep-water circulation in the southeastern Labrador Sea, we used the seismic recordings made across the Eirik Ridge. We are able to carry our seismic-well ties to the Eirik Ridge through correlations between Hudson line 14, which crosses Site 646, through a multichannel line BGR-2 and to a second multichannel line, BGR-1, that runs northwest–southeast, perpendicular to the axis of Eirik Ridge (Fig. 2). A segment of line BGR-1 (Fig. 55) illustrates the correlation and continuity of the reflection characteristics and major seismic units from Site 646 (see Fig. 53) to Eirik Ridge.

Eirik Ridge is a constructional sedimentary feature, which was influenced by the interaction of (1) roughly southwestward-flowing contour currents with (2) topography inherited from the basement (Figs. 2 and 55). A relatively constant thickness of sedimentary strata (about 2 s thick) drapes this basement topography, but most of the existing seafloor relief results from the buildup of the depositional ridge that occurs above the R2 reflector. Because the R2 reflector was dated at Site 646 as the top of the Miocene, we infer that much of the major organized drift-building episode occurred during the late Miocene to Holocene. There is no evidence of significant thickness variations in units underlying R2, except where erosion has truncated unit thickness or where strata have progressively overlapped basement during subsidence, as at the lower part of seismic unit 4 (probable Eocene age).

We constructed the following tentative history of deep-current activity and deposition at Eirik Ridge and environs on the basis of our seismic interpretations and data from Site 646:

1. Deposition of seismic unit 4 (below R3/R4), which fills in troughs and progressively onlaps and drapes the basement, probably encompassed the middle Eocene to late Miocene (52–9.0 Ma). We base this hypothesis on the assumption that the region was not uncommonly uplifted during reorientation of the ridge axis during Chron C24 and was accessible to sedimentation. The seismic record shows no major variations in thickness between any two reflectors in the sequence. Therefore, we have no direct evidence of either major erosional episodes or of episodes of construction of current-influenced sedimentary bodies during seismic unit 4 deposition, except that chaotic, diffracted reflections can be found within seismic unit 4 under Eirik Ridge below R3/R4 and above a deeper reflector that may be equivalent to R4 of Miller and Tucholke (1983). The reflections are similar to those found by Mountain and Tucholke (1985) between reflector Merlin (dated at 11–12 Ma) and Au (intra-Oligocene), inferred to represent current-influenced deposition.

2. Deposition of seismic unit 3 occurred during the upper part of the late Miocene and earliest Pliocene (7.4–4.2 Ma). The base of seismic unit 3 is conformable to disconformable with underlying seismic unit 4. This suggests a hiatus or variation in sedimentation rate at the R3/R4 reflector over the region. The hiatus could have been caused by strong erosive currents.

The preservation and abundance of faunal and floral assemblages below 680 mbsf (R3/R4 reflector) differ from those above. Carbonate contents are <5%, and preservation of calcareous plankton is relatively poor. The low abundance of calcareous-dominated benthic foraminiferal fauna is significantly different from the agglutinated foraminifer-dominated fauna above 680 mbsf. The persistent occurrence of *Nutallides umbonifera*, considered an indicator of Antarctic Bottom Water, and its paucity above 680 mbsf suggest different deep water-mass properties (older, more corrosive bottom water) during deposition of the latter part of seismic unit 4 than during seismic unit 3 sedimentation. The benthic fauna might indicate mixing of a proto-North Atlantic deep water with some Antarctic Bottom Water and less vigorous deep circulation in this region before about 8.2 Ma.

At about 8.2 Ma, significant benthic foraminiferal changes occurred; a high-abundance, agglutinated and calcareous fauna developed that is more typical of North Atlantic deep water ("Biostratigraphy" section, this chapter) and is similar to the late Miocene–early Pliocene fauna around Rockall (Murray, 1984). The agglutinated component of the fauna has affinities to those in the Neogene of the Norwegian Sea and Baffin Bay. This evidence suggests that the "modern" pattern (*sensu* Shor and Poore, 1979) of deep circulation in this part of the North Atlantic began to be established some time in the late Miocene when significant cooling of surface water occurred at high latitudes and the Greenland–Scotland Ridge had subsided sufficiently to allow increasing spillover of deeper waters from the Norwegian–Greenland Sea. These deep-water masses may have been joined in the Labrador Sea by some deep waters formed in Baffin Bay (see Site 645 chapter, this volume).

The thickness of seismic unit 3 is relatively constant over the region, except where erosion of the upper part has taken place. The R2 reflector (Fig. 52) occurs within the upper part of seismic unit 3 and lies close to the Miocene/Pliocene boundary (5.3 Ma). This reflector probably represents a subtle lithologic change at the boundary, mainly an increase in carbonate content above the early Pliocene section. No evidence of an erosional hiatus at R2 either at Site 646 or in the seismic lines occurs. Deposition at apparently high sedimentation rates (96 m/m.y.) continued into the early Pliocene, but again little evidence of formation of a depositional ridge, or even direct evidence of significant current-controlled depositions appears, until the base of seismic unit 2 (about 4.2 Ma). However, the high-sediment-accumulation rates and the lithologic and textural similarity of strata from most of seismic unit 3 to those of seismic unit 2 at Site 646 suggest that deposition was controlled by bottom currents but that they were not particularly strong.

3. Deposition of seismic unit 2 in the late-early to late Pliocene (4.2–2.5 Ma) marked a distinct change in sedimentation in the region. The base of seismic unit 2 lies unconformably above seismic unit 3 over much of the area, except in the lee of the depositional ridges, such as at Site 646 where sedimentation was apparently continuous across the contact between the two units. Buildup of the pronounced depositional ridges of seismic unit 2 occurred mainly during the early to early-late Pliocene. The seismic line across Eirik Ridge (Fig. 55) shows the unconformity between seismic units 2 and 3. Strata of seismic unit 2 apparently climbed the slope at the top of seismic unit 3 and progressively built a large ridge that began to prograde northward across the present position of Eirik Ridge. A segment of the BGR-1 line on

the south flank of Eirik Ridge (Fig. 56) shows that much of seismic unit 3 was eroded before or during deposition of a thin seismic unit 2 sequence. A major flood of sediment, probably from the source region of the IMOC (see DSDP Site 113 report, Laughon, Berggren, et al., 1972), also occurred during seismic unit 2 time. The increased sediment supply was observed just west of DSDP Site 113 in the form of nearly 700 m of Pliocene turbidites, equivalent in age to our seismic unit 2, deposited at rates of 35 cm/k.y. (350 m/m.y.). The high sediment supply coupled with apparently increased current velocities probably caused the episode of drift building. Erosional modification of the drift sequence occurred in the late Pliocene, as can be observed in line 14 near Site 646 (Fig. 52) and on Eirik Ridge (Fig. 55). Several seismic lines show that large sediment waves formed at the top of the drift sequence concomitant with the erosional episode (Fig. 55). The erosion and formation of sediment waves could result from a decrease in sediment supply and/or an increase in current velocities.

Within seismic unit 2, at about the beginning of erosional modification of the drift sequence (about 3.8 Ma), accumulation rates abruptly decrease at Site 646 (Fig. 58). This event just precedes the fairly abrupt appearance of siliceous microfossils just below the early Pliocene/late Pliocene boundary (over the interval of 3.8–3.4 Ma). The event also coincides with another change in the benthic foraminiferal fauna, when the agglutinated fauna nearly disappears and calcareous benthic foraminifers decline in abundance. The benthic fauna is composed mainly of stratigraphically long-ranging species that can be interpreted as being generalists. There is also a change to somewhat better preservation of calcareous plankton remains across this interval. Again, these events precede a significant change in deep-water properties, probably a change to a glacial bottom water derived from major cooling of Norwegian–Greenland Sea surface waters. An interesting correspondence therefore exists between surface- and bottom-water changes at Site 646.

4. Seismic unit 1 primarily represents deposition and smoothing of the seafloor under probably less vigorous deep circulation and waning sediment supply, even with the influx of ice-rafted terrigenous material (Fig. 58) during latest Pliocene and Pleistocene time (2.5–0 Ma). Sediments of seismic unit 1 cover the entire region but vary in thickness; they are thickest on the lee side of the depositional ridges and therefore do not simply drape previous topography.

The history of drift sedimentation on Eirik Ridge contrasts somewhat with that at Gardar and Feni drifts in the northeast Atlantic (Ruddiman, Kidd, et al., in press). Sedimentation rates are about a factor of 2 higher at Site 646 than those at Gardar (5.8 cm/k.y.; 58 m/m.y.) and Feni (5.1 cm/k.y.; 51 m/m.y.) drifts, and the sequence on Eirik Ridge is much more terrigenous than the dominantly pelagic sediment drifts in the northeast Atlantic. Additionally, the major drift-building episode on Eirik Ridge apparently began somewhat later (i.e., at least by 4.2 Ma) than those in the northeast Atlantic.

REFERENCES

- Aksu, A. E., and Mudie, P. J., 1985. Magnetostratigraphy and palynology demonstrate at least 4 million years of Arctic Ocean sedimentation. *Nature*, 318:280–283.
- Backman, J., 1979. Pliocene biostratigraphy of DSDP Sites 111 and 116 from the North Atlantic Ocean and the age of Northern Hemisphere glaciation. *Stockholm Contrib. Geol.* XXXII 3:115–137.
- Baldauf, J. G., 1981. Identification of the Holocene/Pleistocene boundary in the Bering Sea by diatoms. *Boreas*, 11:113–118.
- _____, 1984. Cenozoic diatom biostratigraphy and paleoceanography of the Rockall Plateau region, North Atlantic, Deep Sea Drilling Project Leg 81. In Roberts, D. G., Schnitker, D., et al., *Init. Repts. DSDP*, 81: Washington (U.S. Govt. Printing Office), 439–478.

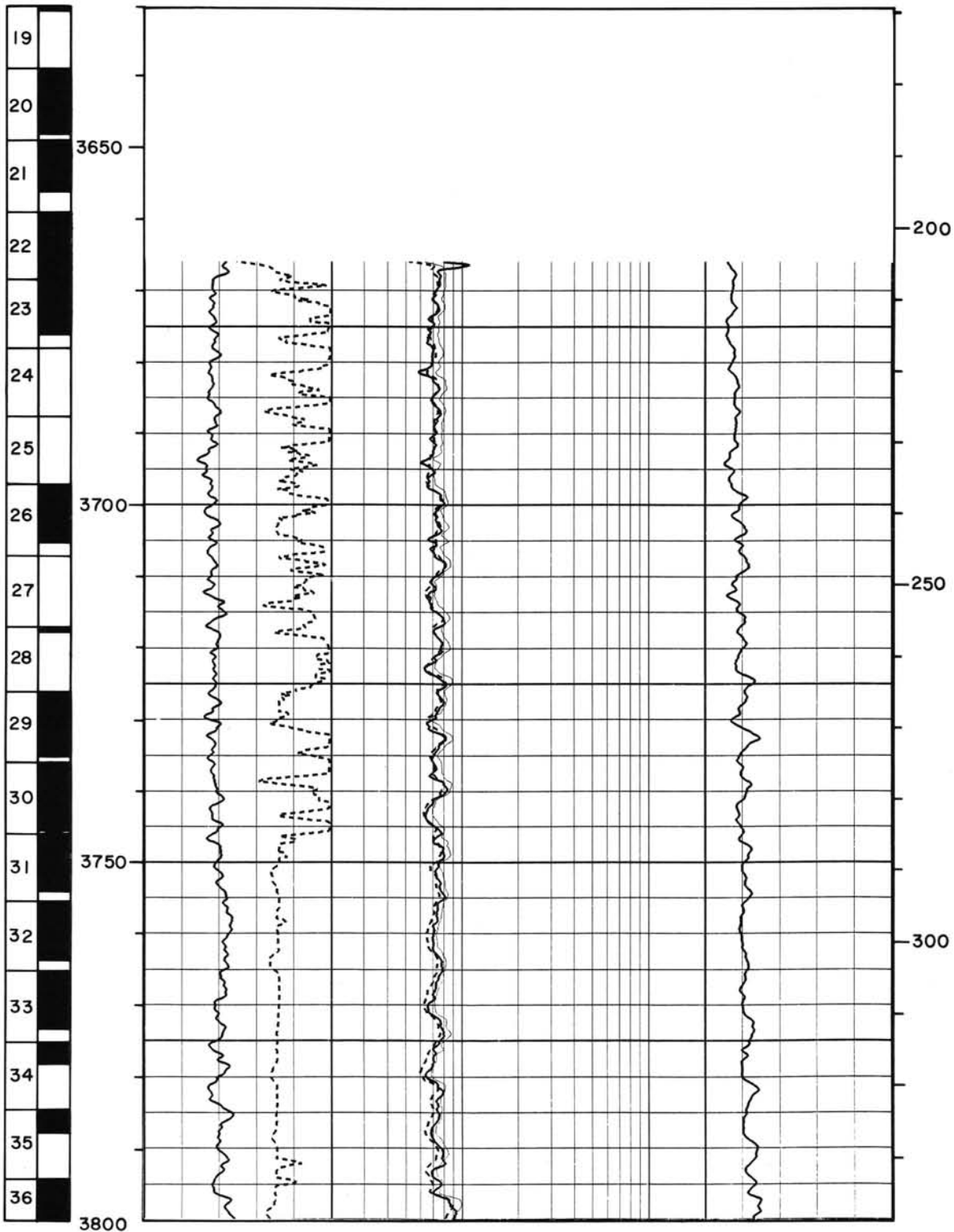
- _____, in press. Diatom biostratigraphy of the middle and high latitude North Atlantic Ocean, Deep Sea Drilling Project Leg 94. In Ruddiman, W., Kidd, R., et al., *Init. Repts. DSDP, 94*: Washington (U.S. Govt. Printing Office).
- Baltes, N., 1971. Pliocene Dinoflagellata and Arcritarche in Romania. *Proc. Second Planktonic Conf.*, 1-16.
- Barron, J., 1980. Lower Miocene to Quaternary biostratigraphy of Leg 57, off Northeastern Japan. In Scientific Party, *Init. Repts. DSDP, 56, 57, Pt. 2*: Washington (U.S. Govt. Printing Office), 641-685.
- _____, 1985. Miocene to Holocene planktic diatoms. In Bolli, H. M., Saunders, J. B., and Perch-Nielsen, K., (Eds.), *Plankton Stratigraphy*: Cambridge (Cambridge Univ. Press), 763-809.
- Barron, J. A., Harper, H. E., Jr., Keller, G., Reynolds, R. A., Sakai, T., Shaffer, B. L., and Thompson, P. R., 1980. Biostratigraphic summary of the Japan Trench transect, Legs 56 and 57, Deep Sea Drilling Project. In Scientific Party, *Init. Repts. DSDP, 56/57, Pt. 1*: Washington (U.S. Govt. Printing Office), 505-520.
- Bé, A.W.H., and Tolderlund, D. S., 1971. Distribution and ecology of living planktonic foraminifera in surface waters of the Atlantic and Indian oceans. In Funnel, B. M., and Riedel, W. R. (Eds.), *The Micropaleontology of Oceans*: Cambridge (Cambridge Univ. Press), 105-149.
- Bergen, J. A., 1982. Calcareous nannoplankton from Deep Sea Drilling Project Leg 78A: evidence for imbricate underthrusting at the Lesser Antillian Active Margin. In Biju-Duval, B., Moore, J. C., et al., *Init. Repts. DSDP, 78*: Washington (U.S. Govt. Printing Office), 411-445.
- Berger, A. L., 1978. Long-term variations of caloric insulation resulting from the earth's orbital elements. *Quat. Res.*, 9:139-167.
- Berggren, W. A., 1972. Cenozoic biostratigraphy and paleobiogeography of the North Atlantic. In Laughton, A. S., Berggren, W. A., et al., *Init. Repts. DSDP, 12*: Washington (U.S. Govt. Printing Office), 965-1001.
- Berggren, W. A., and Schnitker, D., 1983. Cenozoic marine environments in the North Atlantic and Norwegian-Greenland Sea. In Bott, M.H.P., Saxov, S., Talwani, M., and Thiede, J. (Eds.), *Structure and Development of the Greenland-Scotland Ridge*: New York (Plenum Press), 495-548.
- Berggren, W. A., Kent, D. V., and Van Couvering, J. A., 1986. Neogene geochronology and chronostratigraphy. In Snelling, N. J. (Ed.), *Geochronology and the Geologic Time Scale*. Geol. Soc. London, Mem. 10:211-250.
- Bjørklund, K. R., 1976. Radiolarians from the Norwegian Sea, Leg 38 of the Deep Sea Drilling Project. In Talwani, M., Udintsev, G., et al., *Init. Repts. DSDP, 38*: Washington (U.S. Govt. Printing Office), 1101-1168.
- Bryant, W. R., Deflache, A. P., and Trabant, P. K., 1974. Consolidation of clays and carbonates in deep-sea sediments. In Inderbitzen, A. L. (Ed.), *Deep Sea Sediments: Mechanical and Physical Properties*: New York (Plenum Press), 209-244.
- Bujak, J. P., 1984. Cenozoic dinoflagellate cysts and acritarchs from the Bering Sea and northern North Pacific, DSDP Leg 19. *Micropaleontology*, 30:180-212.
- Bujak, J. P., and Davies, E. H., 1981. Neogene dinoflagellate cysts from the Hunt Dome Kopanoar M-13 well, Beaufort Sea, Canada. *Bull. Can. Pet. Geol.*, 29:420-425.
- Bukry, D., 1978. Biostratigraphy of Cenozoic marine sediment by calcareous nannofossils. *Micropaleontology*, 24(1):44-60.
- Chough, S. K., 1978. Morphology, sedimentary facies and processes of the Northwest Atlantic Mid-Ocean Channel between 61° and 52° N, Labrador Sea [Ph.D. thesis]. McGill University, Montreal.
- Chough, S. K., and Hesse, R., 1976. Submarine meandering talweg and turbidity currents flowing for 4,000 km in the Northwest Atlantic Mid-Ocean Channel, Labrador Sea. *Geology*, 4:529-533.
- _____, 1980. The Northwest Atlantic Mid-Ocean Channel of the Labrador Sea: III. head spill vs. body spill deposits from turbidity currents on natural levees. *J. Sed. Pet.*, 50(1):227-234.
- _____, 1985. Contourites from Eirik Ridge, south of Greenland. *Sediment. Geol.*, 41:185-199.
- _____, in press, a. The Northwest Mid-Ocean Channel of the Labrador Sea: V. morphology, sedimentary facies, stratigraphy and processes of a giant deep-sea channel. *Can. J. Earth Sci.*
- Chough, S. K., Hesse, R., and Muller, J., in press, b. The Northwest Atlantic Mid-Ocean Channel of the Labrador Sea: IV. petrography and provenance of the sediments.
- Claypool, G. E., and Kaplan, I. R., 1974. The origin and distribution of methane in marine sediments. In Kaplan, I. R. (Ed.), *Natural Gases in Marine Sediments*: New York (Plenum Press), 99-139.
- Collinson, D. W., 1983. *Methods in Rock Magnetism and Paleomagnetism: Techniques and Instrumentation*: London (Chapman and Hill).
- Davies, T. A., and Laughton, A. S., 1972. Sedimentary processes in the North Atlantic. In Laughton, A. S., Berggren, W. A., et al., *Init. Repts. DSDP, 12*: Washington (U.S. Govt. Printing Office), 905-934.
- De Vernal, A., 1986. Analyses palynologiques et isotopiques de sédiments de la mer du Labrador et de la baie de Baffin: Éléments d'une climatostatigraphie du Pléistocène supérieur dans l'est du Canada [Ph.D. thesis]. Université de Montreal.
- Dixon, J., McNeil, D. H., Dietrich, J. R., Bujak, J. P., and Davies, E. H., 1984. Geology and biostratigraphy of the Dome Gulf et al. Hunt Kopanoar M-13 Well, Beaufort Sea. *Geol. Surv. Can. Pap.* 82-13, 1-28.
- Edwards, L. E., 1985. Miocene dinocysts from Deep Sea Drilling Project Leg 81, Rockall Plateau, eastern North Atlantic Ocean. In Roberts, D. G., Schnitker, D., et al., *Init. Repts. DSDP, 81*: Washington (U.S. Govt. Printing Office), 581-594.
- Eldholm, O., Thiede, J., Taylor, E., et al., in press. *Proc., Init. Repts., ODP (Pt. A)*, 104.
- Gieskes, J. M., 1983. The chemistry of interstitial waters of Deep Sea sediments: interpretation of Deep Sea Drilling data. In Riley, J. P., and Chester, R. (Eds.), *Chemical Oceanography (Vol. 8)*: New York (Academic Press), 221-269.
- Hamilton, E. L., 1974. Prediction of deep-sea sediment properties: state-of-the-art. In Inderbitzen, A. L. (Ed.), *Deep Sea Sediments: Physical and Mechanical Properties*: New York (Plenum Press), 1-43.
- _____, 1976. Variations of density and porosity with depth in deep-sea sediments. *J. Sed. Pet.*, 46:280-300.
- Harland, R., 1979. Dinoflagellate biostratigraphy of Neogene and Quaternary sediments at Holes 400/400A in the Bay of Biscay (DSDP Leg 48). In Montadert, L., Roberts, D. G., et al., *Init. Repts. DSDP, 48*: Washington (U.S. Govt. Printing Office), 531-545.
- Hesse, R., and Chough, S.K., 1980. The Northwest Atlantic Mid-Ocean Channel of the Labrador Sea: II. deposition of parallel laminated levee-muds from the viscous sublayer of low density turbidity currents. *Sedimentology*, 27:697-711.
- Hinz, K., Schluter, H. U., Grant, A. C., Srivastava, S. P., Umpleby, D., and Woodside, J., 1979. Geophysical transects of the Labrador Sea: Labrador to southwest Greenland. In Keen, C. E. (Ed.), *Crustal Properties Across Passive Margins*; Tectonophysics, 59:151-183.
- Hyndman, R. D., 1973. Evolution of the Labrador Sea. *Can. J. Earth Sci.*, 10:637-644.
- Hyndman, R. D., Erickson, A. J., and von Herzen, R. P., 1974. Geothermal measurements on Deep Sea Drilling Project Leg 26. In Davies, T. A., Luyendyk, B. P., et al., *Init. Repts. DSDP, 26*: Washington (U.S. Govt. Printing Office), 451-463.
- Johnson, G. L., and Schneider, E. D., 1969. Depositional ridges in the North Atlantic. *Earth Planet. Sci. Lett.*, 6:416-422.
- Johnson, G. L., Srivastava, S. P., Campsie, J., and Rasmussen, M., 1982. Volcanic rocks in the Labrador Sea and environs and their relation to the evolution of the Labrador Sea. In *Current Research, Pt. B*: Geol. Surv. Can., Pap. 82-1B:7-20.
- Jones, E. J., Ewing, M., Ewing, J. I., and Eittrheim, S. L., 1970. Influences of Norwegian Sea overflow on sedimentation in the northern North Atlantic and the Labrador Sea. *J. Geophys. Res.*, 75:1655-1680.
- Kellog, T. B., 1976. Late Quaternary climatic changes: evidence from deep-sea cores of Norwegian and Greenland Seas. *Geol. Soc. Am. Mem.*, 145:77-110.
- King, R. F., and Rees, A. I., 1962. The measurement of the anisotropy of magnetic susceptibility of rocks by the torque method. *J. Geophys. Res.*, 71:561-571.
- Koizumi, I., 1973. The late Cenozoic diatoms of Sites 183-193, Leg 19, Deep Sea Drilling Project. In Creager, J. C., Scholl, D. W., et al., *Init. Repts. DSDP, 19*: Washington (U.S. Govt. Printing Office), 805-855.
- Kristoffersen, Y., and Talwani, M., 1977. Extinct triple junction south of Greenland and the Tertiary motion of Greenland relative to North America. *Geol. Soc. Am. Bull.*, 88:1037-1049.
- Latouche, C., and Parra, M., 1979. La sédimentation au Quaternaire Récent dans le "Northwest Atlantic Mid-Ocean Canyon"—apport des données minéralogiques et géochimiques. *Mar. Geol.*, 29:137-164.

- Laughton, A. S., and Berggren, W. A., et al., 1972. *Init. Repts. DSDP*, 12: Washington (U.S. Govt. Printing Office).
- Laughton, A. S., Berggren, W. A., Benson, R. N., Davies, T. A., Franz, U., Musich, L. F., Perch-Nielsen, K., Ruffman, A. S., Van Hinte, J. E., and Whitmarsh, R. B., 1972. The Southern Labrador Sea—a key to the Mesozoic and Tertiary evolution of the North Atlantic. In Laughton, A. S., Berggren, W. A., et al., *Init. Repts. DSDP*, 12: Washington (U.S. Govt. Printing Office), 1155–1169.
- Lawrence, J. R., Gieskes, J. M., and Broecker, W. S., 1975. Oxygen isotope and cation composition of DSDP pore waters and the alteration of layer II basalts. *Earth Planet. Sci. Lett.*, 27:1–11.
- Le Pichon, X., Ettreim, S., and Ewing, J., 1971. A sedimentary channel along Gibbs Fracture Zone. *J. Geophys. Res.*, 76:2891–2896.
- Manheim, F. T., Sayles, F. L., and Waterman, L. S., 1972. Interstitial water studies on small core samples, Deep Sea Drilling Project, Leg 12. In Laughton, A. S., Berggren, W. A., et al., *Init. Repts. DSDP*, 12: Washington (U.S. Govt. Printing Office), 1193–1200.
- Manum, S., 1976. Dinocysts in Tertiary Norwegian–Greenland Sea sediments (DSDP Leg 38), with observations on palynomorphs and palynodebris in relation to environment. In Talwani, M., Udintsev, G., et al., *Init. Repts. DSDP*, 38: Washington (U.S. Govt. Printing Office), 897–919.
- Martini, E., 1971. Standard Tertiary and Quaternary calcareous nannoplankton zonation. *Proc. Second Planktonic Conf.*, 1970, 2:739–785.
- _____, 1979. Calcareous nannoplankton and silicoflagellate biostratigraphy at Reykjanes Ridge, Northeastern North Atlantic (DSDP Leg 49, Sites 407 and 409). In Luyendyk, B. P., Cann, J. R., et al., *Init. Repts. DSDP*, 49: Washington (U.S. Govt. Printing Office), 533–549.
- Miller, K. G., 1982. Late Paleogene (Eocene to Oligocene) paleoceanography of the northern North Atlantic [Ph.D. dissert.]. Woods Hole Oceanographic Institution/Massachusetts Institute of Technology.
- Miller, K. G., Gradstein, F. M., and Berggren, W. A., 1982. Late Cretaceous to Early Tertiary agglutinated benthic foraminifera in the Labrador Sea. *Micropaleontology*, 28:1–30.
- Miller, K. G., and Tucholke, B. E., 1983. Development of Cenozoic abyssal circulation south of the Greenland–Scotland Ridge. In Bott, M. H. P., Saxov, S., Talwani, M., and Thiede, J. (Eds.), *Structure and Development of the Greenland–Scotland Ridge*: New York (Plenum Press), 549–589.
- Moore, T. C., 1973. Method of randomly distributing grains for microscopic examination. *J. Sed. Petrol.*, 43:904–906.
- Morley, J. J., and Hays, J. D., 1979. *Cycladophora davisiana*: a stratigraphic tool for Pleistocene North Atlantic and interhemispheric correlation. *Earth Planet. Sci. Lett.*, 44(3):383–389.
- Mountain, G. S., and Tucholke, B. E., 1985. Mesozoic and Cenozoic Geology of the U.S. Atlantic continental slope and rise. In Poag, C. W. (Ed.), *Geologic Evolution of the United States Atlantic Margin*: Stroudsburg, PA (van Nostrand Reinhold).
- Mudie, P. J., in press. Palynology and dinoflagellate biostratigraphy of DSDP Leg 94, Sites 607 and 611, North Atlantic Ocean. In Ruddiman, W. T., Kidd, R., et al., *Init. Repts. DSDP*, 94: Washington (U.S. Govt. Printing Office).
- Mudie, P. J., and Short, S. K., 1985. Marine palynology of Baffin Bay. In Andrews, J. T., and Andrews, M. (Eds.), *Quaternary History of Baffin Island, Baffin Bay and Greenland*: London (Allen and Unwin), 236–308.
- Mueller, P., Erlenkeuser, H., and von Grafenstein, R., 1983. Glacial-interglacial cycles in oceanic productivity inferred from organic carbon content in eastern North Atlantic sediment cores. In Thiede, J., and Suess, E. (Eds.), *Coastal Upwelling*, Pt. B: New York (Plenum Press), 365–398.
- Murray, J. W., 1984. Paleogene and Neogene benthic foraminifers from Rockall Plateau. In Roberts, D. G., Schnitker, D., et al., *Init. Repts. DSDP*, 81: Washington (U.S. Govt. Printing Office), 503–539.
- Okada, H., and Bukry, D., 1980. Supplementary modification and introduction of code numbers to the low-latitude coccolith biostratigraphic zonation (Bukry 1973, 1975). *Mar. Micropaleont.*, 5:321–325.
- Perch-Nielsen, K., 1972. Remarks on Late Cretaceous to Pleistocene coccoliths from the North Atlantic. In Laughton, D. A., Berggren, W. A., et al., *Init. Repts. DSDP*, 12: Washington (U.S. Govt. Printing Office), 1003–1070.
- Piasecki, S., 1980. Dinoflagellate cyst stratigraphy of the Miocene Huddle and Gram Formations. *Bull. Geol. Soc. Den.*, 29:53–76.
- Poore, R. Z., 1979. Oligocene through Quaternary planktonic foraminiferal biostratigraphy of the North Atlantic: DSDP Leg 49. In Luyendyk, B. P., Cann, J. R., et al., *Init. Repts. DSDP*, 49: Washington (U.S. Govt. Printing Office), 447–518.
- Pye, G. D., and Hyndman, R. D., 1972. Heat flow measurements in Baffin Bay and the Labrador Sea. *J. Geophys. Res.*, 77:938–944.
- Rabinowitz, P. D., and Eittreim, S. L., 1974. Bottom current measurements in the Labrador Sea. *J. Geophys. Res.*, 79:4085–4090.
- Raymer, L. I., Hunt, E. R., and Gardner, J. S., 1980. An improved sonic transit time to porosity transform. *Trans. SPWLA*, Annu. Logging Symp., Pap. P.
- Roberts, D. G., 1975. Marine geology of the Rockall Plateau and Trough. *R. Soc. London, Phil. Trans.*, 278A:447–509.
- Roberts, D. G., Montadert, L., and Searle, R. C., 1979. The western Rockall Plateau: stratigraphy and crustal evolution. In Montadert, L., Roberts, D. G., et al., *Init. Repts. DSDP*, 48: Washington (U.S. Govt. Printing Office), 1061–1088.
- Roberts, D. G., Schnitker, D., et al., 1984. *Init. Repts. DSDP*, 81: Washington (U.S. Govt. Printing Office).
- Robinson, S. G., 1986. The late Pleistocene paleoclimatic record of North Atlantic deep-sea sediments revealed by mineral-magnetic measurements. *Physics of the Earth and Planetary Interiors*, 42:22–47.
- Ruddiman, W. F., and McIntyre, A., 1976. Northeast Atlantic paleoclimatic changes over the past 600,000 years. *Geol. Soc. Am. Mem.*, 145:111–146.
- _____, 1981a. Oceanic mechanisms for amplification of the 23,000-year ice-volume cycle. *Science*, 212:617–627.
- _____, 1981b. The North Atlantic Ocean during the last deglaciation. *Palaeogeogr., Palaeoclim., Palaeoecol.*, 35:145–214.
- Ruddiman, W. F., Kidd, R., et al., in press. *Init. Repts. DSDP*, 94: Washington (U.S. Govt. Printing Office).
- Sakai, T., 1980. Radiolarians from Sites 434, 435, and 436, northwest Pacific, Leg 56, Deep Sea Drilling Project. In Langseth, M., Okada, H., et al., *Init. Repts. DSDP*, 56/57, Pt. 2: Washington (U.S. Govt. Printing Office), 695–733.
- Sancetta, C., 1982. Distribution of diatom species in surface sediments of the Bering and Okhotsk seas. *Micropaleontology*, 28:221–257.
- Savin, S. M., and Yeh, H. W., 1981. Stable isotopes in ocean sediments. In Emiliani, C. (Ed.), *The Oceanic Lithosphere*: New York (Wiley), 1521–1554.
- Schnitker, D., 1979. Cenozoic deep water benthic foraminifera, Bay of Biscay. In Montadert, L., Roberts, D. G., et al., *Init. Repts. DSDP*, 48: Washington (U.S. Govt. Printing Office), 377–413.
- Schott, W., 1935. Die Foraminiferen in dem aquatorialen Teil des Atlantischen Ozeans. In *Wissenschaftliche Ergebnisse der deutschen Atlantische Expedition Meteor (1925–1927)* (Vol. 3): West Berlin (de Gruyter), 43–134.
- Schrader, H. J., and Fenner, J., 1976. Norwegian diatom biostratigraphy and taxonomy. In Talwani, M., Udintsev, G., et al., *Init. Repts. DSDP*, 38: Washington (U.S. Govt. Printing Office), 921–1098.
- Sclater, J. G., and Francheteau, J., 1970. The implications of terrestrial heat flow observations on current tectonic and geochemical models of the crust and upper mantle of the earth. *Geophys. J.*, 20:509–542.
- Shackleton, N. J., Backman, J., Zimmerman, H., Kent, D. V., Hall, M. A., Roberts, D. G., Schnitker, D., Baldauf, J. G., Desprairies, A., Homrighausen, R., Huddleston, P., Keene, J. B., Kaltenback, A. J., Krumsiek, K.A.O., Morton, A. C., Murray, J. W., and Westberg-Smith, J., 1984. Oxygen isotope calibration of the onset of ice-rafting and history of glaciation in the North Atlantic region. *Nature*, 307:620–623.
- Shackleton, N. J., and Opdyke, N. D., 1976. Oxygen-isotope and paleomagnetic stratigraphy of Pacific Core V28-239, late Pliocene to latest Pleistocene. *Geol. Soc. Am. Mem.*, 145:449–464.
- Shor, A. N., and Poore, R. Z., 1979. Bottom currents and ice rafting in the North Atlantic; interpretation of Neogene depositional environment of Leg 49 cores. In Luyendyk, B. P., Cann, J. R., et al., *Init. Repts. DSDP*, 49: Washington (U.S. Govt. Printing Office), 859–872.
- Silva, A. J., and Jordan, S., 1984. Consolidation properties and stress history of some deep sea sediments. In Denness, B. (Ed.), *Seabed Mechanics*: London (Graham and Trotman), 25–39.

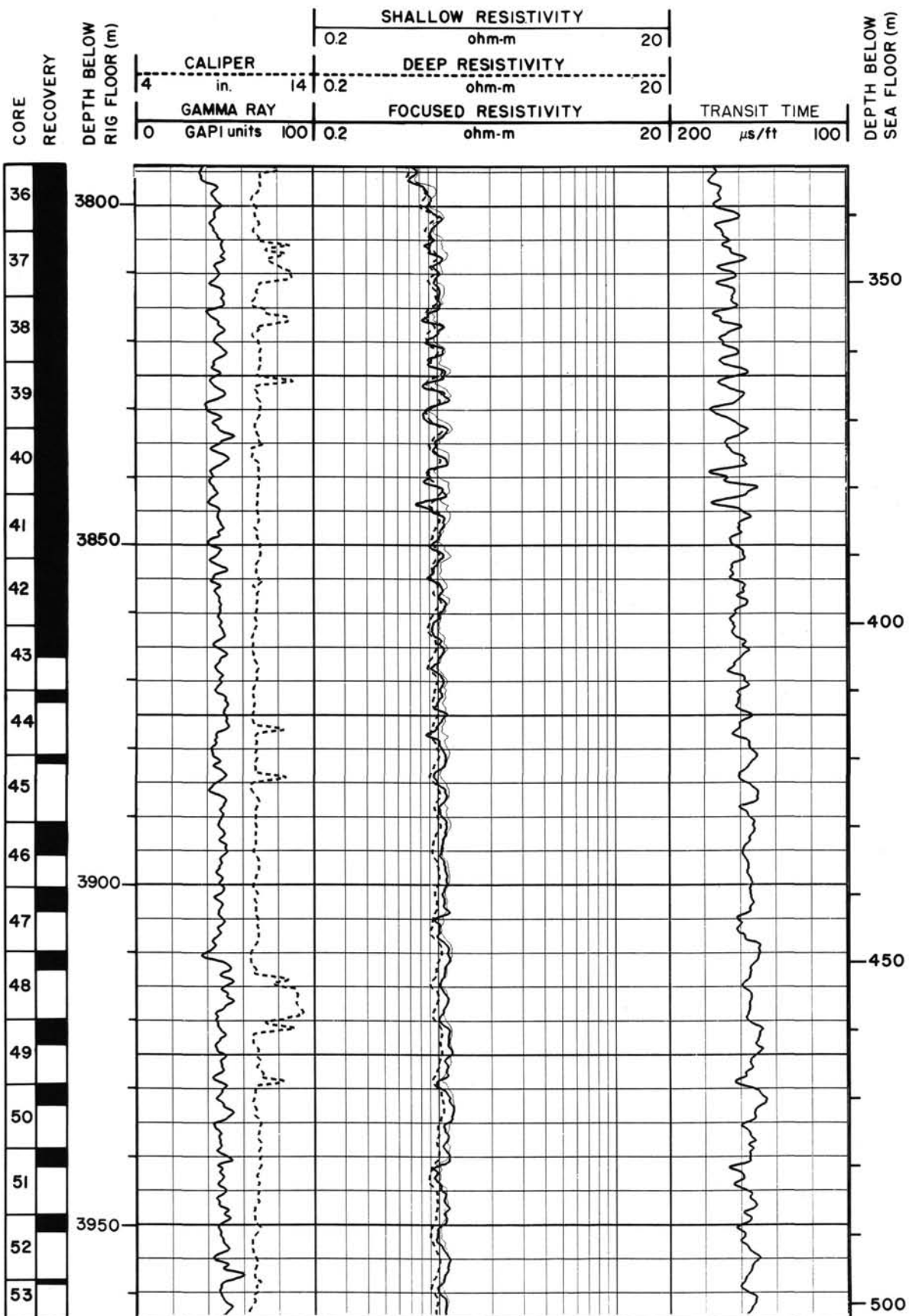
- Skempton, A. W., 1970. The consolidation of clays by gravitational compaction. *Geol. Soc. London Quart. J.*, 125:373-411.
- Srivastava, S. P., 1978. Evolution of the Labrador Sea and its bearing on the early evolution of the North Atlantic. *Geophys. J. R. Astron. Soc.*, 52:313-357.
- , 1985. Geological and geophysical maps of the Labrador Sea and northeast Newfoundland Shelf. *Can. Geol. Surv. Pap.* 85-16.
- Srivastava, S. P., Falconer, R.K.H., and MacLean, B., 1981. Labrador Sea, Davis Strait, Baffin Bay; geology and geophysics; a review. In Kerr, J. W., and Fergusson, A. J. (Eds.), *Geology of the North Atlantic Borderlands*: Can. Soc. Pet. Geol. Mem., 7:333-398.
- Stanley, E. A., 1969. Marine palynology. *Oceanogr. Mar. Biol.*, 7:277-292.
- Stow, D.A.V., 1982. Bottom currents and contourites in the North Atlantic. *Bull. Inst. Geol. Bassin Aquitaine*, 31:151-166.
- Stow, D.A.V., and Holbrook, J. A., 1984. North Atlantic contourites: an overview. In Stow, D.A.V., and Piper, D.J.W. (Eds.), *Fine-Grained Sediments: Deep-Water Processes and Facies*. Geol. Soc. Am. Spec. Publ. 15:245-256.
- Stow, D.A.V., and Lovell, J.P.B., 1979. Contourites: their recognition in modern and ancient sediments. *Earth-Sci. Rev.*, 14:251-291.
- Tucholke, B. E., and Fry, V. A., in press. Basement structure and sediment distribution in the Northwest Atlantic Ocean. *Am. Assoc. Pet. Geol.*
- Williams, D. L., Green, K., van Andel, Tj. H., von Herzen, R. P., Dymond, J. R., and Crane, K., 1979. The hydrothermal mounds of the Galapagos Rift: observations with DSRV *Alvin* and detailed heat flow studies. *J. Geophys. Res.*, 84:7467-7784.
- Worthington, L. V., and Volkmann, G. H., 1965. The volume transport of the Norwegian Sea overflow water in the North Atlantic. *Deep-Sea Res.*, 12:667-676.
- Worthington, L. V., and Wright, W. R., 1970. North Atlantic Ocean atlas of potential temperature and salinity in the deep water including temperature, salinity and oxygen profiles from the Erica Dan cruise of 1962. *Woods Hole Oceanographic Institution Atlas Series*, 2.
- Wyllie, M.R.J., Gregory, A. R., and Gardner, G.H.F., 1956. Elastic wave velocities in heterogeneous and porous media. *Geophysics*, 21:41-70.
- Zimmerman, H. B., Shackleton, N. J., Backman, J., Kent, D. V., Baldauf, J. G., Kaltenback, A. J., and Morton, A. C., 1984. History of Plio-Pleistocene climate in the northeastern Atlantic, Deep Sea Drilling Project Hole 552A. In Roberts, D. G., Schnitker, D., et al., *Init. Repts. DSDP*, 81: Washington (U.S. Govt. Printing Office), 861-875.

Summary log for Hole 646B

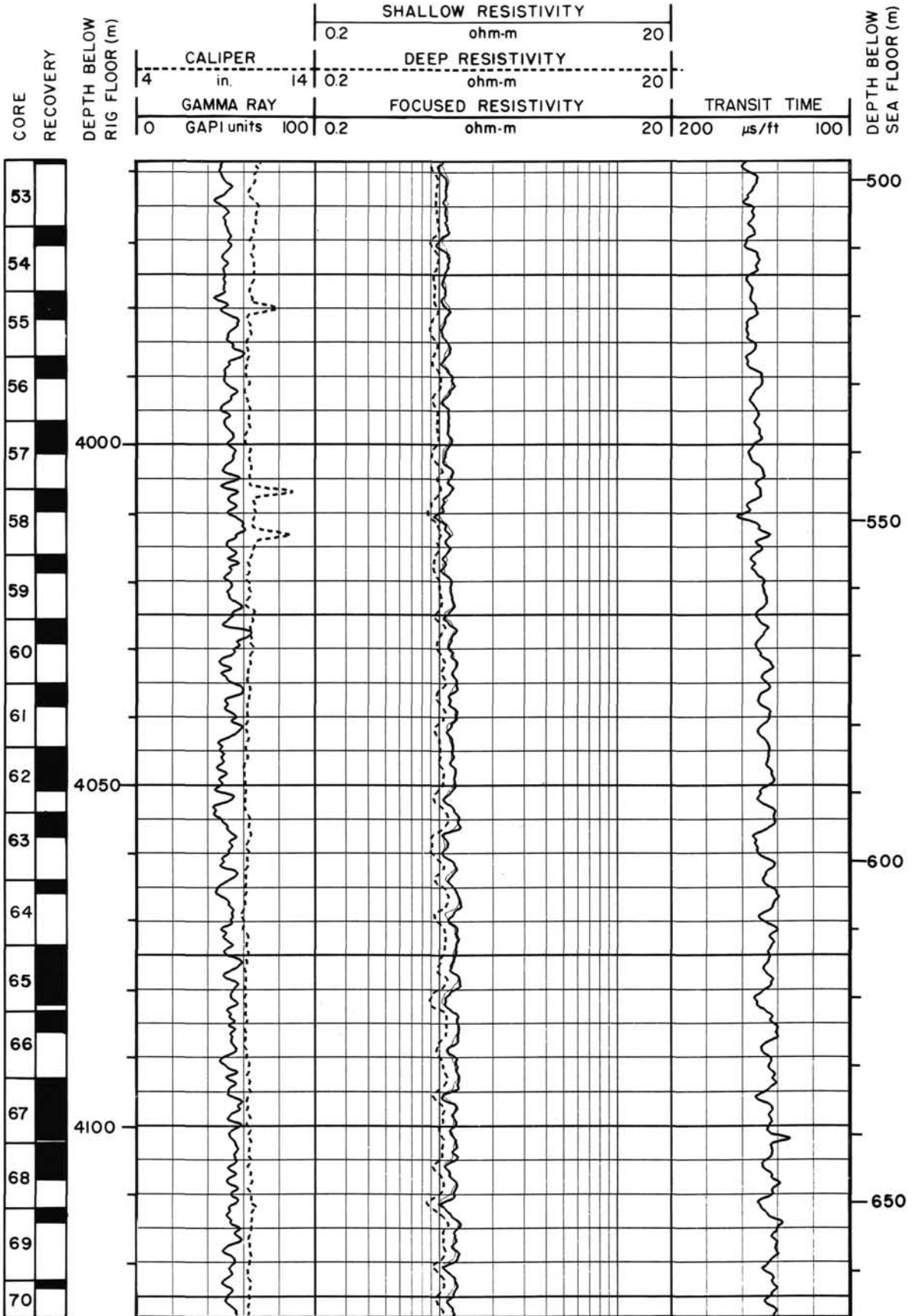
CORE RECOVERY	DEPTH BELOW RIG FLOOR (m)	SHALLOW RESISTIVITY						DEPTH BELOW SEA FLOOR (m)
		0.2		ohm-m		20		
		CALIPER		DEEP RESISTIVITY				
		4 in. 14		0.2		ohm-m 20		
0	GAMMA RAY	FOCUSED RESISTIVITY				TRANSIT TIME		
		0		ohm-m 20		200 μ s/ft 100		



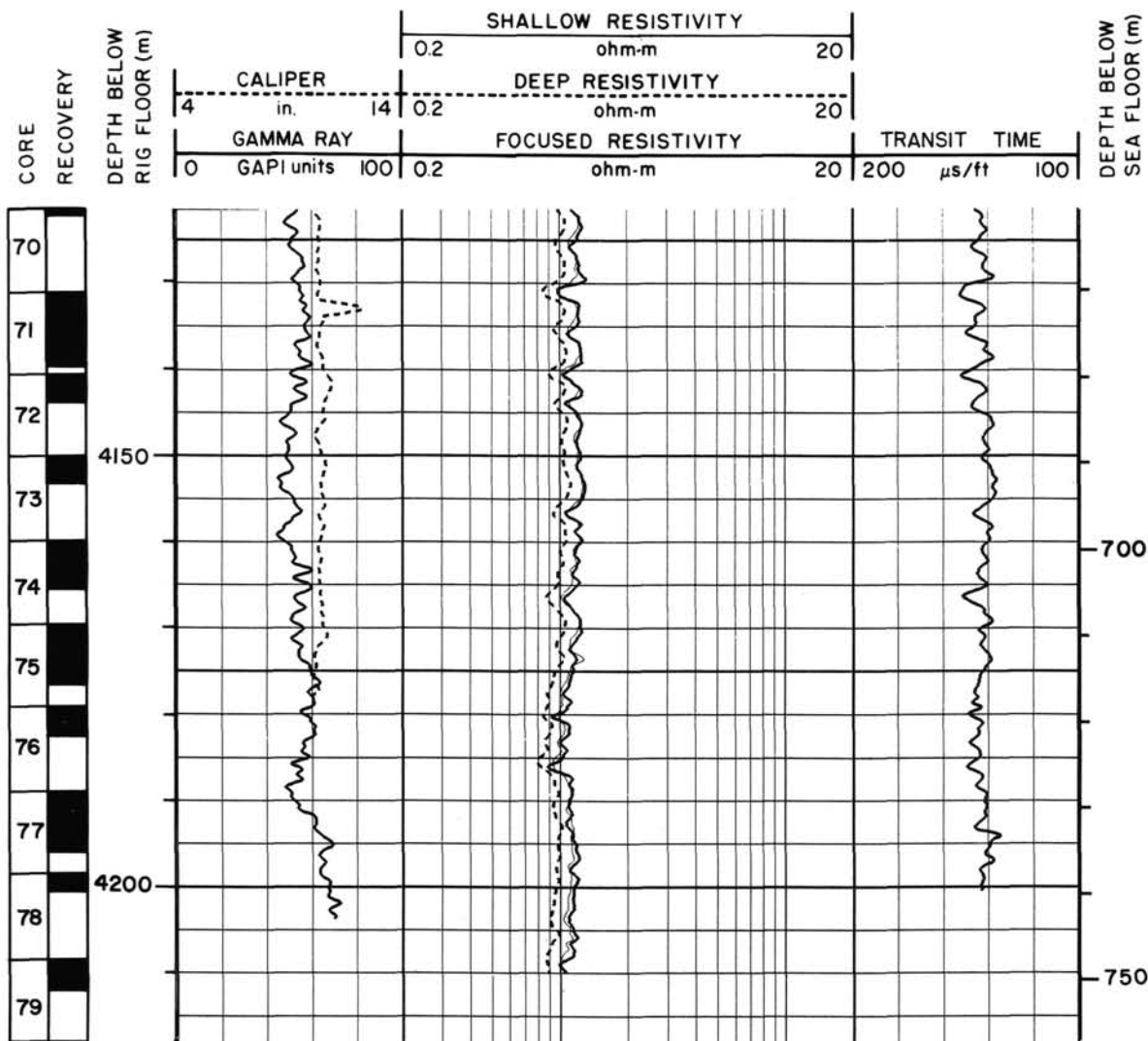
Summary log for Hole 646B (continued)



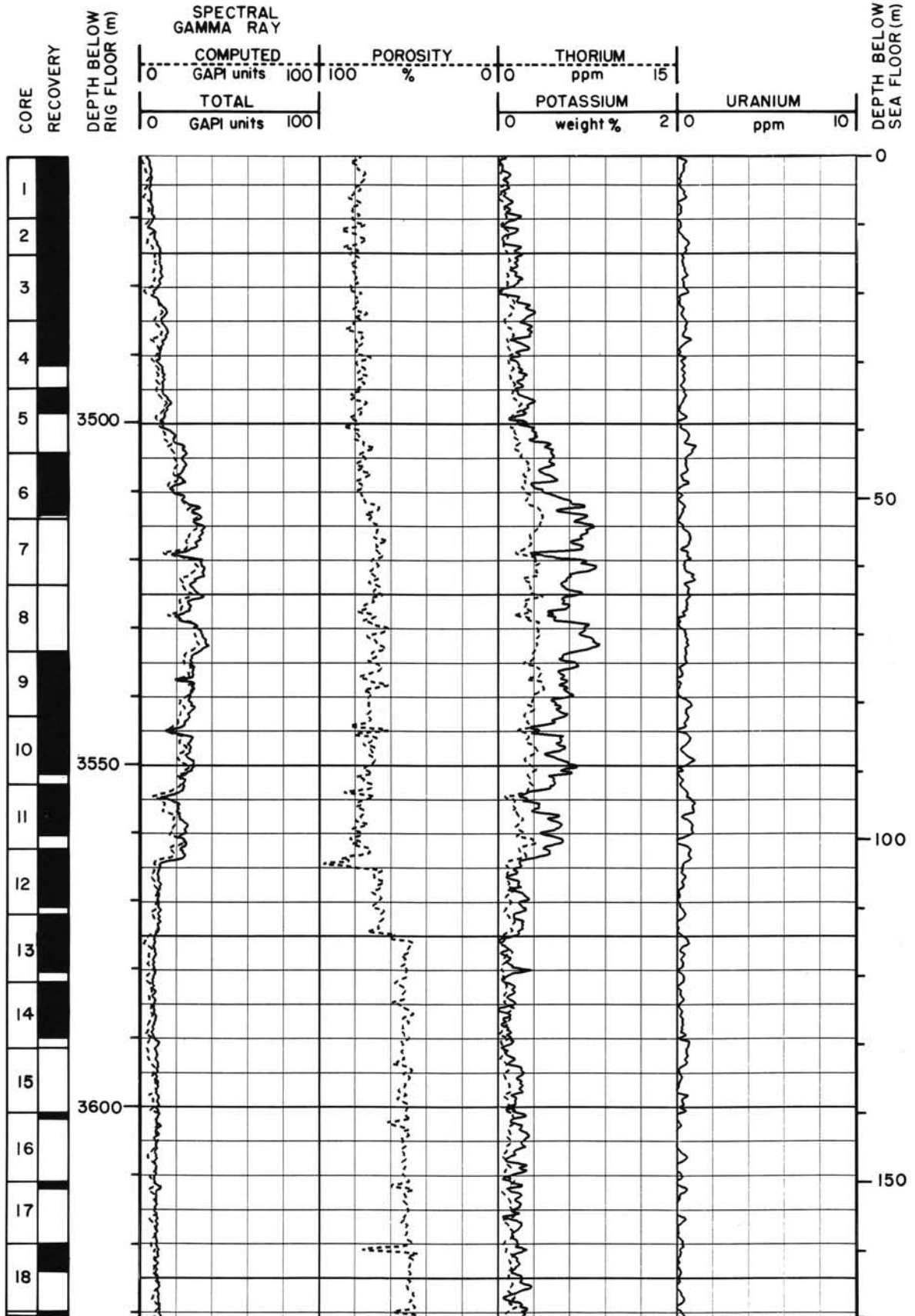
Summary log for Hole 646B (continued)



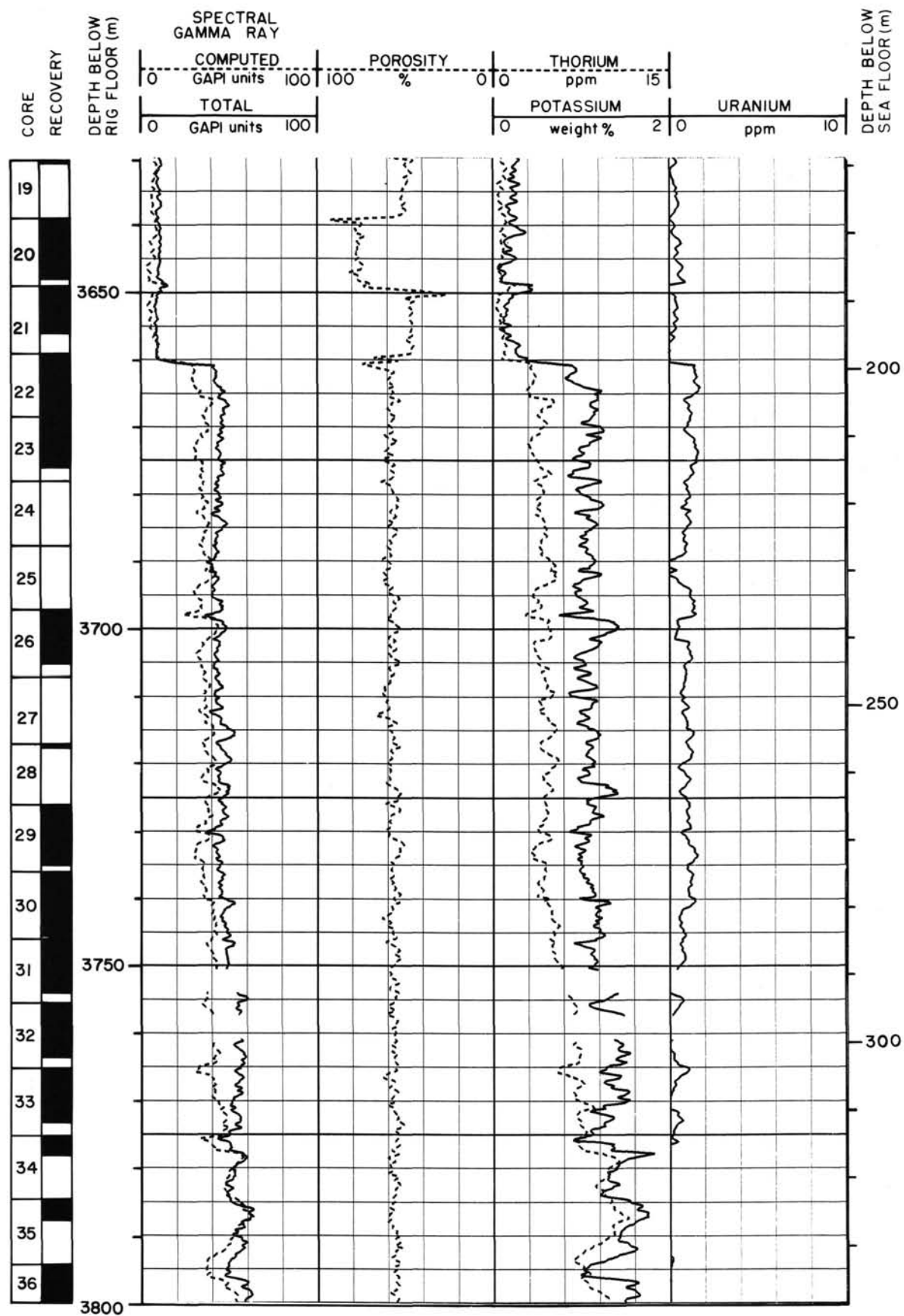
Summary log for Hole 646B (continued)



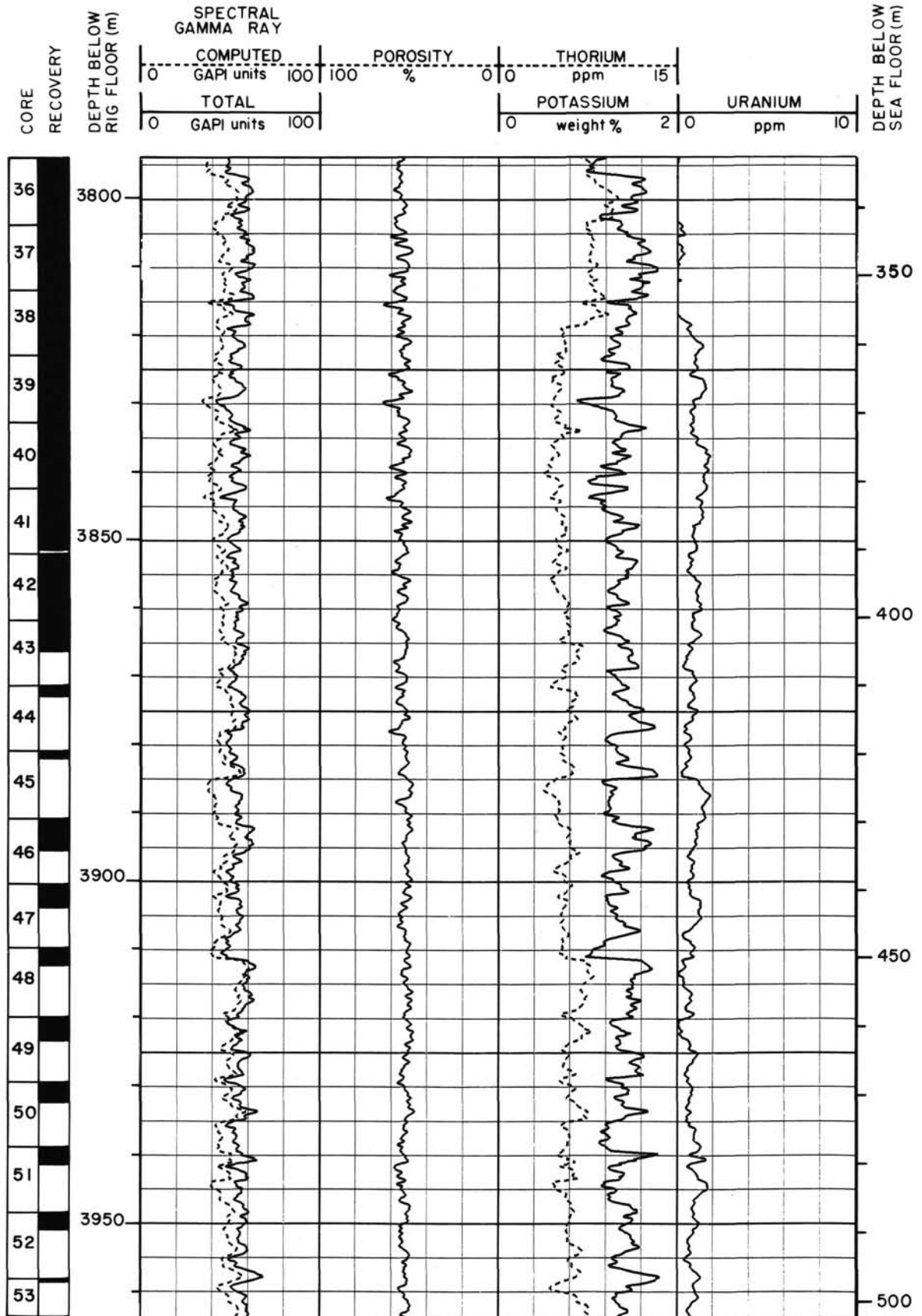
Summary log for Hole 646B (continued)



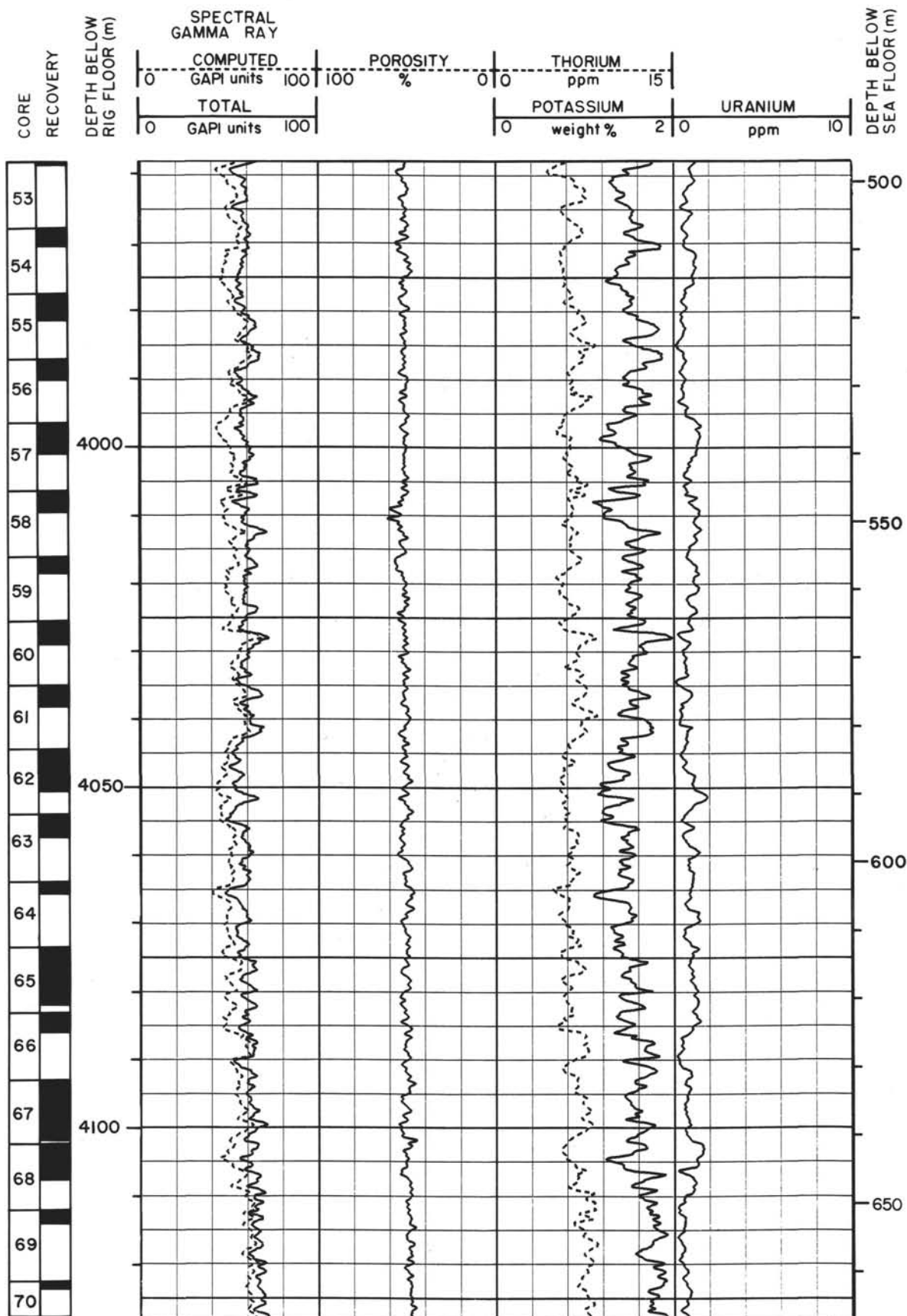
Summary log for Hole 646B (continued)



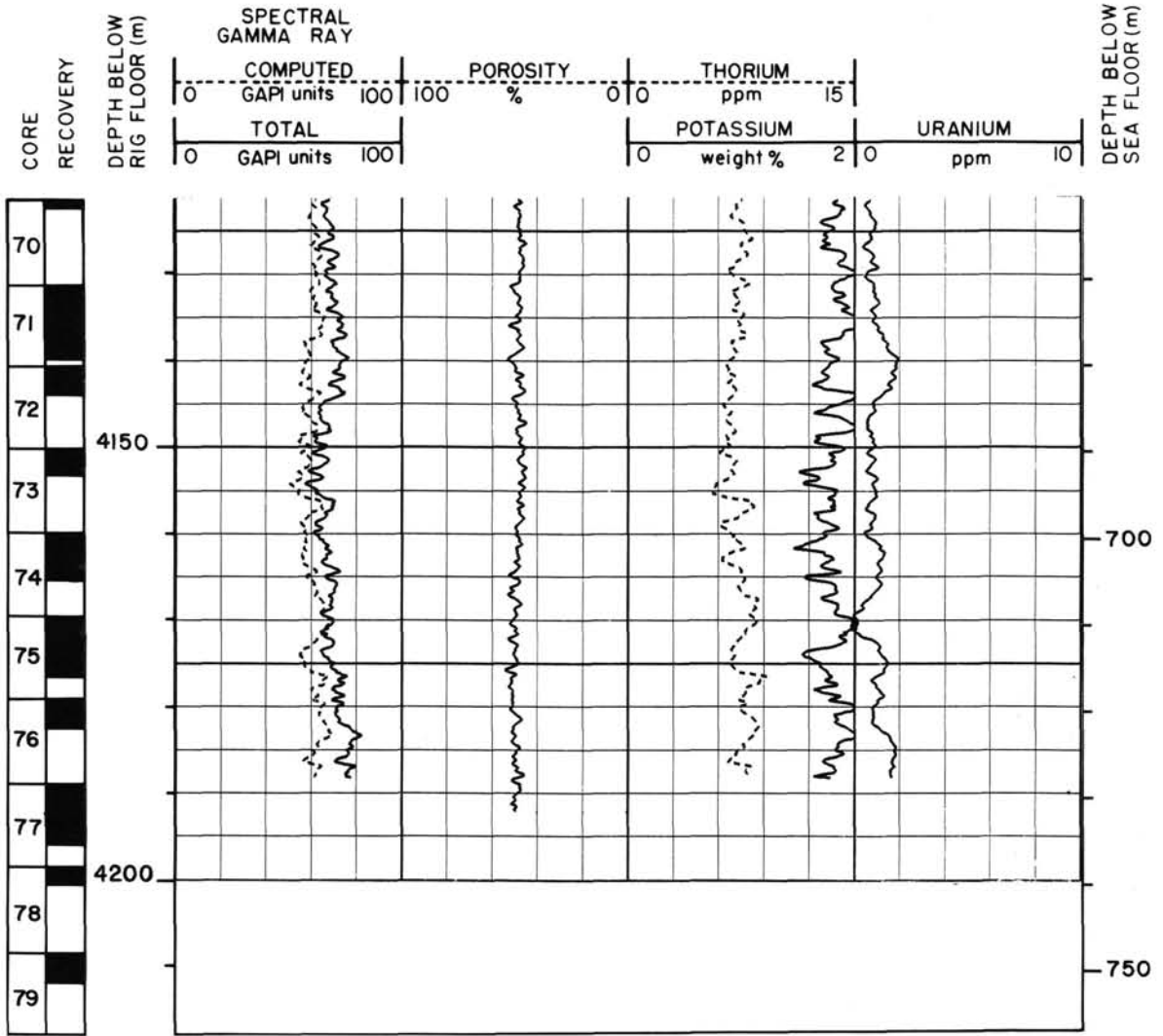
Summary log for Hole 646B (continued)



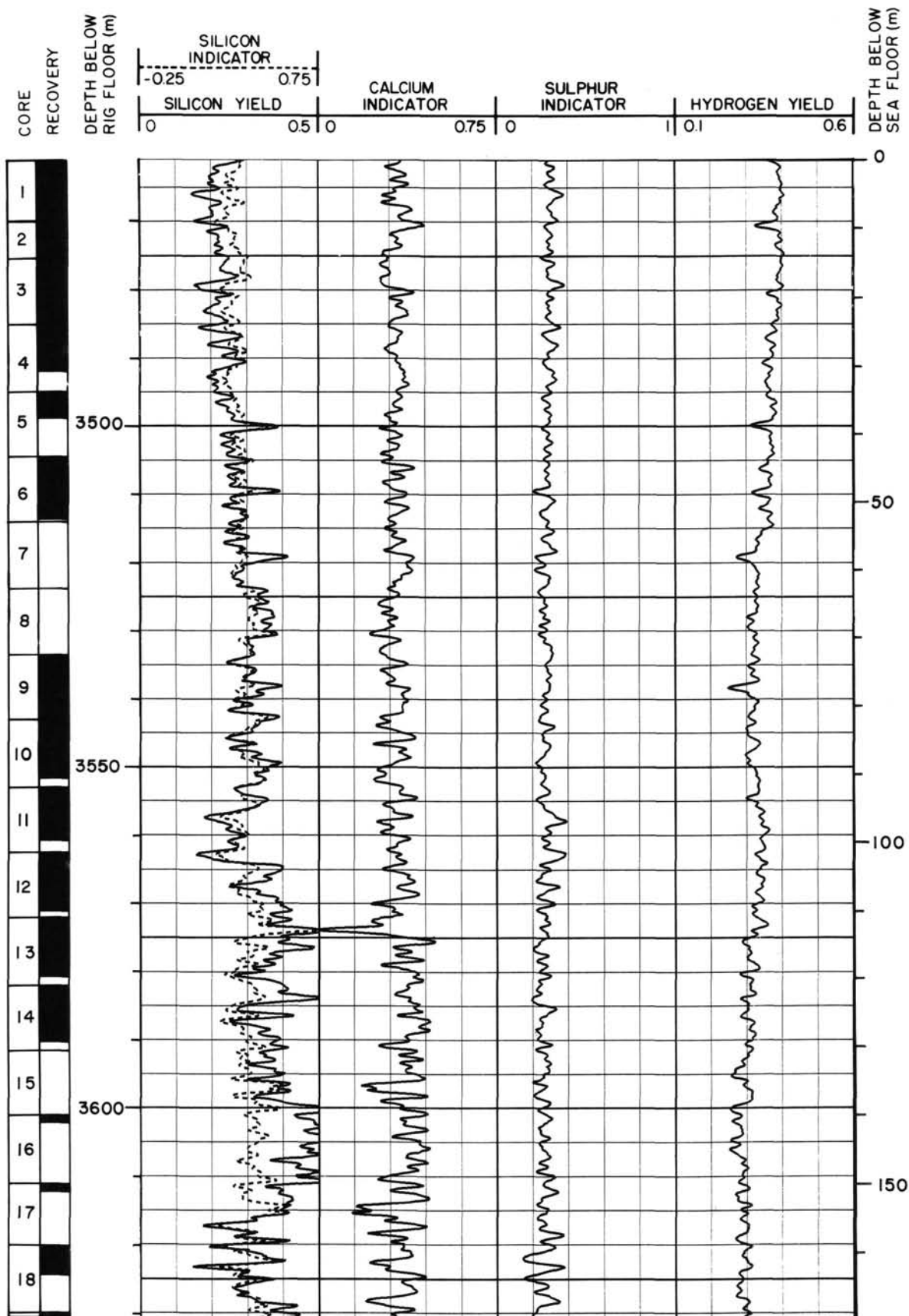
Summary log for Hole 646B (continued)



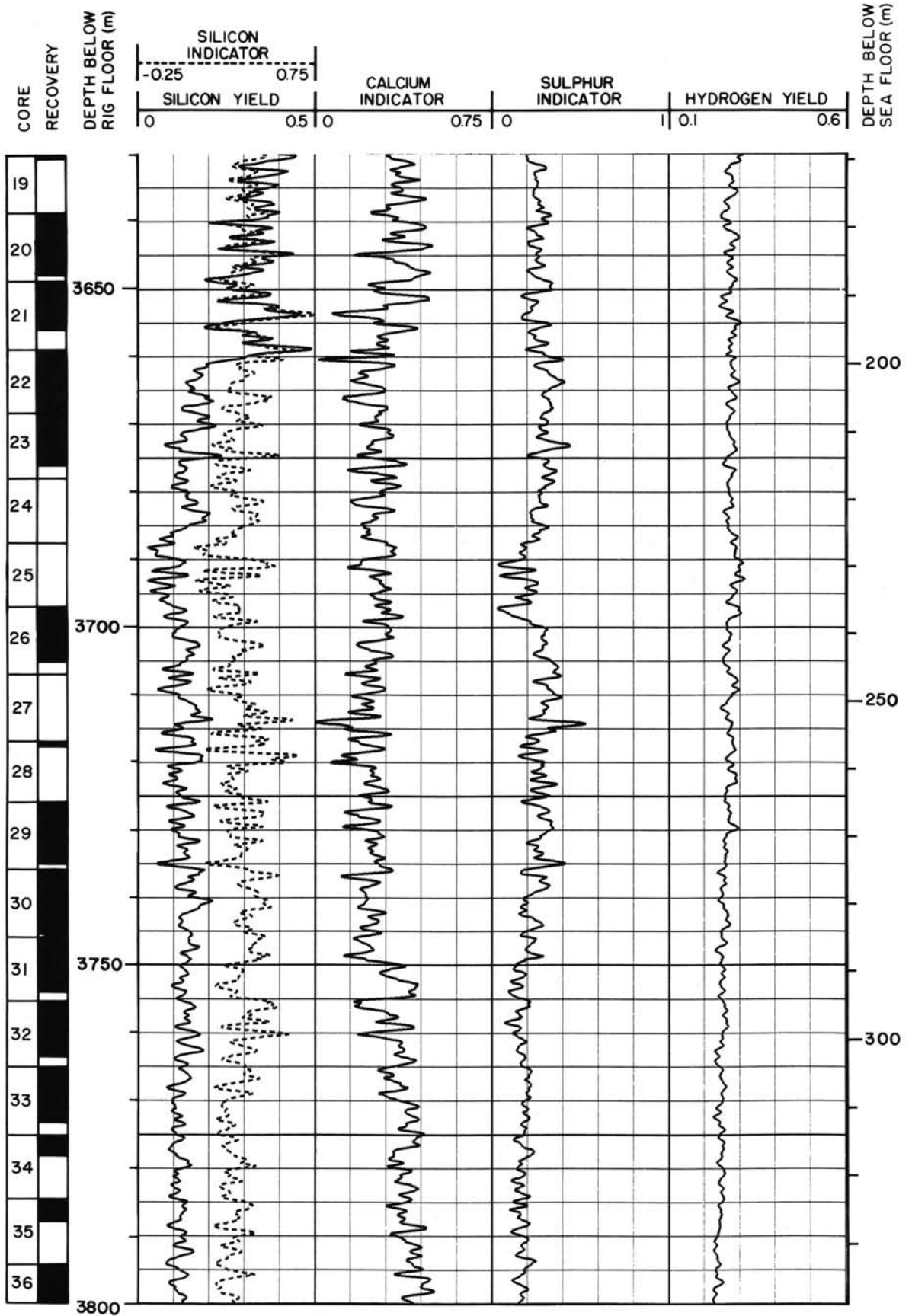
Summary log for Hole 646B (continued)



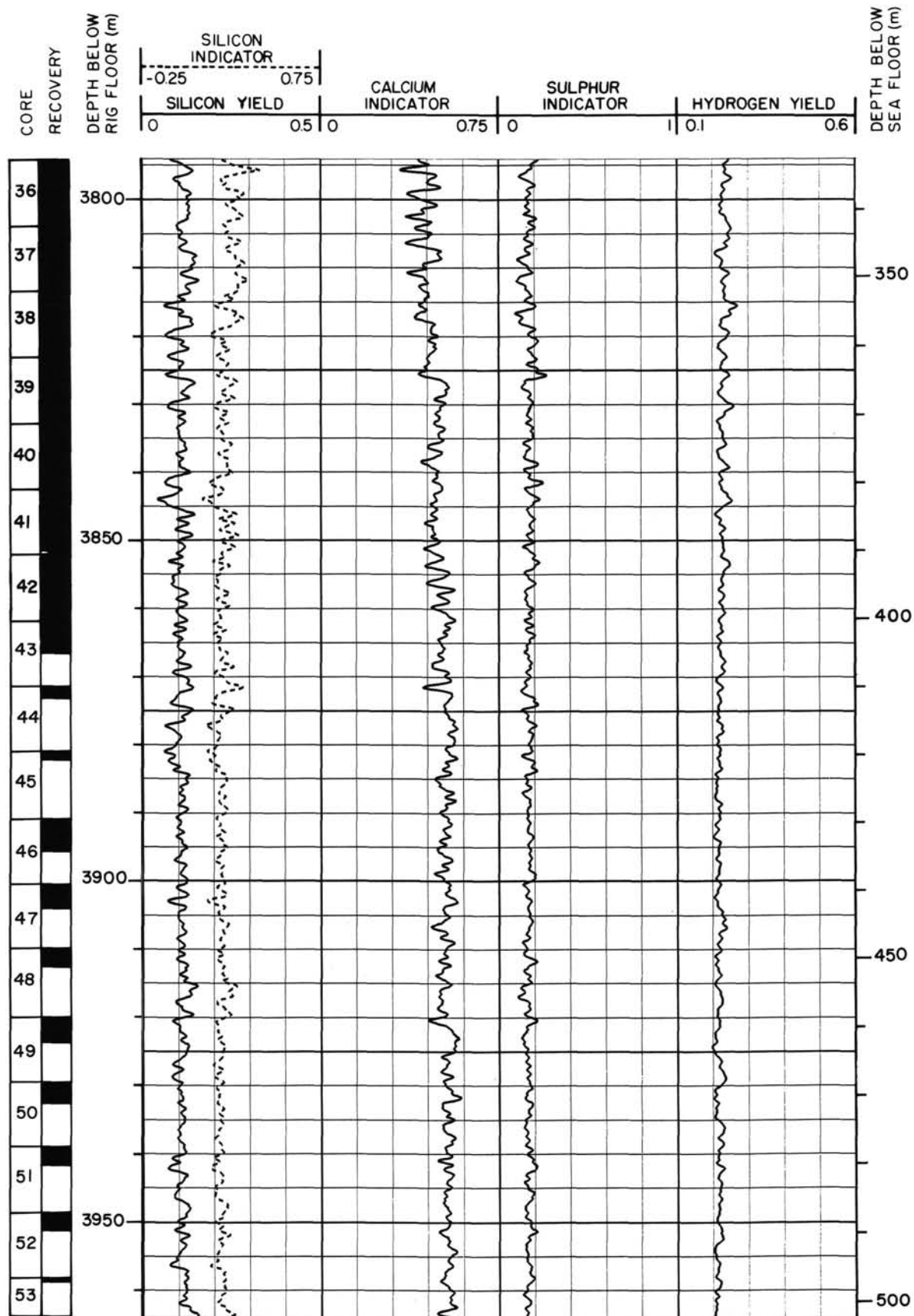
Summary log for Hole 646B (continued)



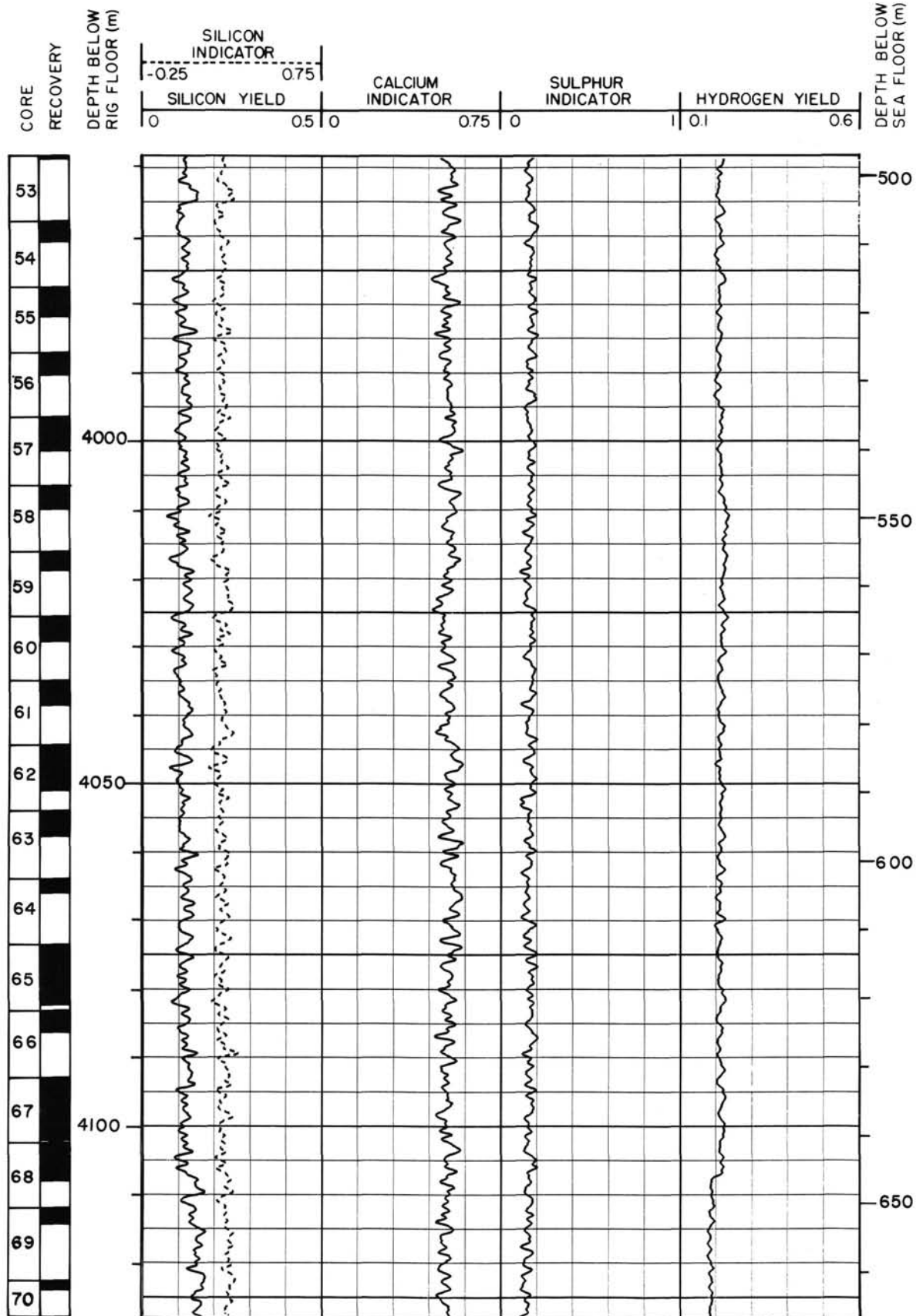
Summary log for Hole 646B (continued)



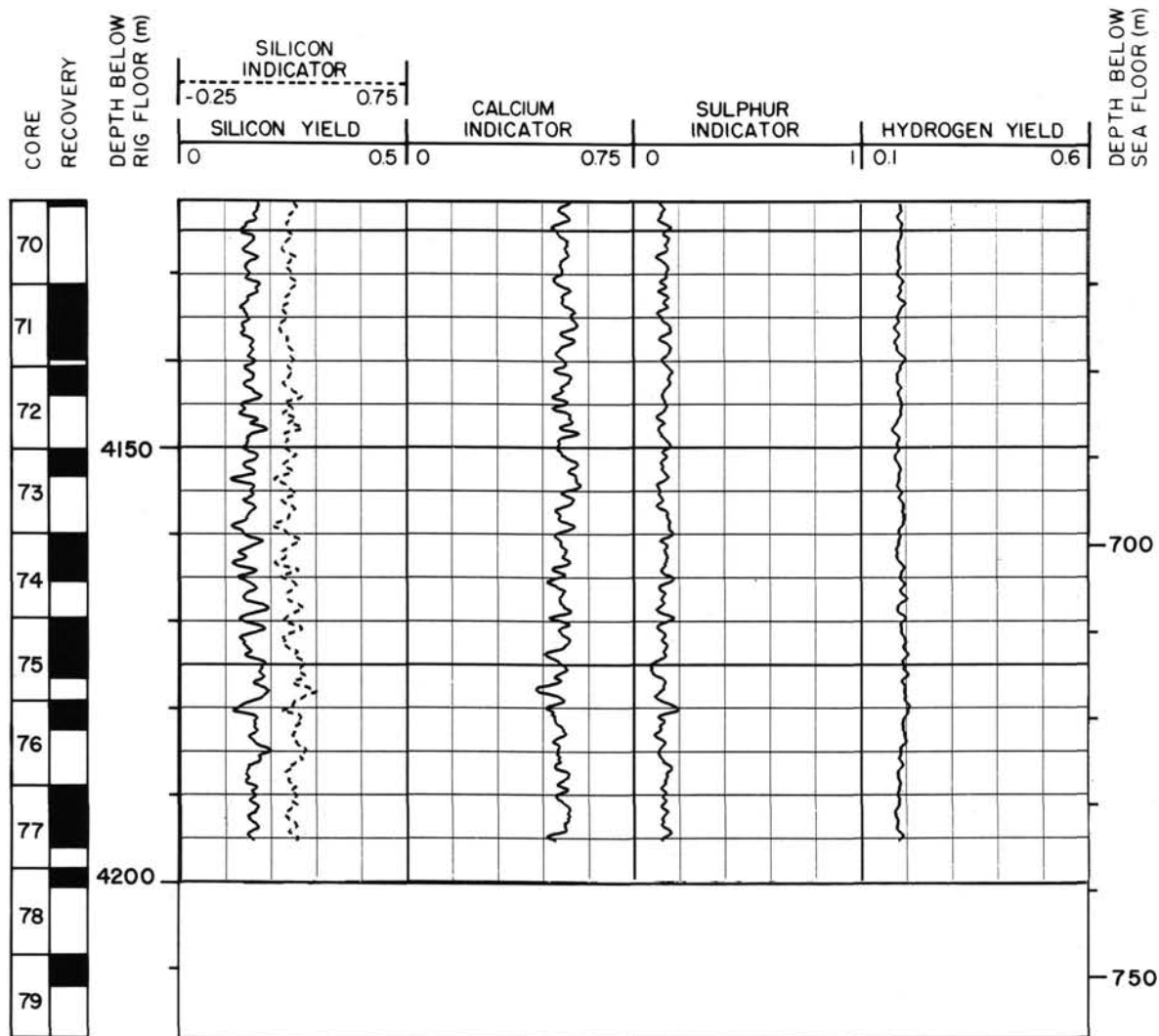
Summary log for Hole 646B (continued)



Summary log for Hole 646B (continued)

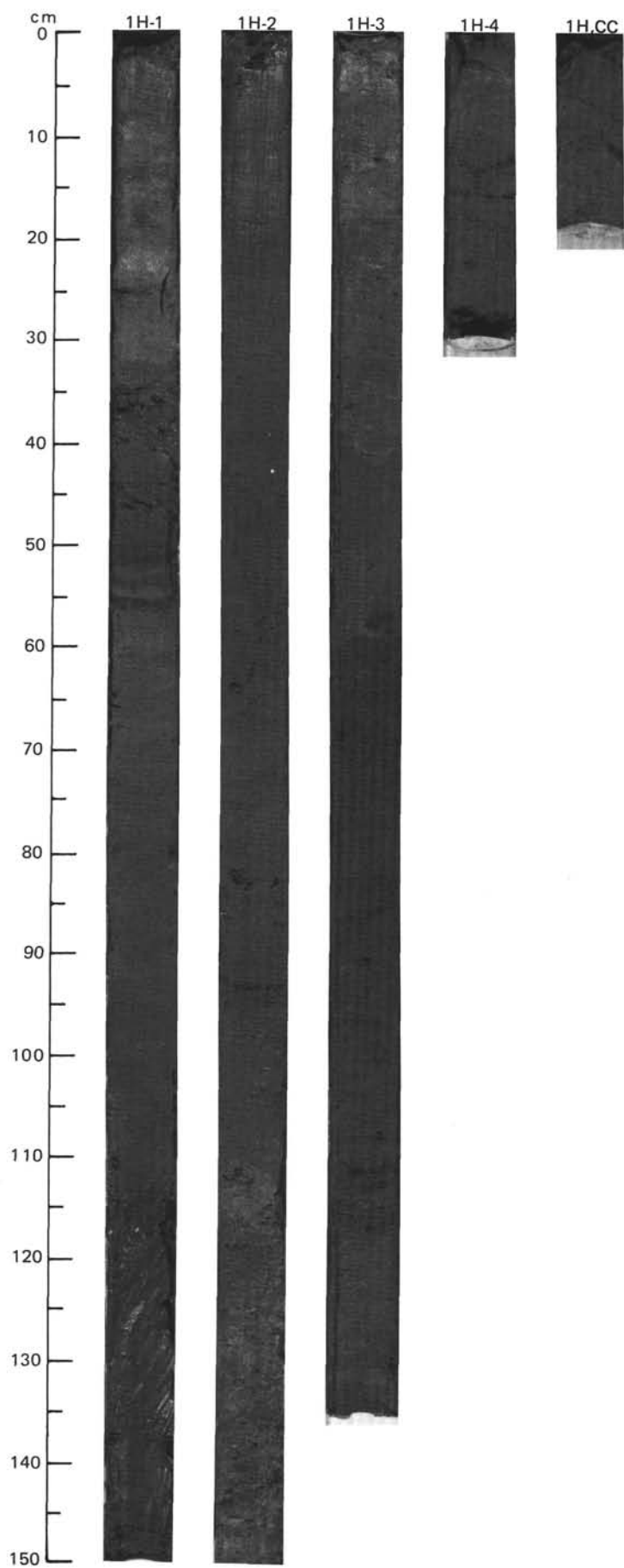


Summary log for Hole 646B (continued)



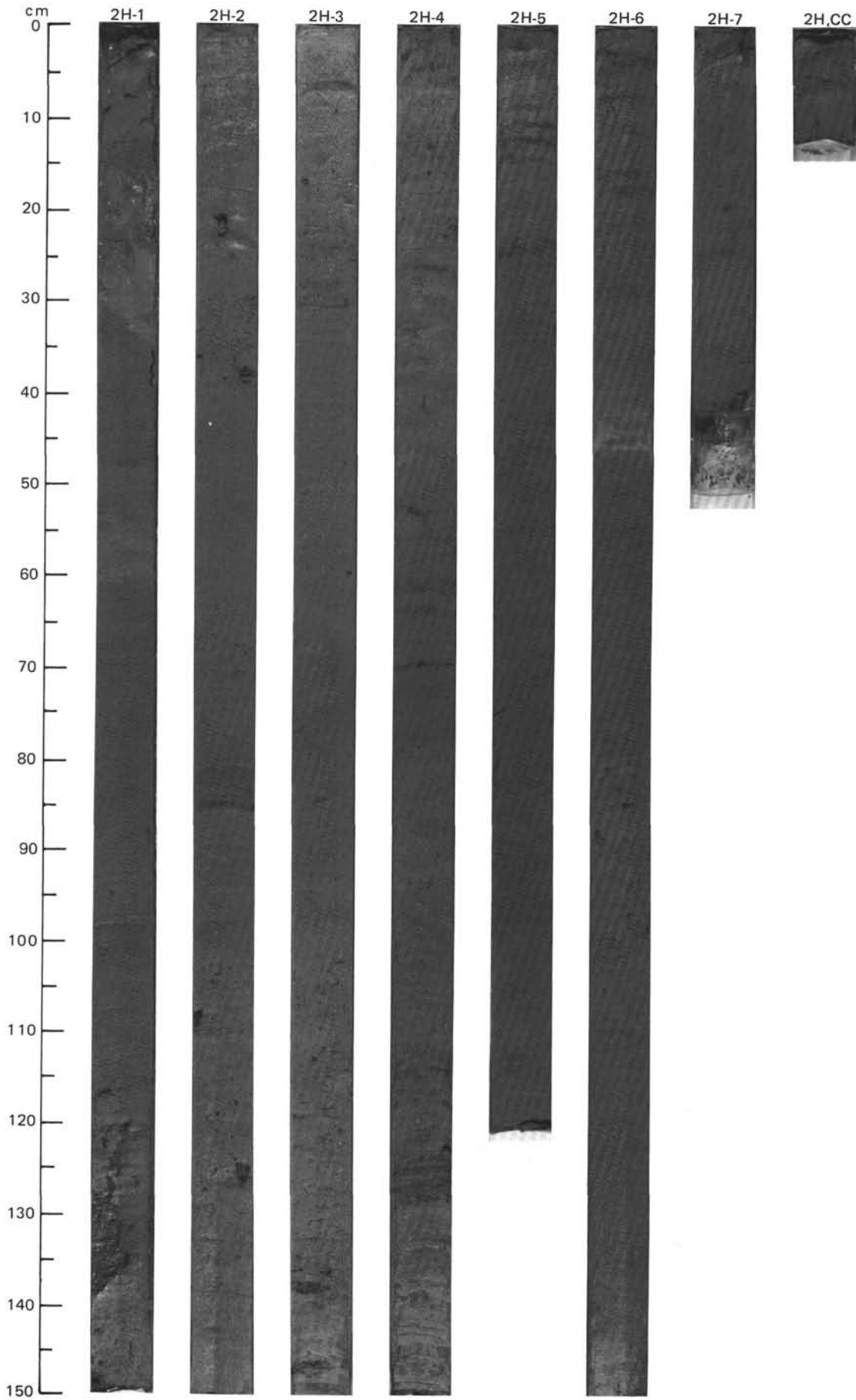
SITE 646 HOLE A CORE 1H CORED INTERVAL 3451.2-3456.2 mbsl; 0.0-5.0 mbsf

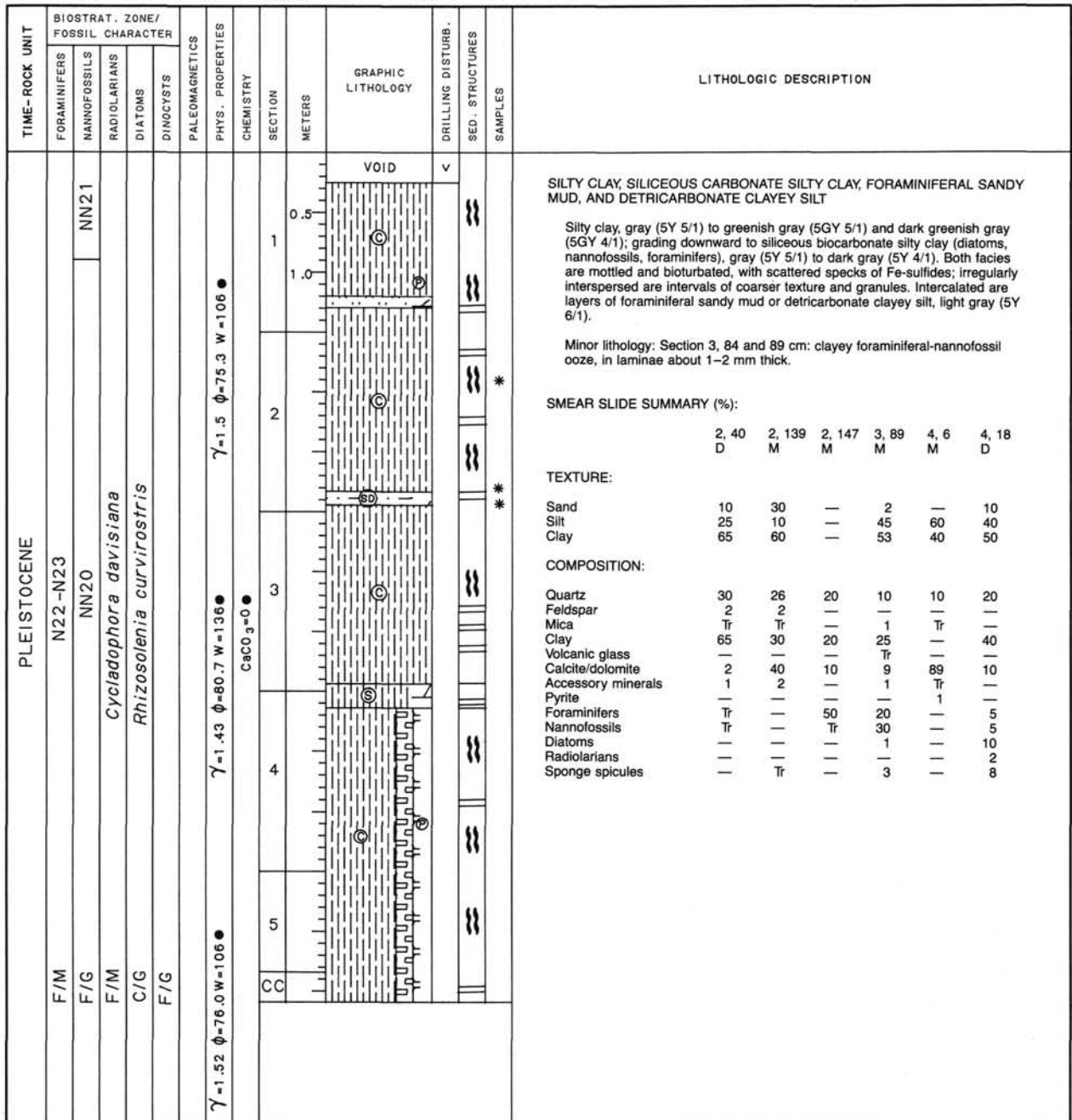
TIME-ROCK UNIT	BIOSTRAT. ZONE/ FOSSIL CHARACTER					PALEOMAGNETICS	PHYS. PROPERTIES	CHEMISTRY	SECTION	METERS	GRAPHIC LITHOLOGY	DRILLING DISTURB.	SED. STRUCTURES	SAMPLES	LITHOLOGIC DESCRIPTION																																																																																			
	FORAMINIFERS	NANNOFOSSILS	RADIOLARIANS	DIATOMS	DINOCYSTS																																																																																													
PLEISTOCENE TO RECENT	A/M	N22 - N23	A/G	A/G	A/G	Brunhes Chronozone	$\gamma_{1.39} \phi = 78.5$ W = 134 ●	CaCO ₃ = 7 ●	1	0.5		*	*	SILTY CLAY, FORAMINIFERAL-NANNOFOSSIL SILTY CLAY, AND NANNOFOSSIL SILTY CLAY																																																																																				
	A/G	NN21 C/G	A/G	A/G	1.0					Silty clay, greenish gray (5GY 6/1), with blebs or streaks of sulfide. Moderately bioturbated, scattered pebbles and coarser sand.																																																																																								
	A/G	<i>Cycladophora davisiana</i>	A/G	A/G	2										Silty clay, greenish gray (5GY 5/1) with few blebs or streaks of sulfide. Moderately bioturbated; scattered sand, granules and pebbles to 3 cm, occasionally concentrated in slightly more greenish intervals.																																																																																			
	A/G		A/G	A/G	3										Foraminiferal-nannofossil silty clay, greenish gray (5GY 6/1); weakly mottled.																																																																																			
C/G		A/G	A/G	4	Nannofossil silty clay, light yellowish brown (10YR 6/4); weakly laminated and bioturbated.																																																																																													
														Minor lithology: Section 2, 112-116 cm: detriticarbonate silty mud, gray (5Y 6/1) with clasts of same composition.																																																																																				
														Smear-slide estimates of nannofossil content (~60%) are too high, as shown by carbonate bomb results of <30% carbonate. Lithologic columns were adjusted.																																																																																				
														SMEAR SLIDE SUMMARY (%):																																																																																				
														<table border="1"> <tr> <td></td> <td>1, 53</td> <td>1, 86</td> <td>2, 114</td> <td>3, 72</td> <td>1, 45</td> <td>2, 12</td> </tr> <tr> <td></td> <td>M</td> <td>D</td> <td>M</td> <td>D</td> <td></td> <td></td> </tr> </table>		1, 53	1, 86	2, 114	3, 72	1, 45	2, 12		M	D	M	D																																																																								
	1, 53	1, 86	2, 114	3, 72	1, 45	2, 12																																																																																												
	M	D	M	D																																																																																														
														TEXTURE:																																																																																				
														<table border="1"> <tr> <td>Sand</td> <td>5</td> <td>10</td> <td>10</td> <td>2</td> <td>—</td> <td>—</td> </tr> <tr> <td>Silt</td> <td>65</td> <td>60</td> <td>70</td> <td>43</td> <td>—</td> <td>—</td> </tr> <tr> <td>Clay</td> <td>30</td> <td>30</td> <td>20</td> <td>55</td> <td>—</td> <td>—</td> </tr> </table>	Sand	5	10	10	2	—	—	Silt	65	60	70	43	—	—	Clay	30	30	20	55	—	—																																																															
Sand	5	10	10	2	—	—																																																																																												
Silt	65	60	70	43	—	—																																																																																												
Clay	30	30	20	55	—	—																																																																																												
														COMPOSITION:																																																																																				
														<table border="1"> <tr> <td>Quartz</td> <td>3</td> <td>5</td> <td>40</td> <td>40</td> <td>—</td> <td>—</td> </tr> <tr> <td>Feldspar</td> <td>Tr</td> <td>Tr</td> <td>2</td> <td>Tr</td> <td>—</td> <td>—</td> </tr> <tr> <td>Clay</td> <td>27</td> <td>22</td> <td>17</td> <td>48</td> <td>—</td> <td>—</td> </tr> <tr> <td>Volcanic glass</td> <td>Tr</td> <td>Tr</td> <td>—</td> <td>Tr</td> <td>—</td> <td>—</td> </tr> <tr> <td>Calcite/dolomite</td> <td>—</td> <td>—</td> <td>40</td> <td>10</td> <td>—</td> <td>—</td> </tr> <tr> <td>Accessory minerals</td> <td>Tr</td> <td>Tr</td> <td>1</td> <td>Tr</td> <td>—</td> <td>—</td> </tr> <tr> <td>Foraminifers</td> <td>5</td> <td>10</td> <td>—</td> <td>1</td> <td>—</td> <td>—</td> </tr> <tr> <td>Nannofossils</td> <td>60</td> <td>60</td> <td>—</td> <td>1</td> <td>—</td> <td>—</td> </tr> <tr> <td>Diatoms</td> <td>3</td> <td>1</td> <td>—</td> <td>Tr</td> <td>—</td> <td>—</td> </tr> <tr> <td>Radiolarians</td> <td>Tr</td> <td>—</td> <td>—</td> <td>Tr</td> <td>—</td> <td>—</td> </tr> <tr> <td>Sponge spicules</td> <td>2</td> <td>2</td> <td>—</td> <td>1</td> <td>—</td> <td>—</td> </tr> <tr> <td>Calcium carbonate bomb(?)</td> <td>—</td> <td>—</td> <td>—</td> <td>—</td> <td>39</td> <td>5</td> </tr> </table>	Quartz	3	5	40	40	—	—	Feldspar	Tr	Tr	2	Tr	—	—	Clay	27	22	17	48	—	—	Volcanic glass	Tr	Tr	—	Tr	—	—	Calcite/dolomite	—	—	40	10	—	—	Accessory minerals	Tr	Tr	1	Tr	—	—	Foraminifers	5	10	—	1	—	—	Nannofossils	60	60	—	1	—	—	Diatoms	3	1	—	Tr	—	—	Radiolarians	Tr	—	—	Tr	—	—	Sponge spicules	2	2	—	1	—	—	Calcium carbonate bomb(?)	—	—	—	—	39	5
Quartz	3	5	40	40	—	—																																																																																												
Feldspar	Tr	Tr	2	Tr	—	—																																																																																												
Clay	27	22	17	48	—	—																																																																																												
Volcanic glass	Tr	Tr	—	Tr	—	—																																																																																												
Calcite/dolomite	—	—	40	10	—	—																																																																																												
Accessory minerals	Tr	Tr	1	Tr	—	—																																																																																												
Foraminifers	5	10	—	1	—	—																																																																																												
Nannofossils	60	60	—	1	—	—																																																																																												
Diatoms	3	1	—	Tr	—	—																																																																																												
Radiolarians	Tr	—	—	Tr	—	—																																																																																												
Sponge spicules	2	2	—	1	—	—																																																																																												
Calcium carbonate bomb(?)	—	—	—	—	39	5																																																																																												

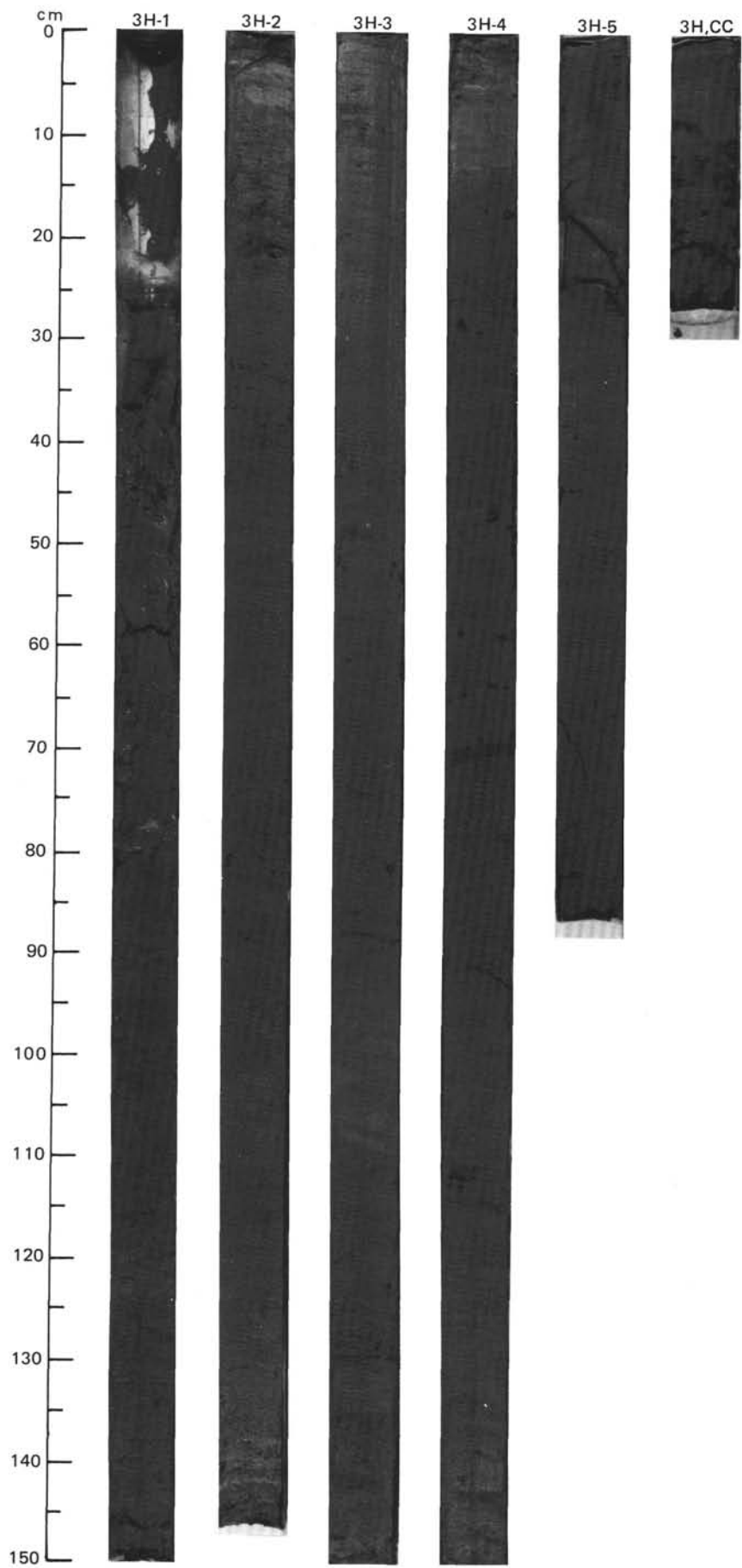


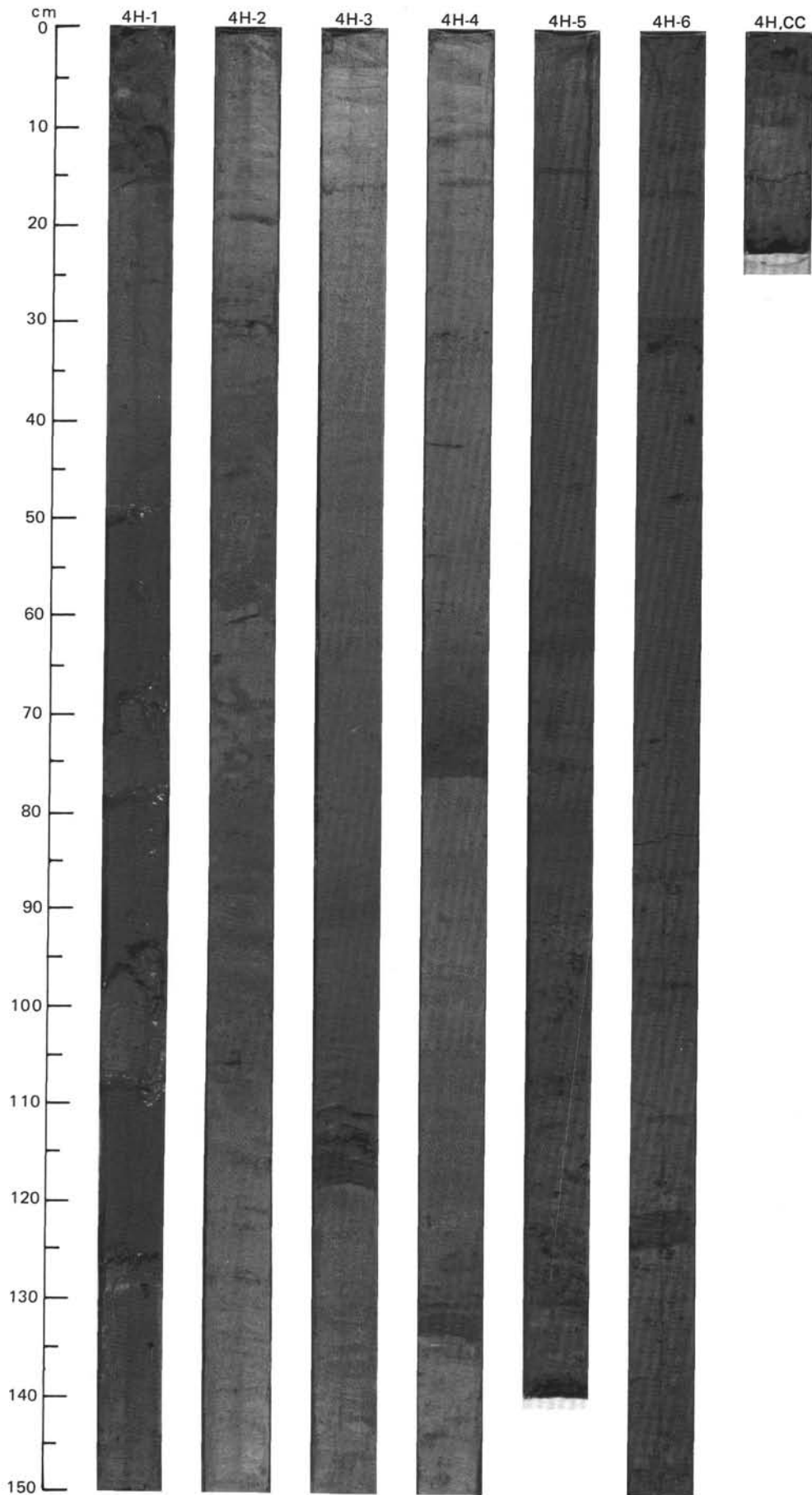
SITE 646 HOLE A CORE 2 H CORED INTERVAL 3456.2-3467.7 mbsl; 5.0-16.5 mbsf

TIME-ROCK UNIT	BIOSTRAT. ZONE/ FOSSIL CHARACTER					PALEOMAGNETICS	PHYS. PROPERTIES	CHEMISTRY	SECTION	METERS	GRAPHIC LITHOLOGY	DRILLING DISTURB.	SED. STRUCTURES	SAMPLES	LITHOLOGIC DESCRIPTION																																																																																																	
	FORAMINIFERS	NANNOFOSSILS	RADIOLARIANS	DIATOMS	DINOCYSTS																																																																																																											
PLEISTOCENE	N22 - N23					Brunhes Chronozone	$\gamma = 1.52 \phi = 75.0 \text{ W} = 102 \bullet$	CaCO ₃ = 8 ●	1	0.5		H	*	*	SILICA-BEARING SILTY CLAY, FORAMINIFER-BEARING SILTY CLAY, AND NANNOFOSSIL CLAYEY SILT																																																																																																	
	NN21																																																																																																															
	<i>Cycladophora davisiana</i>																																																																																																															
	F/G																																																																																																															
	A/G																																																																																																															
	C/G																																																																																																															
	A/G																																																																																																															
C/M																																																																																																																
N22 - N23					Brunhes Chronozone	$\gamma = 1.54 \phi = 75.9 \text{ W} = 102 \bullet$	CaCO ₃ = 10 ●	2	1.0		H	*	*	Silica-bearing silty clay, dark gray (5Y 4/1), and gray (5Y 5/1). Foraminifer-bearing silty clay, gray (5Y 5/1), greenish gray (5GY 5/1), and light gray (5Y 6/1). Foraminifers are concentrated in pockets. Nannofossil clayey silt, light gray (5Y 6/1), gray (5Y 5/1), and dark gray (5Y 4/1). Locally moderate bioturbation is visible. Few granules (dropstones). Minor lithologies: a. Section 1, 53-65 cm: detrital carbonate clayey silt, brown (10YR 5/3) and mottled. b. Section 2, 80-85 cm: well sorted laminated layers of silt, dark gray (5Y 4/1).																																																																																																		
N22 - N23																																																																																																																
NN21																																																																																																																
<i>Cycladophora davisiana</i>																																																																																																																
F/G																																																																																																																
A/G																																																																																																																
C/G																																																																																																																
A/G																																																																																																																
C/M																																																																																																																
N22 - N23					Brunhes Chronozone	$\gamma = 1.47 \phi = 78.7 \text{ W} = 121 \bullet$	CaCO ₃ = 6 ●	3	1.5		H	*	*	SMEAR SLIDE SUMMARY (%):																																																																																																		
N22 - N23																																																																																																																
NN21																																																																																																																
<i>Cycladophora davisiana</i>																																																																																																																
F/G																																																																																																																
A/G																																																																																																																
C/G																																																																																																																
A/G																																																																																																																
C/M																																																																																																																
N22 - N23					Brunhes Chronozone	$\gamma = 1.43 \phi = 81.0 \text{ W} = 139 \bullet$	CaCO ₃ = 9 ●	4	2.0		H	*	*	<table border="1"> <thead> <tr> <th></th> <th>1, 60 D</th> <th>1, 75 D</th> <th>2, 87 M</th> <th>3, 108 D</th> <th>4, 69 M</th> <th>5, 33 D</th> </tr> </thead> <tbody> <tr> <td>Sand</td> <td>5</td> <td>1</td> <td>5</td> <td>4</td> <td>5</td> <td>10</td> </tr> <tr> <td>Silt</td> <td>60</td> <td>80</td> <td>85</td> <td>41</td> <td>35</td> <td>55</td> </tr> <tr> <td>Clay</td> <td>35</td> <td>20</td> <td>10</td> <td>55</td> <td>60</td> <td>35</td> </tr> </tbody> </table>		1, 60 D	1, 75 D	2, 87 M	3, 108 D	4, 69 M	5, 33 D	Sand	5	1	5	4	5	10	Silt	60	80	85	41	35	55	Clay	35	20	10	55	60	35																																																																						
	1, 60 D	1, 75 D	2, 87 M	3, 108 D											4, 69 M	5, 33 D																																																																																																
Sand	5	1	5	4											5	10																																																																																																
Silt	60	80	85	41											35	55																																																																																																
Clay	35	20	10	55											60	35																																																																																																
N22 - N23																																																																																																																
NN21																																																																																																																
<i>Cycladophora davisiana</i>																																																																																																																
F/G																																																																																																																
A/G																																																																																																																
C/G																																																																																																																
A/G																																																																																																																
C/M																																																																																																																
N22 - N23					Brunhes Chronozone	$\gamma = 1.43 \phi = 81.0 \text{ W} = 139 \bullet$	CaCO ₃ = 9 ●	5	2.5		H	*	*	COMPOSITION:																																																																																																		
N22 - N23																																																																																																																
NN21																																																																																																																
<i>Cycladophora davisiana</i>																																																																																																																
F/G																																																																																																																
A/G																																																																																																																
C/G																																																																																																																
A/G																																																																																																																
C/M																																																																																																																
N22 - N23					Brunhes Chronozone	$\gamma = 1.43 \phi = 81.0 \text{ W} = 139 \bullet$	CaCO ₃ = 9 ●	6	3.0		H	*	*	<table border="1"> <tbody> <tr> <td>Quartz</td> <td>35</td> <td>35</td> <td>65</td> <td>30</td> <td>40</td> <td>35</td> </tr> <tr> <td>Feldspar</td> <td>—</td> <td>5</td> <td>10</td> <td>5</td> <td>—</td> <td>5</td> </tr> <tr> <td>Mica</td> <td>—</td> <td>—</td> <td>—</td> <td>—</td> <td>—</td> <td>Tr</td> </tr> <tr> <td>Clay</td> <td>30</td> <td>8</td> <td>10</td> <td>45</td> <td>25</td> <td>25</td> </tr> <tr> <td>Volcanic glass</td> <td>—</td> <td>—</td> <td>Tr</td> <td>—</td> <td>—</td> <td>—</td> </tr> <tr> <td>Calcite/dolomite</td> <td>35</td> <td>7</td> <td>5</td> <td>20</td> <td>25</td> <td>15</td> </tr> <tr> <td>Accessory minerals</td> <td>Tr</td> <td>8</td> <td>5</td> <td>3</td> <td>—</td> <td>Tr</td> </tr> <tr> <td>Pyrite</td> <td>Tr</td> <td>5</td> <td>5</td> <td>2</td> <td>5</td> <td>—</td> </tr> <tr> <td>Foraminifers</td> <td>—</td> <td>3</td> <td>Tr</td> <td>1</td> <td>—</td> <td>2</td> </tr> <tr> <td>Nannofossils</td> <td>—</td> <td>25</td> <td>—</td> <td>3</td> <td>Tr</td> <td>3</td> </tr> <tr> <td>Diatoms</td> <td>—</td> <td>3</td> <td>Tr</td> <td>Tr</td> <td>Tr</td> <td>10</td> </tr> <tr> <td>Radiolarians</td> <td>—</td> <td>Tr</td> <td>—</td> <td>Tr</td> <td>—</td> <td>—</td> </tr> <tr> <td>Sponge spicules</td> <td>—</td> <td>2</td> <td>Tr</td> <td>Tr</td> <td>5</td> <td>5</td> </tr> <tr> <td>Plant debris</td> <td>—</td> <td>—</td> <td>—</td> <td>—</td> <td>—</td> <td>Tr</td> </tr> </tbody> </table>	Quartz	35	35	65	30	40	35	Feldspar	—	5	10	5	—	5	Mica	—	—	—	—	—	Tr	Clay	30	8	10	45	25	25	Volcanic glass	—	—	Tr	—	—	—	Calcite/dolomite	35	7	5	20	25	15	Accessory minerals	Tr	8	5	3	—	Tr	Pyrite	Tr	5	5	2	5	—	Foraminifers	—	3	Tr	1	—	2	Nannofossils	—	25	—	3	Tr	3	Diatoms	—	3	Tr	Tr	Tr	10	Radiolarians	—	Tr	—	Tr	—	—	Sponge spicules	—	2	Tr	Tr	5	5	Plant debris	—	—	—	—	—	Tr
Quartz	35	35	65	30											40	35																																																																																																
Feldspar	—	5	10	5											—	5																																																																																																
Mica	—	—	—	—											—	Tr																																																																																																
Clay	30	8	10	45											25	25																																																																																																
Volcanic glass	—	—	Tr	—											—	—																																																																																																
Calcite/dolomite	35	7	5	20											25	15																																																																																																
Accessory minerals	Tr	8	5	3	—	Tr																																																																																																										
Pyrite	Tr	5	5	2	5	—																																																																																																										
Foraminifers	—	3	Tr	1	—	2																																																																																																										
Nannofossils	—	25	—	3	Tr	3																																																																																																										
Diatoms	—	3	Tr	Tr	Tr	10																																																																																																										
Radiolarians	—	Tr	—	Tr	—	—																																																																																																										
Sponge spicules	—	2	Tr	Tr	5	5																																																																																																										
Plant debris	—	—	—	—	—	Tr																																																																																																										
N22 - N23																																																																																																																
NN21																																																																																																																
<i>Cycladophora davisiana</i>																																																																																																																
F/G																																																																																																																
A/G																																																																																																																
C/G																																																																																																																
A/G																																																																																																																
C/M																																																																																																																
N22 - N23					Brunhes Chronozone	$\gamma = 1.43 \phi = 81.0 \text{ W} = 139 \bullet$	CaCO ₃ = 9 ●	7	3.5		H	*	*	OG																																																																																																		
N22 - N23																																																																																																																
NN21																																																																																																																
<i>Cycladophora davisiana</i>																																																																																																																
F/G																																																																																																																
A/G																																																																																																																
C/G																																																																																																																
A/G																																																																																																																
C/M																																																																																																																



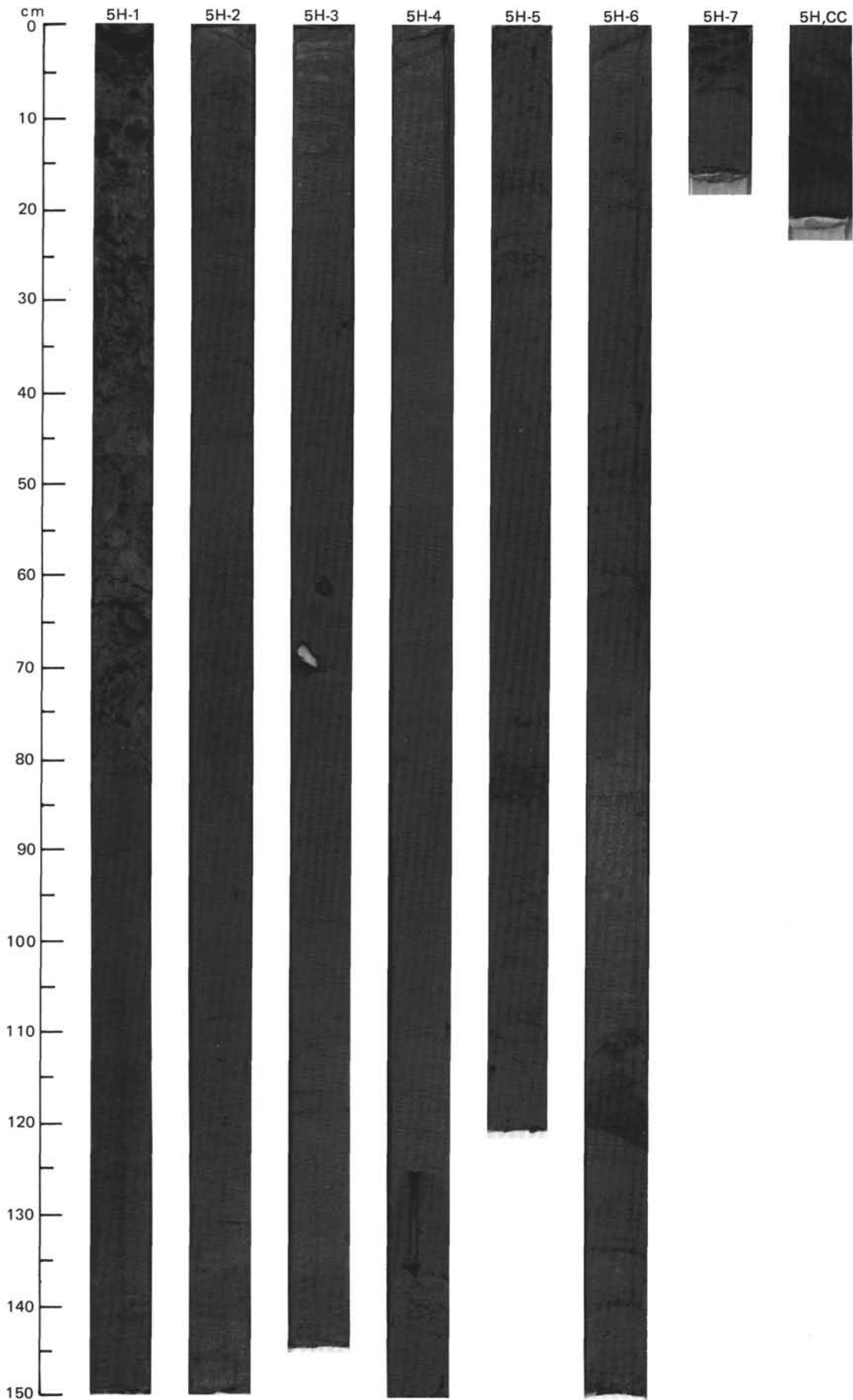




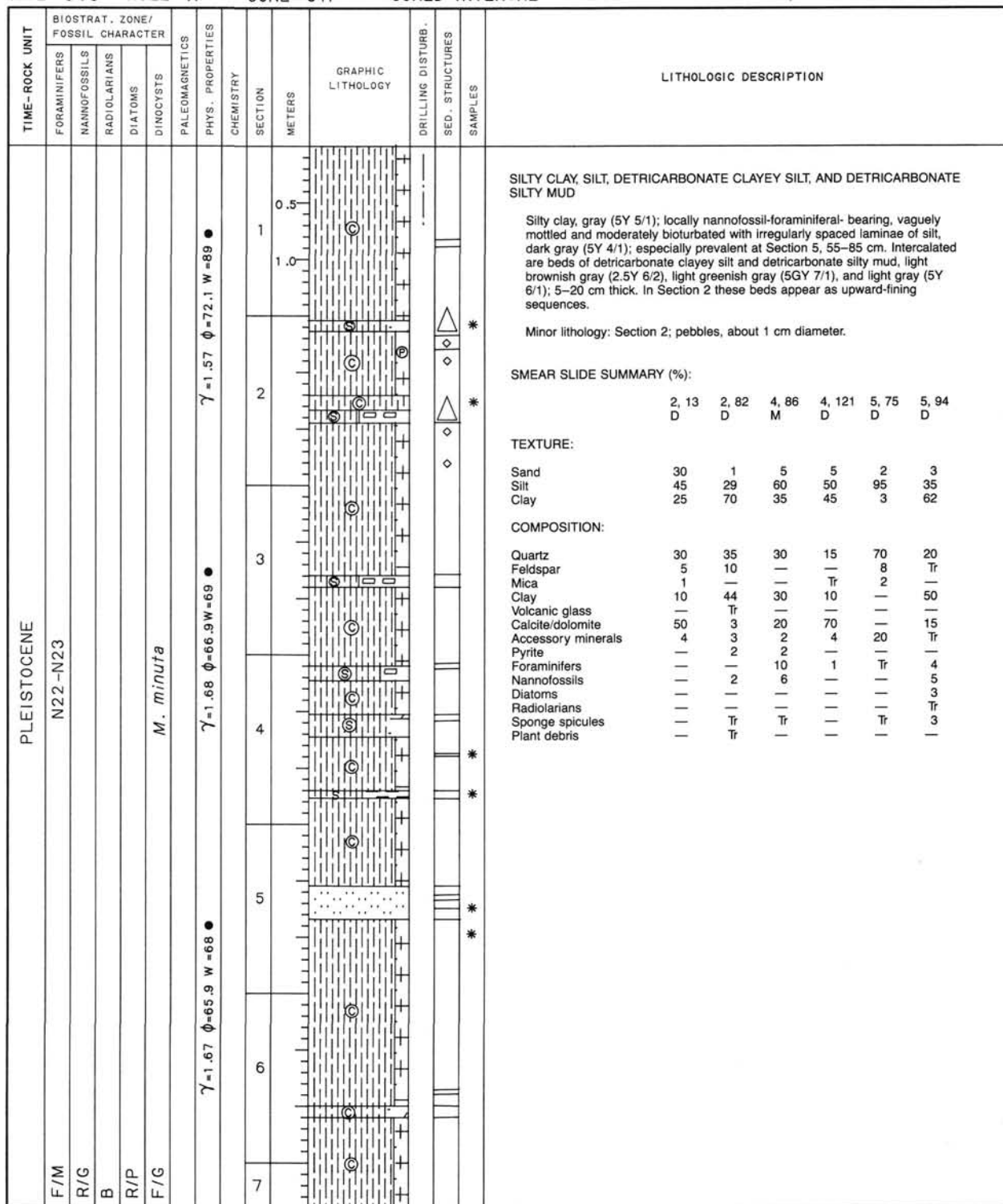


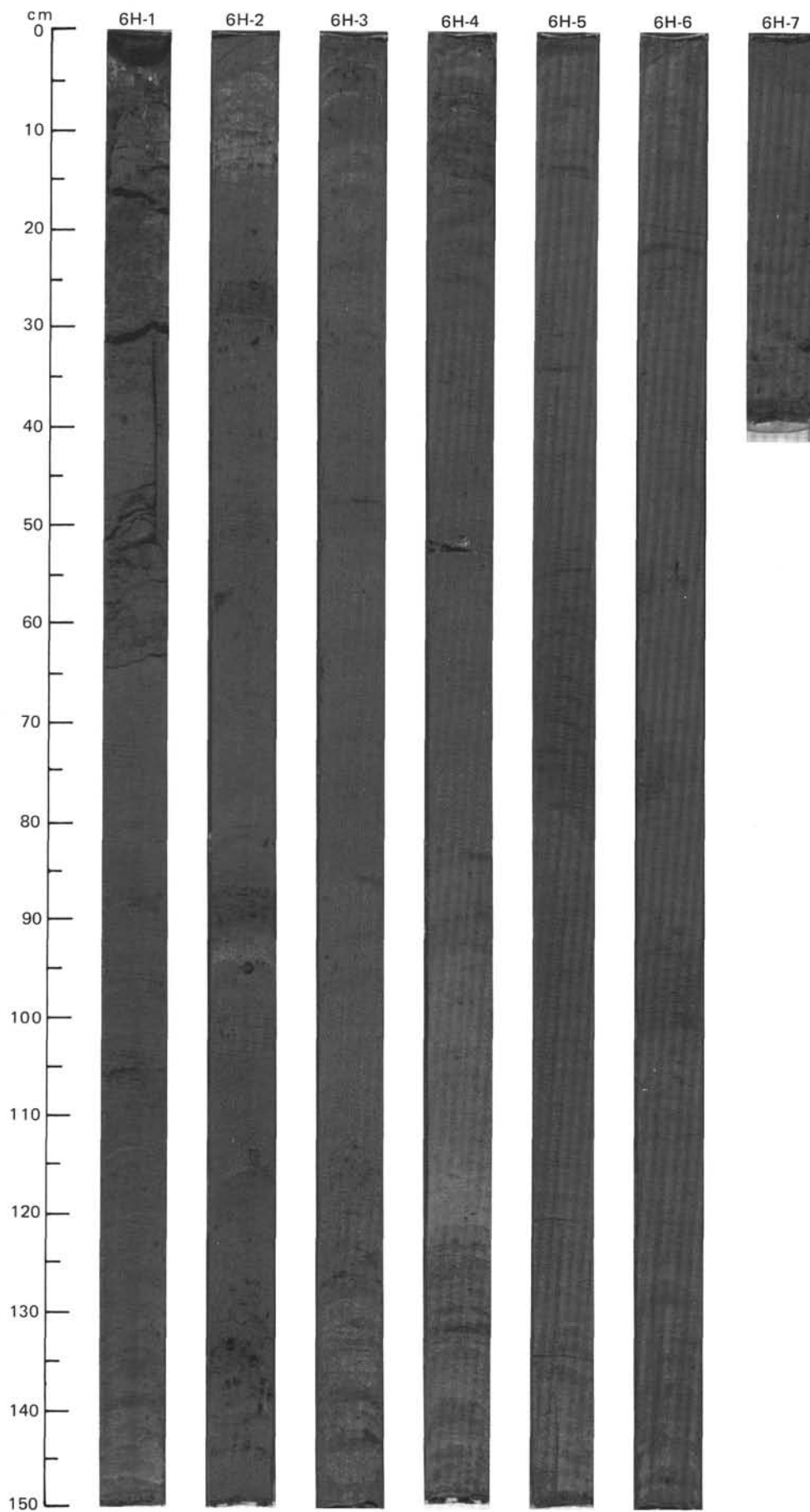
SITE 646 HOLE A CORE 5 H CORED INTERVAL 3487.0-3496.7 mbsl; 35.8-45.5 mbsf

TIME-ROCK UNIT		BIOSTRAT. ZONE/ FOSSIL CHARACTER	SECTION	METERS	GRAPHIC LITHOLOGY	DRILLING DISTURB.	SED. STRUCTURES	SAMPLES	LITHOLOGIC DESCRIPTION																																																																																																												
PLEISTOCENE																																																																																																																					
A/G	N22-N23																																																																																																																				
A/G	NN19																																																																																																																				
F/G	<i>Cycladophora davisiana</i>																																																																																																																				
R/G	<i>Rhizosolenia curvirostris</i>																																																																																																																				
C/G																																																																																																																					
		PALEOMAGNETICS																																																																																																																			
		PHYS. PROPERTIES																																																																																																																			
		CHEMISTRY																																																																																																																			
			1	0.5					<p>SPICULAR-FORAMINIFERAL SILTY MUD AND NANNOFOSSIL CLAY</p> <p>Spicular-foraminiferal silty mud, gray (5Y 5/1), dark gray (5Y 4/1), and light gray (5Y 6/1).</p> <p>Nannofossil clay, gray (5Y 5/1), light gray (5Y 6/1).</p> <p>Locally mottled. Few scattered pebbles.</p> <p>Smear-slide estimates of nannofossil content (~60%) are too high, as shown by carbonate bomb results of <30% carbonate. Lithologic columns have been adjusted.</p> <p>Minor lithologies: a. Section 3, 97-120 cm: nannofossil-foraminifer silty clay, greenish gray (5G 5/1) in some bands. b. Section 6, 118-123 cm: well-sorted silt, dark gray (5Y 4/1) with sharp base and cross-lamination.</p> <p>SMEAR SLIDE SUMMARY (%):</p> <table border="1"> <thead> <tr> <th></th> <th>2, 75 D</th> <th>3, 120 M</th> <th>4, 63 D</th> <th>6, 88 D</th> <th>6, 123 M</th> </tr> </thead> <tbody> <tr> <td>TEXTURE:</td> <td></td> <td></td> <td></td> <td></td> <td></td> </tr> <tr> <td>Sand</td> <td>15</td> <td>30</td> <td>—</td> <td>5</td> <td>—</td> </tr> <tr> <td>Silt</td> <td>60</td> <td>35</td> <td>30</td> <td>40</td> <td>85</td> </tr> <tr> <td>Clay</td> <td>25</td> <td>35</td> <td>70</td> <td>60</td> <td>15</td> </tr> <tr> <td>COMPOSITION:</td> <td></td> <td></td> <td></td> <td></td> <td></td> </tr> <tr> <td>Quartz</td> <td>55</td> <td>10</td> <td>20</td> <td>5</td> <td>45</td> </tr> <tr> <td>Feldspar</td> <td>5</td> <td>—</td> <td>—</td> <td>—</td> <td>5</td> </tr> <tr> <td>Mica</td> <td>—</td> <td>—</td> <td>—</td> <td>—</td> <td>5</td> </tr> <tr> <td>Clay</td> <td>—</td> <td>30</td> <td>20</td> <td>15</td> <td>—</td> </tr> <tr> <td>Calcite/dolomite</td> <td>5</td> <td>10</td> <td>10</td> <td>5</td> <td>5</td> </tr> <tr> <td>Accessory minerals</td> <td>5</td> <td>Tr</td> <td>—</td> <td>1</td> <td>5</td> </tr> <tr> <td>Pyrite</td> <td>5</td> <td>5</td> <td>1</td> <td>—</td> <td>—</td> </tr> <tr> <td>Foraminifers</td> <td>10</td> <td>20</td> <td>5</td> <td>10</td> <td>5</td> </tr> <tr> <td>Nannofossils</td> <td>5</td> <td>15</td> <td>37</td> <td>60</td> <td>Tr</td> </tr> <tr> <td>Diatoms</td> <td>—</td> <td>—</td> <td>2</td> <td>1</td> <td>Tr</td> </tr> <tr> <td>Radiolarians</td> <td>—</td> <td>—</td> <td>—</td> <td>Tr</td> <td>—</td> </tr> <tr> <td>Sponge spicules</td> <td>10</td> <td>10</td> <td>5</td> <td>3</td> <td>Tr</td> </tr> </tbody> </table>		2, 75 D	3, 120 M	4, 63 D	6, 88 D	6, 123 M	TEXTURE:						Sand	15	30	—	5	—	Silt	60	35	30	40	85	Clay	25	35	70	60	15	COMPOSITION:						Quartz	55	10	20	5	45	Feldspar	5	—	—	—	5	Mica	—	—	—	—	5	Clay	—	30	20	15	—	Calcite/dolomite	5	10	10	5	5	Accessory minerals	5	Tr	—	1	5	Pyrite	5	5	1	—	—	Foraminifers	10	20	5	10	5	Nannofossils	5	15	37	60	Tr	Diatoms	—	—	2	1	Tr	Radiolarians	—	—	—	Tr	—	Sponge spicules	10	10	5	3	Tr
	2, 75 D	3, 120 M	4, 63 D	6, 88 D	6, 123 M																																																																																																																
TEXTURE:																																																																																																																					
Sand	15	30	—	5	—																																																																																																																
Silt	60	35	30	40	85																																																																																																																
Clay	25	35	70	60	15																																																																																																																
COMPOSITION:																																																																																																																					
Quartz	55	10	20	5	45																																																																																																																
Feldspar	5	—	—	—	5																																																																																																																
Mica	—	—	—	—	5																																																																																																																
Clay	—	30	20	15	—																																																																																																																
Calcite/dolomite	5	10	10	5	5																																																																																																																
Accessory minerals	5	Tr	—	1	5																																																																																																																
Pyrite	5	5	1	—	—																																																																																																																
Foraminifers	10	20	5	10	5																																																																																																																
Nannofossils	5	15	37	60	Tr																																																																																																																
Diatoms	—	—	2	1	Tr																																																																																																																
Radiolarians	—	—	—	Tr	—																																																																																																																
Sponge spicules	10	10	5	3	Tr																																																																																																																
			2	1.0																																																																																																																	
			3																																																																																																																		
			4																																																																																																																		
			5																																																																																																																		
			6																																																																																																																		
			7																																																																																																																		
CC																																																																																																																					



SITE 646 HOLE A CORE 6 H CORED INTERVAL 3496.7-3506.3 mbsl; 45.5-55.1 mbsf





SITE 646 HOLE A CORE 7H CORED INTERVAL 3506.3-3516.0 mbsl; 55.1-64.8 mbsf

TIME-ROCK UNIT	BIOSTRAT. ZONE/ FOSSIL CHARACTER					PALEOMAGNETICS	PHYS. PROPERTIES	CHEMISTRY	SECTION METERS	GRAPHIC LITHOLOGY	DRILLING DISTURB.	SED. STRUCTURES	SAMPLES	LITHOLOGIC DESCRIPTION					
	FORAMINIFERS	NANNOFOSSILS	RADIOLARIANS	DIATOMS	DINOCYSTS														
PLEISTOCENE	N22-N23 NN19					Brunhes Chronozone		CaCO ₃ =27.0	0.5					CLAYEY MUD, NANNOFOSSIL-FORAMINIFERAL CLAYEY SILT, NANNOFOSSIL-FORAMINIFERAL-BEARING CLAYEY SILT, AND NANNOFOSSIL CLAY					
						1.0	VOID		Clayey mud, dark greenish gray (5GY 4/1), gray (5Y 5/1); bearing scattered granules and some basalt pebbles, very indistinct layering.										
														2	VOID				Nannofossil-foraminifer clayey silt and nannofossil-foraminifer-bearing clayey silt, dark greenish gray (5GY 4/1), gray (5Y 5/1, 5Y 6/1). The clayey silts may contain several distinct, thin silt laminae, more silt-rich beds and some foraminifer pockets. Nannofossil clay, homogeneous.
														3					Smear-slide estimates of nannofossil content (~60%) are too high, as shown by carbonate bomb results of <30% carbonate. Lithologic columns were adjusted.
														4					Minor lithology: Section 5, 60-65 cm: muddy sand layer, dark greenish gray (5G 4/1).
														5					
												Matuyama Chronozone			6				
								7											

SMEAR SLIDE SUMMARY (%):

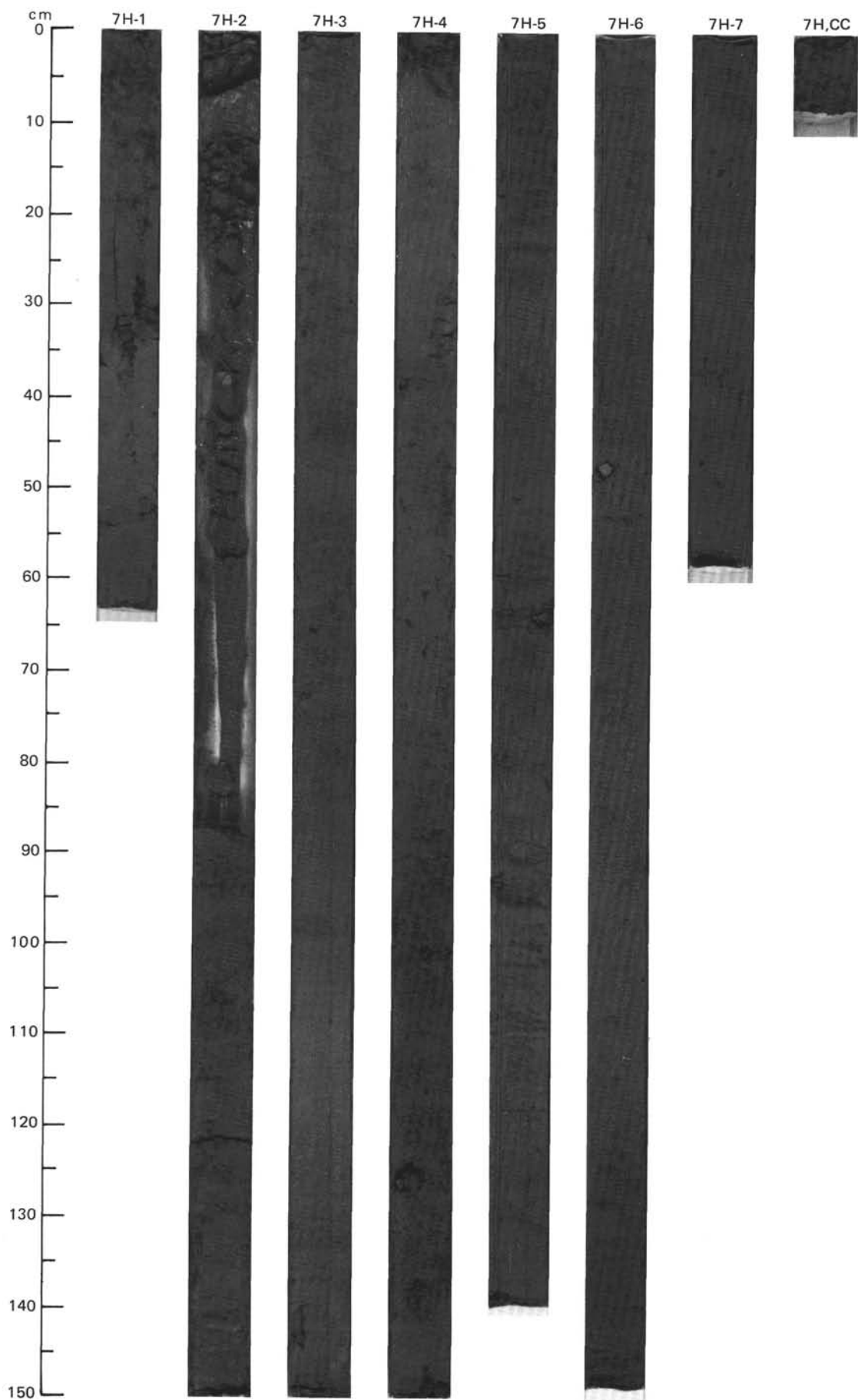
	3, 114 D	4, 117 D	5, 64 D	5, 95 M	6, 105 D	7, 31 D
Sand	15	15	60	15	15	15
Silt	15	35	25	22	45	25
Clay	70	50	15	63	40	60

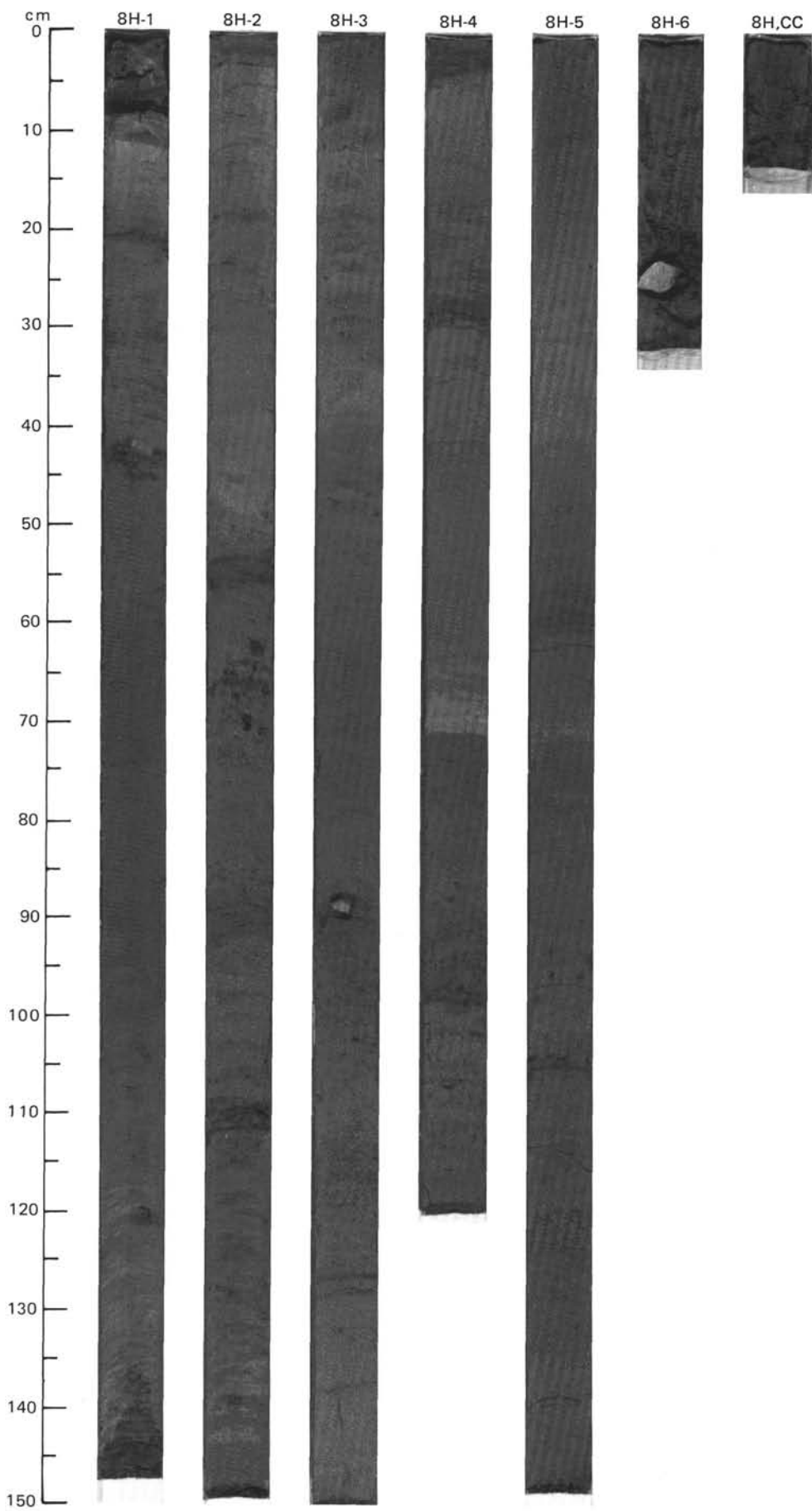
TEXTURE:

	3, 114 D	4, 117 D	5, 64 D	5, 95 M	6, 105 D	7, 31 D
Sand	15	15	60	15	15	15
Silt	15	35	25	22	45	25
Clay	70	50	15	63	40	60

COMPOSITION:

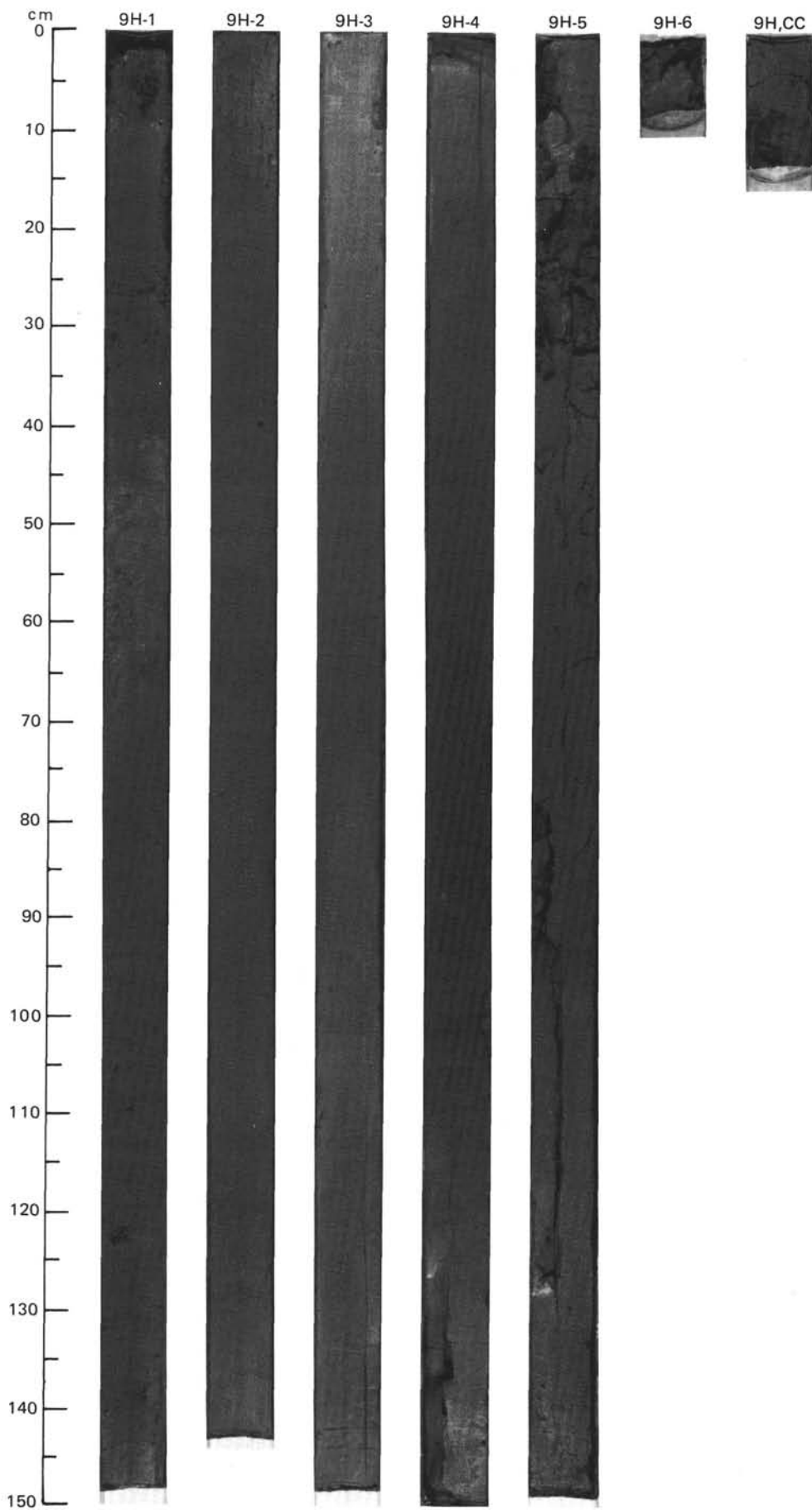
	3, 114 D	4, 117 D	5, 64 D	5, 95 M	6, 105 D	7, 31 D
Quartz	5	34	65	10	25	25
Feldspar	—	2	10	2	—	5
Mica	—	2	Tr	—	—	—
Clay	5	50	15	65	35	60
Calcite/dolomite	2	10	3	10	—	10
Accessory minerals	1	2	5	3	—	—
Pyrite	—	—	2	—	5	—
Foraminifers	20	—	—	8	15	—
Nannofossils	65	—	—	2	15	—
Sponge spicules	2	Tr	—	Tr	5	—

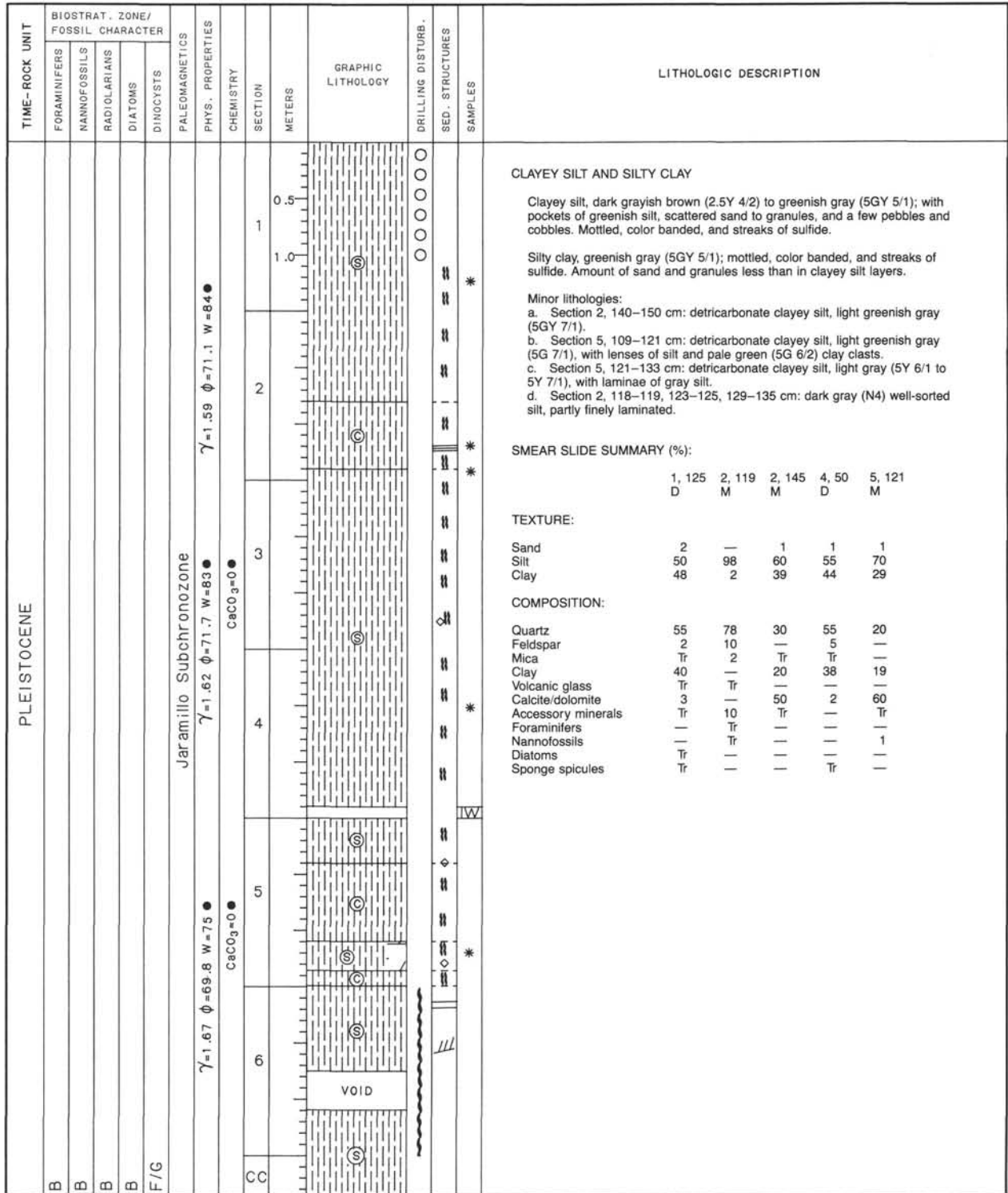


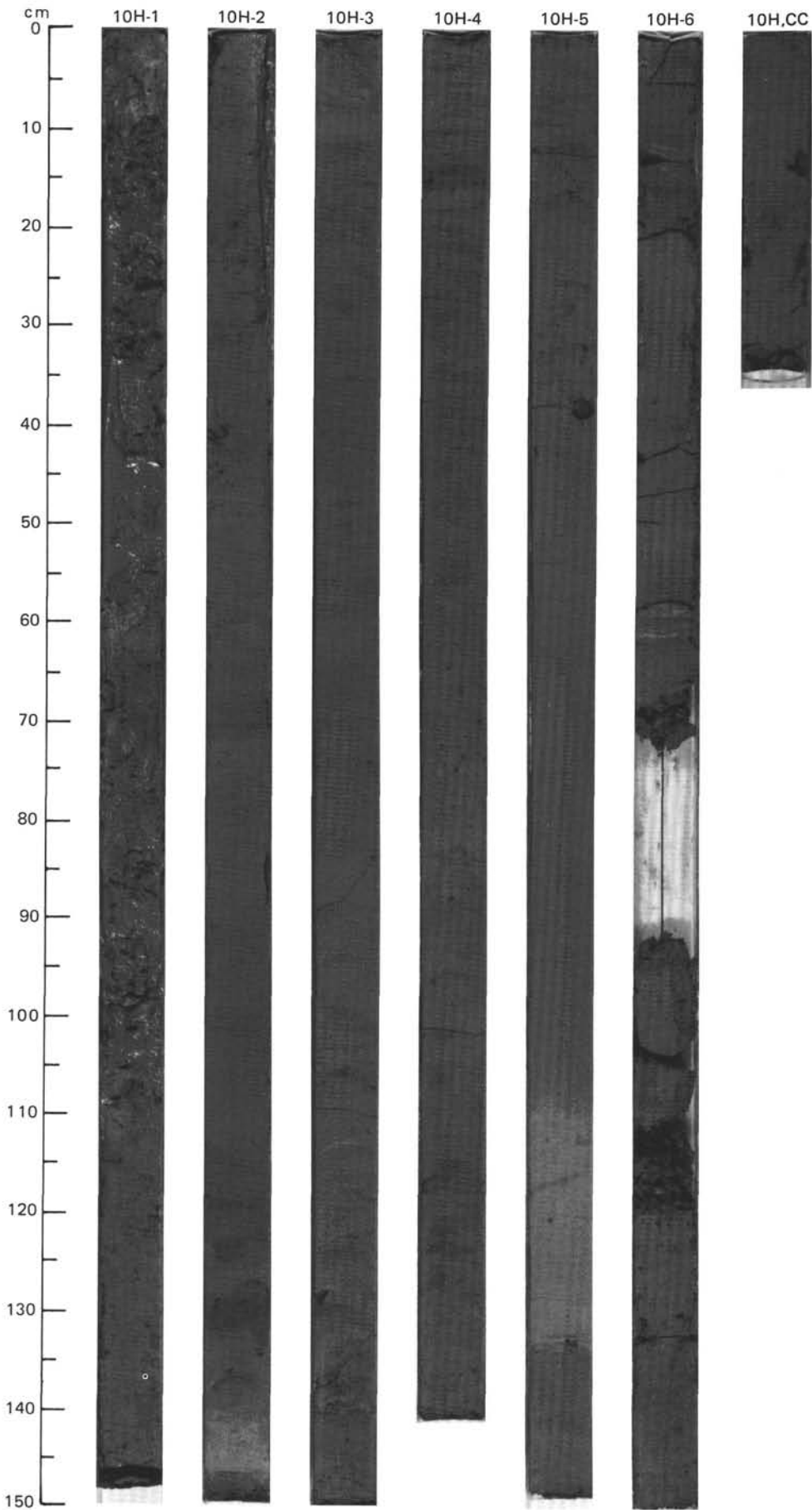


SITE 646 HOLE A CORE 9 H CORED INTERVAL 3525.6-3535.3 mbsl; 74.4-84.1 mbsf

TIME-ROCK UNIT	BIOSTRAT. ZONE/ FOSSIL CHARACTER					PALEOMAGNETICS	PHYS. PROPERTIES	CHEMISTRY	SECTION	METERS	GRAPHIC LITHOLOGY	DRILLING DISTURB.	SED. STRUCTURES	SAMPLES	LITHOLOGIC DESCRIPTION																																																																																																																																			
	FORAMINIFERS	NANNOFOSSILS	RADIOLARIANS	DIATOMS	DINOCCYSTS																																																																																																																																													
PLEISTOCENE	C/M	NN22-NN23							1	0.5				<p>CLAYEY SILT AND SILTY CLAY</p> <p>Clayey silt, dark gray (5Y 4/1) and gray (5Y 5/1), locally slightly bioturbated with rare scattered <5 mm clay clasts in some layers.</p> <p>Silty clay, dark gray (5Y 4/1), with scattered soft silty and clay clasts to about 1 cm.</p> <p>Minor lithologies: a. Section 1, 43-68 cm; Section 3, 80-110 cm; Section 5, 94-130 cm; gray (5Y 5/1), detrital carbonate silty clay, locally with abundant soft detrital carbonate clasts and bioturbated. b. Section 2, 135-145 cm; Section 3, 0-35 cm; gray (N5), foraminiferal-nannofossil-bearing silty clay, perhaps laminated but probably just drilling deformation.</p> <p>Dropped material (silt and clay clasts) is most common in Section 1.</p> <p>SMEAR SLIDE SUMMARY (%):</p> <table border="1"> <thead> <tr> <th></th> <th>1, 110</th> <th>2, 100</th> <th>3, 11</th> <th>3, 100</th> <th>4, 82</th> </tr> <tr> <th></th> <th>D</th> <th>D</th> <th>M</th> <th>M</th> <th>D</th> </tr> </thead> <tbody> <tr> <td>Sand</td> <td>3</td> <td>2</td> <td>8</td> <td>—</td> <td>5</td> </tr> <tr> <td>Silt</td> <td>30</td> <td>50</td> <td>32</td> <td>40</td> <td>55</td> </tr> <tr> <td>Clay</td> <td>67</td> <td>48</td> <td>60</td> <td>60</td> <td>40</td> </tr> </tbody> </table> <p>TEXTURE:</p> <table border="1"> <tbody> <tr> <td>Sand</td> <td>3</td> <td>2</td> <td>8</td> <td>—</td> <td>5</td> </tr> <tr> <td>Silt</td> <td>30</td> <td>50</td> <td>32</td> <td>40</td> <td>55</td> </tr> <tr> <td>Clay</td> <td>67</td> <td>48</td> <td>60</td> <td>60</td> <td>40</td> </tr> </tbody> </table> <p>COMPOSITION:</p> <table border="1"> <tbody> <tr> <td>Quartz</td> <td>40</td> <td>55</td> <td>10</td> <td>20</td> <td>60</td> </tr> <tr> <td>Feldspar</td> <td>Tr</td> <td>Tr</td> <td>Tr</td> <td>—</td> <td>Tr</td> </tr> <tr> <td>Mica</td> <td>—</td> <td>—</td> <td>1</td> <td>—</td> <td>Tr</td> </tr> <tr> <td>Clay</td> <td>54</td> <td>40</td> <td>60</td> <td>55</td> <td>30</td> </tr> <tr> <td>Volcanic glass</td> <td>—</td> <td>Tr</td> <td>Tr</td> <td>—</td> <td>Tr</td> </tr> <tr> <td>Calcite/dolomite</td> <td>5</td> <td>5</td> <td>4</td> <td>25</td> <td>7</td> </tr> <tr> <td>Accessory minerals</td> <td>Tr</td> <td>Tr</td> <td>1</td> <td>Tr</td> <td>—</td> </tr> <tr> <td>Foraminifers</td> <td>Tr</td> <td>—</td> <td>5</td> <td>—</td> <td>2</td> </tr> <tr> <td>Nannofossils</td> <td>1</td> <td>—</td> <td>15</td> <td>—</td> <td>1</td> </tr> <tr> <td>Diatoms</td> <td>Tr</td> <td>Tr</td> <td>—</td> <td>—</td> <td>—</td> </tr> <tr> <td>Radiolarians</td> <td>Tr</td> <td>—</td> <td>1</td> <td>Tr</td> <td>Tr</td> </tr> <tr> <td>Sponge spicules</td> <td>Tr</td> <td>—</td> <td>1</td> <td>Tr</td> <td>Tr</td> </tr> <tr> <td>Bioclasts</td> <td>—</td> <td>—</td> <td>1</td> <td>—</td> <td>—</td> </tr> <tr> <td>Pellets</td> <td>—</td> <td>—</td> <td>2</td> <td>—</td> <td>—</td> </tr> </tbody> </table>		1, 110	2, 100	3, 11	3, 100	4, 82		D	D	M	M	D	Sand	3	2	8	—	5	Silt	30	50	32	40	55	Clay	67	48	60	60	40	Sand	3	2	8	—	5	Silt	30	50	32	40	55	Clay	67	48	60	60	40	Quartz	40	55	10	20	60	Feldspar	Tr	Tr	Tr	—	Tr	Mica	—	—	1	—	Tr	Clay	54	40	60	55	30	Volcanic glass	—	Tr	Tr	—	Tr	Calcite/dolomite	5	5	4	25	7	Accessory minerals	Tr	Tr	1	Tr	—	Foraminifers	Tr	—	5	—	2	Nannofossils	1	—	15	—	1	Diatoms	Tr	Tr	—	—	—	Radiolarians	Tr	—	1	Tr	Tr	Sponge spicules	Tr	—	1	Tr	Tr	Bioclasts	—	—	1	—	—	Pellets	—	—	2	—	—
		1, 110	2, 100	3, 11	3, 100	4, 82																																																																																																																																												
		D	D	M	M	D																																																																																																																																												
	Sand	3	2	8	—	5																																																																																																																																												
	Silt	30	50	32	40	55																																																																																																																																												
	Clay	67	48	60	60	40																																																																																																																																												
Sand	3	2	8	—	5																																																																																																																																													
Silt	30	50	32	40	55																																																																																																																																													
Clay	67	48	60	60	40																																																																																																																																													
Quartz	40	55	10	20	60																																																																																																																																													
Feldspar	Tr	Tr	Tr	—	Tr																																																																																																																																													
Mica	—	—	1	—	Tr																																																																																																																																													
Clay	54	40	60	55	30																																																																																																																																													
Volcanic glass	—	Tr	Tr	—	Tr																																																																																																																																													
Calcite/dolomite	5	5	4	25	7																																																																																																																																													
Accessory minerals	Tr	Tr	1	Tr	—																																																																																																																																													
Foraminifers	Tr	—	5	—	2																																																																																																																																													
Nannofossils	1	—	15	—	1																																																																																																																																													
Diatoms	Tr	Tr	—	—	—																																																																																																																																													
Radiolarians	Tr	—	1	Tr	Tr																																																																																																																																													
Sponge spicules	Tr	—	1	Tr	Tr																																																																																																																																													
Bioclasts	—	—	1	—	—																																																																																																																																													
Pellets	—	—	2	—	—																																																																																																																																													
	F/G	NN19							2	1.0																																																																																																																																								
	C/G		<i>Cycladophora davisiana</i>						3	1.5																																																																																																																																								
	F/G		<i>Actinocyclus oculatus</i>						4	2.0																																																																																																																																								
	C/G								5	2.5																																																																																																																																								
	N/C								6	3.0																																																																																																																																								
									7	3.5																																																																																																																																								
									8	4.0																																																																																																																																								
									9	4.5																																																																																																																																								
									10	5.0																																																																																																																																								
									11	5.5																																																																																																																																								
									12	6.0																																																																																																																																								
									13	6.5																																																																																																																																								
									14	7.0																																																																																																																																								
									15	7.5																																																																																																																																								
									16	8.0																																																																																																																																								
									17	8.5																																																																																																																																								
									18	9.0																																																																																																																																								
									19	9.5																																																																																																																																								
									20	10.0																																																																																																																																								
									21	10.5																																																																																																																																								
									22	11.0																																																																																																																																								
									23	11.5																																																																																																																																								
									24	12.0																																																																																																																																								
									25	12.5																																																																																																																																								
									26	13.0																																																																																																																																								
									27	13.5																																																																																																																																								
									28	14.0																																																																																																																																								
									29	14.5																																																																																																																																								
									30	15.0																																																																																																																																								
									31	15.5																																																																																																																																								
									32	16.0																																																																																																																																								
									33	16.5																																																																																																																																								
									34	17.0																																																																																																																																								
									35	17.5																																																																																																																																								
									36	18.0																																																																																																																																								
									37	18.5																																																																																																																																								
									38	19.0																																																																																																																																								
									39	19.5																																																																																																																																								
									40	20.0																																																																																																																																								
									41	20.5																																																																																																																																								
									42	21.0																																																																																																																																								
									43	21.5																																																																																																																																								
									44	22.0																																																																																																																																								
									45	22.5																																																																																																																																								
									46	23.0																																																																																																																																								
									47	23.5																																																																																																																																								
									48	24.0																																																																																																																																								
									49	24.5																																																																																																																																								
									50	25.0																																																																																																																																								
									51	25.5																																																																																																																																								
									52	26.0																																																																																																																																								
									53	26.5																																																																																																																																								
									54	27.0																																																																																																																																								
									55	27.5																																																																																																																																								
									56	28.0																																																																																																																																								
									57	28.5																																																																																																																																								
									58	29.0																																																																																																																																								
									59	29.5																																																																																																																																								
									60	30.0																																																																																																																																								
									61	30.5																																																																																																																																								
									62	31.0																																																																																																																																								
									63	31.5																																																																																																																																								
									64	32.0																																																																																																																																								
									65	32.5																																																																																																																																								
									66	33.0																																																																																																																																								
									67	33.5																																																																																																																																								
									68	34.0																																																																																																																																								
									69	34.5																																																																																																																																								
									70	35.0																																																																																																																																								

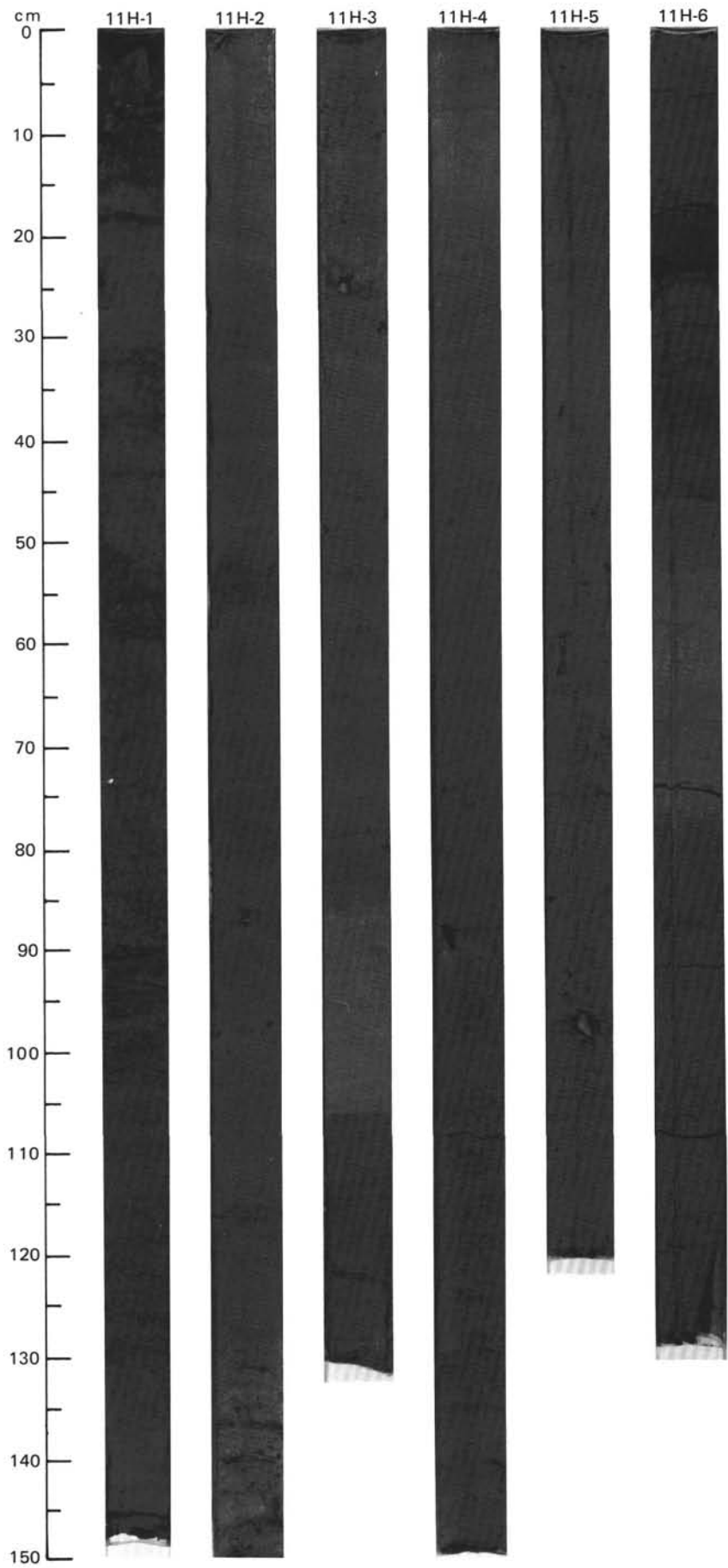


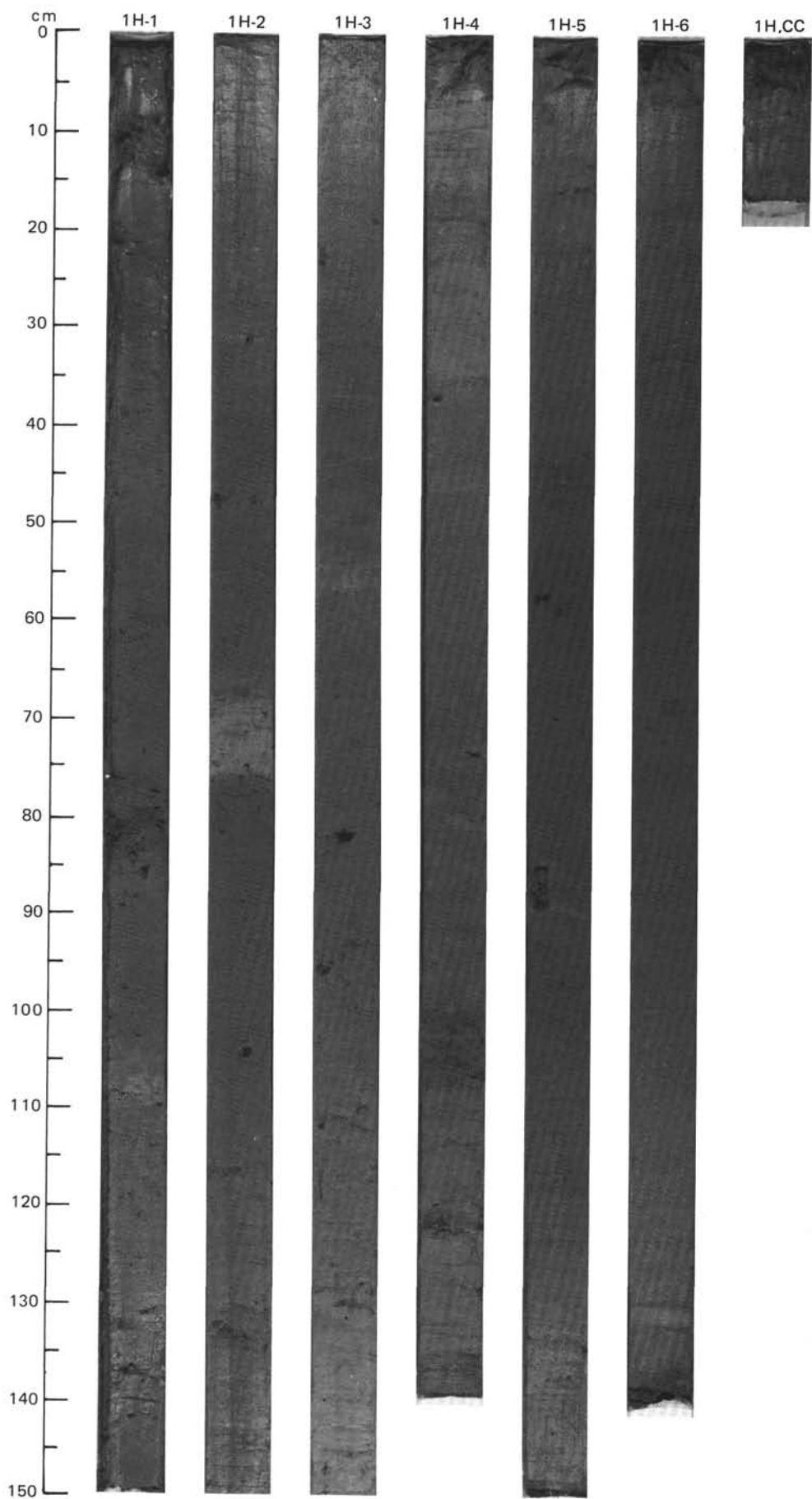


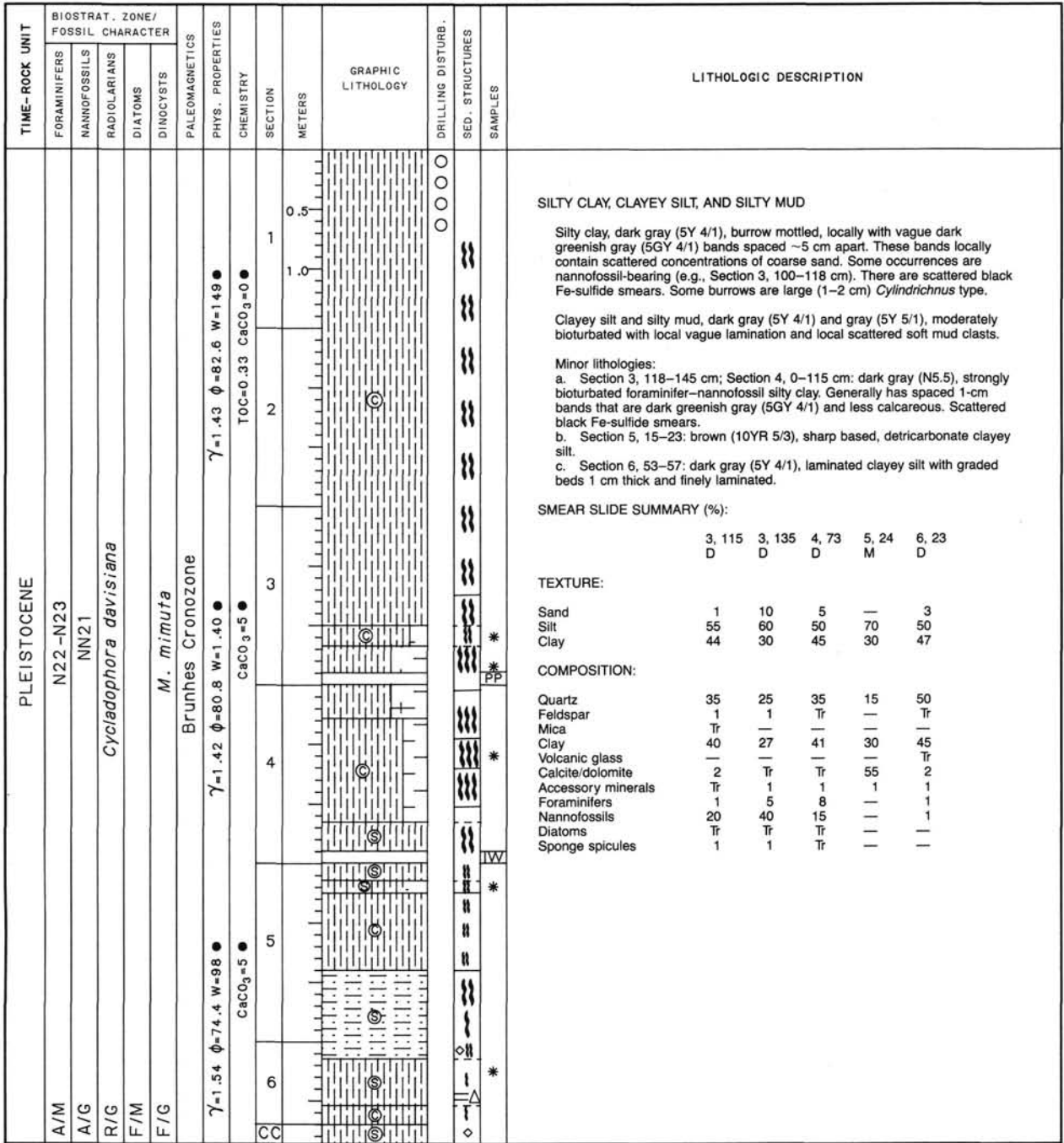


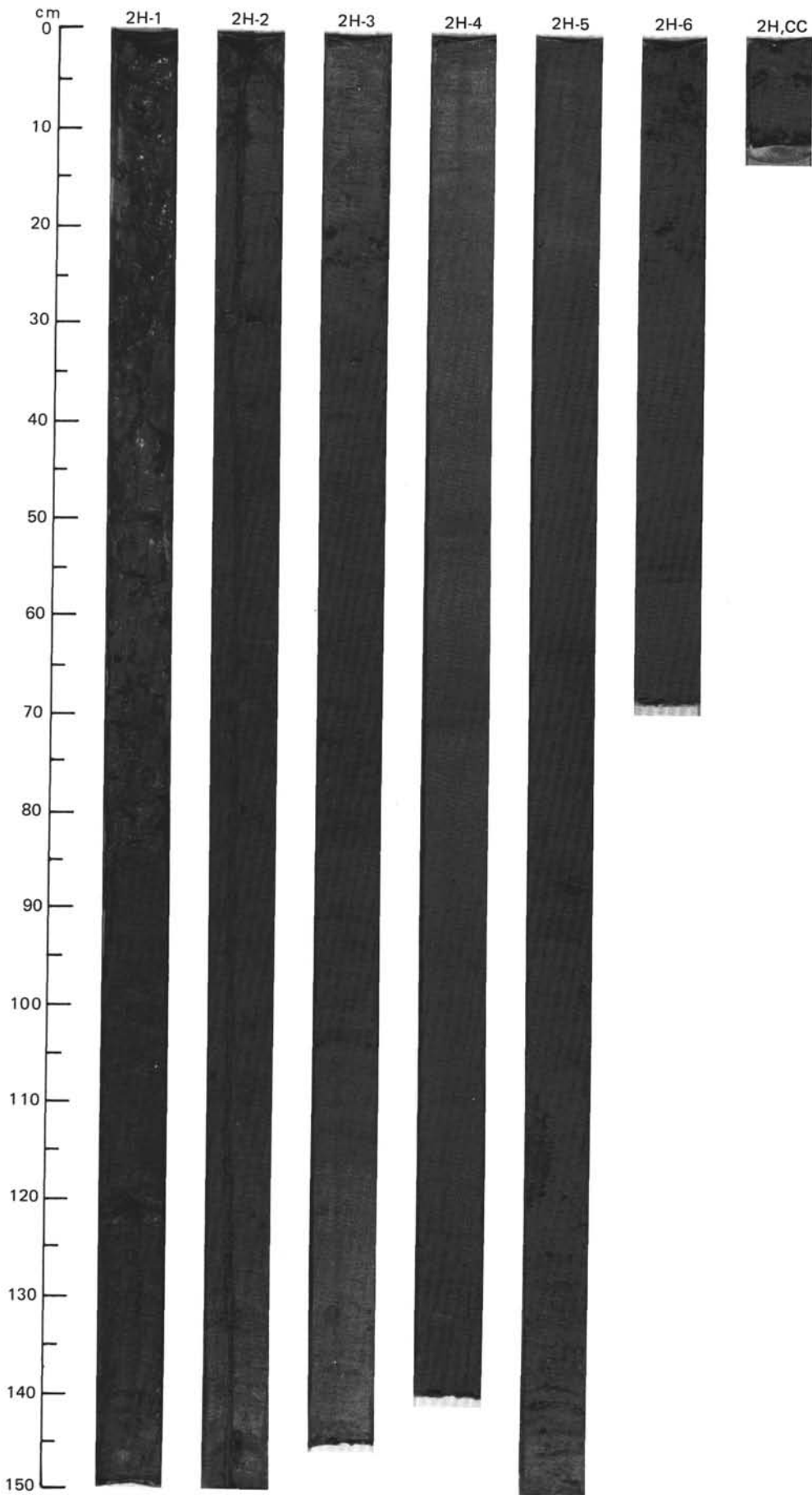
SITE 646 HOLE A CORE 11 H CORED INTERVAL 3545.0-3554.7 mbsl; 93.8-103.5 mbsf

TIME-ROCK UNIT	BIOSTRAT. ZONE/ FOSSIL CHARACTER					PALEOMAGNETICS	PHYS. PROPERTIES	CHEMISTRY	SECTION	METERS	GRAPHIC LITHOLOGY	DRILLING DISTURB.	SED. STRUCTURES	SAMPLES	LITHOLOGIC DESCRIPTION																																																															
	FORAMINIFERS	NANNOFOSSILS	RADIOLARIANS	DIATOMS	DINOCTYSTS																																																																									
PLEISTOCENE	N22-N23					Matuyama Chronozone	$\gamma = 1.71 \phi = 68.5 W = 70$	CaCO ₃ = 0	1	0.5		O	*	*	CLAYEY SILT, SILTY MUD, AND SILTY CLAY																																																															
	C/G	C/G	R/M	A/P	C/G					1.0						2	2	2	2	*	*	*	Clayey silt and silty mud, dark gray (N4, 5Y 4/1), dark grayish brown (2.5Y 4/2), with moderate bioturbation, scattered black Fe-sulfide smears, rare pebbles to ~2 cm, scattered pockets of silt and detrital carbonate silt that may be burrow fillings or dropped clasts.																																																							
																								C/G	C/G	R/M	A/P	C/G	3	3	3	3	*	*	Silty clay, dark gray (5Y 4/1), with moderate bioturbation, Fe-sulfide smears, local <5 mm mud clasts, local vague color banding, scattered sand-bearing intervals.																																											
	C/G	C/G	R/M	A/P	C/G					4						4	4	4	*	*	Minor lithologies: a. Section 3, 10-32, 85-108 cm; Section 6, 64-77 cm: detrital carbonate silty clay, gray (5Y 5/1, 5Y 6/1); with <1 cm-thick, sharp-based, graded, laminated beds of silt. Local cross-lamination. b. Section 6, 17-23 cm; "Black" (5Y 2.5/2), relatively well-sorted silt, with sharp contacts. c. Section 6, 23-46 cm: laminated "black" silt layers and dark gray (5Y 4/1) clayey silt. Laminae to < mm. d. Section 4, 90 cm: low-density clast, phosphatic(?), may be coprolite or bone.																																																									
																						C/G	C/G	R/M	A/P	C/G	5	5	5	5	*	*	*	SMEAR SLIDE SUMMARY (%):																																												
	C/G	C/G	R/M	A/P	C/G					6						6	6	6	*	*	*														<table border="1"> <tr> <td></td> <td>1, 79</td> <td>2, 8</td> <td>3, 98</td> <td>5, 110</td> <td>6, 23</td> </tr> <tr> <td></td> <td>D</td> <td>D</td> <td>M</td> <td>D</td> <td>M</td> </tr> </table>		1, 79	2, 8	3, 98	5, 110	6, 23		D	D	M	D	M																															
						1, 79	2, 8	3, 98	5, 110		6, 23																																																																			
	D	D	M	D	M																																																																									
C/G	C/G	R/M	A/P	C/G	6	6	6	6	6	*	*	*	TEXTURE:																																																																	
														C/G	C/G	R/M	A/P	C/G	6	6	6	6	*	*	*	<table border="1"> <tr> <td>Sand</td> <td>2</td> <td>3</td> <td>—</td> <td>—</td> <td>—</td> </tr> <tr> <td>Silt</td> <td>55</td> <td>40</td> <td>95</td> <td>45</td> <td>95</td> </tr> <tr> <td>Clay</td> <td>43</td> <td>57</td> <td>5</td> <td>55</td> <td>5</td> </tr> </table>	Sand	2	3	—	—	—	Silt	55	40	95	45	95	Clay	43	57	5	55	5																																		
Sand	2	3	—	—	—																																																																									
Silt	55	40	95	45	95																																																																									
Clay	43	57	5	55	5																																																																									
C/G	C/G	R/M	A/P	C/G	6	6	6	6	6	*	*	*	COMPOSITION:																																																																	
														C/G	C/G	R/M	A/P	C/G	6	6	6	6	*	*	*	<table border="1"> <tr> <td>Quartz</td> <td>60</td> <td>35</td> <td>55</td> <td>50</td> <td>74</td> </tr> <tr> <td>Feldspar</td> <td>3</td> <td>Tr</td> <td>—</td> <td>4</td> <td>10</td> </tr> <tr> <td>Mica</td> <td>1</td> <td>—</td> <td>Tr</td> <td>Tr</td> <td>1</td> </tr> <tr> <td>Clay</td> <td>34</td> <td>40</td> <td>—</td> <td>42</td> <td>Tr</td> </tr> <tr> <td>Volcanic glass</td> <td>Tr</td> <td>—</td> <td>—</td> <td>—</td> <td>—</td> </tr> <tr> <td>Calcite/dolomite</td> <td>Tr</td> <td>20</td> <td>45</td> <td>2</td> <td>—</td> </tr> <tr> <td>Accessory minerals</td> <td>1</td> <td>Tr</td> <td>1</td> <td>2</td> <td>15</td> </tr> <tr> <td>Foraminifers</td> <td>—</td> <td>Tr</td> <td>—</td> <td>—</td> <td>—</td> </tr> <tr> <td>Nannofossils</td> <td>—</td> <td>5</td> <td>—</td> <td>—</td> <td>—</td> </tr> <tr> <td>Diatoms</td> <td>—</td> <td>—</td> <td>—</td> <td>—</td> <td>Tr</td> </tr> <tr> <td>Sponge spicules</td> <td>1</td> <td>—</td> <td>—</td> <td>—</td> <td>Tr</td> </tr> </table>	Quartz	60	35	55	50	74	Feldspar	3	Tr	—	4	10	Mica	1	—	Tr	Tr	1	Clay	34	40	—	42	Tr	Volcanic glass	Tr	—	—	—	—	Calcite/dolomite	Tr	20	45	2	—	Accessory minerals	1	Tr	1	2	15	Foraminifers	—	Tr	—	—	—	Nannofossils	—	5	—
Quartz	60	35	55	50	74																																																																									
Feldspar	3	Tr	—	4	10																																																																									
Mica	1	—	Tr	Tr	1																																																																									
Clay	34	40	—	42	Tr																																																																									
Volcanic glass	Tr	—	—	—	—																																																																									
Calcite/dolomite	Tr	20	45	2	—																																																																									
Accessory minerals	1	Tr	1	2	15																																																																									
Foraminifers	—	Tr	—	—	—																																																																									
Nannofossils	—	5	—	—	—																																																																									
Diatoms	—	—	—	—	Tr																																																																									
Sponge spicules	1	—	—	—	Tr																																																																									



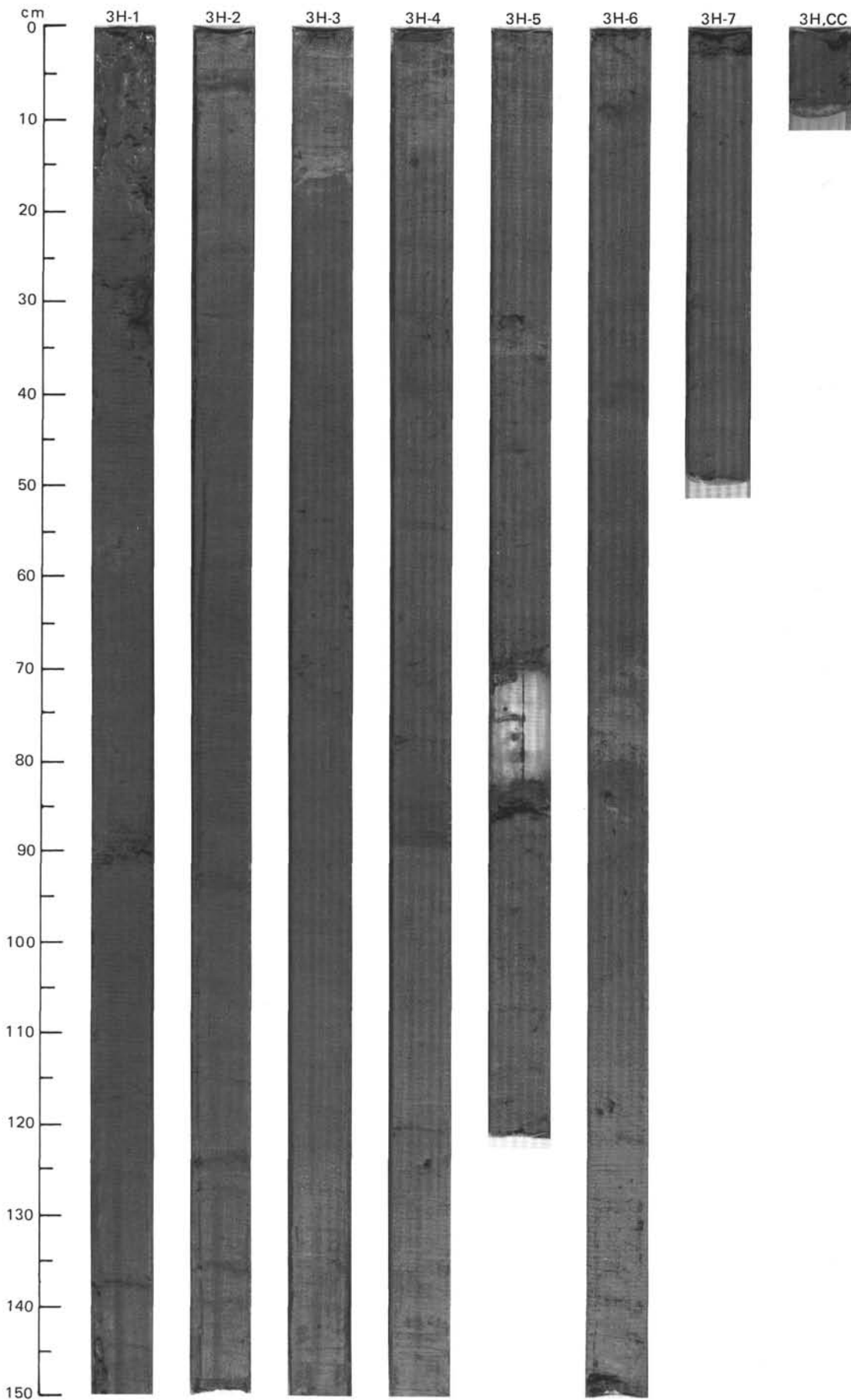




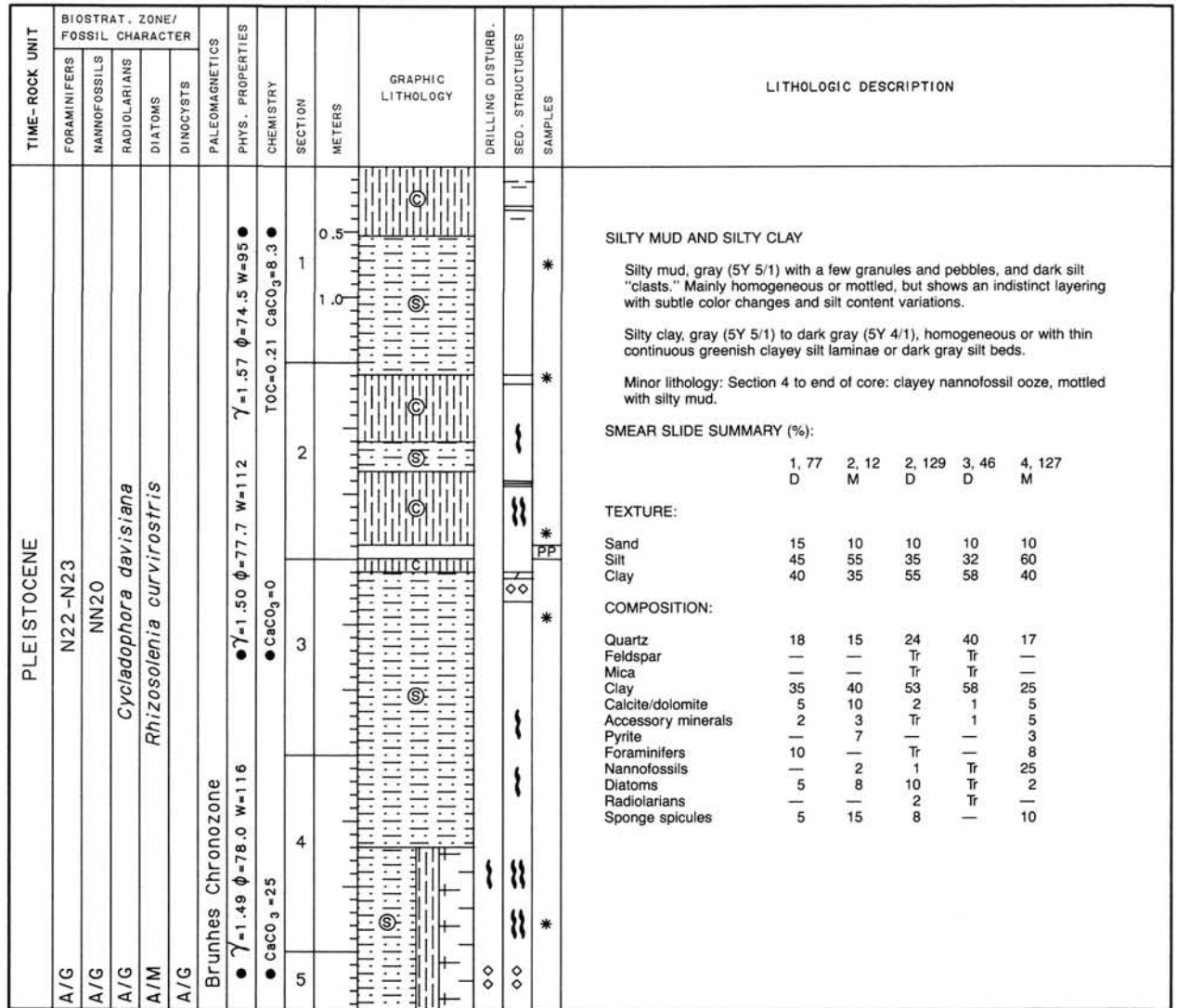


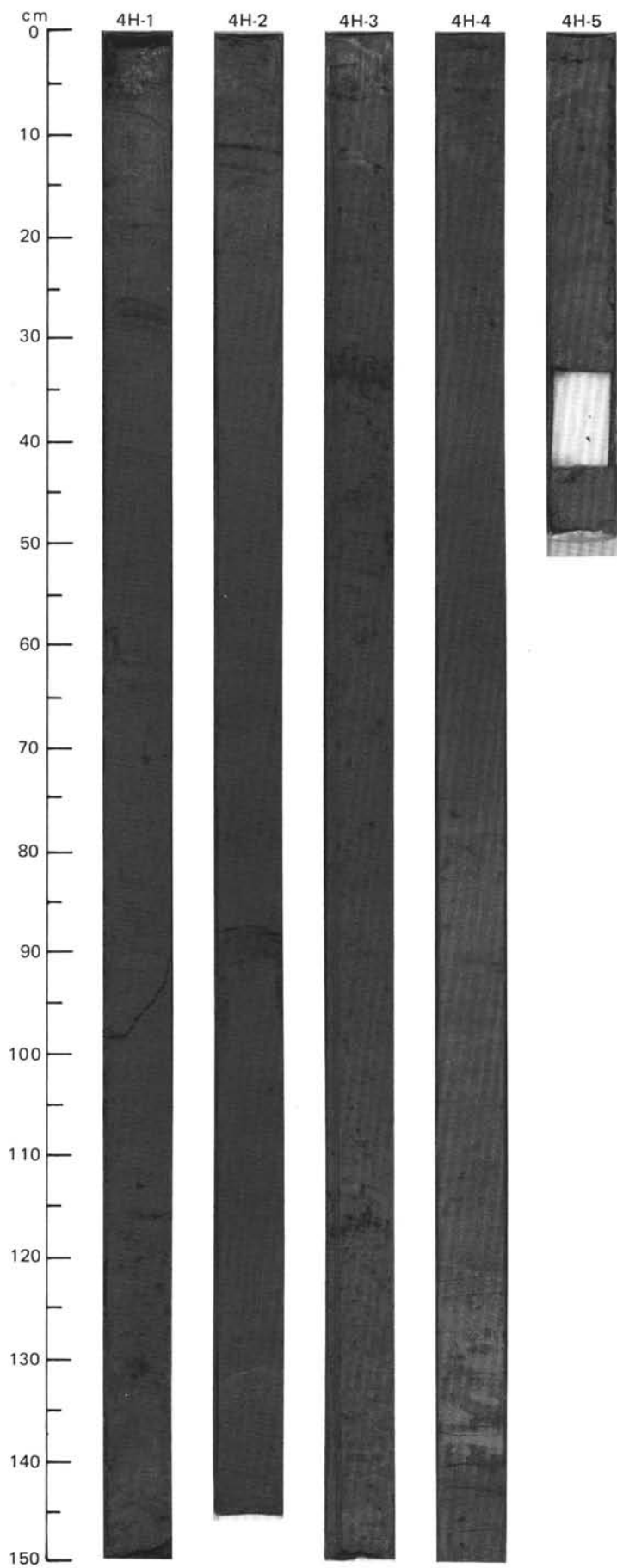
SITE 646 HOLE B CORE 3H CORED INTERVAL 3462.6-3472.3 mbsl; 14.4-24.1 mbsf

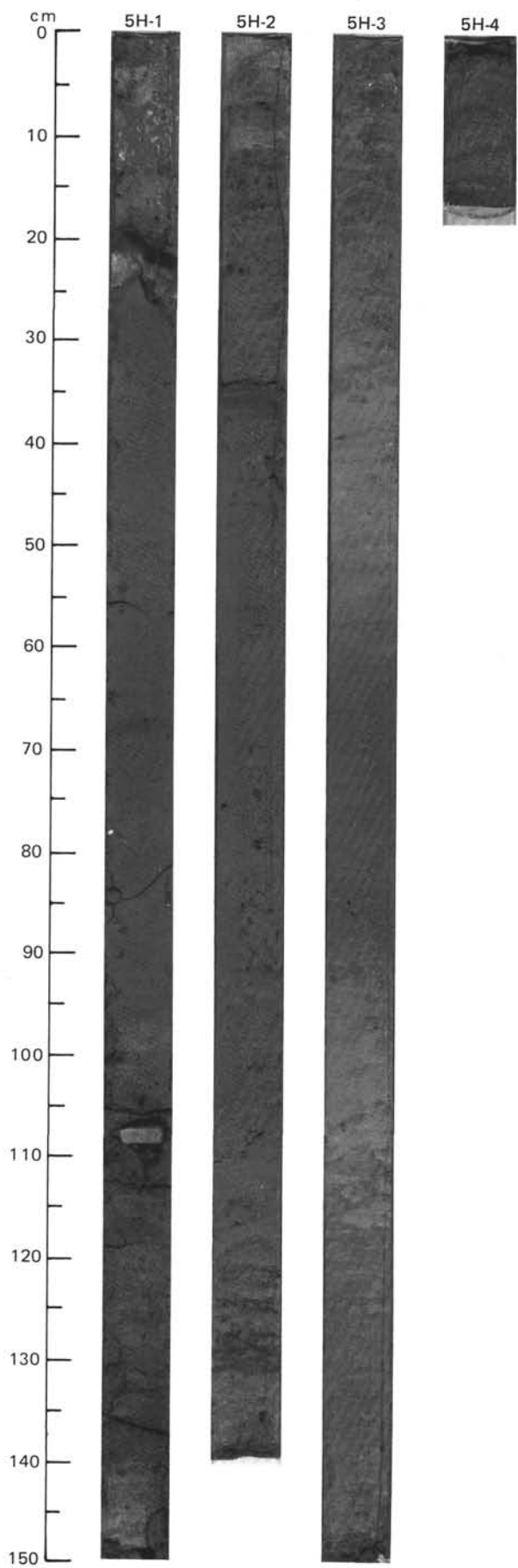
TIME-ROCK UNIT		BIOSTRAT. ZONE/ FOSSIL CHARACTER	PALEOMAGNETICS	PHYS. PROPERTIES	CHEMISTRY	SECTION	METERS	GRAPHIC LITHOLOGY	DRILLING DISTURB.	SED. STRUCTURES	SAMPLES	LITHOLOGIC DESCRIPTION																																																																																																																														
FORAMINIFERS	NANNOFOSSILS																																																																																																																																									
PLEISTOCENE																																																																																																																																										
A/G	N22-N23			$\gamma=1.48 \phi=76.7 W=113$	$CaCO_3=0$	1	0.5				*	<p>SILTY CLAY, CLAYEY SILT, DETRICARBONATE CLAYEY SILT, AND FORAMINIFER-NANNOFOSSIL-BEARING SILTY CLAY</p> <p>Silty clay, greenish gray (5G 5/1) to gray (5Y 5/1), color banded and with streaks of sulfide.</p> <p>Clayey silt, gray (5Y 6/1) mottled with sulfide-rimmed circles of <i>Cylindrichnus</i>.</p> <p>Detriticarbonate clayey silt, light gray (5Y 7/1) with sand and granules.</p> <p>Foraminifer-nannofossil-bearing silty clay, gray (5Y 6/1), slightly mottled.</p> <p>Minor lithology: Section 4, 84-90 cm: weakly laminated dark gray silt.</p> <p>SMEAR SLIDE SUMMARY (%):</p> <table border="1"> <thead> <tr> <th></th> <th>1, 60</th> <th>3, 17</th> <th>4, 92</th> <th>5, 18</th> <th>6, 20</th> <th>7, 20</th> </tr> <tr> <th></th> <th>D</th> <th>D</th> <th>D</th> <th>D</th> <th>D</th> <th>D</th> </tr> </thead> <tbody> <tr> <td>TEXTURE:</td> <td></td> <td></td> <td></td> <td></td> <td></td> <td></td> </tr> <tr> <td>Sand</td> <td>3</td> <td>1</td> <td>2</td> <td>—</td> <td>2</td> <td>5</td> </tr> <tr> <td>Silt</td> <td>30</td> <td>40</td> <td>40</td> <td>55</td> <td>40</td> <td>35</td> </tr> <tr> <td>Clay</td> <td>67</td> <td>59</td> <td>58</td> <td>45</td> <td>58</td> <td>60</td> </tr> <tr> <td>COMPOSITION:</td> <td></td> <td></td> <td></td> <td></td> <td></td> <td></td> </tr> <tr> <td>Quartz</td> <td>30</td> <td>15</td> <td>20</td> <td>50</td> <td>45</td> <td>15</td> </tr> <tr> <td>Feldspar</td> <td>—</td> <td>—</td> <td>—</td> <td>5</td> <td>2</td> <td>—</td> </tr> <tr> <td>Mica</td> <td>—</td> <td>—</td> <td>—</td> <td>Tr</td> <td>—</td> <td>—</td> </tr> <tr> <td>Clay</td> <td>55</td> <td>55</td> <td>58</td> <td>39</td> <td>48</td> <td>60</td> </tr> <tr> <td>Volcanic glass</td> <td>—</td> <td>—</td> <td>—</td> <td>Tr</td> <td>—</td> <td>—</td> </tr> <tr> <td>Calcite/dolomite</td> <td>15</td> <td>30</td> <td>Tr</td> <td>5</td> <td>5</td> <td>—</td> </tr> <tr> <td>Accessory minerals</td> <td>Tr</td> <td>Tr</td> <td>1</td> <td>—</td> <td>Tr</td> <td>2</td> </tr> <tr> <td>Foraminifers</td> <td>—</td> <td>—</td> <td>5</td> <td>—</td> <td>—</td> <td>3</td> </tr> <tr> <td>Nannofossils</td> <td>—</td> <td>—</td> <td>15</td> <td>—</td> <td>—</td> <td>10</td> </tr> <tr> <td>Diatoms</td> <td>—</td> <td>—</td> <td>Tr</td> <td>1</td> <td>Tr</td> <td>10</td> </tr> <tr> <td>Sponge spicules</td> <td>—</td> <td>—</td> <td>1</td> <td>Tr</td> <td>Tr</td> <td>—</td> </tr> </tbody> </table>		1, 60	3, 17	4, 92	5, 18	6, 20	7, 20		D	D	D	D	D	D	TEXTURE:							Sand	3	1	2	—	2	5	Silt	30	40	40	55	40	35	Clay	67	59	58	45	58	60	COMPOSITION:							Quartz	30	15	20	50	45	15	Feldspar	—	—	—	5	2	—	Mica	—	—	—	Tr	—	—	Clay	55	55	58	39	48	60	Volcanic glass	—	—	—	Tr	—	—	Calcite/dolomite	15	30	Tr	5	5	—	Accessory minerals	Tr	Tr	1	—	Tr	2	Foraminifers	—	—	5	—	—	3	Nannofossils	—	—	15	—	—	10	Diatoms	—	—	Tr	1	Tr	10	Sponge spicules	—	—	1	Tr	Tr	—
	1, 60	3, 17	4, 92	5, 18	6, 20	7, 20																																																																																																																																				
	D	D	D	D	D	D																																																																																																																																				
TEXTURE:																																																																																																																																										
Sand	3	1	2	—	2	5																																																																																																																																				
Silt	30	40	40	55	40	35																																																																																																																																				
Clay	67	59	58	45	58	60																																																																																																																																				
COMPOSITION:																																																																																																																																										
Quartz	30	15	20	50	45	15																																																																																																																																				
Feldspar	—	—	—	5	2	—																																																																																																																																				
Mica	—	—	—	Tr	—	—																																																																																																																																				
Clay	55	55	58	39	48	60																																																																																																																																				
Volcanic glass	—	—	—	Tr	—	—																																																																																																																																				
Calcite/dolomite	15	30	Tr	5	5	—																																																																																																																																				
Accessory minerals	Tr	Tr	1	—	Tr	2																																																																																																																																				
Foraminifers	—	—	5	—	—	3																																																																																																																																				
Nannofossils	—	—	15	—	—	10																																																																																																																																				
Diatoms	—	—	Tr	1	Tr	10																																																																																																																																				
Sponge spicules	—	—	1	Tr	Tr	—																																																																																																																																				
A/G	NN20	<i>Cycladophora davisiana</i>		$\gamma=1.50 \phi=79.7 W=119$	$CaCO_3=8$	2	1.0				*																																																																																																																															
A/G		<i>Rhizosolenia curvirostris</i>				3					*																																																																																																																															
F/G			Brunhes Chronozone			4					*																																																																																																																															
				$\gamma=1.58 \phi=73.0 W=90$		5					*																																																																																																																															
				$CaCO_3=3.9$		6					*																																																																																																																															
						7					*																																																																																																																															
CC				TOC=0.54																																																																																																																																						



SITE 646 HOLE B CORE 4 H CORED INTERVAL 3472.3-3482.0 mbsl; 24.1-33.8 mbsf



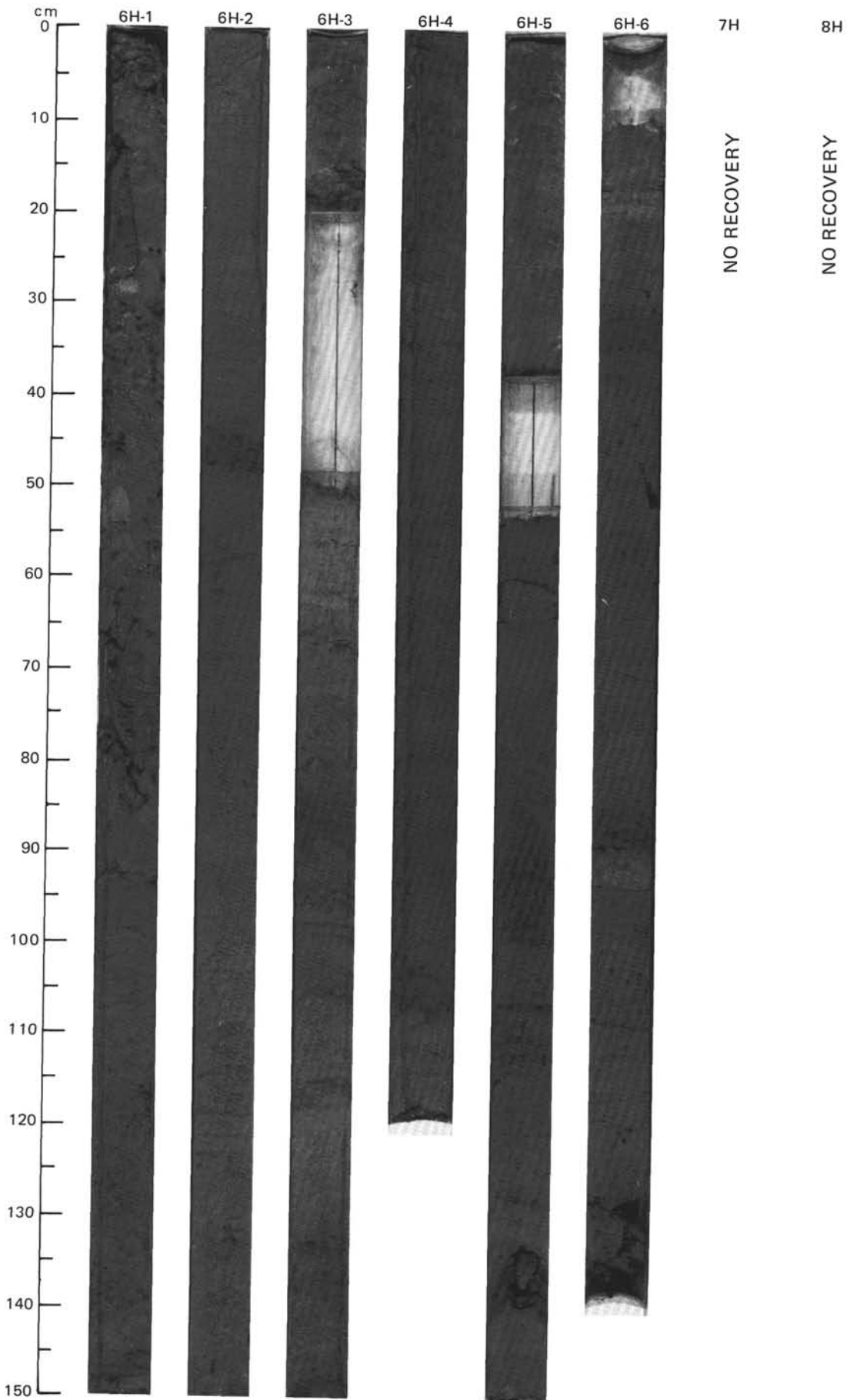




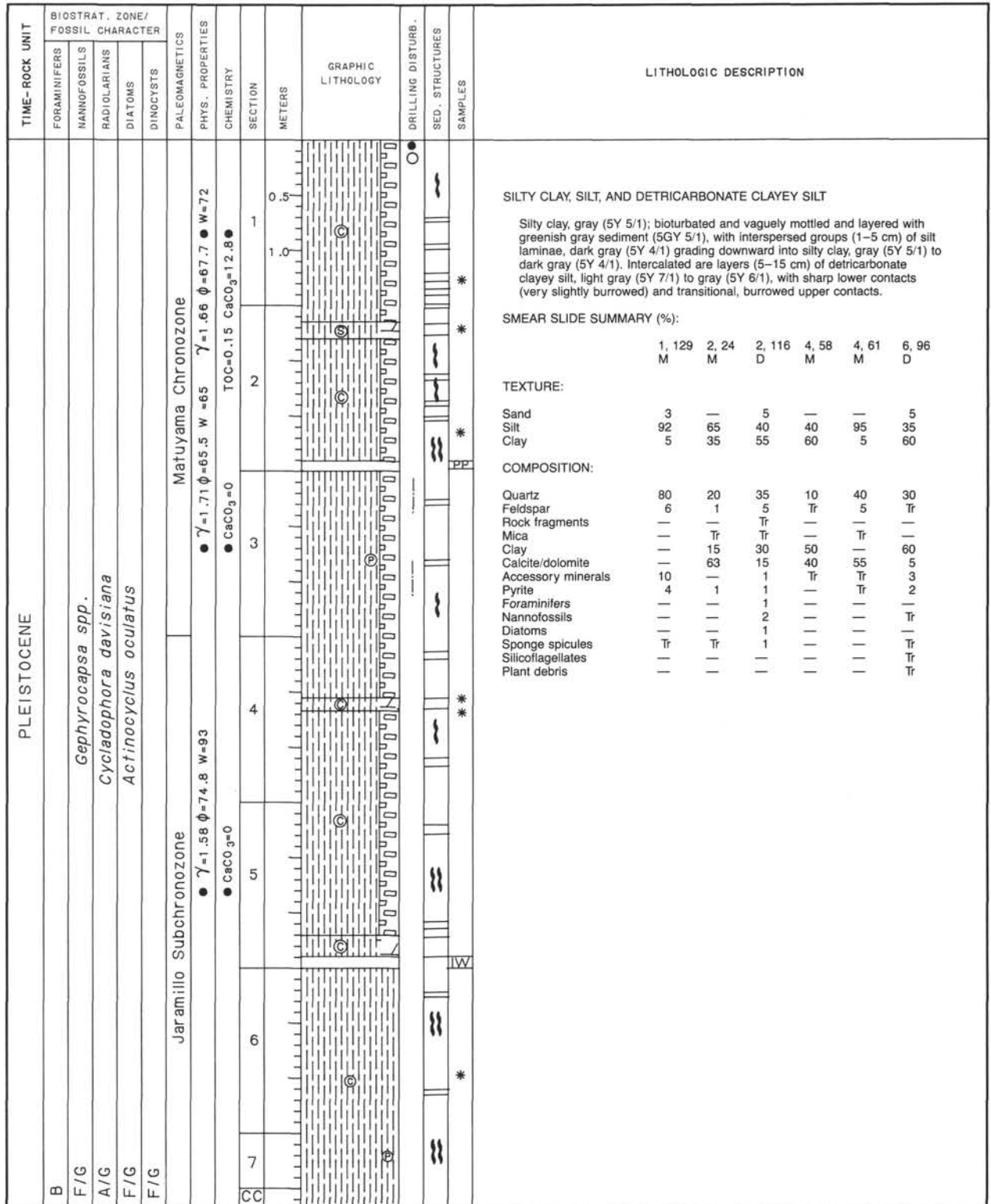
SITE 646 HOLE B CORE 6H CORED INTERVAL 3491.6-3501.3 mbsl; 43.4-53.1 mbsf

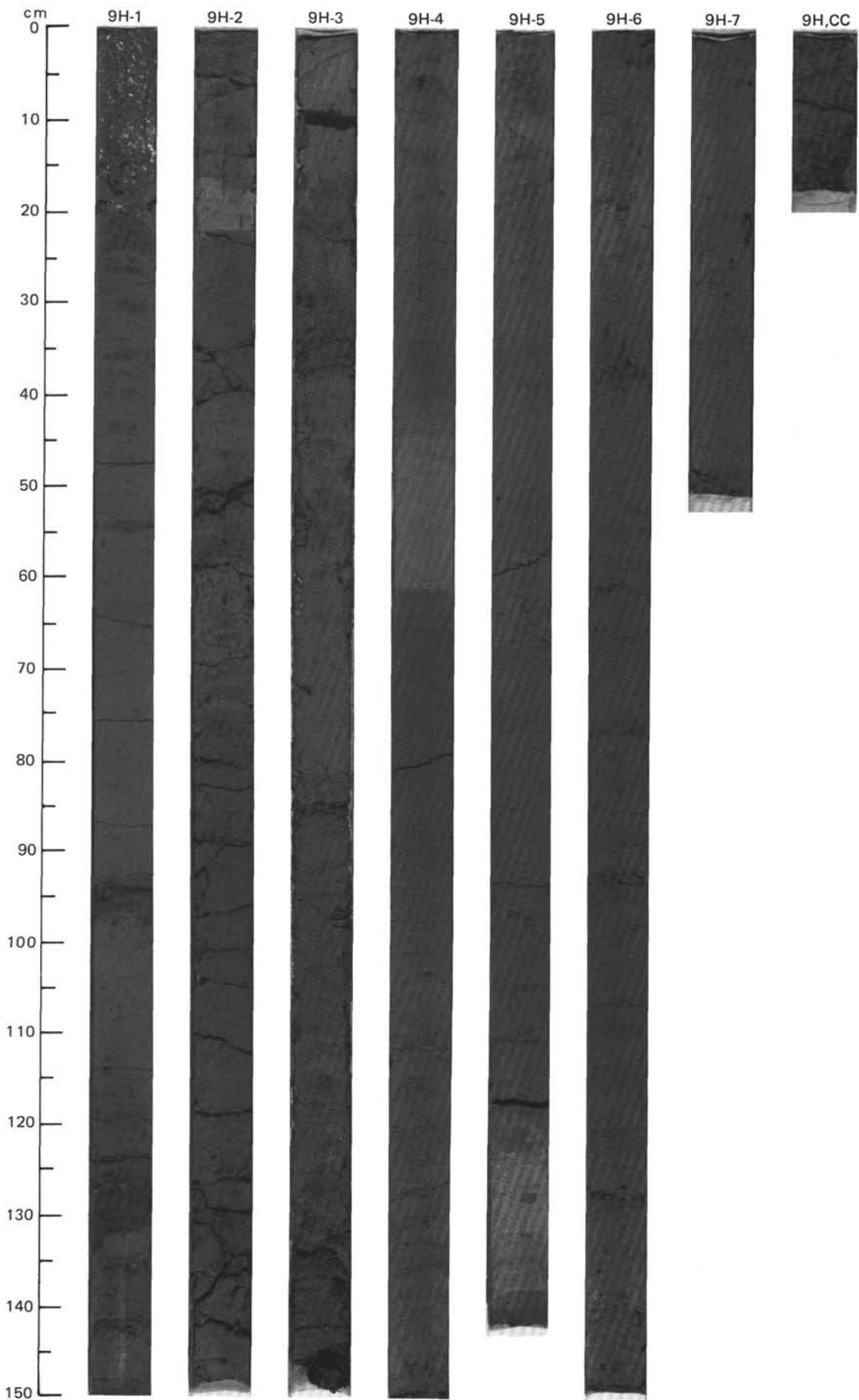
TIME-ROCK UNIT	BIOSTRAT. ZONE/ FOSSIL CHARACTER					PALEOMAGNETICS	PHYS. PROPERTIES	CHEMISTRY	SECTION	METERS	GRAPHIC LITHOLOGY	DRILLING DISTURB.	SED. STRUCTURES	SAMPLES	LITHOLOGIC DESCRIPTION																																																																													
	FORAMINIFERS	NANNOFOSSILS	RADIOLARIANS	DIATOMS	DINOCTYSTS																																																																																							
PLEISTOCENE																																																																																												
A/G	N22-N23						$\gamma=1.64 \phi=69.7 W=77$	TOC=0.31 CaCO ₃ =0.31	1	0.5				*	SILICA-BEARING SILTY CLAY, NANNOFOSSIL-BEARING CLAYEY SILT, CLAYEY SILT, FORAMINIFER-NANNOFOSSIL-BEARING AND FORAMINIFER-NANNOFOSSIL SILTY CLAY																																																																													
C/G	NN19								2	1.0				*	Silica-bearing silty clay, gray (5Y 5/1) and silica and nannofossil-bearing clayey silt, gray (5Y 5/1), and gray (5Y 5/1) mixed with dark gray (5Y 4/1). Foraminifer-nannofossil-bearing and foraminifer-nannofossil silty clay and clayey silt, gray (5Y 4/1). Most parts seem homogeneous, bioturbation is visible locally. Minor lithologies: a. Section 3, 50-65 cm: clayey nannofossil ooze, light gray (5Y 6/1) with gradational contacts. b. Section 6, 43-48 cm; Section 6, 10-20 cm: dark gray silty mud layers (5Y 4/1) with scattered granules. c. Section 6, 80-92 cm: silty mud, pinkish gray (7.5YR 6/2) and dark gray (5Y 4/1) with light gray (5Y 6/1), detrital carbonate layer below and granules. d. Section 3, 80-88: well-sorted laminated silt layers, dark gray (5Y 4/1), with bioturbation in the upper part. 3. Section 3, 135 cm: isolated pebble.																																																																													
B									3		VOID			*	SMEAR SLIDE SUMMARY (%):																																																																													
B							$\gamma=1.63 \phi=1.63 W=79$	CaCO ₃ =1.4	4					*	<table border="1"> <tr> <td></td> <td>1, 107</td> <td>2, 75</td> <td>3, 53</td> <td>4, 43</td> <td>5, 23</td> <td>6, 172</td> </tr> <tr> <td></td> <td>D</td> <td>D</td> <td>M</td> <td>D</td> <td>D</td> <td>D</td> </tr> </table>		1, 107	2, 75	3, 53	4, 43	5, 23	6, 172		D	D	M	D	D	D																																																															
	1, 107	2, 75	3, 53	4, 43	5, 23	6, 172																																																																																						
	D	D	M	D	D	D																																																																																						
F/G							$\gamma=1.59 \phi=73.2 W=89$	TOC=0.16 CaCO ₃ =6.9	5					*	TEXTURE:																																																																													
									6					*	<table border="1"> <tr> <td>Sand</td> <td>20</td> <td>3</td> <td>3</td> <td>—</td> <td>2</td> <td>10</td> </tr> <tr> <td>Silt</td> <td>50</td> <td>40</td> <td>17</td> <td>60</td> <td>50</td> <td>60</td> </tr> <tr> <td>Clay</td> <td>30</td> <td>57</td> <td>80</td> <td>40</td> <td>48</td> <td>30</td> </tr> </table>	Sand	20	3	3	—	2	10	Silt	50	40	17	60	50	60	Clay	30	57	80	40	48	30																																																								
Sand	20	3	3	—	2	10																																																																																						
Silt	50	40	17	60	50	60																																																																																						
Clay	30	57	80	40	48	30																																																																																						
														*	COMPOSITION:																																																																													
														*	<table border="1"> <tr> <td>Quartz</td> <td>35</td> <td>20</td> <td>4</td> <td>25</td> <td>25</td> <td>30</td> </tr> <tr> <td>Feldspar</td> <td>10</td> <td>5</td> <td>—</td> <td>—</td> <td>5</td> <td>—</td> </tr> <tr> <td>Clay</td> <td>25</td> <td>40</td> <td>25</td> <td>35</td> <td>42</td> <td>30</td> </tr> <tr> <td>Calcite/dolomite</td> <td>5</td> <td>10</td> <td>3</td> <td>5</td> <td>15</td> <td>20</td> </tr> <tr> <td>Accessory minerals</td> <td>5</td> <td>2</td> <td>1</td> <td>5</td> <td>1</td> <td>—</td> </tr> <tr> <td>Pyrite</td> <td>—</td> <td>1</td> <td>2</td> <td>5</td> <td>2</td> <td>5</td> </tr> <tr> <td>Foraminifers</td> <td>—</td> <td>7</td> <td>7</td> <td>3</td> <td>4</td> <td>—</td> </tr> <tr> <td>Nannofossils</td> <td>5</td> <td>10</td> <td>57</td> <td>10</td> <td>3</td> <td>8</td> </tr> <tr> <td>Diatoms</td> <td>7</td> <td>2</td> <td>2</td> <td>2</td> <td>1</td> <td>2</td> </tr> <tr> <td>Sponge spicules</td> <td>8</td> <td>3</td> <td>4</td> <td>10</td> <td>2</td> <td>5</td> </tr> <tr> <td>Silicoflagellates</td> <td>—</td> <td>Tr</td> <td>—</td> <td>—</td> <td>—</td> <td>—</td> </tr> </table>	Quartz	35	20	4	25	25	30	Feldspar	10	5	—	—	5	—	Clay	25	40	25	35	42	30	Calcite/dolomite	5	10	3	5	15	20	Accessory minerals	5	2	1	5	1	—	Pyrite	—	1	2	5	2	5	Foraminifers	—	7	7	3	4	—	Nannofossils	5	10	57	10	3	8	Diatoms	7	2	2	2	1	2	Sponge spicules	8	3	4	10	2	5	Silicoflagellates	—	Tr	—	—	—	—
Quartz	35	20	4	25	25	30																																																																																						
Feldspar	10	5	—	—	5	—																																																																																						
Clay	25	40	25	35	42	30																																																																																						
Calcite/dolomite	5	10	3	5	15	20																																																																																						
Accessory minerals	5	2	1	5	1	—																																																																																						
Pyrite	—	1	2	5	2	5																																																																																						
Foraminifers	—	7	7	3	4	—																																																																																						
Nannofossils	5	10	57	10	3	8																																																																																						
Diatoms	7	2	2	2	1	2																																																																																						
Sponge spicules	8	3	4	10	2	5																																																																																						
Silicoflagellates	—	Tr	—	—	—	—																																																																																						

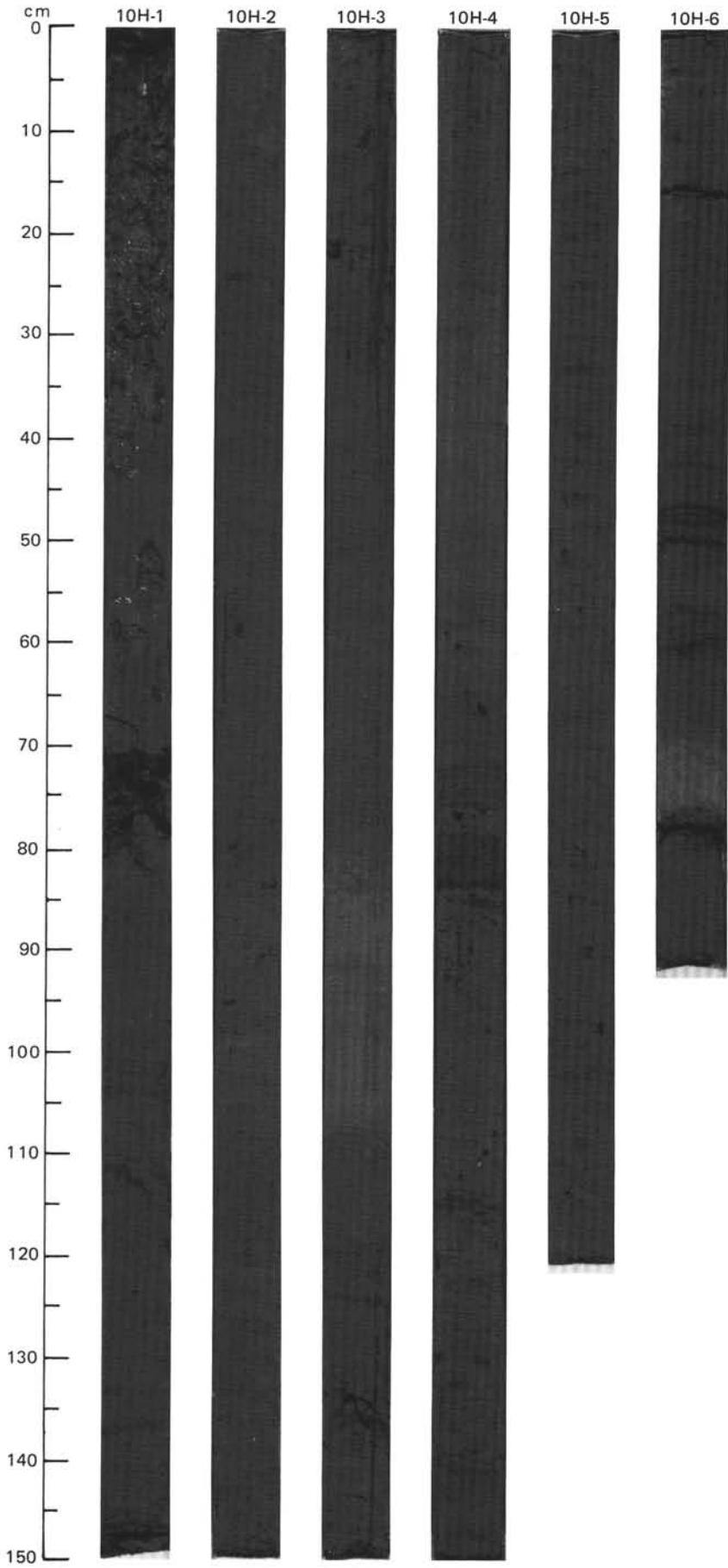
CORE 7H NO RECOVERY
CORE 8H NO RECOVERY

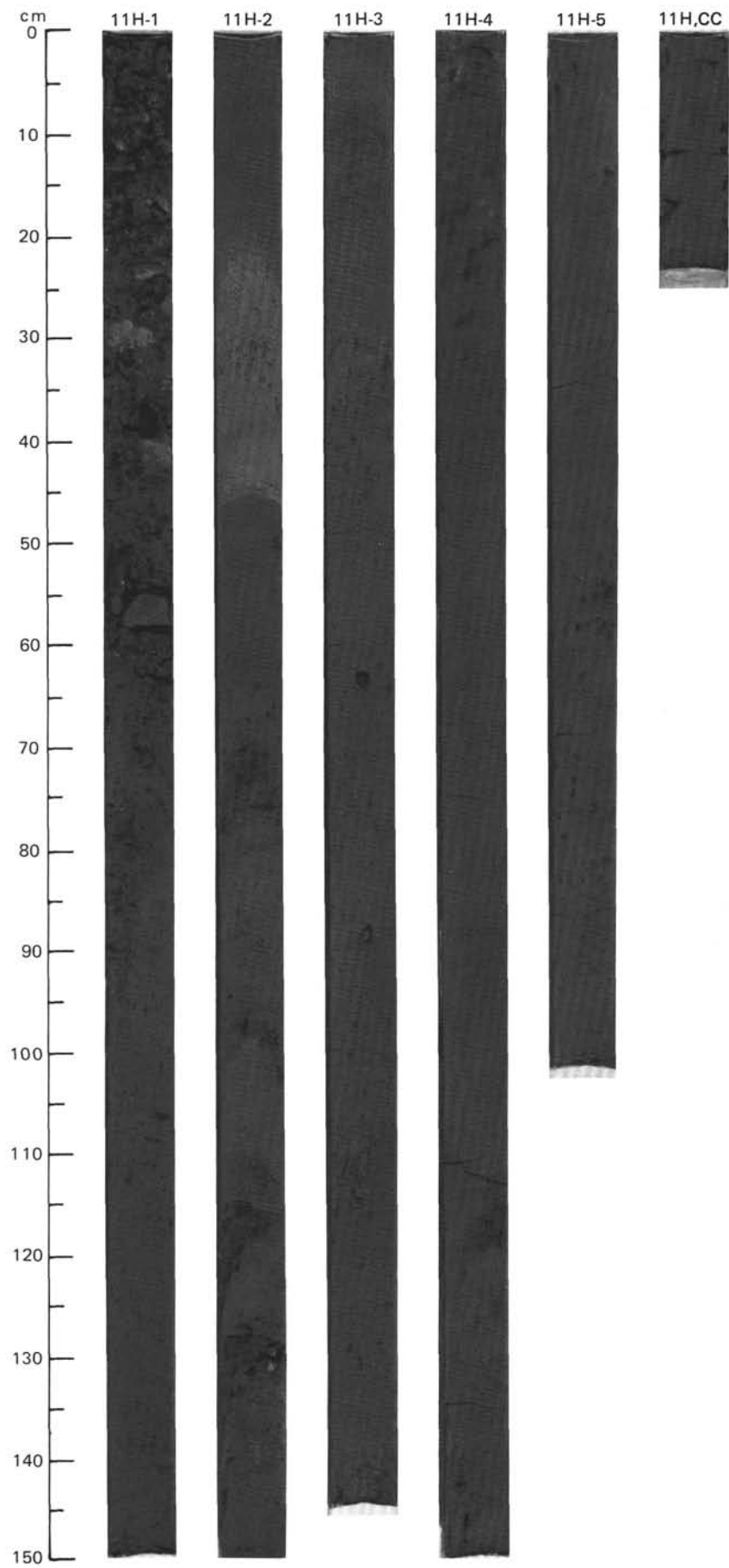


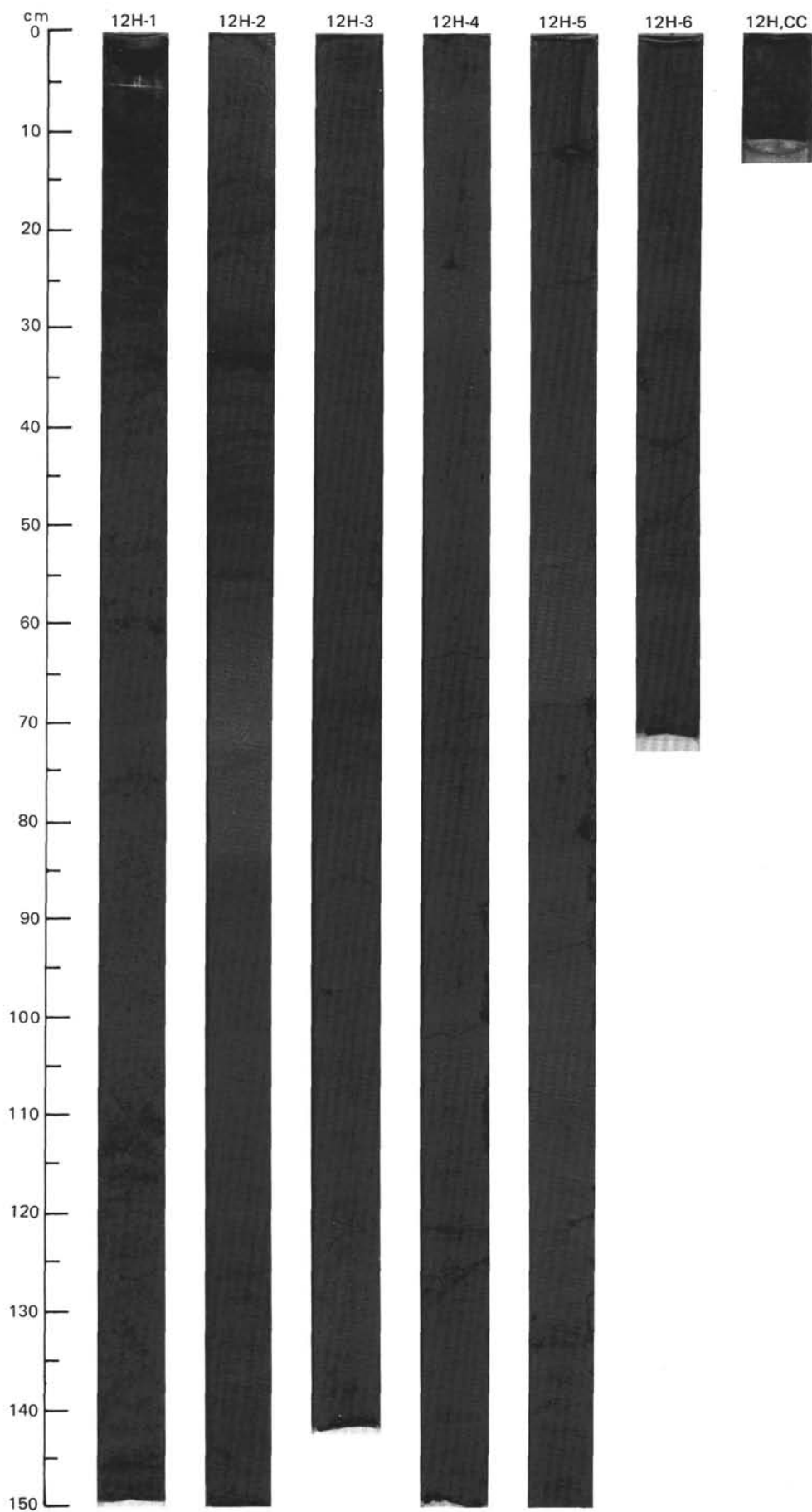
SITE 646 HOLE B CORE 9 H CORED INTERVAL 3520.6-3530.2 mbsl; 72.4-82.0 mbsf

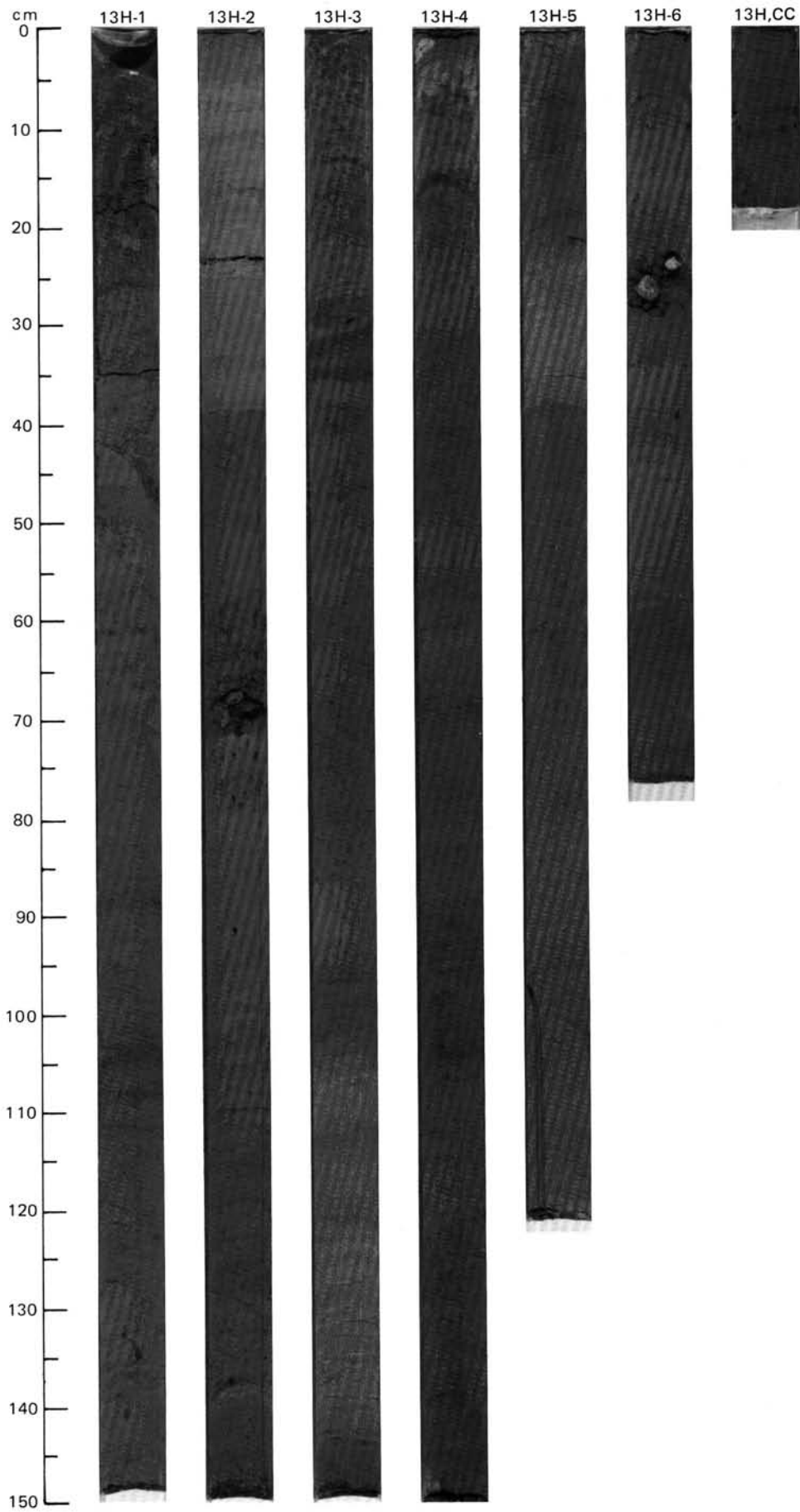












SITE 646 HOLE B CORE 14 H CORED INTERVAL 3569.0-3578.7 mbsl; 120.8-130.5 mbsf

TIME-ROCK UNIT	BIOSTRAT. ZONE/ FOSSIL CHARACTER				FALEOMAGNETICS	PHYS. PROPERTIES	CHEMISTRY	SECTION	METERS	GRAPHIC LITHOLOGY	DRILLING DISTURB.	SED. STRUCTURES	SAMPLES	LITHOLOGIC DESCRIPTION
	FORAMINIFERS	NANNOFOSSILS	RADIOLARIANS	DIATOMS										
LOWER PLEISTOCENE														
R/P	N22-N23													
R/M														
B														
B														
F/G														
					Matuyama Chronozone									
					• $\gamma = 1.84$ $\phi = 62.2$ W=53	• $\gamma = 1.68$ $\phi = 61.5$ W=60	• $\text{CaCO}_3 = 1.0$							
					• $\gamma = 1.78$ $\phi = 63.8$ W=58		• $\text{CaCO}_3 = 0$							
					• $\text{TOC} = 0.24$ $\text{CaCO}_3 = 7.3$									
CC														

CLAYEY SILT, SILTY CLAY, AND NANNOFOSSIL SILTY CLAY

Clayey silt, greenish gray (5GY 5/1 to 5GY 6/1); mottled with greenish bands, bioturbated with pyrite concretions, some intervals slightly calcareous, scattered pockets of light gray, well-sorted fine sand.

Silty clay, greenish gray (5GY 6/1) to gray (5Y 5/1); mottled, bioturbated. Some intervals slightly calcareous with scattered fine sand pockets and pyrite concretions.

Nannofossil silty clay, greenish gray (5GY 6/1); mottled with a few scattered sand pockets.

Minor lithologies:

a. Section 3, 16-100 cm: dark gray (N4) well-sorted silt layers as thick as 1 cm, with sharp boundaries. Some faintly laminated. Intercalated with silty clay or clayey silt.

b. Section 5, 53-69 cm: detrital carbonate clayey silt, light greenish gray (5GY 7/1) to light gray (5Y 7/1).

c. Section 5, 79-100 cm: light gray, well-sorted fine sand laminae and/or lenses, alternating with clayey silt.

SMEAR SLIDE SUMMARY (%):

	1, 80	3, 67	3, 106	5, 68	5, 94
D		M	D	M	M

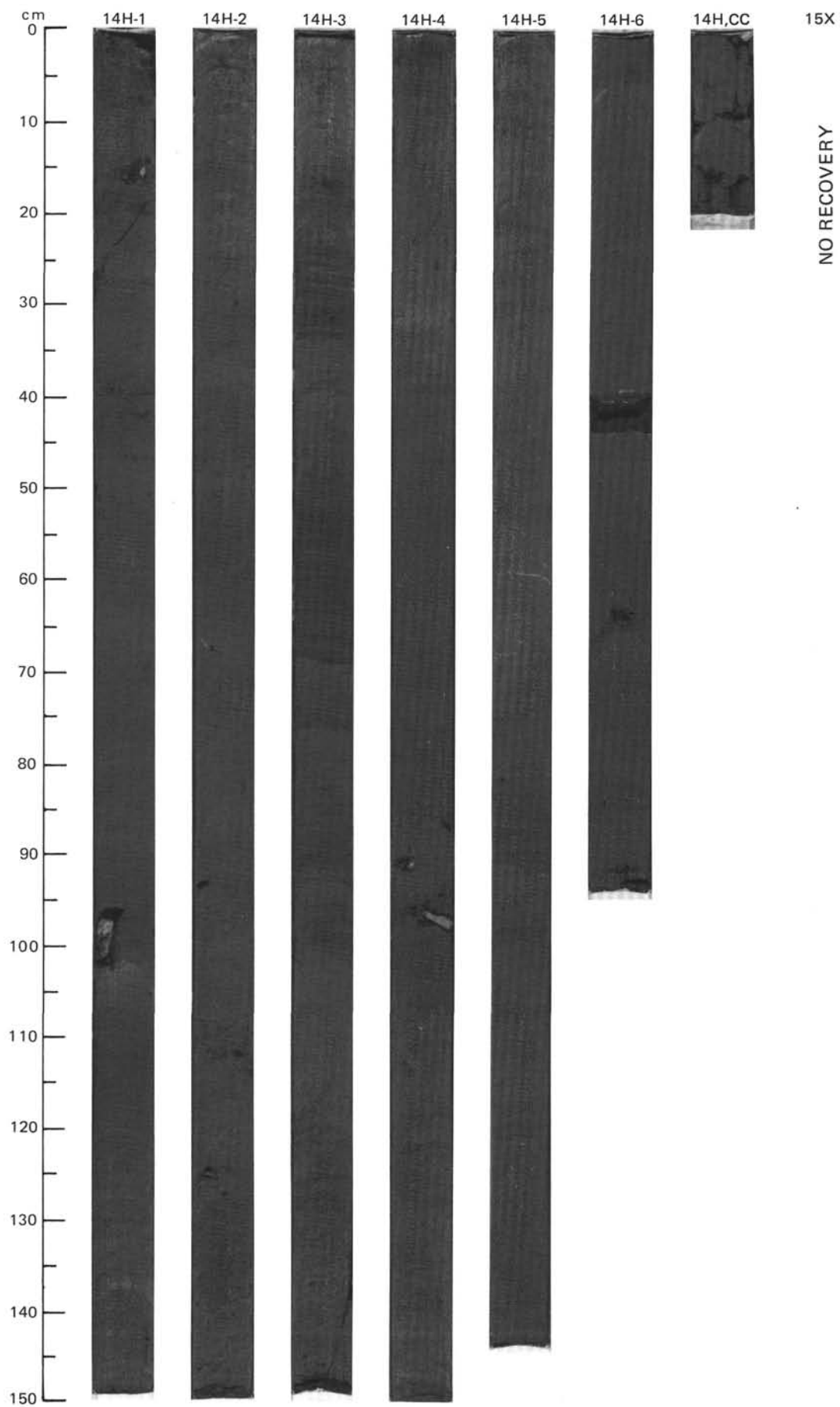
TEXTURE:

Sand	1	—	1	—	85
Silt	45	75	60	60	10
Clay	54	25	39	40	5

COMPOSITION:

Quartz	15	60	65	20	75
Feldspar	—	5	2	Tr	10
Mica	Tr	1	1	—	1
Clay	50	19	27	30	4
Volcanic glass	—	Tr	Tr	—	Tr
Calcite/dolomite	10	—	3	50	—
Accessory minerals	Tr	15	2	Tr	10
Foraminifers	—	—	Tr	—	—
Nannofossils	25	—	—	—	—
Diatoms	—	Tr	—	—	—
Sponge spicules	—	Tr	Tr	Tr	—

CORE 15X NO RECOVERY

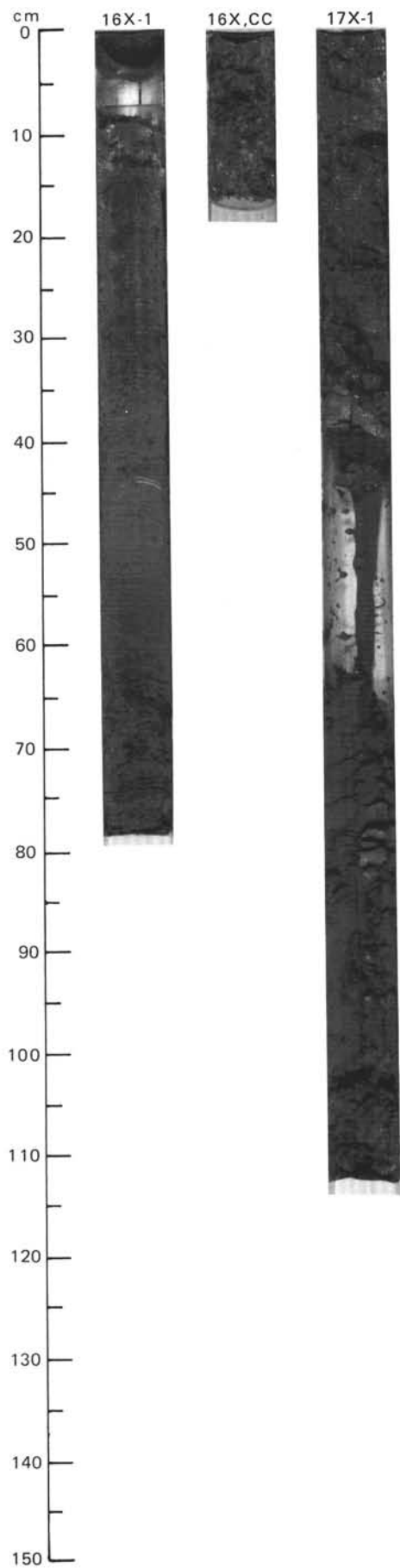


SITE 646 HOLE B CORE 16 X CORED INTERVAL 3588.3-3598.0 mbsl; 140.1-149.8 mbsf

TIME-ROCK UNIT	BIOSTRAT. ZONE/ FOSSIL CHARACTER					PALEOMAGNETICS	PHYS. PROPERTIES	CHEMISTRY	SECTION	METERS	GRAPHIC LITHOLOGY	DRILLING DISTURB.	SED. STRUCTURES	SAMPLES	LITHOLOGIC DESCRIPTION																														
	FORAMINIFERS	NANNOFOSSILS	RADIOLARIANS	DIATOMS	DINOCYSTS																																								
UPPER PLIOCENE	PL3-PL6	C/M							1	0.5					<p>SILTY CLAY</p> <p>Silty clay, greenish gray (5GY 5/1); structureless, with few blebs of pyrite.</p> <p>Minor lithology: Section 1, 44-54 cm: detriticarbonate clayey silt, gray (5Y 6/1), with a few thin laminations, 1-2 mm thick, also light gray.</p> <p>SMEAR SLIDE SUMMARY (%):</p> <table border="1"> <tr> <td></td> <td>1, 25</td> <td>1, 50</td> </tr> <tr> <td>D</td> <td></td> <td>M</td> </tr> </table> <p>TEXTURE:</p> <table border="1"> <tr> <td>Sand</td> <td>—</td> <td>1</td> </tr> <tr> <td>Silt</td> <td>40</td> <td>60</td> </tr> <tr> <td>Clay</td> <td>60</td> <td>39</td> </tr> </table> <p>COMPOSITION:</p> <table border="1"> <tr> <td>Quartz</td> <td>30</td> <td>30</td> </tr> <tr> <td>Clay</td> <td>52</td> <td>29</td> </tr> <tr> <td>Calcite/dolomite</td> <td>15</td> <td>40</td> </tr> <tr> <td>Accessory minerals</td> <td>1</td> <td>1</td> </tr> <tr> <td>Nannofossils</td> <td>2</td> <td>—</td> </tr> </table>		1, 25	1, 50	D		M	Sand	—	1	Silt	40	60	Clay	60	39	Quartz	30	30	Clay	52	29	Calcite/dolomite	15	40	Accessory minerals	1	1	Nannofossils	2	—
	1, 25	1, 50																																											
D		M																																											
Sand	—	1																																											
Silt	40	60																																											
Clay	60	39																																											
Quartz	30	30																																											
Clay	52	29																																											
Calcite/dolomite	15	40																																											
Accessory minerals	1	1																																											
Nannofossils	2	—																																											
							$\gamma = 1.95 \phi = 51.8 W = 37$																																						
							TOC=0.43 CaCO ₃ =24																																						

SITE 646 HOLE B CORE 17 X CORED INTERVAL 3598.0-3607.3 mbsl; 149.8-159.1 mbsf

TIME-ROCK UNIT	BIOSTRAT. ZONE/ FOSSIL CHARACTER					PALEOMAGNETICS	PHYS. PROPERTIES	CHEMISTRY	SECTION	METERS	GRAPHIC LITHOLOGY	DRILLING DISTURB.	SED. STRUCTURES	SAMPLES	LITHOLOGIC DESCRIPTION
	FORAMINIFERS	NANNOFOSSILS	RADIOLARIANS	DIATOMS	DINOCYSTS										
UPPER PLIOCENE	PL3-PL6	F/G	C/G	F/G	R/P	R/G			1	0.5					<p>NANNOFOSSIL-BEARING SILTY CLAY</p> <p>Nannofossil-bearing silty clay, dark gray (5Y 4/1); intensely deformed and probably mixed.</p>

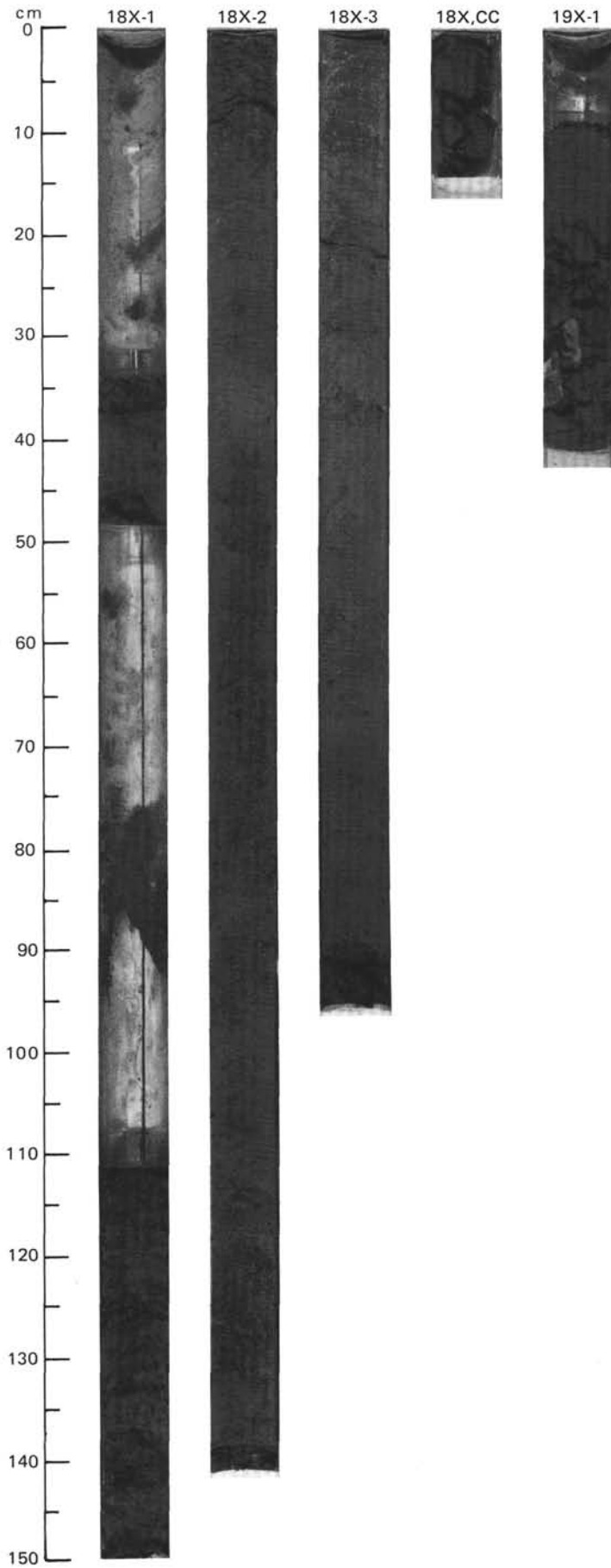


SITE 646 HOLE B CORE 18 X CORED INTERVAL 3607.3-3617.0 mbsl; 159.1-168.8 mbsf

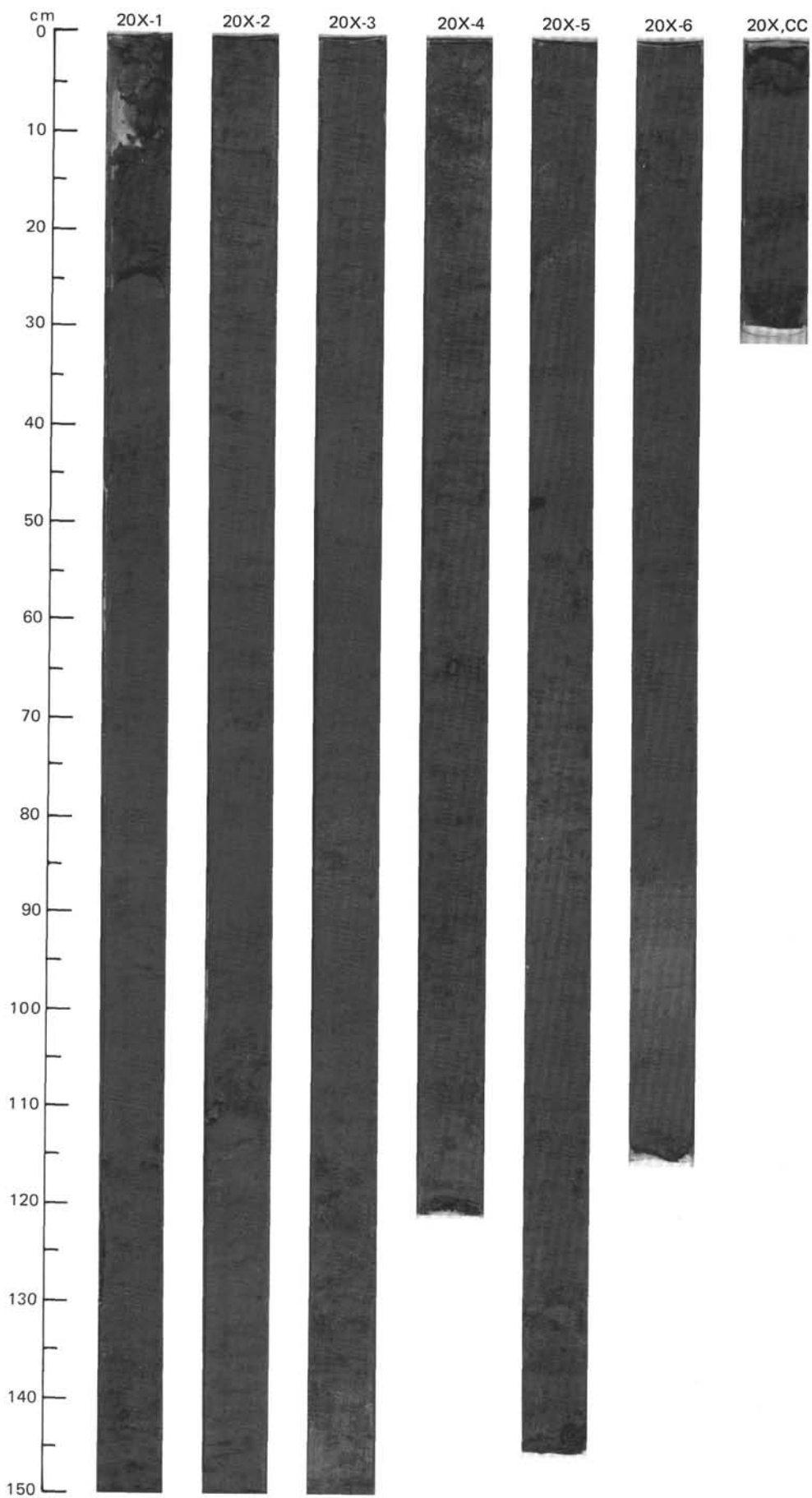
TIME-ROCK UNIT	BIOSTRAT. ZONE/ FOSSIL CHARACTER					PALEOMAGNETICS	PHYS. PROPERTIES	CHEMISTRY	SECTION	METERS	GRAPHIC LITHOLOGY	DRILLING DISTURB.	SED. STRUCTURES	SAMPLES	LITHOLOGIC DESCRIPTION																																																																											
	FORAMINIFERS	NANNOFOSSILS	RADIOLARIANS	DIATOMS	DINOCTYSTS																																																																																					
UPPER PLIOCENE	R/M	B	R/G	R/P	F/G	Matuyama Chronozone	$\gamma = 1.71 \phi = 66.2 \text{ W} = 66$	$\text{CaCO}_3 = 0$	1	0.5 1.0	VOID VOID				<p>CLAYEY SILT AND NANNOFOSSIL SILTY CLAY</p> <p>Clayey silt, dark gray (5Y 4/1); with local vague color banding and scattered ~5 mm dark mud clasts that can be crushed between fingers, local slight bioturbation visible.</p> <p>Nannofossil silty clay, gray (5Y 5/1); with scattered ~5 mm soft mud clasts.</p> <p>Minor lithologies: a. Section 3, 56-65 cm: dark greenish gray (5GY 5/1) silty mud with thin detriticarbonate wispy layers. b. Section 3, 65-72 cm: sharp-based, detriticarbonate clayey silt with ~5 mm thinly laminated layers richer in detriticarbonate silt.</p> <p>SMEAR SLIDE SUMMARY (%):</p> <table border="1"> <tr> <td></td> <td>1, 130</td> <td>2, 38</td> <td>3, 36</td> <td>3, 68</td> </tr> <tr> <td>D</td> <td></td> <td>D</td> <td>D</td> <td>M</td> </tr> </table> <p>TEXTURE:</p> <table border="1"> <tr> <td>Sand</td> <td>—</td> <td>5</td> <td>1</td> <td>—</td> </tr> <tr> <td>Silt</td> <td>55</td> <td>50</td> <td>40</td> <td>65</td> </tr> <tr> <td>Clay</td> <td>45</td> <td>45</td> <td>59</td> <td>35</td> </tr> </table> <p>COMPOSITION:</p> <table border="1"> <tr> <td>Quartz</td> <td>60</td> <td>20</td> <td>20</td> <td>25</td> </tr> <tr> <td>Feldspar</td> <td>5</td> <td>Tr</td> <td>Tr</td> <td>2</td> </tr> <tr> <td>Clay</td> <td>35</td> <td>38</td> <td>45</td> <td>23</td> </tr> <tr> <td>Volcanic glass</td> <td>Tr</td> <td>—</td> <td>Tr</td> <td>—</td> </tr> <tr> <td>Calcite/dolomite</td> <td>—</td> <td>5</td> <td>5</td> <td>50</td> </tr> <tr> <td>Accessory minerals</td> <td>1</td> <td>2</td> <td>1</td> <td>Tr</td> </tr> <tr> <td>Foraminifers</td> <td>—</td> <td>—</td> <td>Tr</td> <td>—</td> </tr> <tr> <td>Nannofossils</td> <td>—</td> <td>35</td> <td>30</td> <td>—</td> </tr> <tr> <td>Diatoms</td> <td>—</td> <td>Tr</td> <td>—</td> <td>—</td> </tr> <tr> <td>Sponge spicules</td> <td>—</td> <td>Tr</td> <td>Tr</td> <td>—</td> </tr> </table>		1, 130	2, 38	3, 36	3, 68	D		D	D	M	Sand	—	5	1	—	Silt	55	50	40	65	Clay	45	45	59	35	Quartz	60	20	20	25	Feldspar	5	Tr	Tr	2	Clay	35	38	45	23	Volcanic glass	Tr	—	Tr	—	Calcite/dolomite	—	5	5	50	Accessory minerals	1	2	1	Tr	Foraminifers	—	—	Tr	—	Nannofossils	—	35	30	—	Diatoms	—	Tr	—	—	Sponge spicules	—	Tr	Tr	—
	1, 130	2, 38	3, 36	3, 68																																																																																						
D		D	D	M																																																																																						
Sand	—	5	1	—																																																																																						
Silt	55	50	40	65																																																																																						
Clay	45	45	59	35																																																																																						
Quartz	60	20	20	25																																																																																						
Feldspar	5	Tr	Tr	2																																																																																						
Clay	35	38	45	23																																																																																						
Volcanic glass	Tr	—	Tr	—																																																																																						
Calcite/dolomite	—	5	5	50																																																																																						
Accessory minerals	1	2	1	Tr																																																																																						
Foraminifers	—	—	Tr	—																																																																																						
Nannofossils	—	35	30	—																																																																																						
Diatoms	—	Tr	—	—																																																																																						
Sponge spicules	—	Tr	Tr	—																																																																																						

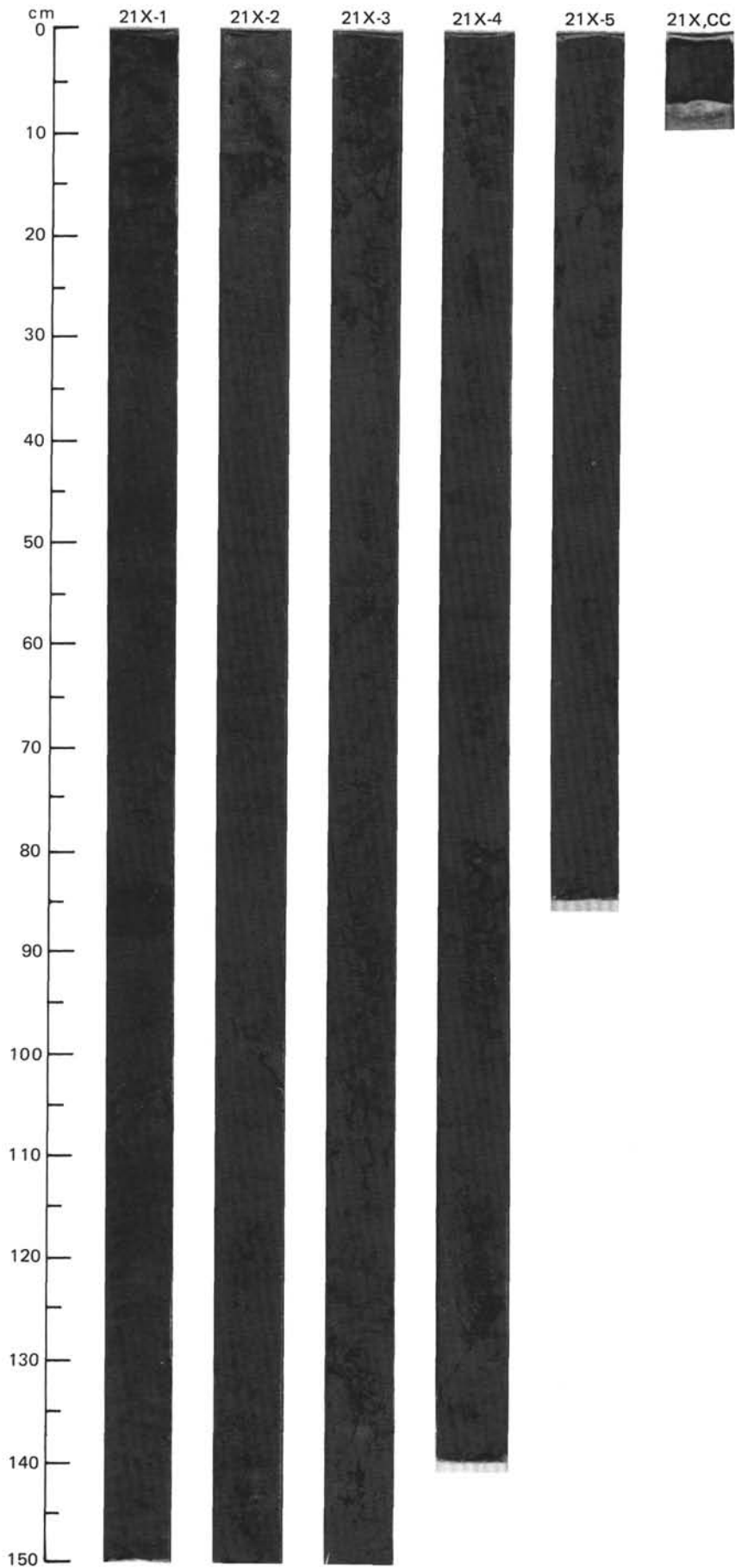
SITE 646 HOLE B CORE 19 X CORED INTERVAL 3617.0-3626.7 mbsl; 168.8-178.5 mbsf

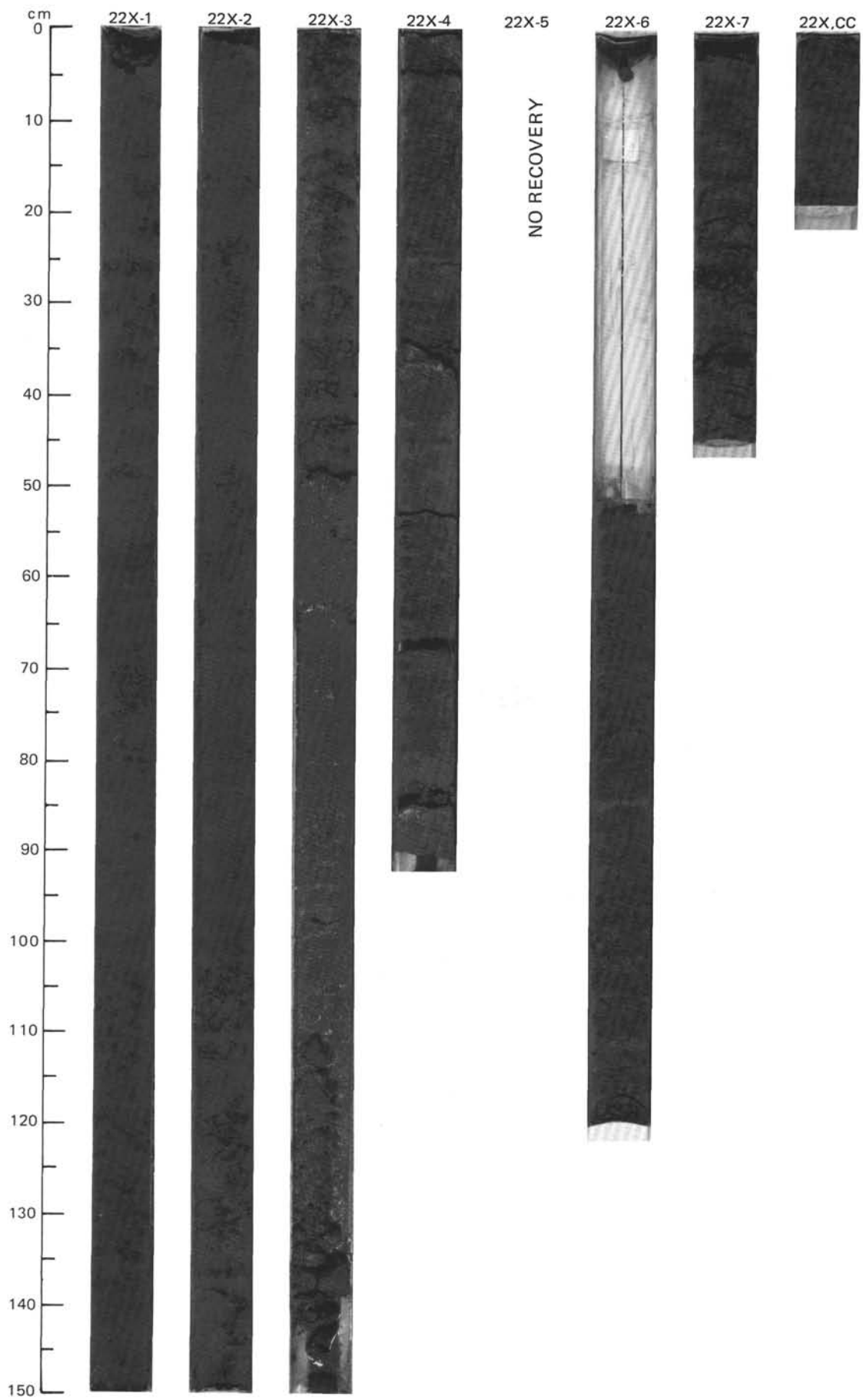
TIME-ROCK UNIT	BIOSTRAT. ZONE/ FOSSIL CHARACTER					PALEOMAGNETICS	PHYS. PROPERTIES	CHEMISTRY	SECTION	METERS	GRAPHIC LITHOLOGY	DRILLING DISTURB.	SED. STRUCTURES	SAMPLES	LITHOLOGIC DESCRIPTION																										
	FORAMINIFERS	NANNOFOSSILS	RADIOLARIANS	DIATOMS	DINOCTYSTS																																				
UPPER PLIOCENE	F/G	B	F/G	R/P	C/G				1						<p>CLAYEY SILT</p> <p>Clayey silt, dark gray (5Y 4/1) with two pebbles of quartz/biotite gneiss and dolerite.</p> <p>SMEAR SLIDE SUMMARY (%):</p> <table border="1"> <tr> <td></td> <td>1, 15</td> </tr> <tr> <td>D</td> <td></td> </tr> </table> <p>TEXTURE:</p> <table border="1"> <tr> <td>Sand</td> <td>1</td> </tr> <tr> <td>Silt</td> <td>55</td> </tr> <tr> <td>Clay</td> <td>44</td> </tr> </table> <p>COMPOSITION:</p> <table border="1"> <tr> <td>Quartz</td> <td>55</td> </tr> <tr> <td>Feldspar</td> <td>3</td> </tr> <tr> <td>Mica</td> <td>1</td> </tr> <tr> <td>Clay</td> <td>38</td> </tr> <tr> <td>Volcanic glass</td> <td>Tr</td> </tr> <tr> <td>Accessory minerals</td> <td>3</td> </tr> <tr> <td>Diatoms</td> <td>Tr</td> </tr> <tr> <td>Sponge spicules</td> <td>Tr</td> </tr> </table>		1, 15	D		Sand	1	Silt	55	Clay	44	Quartz	55	Feldspar	3	Mica	1	Clay	38	Volcanic glass	Tr	Accessory minerals	3	Diatoms	Tr	Sponge spicules	Tr
	1, 15																																								
D																																									
Sand	1																																								
Silt	55																																								
Clay	44																																								
Quartz	55																																								
Feldspar	3																																								
Mica	1																																								
Clay	38																																								
Volcanic glass	Tr																																								
Accessory minerals	3																																								
Diatoms	Tr																																								
Sponge spicules	Tr																																								

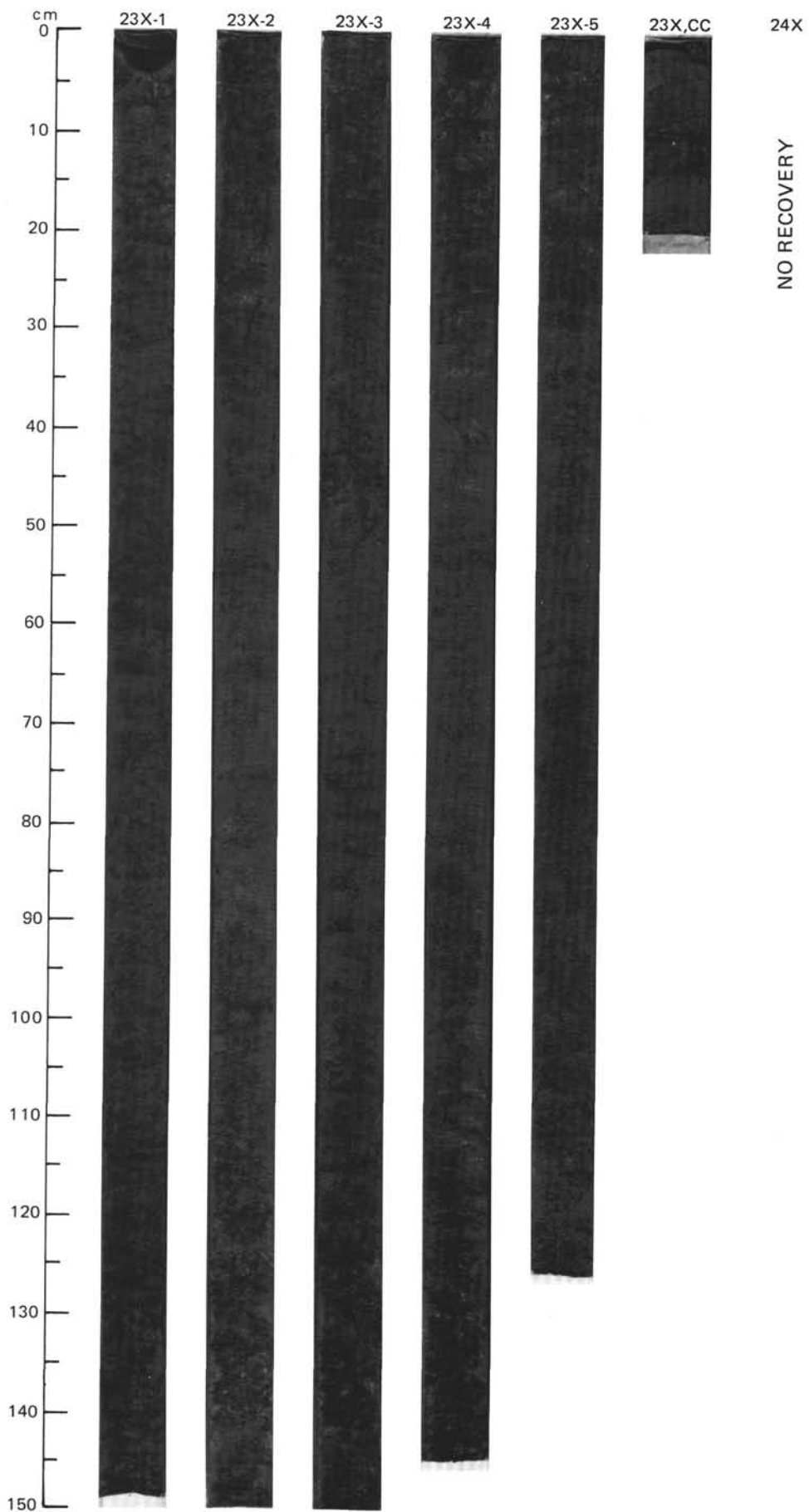


TIME-ROCK UNIT		BIOSTRAT. ZONE/ FOSSIL CHARACTER	PALEOMAGNETICS	PHYS. PROPERTIES	CHEMISTRY	SECTION	METERS	GRAPHIC LITHOLOGY	DRILLING DISTURB.	SED. STRUCTURES	SAMPLES	LITHOLOGIC DESCRIPTION																																																																		
FORAMINIFERS	NANNOFOSSILS												RADIOLARIANS	DIATOMS	DINOCYSTS																																																															
UPPER PLIOCENE																																																																														
C/M	PL3-PL6																																																																													
R/G																																																																														
F/M																																																																														
F/G																																																																														
			Matuyama Chronozone																																																																											
			$\gamma = 1.66 \phi = 65.6 W = 68$ \bullet $\text{CaCO}_3 = 21$ $\gamma = 1.68 \phi = 67.2 W = 70$ \bullet $\text{CaCO}_3 = 5$ $\gamma = 1.65 \phi = 71.2 W = 79$ \bullet $\text{CaCO}_3 = 10$																																																																											
			SECTION 1: 0.5 to 1.0 meters SECTION 2: 1.0 to 2.0 meters SECTION 3: 2.0 to 3.0 meters SECTION 4: 3.0 to 4.0 meters SECTION 5: 4.0 to 5.0 meters SECTION 6: 5.0 to 6.0 meters																																																																											
			DRILLING DISTURB.: 0 SED. STRUCTURES: * SAMPLES: OG, W																																																																											
			CLAYEY SILT, DETRICARBONATE CLAYEY SILT, SILTY CLAY, AND SILTY MUD Clayey silt, olive gray (5Y 4/2), dark gray (5Y 4/1), dark grayish brown (10YR 4/2), grayish green (5G 5/2), and dark greenish gray (5G 4/1). Mostly characterized by regular color banding in intervals 1-2 cm thick with gradational and irregular boundaries; streaks of gray sulfide occur rarely. Local pebbles and pyritic concretions of granule size. Detricarbonate clayey silt, grayish green (5G 5/2), greenish gray (5GY 6/1), gray (5Y 6/1), light gray (5Y 7/1) and light greenish gray (5GY 7/1). Mottled at points with intercalations of noncarbonate clayey silt. No lenses or laminae of well-sorted silt. Gradational boundaries. Occurs in thin to medium beds. Silty clay, gray (5Y 5/1) and silty mud, dark greenish gray (5G 4/1) similar to the clayey silt except for somewhat higher sand content. Minor lithology: Section 5, 48-53, 138 cm; Section 6, 57-58 cm: dark gray (N4) silt.																																																																											
			SMEAR SLIDE SUMMARY (%): <table border="1"> <tr> <td></td> <td>2, 80</td> <td>3, 85</td> <td>4, 115</td> <td>5, 20</td> <td>5, 85</td> </tr> <tr> <td>D</td> <td></td> <td>M</td> <td>D</td> <td>D</td> <td>M</td> </tr> </table>											2, 80	3, 85	4, 115	5, 20	5, 85	D		M	D	D	M																																																						
	2, 80	3, 85	4, 115	5, 20	5, 85																																																																									
D		M	D	D	M																																																																									
			TEXTURE: <table border="1"> <tr> <td>Sand</td> <td>—</td> <td>Tr</td> <td>—</td> <td>10</td> <td>—</td> </tr> <tr> <td>Silt</td> <td>60</td> <td>70</td> <td>45</td> <td>50</td> <td>60</td> </tr> <tr> <td>Clay</td> <td>40</td> <td>30</td> <td>55</td> <td>40</td> <td>40</td> </tr> </table>										Sand	—	Tr	—	10	—	Silt	60	70	45	50	60	Clay	40	30	55	40	40																																																
Sand	—	Tr	—	10	—																																																																									
Silt	60	70	45	50	60																																																																									
Clay	40	30	55	40	40																																																																									
			COMPOSITION: <table border="1"> <tr> <td>Quartz</td> <td>60</td> <td>30</td> <td>50</td> <td>60</td> <td>25</td> </tr> <tr> <td>Feldspar</td> <td>5</td> <td>Tr</td> <td>1</td> <td>8</td> <td>Tr</td> </tr> <tr> <td>Mica</td> <td>1</td> <td>Tr</td> <td>1</td> <td>1</td> <td>Tr</td> </tr> <tr> <td>Clay</td> <td>31</td> <td>24</td> <td>47</td> <td>26</td> <td>25</td> </tr> <tr> <td>Volcanic glass</td> <td>Tr</td> <td>—</td> <td>Tr</td> <td>Tr</td> <td>—</td> </tr> <tr> <td>Calcite/dolomite</td> <td>—</td> <td>45</td> <td>—</td> <td>—</td> <td>50</td> </tr> <tr> <td>Accessory minerals</td> <td>2</td> <td>1</td> <td>1</td> <td>5</td> <td>Tr</td> </tr> <tr> <td>Nannofossils</td> <td>—</td> <td>—</td> <td>Tr</td> <td>—</td> <td>—</td> </tr> <tr> <td>Diatoms</td> <td>1</td> <td>—</td> <td>—</td> <td>Tr</td> <td>—</td> </tr> <tr> <td>Radiolarians</td> <td>—</td> <td>—</td> <td>—</td> <td>Tr</td> <td>—</td> </tr> <tr> <td>Sponge spicules</td> <td>Tr</td> <td>Tr</td> <td>—</td> <td>Tr</td> <td>Tr</td> </tr> </table>										Quartz	60	30	50	60	25	Feldspar	5	Tr	1	8	Tr	Mica	1	Tr	1	1	Tr	Clay	31	24	47	26	25	Volcanic glass	Tr	—	Tr	Tr	—	Calcite/dolomite	—	45	—	—	50	Accessory minerals	2	1	1	5	Tr	Nannofossils	—	—	Tr	—	—	Diatoms	1	—	—	Tr	—	Radiolarians	—	—	—	Tr	—	Sponge spicules	Tr	Tr	—	Tr	Tr
Quartz	60	30	50	60	25																																																																									
Feldspar	5	Tr	1	8	Tr																																																																									
Mica	1	Tr	1	1	Tr																																																																									
Clay	31	24	47	26	25																																																																									
Volcanic glass	Tr	—	Tr	Tr	—																																																																									
Calcite/dolomite	—	45	—	—	50																																																																									
Accessory minerals	2	1	1	5	Tr																																																																									
Nannofossils	—	—	Tr	—	—																																																																									
Diatoms	1	—	—	Tr	—																																																																									
Radiolarians	—	—	—	Tr	—																																																																									
Sponge spicules	Tr	Tr	—	Tr	Tr																																																																									



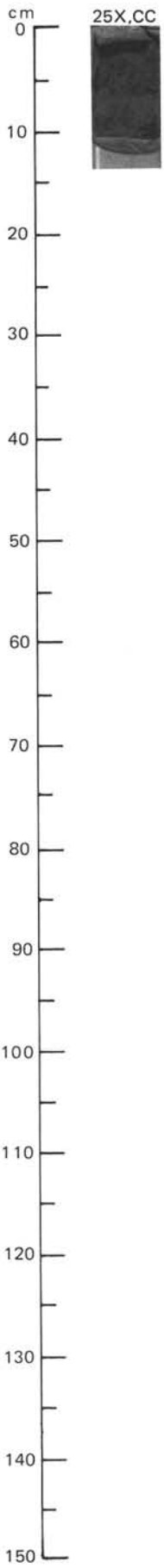


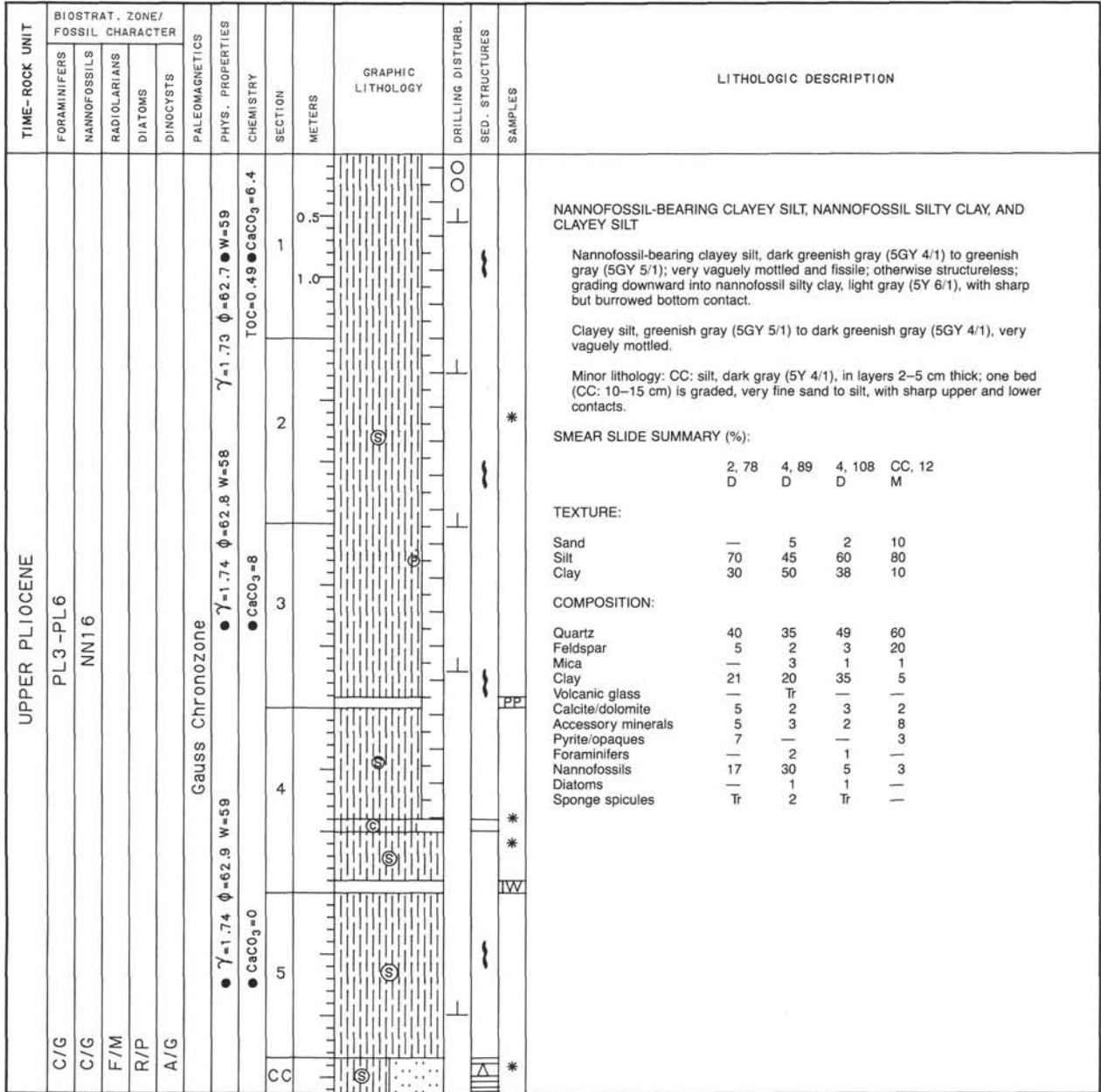




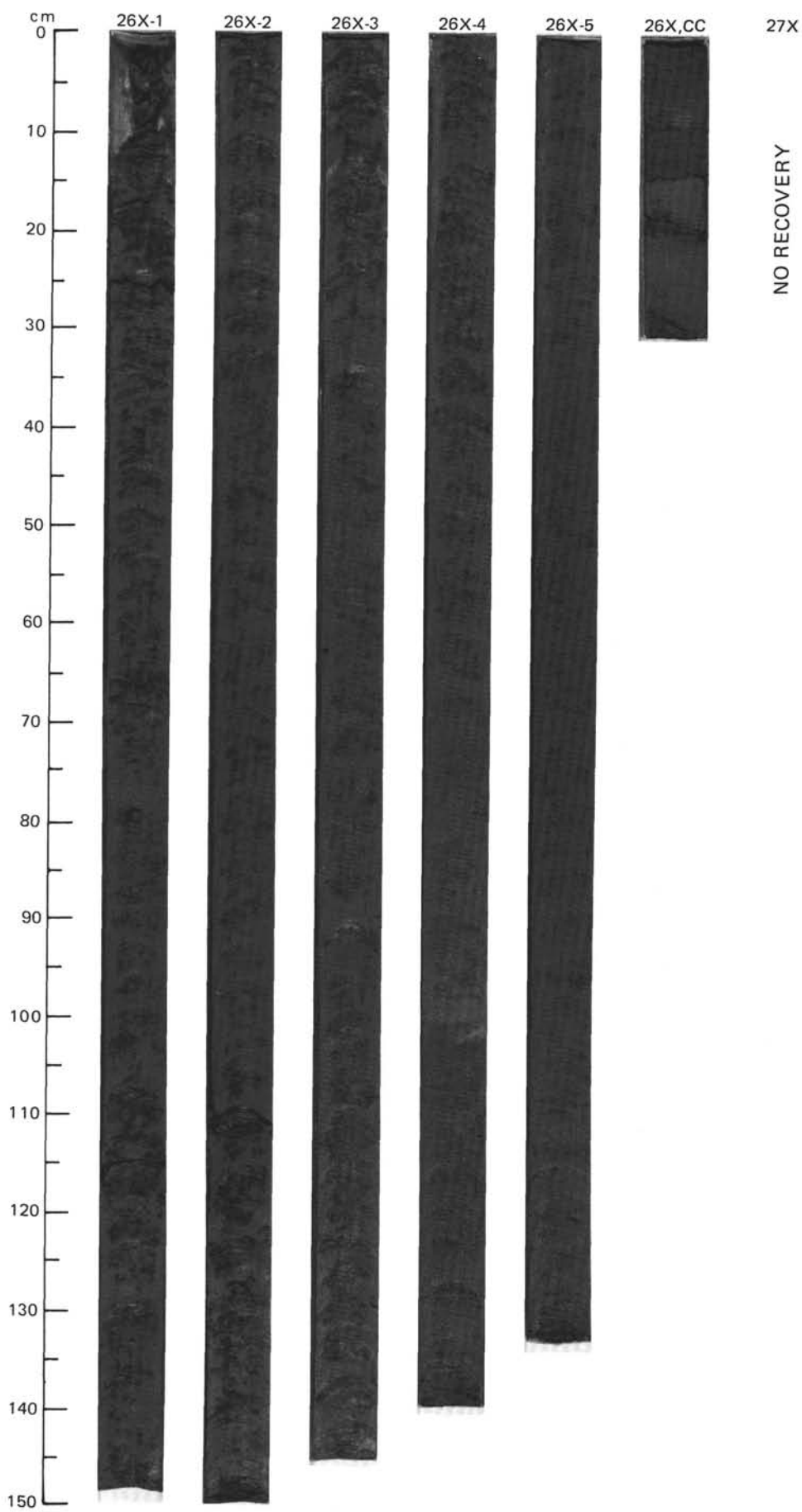
SITE 646 HOLE B CORE 25 X CORED INTERVAL 3674.9-3684.6 mbsl; 226.7-236.1 mbsf

TIME-ROCK UNIT	BIOSTRAT. ZONE/ FOSSIL CHARACTER					PALEOMAGNETICS	PHYS. PROPERTIES	CHEMISTRY	SECTION	METERS	GRAPHIC LITHOLOGY	DRILLING DISTURB.	SED. STRUCTURES	SAMPLES	LITHOLOGIC DESCRIPTION																																																
	FORAMINIFERS	NANNOFOSSILS	RADIOLARIANS	DIATOMS	DINOCYSTS																																																										
UPPER PLIOCENE	A/G	A/G	A/G	R/M	A/G				CC						<p>SILTY MUD AND NANNOFOSSIL- AND SPICULE-BEARING MUDDY SAND</p> <p>The CC consists of silty mud overlain by a nannofossil- and spicule-bearing muddy sand with granules. A caved granite pebble sits at the top of the CC.</p> <p>SMEAR SLIDE SUMMARY (%):</p> <table style="margin-left: 40px;"> <tr> <td></td> <td>CC, 4</td> <td>CC, 9</td> </tr> <tr> <td></td> <td>D</td> <td>D</td> </tr> </table> <p>TEXTURE:</p> <table style="margin-left: 40px;"> <tr> <td>Sand</td> <td>41</td> <td>5</td> </tr> <tr> <td>Silt</td> <td>29</td> <td>53</td> </tr> <tr> <td>Clay</td> <td>30</td> <td>42</td> </tr> </table> <p>COMPOSITION:</p> <table style="margin-left: 40px;"> <tr> <td>Quartz</td> <td>62</td> <td>33</td> </tr> <tr> <td>Feldspar</td> <td>2</td> <td>1</td> </tr> <tr> <td>Mica</td> <td>Tr</td> <td>Tr</td> </tr> <tr> <td>Clay</td> <td>20</td> <td>42</td> </tr> <tr> <td>Volcanic glass</td> <td>3</td> <td>Tr</td> </tr> <tr> <td>Calcite/dolomite</td> <td>—</td> <td>2</td> </tr> <tr> <td>Accessory minerals</td> <td>5</td> <td>5</td> </tr> <tr> <td>Foraminifers</td> <td>2</td> <td>—</td> </tr> <tr> <td>Nannofossils</td> <td>10</td> <td>5</td> </tr> <tr> <td>Diatoms</td> <td>2</td> <td>—</td> </tr> <tr> <td>Sponge spicules</td> <td>4</td> <td>2</td> </tr> </table>		CC, 4	CC, 9		D	D	Sand	41	5	Silt	29	53	Clay	30	42	Quartz	62	33	Feldspar	2	1	Mica	Tr	Tr	Clay	20	42	Volcanic glass	3	Tr	Calcite/dolomite	—	2	Accessory minerals	5	5	Foraminifers	2	—	Nannofossils	10	5	Diatoms	2	—	Sponge spicules	4	2
	CC, 4	CC, 9																																																													
	D	D																																																													
Sand	41	5																																																													
Silt	29	53																																																													
Clay	30	42																																																													
Quartz	62	33																																																													
Feldspar	2	1																																																													
Mica	Tr	Tr																																																													
Clay	20	42																																																													
Volcanic glass	3	Tr																																																													
Calcite/dolomite	—	2																																																													
Accessory minerals	5	5																																																													
Foraminifers	2	—																																																													
Nannofossils	10	5																																																													
Diatoms	2	—																																																													
Sponge spicules	4	2																																																													



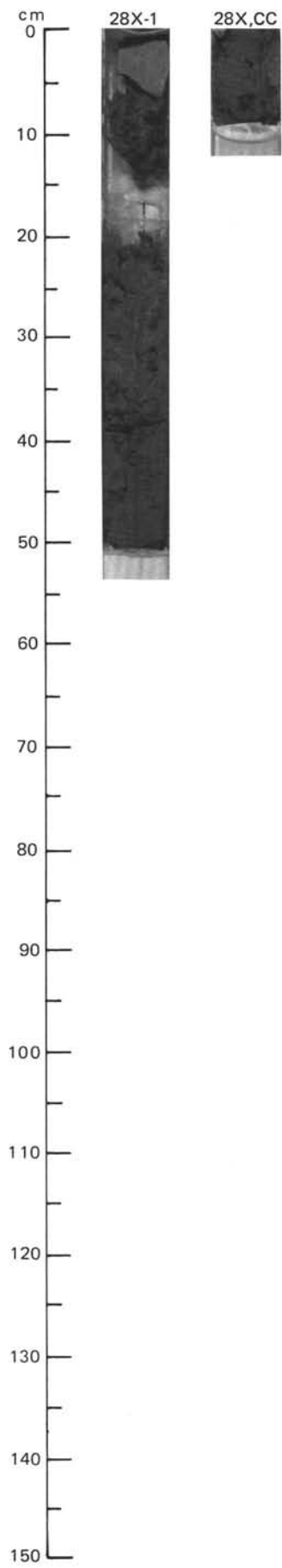


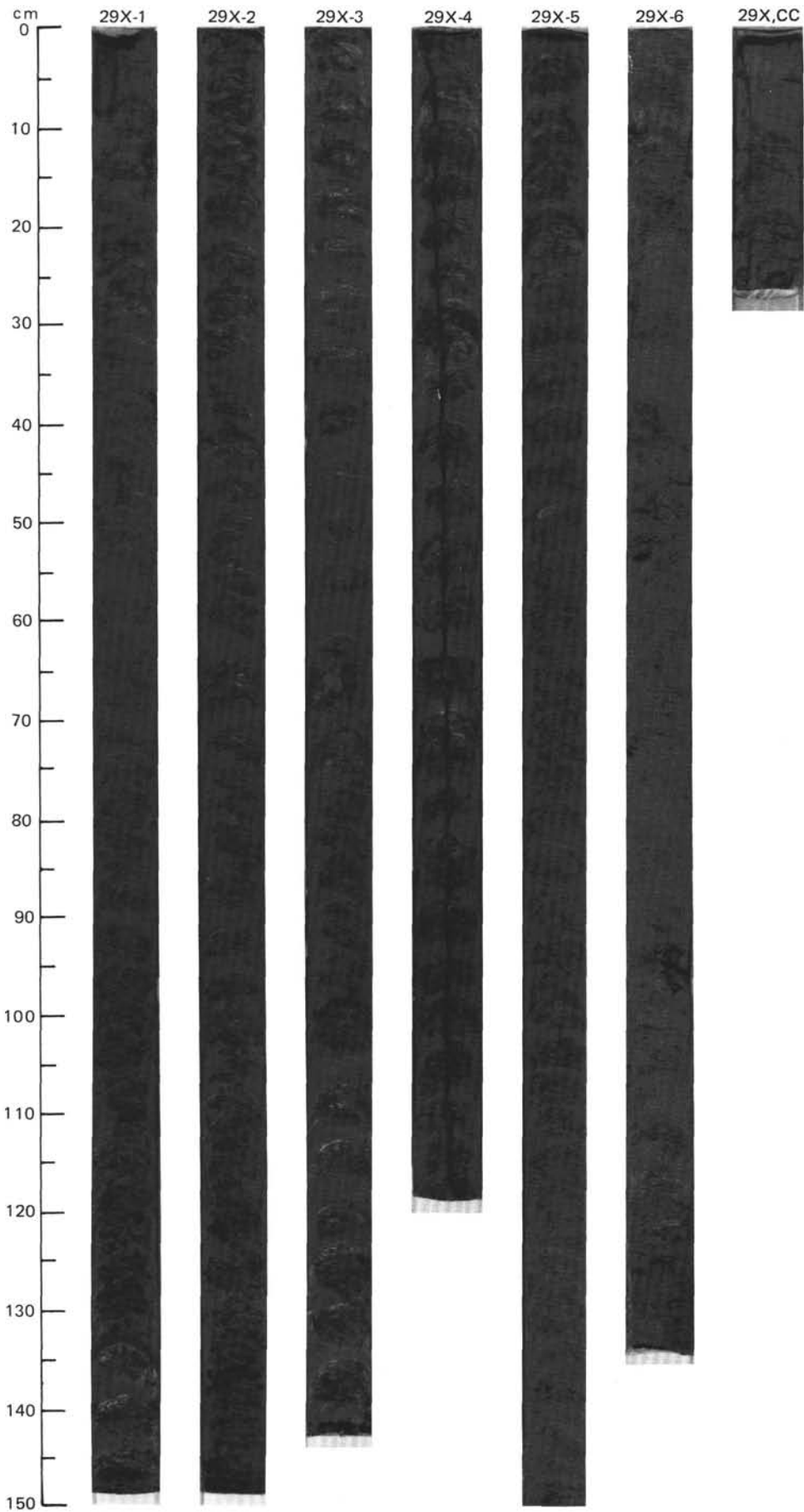
CORE 27X NO RECOVERY

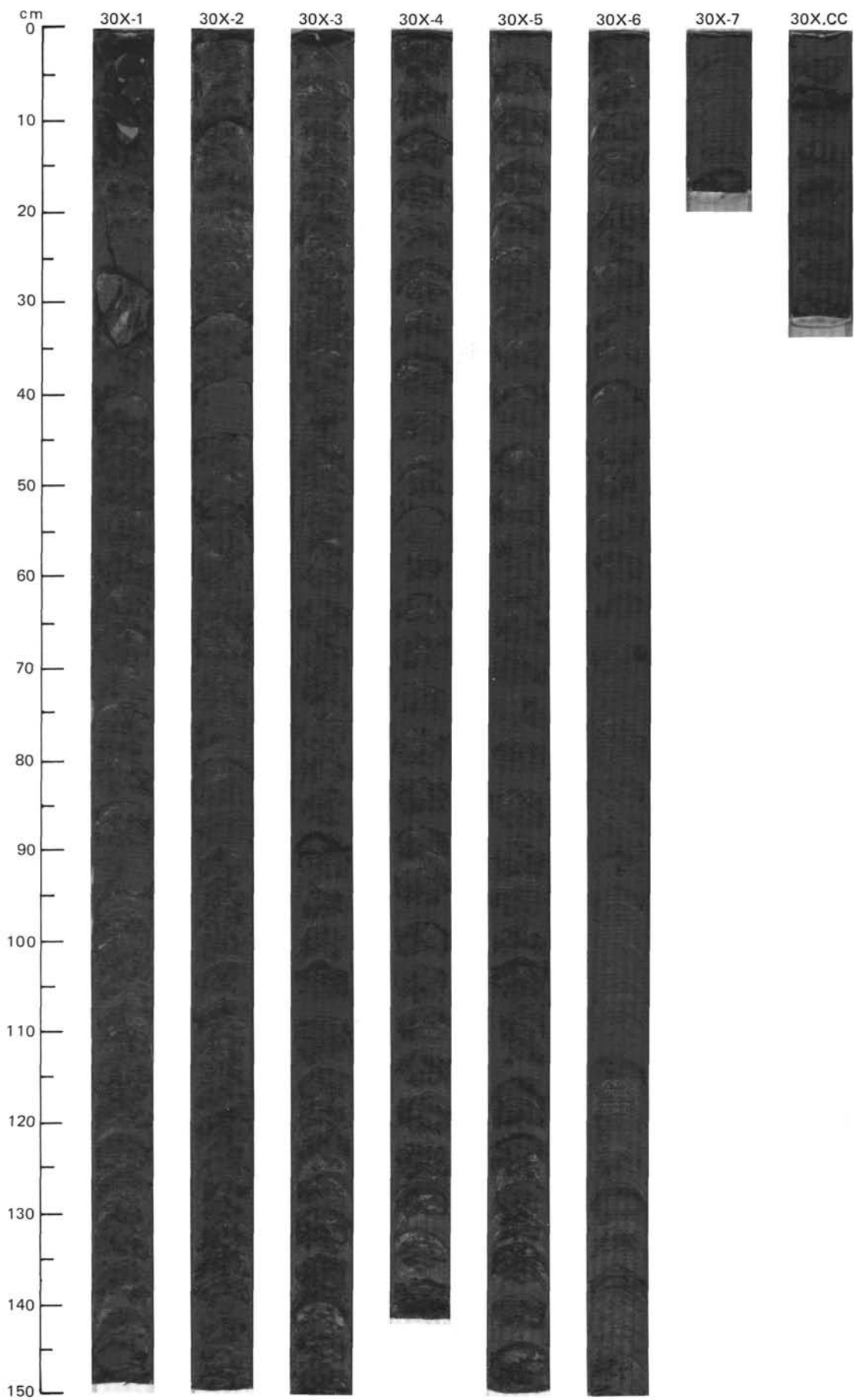


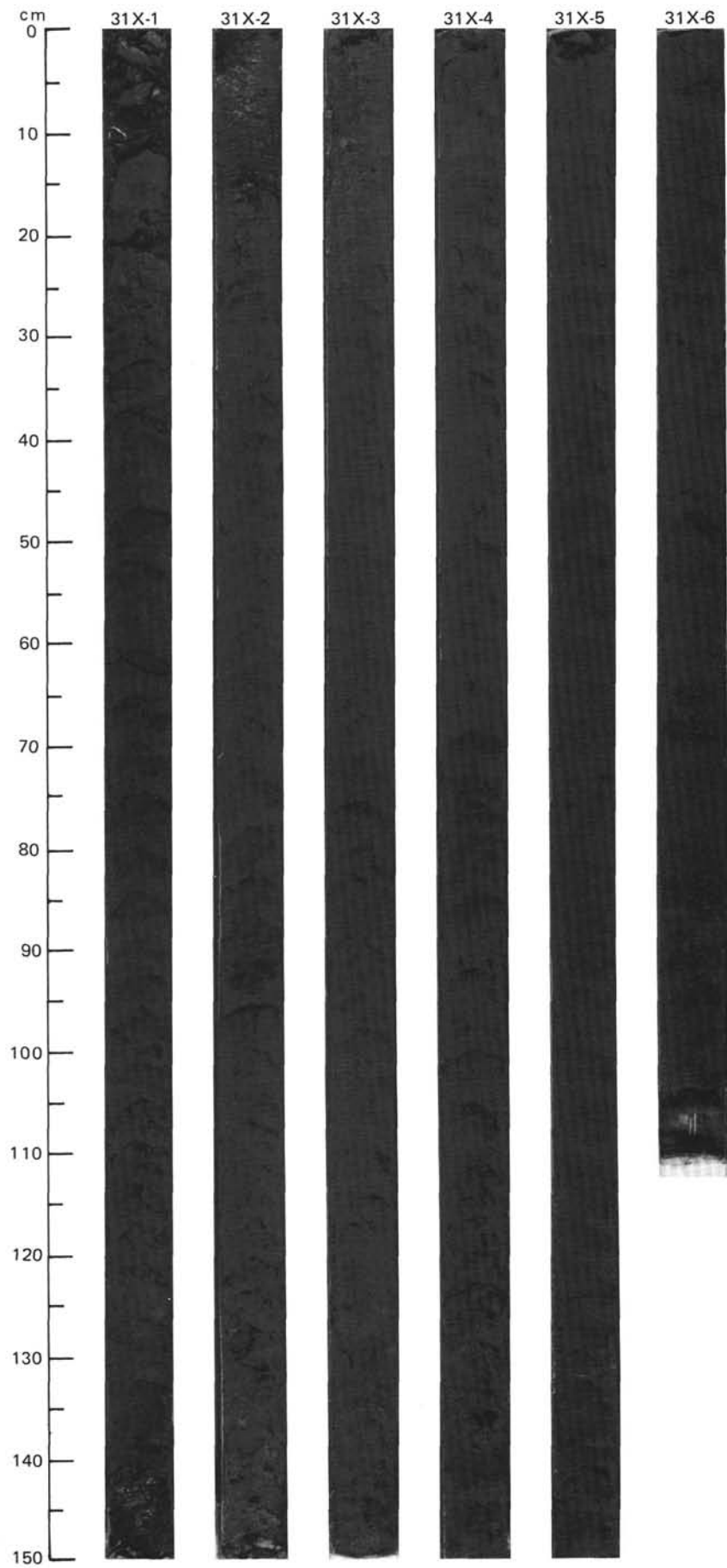
SITE 646 HOLE B CORE 28 X CORED INTERVAL 3703.9-3713.5 mbsl; 255.7-265.3 mbsf

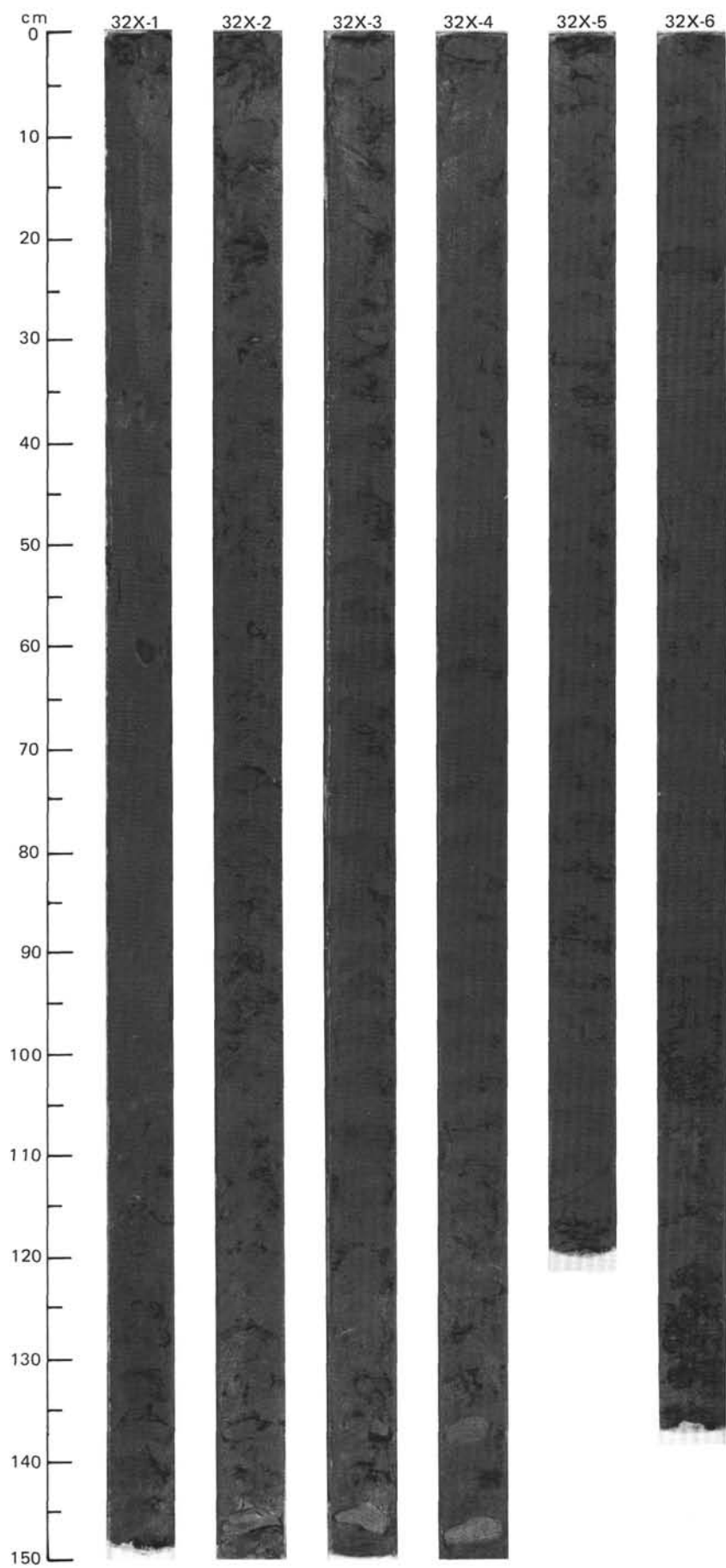
TIME-ROCK UNIT	BIOSTRAT. ZONE/ FOSSIL CHARACTER					SECTION	METERS	GRAPHIC LITHOLOGY	DRILLING DISTURB.	SED. STRUCTURES	SAMPLES	LITHOLOGIC DESCRIPTION																						
	FORAMINIFERS	NANNOFOSSILS	RADIOLARIANS	DIATOMS	DINOCTYSTS																													
UPPER PLIOCENE	F/G	C/G	F/P	R/P	A/G	1	0.5				*	<p>CLAYEY SILT</p> <p>Clayey silt, dark greenish gray (5GY 4/1), very disturbed. Two caved pebbles in the upper part of the core are brachiopod-bearing limestone and basalt.</p> <p>SMEAR SLIDE SUMMARY (%):</p> <table border="0"> <tr> <td></td> <td>1, 48</td> </tr> <tr> <td>D</td> <td></td> </tr> </table> <p>TEXTURE:</p> <table border="0"> <tr> <td>Sand</td> <td>8</td> </tr> <tr> <td>Silt</td> <td>52</td> </tr> <tr> <td>Clay</td> <td>40</td> </tr> </table> <p>COMPOSITION:</p> <table border="0"> <tr> <td>Quartz</td> <td>40</td> </tr> <tr> <td>Feldspar</td> <td>10</td> </tr> <tr> <td>Clay</td> <td>30</td> </tr> <tr> <td>Calcite/dolomite</td> <td>3</td> </tr> <tr> <td>Accessory minerals</td> <td>10</td> </tr> <tr> <td>Pyrite</td> <td>2</td> </tr> </table>		1, 48	D		Sand	8	Silt	52	Clay	40	Quartz	40	Feldspar	10	Clay	30	Calcite/dolomite	3	Accessory minerals	10	Pyrite	2
	1, 48																																	
D																																		
Sand	8																																	
Silt	52																																	
Clay	40																																	
Quartz	40																																	
Feldspar	10																																	
Clay	30																																	
Calcite/dolomite	3																																	
Accessory minerals	10																																	
Pyrite	2																																	



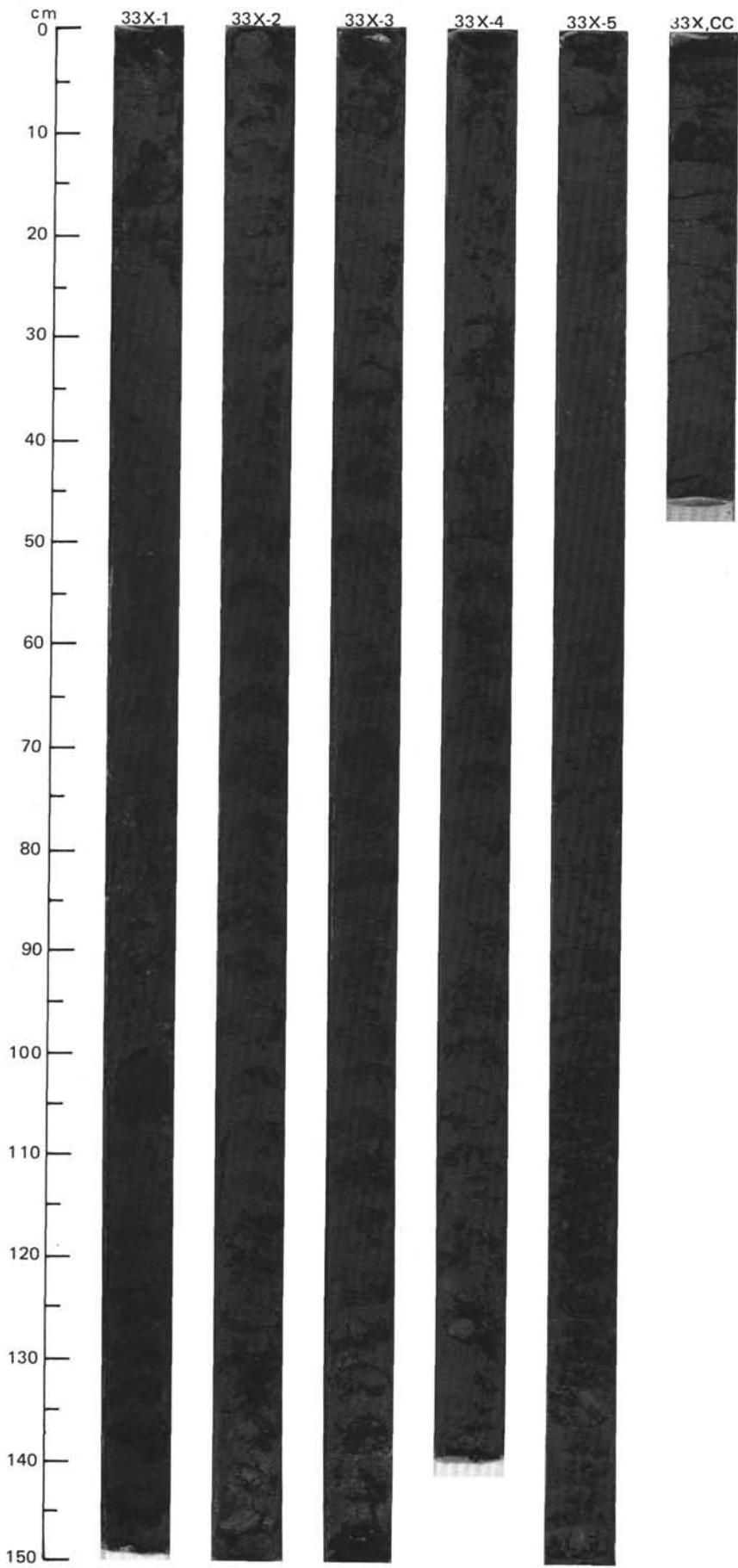








TIME-ROCK UNIT	BIOSTRAT. ZONE/ FOSSIL CHARACTER					PALEOMAGNETICS	PHYS. PROPERTIES	CHEMISTRY	SECTION	METERS	GRAPHIC LITHOLOGY	DRILLING DISTURB.	SED. STRUCTURES	SAMPLES	LITHOLOGIC DESCRIPTION																																																								
	FORAMINIFERS	NANNOFOSSILS	RADIOLARIANS	DIATOMS	DINOCTYSTS																																																																		
UPPER PLIOCENE																																																																							
A/G	M13-PL2						$\gamma = 1.76 \phi = 61.5 W = 56$		1	0.5	Drilling Slurry	X			<p>SILTY CLAY AND NANNOFOSSIL-BEARING SILTY CLAY</p> <p>Silty clay, dark greenish gray (5GY 4/1), moderately bioturbated and subtly color mottled.</p> <p>Nannofossil-bearing silty clay, dark greenish gray (5GY 4/1) and greenish gray (5GY 5/1), moderately bioturbated and subtly color mottled.</p> <p>Core is thoroughly disturbed, often being a mixture of drilling biscuits and slurry. Section 1 is slurry to 112 cm, containing several felsic plutonic pebbles and cobbles, no doubt cavings.</p> <p>SMEAR SLIDE SUMMARY (%):</p> <table border="1"> <tr> <td></td> <td>2, 98</td> <td>4, 79</td> <td>CC, 38</td> </tr> <tr> <td></td> <td>D</td> <td>D</td> <td>D</td> </tr> </table> <p>TEXTURE:</p> <table border="1"> <tr> <td>Sand</td> <td>1</td> <td>—</td> <td>—</td> </tr> <tr> <td>Silt</td> <td>25</td> <td>20</td> <td>40</td> </tr> <tr> <td>Clay</td> <td>74</td> <td>80</td> <td>60</td> </tr> </table> <p>COMPOSITION:</p> <table border="1"> <tr> <td>Quartz</td> <td>16</td> <td>20</td> <td>20</td> </tr> <tr> <td>Feldspar</td> <td>Tr</td> <td>—</td> <td>1</td> </tr> <tr> <td>Mica</td> <td>73</td> <td>Tr</td> <td>Tr</td> </tr> <tr> <td>Clay</td> <td>—</td> <td>80</td> <td>57</td> </tr> <tr> <td>Accessory minerals</td> <td>1</td> <td>Tr</td> <td>1</td> </tr> <tr> <td>Foraminifers</td> <td>—</td> <td>—</td> <td>1</td> </tr> <tr> <td>Nannofossils</td> <td>10</td> <td>Tr</td> <td>20</td> </tr> <tr> <td>Diatoms</td> <td>Tr</td> <td>Tr</td> <td>Tr</td> </tr> <tr> <td>Sponge spicules</td> <td>Tr</td> <td>Tr</td> <td>Tr</td> </tr> </table>		2, 98	4, 79	CC, 38		D	D	D	Sand	1	—	—	Silt	25	20	40	Clay	74	80	60	Quartz	16	20	20	Feldspar	Tr	—	1	Mica	73	Tr	Tr	Clay	—	80	57	Accessory minerals	1	Tr	1	Foraminifers	—	—	1	Nannofossils	10	Tr	20	Diatoms	Tr	Tr	Tr	Sponge spicules	Tr	Tr	Tr
	2, 98	4, 79	CC, 38																																																																				
	D	D	D																																																																				
Sand	1	—	—																																																																				
Silt	25	20	40																																																																				
Clay	74	80	60																																																																				
Quartz	16	20	20																																																																				
Feldspar	Tr	—	1																																																																				
Mica	73	Tr	Tr																																																																				
Clay	—	80	57																																																																				
Accessory minerals	1	Tr	1																																																																				
Foraminifers	—	—	1																																																																				
Nannofossils	10	Tr	20																																																																				
Diatoms	Tr	Tr	Tr																																																																				
Sponge spicules	Tr	Tr	Tr																																																																				
A/G	NN13-NN15						$\gamma = 1.77 \phi = 62.4 W = 57$		2	1.0		X																																																											
R/P							$\text{CaCO}_3 = 0$		3			X																																																											
R/P									4			X																																																											
A/G									5			X																																																											
CC												X																																																											

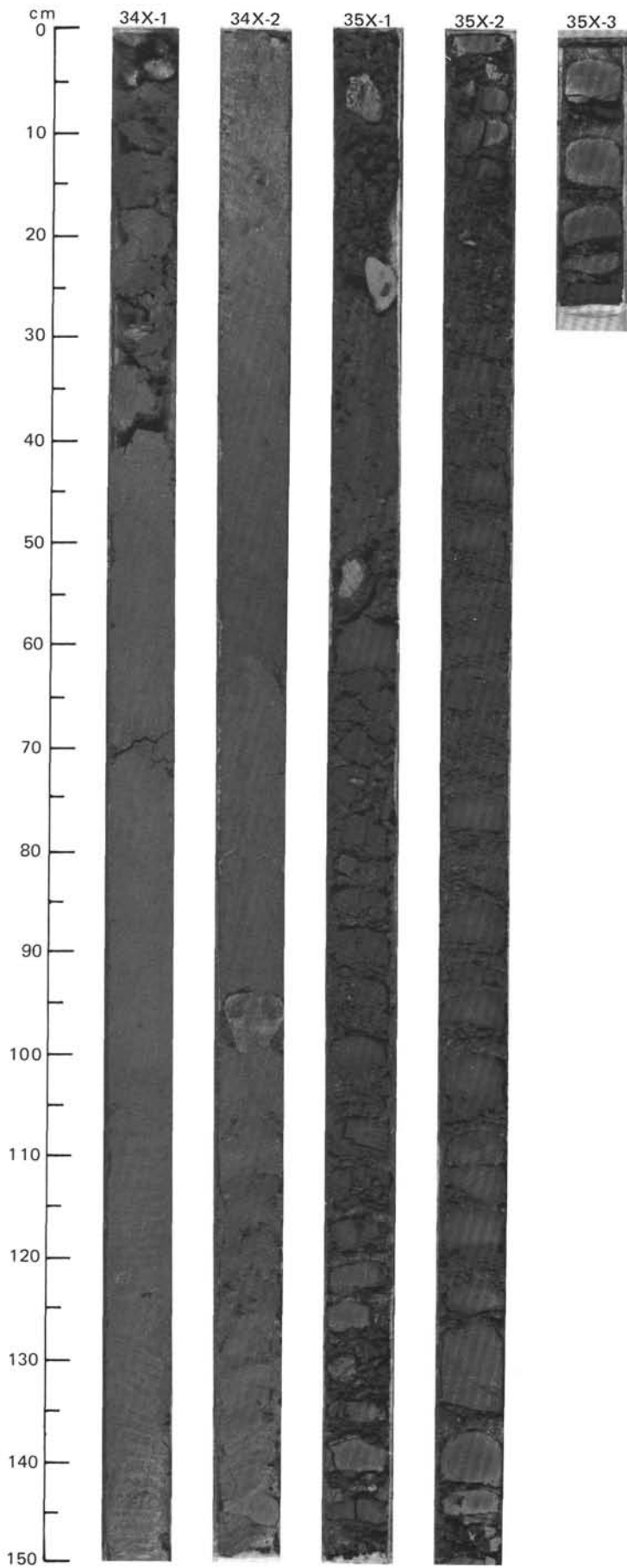


SITE 646 HOLE B CORE 34 X CORED INTERVAL 3762.0-3771.6 mbsl; 313.8-323.4 mbsf

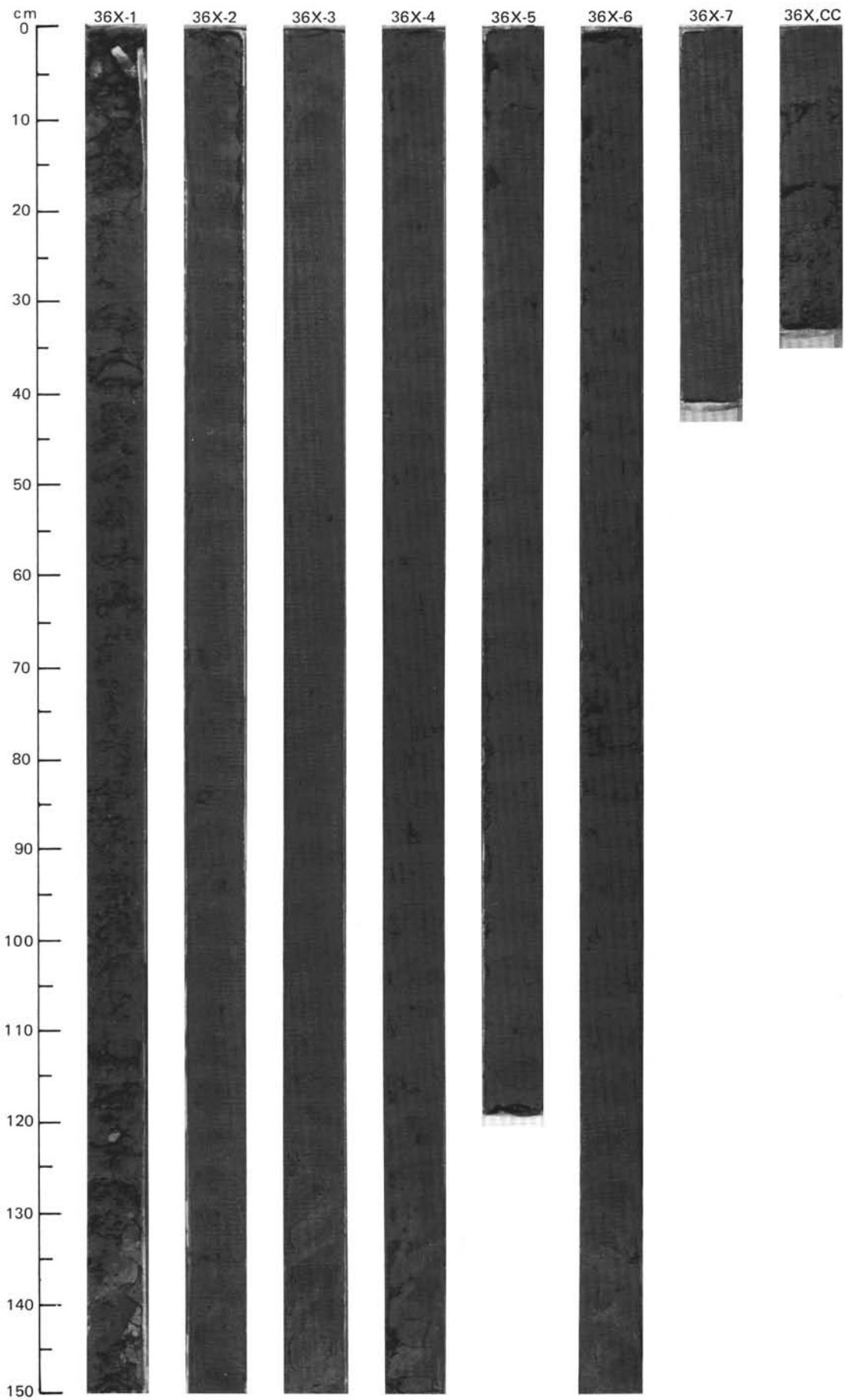
TIME-ROCK UNIT	BIOSTRAT. ZONE/ FOSSIL CHARACTER					PALEOMAGNETICS	PHYS. PROPERTIES	CHEMISTRY	SECTION	METERS	GRAPHIC LITHOLOGY	DRILLING DISTURB.	SED. STRUCTURES	SAMPLES	LITHOLOGIC DESCRIPTION
	FORAMINIFERS	NANNOFOSSILS	RADIOLARIANS	DIATOMS	DINOCYSTS										
LOWER PLIOCENE	A/M	M13-PL2	A/G	NN13-NN15	A/M	<i>Antarctissa whitei</i>	R/P	A/G	● $\gamma = 1.76$ $\phi = 60.9$ W=55						<p>NANNOFOSSIL CLAY</p> <p>Nannofossil clay, gray to dark gray (5Y 5/1) with greenish mottling.</p> <p>SMEAR SLIDE SUMMARY (%):</p> <p>2, 139 D</p> <p>TEXTURE:</p> <p>Silt 40 Clay 60</p> <p>COMPOSITION:</p> <p>Quartz 10 Feldspar 1 Clay 57 Accessory minerals 1 Nannofossils 30 Sponge spicules 1</p>

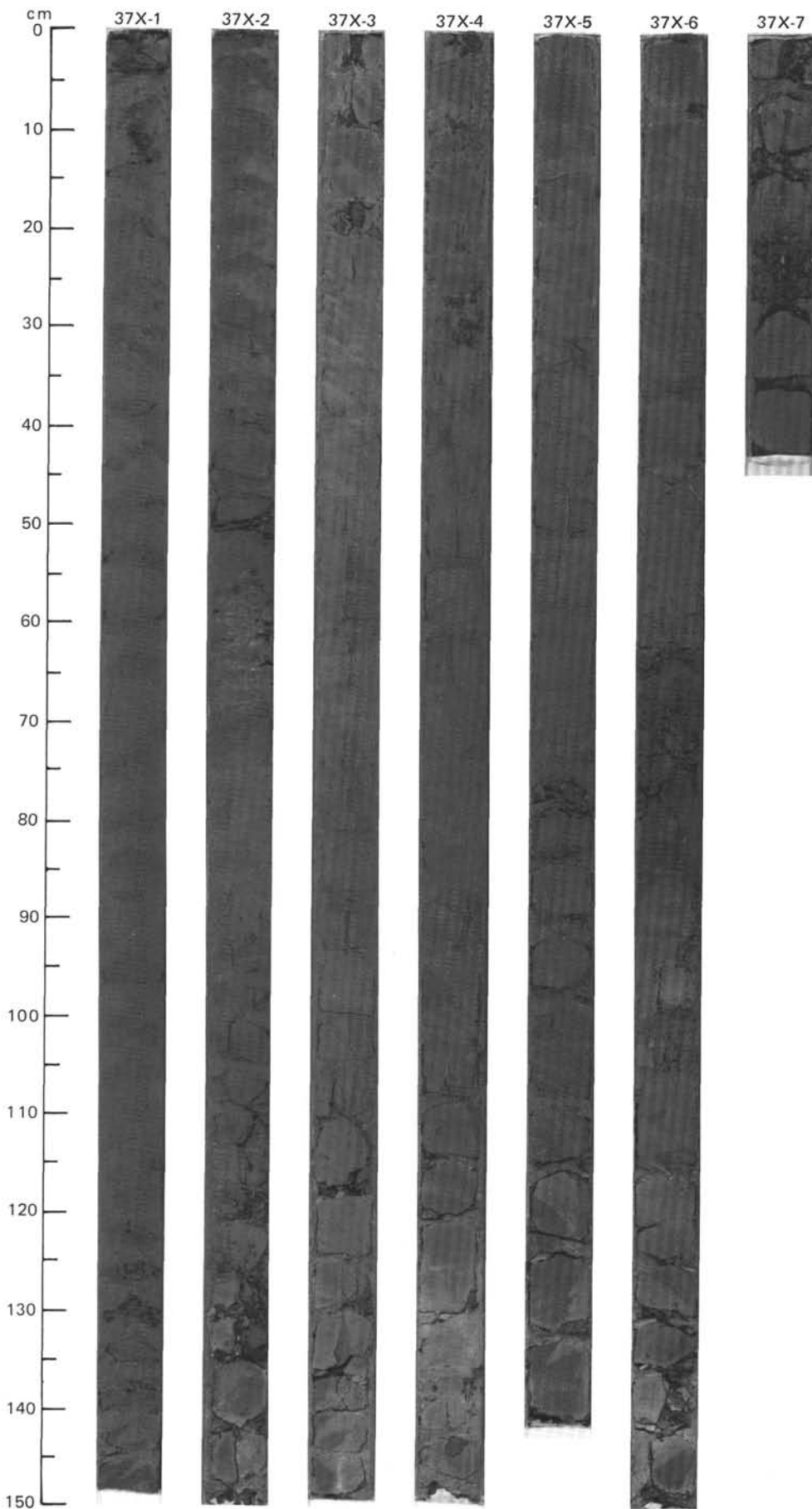
SITE 646 HOLE B CORE 35 X CORED INTERVAL 3771.6-3781.3 mbsl; 323.4-333.1 mbsf

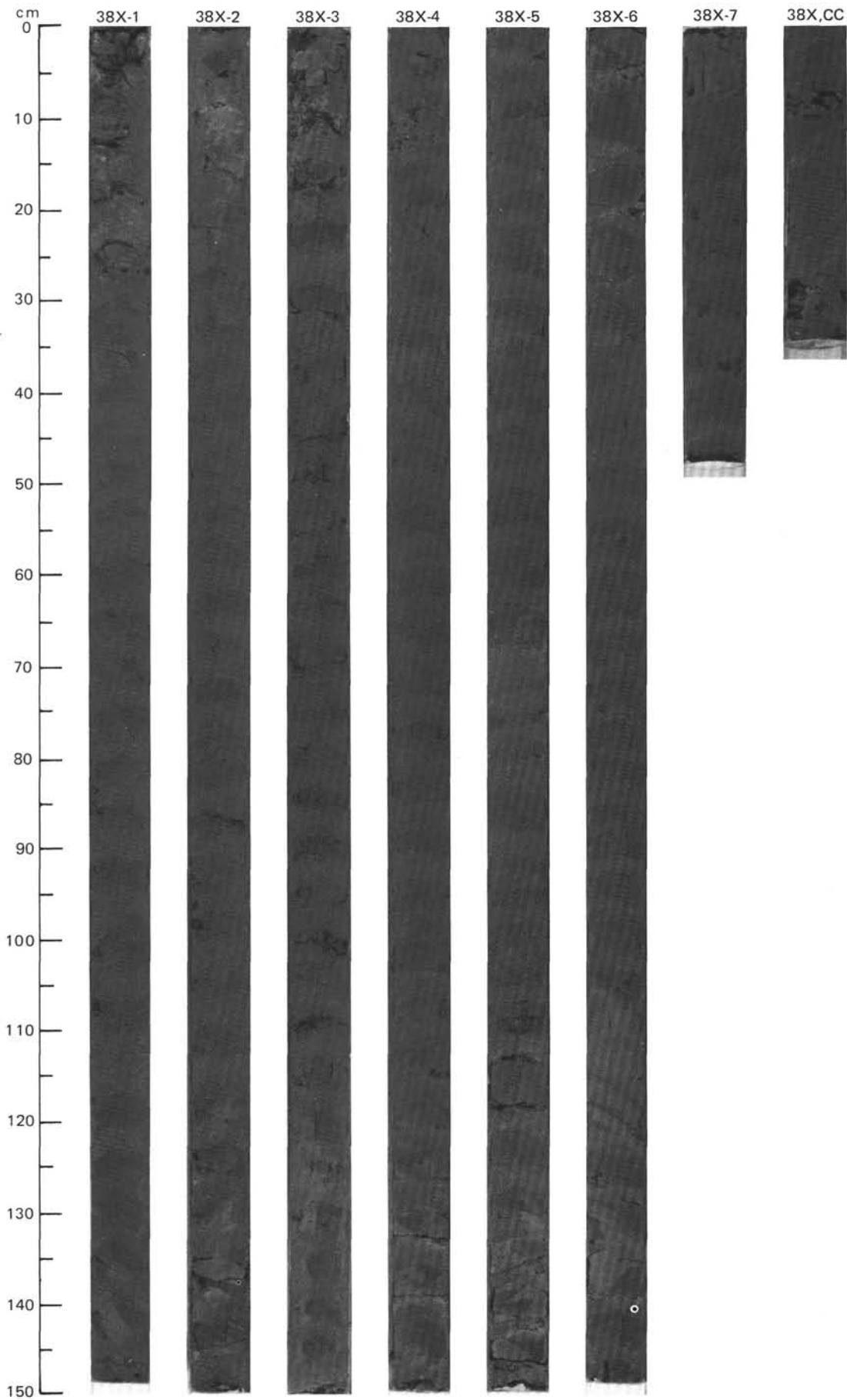
TIME-ROCK UNIT	BIOSTRAT. ZONE/ FOSSIL CHARACTER					PALEOMAGNETICS	PHYS. PROPERTIES	CHEMISTRY	SECTION	METERS	GRAPHIC LITHOLOGY	DRILLING DISTURB.	SED. STRUCTURES	SAMPLES	LITHOLOGIC DESCRIPTION
	FORAMINIFERS	NANNOFOSSILS	RADIOLARIANS	DIATOMS	DINOCYSTS										
LOWER PLIOCENE		B				Gilbert Chronozone	● $\gamma = 1.76$ $\phi = 59.9$ W=54 ● TOC=0.36 CaCO ₃ =3.4								<p>NANNOFOSSIL-BEARING SILTY CLAY</p> <p>Nannofossil-bearing silty clay, dark greenish gray (5GY 4/1), moderately to strongly bioturbated. Very distinct horizontal layering is shown by color variations. Subtle variations in grain size and nannofossil content.</p> <p>SMEAR SLIDE SUMMARY (%):</p> <p>1, 70 2, 102 3, 4 D D D</p> <p>TEXTURE:</p> <p>Sand — — 5 Silt 40 40 50 Clay 60 60 45</p> <p>COMPOSITION:</p> <p>Quartz 30 30 20 Clay 50 40 35 Calcite/dolomite 2 — 5 Accessory minerals 5 — 5 Pyrite 3 2 5 Nannofossils 10 20 20 Diatoms — Tr 5 Sponge spicules — 8 5</p>

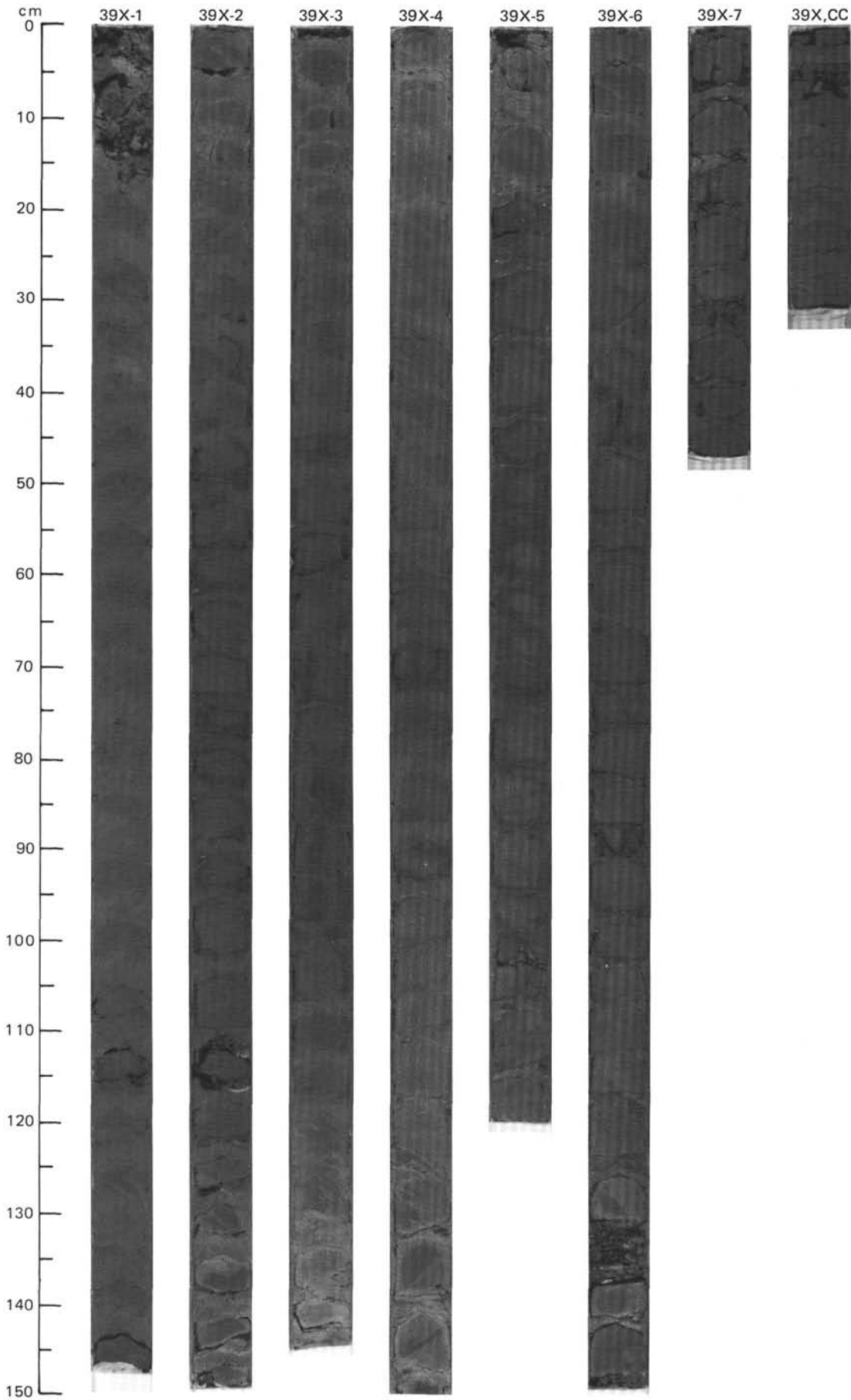


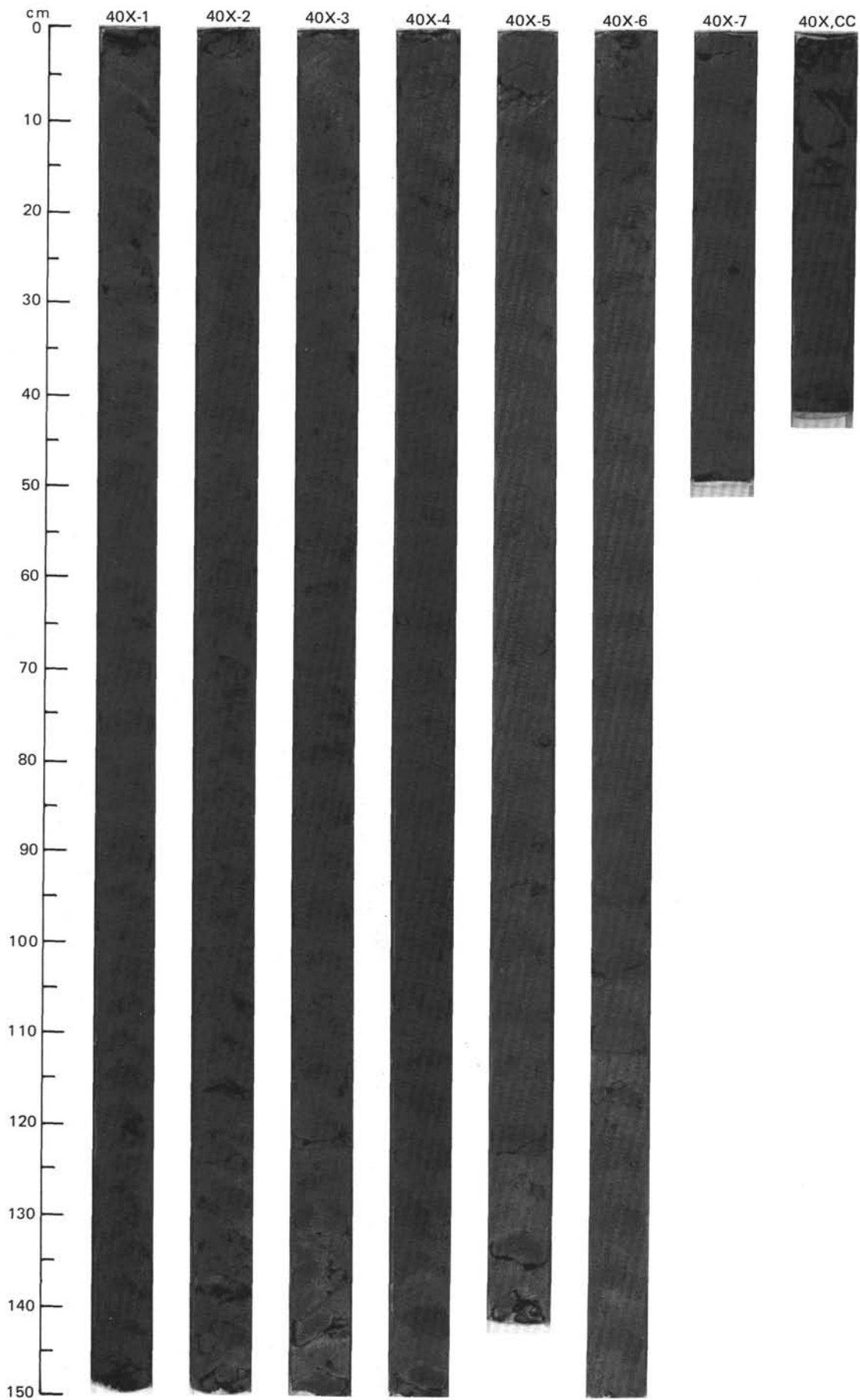
TIME-ROCK UNIT		BIOSTRAT. ZONE/ FOSSIL CHARACTER	PALEOMAGNETICS	PHYS. PROPERTIES	CHEMISTRY	SECTION	METERS	GRAPHIC LITHOLOGY	DRILLING DISTURB.	SED. STRUCTURES	SAMPLES	LITHOLOGIC DESCRIPTION																																																																						
FORAMINIFERS	NANNOFOSSILS												RADIOLARIANS	DIATOMS	DINOCYSTS																																																																			
LOWER PLIOCENE																																																																																		
A/M	M1 3-PL2			$\gamma = 1.75 \phi = 65.6 W = 62$	$CaCO_3 = 12$	1	0.5				*	<p>NANNOFOSSIL SILTY CLAY, CLAYEY NANNOFOSSIL OOZE, SILTY CLAY, AND CLAYEY SILTY</p> <p>Nannofossil silty clay and clayey nannofossil ooze, gray to dark gray (5Y 5/1 to 5Y 4/1).</p> <p>Silty clay and clayey silt, gray (5Y 5/1) and dark gray (5Y 4/1).</p> <p>Sediments are moderately to strongly bioturbated. Larger burrow traces are mostly dark gray (5Y 4/1) and dark greenish gray (5GY 4/1). Drilling biscuits occur throughout.</p> <p>SMEAR SLIDE SUMMARY (%):</p> <table border="1"> <tr> <td></td> <td>1, 58</td> <td>3, 55</td> <td>5, 58</td> <td>7, 25</td> </tr> <tr> <td>D</td> <td>D</td> <td>D</td> <td>D</td> <td>D</td> </tr> </table> <p>TEXTURE:</p> <table border="1"> <tr> <td>Sand</td> <td>5</td> <td>—</td> <td>—</td> <td>—</td> </tr> <tr> <td>Silt</td> <td>35</td> <td>65</td> <td>40</td> <td>60</td> </tr> <tr> <td>Clay</td> <td>60</td> <td>35</td> <td>60</td> <td>40</td> </tr> </table> <p>COMPOSITION:</p> <table border="1"> <tr> <td>Quartz</td> <td>25</td> <td>45</td> <td>23</td> <td>7</td> </tr> <tr> <td>Feldspar</td> <td>—</td> <td>—</td> <td>9</td> <td>—</td> </tr> <tr> <td>Mica</td> <td>—</td> <td>—</td> <td>Tr</td> <td>—</td> </tr> <tr> <td>Clay</td> <td>40</td> <td>35</td> <td>60</td> <td>18</td> </tr> <tr> <td>Calcite/dolomite</td> <td>2</td> <td>—</td> <td>Tr</td> <td>8</td> </tr> <tr> <td>Accessory minerals</td> <td>5</td> <td>5</td> <td>3</td> <td>1</td> </tr> <tr> <td>Pyrite</td> <td>3</td> <td>5</td> <td>4</td> <td>1</td> </tr> <tr> <td>Foraminifers</td> <td>Tr</td> <td>—</td> <td>1</td> <td>Tr</td> </tr> <tr> <td>Nannofossils</td> <td>25</td> <td>5</td> <td>—</td> <td>55</td> </tr> </table>		1, 58	3, 55	5, 58	7, 25	D	D	D	D	D	Sand	5	—	—	—	Silt	35	65	40	60	Clay	60	35	60	40	Quartz	25	45	23	7	Feldspar	—	—	9	—	Mica	—	—	Tr	—	Clay	40	35	60	18	Calcite/dolomite	2	—	Tr	8	Accessory minerals	5	5	3	1	Pyrite	3	5	4	1	Foraminifers	Tr	—	1	Tr	Nannofossils	25	5	—	55
	1, 58	3, 55	5, 58	7, 25																																																																														
D	D	D	D	D																																																																														
Sand	5	—	—	—																																																																														
Silt	35	65	40	60																																																																														
Clay	60	35	60	40																																																																														
Quartz	25	45	23	7																																																																														
Feldspar	—	—	9	—																																																																														
Mica	—	—	Tr	—																																																																														
Clay	40	35	60	18																																																																														
Calcite/dolomite	2	—	Tr	8																																																																														
Accessory minerals	5	5	3	1																																																																														
Pyrite	3	5	4	1																																																																														
Foraminifers	Tr	—	1	Tr																																																																														
Nannofossils	25	5	—	55																																																																														
A/G	NN13-NN15			$\gamma = 1.94 \phi = 52.1 W = 38$	$CaCO_3 = 5$	2	1.0																																																																											
B						3					*																																																																							
B						4																																																																												
A/G				$\gamma = 1.93 \phi = 57.5 W = 44$	$CaCO_3 = 0$	5					*																																																																							
				$TOC = 0.53$		6					OG																																																																							
						7					*																																																																							
CC																																																																																		

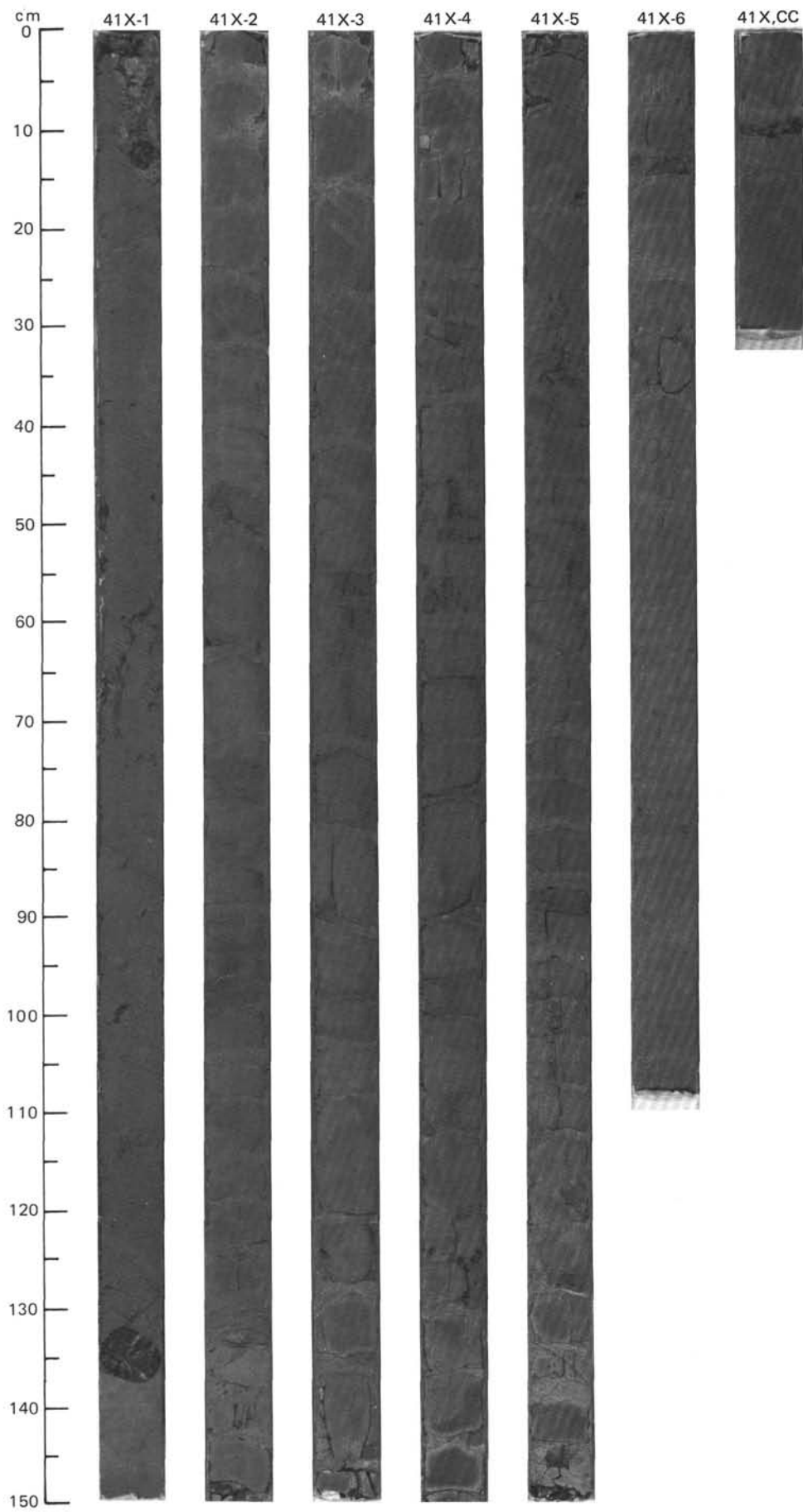


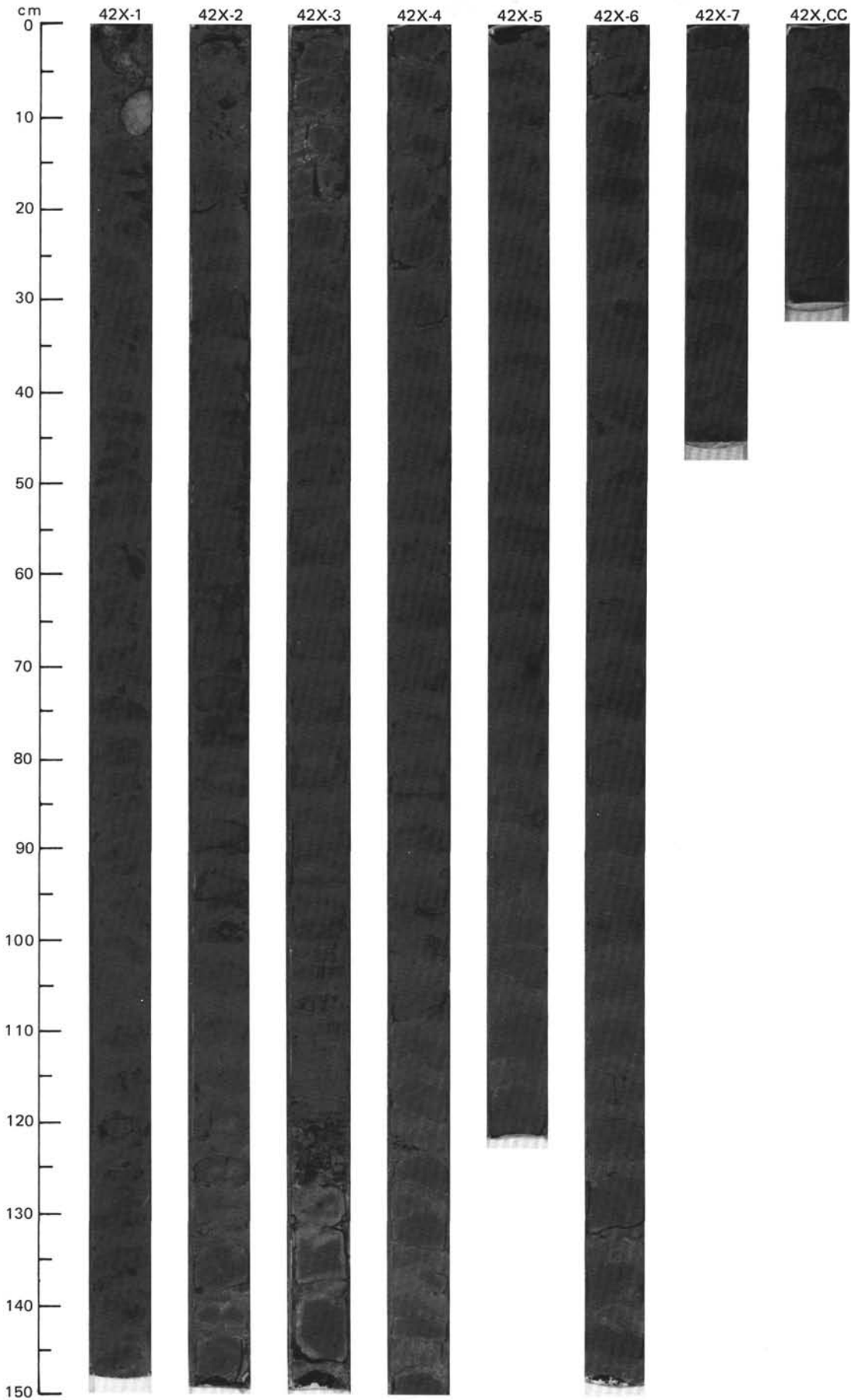










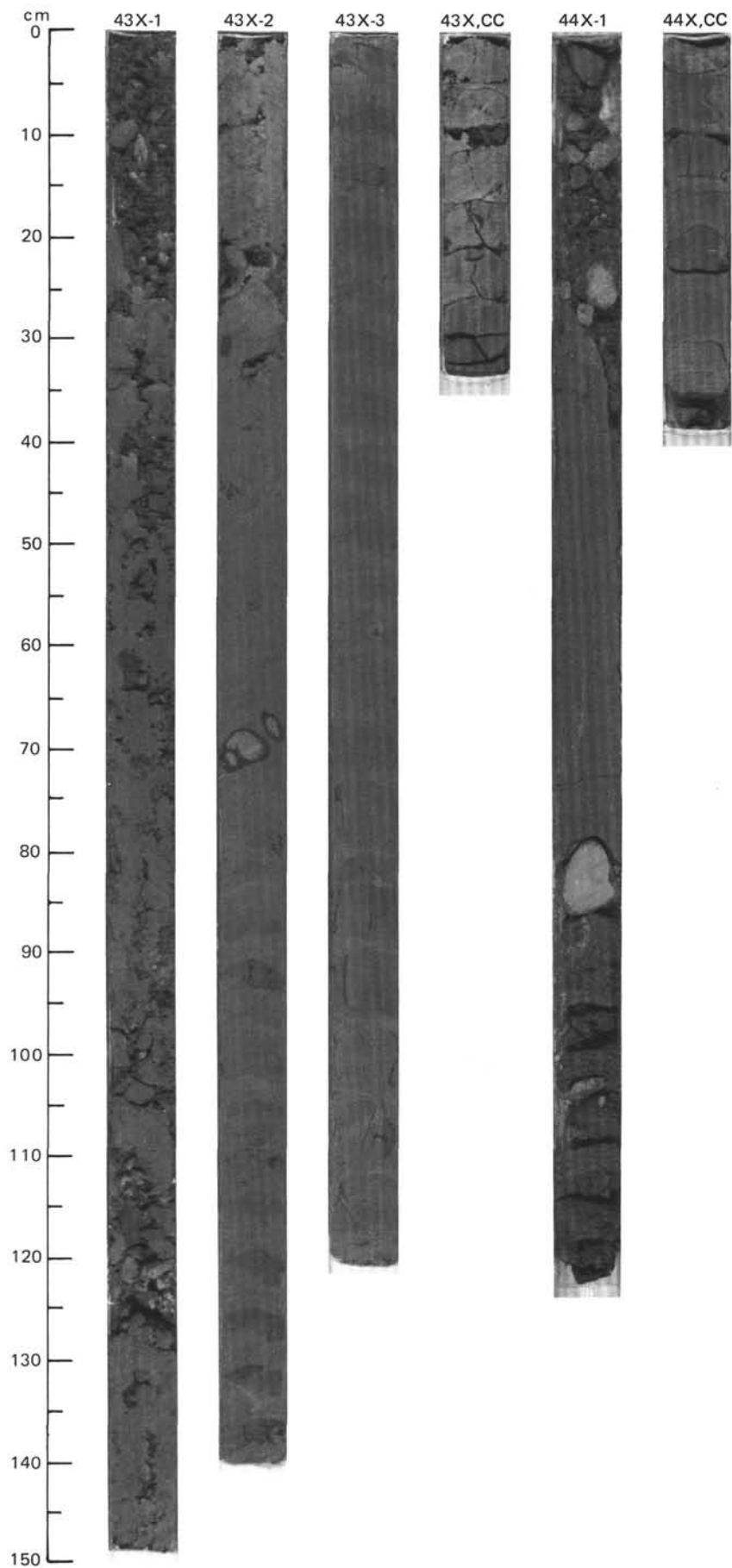


SITE 646 HOLE B CORE 43 X CORED INTERVAL 3848.9-3858.6 mbsl; 400.7-410.4 mbsf

TIME-ROCK UNIT	BIOSTRAT. ZONE/ FOSSIL CHARACTER					PALEOMAGNETICS	PHYS. PROPERTIES	CHEMISTRY	SECTION	METERS	GRAPHIC LITHOLOGY	DRILLING DISTURB.	SED. STRUCTURES	SAMPLES	LITHOLOGIC DESCRIPTION																								
	FORAMINIFERS	NANNOFOSSILS	RADIOLARIANS	DIATOMS	DINOCYSTS																																		
LOWER PLIOCENE	A/M	M13-PL1													<p>NANNOFOSSIL-BEARING CLAY</p> <p>Highly deformed core, with upper Section 1 and Section 2-77 cm being drilling slurry with a few scattered basalt caved pebbles. Rest of core is about 50% partly tipped biscuits surrounded by slurry.</p> <p>Nannofossil-bearing clay, dark gray (5Y 4/1), moderately bioturbated, subtly color mottled.</p> <p>SMEAR SLIDE SUMMARY (%):</p> <table style="margin-left: 20px;"> <tr><td></td><td>3, 79</td></tr> <tr><td>D</td><td></td></tr> </table> <p>TEXTURE:</p> <table style="margin-left: 20px;"> <tr><td>Silt</td><td>30</td></tr> <tr><td>Clay</td><td>70</td></tr> </table> <p>COMPOSITION:</p> <table style="margin-left: 20px;"> <tr><td>Quartz</td><td>15</td></tr> <tr><td>Feldspar</td><td>Tr</td></tr> <tr><td>Mica</td><td>Tr</td></tr> <tr><td>Clay</td><td>68</td></tr> <tr><td>Calcite/dolomite</td><td>1</td></tr> <tr><td>Accessory minerals</td><td>1</td></tr> <tr><td>Foraminifers</td><td>Tr</td></tr> <tr><td>Nannofossils</td><td>15</td></tr> </table>		3, 79	D		Silt	30	Clay	70	Quartz	15	Feldspar	Tr	Mica	Tr	Clay	68	Calcite/dolomite	1	Accessory minerals	1	Foraminifers	Tr	Nannofossils	15
	3, 79																																						
D																																							
Silt	30																																						
Clay	70																																						
Quartz	15																																						
Feldspar	Tr																																						
Mica	Tr																																						
Clay	68																																						
Calcite/dolomite	1																																						
Accessory minerals	1																																						
Foraminifers	Tr																																						
Nannofossils	15																																						
									1	0.5	Drilling																												
									2	1.0	Slurry																												
									3																														
									CC																														

SITE 646 HOLE B CORE 44 X CORED INTERVAL 3858.6-3868.3 mbsl; 410.4-420.1 mbsf

TIME-ROCK UNIT	BIOSTRAT. ZONE/ FOSSIL CHARACTER					PALEOMAGNETICS	PHYS. PROPERTIES	CHEMISTRY	SECTION	METERS	GRAPHIC LITHOLOGY	DRILLING DISTURB.	SED. STRUCTURES	SAMPLES	LITHOLOGIC DESCRIPTION																								
	FORAMINIFERS	NANNOFOSSILS	RADIOLARIANS	DIATOMS	DINOCYSTS																																		
LOWER PLIOCENE	A/M	M13-PL1													<p>NANNOFOSSIL-BEARING CLAY</p> <p>Entire first section is drilling slurry with caved basalt, gabbro, and limestone pebbles and cobbles. Only recovery is in the CC.</p> <p>Nannofossil-bearing clay, dark gray (5Y 4/1), moderately bioturbated, subtly color banded.</p> <p>SMEAR SLIDE SUMMARY (%):</p> <table style="margin-left: 20px;"> <tr><td></td><td>2, 24</td></tr> <tr><td>D</td><td></td></tr> </table> <p>TEXTURE:</p> <table style="margin-left: 20px;"> <tr><td>Silt</td><td>30</td></tr> <tr><td>Clay</td><td>70</td></tr> </table> <p>COMPOSITION:</p> <table style="margin-left: 20px;"> <tr><td>Quartz</td><td>10</td></tr> <tr><td>Feldspar</td><td>Tr</td></tr> <tr><td>Mica</td><td>Tr</td></tr> <tr><td>Clay</td><td>69</td></tr> <tr><td>Calcite/dolomite</td><td>1</td></tr> <tr><td>Accessory minerals</td><td>Tr</td></tr> <tr><td>Foraminifers</td><td>Tr</td></tr> <tr><td>Nannofossils</td><td>20</td></tr> </table>		2, 24	D		Silt	30	Clay	70	Quartz	10	Feldspar	Tr	Mica	Tr	Clay	69	Calcite/dolomite	1	Accessory minerals	Tr	Foraminifers	Tr	Nannofossils	20
	2, 24																																						
D																																							
Silt	30																																						
Clay	70																																						
Quartz	10																																						
Feldspar	Tr																																						
Mica	Tr																																						
Clay	69																																						
Calcite/dolomite	1																																						
Accessory minerals	Tr																																						
Foraminifers	Tr																																						
Nannofossils	20																																						
									1	0.5	Drilling																												
										1.0	Slurry																												
									CC		VOID																												

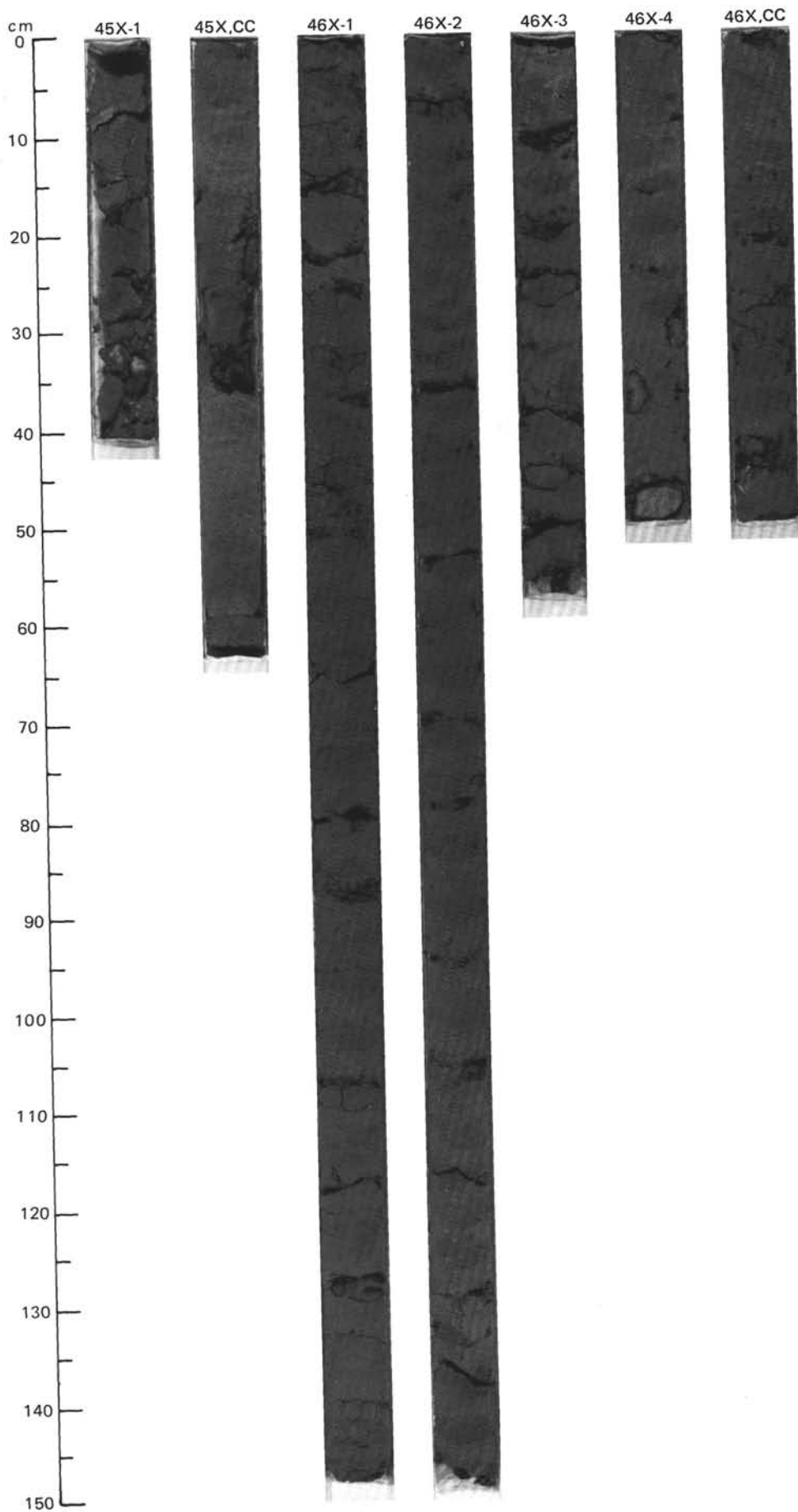


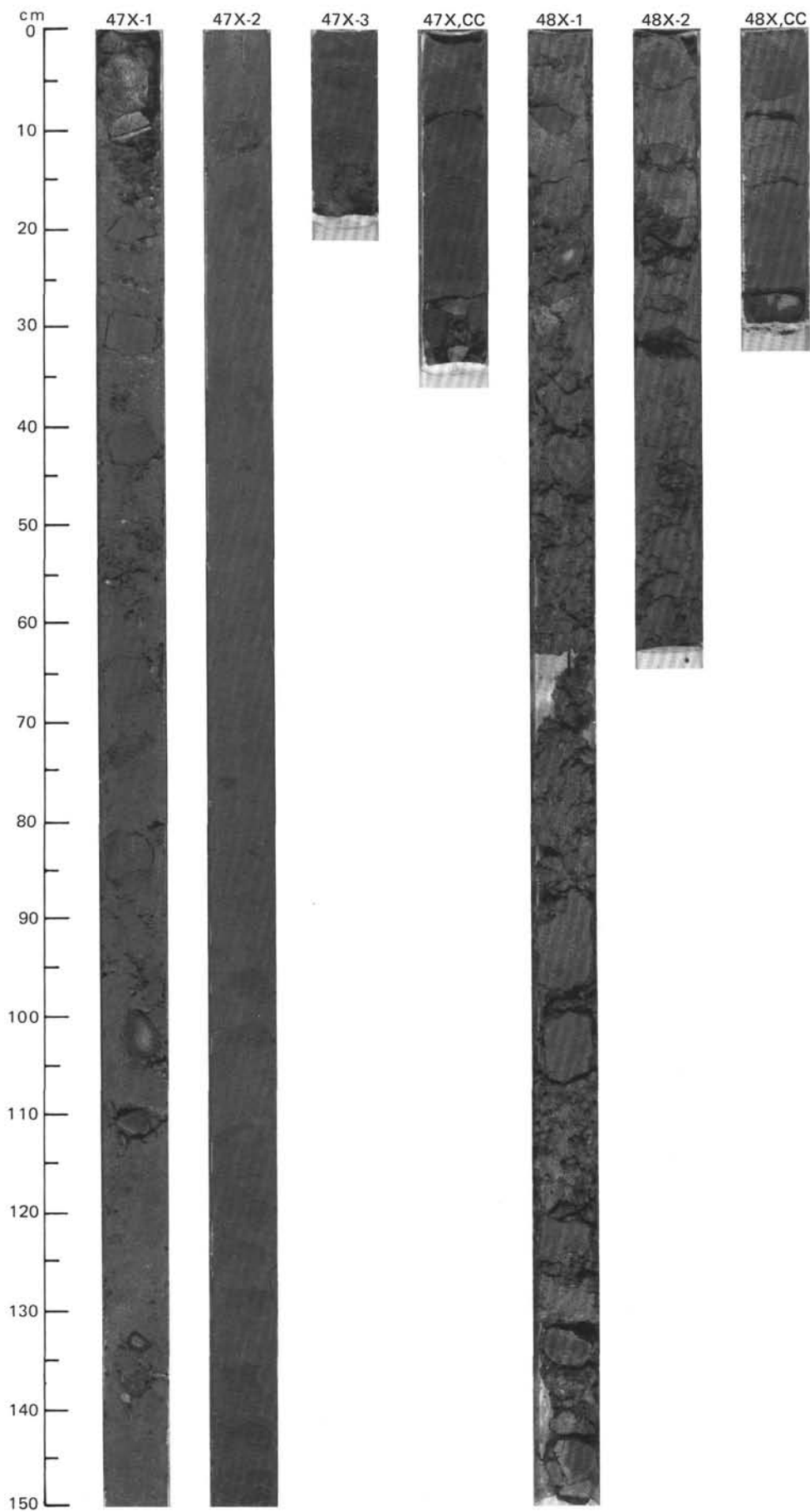
SITE 646 HOLE B CORE 45 X CORED INTERVAL 3868.3-3878.0 mbsl; 420.1-429.8 mbsf

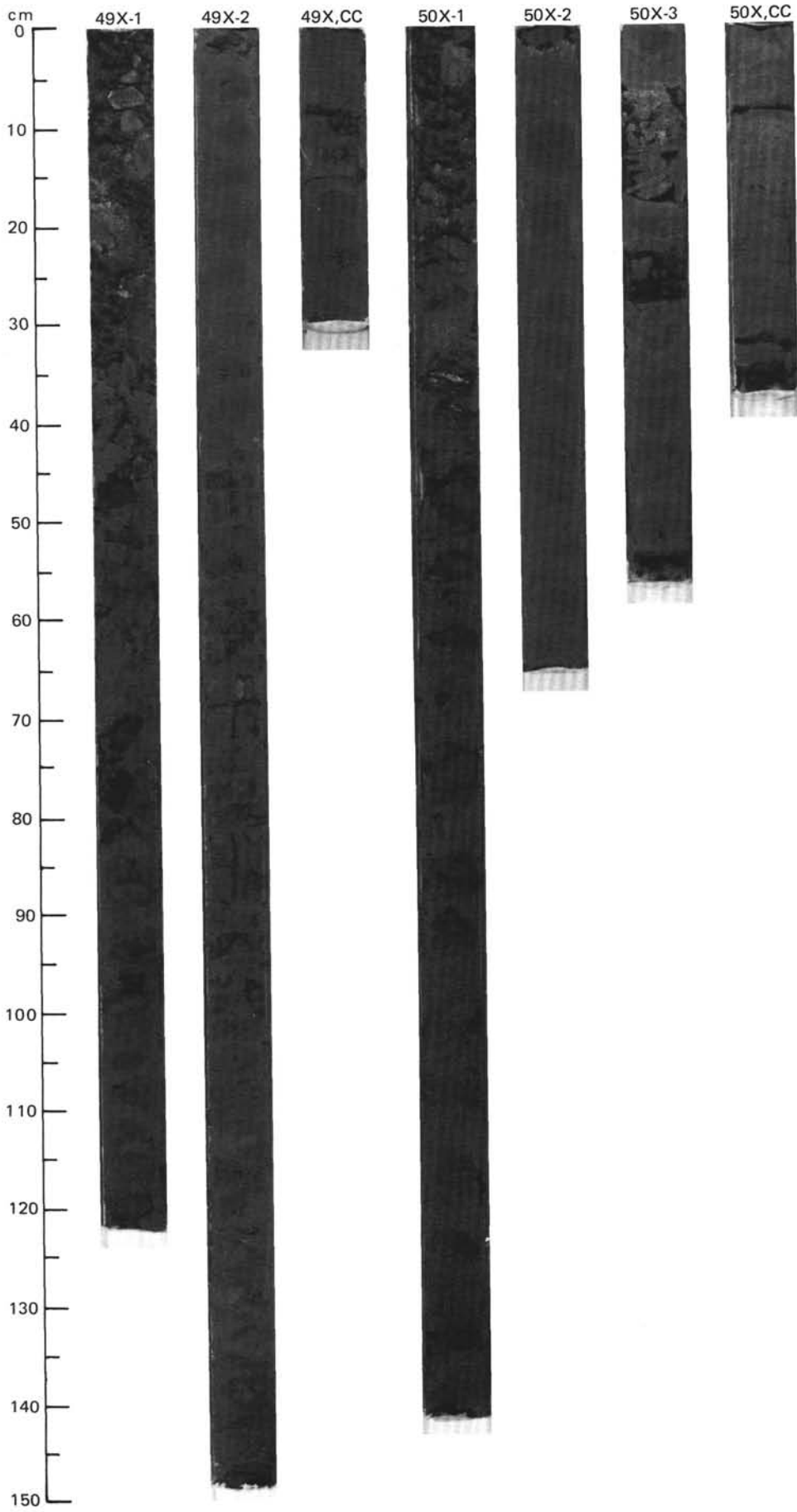
TIME-ROCK UNIT	BIOSTRAT. ZONE/ FOSSIL CHARACTER				PALEOMAGNETICS	PHYS. PROPERTIES	CHEMISTRY	SECTION	METERS	GRAPHIC LITHOLOGY	DRILLING DISTURB.	SED. STRUCTURES	SAMPLES	LITHOLOGIC DESCRIPTION
	FORAMINIFERS	NANNOFOSSILS	RADIOLARIANS	DIATOMS										
LOWER PLIOCENE	A/G	C/G	B	B	A/G			1		Drilling Slurry				<p>NANNOFOSSIL-BEARING CLAY</p> <p>Nannofossil-bearing clay, greenish gray (5GY 5/1), probably drilling slurry.</p> <p>SMEAR SLIDE SUMMARY (%):</p> <p style="text-align: right;">CC, 50 D</p> <p>TEXTURE:</p> <p>Silt 25 Clay 75</p> <p>COMPOSITION:</p> <p>Quartz 10 Rock fragments Tr Clay 74 Calcite/dolomite Tr Accessory minerals 1 Nannofossils 15</p>
	M13-PL1	NN12						CC						

SITE 646 HOLE B CORE 46 X CORED INTERVAL 3878.0-3887 mbsl; 429.8-439.5 mbsf

TIME-ROCK UNIT	BIOSTRAT. ZONE/ FOSSIL CHARACTER				PALEOMAGNETICS	PHYS. PROPERTIES	CHEMISTRY	SECTION	METERS	GRAPHIC LITHOLOGY	DRILLING DISTURB.	SED. STRUCTURES	SAMPLES	LITHOLOGIC DESCRIPTION
	FORAMINIFERS	NANNOFOSSILS	RADIOLARIANS	DIATOMS										
LOWER PLIOCENE	A/G	A/G	B	C/M		$\gamma = 1.98$ $\phi = 48.5$ $W = 33$	$TOC = 0.36$ $CaCO_3 = 8.8$	1	0.5					<p>NANNOFOSSIL CLAYEY SILT, NANNOFOSSIL SILTY CLAY, AND SILTY CLAY</p> <p>All lithologies are moderately bioturbated.</p> <p>Nannofossil clayey silt, gray (5Y 5/1, and 5Y 5/1 to N5).</p> <p>Nannofossil silty clay, light gray (5Y 6/1).</p> <p>Silty clay, gray (5Y 5/1 to N5).</p> <p>SMEAR SLIDE SUMMARY (%):</p> <p style="text-align: right;">1, 65 4, 24 CC, 38 D D D</p> <p>TEXTURE:</p> <p>Sand 5 — 5 Silt 60 40 35 Clay 35 60 60</p> <p>COMPOSITION:</p> <p>Quartz 35 30 60 Clay 35 25 30 Calcite/dolomite — — 2 Accessory minerals — 5 2 Pyrite 5 5 3 Nannofossils 30 35 3</p>
	M13-PL1	NN15 or older						2	1.0				*	
								3		VOID				
								4					*	
								CC					*	





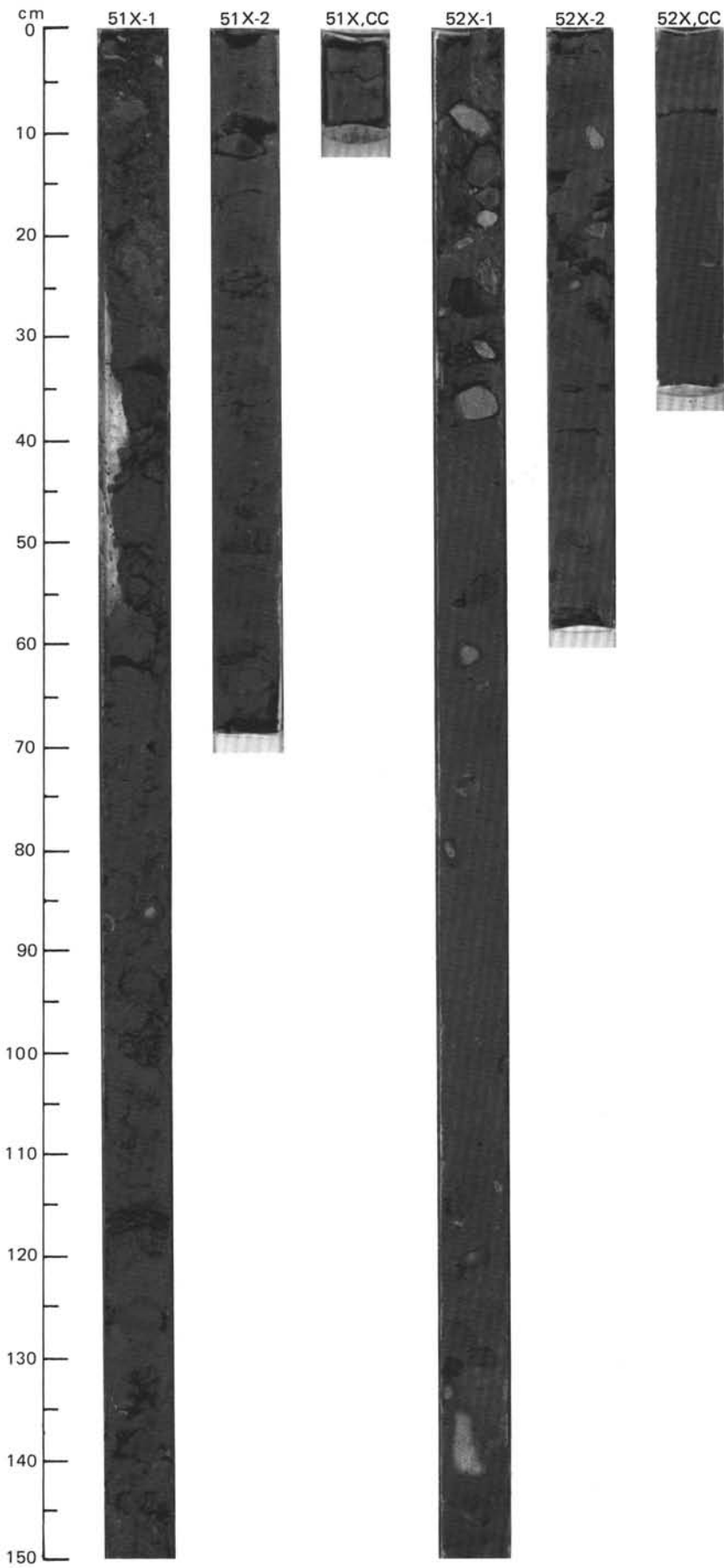


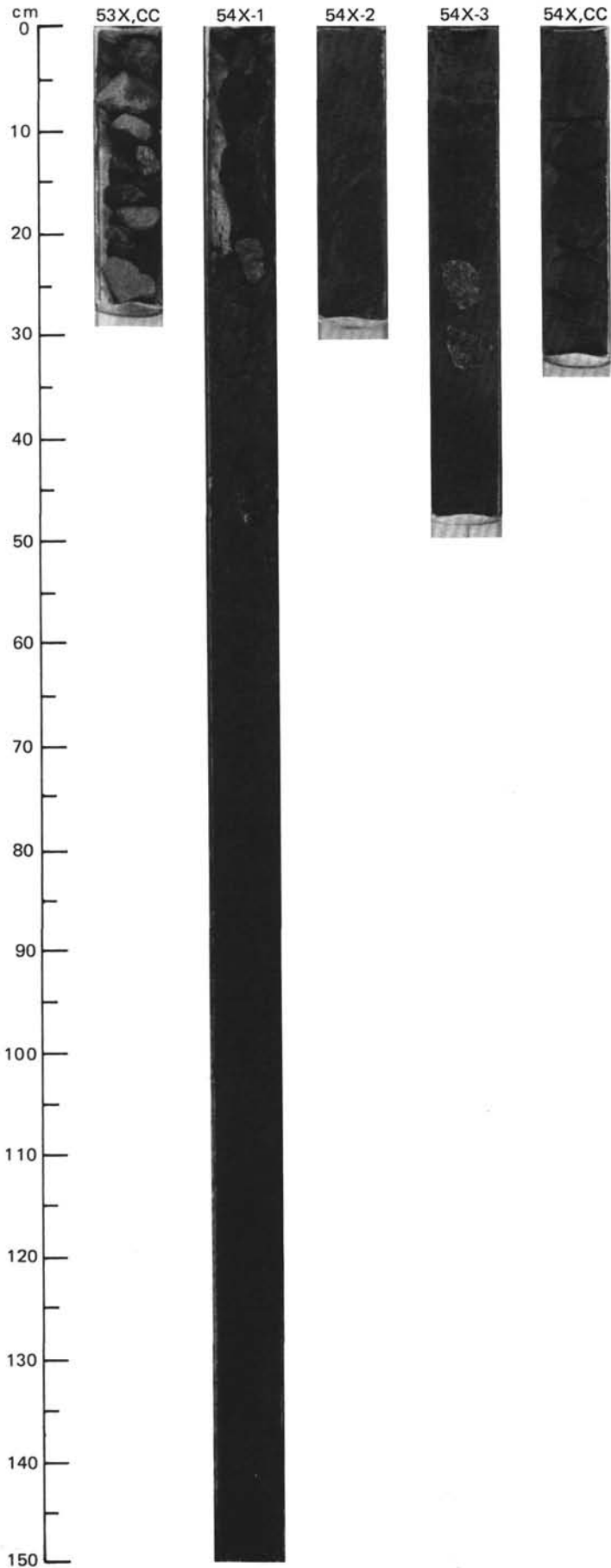
SITE 646 HOLE B CORE 51X CORED INTERVAL 3926.3 3935.7 mbsf; 478.1-487.4 mbsf

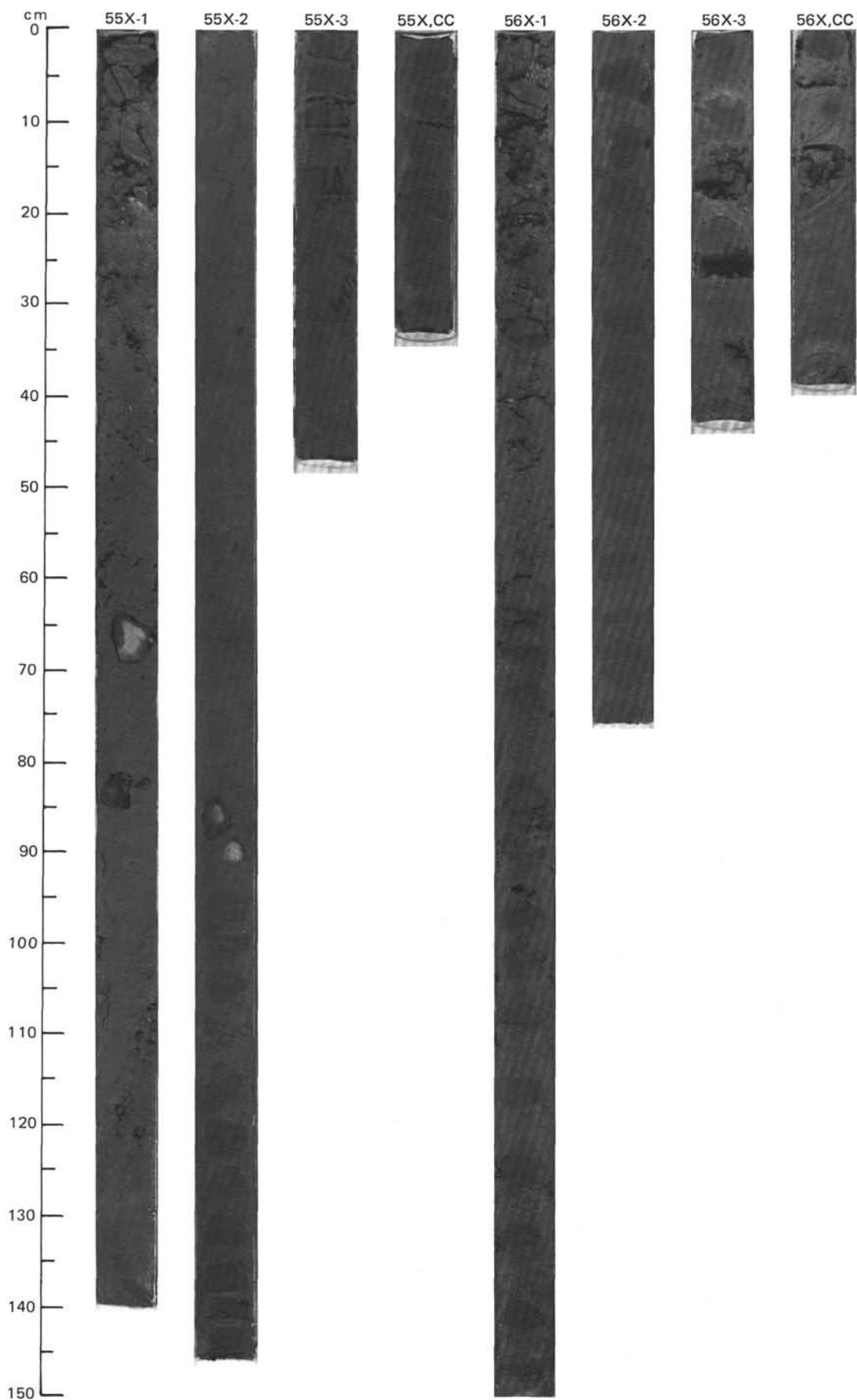
TIME-ROCK UNIT	BIOSTRAT. ZONE/ FOSSIL CHARACTER					PALEOMAGNETICS	PHYS. PROPERTIES	CHEMISTRY	SECTION	METERS	GRAPHIC LITHOLOGY	DRILLING DISTURB.	SED. STRUCTURES	SAMPLES	LITHOLOGIC DESCRIPTION
	FORAMINIFERS	NANNOFOSSILS	RADIOLARIANS	DIATOMS	DINOCYSTS										
UPPER MIOCENE TO LOWER PLIOCENE	A/G	M13-PL1													<p>CLAYSTONE</p> <p>Claystone, dark gray (5Y 4/1), moderately bioturbated, strongly disturbed biscuits surrounded by slurry. Basalt and gabbro caved pebbles in Section 1.</p>
	C/G	NN15 or older	B	B	C/G	$\gamma = 2.02$	$\phi = 49.6$	W-34	1	0.5 1.0	Drilling Slurry	X			
									2			X			
									CC			X			

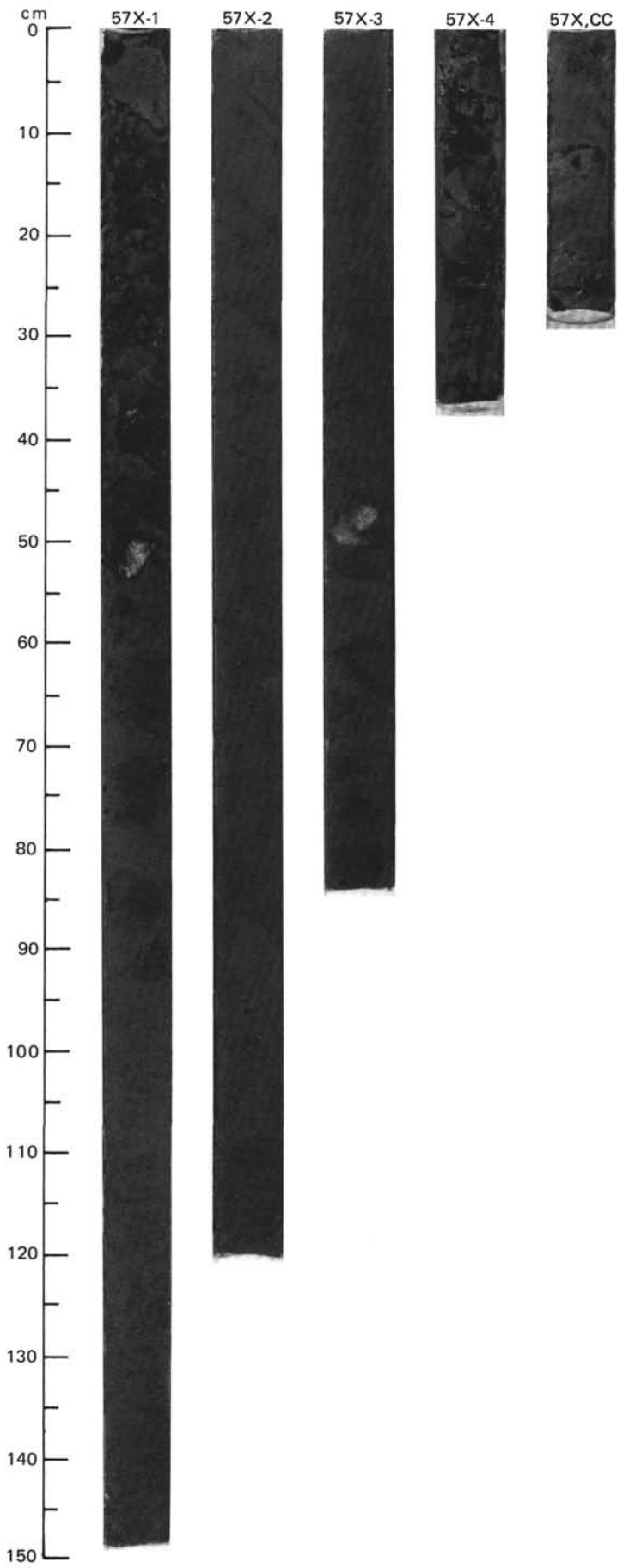
SITE 646 HOLE B CORE 52 X CORED INTERVAL 3935.7-3945.4 mbsf; 487.4-497.1 mbsf

TIME-ROCK UNIT	BIOSTRAT. ZONE/ FOSSIL CHARACTER					PALEOMAGNETICS	PHYS. PROPERTIES	CHEMISTRY	SECTION	METERS	GRAPHIC LITHOLOGY	DRILLING DISTURB.	SED. STRUCTURES	SAMPLES	LITHOLOGIC DESCRIPTION
	FORAMINIFERS	NANNOFOSSILS	RADIOLARIANS	DIATOMS	DINOCYSTS										
UPPER MIOCENE TO LOWER PLIOCENE	C/G	M13-PL1													<p>CLAYSTONE</p> <p>Claystone, greenish gray (5GY 5/1), moderately bioturbated, strongly disturbed biscuits surrounded by slurry.</p> <p>SMEAR SLIDE SUMMARY (%):</p> <p>CC, 26 D</p> <p>TEXTURE:</p> <p>Silt 15 Clay 85</p> <p>COMPOSITION:</p> <p>Quartz 10 Feldspar Tr Mica Tr Clay 85 Calcite/dolomite Tr Accessory minerals Tr Nannofossils 5</p>
	A/G	NN15-NN11	B	B	A/G				1	0.5 1.0	Drilling Slurry				
									2						
									CC				*		







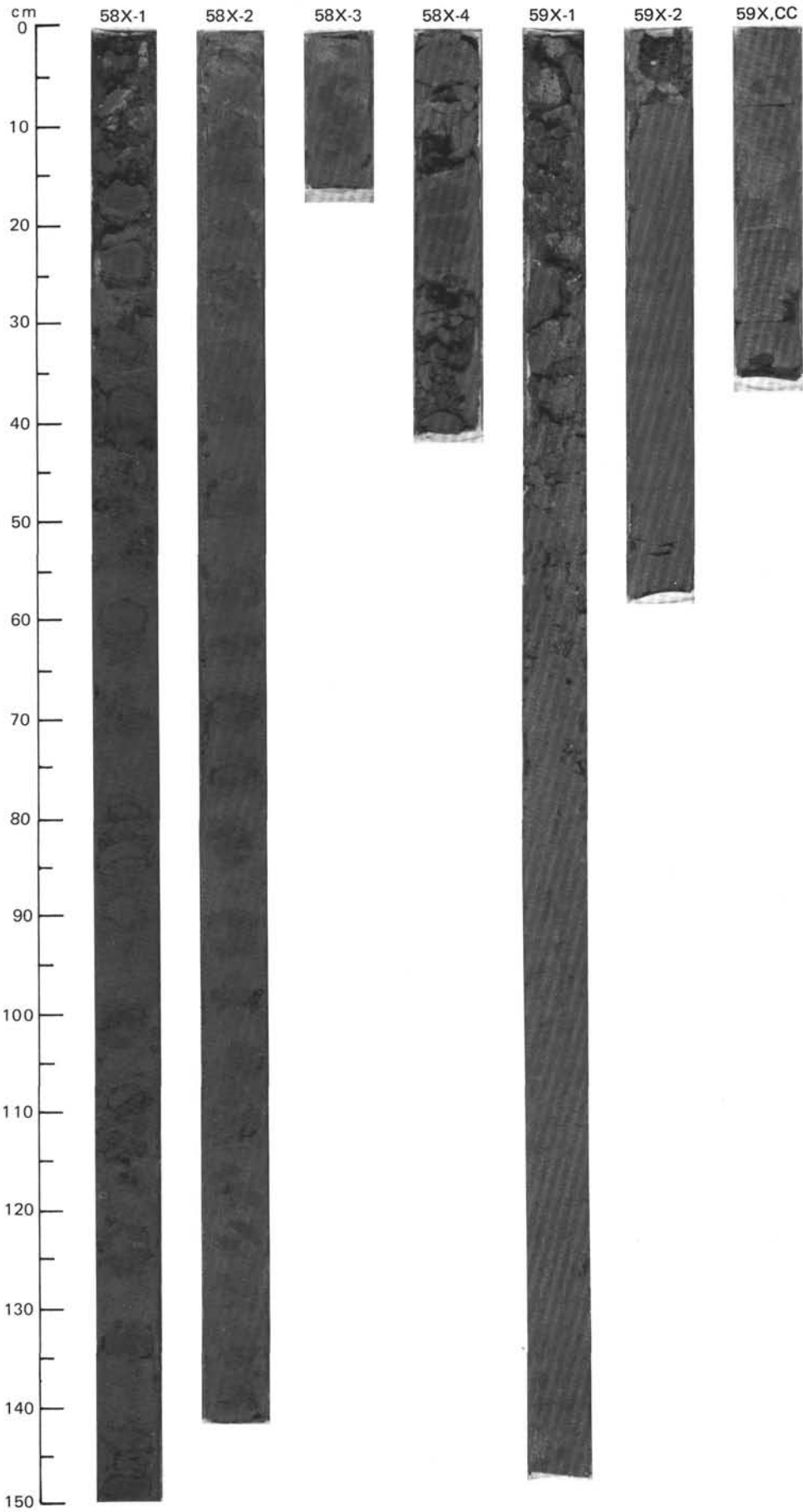


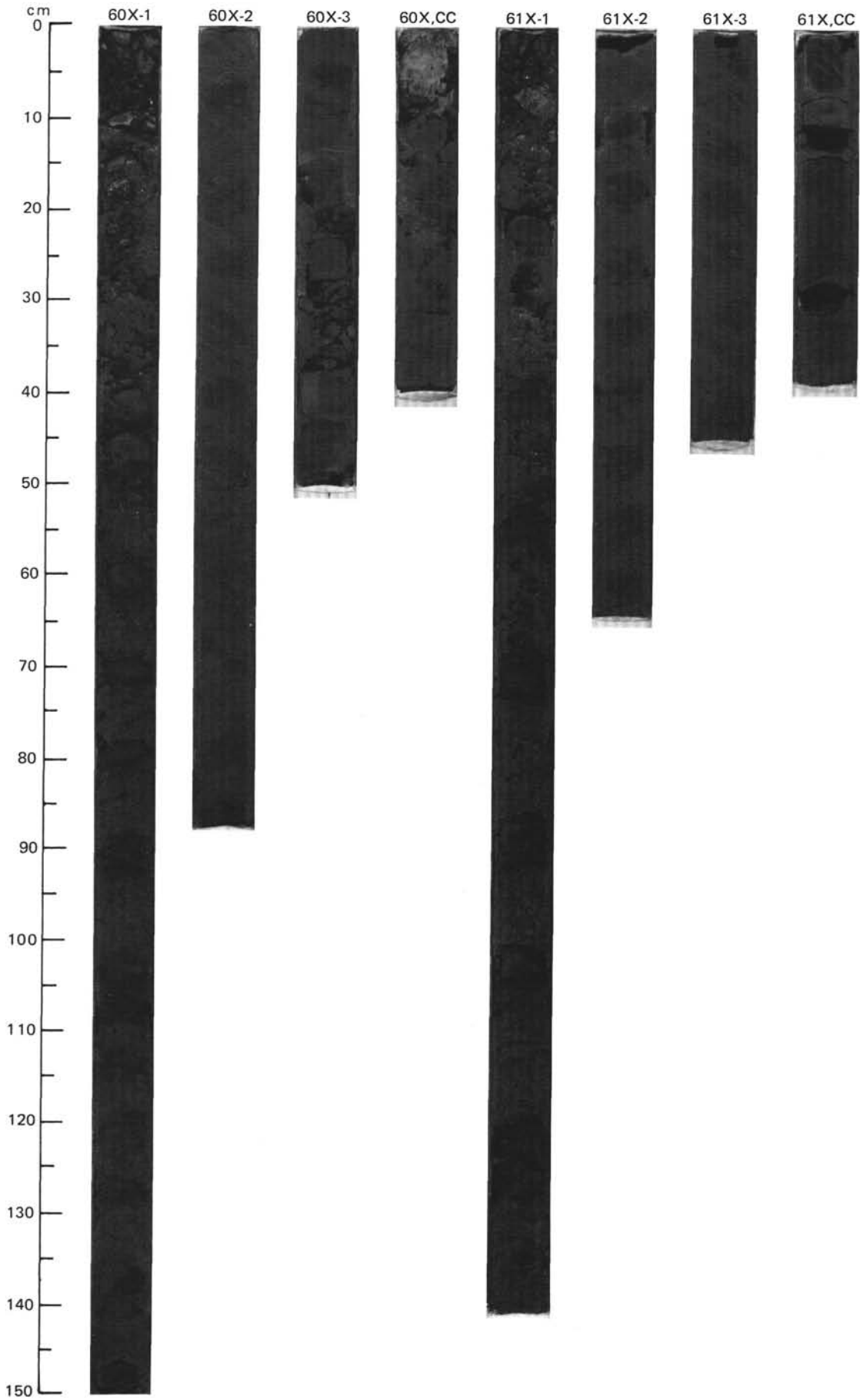
SITE 646 HOLE B CORE 58 X CORED INTERVAL 3993.7-4003.4 mbsf; 545.5-555.2 mbsf

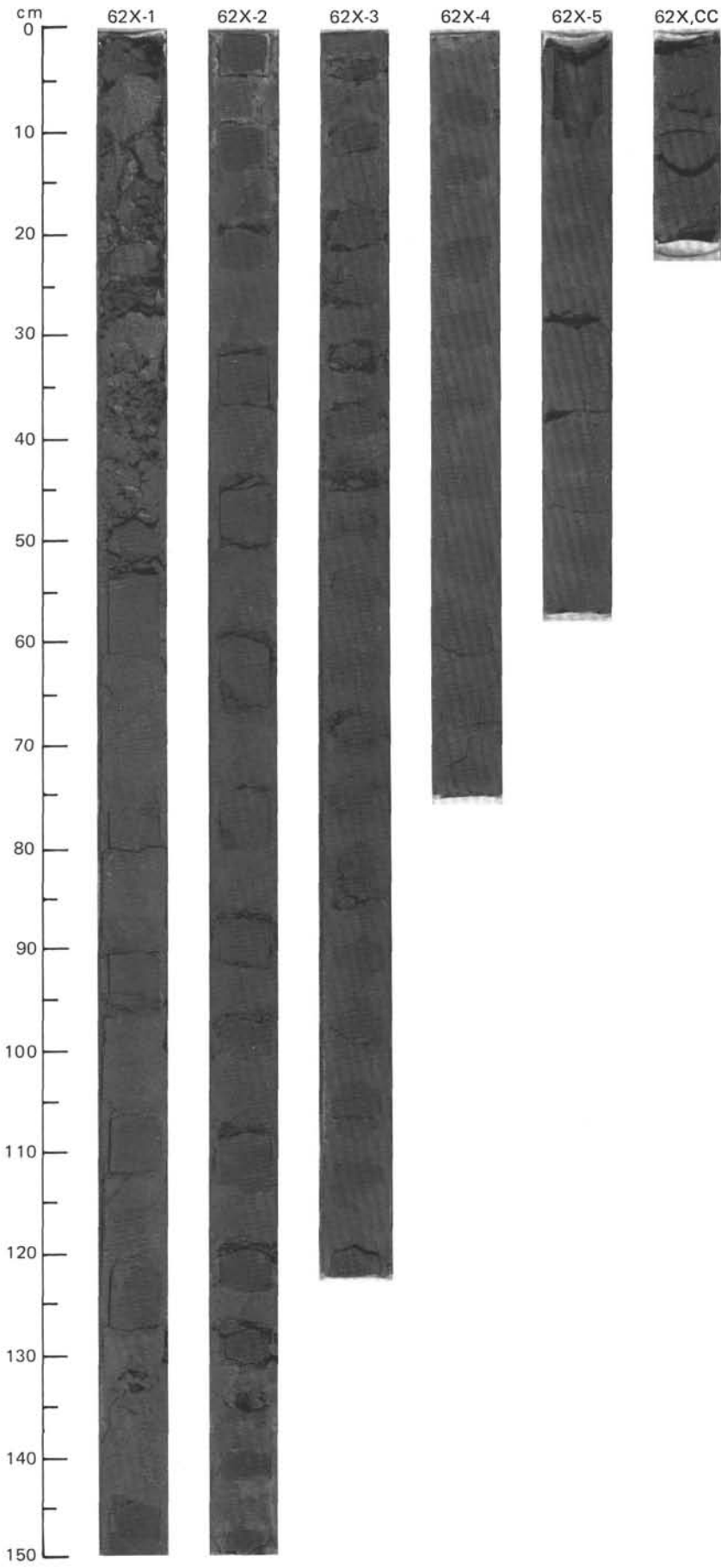
TIME-ROCK UNIT	BIOSTRAT. ZONE/ FOSSIL CHARACTER					PALEOMAGNETICS	PHYS. PROPERTIES	CHEMISTRY	SECTION	METERS	GRAPHIC LITHOLOGY	DRILLING DISTURB.	SED. STRUCTURES	SAMPLES	LITHOLOGIC DESCRIPTION																														
	FORAMINIFERS	NANNOFOSSILS	RADIOLARIANS	DIATOMS	DINOCTYSTS																																								
UPPER MIOCENE	C/P	?M11-M12													<p>SILTY CLAYSTONE</p> <p>Silty claystone, dark greenish gray to dark gray (5GY 4/1 - 5Y 4/1), bioturbated but otherwise homogeneous. Few or no nannofossils.</p> <p>SMEAR SLIDE SUMMARY (%):</p> <table border="1"> <tr> <td></td> <td>1, 124</td> <td>2, 56</td> </tr> <tr> <td>D</td> <td>D</td> <td>D</td> </tr> </table> <p>TEXTURE:</p> <table border="1"> <tr> <td>Silt</td> <td>30</td> <td>25</td> </tr> <tr> <td>Clay</td> <td>70</td> <td>75</td> </tr> </table> <p>COMPOSITION:</p> <table border="1"> <tr> <td>Quartz</td> <td>35</td> <td>25</td> </tr> <tr> <td>Feldspar</td> <td>2</td> <td>1</td> </tr> <tr> <td>Mica</td> <td>Tr</td> <td>Tr</td> </tr> <tr> <td>Clay</td> <td>63</td> <td>74</td> </tr> <tr> <td>Accessory minerals</td> <td>Tr</td> <td>Tr</td> </tr> <tr> <td>Nannofossils</td> <td>—</td> <td>Tr</td> </tr> </table>		1, 124	2, 56	D	D	D	Silt	30	25	Clay	70	75	Quartz	35	25	Feldspar	2	1	Mica	Tr	Tr	Clay	63	74	Accessory minerals	Tr	Tr	Nannofossils	—	Tr
	1, 124	2, 56																																											
D	D	D																																											
Silt	30	25																																											
Clay	70	75																																											
Quartz	35	25																																											
Feldspar	2	1																																											
Mica	Tr	Tr																																											
Clay	63	74																																											
Accessory minerals	Tr	Tr																																											
Nannofossils	—	Tr																																											
	B					● $\gamma = 2.06$ $\phi = 47.7$ $W = 31$	● $TOC = 0.45$ $CaCO_3 = 0.45$	1	0.5		X																																		
	B							2	1.0		X		*																																
	B							3		VOID	X		IV																																
	F/G							4			X																																		

SITE 646 HOLE B CORE 59 X CORED INTERVAL 4003.4-4012.6 mbsf; 555.2-564.4 mbsf

TIME-ROCK UNIT	BIOSTRAT. ZONE/ FOSSIL CHARACTER					PALEOMAGNETICS	PHYS. PROPERTIES	CHEMISTRY	SECTION	METERS	GRAPHIC LITHOLOGY	DRILLING DISTURB.	SED. STRUCTURES	SAMPLES	LITHOLOGIC DESCRIPTION																				
	FORAMINIFERS	NANNOFOSSILS	RADIOLARIANS	DIATOMS	DINOCTYSTS																														
UPPER MIOCENE	C/M	?M11-M12													<p>SILTY CLAYSTONE</p> <p>Silty claystone, dark gray (5Y 4/1), burrow mottled with a small percentage of nannofossils.</p> <p>SMEAR SLIDE SUMMARY (%):</p> <table border="1"> <tr> <td></td> <td>CC, 17</td> </tr> <tr> <td>D</td> <td>D</td> </tr> </table> <p>TEXTURE:</p> <table border="1"> <tr> <td>Silt</td> <td>30</td> </tr> <tr> <td>Clay</td> <td>70</td> </tr> </table> <p>COMPOSITION:</p> <table border="1"> <tr> <td>Quartz</td> <td>35</td> </tr> <tr> <td>Feldspar</td> <td>Tr</td> </tr> <tr> <td>Mica</td> <td>Tr</td> </tr> <tr> <td>Clay</td> <td>64</td> </tr> <tr> <td>Accessory minerals</td> <td>Tr</td> </tr> <tr> <td>Nannofossils</td> <td>1</td> </tr> </table>		CC, 17	D	D	Silt	30	Clay	70	Quartz	35	Feldspar	Tr	Mica	Tr	Clay	64	Accessory minerals	Tr	Nannofossils	1
	CC, 17																																		
D	D																																		
Silt	30																																		
Clay	70																																		
Quartz	35																																		
Feldspar	Tr																																		
Mica	Tr																																		
Clay	64																																		
Accessory minerals	Tr																																		
Nannofossils	1																																		
	F/G	NN15 or older					● $TOC = 0.30$ $CaCO_3 = 10$	1	0.5	Drilling																									
	B							2	1.0	Slurry																									
	B							CC			X		*																						





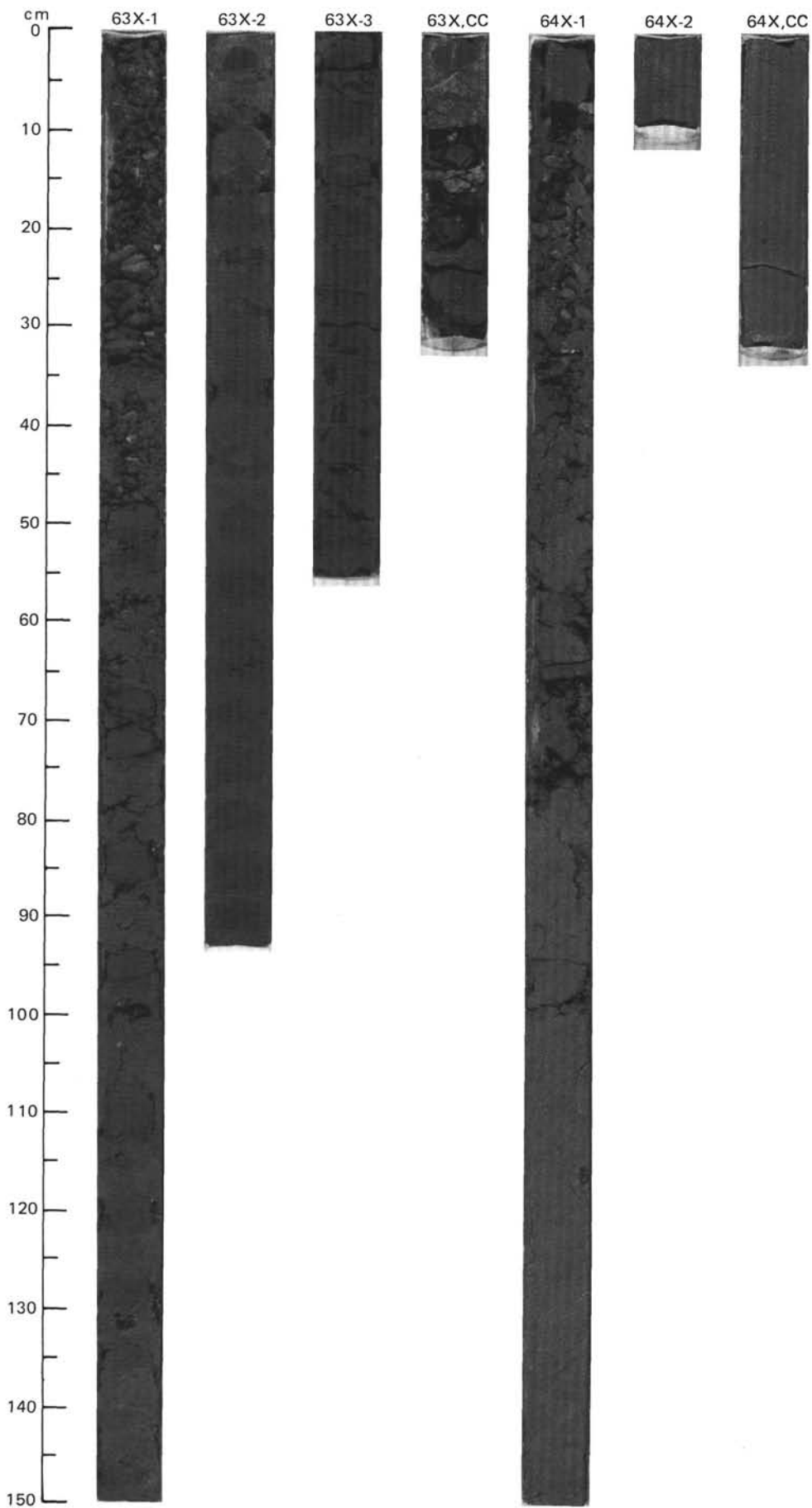


SITE 646 HOLE B CORE 63 X CORED INTERVAL 4041.4-4051.1 mbsl; 593.2-602.9 mbsf

TIME-ROCK UNIT	BIOSTRAT. ZONE/ FOSSIL CHARACTER					PALEOMAGNETICS	PHYS. PROPERTIES	CHEMISTRY	SECTION	METERS	GRAPHIC LITHOLOGY	DRILLING DISTURB.	SED. STRUCTURES	SAMPLES	LITHOLOGIC DESCRIPTION																																																
	FORAMINIFERS	NANNOFOSSILS	RADIOLARIANS	DIATOMS	DINOCTYSTS																																																										
UPPER MIOCENE	F/P	F/G	B	B	F/M	Chronozone 6	$\gamma = 2.15$ $\phi = 44.5$ $W = 27$	TOC=0.32 $CaCO_3 = 11$	1	0.5					<p>NANNOFOSSIL-BEARING SILTY CLAYSTONE AND SILTY CLAYSTONE</p> <p>Nannofossil-bearing silty claystone and silty claystone, dark gray (5Y 4/1), with large burrows parallel to bedding, and smaller burrows more or less concentrated in layers. In the top of Section 3, there are thinly laminated beds, ~1 cm thick, each capped by burrowed sediment, suggesting emplacement by turbidity currents.</p> <p>SMEAR SLIDE SUMMARY (%):</p> <table border="0"> <tr> <td></td> <td>1, 83</td> <td>CC, 28</td> </tr> <tr> <td>D</td> <td></td> <td>D</td> </tr> </table> <p>TEXTURE:</p> <table border="0"> <tr> <td>Sand</td> <td>Tr</td> <td>—</td> </tr> <tr> <td>Silt</td> <td>40</td> <td>45</td> </tr> <tr> <td>Clay</td> <td>60</td> <td>55</td> </tr> </table> <p>COMPOSITION:</p> <table border="0"> <tr> <td>Quartz</td> <td>40</td> <td>30</td> </tr> <tr> <td>Mica</td> <td>—</td> <td>Tr</td> </tr> <tr> <td>Clay</td> <td>50</td> <td>50</td> </tr> <tr> <td>Calcite/dolomite</td> <td>2</td> <td>Tr</td> </tr> <tr> <td>Accessory minerals</td> <td>2</td> <td>4</td> </tr> <tr> <td>Pyrite</td> <td>1</td> <td>3</td> </tr> <tr> <td>Unspecified</td> <td>—</td> <td>13</td> </tr> <tr> <td>Foraminifers</td> <td>—</td> <td>Tr</td> </tr> <tr> <td>Nannofossils</td> <td>10</td> <td>1</td> </tr> <tr> <td>Sponge spicules</td> <td>—</td> <td>Tr</td> </tr> <tr> <td>Plant debris</td> <td>—</td> <td>Tr</td> </tr> </table>		1, 83	CC, 28	D		D	Sand	Tr	—	Silt	40	45	Clay	60	55	Quartz	40	30	Mica	—	Tr	Clay	50	50	Calcite/dolomite	2	Tr	Accessory minerals	2	4	Pyrite	1	3	Unspecified	—	13	Foraminifers	—	Tr	Nannofossils	10	1	Sponge spicules	—	Tr	Plant debris	—	Tr
	1, 83	CC, 28																																																													
D		D																																																													
Sand	Tr	—																																																													
Silt	40	45																																																													
Clay	60	55																																																													
Quartz	40	30																																																													
Mica	—	Tr																																																													
Clay	50	50																																																													
Calcite/dolomite	2	Tr																																																													
Accessory minerals	2	4																																																													
Pyrite	1	3																																																													
Unspecified	—	13																																																													
Foraminifers	—	Tr																																																													
Nannofossils	10	1																																																													
Sponge spicules	—	Tr																																																													
Plant debris	—	Tr																																																													
								2	1.0																																																						
								3		VOID																																																					
								CC																																																							

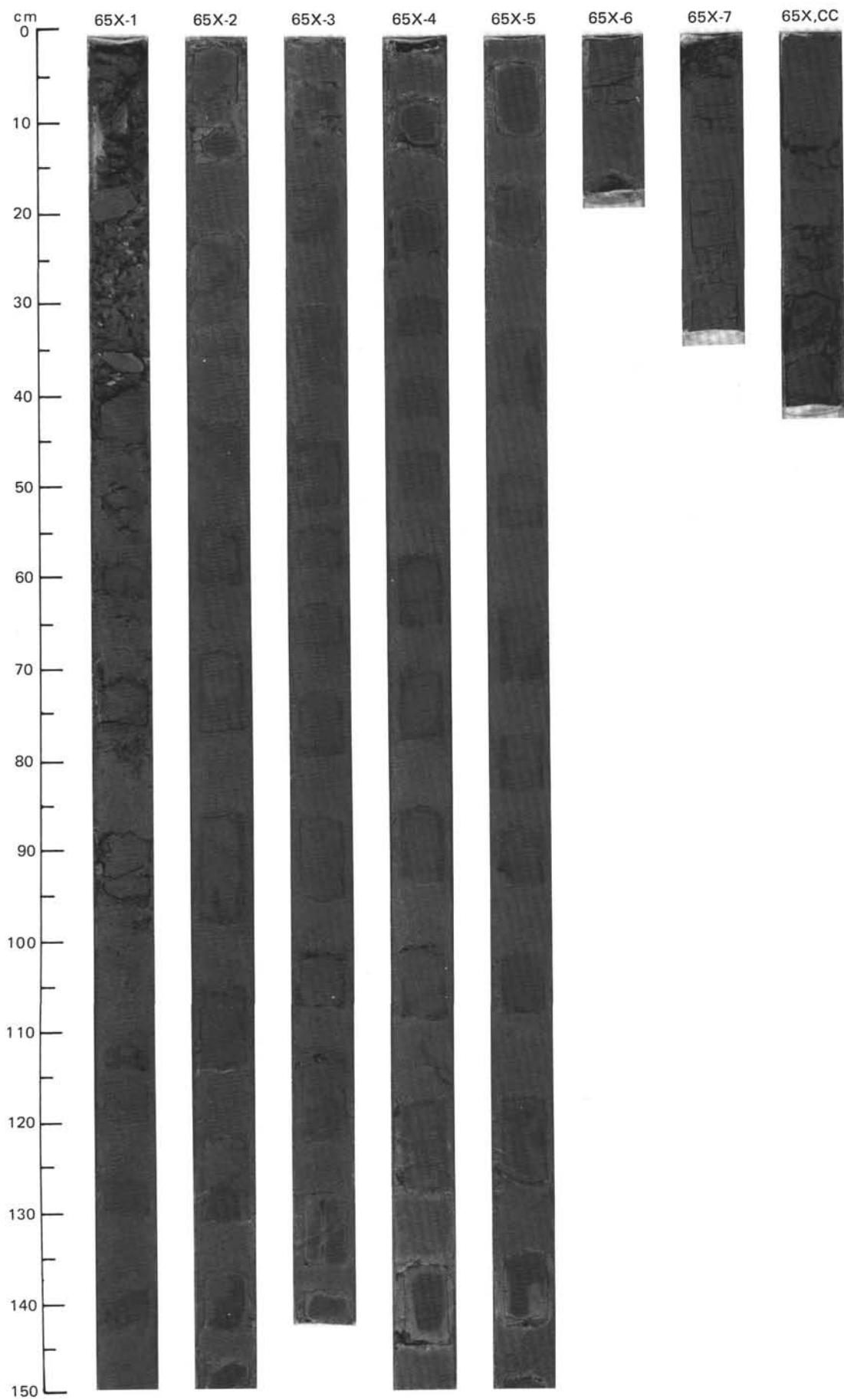
SITE 646 HOLE B CORE 64 X CORED INTERVAL 4051.1-4060.7 mbsl; 602.9-612.5 mbsf

TIME-ROCK UNIT	BIOSTRAT. ZONE/ FOSSIL CHARACTER					PALEOMAGNETICS	PHYS. PROPERTIES	CHEMISTRY	SECTION	METERS	GRAPHIC LITHOLOGY	DRILLING DISTURB.	SED. STRUCTURES	SAMPLES	LITHOLOGIC DESCRIPTION																				
	FORAMINIFERS	NANNOFOSSILS	RADIOLARIANS	DIATOMS	DINOCTYSTS																														
UPPER MIOCENE	A/G	A/M	B	B	F/M				1	0.5					<p>NANNOFOSSIL SILTY CLAYSTONE</p> <p>This core is entirely drilling slurry, except for a single biscuit taken from the top of Section 1, and consisting of gray (5Y 5/1) nannofossil silty claystone with scattered foraminifers.</p> <p>SMEAR SLIDE SUMMARY (%):</p> <table border="0"> <tr> <td></td> <td>1, 20</td> </tr> <tr> <td>D</td> <td></td> </tr> </table> <p>TEXTURE:</p> <table border="0"> <tr> <td>Silt</td> <td>45</td> </tr> <tr> <td>Clay</td> <td>55</td> </tr> </table> <p>COMPOSITION:</p> <table border="0"> <tr> <td>Quartz</td> <td>15</td> </tr> <tr> <td>Clay</td> <td>48</td> </tr> <tr> <td>Accessory minerals</td> <td>1</td> </tr> <tr> <td>Pyrite</td> <td>1</td> </tr> <tr> <td>Foraminifers</td> <td>Tr</td> </tr> <tr> <td>Nannofossils</td> <td>35</td> </tr> </table>		1, 20	D		Silt	45	Clay	55	Quartz	15	Clay	48	Accessory minerals	1	Pyrite	1	Foraminifers	Tr	Nannofossils	35
	1, 20																																		
D																																			
Silt	45																																		
Clay	55																																		
Quartz	15																																		
Clay	48																																		
Accessory minerals	1																																		
Pyrite	1																																		
Foraminifers	Tr																																		
Nannofossils	35																																		
								2	1.0	Drilling Slurry																									
								CC																											



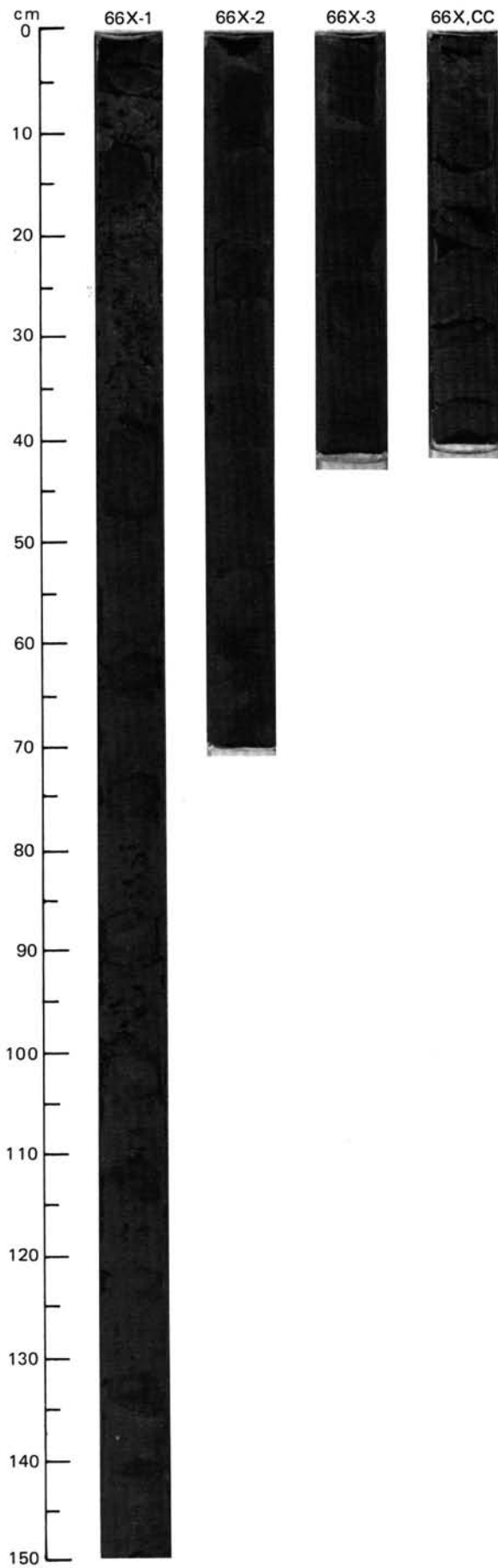
SITE 646 HOLE B CORE 65 X CORED INTERVAL 4060.7-4070.4 mbsl; 612.5-622.2 mbsf

TIME-ROCK UNIT		BIOSTRAT. ZONE/ FOSSIL CHARACTER	SECTION	METERS	GRAPHIC LITHOLOGY	DRILLING DISTURB.	SED. STRUCTURES	SAMPLES	LITHOLOGIC DESCRIPTION																																																				
FORAMINIFERS	NANNOFOSSILS																																																												
C/M	A/G	UPPER MIOCENE ?M11-M12 NN15 or older							<p>SILTY CLAYSTONE AND NANNOFOSSIL-BEARING SILTY CLAYSTONE</p> <p>Silty claystone, dark gray (5Y 4/1), distinctly bioturbated with burrows parallel to bedding, mostly of <i>Zoophycos</i> and <i>Planolites</i> type. A few scattered white foraminifers occur.</p> <p>Nannofossil-bearing silty claystone, greenish gray (5GY 5/1), very distinctly bioturbated by bedding-parallel <i>Zoophycos</i> and <i>Planolites</i>. A third type, as much as 12 mm in diameter, and without internal structure, was noted. White foraminifers are common.</p> <p>SMEAR SLIDE SUMMARY (%):</p> <table border="1"> <tr> <td></td> <td>2, 92</td> <td>4, 121</td> <td>5, 67</td> </tr> <tr> <td>D</td> <td>D</td> <td>D</td> <td>D</td> </tr> </table> <p>TEXTURE:</p> <table border="1"> <tr> <td>Silt</td> <td>25</td> <td>35</td> <td>40</td> </tr> <tr> <td>Clay</td> <td>75</td> <td>65</td> <td>60</td> </tr> </table> <p>COMPOSITION:</p> <table border="1"> <tr> <td>Quartz</td> <td>25</td> <td>35</td> <td>15</td> </tr> <tr> <td>Feldspar</td> <td>2</td> <td>3</td> <td>1</td> </tr> <tr> <td>Mica</td> <td>Tr</td> <td>Tr</td> <td>Tr</td> </tr> <tr> <td>Clay</td> <td>69</td> <td>47</td> <td>67</td> </tr> <tr> <td>Volcanic glass</td> <td>—</td> <td>Tr</td> <td>—</td> </tr> <tr> <td>Calcite/dolomite</td> <td>1</td> <td>5</td> <td>1</td> </tr> <tr> <td>Accessory minerals</td> <td>1</td> <td>Tr</td> <td>1</td> </tr> <tr> <td>Foraminifers</td> <td>—</td> <td>Tr</td> <td>—</td> </tr> <tr> <td>Nannofossils</td> <td>2</td> <td>10</td> <td>15</td> </tr> </table>		2, 92	4, 121	5, 67	D	D	D	D	Silt	25	35	40	Clay	75	65	60	Quartz	25	35	15	Feldspar	2	3	1	Mica	Tr	Tr	Tr	Clay	69	47	67	Volcanic glass	—	Tr	—	Calcite/dolomite	1	5	1	Accessory minerals	1	Tr	1	Foraminifers	—	Tr	—	Nannofossils	2	10	15
	2, 92		4, 121	5, 67																																																									
D	D		D	D																																																									
Silt	25		35	40																																																									
Clay	75		65	60																																																									
Quartz	25		35	15																																																									
Feldspar	2		3	1																																																									
Mica	Tr	Tr	Tr																																																										
Clay	69	47	67																																																										
Volcanic glass	—	Tr	—																																																										
Calcite/dolomite	1	5	1																																																										
Accessory minerals	1	Tr	1																																																										
Foraminifers	—	Tr	—																																																										
Nannofossils	2	10	15																																																										
B	B																																																												
F/G																																																													
		Chronozone 6																																																											
		● $\gamma = 2.15$ $\phi = 45.8$ $w = 28$ ●																																																											
		● $\gamma = 2.24$ $\phi = 46.2$ $w = 27$ ●																																																											
		● TOC=0.32 CaCO ₃ =16.0 ●																																																											
		● CaCO ₃ =13.0 ●																																																											
			1	0.5																																																									
			2	1.0																																																									
			3																																																										
			4																																																										
			5																																																										
			6		VOID																																																								
			7																																																										
C/C																																																													

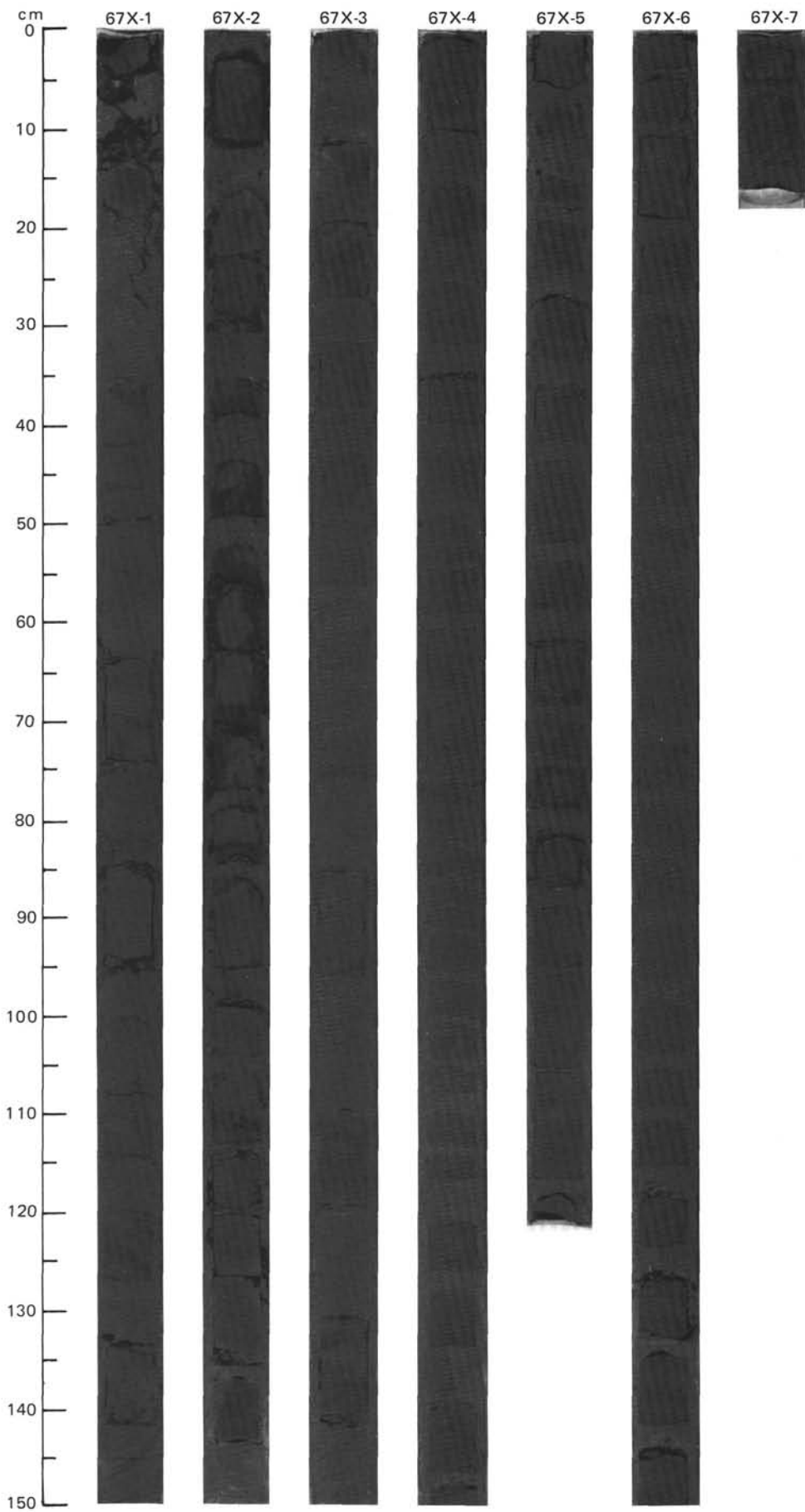


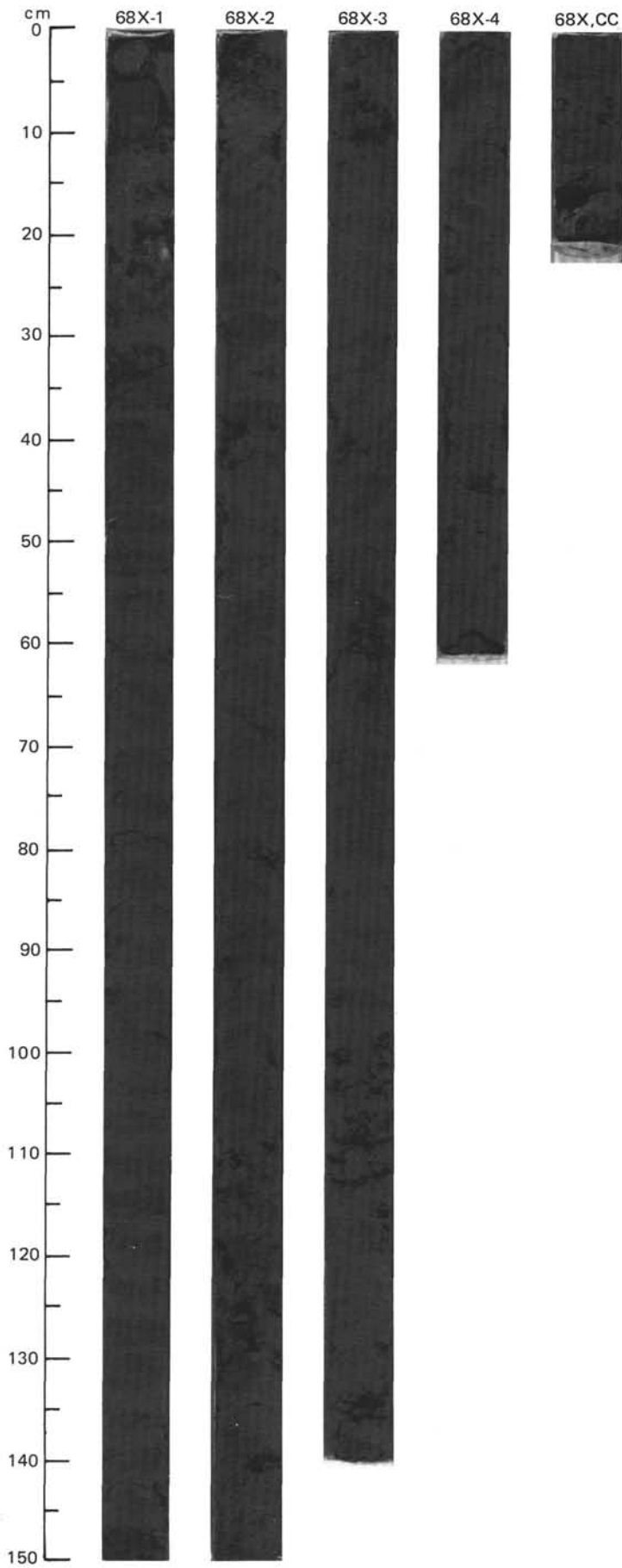
SITE 646 HOLE B CORE 66X CORED INTERVAL 4070.4-4080.0 mbsl; 622.2-631.8 mbsf

TIME-ROCK UNIT		BIOSTRAT. ZONE/ FOSSIL CHARACTER		PALEOMAGNETICS	PHYS. PROPERTIES	CHEMISTRY	SECTION	METERS	GRAPHIC LITHOLOGY	DRILLING DISTURB.	SED. STRUCTURES	SAMPLES	LITHOLOGIC DESCRIPTION
FORAMINIFERS	NANNOFOSSILS	RADIOLARIANS	DIATOMS										
UPPER MIOCENE													
C/M	?M11 -M12							0.5					<p>NANNOFOSSIL-BEARING SILTY CLAYSTONE</p> <p>Nannofossil-bearing silty claystone, dark gray (5Y 4/1) with mottles and vague bands as dark as black. Burrows are abundant, resulting in color mottling. Some darker (nearly black) bands ~1 cm thick may reflect primary layering. Coiled foraminifers are scattered. Burrows are of <i>Planolites</i> type.</p> <p>SMEAR SLIDE SUMMARY (%):</p> <p style="text-align: right;">1, 88 D</p> <p>TEXTURE:</p> <p>Sand 2 Silt 43 Clay 55</p> <p>COMPOSITION:</p> <p>Quartz 20 Clay 40 Calcite/dolomite 1 Accessory minerals 4 Nannofossils 20 Pellets 15</p>
A/G	NN11						1.0	VOID					
B							2						
B							3						
F/G							C						
<p>● TOC=0.32 CaCO₃ = 6.5</p>													



TIME-ROCK UNIT	BIOSTRAT. ZONE/ FOSSIL CHARACTER					PHYS. PROPERTIES	CHEMISTRY	SECTION	METERS	GRAPHIC LITHOLOGY	DRILLING DISTURB.	SED. STRUCTURES	SAMPLES	LITHOLOGIC DESCRIPTION																																												
	FORAMINIFERS	NANNOFOSSILS	RADIOLARIANS	DIATOMS	DINOCTYSTS																																																					
UPPER MIOCENE																																																										
R/P	?M11-M12								0.5		X			<p>SILTY CLAYSTONE</p> <p>Silty claystone, dark gray (5Y 4/1) to greenish gray (5GY 5/1) and dark greenish gray (5GY 4/1), distinctly bioturbated with burrows, approximately parallel to bedding, of <i>Zoophycos</i>, <i>Planolites</i>, and other unidentified types. Silt-lined white tubes are scattered. Foraminifers and nannofossils are present and are most abundant in the more greenish lithologies. There are a few greenish color bands, 1-3 mm thick.</p> <p>SMEAR SLIDE SUMMARY (%):</p> <table border="1"> <tr> <td></td> <td>1, 138</td> <td>3, 86</td> <td>6, 18</td> </tr> <tr> <td>D</td> <td>D</td> <td>D</td> <td>D</td> </tr> </table> <p>TEXTURE:</p> <table border="1"> <tr> <td>Silt</td> <td>25</td> <td>35</td> <td>20</td> </tr> <tr> <td>Clay</td> <td>75</td> <td>65</td> <td>70</td> </tr> </table> <p>COMPOSITION:</p> <table border="1"> <tr> <td>Quartz</td> <td>25</td> <td>35</td> <td>35</td> </tr> <tr> <td>Feldspar</td> <td>Tr</td> <td>2</td> <td>1</td> </tr> <tr> <td>Mica</td> <td>Tr</td> <td>1</td> <td>Tr</td> </tr> <tr> <td>Clay</td> <td>72</td> <td>57</td> <td>62</td> </tr> <tr> <td>Calcite/dolomite</td> <td>Tr</td> <td>1</td> <td>1</td> </tr> <tr> <td>Accessory minerals</td> <td>1</td> <td>1</td> <td>1</td> </tr> <tr> <td>Nannofossils</td> <td>2</td> <td>3</td> <td>Tr</td> </tr> </table>		1, 138	3, 86	6, 18	D	D	D	D	Silt	25	35	20	Clay	75	65	70	Quartz	25	35	35	Feldspar	Tr	2	1	Mica	Tr	1	Tr	Clay	72	57	62	Calcite/dolomite	Tr	1	1	Accessory minerals	1	1	1	Nannofossils	2	3	Tr
	1, 138	3, 86	6, 18																																																							
D	D	D	D																																																							
Silt	25	35	20																																																							
Clay	75	65	70																																																							
Quartz	25	35	35																																																							
Feldspar	Tr	2	1																																																							
Mica	Tr	1	Tr																																																							
Clay	72	57	62																																																							
Calcite/dolomite	Tr	1	1																																																							
Accessory minerals	1	1	1																																																							
Nannofossils	2	3	Tr																																																							
F/G	NN15 or older								1.0			*																																														
B																																																										
B																																																										
R/G	Chronozone 7																																																									
						<ul style="list-style-type: none"> • $\gamma = 2.14$ $\phi = 47.3$ $w = 29$ • $\text{CaCO}_3 = 0$ 			2																																																	
						<ul style="list-style-type: none"> • $\gamma = 2.21$ $\phi = 45.5$ $w = 26$ • $\text{TOC} = 0.30$ $\text{CaCO}_3 = 7.1$ 			3			*																																														
									4																																																	
									5																																																	
									6			OG																																														
									7																																																	



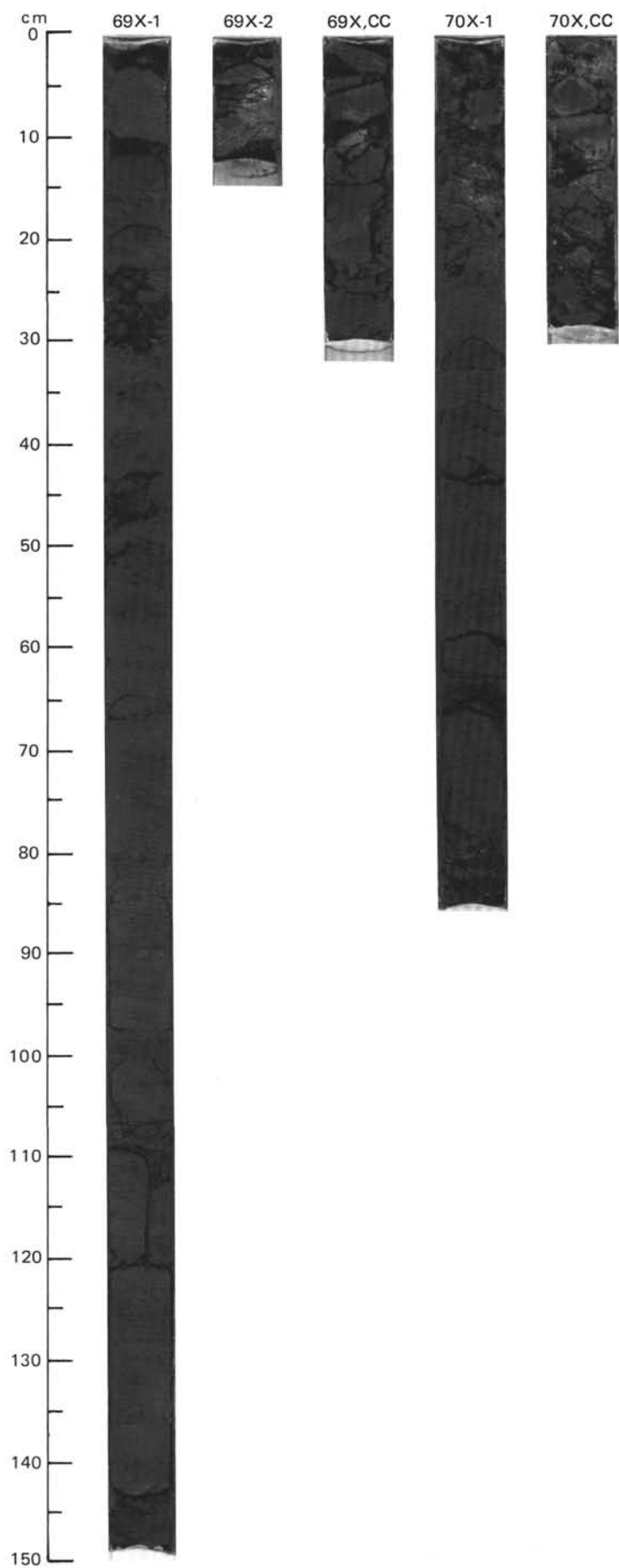


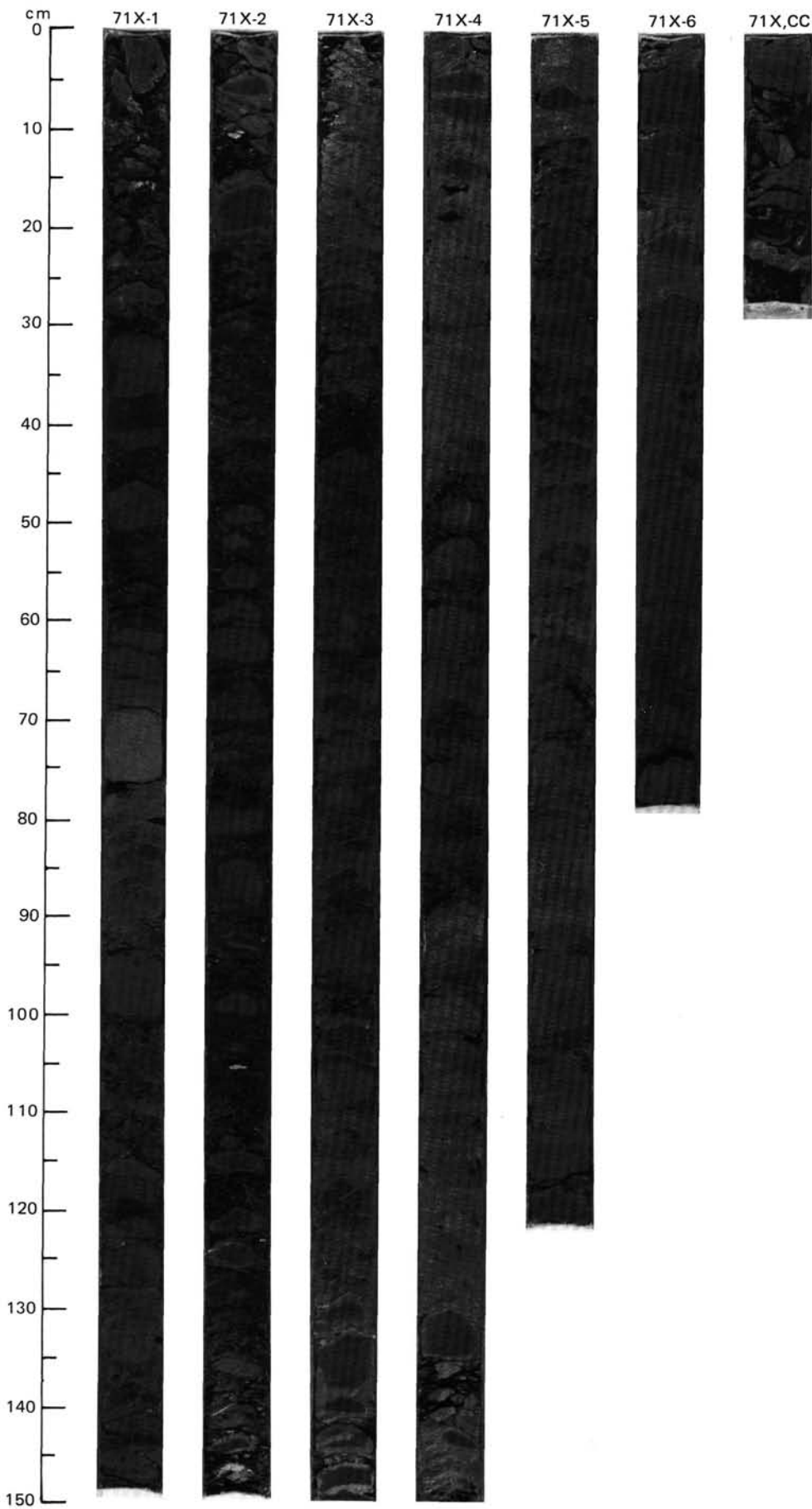
SITE 646 HOLE B CORE 69 X CORED INTERVAL 4099.1-4108.7 mbsl; 650.9-660.5 mbsf

TIME-ROCK UNIT	BIOSTRAT. ZONE/ FOSSIL CHARACTER					PALEOMAGNETICS	PHYS. PROPERTIES	CHEMISTRY	SECTION	METERS	GRAPHIC LITHOLOGY	DRILLING DISTURB.	SED. STRUCTURES	SAMPLES	LITHOLOGIC DESCRIPTION																																												
	FORAMINIFERS	NANNOFOSSILS	RADIOLARIANS	DIATOMS	DINOCTYSTS																																																						
UPPER MIOCENE	C/M	?M11-M12	R/G	NN15 or older	B		$\gamma = 2.18$ $\phi = 41.4$ $W = 24$	CaCO ₃ = 22	1	0.5 1.0	Drilling Slurry ⊗	⊗	**	<p>NANNOFOSSIL-BEARING SILTY CLAYSTONE AND SILTY CLAYSTONE</p> <p>Nannofossil-bearing silty claystone, dark gray (5Y 4/1), with intercalated layers and laminae (<1 cm thick) of silty claystone, black (5Y 2.5/1), thoroughly bioturbated with distinct gray (5Y 5/1) burrows. Scattered throughout are white silt-lined worm tubes and foraminifer tests.</p> <p>SMEAR SLIDE SUMMARY (%):</p> <table border="0"> <tr> <td></td> <td>1, 136</td> <td>1, 140</td> </tr> <tr> <td>D</td> <td>D</td> <td>D</td> </tr> </table> <p>TEXTURE:</p> <table border="0"> <tr> <td>Sand</td> <td>1</td> <td>3</td> </tr> <tr> <td>Silt</td> <td>39</td> <td>47</td> </tr> <tr> <td>Clay</td> <td>60</td> <td>50</td> </tr> </table> <p>COMPOSITION:</p> <table border="0"> <tr> <td>Quartz</td> <td>29</td> <td>40</td> </tr> <tr> <td>Feldspar</td> <td>—</td> <td>6</td> </tr> <tr> <td>Clay</td> <td>40</td> <td>45</td> </tr> <tr> <td>Calcite/dolomite</td> <td>—</td> <td>1</td> </tr> <tr> <td>Accessory minerals</td> <td>3</td> <td>5</td> </tr> <tr> <td>Pyrite</td> <td>1</td> <td>1</td> </tr> <tr> <td>Glaucinite</td> <td>—</td> <td>Tr</td> </tr> <tr> <td>Nannofossils</td> <td>20</td> <td>2</td> </tr> <tr> <td>Plant debris</td> <td>—</td> <td>Tr</td> </tr> <tr> <td>Pellets</td> <td>7</td> <td>5</td> </tr> </table>		1, 136	1, 140	D	D	D	Sand	1	3	Silt	39	47	Clay	60	50	Quartz	29	40	Feldspar	—	6	Clay	40	45	Calcite/dolomite	—	1	Accessory minerals	3	5	Pyrite	1	1	Glaucinite	—	Tr	Nannofossils	20	2	Plant debris	—	Tr	Pellets	7	5
	1, 136	1, 140																																																									
D	D	D																																																									
Sand	1	3																																																									
Silt	39	47																																																									
Clay	60	50																																																									
Quartz	29	40																																																									
Feldspar	—	6																																																									
Clay	40	45																																																									
Calcite/dolomite	—	1																																																									
Accessory minerals	3	5																																																									
Pyrite	1	1																																																									
Glaucinite	—	Tr																																																									
Nannofossils	20	2																																																									
Plant debris	—	Tr																																																									
Pellets	7	5																																																									

SITE 646 HOLE B CORE 70 X CORED INTERVAL 4108.7-4118.4 mbsl; 660.5-670.2 mbsf

TIME-ROCK UNIT	BIOSTRAT. ZONE/ FOSSIL CHARACTER					PALEOMAGNETICS	PHYS. PROPERTIES	CHEMISTRY	SECTION	METERS	GRAPHIC LITHOLOGY	DRILLING DISTURB.	SED. STRUCTURES	SAMPLES	LITHOLOGIC DESCRIPTION																			
	FORAMINIFERS	NANNOFOSSILS	RADIOLARIANS	DIATOMS	DINOCTYSTS																													
UPPER MIOCENE	R/P	?M11-M12	C/G	NN11	B		$\gamma = 2.09$ $\phi = 43.4$ $W = 27$	TOC = 0.39 CaCO ₃ = 8.1	1	0.5			*	<p>NANNOFOSSIL-BEARING CLAYSTONE AND CLAYSTONE.</p> <p>Nannofossil-bearing claystone, dark gray (5Y 4/1) with intercalated layers of silty claystone, black (5Y 2.5/1), moderately bioturbated, with some larger burrows and scattered white silt-lined worm tubes.</p> <p>SMEAR SLIDE SUMMARY (%):</p> <table border="0"> <tr> <td></td> <td>1, 74</td> </tr> <tr> <td>D</td> <td>D</td> </tr> </table> <p>TEXTURE:</p> <table border="0"> <tr> <td>Silt</td> <td>10</td> </tr> <tr> <td>Clay</td> <td>90</td> </tr> </table> <p>COMPOSITION:</p> <table border="0"> <tr> <td>Quartz</td> <td>5</td> </tr> <tr> <td>Mica</td> <td>1</td> </tr> <tr> <td>Clay</td> <td>75</td> </tr> <tr> <td>Calcite/dolomite</td> <td>2</td> </tr> <tr> <td>Accessory minerals</td> <td>2</td> </tr> <tr> <td>Nannofossils</td> <td>15</td> </tr> </table>		1, 74	D	D	Silt	10	Clay	90	Quartz	5	Mica	1	Clay	75	Calcite/dolomite	2	Accessory minerals	2	Nannofossils	15
	1, 74																																	
D	D																																	
Silt	10																																	
Clay	90																																	
Quartz	5																																	
Mica	1																																	
Clay	75																																	
Calcite/dolomite	2																																	
Accessory minerals	2																																	
Nannofossils	15																																	



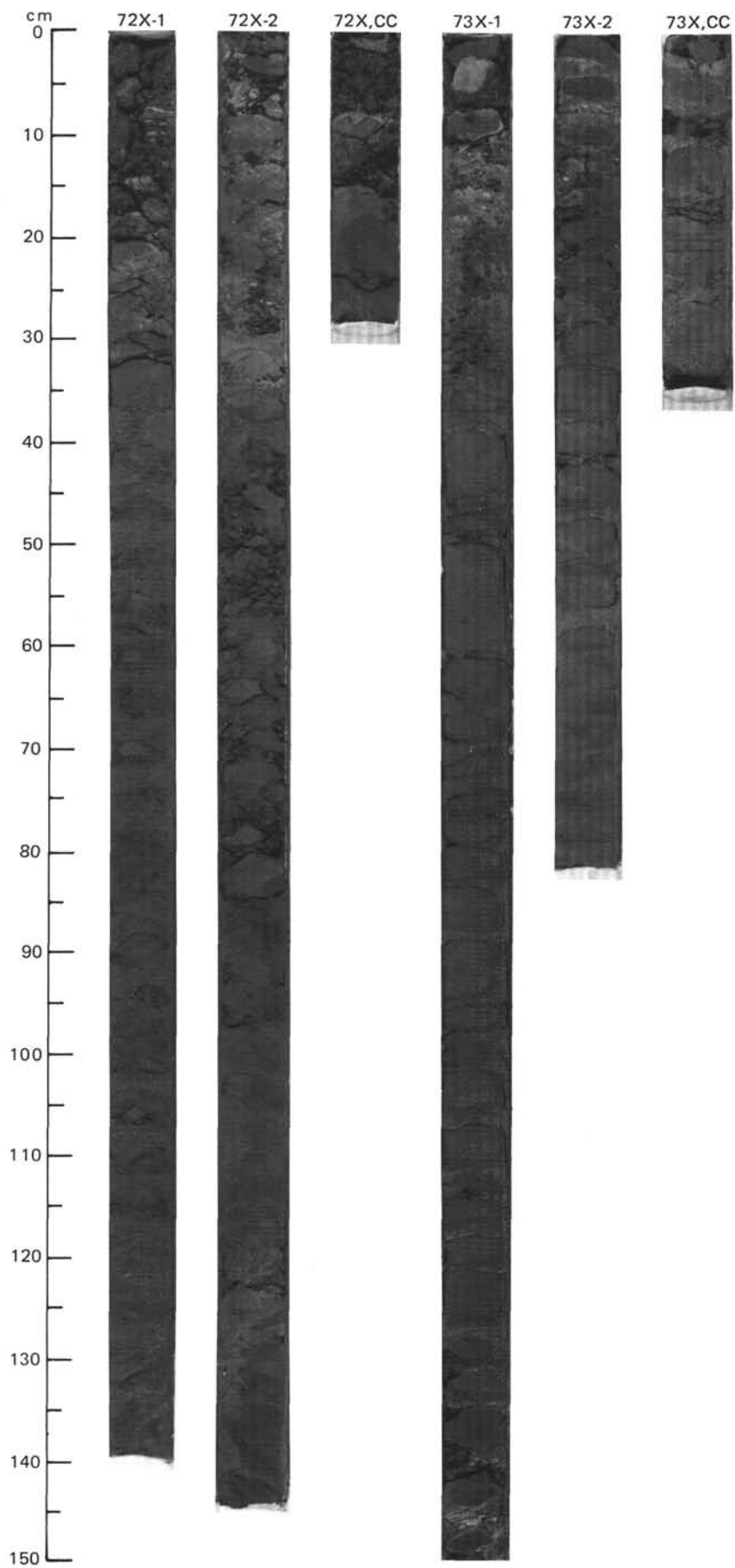


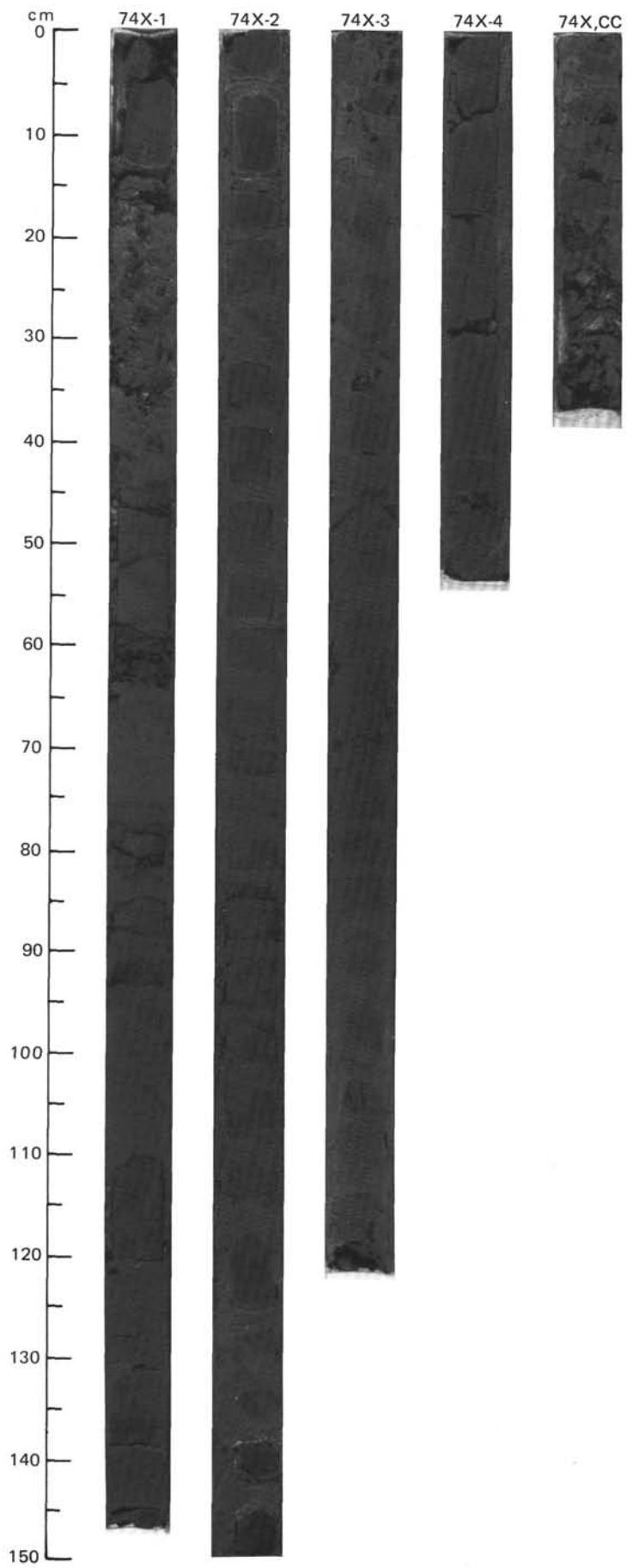
SITE 646 HOLE B CORE 72 X CORED INTERVAL 4127.9-4137.5 mbsl; 679.7-689.3 mbsf

TIME-ROCK UNIT	BIOSTRAT. ZONE/ FOSSIL CHARACTER					PALEOMAGNETICS	PHYS. PROPERTIES	CHEMISTRY	SECTION	METERS	GRAPHIC LITHOLOGY	DRILLING DISTURB.	SED. STRUCTURES	SAMPLES	LITHOLOGIC DESCRIPTION																																																				
	FORAMINIFERS	NANNOFOSSILS	RADIOLARIANS	DIATOMS	DINOCYSTS																																																														
UPPER MIOCENE	C/M	?	M11-M12												<p>NANNOFOSSIL-BEARING SILTY CLAYSTONE</p> <p>Nannofossil-bearing silty claystone, olive gray (5Y 4/2) to dark gray (5Y 4/1); grading downward to silty claystone, very dark gray (10YR 3/1 and 5YR 3/1) to black (5YR 2.5/1); moderately bioturbated, with burrow fillings of dark grayish brown (2.5Y 4/2) sediment. Burrows become increasingly indistinct in the darker sediments at the bottom of the core.</p> <p>Minor lithologies: a. Section 2, 25-35 cm: nannofossil-bearing calcareous clayey siltstone, light brownish gray (2.5Y 6/2). b. Section 2, 118 cm: pyrite nodule, 1 x 3 cm.</p> <p>SMEAR SLIDE SUMMARY (%):</p> <table border="1"> <tr> <td></td> <td>1, 125</td> <td>2, 32</td> <td>CC, 21</td> </tr> <tr> <td></td> <td>D</td> <td>D</td> <td>D</td> </tr> </table> <p>TEXTURE:</p> <table border="1"> <tr> <td>Sand</td> <td>Tr</td> <td>1</td> <td>—</td> </tr> <tr> <td>Silt</td> <td>45</td> <td>54</td> <td>35</td> </tr> <tr> <td>Clay</td> <td>55</td> <td>45</td> <td>65</td> </tr> </table> <p>COMPOSITION:</p> <table border="1"> <tr> <td>Quartz</td> <td>25</td> <td>15</td> <td>41</td> </tr> <tr> <td>Feldspar</td> <td>5</td> <td>—</td> <td>—</td> </tr> <tr> <td>Mica</td> <td>Tr</td> <td>2</td> <td>—</td> </tr> <tr> <td>Clay</td> <td>45</td> <td>30</td> <td>55</td> </tr> <tr> <td>Calcite/dolomite</td> <td>5</td> <td>40</td> <td>—</td> </tr> <tr> <td>Accessory minerals</td> <td>—</td> <td>1</td> <td>2</td> </tr> <tr> <td>Pyrite</td> <td>Tr</td> <td>1</td> <td>2</td> </tr> <tr> <td>Nannofossils</td> <td>20</td> <td>10</td> <td>—</td> </tr> </table>		1, 125	2, 32	CC, 21		D	D	D	Sand	Tr	1	—	Silt	45	54	35	Clay	55	45	65	Quartz	25	15	41	Feldspar	5	—	—	Mica	Tr	2	—	Clay	45	30	55	Calcite/dolomite	5	40	—	Accessory minerals	—	1	2	Pyrite	Tr	1	2	Nannofossils	20	10	—
	1, 125	2, 32	CC, 21																																																																
	D	D	D																																																																
Sand	Tr	1	—																																																																
Silt	45	54	35																																																																
Clay	55	45	65																																																																
Quartz	25	15	41																																																																
Feldspar	5	—	—																																																																
Mica	Tr	2	—																																																																
Clay	45	30	55																																																																
Calcite/dolomite	5	40	—																																																																
Accessory minerals	—	1	2																																																																
Pyrite	Tr	1	2																																																																
Nannofossils	20	10	—																																																																
	A/G	NN11																																																																	

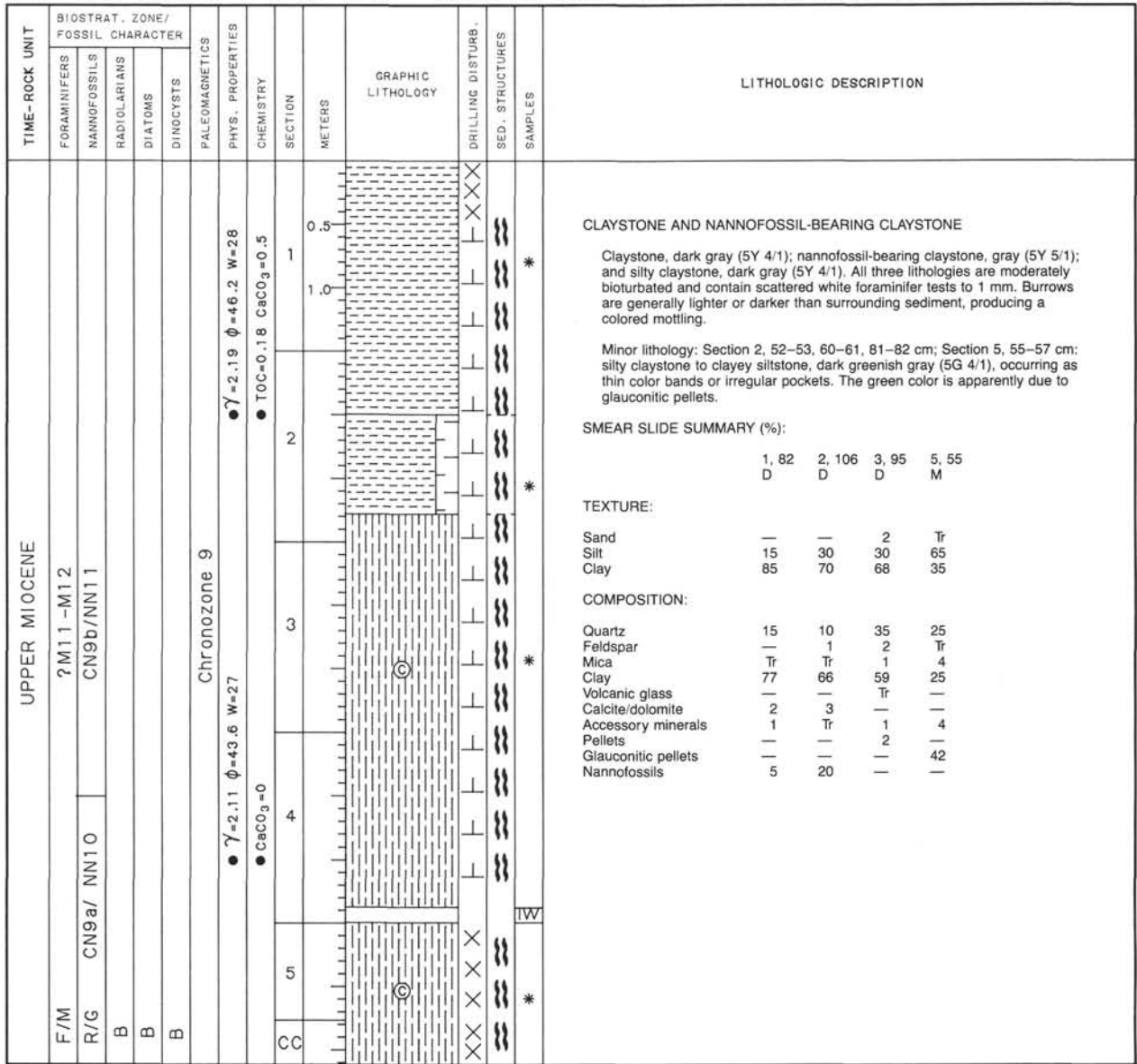
SITE 646 HOLE B CORE 73 X CORED INTERVAL 4137.5-4147.2 mbsl; 689.3-699.0 mbsf

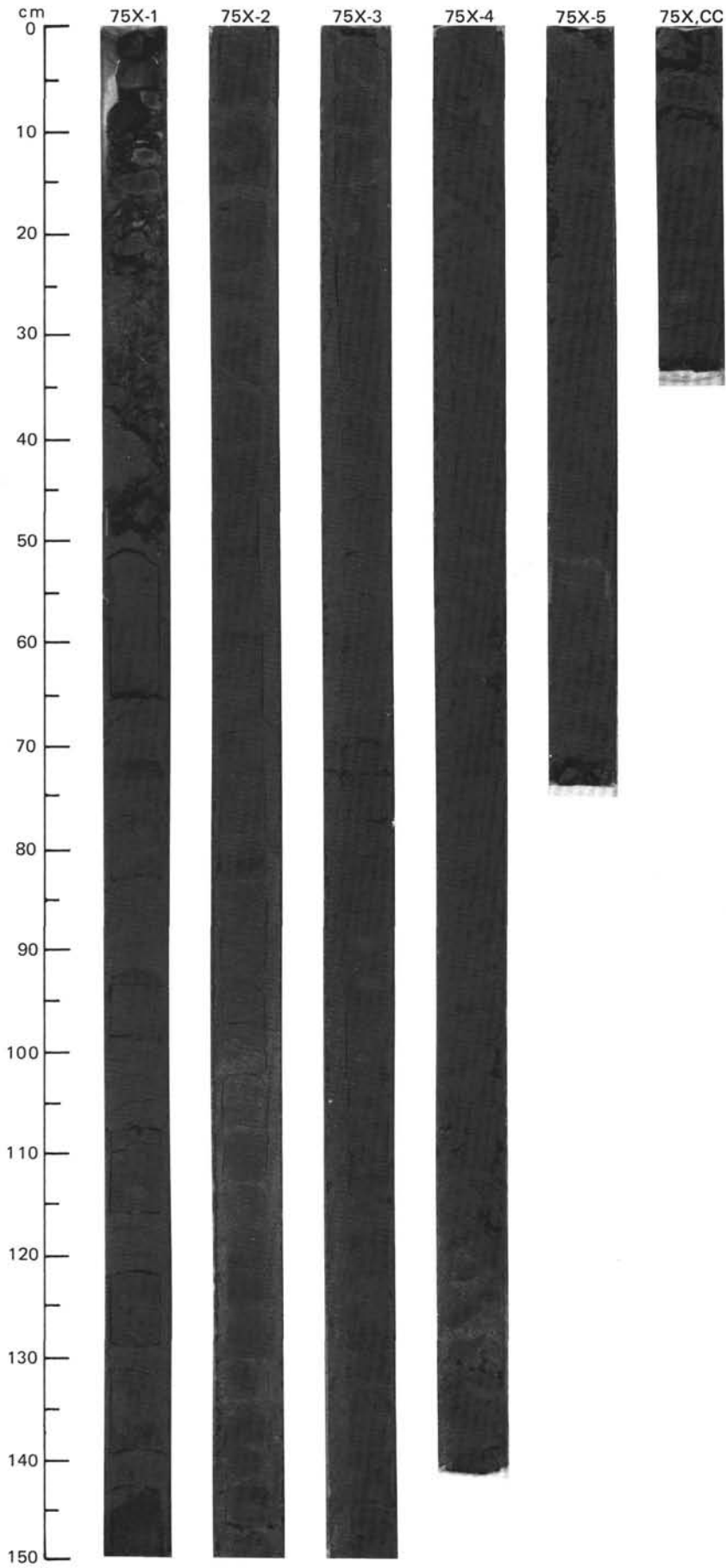
TIME-ROCK UNIT	BIOSTRAT. ZONE/ FOSSIL CHARACTER					PALEOMAGNETICS	PHYS. PROPERTIES	CHEMISTRY	SECTION	METERS	GRAPHIC LITHOLOGY	DRILLING DISTURB.	SED. STRUCTURES	SAMPLES	LITHOLOGIC DESCRIPTION																																										
	FORAMINIFERS	NANNOFOSSILS	RADIOLARIANS	DIATOMS	DINOCYSTS																																																				
UPPER MIOCENE	C/M	?	M11-M12												<p>NANNOFOSSIL-BEARING CLAYSTONE AND NANNOFOSSIL CLAYSTONE</p> <p>Nannofossil-bearing claystone, dark gray (5Y 4/1), moderately bioturbated, including <i>Planolites</i>. Burrows commonly have dark rims (sulfides?). Sediment is subtly color mottled. Some white silt-lined tubes and foraminifers are present.</p> <p>Nannofossil claystone, gray (5Y 5/1) with ~1-cm-spaced color bands of greenish gray (5G5/1) and gray (N5). Moderately bioturbated.</p> <p>SMEAR SLIDE SUMMARY (%):</p> <table border="1"> <tr> <td></td> <td>1, 92</td> <td>2, 55</td> </tr> <tr> <td></td> <td>D</td> <td>D</td> </tr> </table> <p>TEXTURE:</p> <table border="1"> <tr> <td>Sand</td> <td>1</td> <td>1</td> </tr> <tr> <td>Silt</td> <td>25</td> <td>40</td> </tr> <tr> <td>Clay</td> <td>74</td> <td>59</td> </tr> </table> <p>COMPOSITION:</p> <table border="1"> <tr> <td>Quartz</td> <td>15</td> <td>7</td> </tr> <tr> <td>Feldspar</td> <td>Tr</td> <td>Tr</td> </tr> <tr> <td>Mica</td> <td>Tr</td> <td>Tr</td> </tr> <tr> <td>Clay</td> <td>72</td> <td>54</td> </tr> <tr> <td>Calcite/dolomite</td> <td>2</td> <td>3</td> </tr> <tr> <td>Accessory minerals</td> <td>Tr</td> <td>Tr</td> </tr> <tr> <td>Pellets</td> <td>1</td> <td>1</td> </tr> <tr> <td>Foraminifers</td> <td>Tr</td> <td>Tr</td> </tr> <tr> <td>Nannofossils</td> <td>10</td> <td>35</td> </tr> </table>		1, 92	2, 55		D	D	Sand	1	1	Silt	25	40	Clay	74	59	Quartz	15	7	Feldspar	Tr	Tr	Mica	Tr	Tr	Clay	72	54	Calcite/dolomite	2	3	Accessory minerals	Tr	Tr	Pellets	1	1	Foraminifers	Tr	Tr	Nannofossils	10	35
	1, 92	2, 55																																																							
	D	D																																																							
Sand	1	1																																																							
Silt	25	40																																																							
Clay	74	59																																																							
Quartz	15	7																																																							
Feldspar	Tr	Tr																																																							
Mica	Tr	Tr																																																							
Clay	72	54																																																							
Calcite/dolomite	2	3																																																							
Accessory minerals	Tr	Tr																																																							
Pellets	1	1																																																							
Foraminifers	Tr	Tr																																																							
Nannofossils	10	35																																																							
	A/G	NN11																																																							

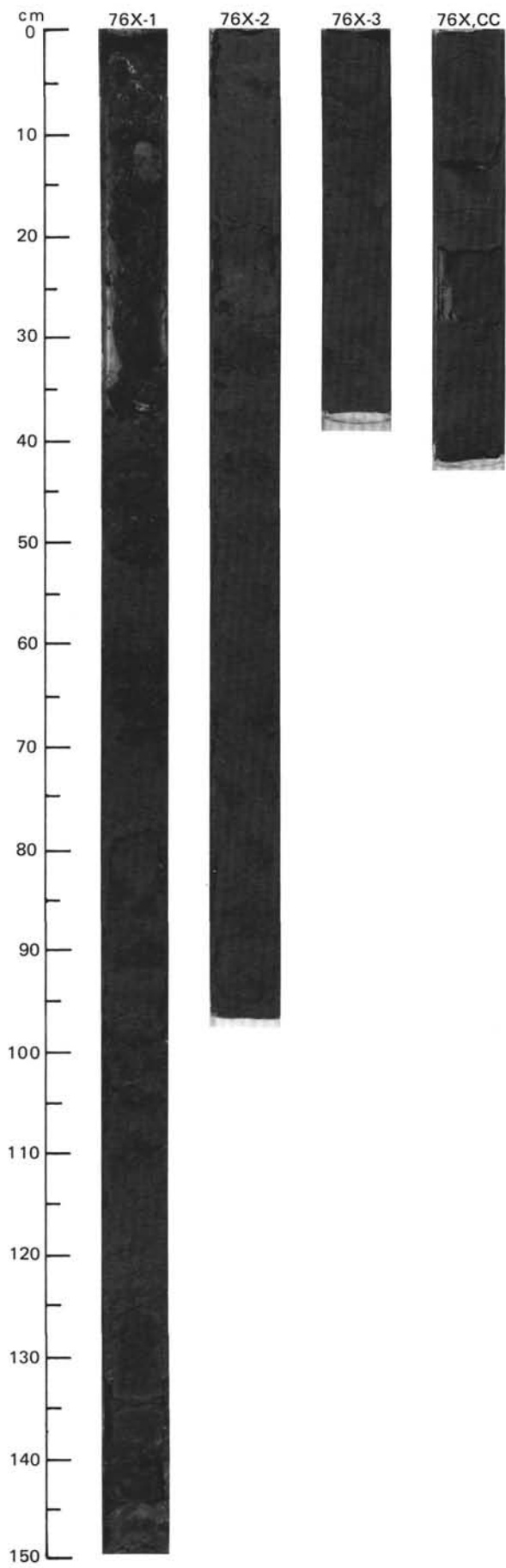


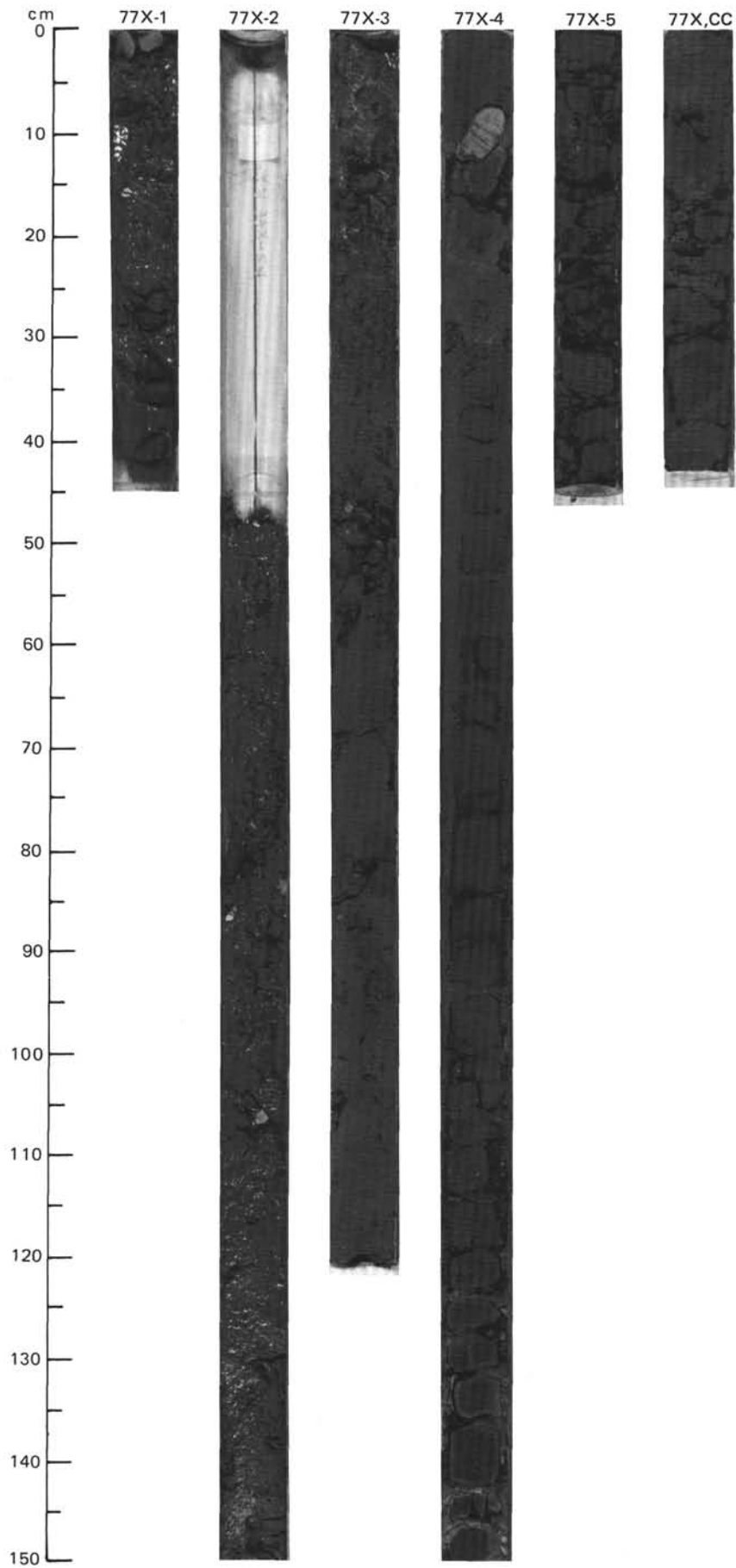


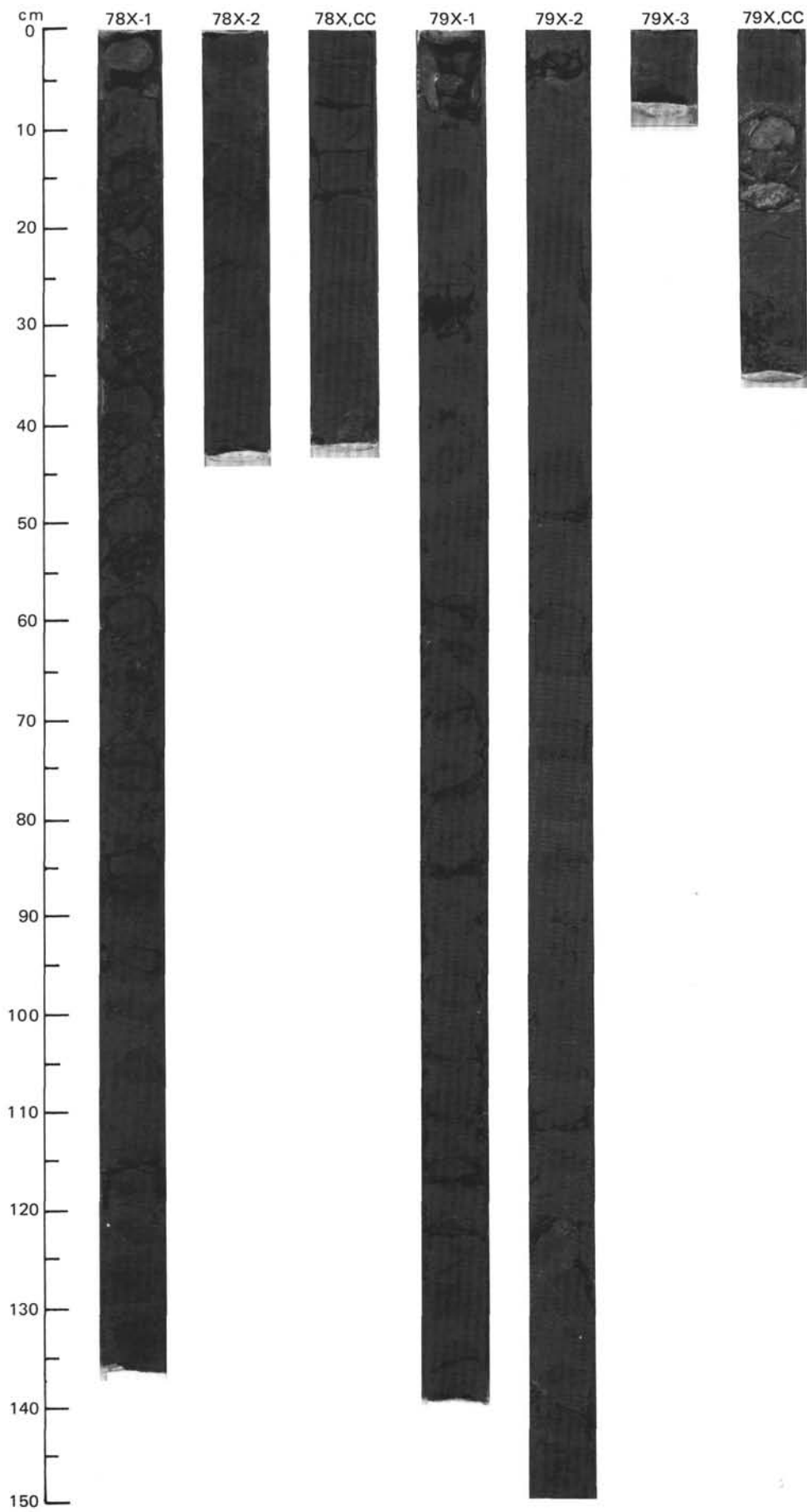
SITE 646 HOLE B CORE 75 X CORED INTERVAL 4156.8-4166.5 mbsf; 708.6-718.3 mbsf

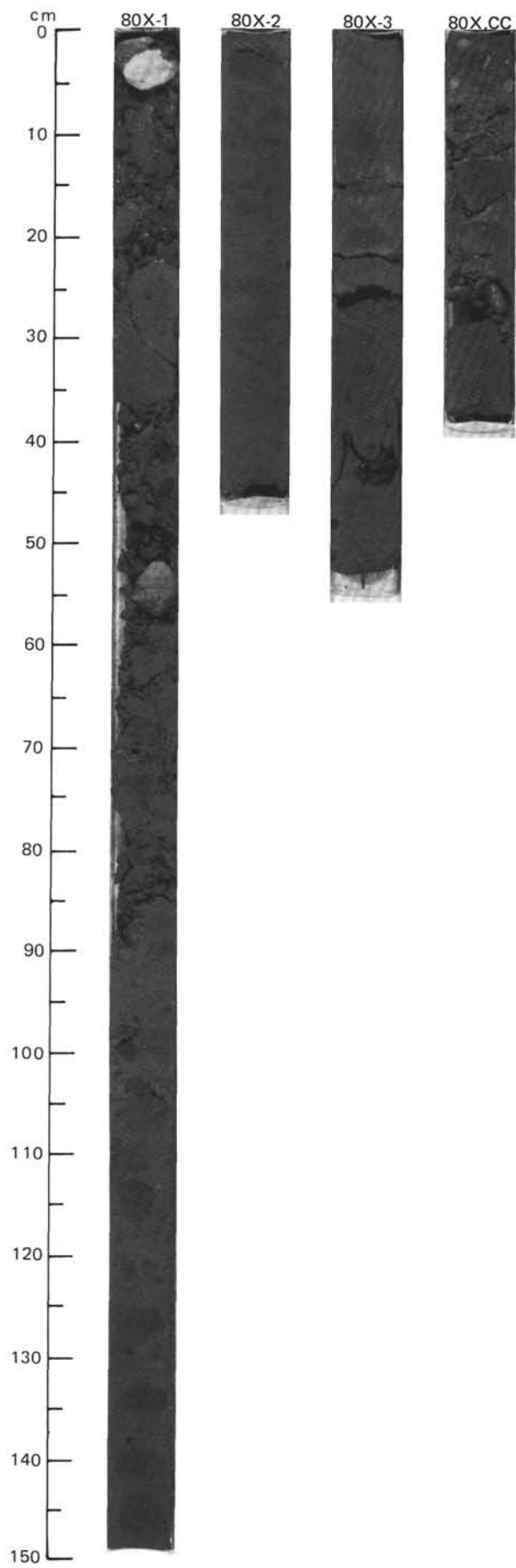




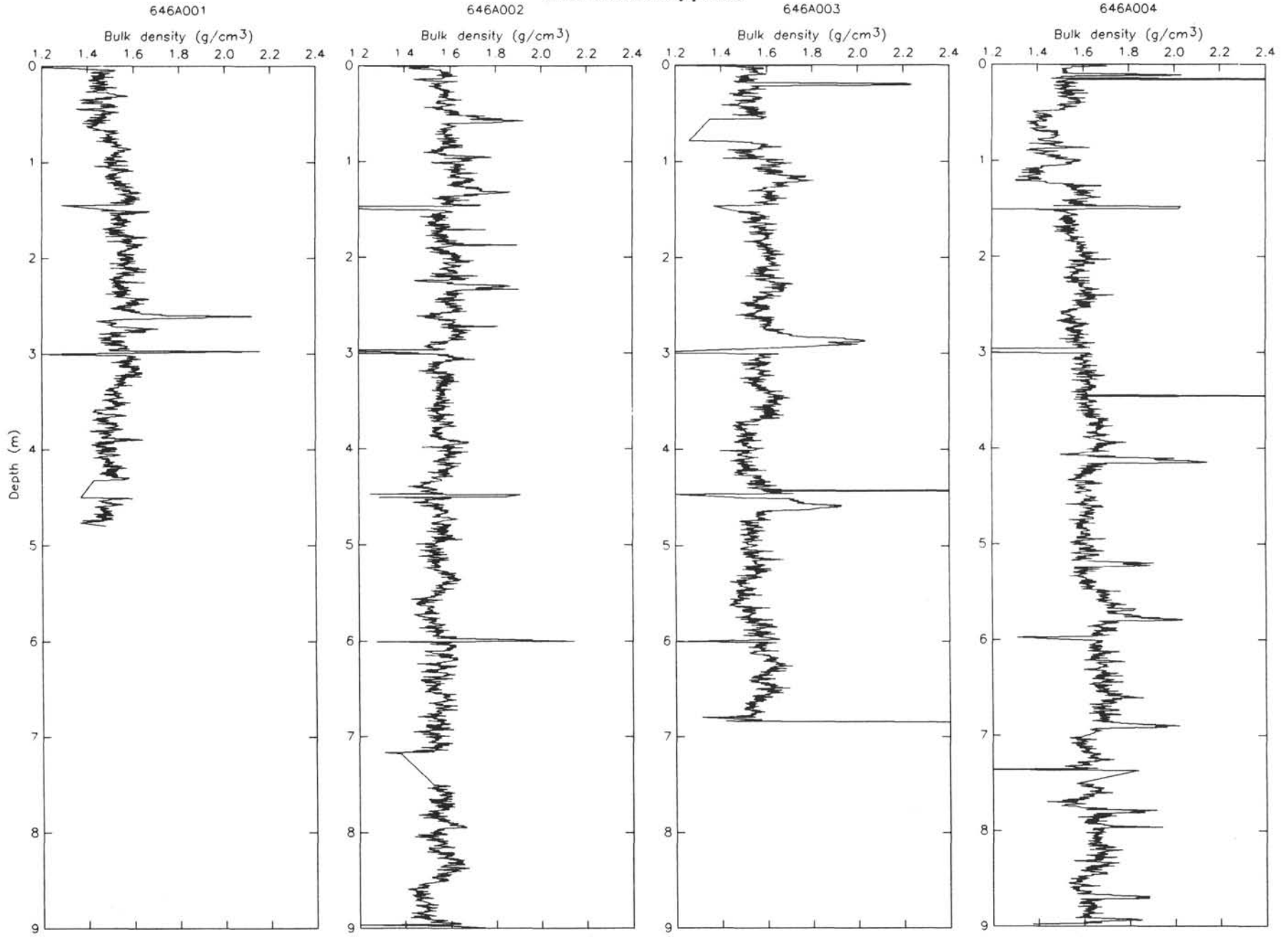




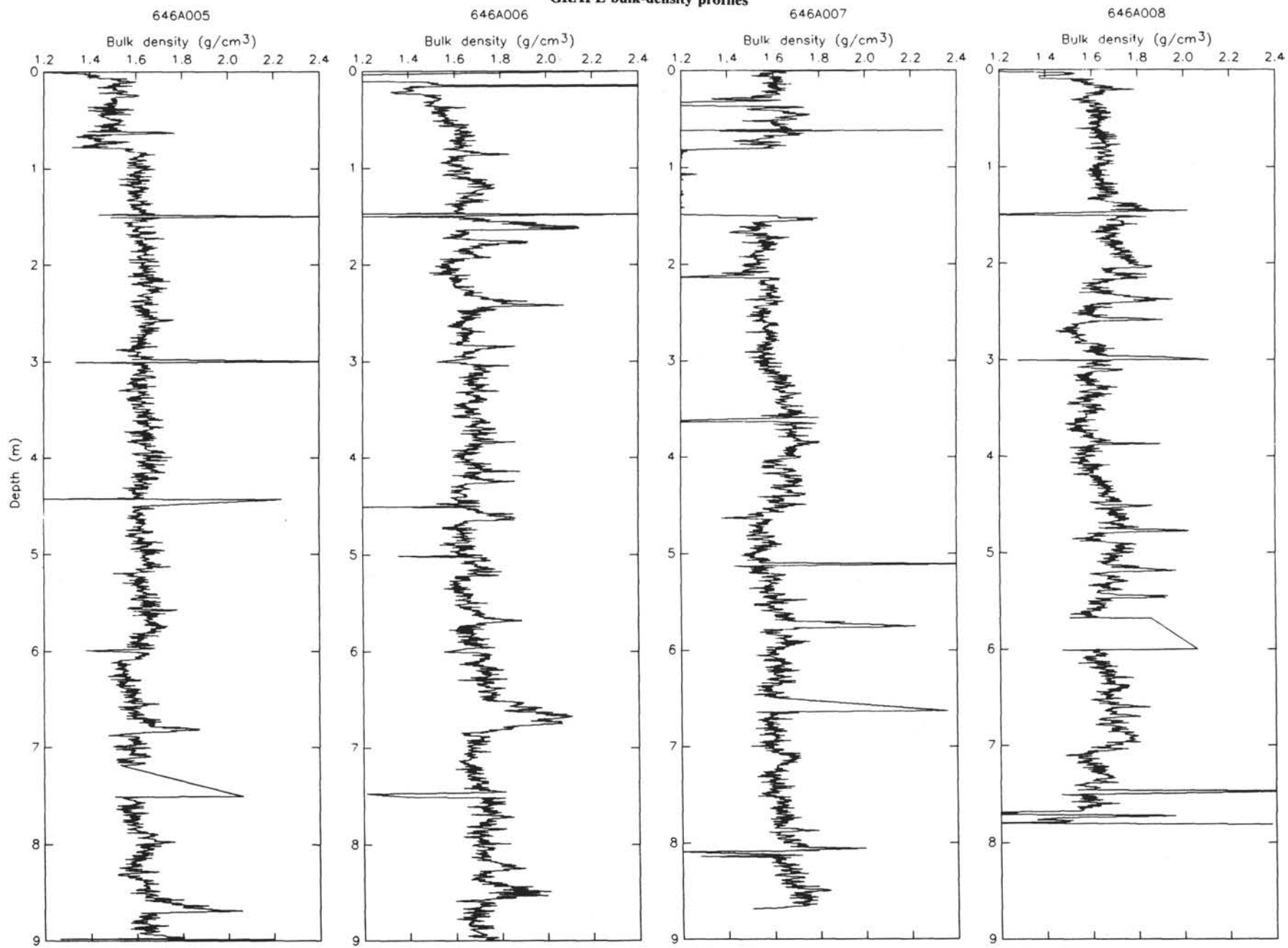




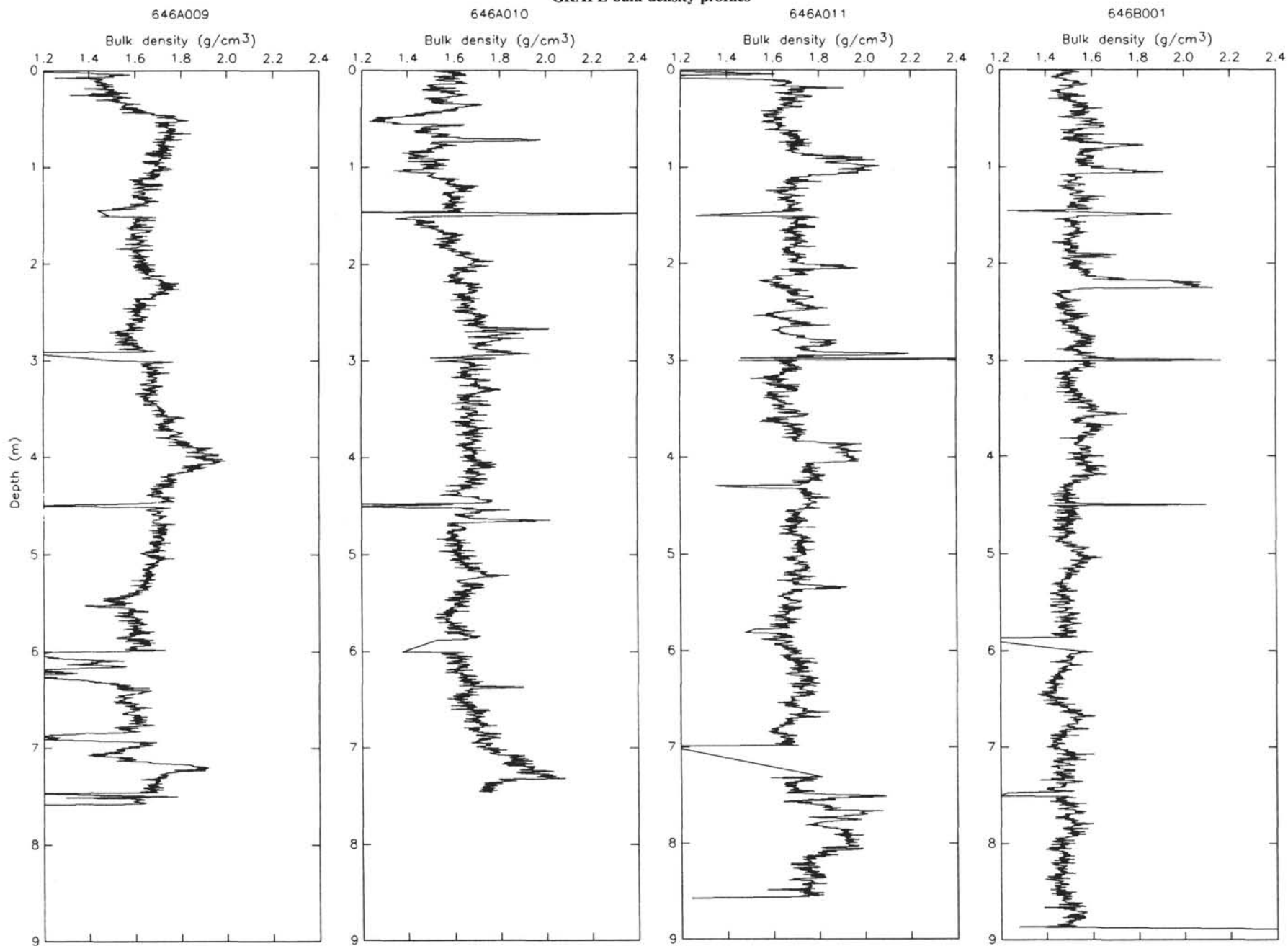
GRAPE bulk-density profiles



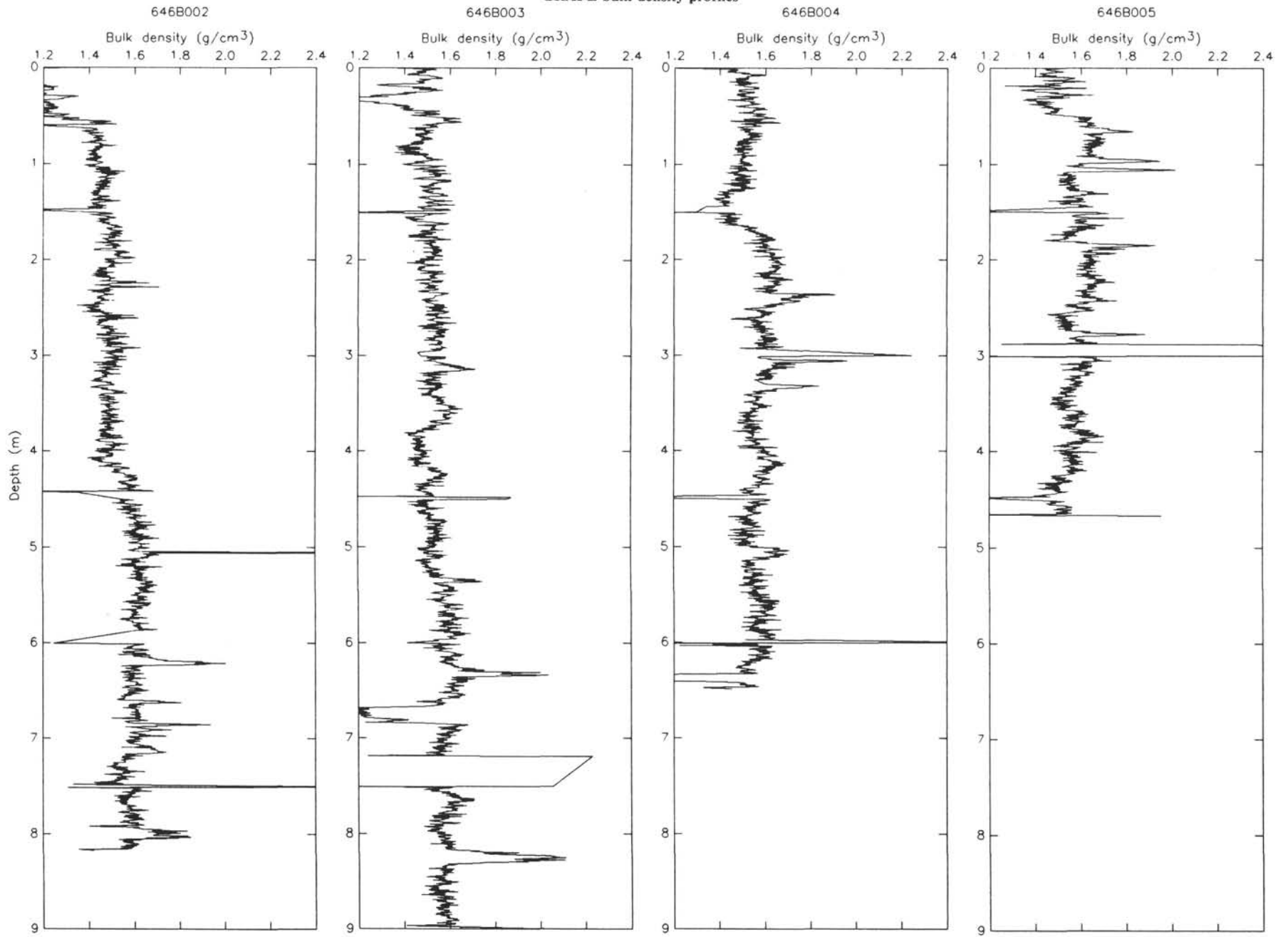
GRAPE bulk-density profiles



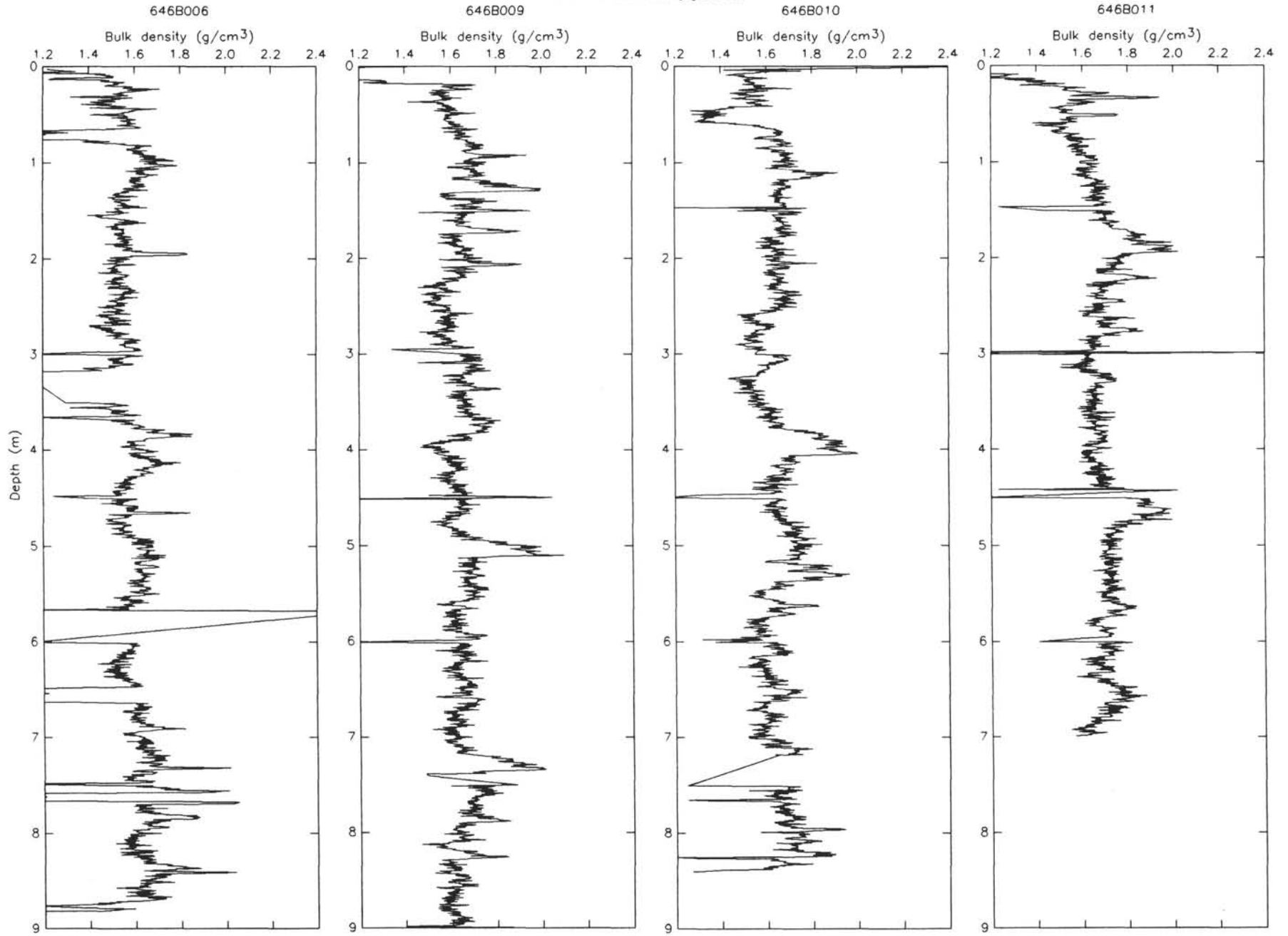
GRAPE bulk-density profiles



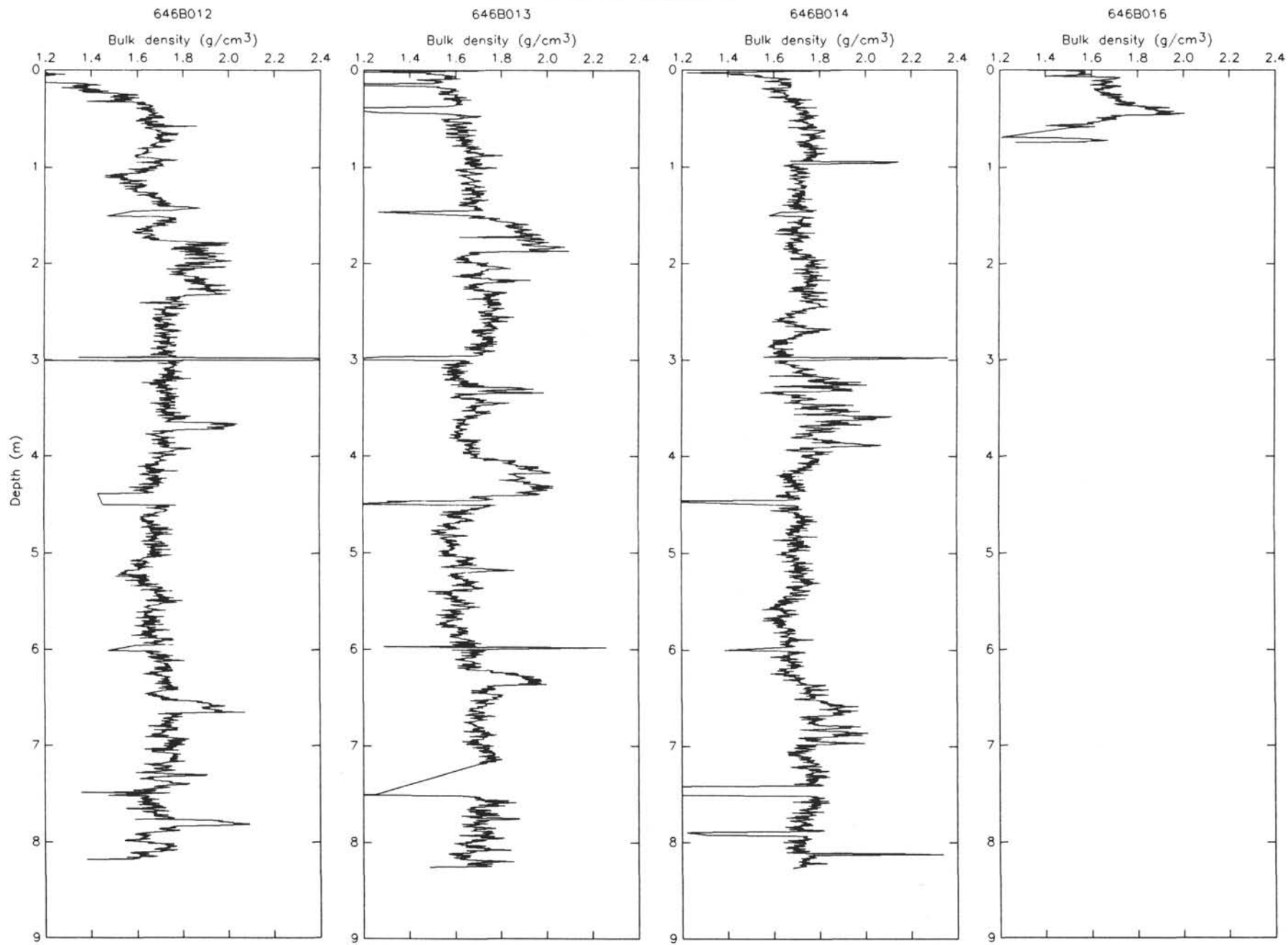
GRAPE bulk-density profiles



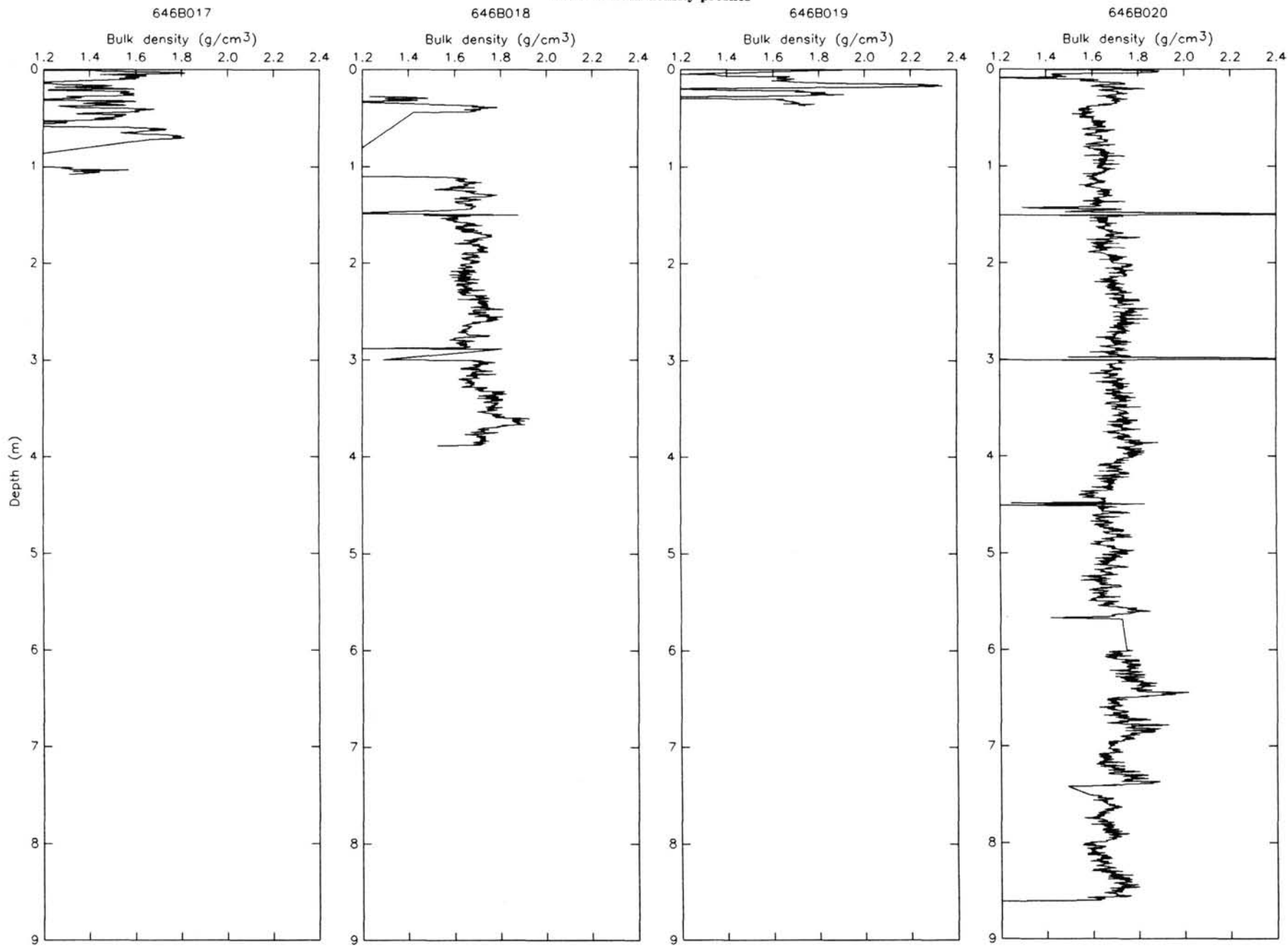
GRAPE bulk-density profiles



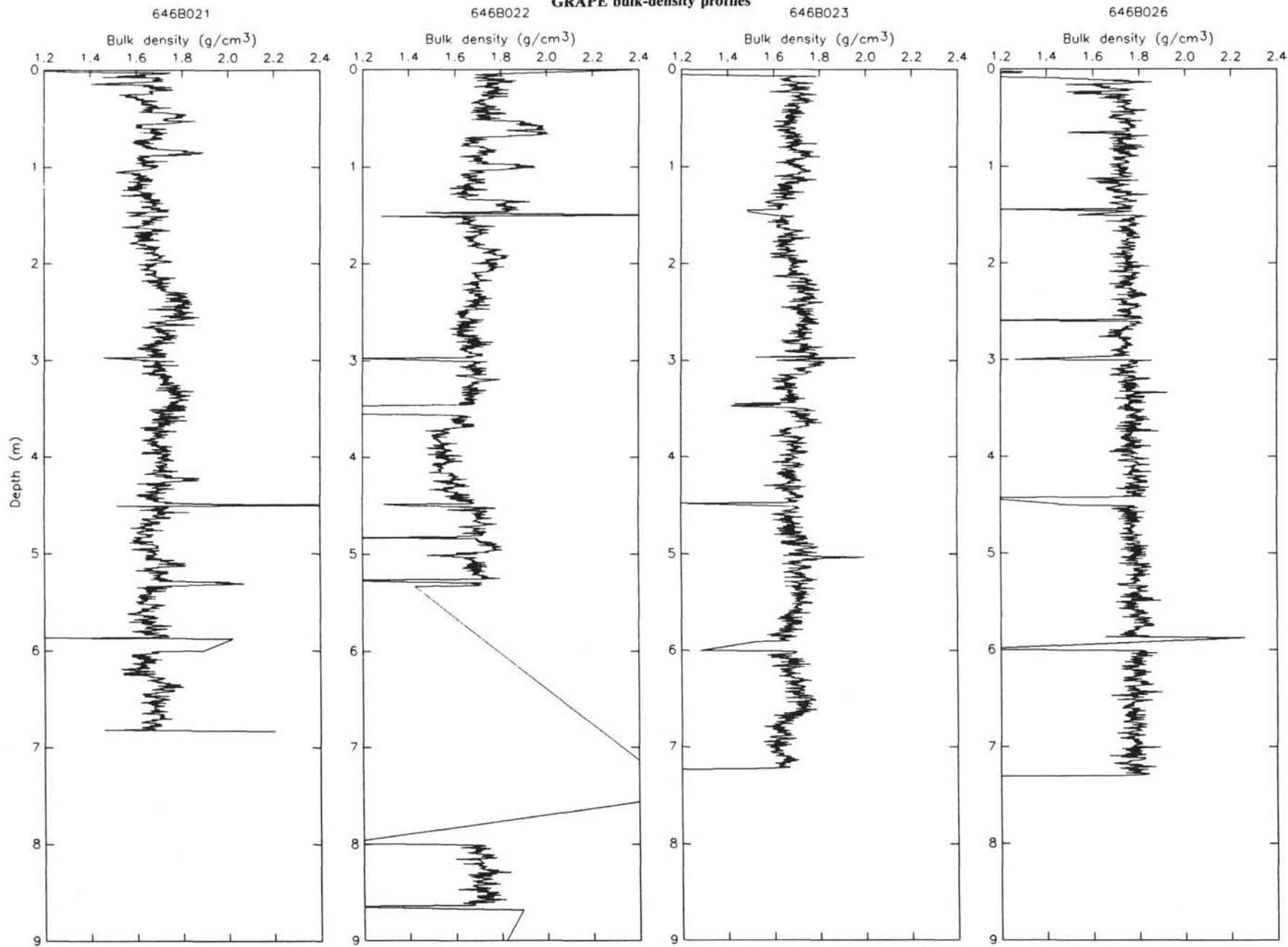
GRAPE bulk-density profiles



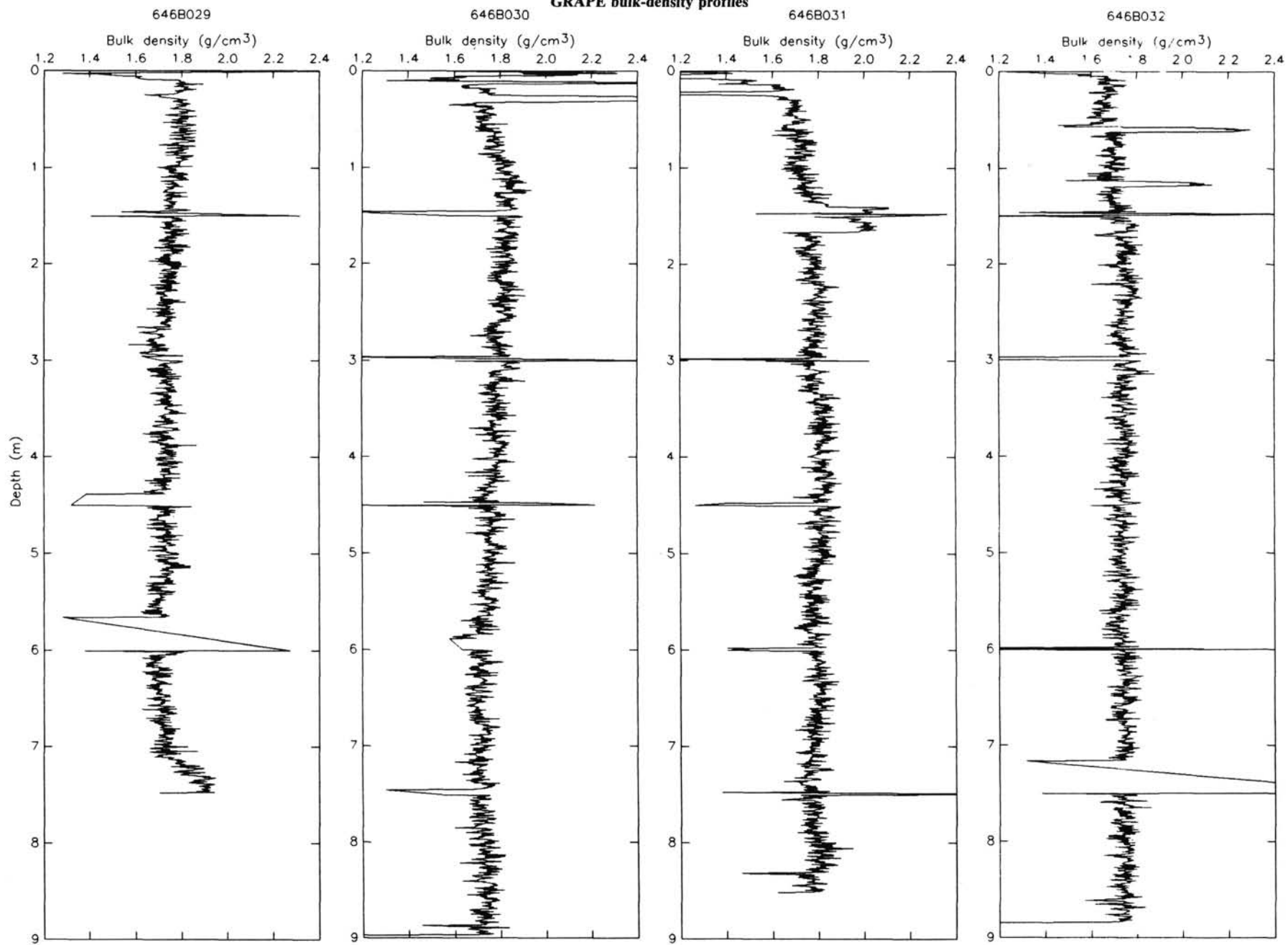
GRAPE bulk-density profiles



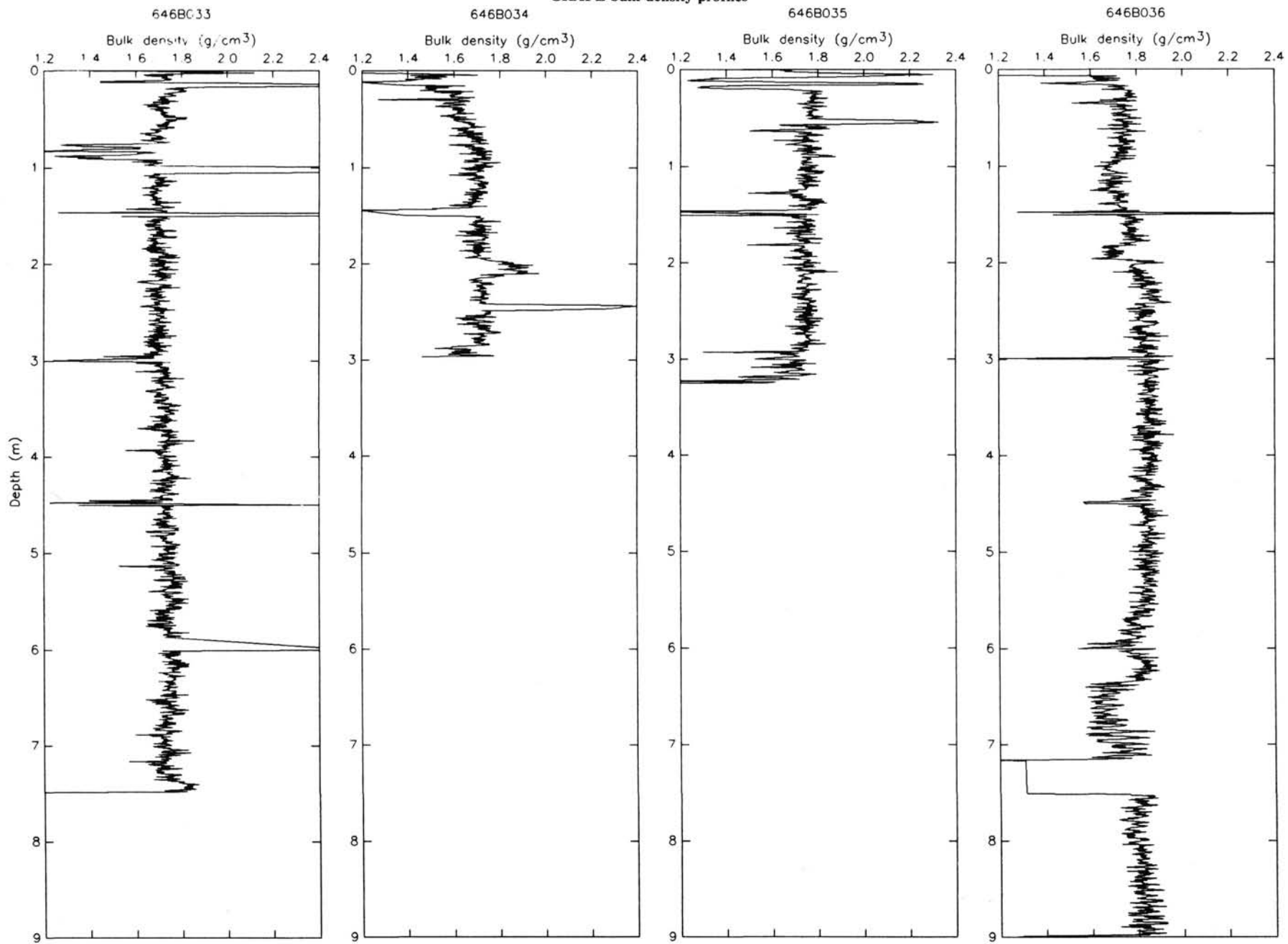
GRAPE bulk-density profiles



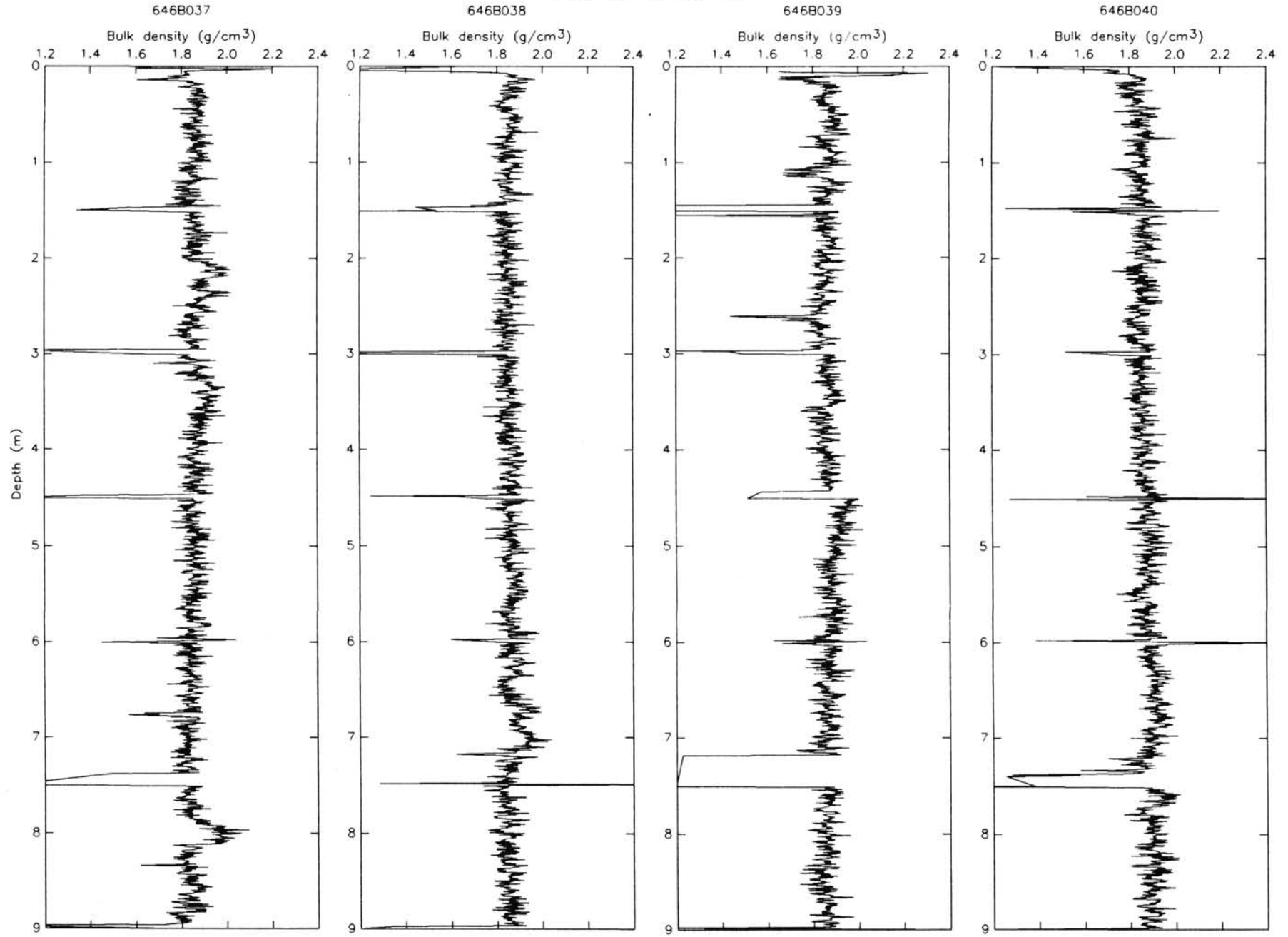
GRAPE bulk-density profiles



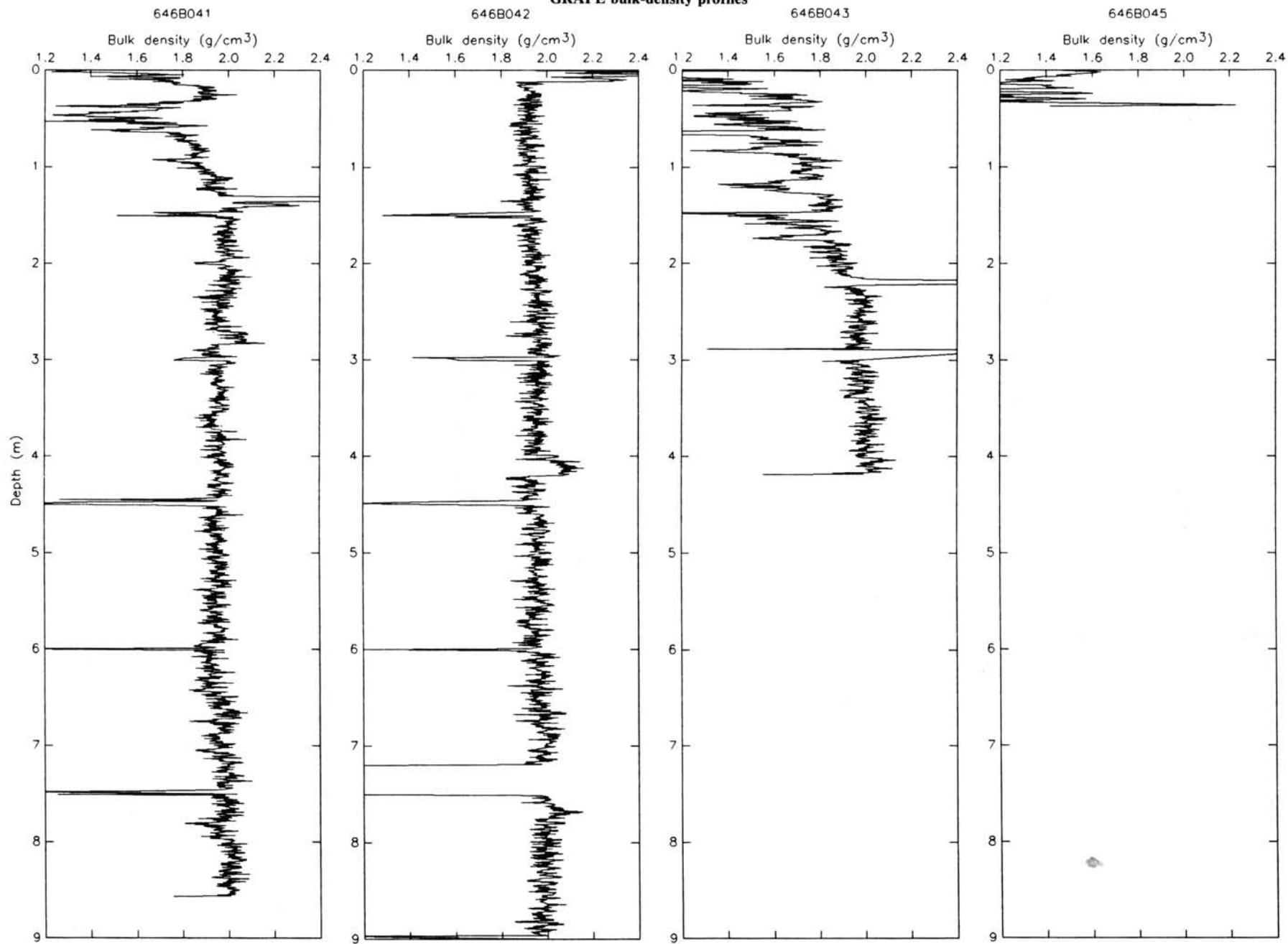
GRAPE bulk-density profiles



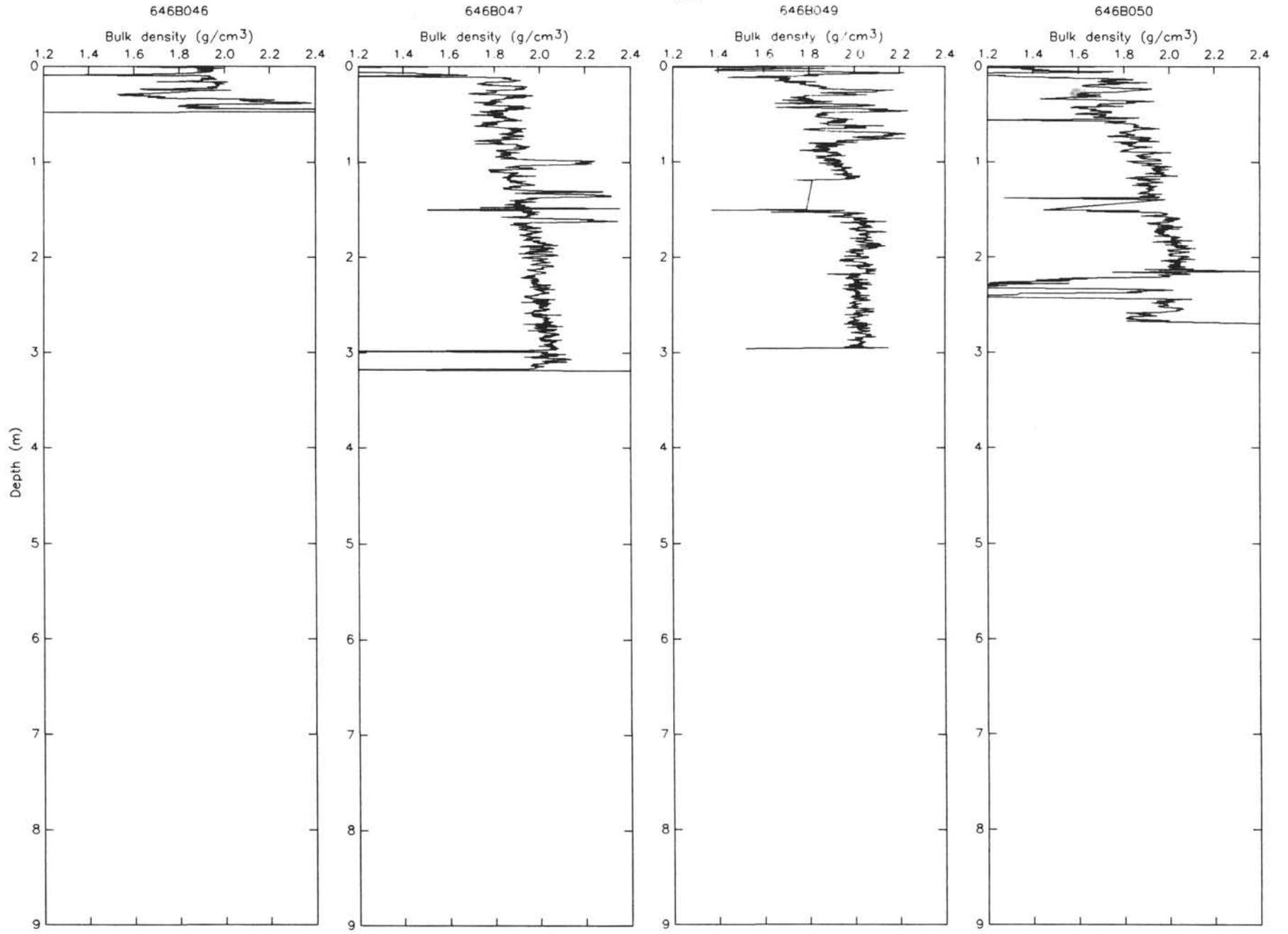
GRAPE bulk-density profiles



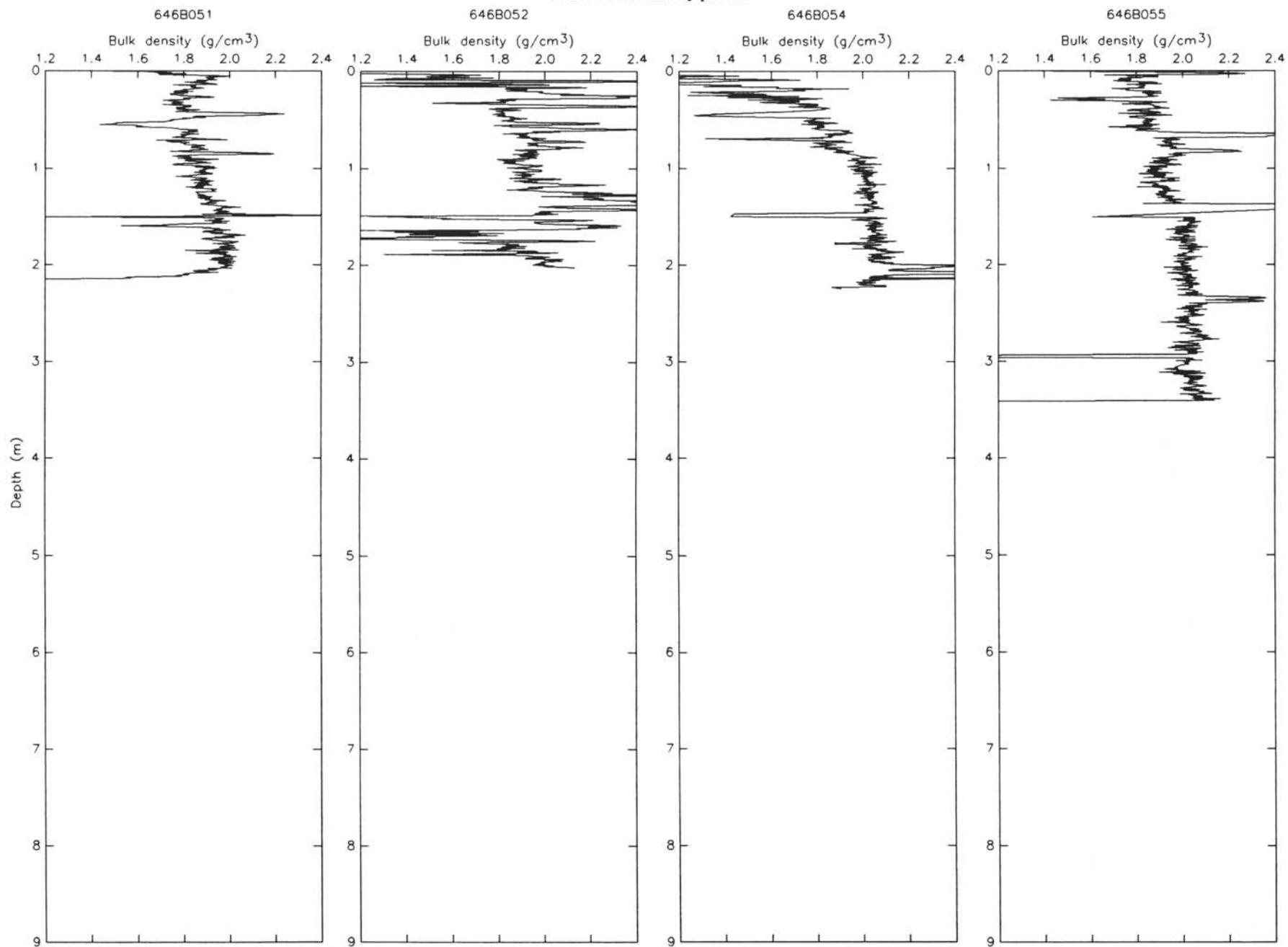
GRAPE bulk-density profiles



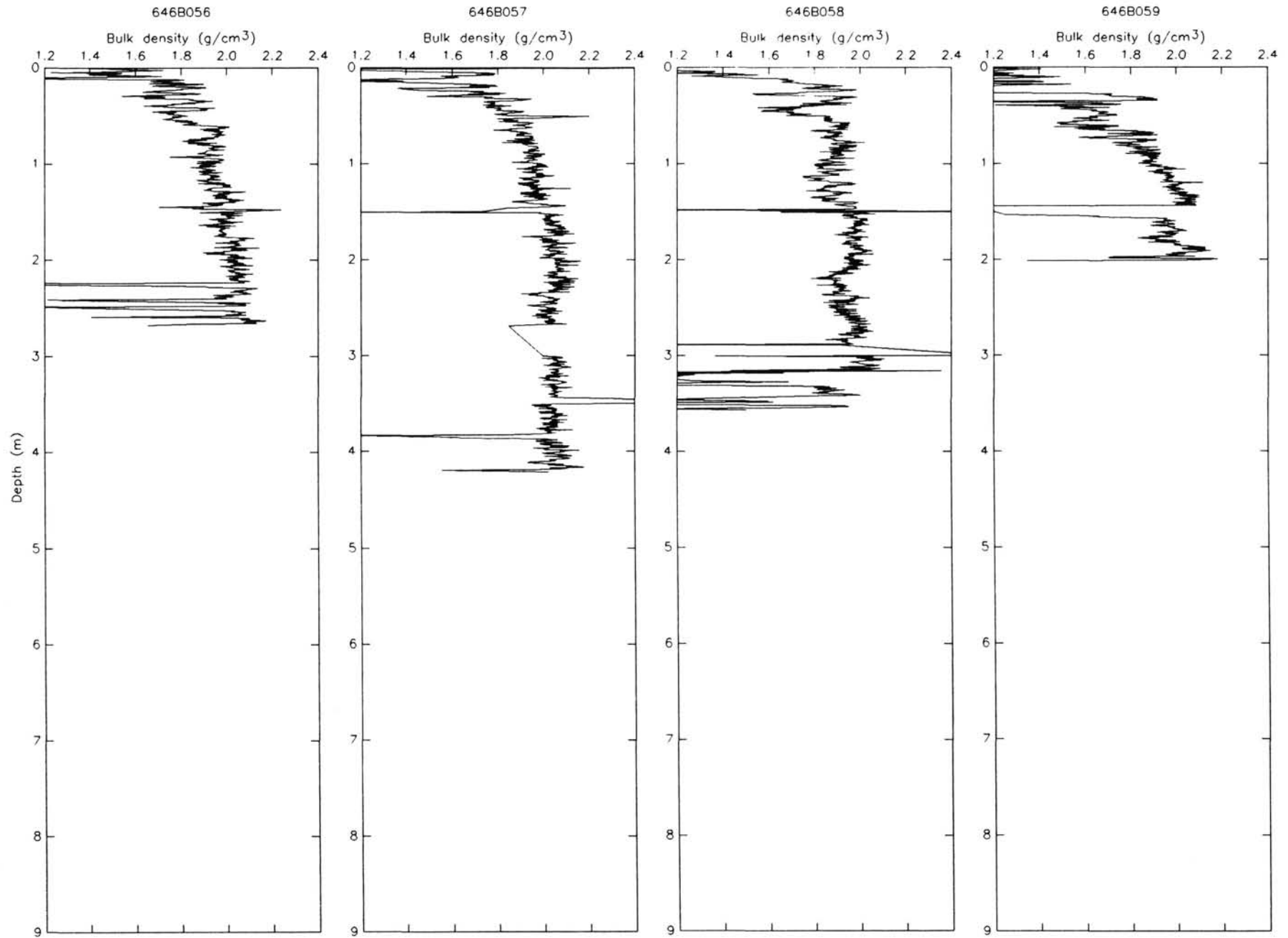
GRAPE bulk-density profiles



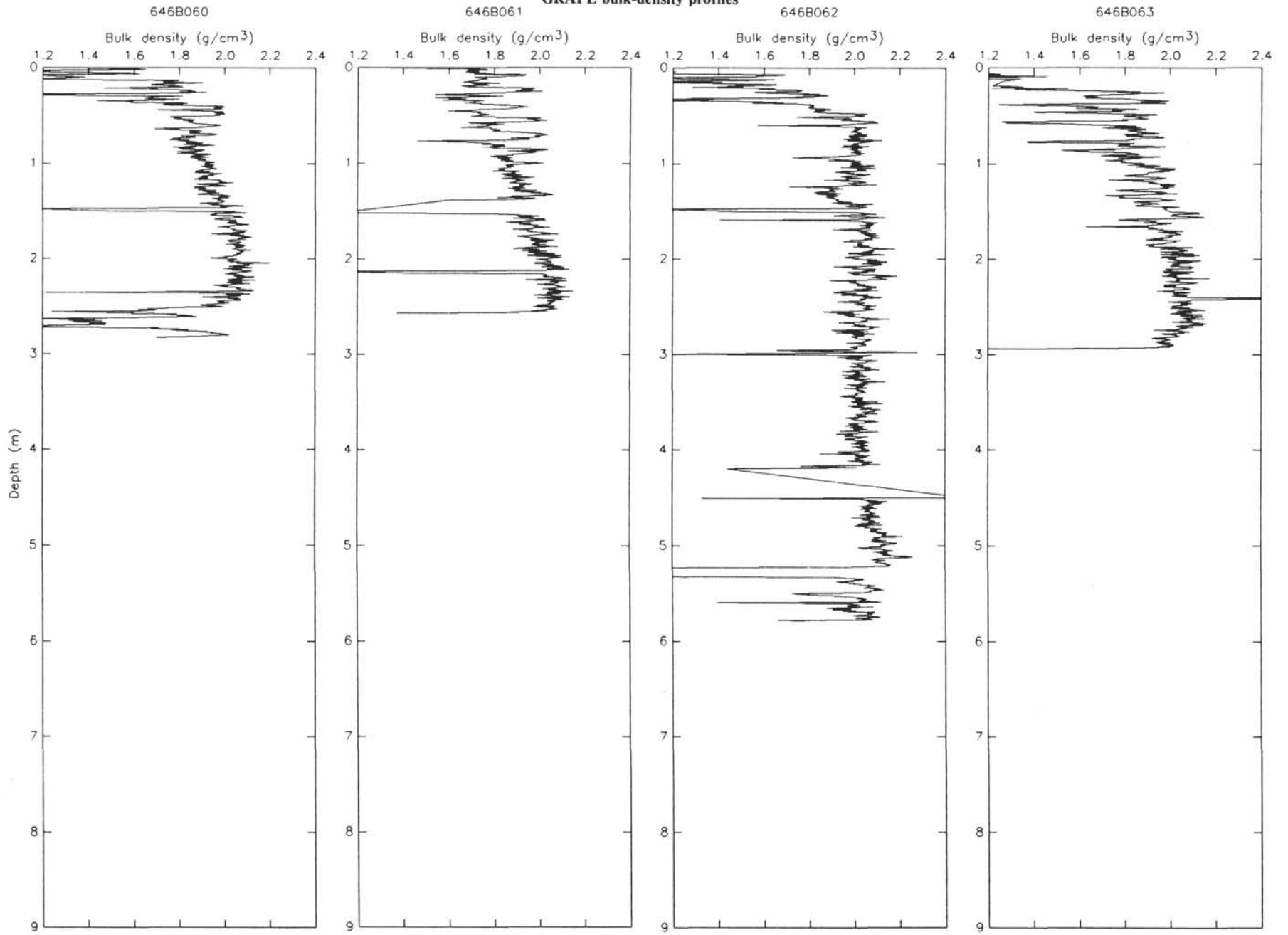
GRAPE bulk-density profiles



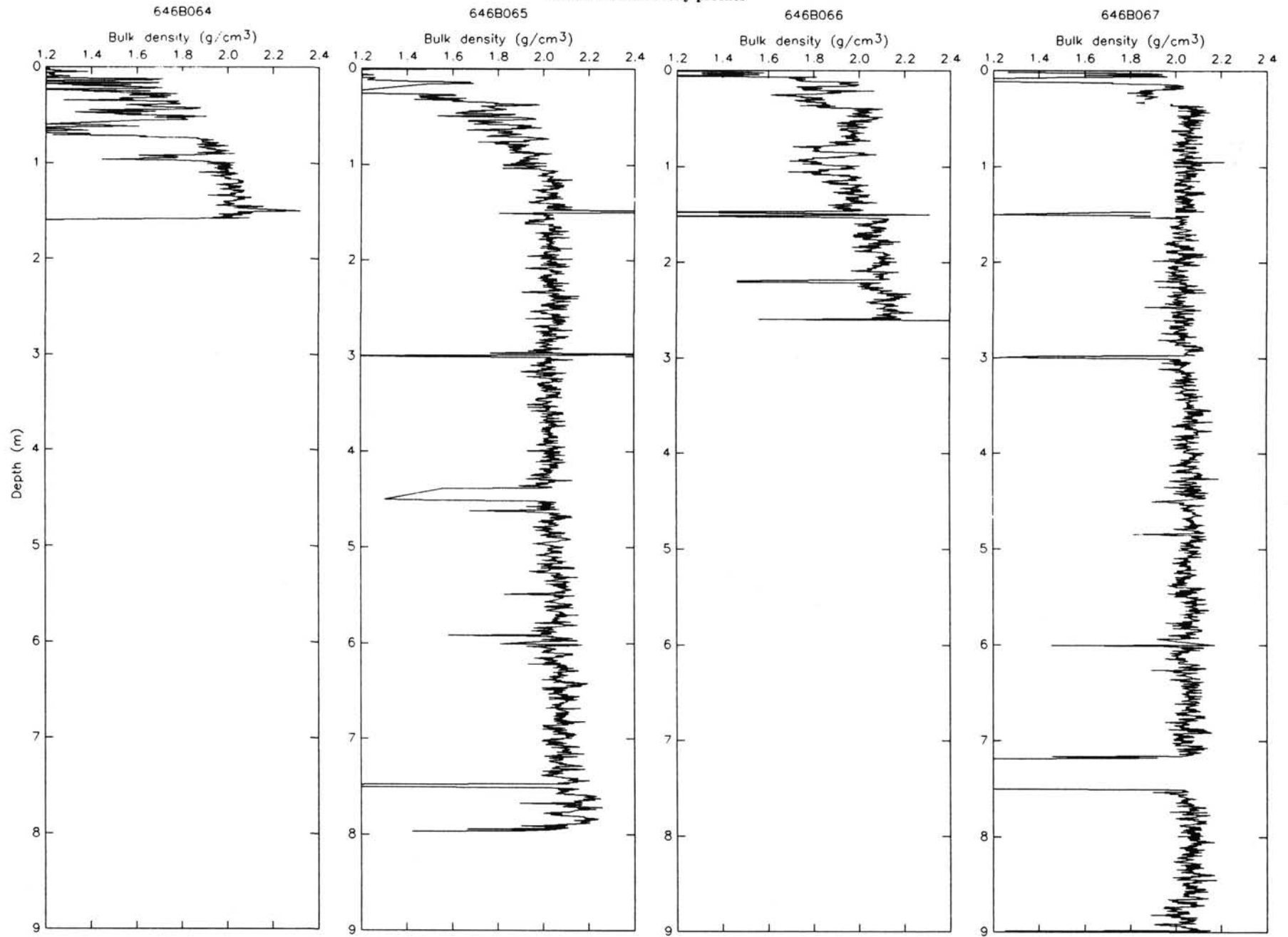
GRAPE bulk-density profiles



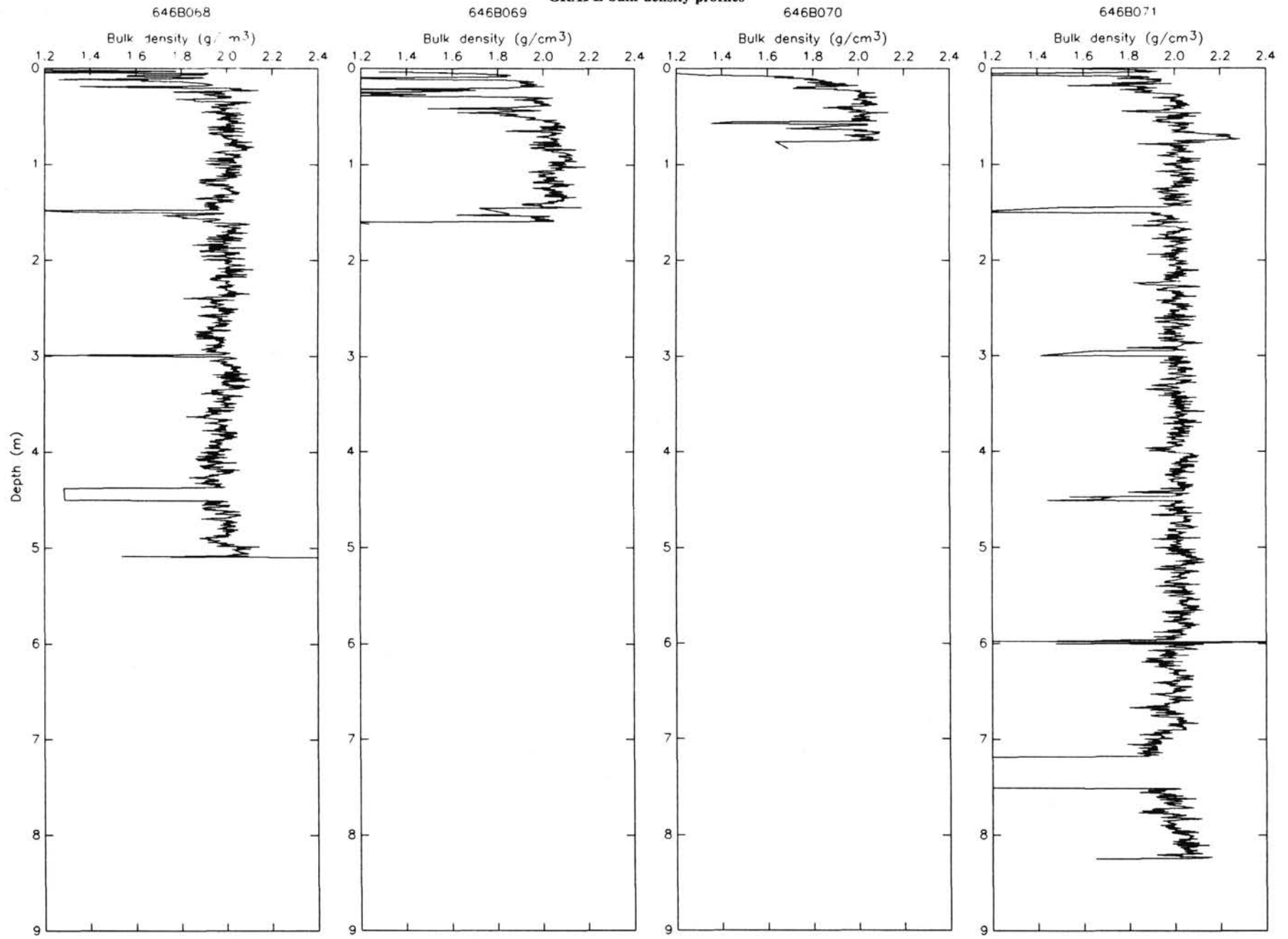
GRAPE bulk-density profiles



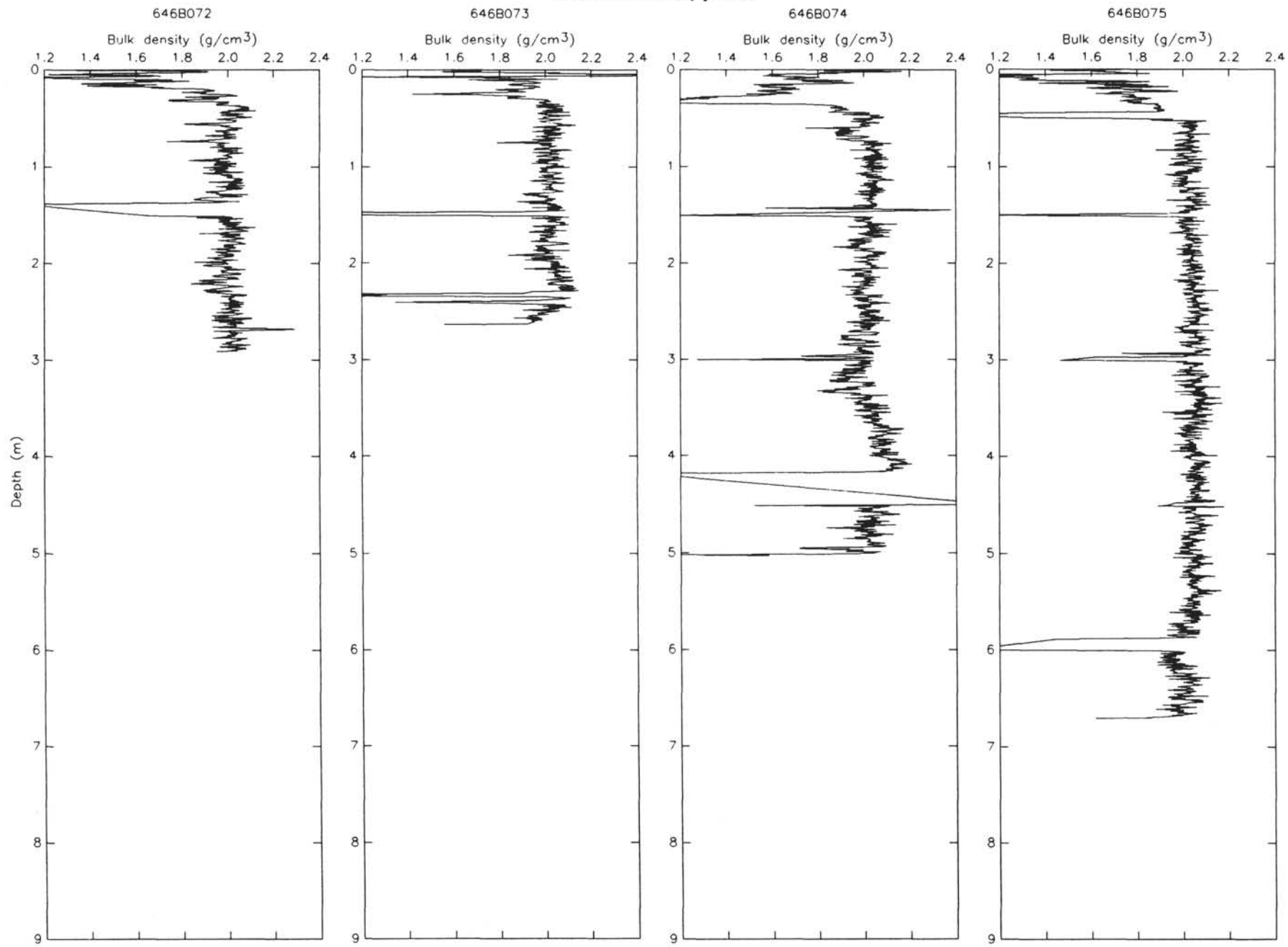
GRAPE bulk-density profiles



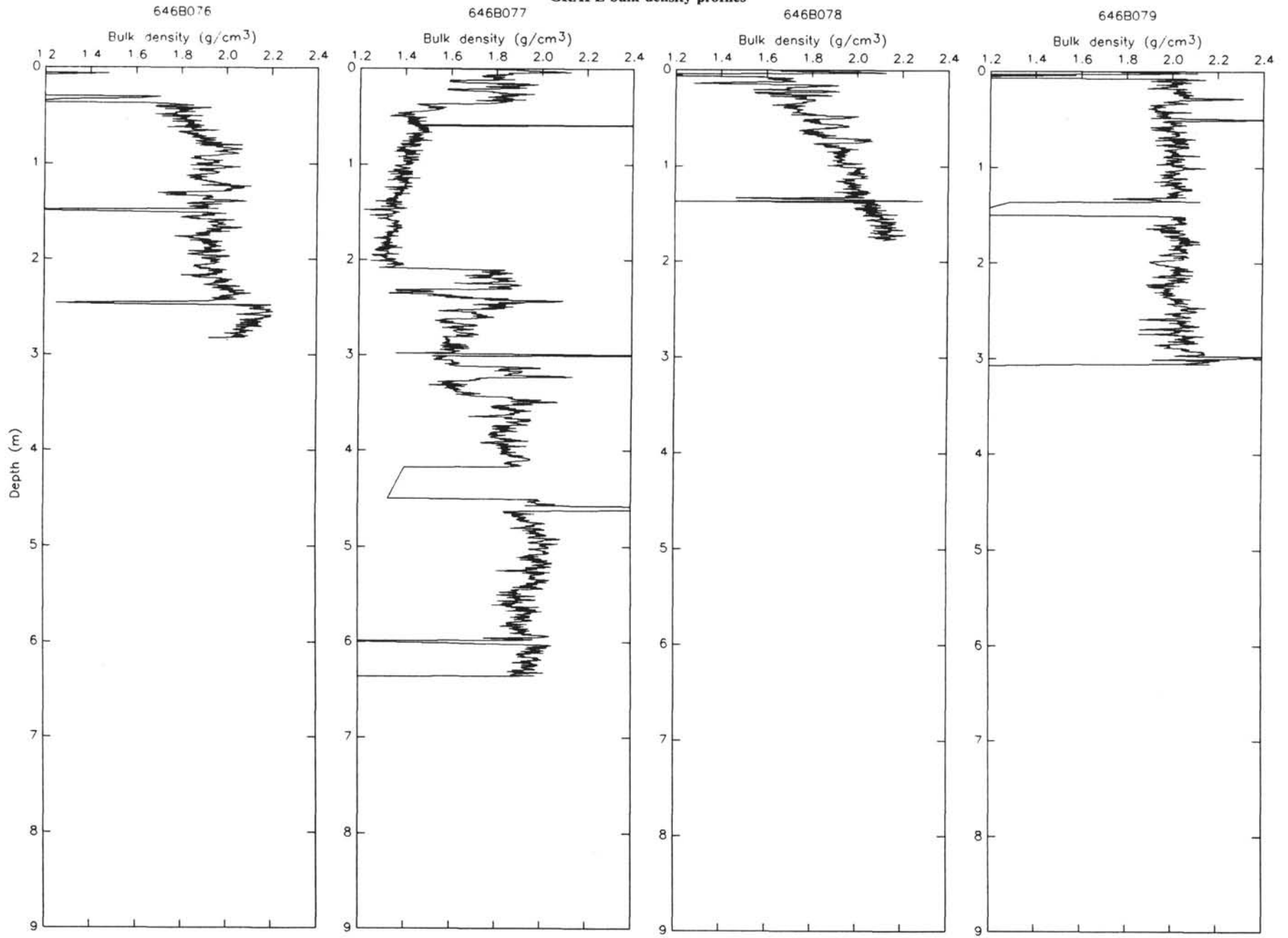
GRAPE bulk-density profiles



GRAPE bulk-density profiles



GRAPE bulk-density profiles



GRAPE bulk-density profiles

646B080

